B. Scatlle
JA52

PLASMA DIAGNOSTICS PACKAGE

FINAL SCIENCE REPORT

Volume 1

OSS-1 SECTION

NASA/MSFC Contract No. NAS8-32807

Department of Physics and Astronomy

THE UNIVERSITY OF IOWA

Iowa City, Iowa 52242

PLASMA DIAGNOSTICS PACKAGE

FINAL SCIENCE REPORT

Volume 1

OSS-1 SECTION

NASA/MSFC Contract No. NAS8-32807

Compiled By

J. S. Pickett
L. A. Frank
W. S. Kurth

Department of Physics and Astronomy
University of Iowa
Iowa City, Iowa 52242

June, 1988

I. INTRODUCTION

This volume (1) of the Plasma Diagnostics Package (PDP) Final Science Report contains a summary of all of the data reduction and scientific analyses which were performed using PDP data obtained on STS-3 as a part of the Office of Space Science first payload (OSS-1). This work was performed under NASA/Marshall Space Flight Center Contract No. NAS8-32807 with the University of Iowa during the period of launch, March 22, 1982, through June 30, 1983. During this period the primary data reduction effort consisted of processing summary plots of the data received by the 14 instruments located on the PDP and submitting these data to the National Space Science Data Center (NSSDC).

The scientific analyses during the performance period consisted of general studies which incorporated the results of several of the PDP's instruments, detailed studies which concentrated on data from only one or two of the instruments, and joint studies of beam-plasma interactions with the OSS-1 Fast Pulse Electron Generator (FPEG) of the Vehicle Charging and Potential Investigation (VCAP). Internal reports, published papers and oral presentations which involve PDP/OSS-1 data are listed in Sections III and IV. A PDP/OSS-1 scientific results meeting was held at the University of Iowa on April 19-20, 1983. This meeting was attended by most of the PDP and VCAP investigators and provided a forum for discussing and comparing the various results, particularly with regard to the shuttle orbiter environment. One of the most important functional objectives of the PDP on OSS-1 was to characterize the orbiter environment.

II. SUMMARY OF DATA PROCESSED

During the period March 22, 1982 through June 30, 1983, the University of Iowa generated 10-minute color survey slides for all of the times when the PDP was turned on during the OSS-1 flight, March 22, 1982 to March 27, 1982. These slides contain 15 panels of data representing the output from each of the instruments mounted on the PDP structure. Two sets of slides, together with a Data User's Guide, were submitted to NSSDC on April 28, 1983 and were given the identifying number NSSDC ID 82-022A-01A. In addition, 70 mm black and white wideband analog film was generated showing high time and frequency resolution of the electric and magnetic noise signals (0-30 kHz) received by the wideband analog receiver mounted on the PDP on the OSS-1 flight. This film, together with a Data User's Guide, was sent to NSSDC on June 23, 1983 and was given the identifying number NSSDC ID 82-022A-01B with film roll accession numbers IM00001 to IM00016.

III. INTERNAL REPORTS

A list of University of Iowa internally-generated reports, which pertain to the PDP on OSS-1, is given below. None of these reports was published (unless otherwise noted), but each is on file in the PDP Project Office in the Department of Physics and Astronomy.

STS-3/OSS-1 Plasma Diagnostics Package (PDP): 30 Day Engineering Report, Stanley Shawhan, Roger Anderson, and Gerald Murphy, Report No. 82-03, Dept. of Physics and Astronomy, University of Iowa, April, 1982.

STS-3/OSS-1 Plasma Diagnostics Package (PDP): 90 Day Summary Science Report, Stanley D. Shawhan and Gerald B. Murphy, Report No. 82-07, Dept. of Physics and Astronomy, University of Iowa, July, 1982. (Incorporated in its entirety in "STS/OSS-1 Plasma Diagnostics Package (PDP) Measurements of the Temperature, Pressure and Plasma Environment, S. D. Shawhan and G. Murphy, proceedings of the Shuttle Environment Workshop, Calverton, MD, Oct. 5-7, 1982.)

STS-3 Electromagnetic Interference: OSS-1/PDP Measurements, Stanley D. Shawhan, Report No. 82-06-01, Dept. of Physics and Astronomy, University of Iowa, August, 1982.

STS-3/PDP Microprocessor and Power Buss Performance, Richard L. Kroeger, Donald C. Enemark, and Stanley D. Shawhan, Report No. 82-08, Dept. of Physics and Astronomy, University of Iowa, August, 1982.

STS-3/PDP Thermal History and Time Constants, Martin E. Kerl, Timothy W. Clark, and Stanley D. Shawhan, Report No. 82-09, Dept. of Physics and Astronomy, University of Iowa, September, 1982.

Report on S-Band Field Strengths Due to the Transmitters of the Columbia as Measured on STS-3 by the University of Iowa Plasma Diagnostics Package, Gerald B. Murphy, Stanley D. Shawhan, and Kerry L. Neal, Report Nos. 82-10 and 83-04, Dept. of Physics and Astronomy, University of Iowa, September, 1982 and May 1983.

Data Users Guide to Plasma Diagnostics Package Survey Slides, Stanley D. Shawhan, Gerald B. Murphy, and Jolene S. Pickett, Report No. 83-02, Dept. of Physics and Astronomy, University of Iowa, April, 1983.

Data Users Guide to Plasma Diagnostics Package Wideband Analog Film, Stanley D. Shawhan, Gerald B. Murphy, and Jolene S. Pickett, Report No. 83-07, Dept. of Physics and Astronomy, University of Iowa, June, 1983.

IV. PUBLICATIONS AND PRESENTATIONS

A list of publications and oral presentations, which contain PDP/OSS-1 data, is given below. Copies of most of the publications are included in the remainder of this volume.

A. LIST OF PUBLICATIONS IN REFEREED JOURNALS

Description of the Plasma Diagnostics Package (PDP) for the OSS-1 Shuttle Mission and JSC Plasma Chamber Test in Conjunction with the Fast Pulse Electron Gun (FPEG), Stanley D. Shawhan, in Artificial Particle Beams Utilized in Space Plasma Studies, B.Grandal (ed.); NATO Conference Publications Series, Plenum Press, pp. 419-429, 1982.

Science on the Space Shuttle, W. M. Neupert, P. M. Banks, G. E. Brueckner, E. G. Chipman, J. Cowles, J. A. M. McDonnell, R. Novick, S. Ollendorf, S. D. Shawhan, J. J. Triolo, and J. L. Weinberg, Nature, Vol. 296, pp. 193-197, 1982.

Subsatellite Studies of Wave, Plasma and Chemical Injections from Spacelab, Stanley D. Shawhan, James L. Burch, and Robert W. Fredricks, J. of Spacecraft and Rockets, Vol. 20, pp. 238-244, 1983.

A Spacelab Principal Investigator's Guidance for Planning Scientific Experiments Using the Shuttle, Stanley D. Shawhan, J. of Spacecraft and Rockets, Vol. 20, pp. 477-483, 1983.

Multiple Ion Streams in the Near Vicinity of the Space Shuttle, N. H. Stone, U. Samir, K. H. Wright, Jr, D. L. Reasoner, and S. D. Shawhan, Geophys. Res. Lett., Vol. 10, pp. 1215-1218, 1983.

Plasma Diagnostics Package Initial Assessment of the Shuttle Orbiter Plasma Environment, Stanley D. Shawhan, Gerald B. Murphy, and Jolene S. Pickett, J. of Spacecraft and Rockets, Vol. 21, No. 4, pp. 387-391, 1984.

Measurements of Electromagnetic Interference on OV102 Columbia Using the Plasma Diagnostics Package, Stanley D. Shawhan, Gerald B. Murphy, and Dwight L. Fortna, J. of Spacecraft and Rockets, Vol. 21, No. 4, pp. 392-397, 1984.

Radio Frequency Fields Generated by the S-Band Communication Link on OV102, Gerald B. Murphy and Stanley D. Shawhan, J. of Spacecraft and Rockets, Vol. 21, No. 4, pp. 398-399, 1984.

Wave emissions from DC and Modulated Electron Beams on STS 3, Stanley D. Shawhan, Gerald B. Murphy, Peter M. Banks, P. Roger Williamson, and W. John Raitt, Radio Science, Vol. 19, No. 2, pp. 471-486, 1984.

Modulated Beam Injection from the Space Shuttle during Magnetic Conjunctions of STS 3 with the DE 1 Satellite, U. S. Inan, M. Pon, P. M. Banks, P. R. Williamson, W. J. Raitt, and S. D. Shawhan, Radio Science, Vol. 19, No. 2, pp. 487-495, 1984.

Effects of Chemical Releases by the STS-3 Orbiter on the Ionosphere, Jolene S. Pickett, Gerald B. Murphy, William S. Kurth, Christoph K. Goertz, and Stanley D. Shawhan, J. Geophys. Res., Vol. 90, No. 4A, pp. 3487-3497, 1985.

Further Observations of Space Shuttle Plasma-Electrodynamic Effects from OSS-1/STS-3, N. H. Stone, K. H. Wright, Jr., K. S. Hwang, U. Samir, G. B. Murphy, and S. D. Shawhan, Geophys. Res. Lett., Vol. 13, No. 3, pp. 217-220, 1986.

Measurements of Plasma Parameters in the Vicinity of the Space Shuttle, G. Murphy, J. Pickett, N. D'Angelo, and W. S. Kurth, Planet. Space Sci., Vol. 34, No. 10, pp. 993-1004, 1986.

Plasma Diagnostics Package Measurements of Ionospheric Ions and Shuttle-Induced Perturbations, David L. Reasoner, Stanley D. Shawhan, and Gerald B. Murphy, J. Geophys. Res., Vol. 91, No. A12, pp. 13,463-13,471, 1986.

The Emissions of Broadband Electrostatic Noise in the Near Vicinity of the Shuttle Oribter, K. S. Hwang, N. H. Stone, K. H. Wright, Jr., and U. Samir, Planet. Space Sci., Vol. 35, 1373-1379, 1987.

The Space Shuttle as a Platform for Observations of Ground-Based Transmitter Signals and Whistlers, T. Neubert, T. F. Bell, L. R. O. Storey, D. A. Gurnett, J. Geophys. Res., Vol. 92, 11262-11268, 1987.

Comment on "Ram Ion" Scattering by Space Shuttle V x B Induced Differential Charging, N. H. Stone, U. Samir, K. H. Wright, Jr., and K. S. Hwang, J. Geophys. Res., Vol. 93, No. A5, pp. 4143-4147, 1988.

VLF Wave Stimulation by Pulsed Electron Beams Injected from the Space Shuttle, G. D. Reeves, P. M. Banks, A. C. Fraser-Smith, T. Neubert, R. I. Bush, D. A. Gurnett, and W. J. Raitt, J. Geophys. Res., Vol. 93, 162-174, 1988.

B. LIST OF PUBLICATIONS IN PROCEEDINGS

Measurements by the Plasma Diagnostics Package on STS-3, Stanley D. Shawhan and Gerald B. Murphy, Proceedings of the Twelfth Space Simulation Conference "Shuttle Plus One--A New View of Space", Institute of Environmental Sciences, Pasadena, CA, 17-19 May, 1982.

STS-3/OSS-1 Plasma Diagnostics Package (PDP) Measurements of Orbiter-Generated V x B Potentials and Electrostatic Noise, S. D. Shawhan and G. B. Murphy, Proceedings of the Workshop on Natural Charging of Large Space Structures in Near Earth Polar Orbit, Air Force Geophysics Laboratory and Boston College, Hanscom AFB, MA, 14-15 Sept., 1982.

STS-3/OSS-1 Plasma Diagnostics Package (PDP) Measurements of the Temperature, Pressure and Plasma Environment, S. D. Shawhan and G. Murphy, Proceedings of the Shuttle Environment Workshop, NASA Office of Space Science and Applications, Calverton, MD, 5-7 Oct., 1982.

STS-3/OSS-1 Plasma Diagnostics Package (PDP) Measurements of Orbiter Transmitter and Subsystem Electromagnetic Interference, S. D. Shawhan and G. Murphy, Proceedings of the Shuttle Environment Workshop, NASA Office of Space Science and Applications, Calverton, MD, 5-7 Oct., 1982.

Electron Beam Experiments Aboard the Space Shuttle, P. M. Banks, P. R. Williamson, W. J. Raitt, and S. D. Shawhan, Proceedings of the International Symposium on Active Experiments in Space, European Space Agency, Alpbach, Austria, 24-28 May, 1983.

Interaction of the Space Shuttle Orbiter with the Ionospheric Plasma, G. B. Murphy, S. D. Shawhan, L. A. Frank, N. D'Angelo, D. A. Gurnett, J. M. Grebowsky, D. L. Reasoner and N. Stone, Proceedings of the 17th ESLAB Symposium on Spacecraft/Plasma Interactions and their Influence on Field and Particle Measurements, European Space Agency, Noordwijk, Netherlands, pp. 73-78, 13-16 Sept., 1983.

Suprathermal Plasma Observed on the STS-3 Mission by the Plasma Diagnostics Package, W. Paterson, L. A. Frank, H. Owens, J. S. Pickett, G. B. Murphy and S. D. Shawhan, Proceedings of the USAF/NASA Spacecraft Environmental Interactions Technology Conference, U.S. Air Force Academy, Colorado Springs, CO, 4-6 Oct., 1983.

Electron and Ion Density Depletions Measured in the STS-3 Orbiter Wake, G. B. Murphy, J. S. Pickett, W. J. Raitt, and S. B. Shawhan, Proceedings of the USAF/NASA Spacecraft Environmental Interactions Technology Conference, U. S. Air Force Academy, Colorado Springs, CO, 4-6 Oct., 1983.

Perturbations to the Plasma Environment Induced by the Orbiter's Maneuvering Thrusters, Gerald B. Murphy, Stanley D.Shawhan, and Jolene S. Pickett, Proceedings of the AIAA Shuttle Environment and Operations Meeting, American Institute of Aeronautics and Astronautics, Washington, D.C., pp. 59-65, 31 Oct.-2 Nov., 1983.

Measured Thermal Ion Environment of STS-3, J. M. Grebowsky, M. W. Pharo III, H. A. Taylor, Jr., and I. J. Eberstein, Proceedings of the AIAA Environment and Operations Meeting, American Institute of Aeronautics and Astronautics, Washington, D.C., pp. 47-51, 31 Oct.-2 Nov., 1983.

C. LIST OF ORAL PRESENTATIONS

Subsatellite Studies of Wave, Plasma and Chemical Injections from Spacelab, S. D. Shawhan, J. L. Burch, and R. W. Fredricks, AIAA 20th Aerospace Sciences Meeting, American Institute of Aeronautics and Astronautics, Orlando, FL, Jan., 1982.

Results from the Plasma Diagnostics Package, S.D.Shawhan, OSS-1 Press Conference, NASA/HQ, Washington, D.C., May, 1982.

Measurements by the Plasma Diagnostics Package on STS-3, Stanley D. Shawhan and Gerald B. Murphy, Twelfth Space Simulation Conference "Shuttle Plus One—A View of Space", Institute of Environmental Sciences, Pasadena, CA, 17-19 May, 1982.

Plasma Diagnostics Package of the OSS-1 Pallet on STS-3: The Mission and First Results, S. D. Shawhan, AGU 1982 Spring Meeting, Philadelphia, PA, June, 1982.

Beam-Plasma Experiments from the Space Shuttle STS-3 Mission, S. D. Shawhan, European Geophysical Society, Leeds, England, Aug., 1982.

STS-3/OSS-1 Plasma Diagnostics Package (PDP) Measurements of Orbiter-Generated V x B Potentials and Electrostatic Noise, Workshop on Natural Charging of Large Space Structures in Near Earth Polar Oribt, Air Force Geophysics Laboratory, Hanscom AFB, MA, 14-15 Sept., 1982.

STS-3/OSS-1 Plasma Diagnostics Package (PDP) Measurements of Orbiter Transmitter and Subsystem Electromagnetic Interference, S. D. Shawhan and G. Murphy, The Shuttle Environment Workshop, NASA Office of Space Science and Applications, Calverton, MD, 5-7 Oct., 1982.

STS-3/OSS-1 Plasma Diagnostics Package Measurements of the Temperature, Pressure and Plasma Environment, S. D. Shawhan and G. Murphy, The Shuttle Environment Workshop, NASA Office of Space Science and Applications, Calverton, MD, 5-7 Oct., 1982.

PDP Measurements of Beam-Plasma Interactions on STS-3/OSS-1, S. D. Shawhan, G. B. Murphy, L. A. Frank, D. A. Gurnett, and H. D. Owens, AGU 1982 Fall Meeting, American Geophysical Union, San Francisco, CA, 6-11 Dec., 1982.

STS-3/OSS-1 Plasma Diagnostics Package (PDP) Measurements of Orbiter-Generated V x B Potentials and Electrostatic Noise, G. B. Murphy, S. D. Shawhan, and D. A. Gurnett, AGU 1982 Fall Meeting, American Geophysical Union, San Francisco, CA, 6-11 Dec., 1982.

Orbiter-Excited Electrostatic Emission, Stanley D. Shawhan, Gerald B. Murphy, and Donald A. Gurnett, National Radio Science Meeting, U. S. National Committee for International Union of Radio Science, Boulder, CO, 5-7 Jan., 1983.

Wave Emission from the FPEG Electron Beam Measured with the PDP, Stanley D. Shawhan, Gerald B. Murphy, and Peter Banks, National Radio Science Meeting, U. S. National Committee for International Union of Radio Science, Boulder, CO, 5-7 Jan., 1983.

Plasma Diagnostics Package Assessment of the STS-3 Orbiter Environment and Systems for Science, Gerald B. Murphy and Stanley D. Shawhan, AIAA 21st Aerospace Sciences Meeting, American Institute of Aeronautics and Astronautics, Reno, NV, 10-13 Jan., 1983.

Beam-Plasma Interactions and Orbiter Environment Measurements with the PDP on STS-3, S. D. Shawhan, R. R. Anderson, N. D'Angelo, L. A. Frank, D. A. Gurnett, G. B. Murphy, H. D. Owens, D. Reasoner, N. Stone, H. Brinton, and D. Fortna, AIAA 21st Aerospace Sciences Meeting, American Institute of Aeronautics and Astronautics, Reno, NV, 10-13 Jan., 1983.

Orbiter-Associated Wave Phenomena, Stanley D. Shawhan, Donald A. Gurnett, Gerald B. Murphy, and Peter M. Banks, Waves in Magnetospheric Plasmas, Hawaii, 7-11 Feb., 1983.

Interaction of the Space Shuttle Orbiter with the Ionospheric Plasma, G. B. Murphy, S. D. Shawhan, L. A. Frank, N. D'Angelo, D. A. Gurnett, J. M. Grebowsky, D. L. Reasoner, and N. Stone, 17th ESLAB Symposium on Spacecraft/Plasma Interactions and their Influence on Field and Particle Measurements, European Space Agency, Noordwijk, Netherlands, 13-16 Sept., 1983.

Suprathermal Plasma Observed on the STS-3 Mission by the Plasma Diagnostics Package, S. D. Shawhan, L. A. Frank, H. Owens, W. Paterson, J. Pickett, and G. B. Murphy, USAF/NASA Spacecraft Environmental Interactions Technology Conference, U. S. Air Force Academy, Colorado Springs, CO, 4-6 Oct., 1983.

Electron and Ion Density Depletions in the STS-3 Orbiter Wake, S. D. Shawhan, G. B. Murphy, A. Dresselhaus, J. Pickett, J. Grebowsky, D. L. Reasoner, and W. J. Raitt, USAF/NASA Spacecraft Environmental Interactions Technology Conference, U. S. Air Force Academy, Colorado Springs, CO, 4-6 Oct., 1983.

Perturbations to the Plasma Environment Induced by the Orbiter's Maneuvering Thrusters, Gerald B. Murphy, Stanley D. Shawhan, and Jolene S. Pickett, AIAA Shuttle Environment and Operations Meeting, American Institute of Aeronautics and Astronautics, Washington, D.C., 31 Oct. -2 Nov., 1983.

Plasma Measurements on Space Shuttle, S. D. Shawhan and G. B. Murphy, AIAA Shuttle Environment and Operations Meeting, American Institute of Aeronautics and Astronautics, Washington, D.C., 31 Oct. -2 Nov., 1983.

Observations of a Return Current Induced by an Electron Beam Emitted from the Space Shuttle, W. R. Paterson, W. S. Kurth, L. A. Frank, T. E. Eastman, G. B. Murphy, J. S. Pickett, H. Owens, and S. D. Shawhan, AGU 1983 Fall Meeting, American Geophysical Union, San Francisco, CA, 5-9 Dec., 1983.

Broadband Orbiter-Generated Electrostatic Noise, G. B. Murphy, W. S. Kurth, J. S. Pickett, S. D. Shawhan, and K. Papadopoulos, AGU 1983 Fall Meeting, American Geophysical Union, San Francisco, CA, 5-9 Dec., 1983.

Effects of Chemical Releases by the STS-3 Orbiter on the Ionosphere, J. S. Pickett, G. B. Murphy, W. S. Kurth, and S.D. Shawhan, National Radio Science Meeting, U. S. National Committee for International Union of Radio Science, Boulder, CO, 11-14 Jan., 1984.

Characteristics of Strong Plasma Turbulence Created by the STS Orbiter, G. B. Murphy, N. D'Angelo, W. S. Kurth, J. S. Pickett, and S. D. Shawhan, National Radio Science Meeting, U. S. National Committee for International Union of Radio Science, Boulder, CO, 11-14 Jan., 1984.

Effects of Varying Plasma Density and Turbulence on the Operation of a Large VLF Dipole Antenna, G. B. Murphy and J. S. Pickett, National Radio Science Meeting, U. S. National Committee for International Union of Radio Science, Boulder, CO, 11-14 Jan., 1984.

Observations of an Electron Beam Emitted from the Space Shuttle, W. R. Paterson, L. A. Frank, W. S. Kurth, G. B. Murphy, J. S. Pickett and S. D. Shawhan, Conference on Beam Plasma Interactions in Space, NASA and Science Applications, Inc., Eastsound, WA, 12-16 Aug., 1984.

Wave emissions from dc and modulated electron beams on STS-3, Gerald B. Murphy, Stanley D. Shawhan, Peter M. Banks, P. Roger Williamson and W. John Raitt, Conference on Beam Plasma Interactions in Space, NASA and Science Applications, Inc., Eastsound, WA, 12-16 Aug., 1984.

Effects of Chemical Releases by the STS-3 Orbiter on the Ionosphere, W. S. Kurth, J. S. Pickett, C. K. Goertz, G. B. Murphy, and S. D. Shawhan, XXIst General Assembly of the International Union of Radio Science, Italian National Committee for URSI, Florence, Italy, 29 Aug. -5 Sept., 1984.

Elevated Plasma "Temperature" in the Near Wake of the Shuttle Orbiter, G. B. Murphy, J. S. Pickett, N. D'Angelo, S. D. Shawhan, U. Samir, N. Stone, K. Wright, AGU 1984 Fall Meeting, American Geophysical Union, San Francisco, CA ,6 Dec., 1984.

OSS-1/PDP Langmuir Probe Results, G. B. Murphy, J. S. Pickett, N. D'Angelo, NASA Lewis Research Center, Cleveland, OH, 24 Jan., 1985.

OSS-1/PDP LEPEDEA Results, W. R. Paterson, L. A. Frank, NASA Lewis Research Center, San Francisco, CA, 24 Jan., 1985.

Plasma Oscillations Associated with the Wake Structure of the Space Shuttle, G. B. Murphy, J. S. Pickett, N. D'Angelo, W. S. Kurth, AGU 1985 Fall Meeting, American Geophysical Union, San Francisco, CA, 12 Dec., 1985.

Conditions for the Emission of Broadband Electrostatic Waves Near the Shuttle Orbiter, K. S. Hwang, N. H. Stone, K. H. Wright, Jr., U. Samir, poster paper presented at 1986 Spring AGU Meeting, American Geophysical Union, Baltimore, MD, 19-23 May, 1986.

D. STS-3/OSS-1 PUBLICATIONS

From: ARTIFICIAL PARTICLE BEAMS IN SPACE PLASMA STUDIES
Edited by [illegible]
(Plenum Publishing Corporation, 1982)

DESCRIPTION OF THE PLASMA DIAGNOSTICS PACKAGE (PDP) FOR THE OSS-1 SHUTTLE MISSION AND JSC PLASMA CHAMBER TEST IN CONJUNCTION WITH THE FAST PULSE ELECTRON GUN (FPEG)

Stanley D. Shawhan

Department of Physics and Astronomy
The University of Iowa
Iowa City, Iowa 52242 USA

INTRODUCTION

The Plasma Diagnostics Package (PDP) and support systems are being readied for flight on the OSS-1 Space Shuttle Mission (STS-4 in 1982) and on the Spacelab-2 Shuttle Mission (1983 or 1984). In March 1981 in the Johnson Space Center Plasma Chamber A, the PDP was utilized to measure the state of the ambient plasma and of phenomena induced by operation of the Utah State University Fast Pulse Electron Gun (FPEG). The FPEG is an element of the Vehicle Charging and Potential (VCAP) investigation on the OSS-1 Mission. On the OSS-1 Mission, the PDP will make plasma measurements as it is swept through the FPEG beam region by the Shuttle Remote Manipulator System (RMS).

In this paper, objectives of the PDP investigations are stated, features of the PDP systems are described and measurement characteristics of the PDP instruments are listed. Sample results from the JSC Plasma Chamber Tests are presented and these results are discussed in the context of results obtained, for example, by Bernstein, et al. (1978, 1979) and by Jost, et al. (1980) and of the theory developed by Rowland, et al. (1980).

DESCRIPTION OF THE OSS-1 PLASMA DIAGNOSTICS PACKAGE (PDP)

Each of the investigations for the Shuttle OSS-1 "Pathfinder" Mission and for the Spacelab-2 Missions are described by Neupert (1979) and Clifton (1978), respectively. A brief summary of the PDP investigation objectives, instrument characteristics and on-orbit operations is given here.

Science and Technical Objectives

For the OSS-1 Mission, the primary scientific and technical objectives are as follows and these are depicted in Figure 1:

- Study the Orbiter-magnetoplasma interactions within 15 meters of the Orbiter through measurement of electric and magnetic fields, ionized particle wakes and generated waves;

- Determine the characteristics of the electron beam emitted from the Fast Pulse Electron Gun (FPEG) out to a range of 15 meters from the Orbiter and measure the resulting beam-plasma interactions in terms of fields, waves and particle distribution functions;

- Locate and measure sources of fields, electromagnetic interference (EMI) and plasma contamination in the environment of the Orbiter out to 15 meters; and

- Flight-test the systems and procedures associated with the Spacelab-2 PDP experiment with particular emphasis on operations with the Remote Manipulator System, on unlatching and relatching the PDP unit, and on evaluating the telemetry link.

The first two objectives utilize the Orbiter for carrying out active experiments in the ionosphere. Since the Orbiter itself is very large compared to an electron gyroradius, comparable to an ion gyroradius, partially conducting and partially insulating, its motion through the magnetoplasma will cause a variety of wake effects including density perturbations, currents, wave excitation and particle energization. On OSS-1 these wake phenomena are to be studied out to the 15m extent of the RMS but on Spacelab-2, when the PDP functions as an Orbiter subsatellite, the wake region out to 10km can be explored.

OSS-1 offers the only Shuttle opportunity before 1985 to perform active beam-plasma interaction studies with in-beam diagnostics. OSS-1 will carry both the VCAP Fast Pulse Electron Gun and the PDP which is articulated through the electron beam by the RMS. The Space Experiments With Particle Accelerations (SEPAC) particle injection system with some near-beam diagnostics will be flown on Spacelab-1 but the PDP is assigned for reflight on Spacelab-2. Only after 1985 with the follow-on Spacelab missions are there plans to fly the SEPAC with in-beam and subsatellite diagnostics. The JSC Plasma Chamber test of March 1981, described in the next major section, was motivated by the desire to obtain more data on beam-plasma interactions, to further describe the beam-plasma-discharge (BPD) phenomena (e.g., Rowland, et al., 1980) for identification of its occurrence on-orbit and to better understand the joint operation of the PDP and VCAP systems.

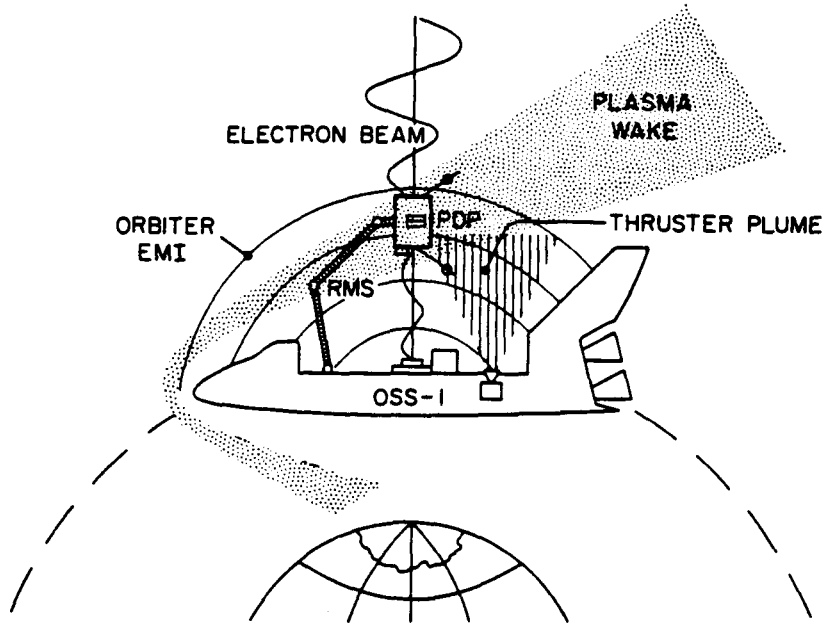

Fig. 1. Depiction of scientific and technical objectives for the Plasma Diagnostics Package (PDP) on the Shuttle OSS-1 Mission. Through articulation by the Remote Manipulator System (RMS), the PDP can be used to diagnose Orbiter-induced plasma wakes and the Fast Pulse Electron Gun-initiated electron beam-plasma phenomena.

As a subsatellite of the Spacelab-2 Orbiter, the PDP will penetrate regions of plasma depletion created by scheduled OMS burns exhausting 100-1000 kg of propellant. These active plasma depletion experiments of Mendillo and da Rosa (see Clifton, 1978) offer the opportunity to compare ground-radar global measurements of the depletion regions with PDP in situ samples to assess chemical reaction rates and associated fields, waves and energized plasma. A Recoverable PDP is being developed to continue these studies after 1985 with active particle, wave, moving body, and chemical perturbations of the ionospheric plasma.

PDP INSTRUMENT CHARACTERISTICS

The PDP carries a complement of new and of flight-spare instruments from previous NASA programs, to provide a comprehensive set of fields, waves, thermal plasma and energized plasma measurements. A detailed listing of the measured parameters and the measurement ranges is given in Table 1 for OSS-1. For Spacelab-2 the electric field dipole length will be increased to 4 meters through the use of hinged booms. Indicated in Figure 2 are the locations of the apera-

Table 1. PDP Scientific Instruments Performance Specifications

MEASUREMENT	TECHNIQUE	PARAMETERS	VALUE/RANGE
DC Magnetic Field	Triaxial Fluxgate Magnetometer	Dynamic Range	±12 milligauss to ±1.5 gauss each axis
		Temporal Resolution	10 samples/second each axis
DC Electric Field	1m Double Probe with Spherical Sensors	Dynamic Range	±2 mV/m to ±2 V/m (average and differential
		Temporal Resolution	20 samples/second
AC Magnetic Waves	Searchcoil Sensor; Wideband Receiver	Frequency Range	5Hz-1kHz & 0.65-10, 10-20, 20-30kHz
		Amplitude Range	100db @ 0.4db resolution; $3m\gamma$-300γ
		Duty Cycle	12.8 seconds out of 51.2 sec.
	Searchcoil Sensor; VLF Spectrum Analyzer (IMP)	Frequency Range	16 channels 35.5 Hz to 178kHz
		Frequency Resolution	±15% bandwidth
		Amplitude Resolution	100db @ 0.4dB resolution; $3x10^{-5}$ - $3\gamma Hz^{-1/2}$ (peak and average)
		Temporal Resolution	0.6 sample/second each channel
		Duty Cycle	12.8 seconds out of 51.2 sec.
AC Electric and Electrostatic Waves	1m Dipole Antenna Wideband Receiver	Frequency Range	5Hz-1kHz, 0.65-10kHz, 10-20kHz & 20-30kHz
		Amplitude Range	100db @ 0.4db resolution; 3uV/m - 300 mV/m
		Duty Cycle	38.4 seconds out of 51.2 sec.
	1m Dipole Antenna VLF Spectrum Analyzer (Helios)	Frequency Range	16 channels-31.2Hz to 178kHz
		Frequency Resolution	±15% bandwidth
		Amplitude Resolution	100db @ 0.4dB resolution; $3x10^{-8}$ - $3x10^{-3}Vm^{-1}Hz^{-1/2}$ (peak and average)
		Temporal Resolution	0.6 sample/second each channel
		Duty Cycle	100%
	1m Dipole Antenna, Mid Frequency Receiver	Frequency Range	8 channels-31.6Hz to 17.8 MHz
		Frequency Resolution	±30% bandwidth
		Amplitude Resolution	70db @ 1dB resolution; $3x10^{-3}$ - 10 V/m (peak and average)
		Temporal Resolution	1.6 second/scan
VHF/UHF EMI Levels	Horn Antenna VHF/UHF Receiver	Frequency Range	4 channels--25-65, 65-160, 160-400, 400-800 MHz
		Frequency Resolution	±50%
		Amplitude Resolution	70db @ 1db resolution; 10^{-2} - 30 V/m; (peak and average)
		Temporal Resolution	1.6 sec/scan
S-Band Field Strength Monitor	Horn Antenna VHF/UHF Receiver + Mixer and L.O.	Frequency Range	2000-2330 MHz
		Amplitude Range	.01 to 30 V/m (peak & average)
		Temporal Resolution	1.6 sec.
Suprathermal Particles	Low Energy Proton & Electron Differential Energy Analyzer (LEPEDEA)	Energy Range	2eV-50keV in 42 steps: electrons and ions
		Energy Resolution	34%
		Field of View	6^o x 162^o (7 detectors)
		Flux: Electrons	$30-1x10^7$, electrons/cm^2 sec sr eV
		Protons	$6-2x10^8$ protons/cm^2 sec sr eV
		Temporal Resolution	1.6 sec for spectrum
	Electrometer	Flux Range	10^9 -10^{14} elect cm^{-2} sec^{-1}
		Temporal Resolution	10 samples/second
	Retarding Potential Analyzer/Differential Ion Flux Probe	Density Range	$2x10^1$ -$1x10^7$ ions cm^{-3}
		Energy Range	0-16 eV
		Velocity Range	0-15km sec^{-1}
		Temporal Resolution	0.8 sec/scan; 51.2 sec/analysis
Thermal Electrons	Langmuir Probe, Density	Dynamic Range	10^3 -10^7 electrons cm^{-3}
		Temporal Resolution	1 second sweep every 12.8 sec.
	Langmuir Probe, Density Irregularities	Scale Sizes	10 meters to 100 km
		Dynamic Range	80db @ 5db resolution; 10^2 - 10^8 cm^{-3}
Thermal Ions	Ion Mass Spectrometer	Dynamic Range	$20-2x10^8$ ions cm^{-3}
		Mass Range	1-64 AMU @ < 1% overlap
		Temporal Resolution	1.6 seconds for mass scan
Ambient Pressure	Ionization Gauge	Pressure Range	10^{-7} to 10^{-3} torr

tures for the High Frequency Antenna, the Ion Mass Spectrometer, the Electron Fluxmeter, the Retarding Potential Analyzer/Differential Ion Flux Probe and the Low Energy Differential Energy Analyzer (LEPEDEA) around the spacecraft belly. Also indicated are the locations of the search coil magnetometer, the AC-DC electric antennas and the Langmuir Probe sensors which are supported on short booms for OSS-1. Sample results from the JSC Plasma Chamber Tests are presented for some of these instruments in the next major section.

PDP On-Orbit Operations

For the OSS-1 Mission, the primary PDP measurements are made during two 6 hour periods attached to the RMS. The PDP is moved and articulated on the RMS by a series of Automode Sequences which specify a trajectory of locations and the PDP attitude at each location. These sequences are initiated by the crew and the crew can take over manual control at any point. In support of the FPEG, one sequence positions the PDP above the FPEG to measure any Orbiter-

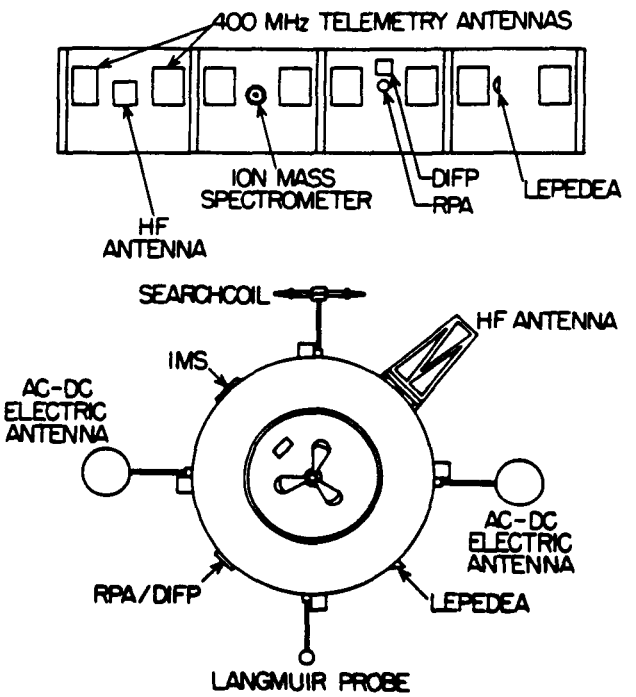

Fig. 2. Location of PDP instrument aperatures around the belly and of the boom-mounted sensors protruding above the top for OSS-1.

generated dc magnetic fields that might affect the predicted beam trajectory. Two sequences are set up to sweep the PDP through the predicted beam trajectory region. The OSS-1 crew will have a display of a few parameters from the PDP in order to judge which Automode Sequence to use. However, the bulk of the telemetry data is tape recorded on-board for playback after the mission. On Spacelab-2 the bulk of the data will be relayed to the Payload Operator's Control Center (POCC) at JSC. Therefore, realtime analysis is possible by the PDP Team as the PDP is operated on the RMS or as the Orbiter moves with respect to the PDP to pass the wake or the exhaust plume past the PDP.

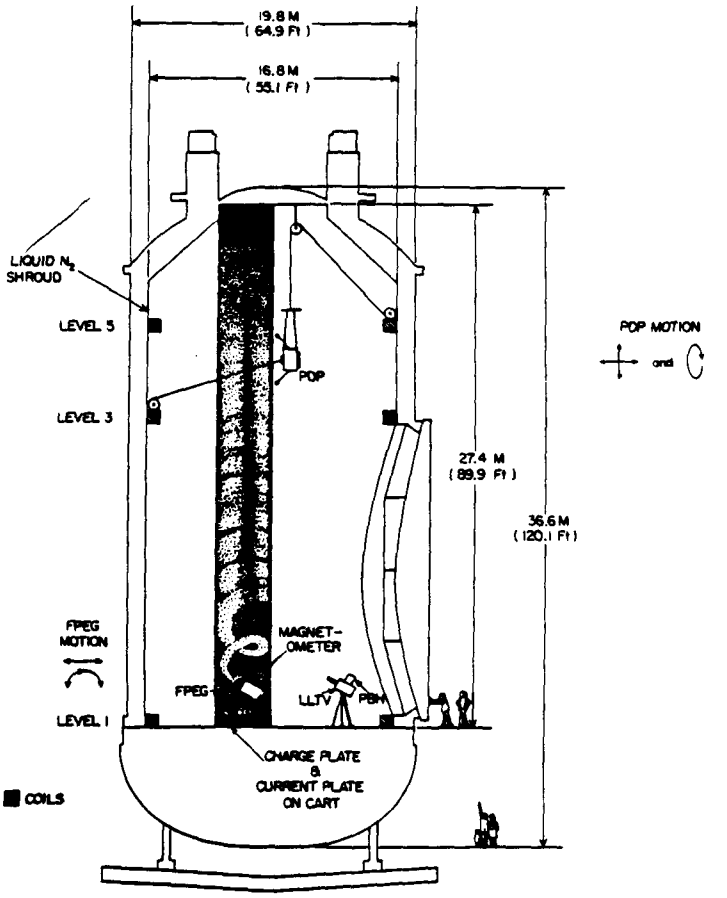

Fig. 3. Dimensions of JSC Chamber A and the relative locations of the PDP and FPEG systems within the chamber. The PDP can be rotated, moved back and forth and moved up and down. The FPEG can be moved across the floor.

JSC PLASMA CHAMBER TESTS

Use of the JSC Chamber A for ionospheric-type plasma experiments has been described by Bernstein, et al. (1978). This unique facility has dimensions of 17m in diameter by 27m in height and the pressure is reduced to below 10^{-5} torr in less than 8 hours pumping time. External coils can be used to impose a magnetic field up to 2 gauss to boost or buck the earth's field. As indicated in Figure 3, the FPEG and other elements of the VCAP system were mounted to a moveable cart on the chamber floor. This set-up was similar to that of Raitt, et al. (1980). A magnetometer mounted to the FPEG was used to set the beam pitch angle. The PDP was suspended at ~ 15 meters above the FPEG with a rope and pulley system that allowed for it to move up/down and in/out of the beam. In addition, it was possible to rotate the PDP ±180°.

Measurements were made with the PDP under variation of a wide number of parameters including magnetic field (0.2-1.5 gauss) and direction (up/down), chamber pressure (6×10^{-6} to 6×10^{-5} torr), plasma (5×10^{6} cm^{-3}) or not, FPEG pitch angle (±90°), FPEG beam current (0.5-85 ma), PDP location with respect to the beam and PDP roll angle. Some sample results regarding fluxes, fields, wave amplitudes, and particle energy spectra under BPD and non-BPD conditions and the variation of these parameters with distance from the beam are presented in the next sections.

Non-BPD vs BPD Characteristics

The data of Bernstein, et al. (1978, 1979) and the theory of Rowland, et al. (1980) give a relation for the critical current I_c for onset of the beam-plasma-discharge:

$$I_c > 150\ E_b(keV)^{1.8}\ U(km/s)/(P(\mu torr)L(cm))$$

For parameters of $E_b = 1$, $U = 1$, $P = 6$ and $L = 2000$, $I_c > 12.5$ ma. The beam-plasma-discharge was recognized to occur for beam currents between 15 and 20 ma depending on the pitch angle. Distinctive characteristics between non-BPD and BPD are illustrated in Figures 4 and 5. For this case B = 1.2 gauss, the pitch angle is 30° and the gun current starts at 16.5 ma rising to 17.5 ma at the end of a 26 second gun pulse. In the last 4 seconds the BPD is ignited apparently due to the increasing plasma density in the beam. As shown in Figure 4, the electron spectrum did not change significantly (except below 10 eV which may be a charging effect) for this detector look angle (perpendicular to B) but the ion flux increased dramatically by more than an order of magnitude and increased in average energy with a broad peak between 10 eV and 250 eV. Electric field emissions below 10 kHz have intensities of up to 1 V/m when the beam is on but generally decrease after onset of BPD. Between the lower hybrid frequency and the gyrofrequency, intensities are greater by 5-15 dB after BPD onset.

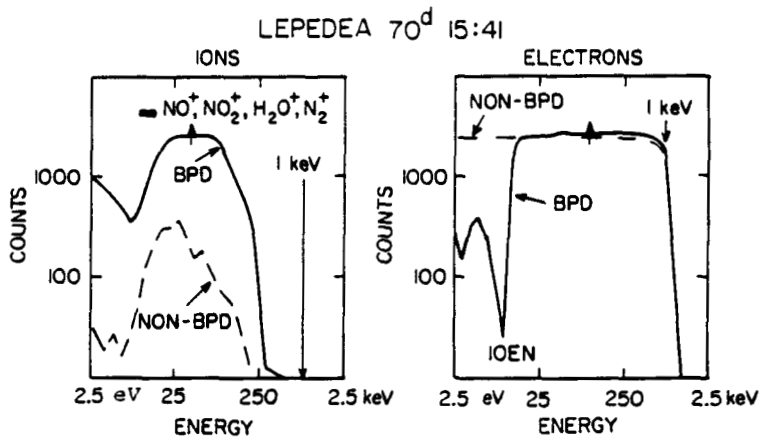

Fig. 4. Energetic ion and electron fluxes under non-BPD and BPD conditions. Note that the electron energy distribution changes very little except at low energies, whereas the ion flux increase by an order of magnitude and becomes more energetic. The ion enhancement between 10 and 100 eV correlates with ionization potentials. The primary electron beam was 1 keV with a current of 16 ma for non-BPD and 17.5 ma for BPD at a 30° pitch angle and B = 1.2 gauss.

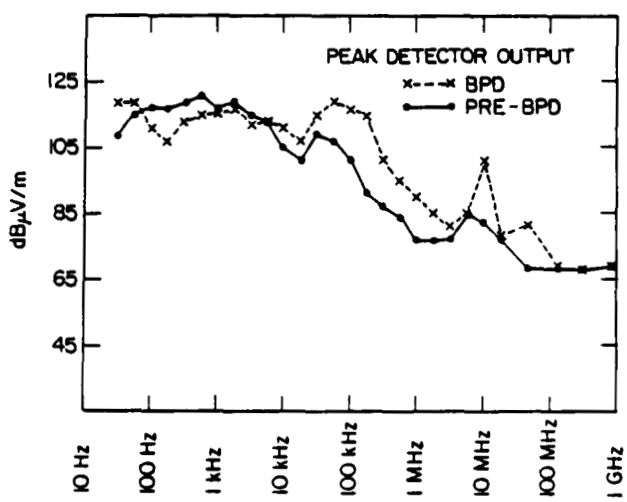

Fig. 5. Electric field intensities for wave emissions under non-BPD and BPD conditions with same plasma and FPEG parameters as in Fig. 4. Note the enhanced emission above the lower hybrid frequency (~ 15 kHz) and at the plasma frequency (~ 10 MHz). Intensities range up to 1 volt/m.

There is also a 20 dB enhancement near the plasma frequency to fields of ~ .1 V/m during BPD.

Also noted under these critical current conditions was the 1-5 Hz oscillatory behavior of the plasma which is probably the same flickering phenomena reported by Bernstein, et al. (1978) and Jost, et al. (1980). This occurred only before BPD onset. Order of magnitude variations were observed in the Langmuir Probe current and in the electron flux; ~ 1 V/m electric field fluctuations were measured and the energetic particle spectra were modulated. Visually, it appeared as if sections of the plasma column were torn loose and driven perpendicular to the magnetic field lines to the chamber walls.

Spatial Variation of Parameters

Spatial variations for the total electron upward flux and for the dc electric field perpendicular to the downward magnetic field of 1.18 gauss are shown in Figure 6 for an 80 ma, 80° pitch angle beam. Two parallel electric field values are also indicated. The upward flux is minimum in the region of one gyroradius where the primary beam electrons are perpendicular to $\vec{B}$ and seems to go to zero near the chamber walls. Directions of the perpendicular E-field indicate an excess of positive charge inside of one gyroradius (beam center) and an excess

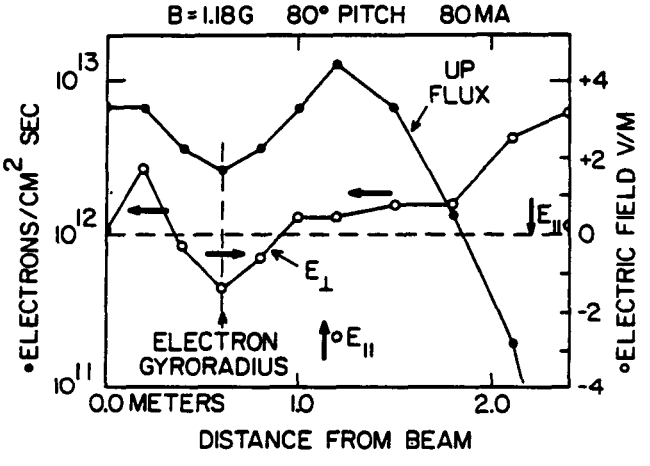

Fig. 6. Variation of the energetic electron flux and the DC electric field with distance from the electron beam center. A 1 keV, 80 ma beam was injected into a 1.18 gauss field at an 80° pitch angle. Note that there is a significant electron flux outside of the illuminated column (1 gyroradius) and that the electric field perpendicular to B reverses twice near 0.6 meters.

of negative charge outside. The upward directed field component at 1.2 meters (2 gyroradii) indicates that upward going electrons are being decelerated. The 10 MHz plasma frequency emission peaks at one gyroradius then decreases by 20 dB at two gyroradii.

Discussion

The energetic electron spectrum results and the electric field wave emission results are consistent with those of Bernstein, et al. (1978, 1979), Jost, et al. (1980) and others. Unique to this experiment with the PDP are the measurements of the energetic ion spectra, the electron flux, the dc electric field and the ion composition of the chamber which are yet to be processed and interpreted for the many cases available. The PDP is limited to a temporal resolution of ~ 1.6 seconds so that onset characteristics cannot be determined.

ACKNOWLEDGEMENTS

The PDP is being developed for the OSS-1 and Spacelab-2 Shuttle Missions through Contract NAS8-32807 with Marshall Space Flight Center. Funding for the JSC Plasma Chamber Tests was provided by NASA/HQ through Grant NAGW-190. I thank the contractors and staff of the JSC Chamber A, especially Jerry Jost, for the set-up and operation of the experiments and I thank John Raitt, Peter Banks, Bill Denig and Brent White for our collaborative effort with the FPEG. I am especially appreciative of the PDP Co-Investigators and Engineering staff with special thanks to Roger D. Anderson as Project Manager, and to Marty Kerl, Terry Clausen, Harry Owens, Gerry Murphy, Dave Cramer and Lowell Swartz for the JSC operations.

REFERENCES

Bernstein, W., Leinbach, H., Kellogg, P. J., Monson, S. J. and Hallinan, T., 1979, Further Laboratory Measurements of the Beam-Plasma Discharge, J. Geophys. Res., 84:7271.

Bernstein, W., Leinbach, H., Kellogg, P., Monson, S., Hallinan, T., Garriott, O. K., Konradi, A., McCoy, J., Daly, P., Baker, B. and Anderson, H. R., 1978, Electron Beam Injecton Experiments: The Beam-Plasma Discharge at Low Pressures and Magnetic Field Strengths, Geophys. Res. Lett., 5:127.

Clifton, K. Stuart (ed.), "Spacelab Mission-2 Experiment Descriptions," 1978, NASA TM-78198, Marshall Space Flight Center, Huntsville, Alabama.

Jost, R. J., Anderson, H. R. and McGarity, J. O., Electron Energy Distributions Measured During Electron Beam/Plasma Interactions, 1980, Geophys. Res. Lett., 7:509.

Neupert, Werner M. (ed.), 1979, "Office of Space Sciences-1 Experiment Investigation Descriptions," NASA/Goddard Space Flight Center, Greenbelt, Maryland.

Raitt, W. J. Banks, P. M., Denig, W. F., White, A. B. and Jost, R. J., 1980, Studies of Electron-Beam Plasma Interactions In a Space Simulation Environment, preprint, Utah State University, Logan, Utah.

Rowland, H. L., Chang, C. L. and Papadopoulos, K., 1980, Scaling of the Beam Plasma Discharge, preprint, Science Applications, Inc., McLean, Virginia.

DISCUSSION

Szuszczewicz: What were the relative populations of energized ions (25 eV or greater) compared with their thermal counterparts?

Shawhan: The ion flux was about 10^8 ions/cm^2 sec eV str and for 100 eV ions (NO^+) the velocity is 10^6 cm/sec so the net density is greater than 100 cm^{-3} which is very small compared to the 10^5-10^7 cm^{-3} "ambient" densities.

Szuszczewicz: If your DC electric field measurement perpendicular to the magnetic field (or perpendicular to the beam axis) is a standard differential floating potential measurement, then there appears to be a distinct possibility that the results could be in substantial error if the sensors are in different plasma environments. Our own results have shown significant variations in plasma-electron energy populations over short perpendicular distances (1-2 meters) (e g change from a single component "cold" Maxwellian distribution to a two-component plasma-electron population with a high energy component) that result in a much greater change in floating potential than in the local plasma potential. Sensors immersed in these two environments would therefore measure potential changes which suggest a higher field than actually exists. Could you comment on this potential problem?

Shawhan: That condition is possible. We do have a Langmuir probe that extends to the same radius as that of the spheres so that as the PDP is rotated the plasma state at each sphere location can be determined. Probably we cannot correct the electric field measurement but we can know if it is not valid.

Reprinted from Nature, Vol. 296, No. 5854, pp. 193-197, 18 March 1982

Science on the Space Shuttle

W.M. Neupert, P.M. Banks, G.E. Brueckner, E.G. Chipman, J. Cowles, J.A.M McDonnell, R. Novick, S. Ollendorf, S.D. Shawhan, J.J. Triolo & J.L. Weinberg

THE third flight of the Space Shuttle, chiefly intended to test the orbiting portion of the Shuttle in extreme thermal conditions in space, nevertheless carries a scientific payload. The investigations will demonstrate the Shuttle's capability for research in space plasma physics, solar physics, astronomy, life sciences and technology and will also determine the effects that the presence of the Orbiter may have on its immediate environment. The information to be gathered is thus the foundation for planning of future investigations with the Space Shuttle.

The scientific payload is designated OSS-1 because the programme was originally managed by the Office of Space Science (now the Office of Space Science and Applications) at NASA headquarters. Responsibility for development of the payload was assigned to the Goddard Space Flight Center. The manager for the scientific payload is Kenneth Kissin. The OSS-1 instruments will study the Orbiter's plasma environment and the propagation of an electron beam in space, record the Sun's UV and X-ray fluxes, observe the zodiacal light and Milky Way, record interplanetary dust particle impacts, operate a sophisticated heat pipe system and also grow plants in the Orbiter's cabin. Demonstrating the Orbiter's research capability demands accurate control of the Orbiter's orientation during solar observations and use of a Remote Manipulator System to carry a package of sensors that will map charged particle and magnetic and electric field distributions around the vehicle.

The same instruments will make sensitive measurements of how the Orbiter alters its environments by the emission of particles or electromagnetic fields. Although the spacecraft has been designed to minimize such effects some, such as propellant plumes from thruster engine firings or electromagnetic radiation from the electrical circuits, are unavoidable.

Werner Neupert is OSS-1 Mission Scientist and Head of the Solar Plasmas Branch, Laboratory for Astronomy and Solar Physics, at NASA Goddard Space Flight Center, Greenbelt, Maryland; Peter Banks, Principal Investigator of the Vehicle Charging and Potential Experiment, is Adjunct Professor Physics at Utah State University, Logan, Utah, and Professor of Electrical Engineering at Stanford University, Stanford, California; Guenter Brueckner, Principal Investigator of the Solar Ultraviolet Irradiance Monitor, is Head of the Solar Physics Branch at the Naval Research Laboratory, Washington DC; Eric Chipman is Program Scientist for the OSS-1 mission at NASA Headquarters, Washington DC; Joe Cowles, Principal Investigator of the Plant Lignification Experiment is Professor of Biology, University of Houston, Houston, Texas; J.A.M. McDonnell is Principal Investigator of the Microfoil Abrasion Experiment and Reader in Space Sciences at the University of Kent, Canterbury, UK; Robert Novick, Principal Investigator of the Solar Flare X-ray Polarimeter, is Professor of Physics, Columbia University, New York; Stanford Ollendorf, Principal Investigator of the Thermal Canister Experiment is Head, Spacecraft Component Development and Analysis Section, Goddard Space Flight Center; Stanley Shawhan, Principal Investigator of the Plasma Diagnostics Package, is Professor of Physics, University of Iowa, Iowa City, Iowa; Jack Triolo, Principal Investigator of the Contamination Monitor Package is in the Spacecraft Component Development and Analysis Section, Goddard Space Flight Center, Greenbelt, Maryland; and J.L. Weinberg, Principal Investigator of the Shuttle Spacelab Induced Atmospheres Experiment, is Research Scientist and Director of the Space Astronomy Laboratory at the University of Florida, Gainesville, Florida.

The nine instrument packages on the third Shuttle flight should yield important data for space plasma physicists, astronomers, life scientists and engineers and also pave the way for future scientific payloads.

All but one of the OSS-1 instruments are mounted on an engineering model of the Spacelab pallet manufactured by the European Space Agency (Fig. 1). The instruments, pallet and the various subsystems for command, data handling, power and thermal control weigh 3,132 kg. The Plant Lignification Experiment is located in mid-deck lockers of the Orbiter cabin and two OSS-1 tape recorders and two control panels are located in the aft flight deck on the upper level of the cabin. Most internal experiment operations will be carried out via commands from the investigators located at the Payload Operations Control Center at Johnson Space Center in Houston, Texas.

On the third Shuttle flight, scheduled for late March, the Orbiter will be placed in a circular orbit of 241 km with an inclination of 38°. During the seven-day flight, the Orbiter will be held in several attitudes as part of the mission's thermal test objectives. The 28-hour long orientation of the Orbiter bay towards the Sun is suitable for solar observations. The planned 80-hour long period when the Orbiter will be maintained with its nose towards the Sun is a prime observing interval for the plasma physics investigations.

The nine experiments will now be described separately.

Electromagnetic environment

During the next decade, active electron and ion beam experiments in space will become an important tool for probing the environment above the Earth's atmosphere. This region contains plasma and magnetic fields of both solar and terrestrial origin. Hitherto, actively controlled charged particle experiments carried by rockets and unmanned satellites have been used to probe the structure of the Earth's magnetic field and to create the physical conditions that led to the formation of the aurorae, seen at high latitudes[1].

The Vehicle Charging and Potential Experiment is the first opportunity to make vehicle charging and electron beam studies from a manned spacecraft. In the first instance, measurements will be made of the effect of the natural ionospheric environment on the gross electrical characteristics of the Orbiter using two pairs of charge and current probes, situated on opposite corners of the pallet, which simulate both the electrically insulating and conducting portions of the Orbiter's surface, and with a Langmuir Probe–Spherical Retarding Potential Analyser located on the sill of the pallet.

Active electron emissions will be used to change the natural electrical balance to determine how a charged Orbiter will affect electron beam and direct plasma measurements. The electron source (the Fast Pulse Electron Generator) emits a 100-mA beam of nearly monoenergetic 1 keV electrons. Pulses as short as 600 ns or as long as 109 s can be generated (Fig. 2*a*).

The Fast Pulse Electron Generator will also be used to investigate the effectiveness

Table 1 OSS-1 Plasma Diagnostics Package instrumentation and measurement ranges

●Low energy proton and electron differential energy analyser
Nonthermal electron and ion energy spectra and pitch angle distributions for particle energies between 2 and 50 keV

●A.c. magnetic wave search coil sensor
Magnetic fields with a frequency range of 10–30 kHz

●Total energetic electron fluxmeter
Electron fluxes between 10^9 and 10^{14} electrons cm^{-2} s^{-1}

●A.c. electric and electrostatic wave analysers
Electric fields with a frequency range of 10 Hz–1 GHz
S-band field strength meter

●D.c. electrostatic double probe with spherical sensors
Electric fields in one axis from 2 mV m^{-1} to 2 V m^{-1}

●D.c. triaxial fluxgate magnetometer
Magnetic fields from 12 mG to 1.5 G

●Langmuir probe
Thermal electron densities between 10^4 and 10^7 cm^{-3}
Density irregularities with 10 m–10 km scale size

●Retarding potential analyser/Differential velocity probe
Ion number density from 10^2 to 10^7 cm^{-3}
Energy distribution function below 16 eV
Directed ion velocities up to 15 km s^{-1}

●Ion mass spectrometer
Mass ranges of 1–64 AMU
Ion densities from 20 to 2×10^7 ions cm^{-3}

●Pressure gauge
Ambient pressure from 10^{-3} to 10^{-7} torr

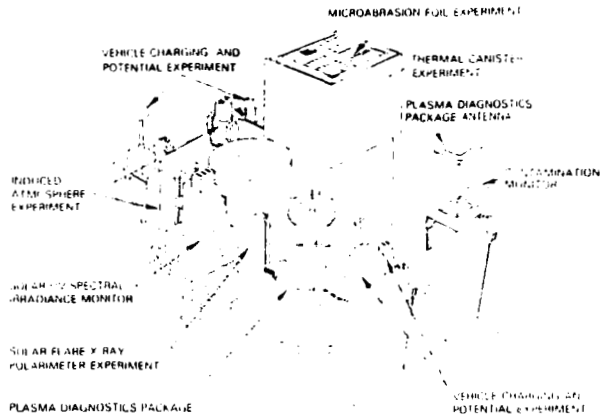

Fig. 1 OSS-1 instrumentation mounted on an engineering model pallet supplied by the European Space Agency. An additional OSS-1 experiment is carried in the mid-deck section of the Orbiter cabin.

of generating electromagnetic radiation by pulsing the electron beam at frequencies as high as 1 MHz. Several ground-based observatories will attempt to receive this radiation. Of particular interest is the extent to which VLF radiation can be generated using special electron beam modulation sequences. Detection will be attempted both at ground observatories and with VLF receivers aboard the recently launched Dynamics Explorer satellites.

Evidence will also be sought for a laboratory phenomenon termed beam-plasma discharge, in which an electron beam energizes a plasma column which then emits intense optical radiation and radio waves (Fig. 2*a*). It is thought that the electron beam initially ionizes residual gas, producing a columnar plasma. As the plasma density builds up, the beam creates electrostatic plasma waves which impart additional energy to the plasma, leading to further ionization and excitation and causing the column to emit optical and radio waves. In Earth-orbit, the different conditions may mean that beam plasma discharge does not occur — the gas density is less, the beam is not terminated by the metallic top of a chamber and the Orbiter moves the beam across magnetic field lines so that plasma may not build up. The Vehicle Charging and Potential Experiment will be used with the Plasma Diagnostics Package to tell whether beam plasma discharge is initiated by the beam from the orbiting electron generator (Fig. 2*b*).

Ionosphere studies

The Earth's ionosphere can be studied by introducing perturbations such as chemical tracers, radio waves and particle beams and by creating plasma wakes around solid bodies. The objectives of the Plasma Diagnostics Package, an assembly of electromagnetic and particle sensors, are to assess the electromagnetic and plasma environment of the Orbiter, to study the interaction of the vehicle with the surrounding plasma, to test the capabilities of the Remote Manipulator System and to carry out active beam–plasma experiments in conjunction with the Fast Pulse Electron Generator. Measurements will be made of electric and magnetic fields, plasma waves, energetic ions and electrons and plasma parameters — density, composition, temperature and directed velocity (see Table 1).

The Plasma Diagnostics Package will be operated both on the OSS-1 pallet and while deployed by the Remote Manipulator System. As the Plasma Diagnostics Package is moved in and around the Orbiter bay, measurements will be made of the ambient pressure and of the spectrum of electromagnetic interference generated by the Orbiter's electrical subsystems. The pressure profiles in time and in distance from the Orbiter are relevant for the design of instruments sensitive to gaseous contamination and those requiring low operating pressures. The sensitivity of wave receivers and of topside ionospheric sounders to be flown on future Spacelabs will be determined by the levels now measured, while measurements of electric fields and particles by the Plasma Diagnostics Package will provide an independent assessment of the charge condition of the Orbiter.

The Orbiter will move in the ionosphere, at supersonic velocity (Mach number 6 relative to the characteristic plasma sound speed or the ion acoustic sound speed[2]) and so will create a plasma wake that may be identified by plasma depletion, energization of particles and the creation of Alfven waves behind the Orbiter. Such processes are thought to be important consequences of the motion of other bodies through plasmas — for example, Alfven waves behind the jovian moon Io may accelerate the particles which cause decametric radio noise bursts[3]. Remote Manipulator System trajectories have been designed to move the Plasma Diagnostics Package through the wake boundary, thus providing direct observations of its physical properties. When the package flies again on the Spacelab-2 mission as a subsatellite, the wake will be examined out to 20 km behind the Orbiter[4].

The combination of the Fast Pulse Electron Generator and the Plasma Diagnostics Package provides an opportunity to study the interactions of a beam of accelerated electrons with the ambient space environment (see Fig. 2*b*). Radio waves over a wide frequency range may be stimulated by both pulsed and continuous operation of the electron beam and measured with the Plasma Diagnostics Package. The two instruments will also operate together to investigate beam–plasma interactions such as the beam plasma discharge. Similar experiments will be conducted with more intense beams on Spacelab-1 and on later missions[5].

Solar ultraviolet radiation

Solar UV radiation in the spectral range 120–300 nm has an important role in the energy balance and photochemistry of the Earth's upper atmosphere. Molecular oxygen absorbs radiation at wavelengths below 242 nm, resulting in its dissociation into atomic oxygen; ozone is dissociated into molecular and atomic oxygen by UV radiation below 310 nm. These reactions

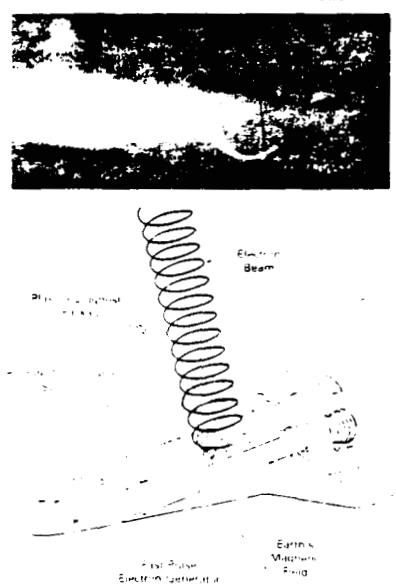

Fig. 2*a*, Photograph of light emission resulting from the interaction of electrons generated by Fast Pulse Electron Generator with residual atmosphere in a space simulation chamber at the Johnson Space Center. The column of luminosity enclosing the helical path of the primary electron beam is due to the occurrence of a beam plasma discharge for the conditions pertaining to this particular operation of the electron generator. *b*, Scheme for the joint Fast Pulse Electron Generator and Plasma Diagnostics Package operations. As the electron beam is emitted along some angle to the Earth's magnetic field, the Remote Manipulator System sweeps the Plasma Diagnostics Package back and forth across the beam region to make measurements of plasma fields and waves and of the energy distributions of electrons and ions.

take place at altitudes from 30 to 160 km in the Earth's atmosphere. Ozone is formed from molecular and atomic oxygen by a catalytic reaction which involves trace species such as NO, NO_x or Cl. Quantitative description of these reactions requires precise knowledge of the absolute amount of solar UV radiation as a function of wavelength. Although many attempts have been made to measure this quantity, large experimental discrepancies still exist[6] (Fig. 3). The objective of this first flight of the Solar Ultraviolet Spectral Irradiance Monitor experiment is to establish a more accurate base of solar UV irradiance measurements with an absolute error of 10 per cent or less over the wavelength region 120–400 nm. During the STS-3 flight, it will accumulate approximately 20 hours of solar measurements, compared with 5 minutes during a typical sounding rocket flight.

Calibration is important. The instrument carries two independent spectrometers and an in-flight calibration light source which allows tracking of any sensitivity change due to vibration at lift-off or contamination during flight. Its seven detectors will allow cross-checks of possible detector changes. It can be operated in broadband (5 nm) or narrow band (0.15 nm) modes over the wavelength region 120–400 nm. During 17 orbits amounting to approximately 28 hours, the bay of the Orbiter will be pointed to the Sun by the crew, using Sun sensors mounted on the Solar Ultraviolet Irradiance Monitor and measurements of solar intensities will be interleaved with periodic in-flight calibrations[7].

The measurement of the solar UV irradiance on OSS-1 is only the first step of a programme to measure the variability of the solar UV radiation over an 11-year solar cycle. This variability has been estimated to be less than 20 per cent in the 170–210 nm region and less than 2 per cent in the 210–300 nm region[8], and Fig. 3 shows that a decisive improvement of accuracy is needed if the Sun's UV variability is to be determined.

Solar flares

Although it is known that there are high-energy electrons in the Sun's atmosphere during solar flares, fundamental questions remain about the nature and location of the mechanisms by which the electrons are energized and their energy dissipated. It is, however, believed that a flux of magnetic energy from the solar interior provides the energy for these events, and that interactions of the accelerated particles with the Sun's atmosphere dissipate this energy, leading to observable flare phenomena including X-ray emission. Similar bursts of energy observed by the Einstein Observatory from other stellar objects have established that flares are relatively common. Hard X rays emitted during flares carry unique information about the motion of the electrons producing the radiation[9]. A definitive observation of the state of polarization of the radiation could provide important data to test theoretical models of the flare phenomenon.

The Solar Flare X-ray Polarimeter on OSS-1 aims to observe flare X rays emitted between 5 and 30 keV and to measure their polarization as a function of time and photon energy. The instrument uses blocks of metallic lithium surrounded by xenon-filled proportional counters as detectors. If polarized, the incident X rays will be scattered preferentially by the lithium into directions normal to the plane of the electric vector of the incoming radiation. To avoid instrumental effects that have plagued previous measurements, the instrument uses three independent sets of scattering blocks and detectors, with each unit rotated by 120° with respect to the other two about a line passing through the Sun. A minimum of two units is necessary to determine the magnitude and orientation of polarization; the use of a third provides redundancy and increased effective area[10].

The instrument will be aimed at the Sun by orienting the entire bay of the Orbiter and it is planned to maintain the Orbiter in this orientation for approximately 28 hours. Solar flares occur only sporadically on the Sun, so that the observation of flare emission is not assured. However, the instrument has sufficient sensitivity that even a small event can yield a usable signal. Such events can be expected to occur about once a day on average.

Zodiacal light

The zodiacal light arises from sunlight scattered or absorbed by interplanetary dust particles, the characteristics of which have been partly defined by rockets and unmanned Earth-orbiting satellites[11]. Observations of colour, polarization and angular dependence are needed to determine dust particle size and composition[12]. Unfortunately, accurate data are scarce. Thus, polarization results at different wavelengths are often combined. There are some observations of brightness, but few of polarization and colour in regions off the ecliptic, closer than 30° to the Sun and near the anti-solar point — the regions which contain the most information on the dust. The Shuttle Spacelab Induced Atmosphere Experiment will provide observations to determine more precisely the position of maximum concentration of interplanetary dust and will search for evidence of different particle characteristics for dust near the Sun.

Although astronomical observations from space avoid the effects of the Earth's atmosphere, the observing platform releases particulates which may form a local contaminant cloud that will also scatter sunlight into the detector. The presence of such an induced atmosphere can be established by comparing observations made when the spacecraft is in sunlight and in the Earth's shadow. The photopolarimeter system on OSS-1 will measure the light scattered from any local cloud of particulates and will record the brightness, polarization, colour and angular dependence of the diffuse astronomical background (zodiacal light and background starlight) at visual and near IR wavelengths.

The instrumentation to be used is the spare unit of the Skylab S073 photopolarimeter and bore-sighted 16 mm camera. The system, which includes an optical train, optical filters for 10 wavelength bands between 400 and 820 nm, a polarization analyser, a brightness calibration source and a photoelectric sensor, can carry out observing sequences according to pre-programmed routines. Although the instrument was operated on Skylab, difficulties with the airlock precluded observations closer than 80° to the Sun. A new gimbal mount has been designed for this mission, allowing the instruments to be scanned in a vertical plane running fore and aft along the Orbiter axis. The instrument will view the entire sky between 20° and 120° from the Sun. Limited observations will also be possible at larger angles.

Fig. 3 Recent measurements of solar UV irradiance in the spectral region between 170 and 200 nm (after ref. 6).

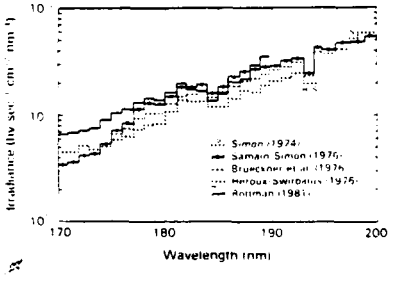

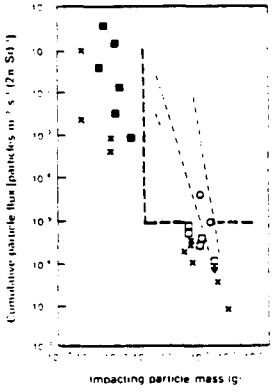

Fig. 4 Measurements of near-Earth microparticle fluxes by various techniques ■ impact plasma sensors; ×, capacitor discharge sensors; O, recovered surface examination, perforation of pressurized cylinders; dashed lines, models derived from microphone sensors. The area to the upper right of the heavy dashed line is the sampling regime of the Microabrasion Foil Experiment on OSS-1. The cumulative particle flux is the flux of particles above a specific mass. Adapted from ref. 14.

Interplanetary dust

Direct sampling of interplanetary particulate matter has been carried out from balloons, U-2 airplanes, rockets, Earth-orbiting spacecraft[13]. Remote measurements have been made with sensors in Earth orbit and interplanetary space[14]. Even impact craters in lunar samples have provided valuable information. A wide range of particle masses, down to 10^{-15}g have been observed, with the cumulative particle flux increasing strongly with decreasing mass (Fig. 4). While comets are thought to be the most likely source of interplanetary dust, direct measurement of particle composition could discriminate between cometary and asteroidal sources for the dust.

The Microabrasion Foil Experiment aims to measure the high velocity microparticle flux in near-Earth orbit, for particle masses greater than 10^{-12}g, to investigate the density distributions of the impacting particles and to study their chemical properties by analysis of residues remaining in the impact craters. The sensor, attached to the thermal blanket on top of the thermal canister experiment, consists of approximately 1 m^2 of 5μm thick aluminium foil bonded to a gold-coated brass support mesh bonded to a Kapton sheet to form a double layer detector.

Differing types of impacts may be recorded. A particle of mass < 10^{-12}g will form a hypervelocity impact crater on the foil surface, without penetrating the foil. More massive particles will penetrate the foil forming a characteristic 'penetration profile', dependent on the particle's incident velocity. Particles penetrating the foil may survive intact to produce a single impact crater on the rear Kapton sheet, or the particle may split into fragments and produce a corresponding number of impact craters on the sheet. Low density "fluffy" particles readily fragment whereas high density iron or stony micrometeorites survive almost intact.

Unlike the other experiments, the Microabrasion Foil Experiment is passive. Post-flight measurements of the craters with scanning electron microscopy and energy dispersive X-ray microprobe analysis of residues will provide information on elemental composition, density and shape, and thus on the origin of these particles.

Plant lignification

Although few plants have been grown in space, Russian experiments have demonstrated that near-zero gravity disorients root and shoot growth, enhances plant sensitivity to substrate moisture conditions and generally results in a high mortality rate. However, little is known about the physiological changes that occur. Understanding of gravity's effects on plant growth and metabolism will provide an insight into plant physiology and aid development of an effective biological life support system.

After cellulose, lignin is the most abundant carbon compound in plants and provides both their strength and form. As gravity is believed to be a primary controlling stimulus for lignification the Plant Lignification Experiment will evaluate how near zero gravity affects the quantity and rate of lignin formation in different plant species during early stages of development.

Of the major groups of higher plants the gymnosperms will be represented by slash pine, the monocotyledonous angiosperm by oat, and the dicotyledonous angiosperm by the mung bean. All are compact species that may be grown in the limited space and relatively low light levels provided by the compact flight Plant Growth Unit. Oat and mung bean seeds and young pine seedlings will be planted in the growth chambers (Fig 5) before launch so that most seedling development will take place in a weightless environment. Electronics for controlling and monitoring temperature and light cycles are incorporated into the Plant Growth Unit. At the latest convenient time (about 7 hours before launch) the unit will be carried on board and installed in a mid-deck locker of the Orbiter cabin, where it will remain throughout the flight.

On landing, the Plant Growth Unit will immediately be removed from the Shuttle, the plants photographed, and the gaseous atmosphere of the plant chambers analysed. The seedlings will then be removed and analysed for lignin content.

Control experiments, with the plants growing in a 1-*g* environment, will be conducted after the flight using the flight hardware and flight environmental data. Lignin data from the flight and control plants will be compared for patterns of lignin deposition to assess whether lignin is reduced in plants grown in zero gravity.

Because the reduced flight time of the previous Orbiter flight prevented completion of the Heflex (plant) Bioengineering Test that it carried, this experiment has been added to the current flight and is also carried[16] in the Orbiter cabin.The test is being conducted specifically to determine the optimal soil moisture conditions for germination and growth of the sunflower ***Helianthus annus*** in near zero gravity. It is a prelude to a plant growth experiment to be conducted on the first Spacelab mission to be flown on the Shuttle in 1983.

Fig. 5 View of a growth chamber, one of six used in the Plant Growth Unit of the Plant Lignification Experiment.

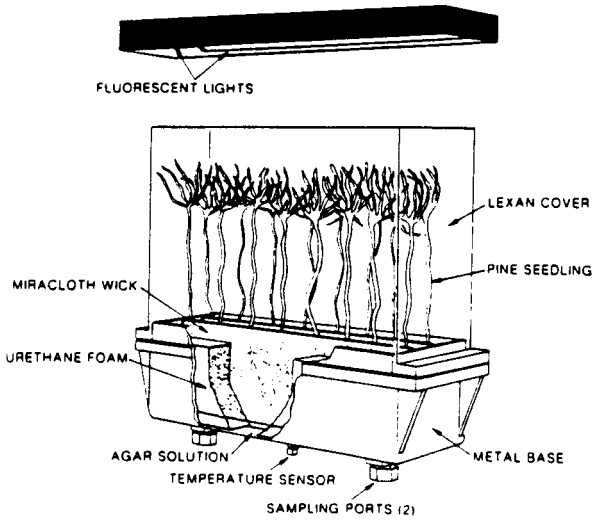

Thermal canister

The long-term use of Space Shuttle means that many scientific and technical investigations can be performed in the Orbiter bay. However, the extreme thermal environmental conditions ranging from equivalent sink temperatures of + 100°C in full Sun, to -100°C, in shadow may cause problems. In the past such conditions were accommodated using coatings, insulation and heaters. With the Shuttle, an instrument designed for one set of conditions may have to survive in an entirely different environment if flown again with different orbit attitudes. If a thermal enclosure were provided which decoupled instruments from the wide extremes in external tempeature whilst maintaining them in a benign environment, simpler thermal designs for instruments, with limited maintenance between flights, might be realized.

To this end the Thermal Canister Experiment aims to determine whether a device using controllable heat pipes could maintain simulated instruments at several selectable temperature levels in zero gravity, and under widely varying internal and external thermal loads. It is hoped to demonstrate ±3°C temperature stability at various control points in the canister while dissipating up to 400 W in cold Orbiter attitudes (bay away from the Sun)

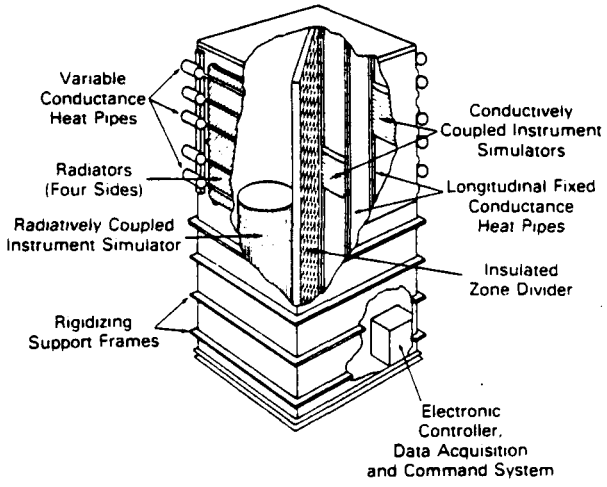

Fig. 6 Cutaway view of the Thermal Canister Experiment showing controllable heat pipes. In flight conditions, the lower half of the unit is covered with multi-layer insulation to provide a measure of isolation from temperature extremes in the Orbiter bay.

and 100 W hot (bay towards the Sun) conditions.

The Thermal Canister Experiment (Fig. 6) consists of a rectangular enclosure 3m high × 1m long × 1m wide with its aluminum sides equalized in temperature by a system of longitudinal fixed conductance heat pipes. These heat pipes collect the thermal energy dissipated internally by electrical heaters simulating instruments in operation and the energy absorbed from direct and reflected sunlight. This heat is then conducted to variable conductance heat pipes mounted to external radiators at the upper end of the canister and radiated to space. The heat pipes are long narrow closed chambers with internal capillary wicking which provides pumping action. The wick is saturated with a volatile liquid (ammonia) in equilibrium with its vapour. Heat transport is established by applying heat at one end (the evaporator) and providing cooling at the other end (the condenser) with the heat being trasferred as latent heat of vaporization. The flow path is completed by capillary forces in the wick.

The variable conductance heat pipes are more complex than the fixed conductance type in that they contain a non-condensible gas (nitrogen) stored in a reservoir at the condenser end of each pipe. As the temperature of the evaporator end of the pipe falls a heating element raises the temperature of the reservoir, causing the gas to expand into the condenser, blocking the condenser region and effectively stopping heat pipe action. The length of condenser rendered inactive depends on the temperature level along the pipe. Conversely, with increasing evaporator-end temperature, the gas will recede into the reservoir making more active area of the radiators available for heat rejection to space. The signal for activating the reservoir heaters is supplied through a feedback loop consisting of a temperature control sensor and either a hardwire proportional controller or a computer-driven controller. The sensors are attached to the canister side walls or on simulated instruments located in two different zones separated by an insulating barrier. The simulators are either radiatively or conductively coupled to the canister walls.

During the mission, it is planned to: (1) operate the canister over set points (5–25°C) located on the walls and on the simulators themselves; (2) change the internal dissipation (in the simulators); and (3) demonstrate control in maintaining the two zones at differing temperatures. The system can be operated by a proportional controller maintaining a specific temperature at one sensor, or by a microprocessor that uses all available data to maintain the overall temperature of the canister at some level, in balance with the environment, irrespective of the preselected set point.

Contamination monitoring

Payloads operating in the bay of the Orbiter will be exposed to a variable gaseous environment. In addition to outgassing of the vehicle and the payloads themselves, the operation of altitude control systems, the venting of relief valves and the dumping of water for thermal control of the vehicle all represent molecular sources that may affect sensitive instrumentation, particularly equipment at cryogenic temperatures. Measurements have been planned for the series of four orbital test flights using the Induced Environment Contamination Monitor provided by the Marshall Space Flight Center and located, on this flight, behind the OSS-1 pallet in the Orbiter bay. Particulate measurements will be provided by the Shuttle/Spacelab Induced Atmosphere Experiment. A molecular contamination monitor on the OSS-1 pallet provides information on molecular species around the OSS-1 instruments, supplementing measurements from the Induced Environment Contamination Monitor.

The Contamination Monitor Package, sponsored by the United States Air Force, contains four temperature-controlled Quartz Crystal Microbalances which measure the accreted mass of molecular fluxes. These microbalances are identical to those contained in the Induced Environment Contamination Monitor but their operation can be monitored and the data analysed during the flight. Their temperatures may be reset by command after initial results have been analysed to optimize the operation of the sensors.

The instrument will monitor the mass accretion of condensible volatile materials during ascent, on-orbit operations and descent. After the mission, the data on mass build-up will be correlated with payload activities, Orbiter operational events, performance of other OSS-1 instruments and Induced Environment Contamination Monitor results. The activation energy of the major species of the accreted materials can also be estimated.

While minimal impact is expected for most instruments that may fly on Shuttle, long-term exposures of particularly sensitive optical components or cryogenic surfaces to the Orbiter environment may require special precautions.

Future prospects

The OSS-1 instruments will point the way to future developments in the use of the Shuttle for space science investigations. Two of the OSS-1 instruments will fly again on the Spacelab-2 mission: the Plasma Diagnostics Package will be released from the Remote Manipulator System to become a subsatellite and make measurements of the spacecraft wake at distances up to 20 km behind the Orbiter, while the Solar Ultraviolet Irradiance Monitor will be mounted on a solar pointer to continue UV irradiance measurements through the solar cycle. The data from other experiments will be used to design large UV and IR telescopes and other instruments for future flights in the Orbiter. Ultimately, the Shuttle program will include discipline-dedicated flights and the development of space platforms serviced by the Shuttle.

1. Grandal, B. (ed.) *Artificial Particle Beams Utilized in Space Plasma Physics* (Plenum, New York, 1982).
2. Samir, U. & Stone, N.H. *Acta Astronaut.* **1**, 1001–1141 (1980).
3. Gurnett, D.A. & Goertz, C.K. *J. geophys. Res.* **86**, 717 (1981).
4. Shawhan, S.D., Burch, J.L. & Fredricks, R.W. *AIAA Paper 82-0085*, Florida (1982).
5. Raitt, W.J. *et al. AIAA Paper 82-0083*, Florida (1982).
6. Simon, P.C. *Solar Phys.* **74**, 273 (1981).
7. VanHooser, M.E., Bartoe, J.-D.F., Brueckner, G.E., Prinz, D.K. & Cook, J.W. *Solar Phys.* **74**, 521 (1981).
8. Cook, J.W., Brueckner, G.E. & VanHooser, M.E. *J. geophys. Res.* **85**, 2257 (1980).
9. Ewert, G. & Haug, E. *Solar Phys.* **20**, 413 (1971).
10. Lemen, J.R. *et al. Solar Phys.* (submitted).
11. Weinberg, J.L. in *Lecture Notes in Physics* Vol. 38 (eds Elsässer H. & Fechig, H.) 3–18 (Springer, Berlin, 1976).
12. Giese, R.H., Hanner, M.S. & Lemert, C. *Planet Space Sci.* **21**, 2061 (1973).
13. Brownlee, D.E. in *Cosmic Dust* (ed. McDonnell, J.A.M.) 295–336 (Wiley, New York, 1978).
14. McDonnell, J.A.M. in *Cosmic Dust* (Wiley, New York, 1978).
15. Lemert, C. *Space Sci. Rev.* **18**, 281 (1975).
16. Tarantick, J.V. & Settle, M. *Science* **214**, 619 (1981).

Subsatellite Studies of Wave, Plasma, and Chemical Injections from Spacelab

S.D. Shawhan, J.L. Burch, R.W. Fredricks

Reprinted from

Journal of Spacecraft and Rockets Volume 20. Number 3. May-June 1983. Page 238

Subsatellite Studies of Wave, Plasma, and Chemical Injections from Spacelab

Stanley D. Shawhan*
University of Iowa, Iowa City, Iowa
James L. Burch†
Southwest Research Institute, San Antonio, Texas
and
Robert W. Fredricks‡
TRW, Redondo Beach, California

Three classes of Orbiter subsatellites have been identified to support Spacelab active plasma investigations: 1) small, throw-away detectors which are not reusable; 2) medium-sized, recoverable subsatellites, and 3) large, maneuverable subsatellites with a significant orbit-adjust capability. A class 1 subsatellite—the Plasma Diagnostics Package (PDP)—was utilized attached to the Remote Manipulator System on the STS-3 flight to diagnose effects of the fast pulse electron generator electron beam and of Orbiter-produced plasma wakes. On the Spacelab-2 mission, the PDP will be released as a subsatellite to examine Orbiter wakes out to 20 km and the ionospheric plasma depletion effects resulting from planned Orbiter engine-burns. Class 1 Magnetospheric Multiprobes and a class 2 Recoverable Plasma Diagnostics Package are under development for the follow-on Spacelab missions. In addition, a study has been completed on a class 3 Solar-Terrestrial Subsatellite. All of these planned subsatellites provide measurements of plasma composition, wave fields, particle spectra, and optical emissions.

Introduction

THE Shuttle/Spacelab system now offers the possibility to provide the platform, the weight and power, and the manned control of space plasma investigations in low Earth orbit.[1] Planned active space plasma physics investigations include the emission of very low frequency (vlf) waves to study propagation and particle interaction effects; the emission of high-frequency (hf) waves to sound the local and remote ionospheric density structure; the injection of energetic electron beams and of hot plasma to examine stability criteria and to remotely measure electric fields along the magnetic field line path; the stimulation of low-frequency waves and the establishment of large-scale current systems by an electrically conducting tether associated with a modulated electron emission source; the release of known materials such as water or H_2 in the vicinity of the Orbiter to emphasize particular chemical reactions and the release of materials such as Ba^+ at high altitudes to trace magnetic field lines and to enhance electric field phenomena; and the diagnostics of wakes of bodies with known shapes and electrical properties.

Diagnostic measurements of the effects stimulated by these active investigations can be carried out with instruments located in the Spacelab payload, manipulated by the 15-m Remote Manipulator System (RMS), carried by other free-flying satellites or stationed along the ground track—such as incoherent scatter radars and optical observatories. Probably the most effective diagnostic element is that of instrumented subsatellites which operate in the vicinity of the Orbiter from the range of the RMS out to several hundred kilometers. Table 1 lists estimates for a few scale lengths that are important for defining the regions to be explored in detail in the active space plasma investigations. These scale lengths range from 10-100 km.

Presented as Paper 82-0085 at the AIAA 20th Aerospace Sciences Meeting, Orlando, Fla., Jan. 11-14, 1982; submitted Feb. 22, 1982; revision received Nov. 2, 1982.

*Professor of Physics, Dept. of Physics and Astronomy.
†Director, Space Sciences Laboratory.
‡Manager, Space Sciences Department.

Heritage of the Spacelab Subsatellite Systems

In the mid-1970s at the conclusion of the successful Skylab program, groups of international scientists began to consider the investigations which might be conducted using the upcoming Shuttle/Spacelab system. These scientists identified scientific objectives for both active and passive measurements, defined instrument complements, and considered mission scenarios in some detail. These studies were coordinated under the Atmosphere, Magnetosphere, and Plasmas-In-Space (AMPS) program.

AMPS scientists defined a set of experiments and the type of major instrument facilities necessary to carry out these experiments.[2] The requirement for subsatellites to make in situ measurements was identified for 8 of these 17 diverse experiments. In the polar region, subsatellites were required for four of the five investigations of natural phenomena. Table 2 gives a list of specific instruments forming model payloads for a subsatellite to make the measurements required for a particular set of investigations.[3,4] These instruments were assumed to be similar to those flown on numerous free-flying satellites.

In 1976 the AMPS Working Group completed its work to suggest a comprehensive and coordinated set of instrumentation and investigations to acquire information on the processes that control the Earth's environment and its susceptibility to modification by human and natural forces.[4] The work and recommendations of the AMPS group were reviewed by an independent panel of scientists.[5] Based on this report, facility definition teams were established to study further the objectives and the implementation of these major Spacelab facilities: LIDAR, spectroscopy, particle beams, chemical releases, subsatellites, and wave injection. An important goal of these teams was to produce specifications and schedules for the evolutionary development and use of the facilities.

The subsatellite facility definition team met between 1977 and 1979. This committee reiterated the need for Spacelab subsatellites as follows[6]:

1) The subsatellites can be equipped with instrumentation to measure/map perturbations generated at or by the Shuttle.

2) The subsatellites can be used in a cooperative mode in

support of active experiments conducted from Spacelab wherein remotely located sensors are required.

3) Subsatellites can be used to make measurements that might otherwise be masked by the Shuttle environment.

4) The subsatellites can be equipped with instrumentation to obtain simultaneous measurements at several points in space.

Table 1 Scale lengths for active space plasma investigations

Wavelength for 300 Hz whistler mode wave, km	10-100
Far field of Orbiter antenna at 30 MHz, km	9
Gyrodiameter for 7.5 keV electron, m	8
Orbiter motion during energetic electron transit to opposite hemisphere and back, km	5-20
Size of plasma depletion regions from Orbiter burns, km	100
Extension of Orbiter-induced plasma wake, km	3

Further consideration of specific requirements for subsatellites and the resources that might be available to develop them lead to three classes of subsatellite systems.[7] Table 3 identifies these classes, some performance characteristics, and approximate cost estimates. Both the single mission/class 1 and the recoverable/class 2 subsatellites seem to be within the capabilities of a principal investigator's institution whereas the maneuverable-recoverable/class 3 subsatellite would be a facility to be developed and managed by a NASA Center or by industry. In 1979, industry was invited to submit proposals on the adaptation of existing qualified spacecraft to the class 3 subsatellite requirements; this satellite program was named the Solar-Terrestrial Subsatellite (S-TSS).[8] More details on the development of all three classes are given in the following sections.

Current Plasma Diagnostics Package Flight Program

A throw-away subsatellite falling within the class 1 category has been developed for flight on two Shuttle missions. On the

TABLE 2. INSTRUMENT COMPLEMENT FOR ATMOSPHERE, MAGNETOSPHERE AND PLASMAS-IN-SPACE MODEL PAYLOADS[3]

EXPERIMENTS / MODEL PAYLOADS	LANGMUIR PROBE	ELECTRON DETECTOR 0.1 - 20 keV	ELECTRON DETECTOR 15 keV - 3 MeV	NEUTR. TEMP. & WIND EXPERIMENT	NEUTRAL MASS SPECTROMETER	ION MASS SPECTROMETER	ION DRIFT DETECTOR (RPA)	PROTON DETECTOR 0.5 - 20 keV	ION ENERGY & MASS ANALYSIS 10 keV < E/Q < 30 keV	ION ENERGY & MASS ANALYSIS 25 keV < E/Q < 10 MeV	TRIAXIAL MICRO ACCELEROMETER	AC/DC ELECTRIC FIELD	DC MAGNETIC FIELD (FLUXGATE)	AC MAGNETIC FIELD (SEARCH COIL)	RESONANCE CONE EXPERIMENT	QUADRUPOLE PROBE	GRID ANTENNA	NEAR IR - TELESCOPE	UV - TELESCOPE
1. AERONOMY	X	X		X	X	X	X	X			X								
2. MAGNETOSPHERIC (PLASMA & FIELDS)	X	X					X	X	X			X	X	X					
3. MAGNETOSPHERIC (PARTICLES)	X	X	X				X	X	X	X				X					
4. PLASMA ACCEL. MONITORING	X	X	X			X	X	X	X			X	X	X					
5. DEVELOPMENT PAYLOAD	X						X					X	X	X	X	X	X		
6. CONTAMINATION (EMI, CHEMICAL)	X				X	X	X					X	X	X					
7. OPTICAL	X				X	X	X											X	X

TABLE 3. COMPARISON OF SUBSATELLITE CLASSES[A]

SUBSATELLITE PERFORMANCE	PRINCIPAL INVESTIGATOR CLASS: SINGLE MISSION (CLASS 1)	PRINCIPAL INVESTIGATOR CLASS: RECOVERABLE (CLASS 2)	FACILITY CLASS: MANEUVERABLE (CLASS 3)
NUMBER PER MISSION	1 TO 6	1 TO 4	1 TO 2
MAXIMUM SIZE	42" DIA, 27" H	60" DIA, 42" H	> 60" DIA, > 42" H
WEIGHT	25 TO 250 KG	250 TO 500 KG	> 500 KG
POWER B = BATTERIES S = SOLAR CELLS F = FUEL CELL	20-40 WATTS (B)	50-150 WATTS (B & S)	100-1000 WATTS (B & S OR F)
DATA: TELEMETRY	10-100 KBPS + 50 KHZ	16-512 KBPS + 250 KHZ	256 KBPS + 250 KHZ + TV
TAPE RECORDER	NONE	512 KBPS + 250 KHZ	MBPS + 250 KHZ + TV
COMMANDS	NONE-6 (DISCRETE)	16-64 (SERIAL)	> 256 (SERIAL)
ANTENNAS AND BOOMS	< 10M, ONE SHOT	< 10M, RETRACTABLE	< 100M, RETRACTABLE
ALTITUDE/ORBIT ADJUST	NONE SPIN STABILIZED	CRUDE ACS FOR SPIN AXIS	3 AXIS STABILIZED, ΔV ~ 2500-FT/SEC
LIFETIME ON-ORBIT	DAYS	MONTHS	MONTH UP TO YEARS
NUMBER OF INSTRUMENTS	3-8	6-12	10-16
DEVELOPMENT COST	$3-5M	$10-20M	$50-100M
REFLIGHT COST	~ $2M	~ $2M	~ $5M

(A) ADOPTED FROM REFERENCE 87.

first flight—STS-3, which was flown in March 1982 as part of the Office of Space Science-1 pallet—this Plasma Diagnostics Package (PDP) was not released into orbit but was manipulated by the systems RMS out to distances of 15 m from the Orbiter. On the second flight—the Spacelab-2 mission scheduled for November 1984—the PDP is spun up and released by a special end effector on the RMS. The Orbiter will keep the PDP within telemetry range (~ 100 km) for several days.

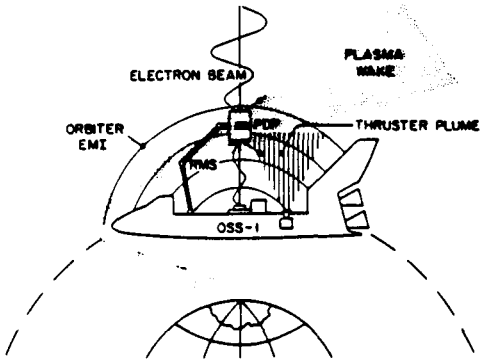

Fig. 1 OSS-1/PDP science objectives.

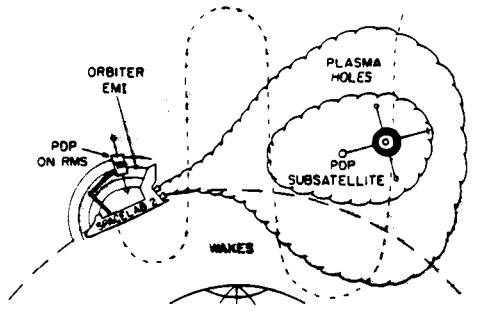

Fig. 2 Spacelab-2/PDP science objectives.

In Fig. 1 the PDP on the RMS is depicted making measurements in and about the Orbiter. The specific objectives for the PDP on the STS-3 flight included:

1) Study the Orbiter-magnetoplasma interactions within 15 m of the Orbiter through the measurement of electric and magnetic fields, ionized particle wakes, and generated waves.

2) Determine the characteristics of the electron beam emitted from the fast pulse electron generator (FPEG) experiment out to a range of 15 m from the Orbiter and measure the results of beam-plasma interactions in terms of fields, waves, and particle distribution functions.

3) Measure and locate the sources of fields, electromagnetic interference (EMI), and plasma contamination in the environment of the Orbiter out to 15 m.

4) Flight-test the systems and procedures associated with the Spacelab-2 Plasma Diagnostics Package experiment with particular emphasis on operations with the Remote Manipulator System (RMS), on unlatching and relatching the PDP unit, and on evaluating the radio frequency (rf) telemetry link.

The PDP is cylindrical in shape with a 107 cm diam by 69 cm height with electric field, magnetic search coil, and Langmuir probe sensors extending ~30 cm beyond the cylinder. On top of the PDP is the special electrical grapple fixture for mating to the RMS standard end effector. For STS-3 the PDP weighed 159 kg and used 45 W of Orbiter power. Other flight systems included the release/engagement mechanism (REM), a 400 MHz rf receiving antenna, and an electronics assembly with rf receivers and logic for processing commands and for generating onboard displays.[9]

Within the PDP housing are instruments for measuring characteristics of the plasma environments in the vicinity of the Orbiter and of the phenomena induced by operation of the fast pulse electron generator (FPEG), which is part of the vehicle charging and potential (VCAP) investigation.[9,10] The measurements made by the PDP include magnetic and electric fields, plasma waves, plasma composition, temperature and directed velocity, and energetic particle flux and pitch angle distributions.

For Spacelab-2, the PDP is equipped with batteries (adding 91 kg in weight) for ~7 days of energy and with folding booms to extend the sensors about 1.5 m from the spacecraft body. The PDP is to be released into orbit with the

TABLE 4. PHASED DEVELOPMENT OF SPACELAB FACILITIES[A]

	CY 82	CY 83	CY 84	CY 85	CY 86	CY 87	CY 88
PHASE I (UNDER DEVELOPMENT)							
A. OSS-1 MISSION ----------?							
1. PLASMA DIAGNOSTICS PACKAGE ON RMS							
2. VCAP FAST PULSE ELECTRON GENERATOR							
B. SPACELAB-1 MISSION ----------?							
1. SEPAC							
C. SPACELAB-2 MISSION ----------?							
1. EJECTABLE PLASMA DIAGNOSTICS PACKAGE							
2. PLASMA DEPLETION EXPERIMENTS							
PHASE II (SELECTED FOR DEFINITION)---------- -AVAILABLE--							
1. RECOVERABLE PDP							
2. MULTIPROBES							
3. AUGMENTED SEPAC							
4. WISP							
5. CHEMICAL RELEASE MODULE							
6. TETHER							
7. LIDAR							
PHASE III (PROPOSAL STAGE) ----------?							
1. S-TSS							
2. OPEN FREE-FLYERS (4)							
3. UARS FREE-FLYERS (2)							

(A) ADAPTED FROM REFERENCE 8

TABLE 5. ACTIVE SPACE PLASMA LAB INVESTIGATIONS

ACTIVE INVESTIGATION/TECHNIQUE	PRIMARY OBJECTIVES	SUBSATELLITE OBJECTIVES
WISP-WAVES IN SPACE PLASMA[1] • 1 KW VLF TRANSMITTER, 1 TO 10 KHZ • 100 METER TIP-TO-TIP ELECTRIC ANTENNA • VLF RECEIVERS ON SUBSATELLITE • HF SOUNDER TRANSMITTER ON ORBITER 0.1 TO 10 MHZ • HF SOUNDER RECEIVERS ON ORBITER AND ON SUBSATELLITE	• EMIT ELECTROMAGNETIC AND ELECTROSTATIC PLASMA WAVES • EFFECT MODE COUPLING AT CRITICAL PLASMA REGIONS FOR CRITICAL PLASMA FREQUENCIES • STIMULATE WAVE-PARTICLE INTERACTIONS LEADING TO WAVE GROWTH AND PARTICLE MODIFICATION • SOUND THE PLASMA VOLUME FOR DENSITY IRREGULARITY STRUCTURES	• MEASURE VLF AND HF WAVE AMPLITUDE AND SPECTRA FOR ELECTROMAGNETIC AND ELECTROSTATIC MODES OUT TO RANGES OF 10^{4}S KM • OBSERVE WAVE GROWTH STIMULATED BY VLF WAVES • OBSERVE RETURNING HF WAVES FROM REMOTE DENSITY IRREGULARITIES
SEPAC-SPACE EXPERIMENTS WITH PARTICLE ACCELERATORS[1] • ELECTRON ACCELERATOR, 7.5 KV, 1.5A, 10 MS - 1 SEC PULSE • MPD ARCJET, 2 KJ/PULSE, 10^{19} IONS/PULSE, 250 V ENERGY, 1 MS PULSE, ARGON GAS • DIAGNOSTIC INSTRUMENTS IN ORBITER BAY	• EMIT ENERGETIC ELECTRON AND PLASMA BEAMS TO INVESTIGATE BEAM STABILITY AND BEAM PROPAGATION • UTILIZE ELECTRON BEAM TO STIMULATE ARTIFICIAL AURORAL SPOTS • DIRECT ELECTRON BEAM TO EXAMINE ELECTRIC FIELDS IN THE MAGNETOSPHERE	• MEASURE THE ELECTRON AND PLASMA BEAM EVOLUTION IN SPACE OUT TO RANGES OF 200 KM • REMOTELY SENSE THE PLASMA PARAMETERS ASSOCIATED WITH THE ARTIFICIAL AURORA MAGNETIC FLUX TUBE • TRAIL THE ORBITER TO INTERCEPT ELECTRON BEAMS MODIFIED BY MAGNETOSPHERIC ELECTRIC FIELDS
ELECTRODYNAMICS TETHER SYSTEM[1,4] • CONDUCTING WIRE EXTENDED UPWARD FROM ORBITER BY 1-10 KM • CONDUCTING BALLOON OF 20-100 METER DIAMETER TETHERED TO END OF WIRE • ELECTRON GUN ON ORBITER	• EXCITE ALFVEN WAVE STRUCTURES BY THE MOTION OF THE TETHER THROUGH THE GEOMAGNETIC FIELD • CREATE A FIELD-ALIGNED CURRENT SYSTEM WITH CLOSURE IN THE IONOSPHERE • SERVE AS AN EFFICIENT VLF WAVE TRANSMITTING ANTENNA	• MEASURE WAVE AMPLITUDES AND SPECTRA FROM ULF THROUGH VLF IN THE NEAR AND FAR FIELD OF THE TETHER • LOCATE FLUX TUBES WITH TETHER INDUCED CURRENT SYSTEMS • DIAGNOSE PLASMA ENERGIZED BY THE POTENTIAL SYSTEM ASSOCIATED WITH THE TETHER
SPACELAB-2 PLASMA DEPLETION EXPERIMENTS[1] • ORBITER OMS ENGINES EMITTING 200-2000 KG OF PROPELLANT COMBUSTION PRODUCTS • SUBSATELLITE, GROUND RADAR, GROUND OPTICAL DIAGNOSTICS OF IONOSPHERIC DEPLETION EFFECTS	• INTRODUCE COMBUSTION PRODUCTS INTO IONOSPHERE TO STUDY CHEMICAL REACTIONS LEADING TO DEPLETION AND REPLENISHMENT OF THE IONSPHERIC PLASMA • STUDY ASSOCIATED OPTICAL EMISSIONS AND RADIO PROPAGATION PERTURBATIONS	• CHARACTERIZE THE PLASMA PROPERTIES BEFORE, DURING AND AFTER RELEASE OF THE COMBUSTION PRODUCTS • MEASURE ASSOCIATED EFFECTS SUCH AS THE STIMULATION OF PLASMA WAVES AND THE ESTABLISHMENT OF PLASMA FLOWS
CHEMICAL RELEASE EXPERIMENTS[1] • TRACE CHEMICALS SUCH AS Ba^{+} ARE RELEASED FROM ORBITER-BORNE CANISTERS OR FROM A FREE-FLYING SATELLITE ~ 10^{+5} KG PER CANISTER	• CREATE CHEMICAL REACTIONS AT LOW ALTITUDE TO STUDY ATMOSPHERIC PROCESSES • TRACE MAGNETIC FIELDLINES EXTENDING INTO THE MAGNETOSPHERE TO DETECT ELECTRIC FIELD REGIONS	• MAKE IN SITU MEASUREMENTS OF PLASMA CHANGES AS CHEMICAL IS INTRODUCED • DETECT FIELDS, WAVES AND PARTICLE CHARACTERISTICS ASSOCIATED WITH MAGNETOSPHERIC FIELD LINES WITH TRACES

spin axis perpendicular to the orbital plane with a spin rate of 6 rpm.[11] By using the Orbiter propulsion system, the Orbiter maneuvers about the PDP and also releases combustion products to create local depletion of the ionosphere.[12] As depicted in Fig. 2 the Spacelab-2 PDP is to meet the following objectives:

1) Provide in situ measurements of the ionospheric plasma "holes" induced by the Orbiter engine burns in support of ground radar observations of the plasma depletion experiment.

2) Observe natural waves, fields, and plasmas in the unperturbed magnetosphere.

3) Assess the Spacelab system for performance of active and passive magnetospheric experiments.

Evolution of Space Plasma Lab Investigations

Instrumentation has been developed for the conduct of investigations in the space plasma physics disciplines. These investigations are listed in Table 4 under phase I for the OSS-1, Spacelab-1, and Spacelab-2 missions[9,11,13] by the calendar year of the Shuttle launch. At the same time there is another set of Spacelab facilities and principal investigator class instruments which have been selected for possible follow-on Spacelab missions, phase II. Some of these phase II items are being defined and others are in an early definition phase for development starting in 1984 pointing toward a Spacelab-6 flight opportunity in mid-1987, the Space Plasma Lab-1.

Orbiter subsatellites are to be developed under phase II. The recoverable PDP (RPDP) is a class 2 system that follows from the Spacelab-2 PDP. Magnetospheric Multiprobes (MMP) is a system of up to six class 1 subsatellites to make the first set of simultaneous but spatially separated measurements. These subsatellite systems are to be joined by the Solar-Terrestrial Subsatellite toward the end of the decade and with other free-flyer satellite systems, such as the Origin of Plasmas in the Earth's Neighborhood (OPEN) and the Upper Atmosphere Research Satellites (UARS).

Table 5 gives the features of several active Space Plasma Lab perturbation sources—waves, particles, currents, and chemical tracers—that may be available as part of phase II. This table gives a summary of the investigation technique, the primary objectives, and the objectives to be met by the subsatellites and free-flyers (if available). As the Spacelab instrumentation and investigation experience evolves, these space plasma active experiments can be conducted and diagnosed by any and all of the subsatellite systems—MMP, RPDP, of S-TSS. These systems are described in more detail in the following sections.

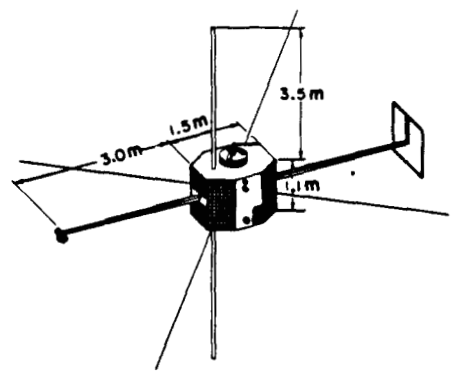

Fig. 3 Recoverable plasma diagnostics concept.

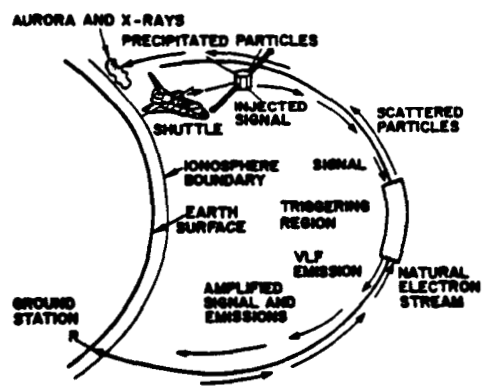

Fig. 4 Diagnostics of WISP stimulated vlf waves and precipitated particles.

Recoverable Plasma Diagnostics Package Scheme

Presently, the Recoverable Plasma Diagnostics Package (RPDP)—derived from the Spacelab-2 PDP—is being designed for a flight as part of the Space Plasma Lab-1 (tentatively, Spacelab-6) complement of hardware.

In Fig. 3, the RPDP is shown in its subsatellite configuration with deployed sensors on booms and with electric long-wire antennas. Energy is supplied by primary batteries and supplemented by solar cells with a secondary battery system to meet the ~100-W operational demand. The 500-kg

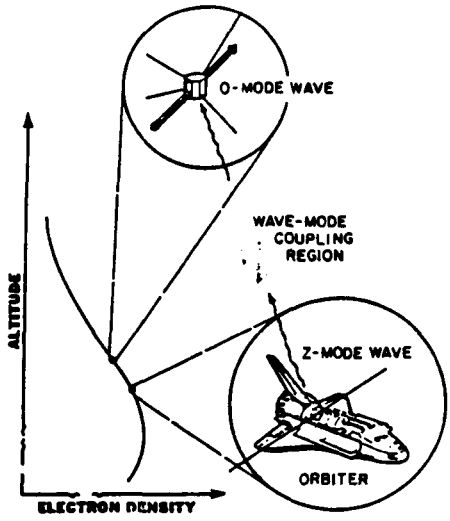

Fig. 5 Diagnostics of WISP emitted hf waves.

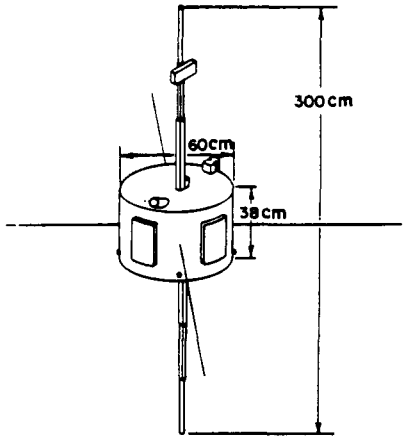

Fig. 6 Magnetospheric multiprobes concept.

unit is spun up to 6 rpm and despun by the combination of a reaction wheel and a cold gas thruster system. The cylindrical dimensions are 152 cm diam by 107 cm height to house up to 12 instrument systems and the supporting spacecraft subsystems. Data are downlinked to the Orbiter over two 400 MHz links and commands are uplinked at S-band. Overall the RPDP satisfies the general specifications of the class 2 recoverable subsatellite in Table 3.

An example of a WISP vlf investigation (see Table 5) utilizing the RPDP is given in Fig. 4. The WISP vlf transmitter illuminates a magnetic flux tube that contains energetic electrons near the equator. These emitted vlf waves can partially organize the particles to stimulate wave growth leading to amplified waves and to particles precipitating into the atmosphere creating an artificial aurora. Very low-frequency sensors on the RPDP can measure both the injected wave characteristics and those of the stimulated waves; other RPDP sensors can detect precipitated electrons in the flux tube and can remotely sense the light of the artificial auroral spot.

For WISP high-frequency (hf) transmissions, the RPDP provides a receiving point which is remote from the Orbiter-borne sounder transmitter/receiver itself. Consequently, these bistatic sounding measurements enhance the information on the dimensionality of the detected density irregularity features. The RPDP can also be used to examine hf wave propagation and mode coupling phenomena as depicted in Fig. 5. A Z-mode wave emitted at the Orbiter may be coupled

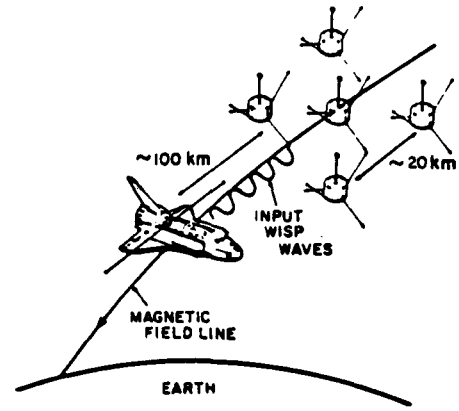

Fig. 7 MMP diagnostics of wave and wave-particle interactions.

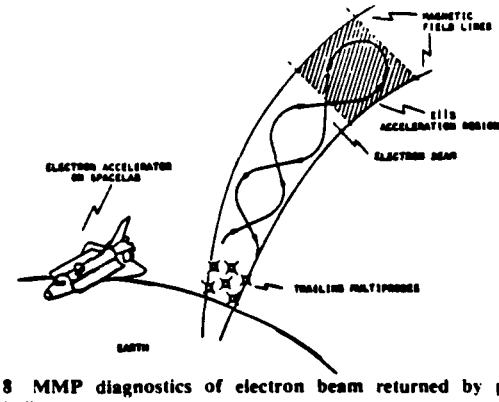

Fig. 8 MMP diagnostics of electron beam returned by parallel electric field region.

to an O-mode wave in the presence of a strong gradient in electron density. Such experiments require careful positioning of the Orbiter with respect to the RPDP.

As part of the Space Plasma Lab-1, the RPDP can also be utilized with other phase II instruments to diagnose the SEPAC electron and plasma beams[10] and to characterize reactions to chemical releases.[12]

Magnetospheric Multiprobes Scheme

Multiple throw-away detectors are particularly important for providing a spatial sample of natural and induced phenomena. A system of up to six Magnetospheric Multiprobes (MMPs) is being defined under phase II of the Space Plasma Lab facility.[13]

A possible configuration for the MMP is shown in Fig. 6. Each unit is 60 cm in diameter by about 30 cm high with a telescoping antenna/boom system along the spin axis and four wire antennas perpendicular to the spin axis. These units are battery powered with an uplink command/link and a data downlink in the 400-MHz band at data rates up to 128 kilobit/s. For some missions the units are to be instrumented to measure dc electric fields, particle spectra and pitch angles, magnetic perturbations due to currents, and possibly the vlf plasma wave spectrum. For other missions an ion drift meter and ion mass spectrometer might be substituted for or added to the instrument complement.

Spin up to ~20 rpm and ejection of each unit with an Δv up to 10 m/s is accomplished by a special ejection mechanism. The mechanism operates with cold gas to effect the Δv and with an electric motor to provide the spin up. Positioning of the MMPs is accomplished by selecting the correct Orbiter attitude to direct the Δv; 10 m/s yields a peak separation of approximately 10 km from the Orbiter (although the separation varies sinusoidally to ± 10 km peak). With time the

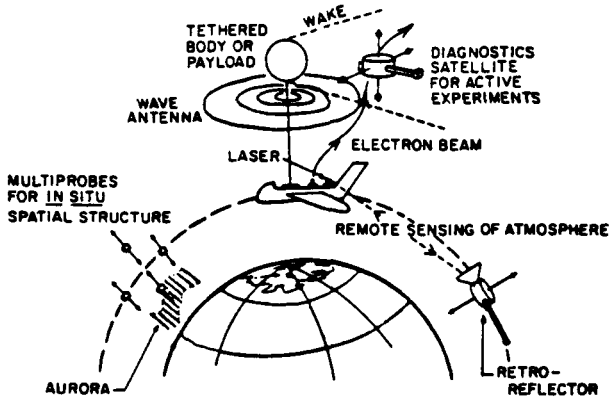

Fig. 9 Summary S-TSS science opportunities.

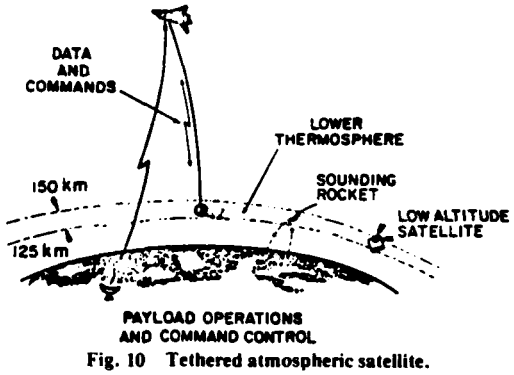

Fig. 10 Tethered atmospheric satellite.

MMP cluster deforms into a string along the orbital track due to atmospheric drag.

Multipoint measurements can provide a snapshot of the WISP antenna pattern for a particular geometry and plasma parameters as indicated in Fig. 7. Also wave-particle phenomena at particular, but not entirely predictable, spatial locations (such as the density gradient in Fig. 5) are more likely to be encountered with multiple probes. Likewise experiments with the electron beam sounding of magnetic field lines for electric field regions depicted in Fig. 8 has a higher chance of success if multipoint measurements of the return electrons are made.[10,13] Similarly, measurements in and near flux tubes containing chemical releases can give estimates of spatial gradients as well as of temporal evolution.[12,13]

Solar-Terrestrial Subsatellite Scheme

Four adaptations of the Solar-Terrestrial Subsatellite based on existing technology were proposed: the inertial upper stage (IUS), the Teleoperator Retrieval System, the Detached Experiment Carrier, and the AE/DE technology.[8]

As implied in Table 3, the class 3 S-TSS is bigger and better than the other two classes. Besides providing for nearly twice the number of instruments, for increased data handling capabilities, and for sustained management from a NASA Center, the S-TSS is to provide both an orbit adjust and stabilized attitude capability. This orbit adjust capability is required to: 1) minimize Orbiter resource requirements in terms of propulsion, rendezvous time, and data handling; 2) carry sensitive instruments outside of the Orbiter contamination envelope; 3) provide lower atmosphere (50-200 km) scan capability by carrying a retroreflector or detector for LIDAR or similar optical source; 4) perform diagnostic measurements of plasma flow around bodies tethered to the Orbiter; and 5) provide numerous experiment opportunities that require specific Orbiter/S-TSS alignments such as along B lines.

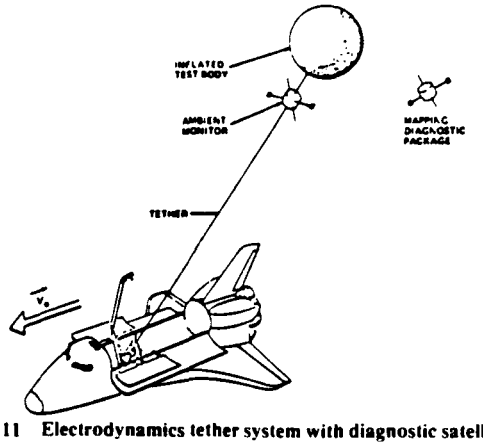

Fig. 11 Electrodynamics tether system with diagnostic satellites.

The stabilized attitude capability is required to: 1) direct mass spectrometers and RPAs into velocity ram direction; 2) point imagers, spectrometers, interferometers, and radiometers toward atmospheric targets such as the limb and auroral regions; 3) position magnetometers, electric field detectors, and energetic particle detectors with respect to the geomagnetic field; 4) establish solar inertial pointing for solar viewing instruments such as imagers and spectrometers; and 5) change attitude according to experiment requirements during the mission.

With the added capabilities of the S-TSS, subsatellite support can be provided to a full range of Spacelab-based facilities as illustrated in Fig. 9.

Electrodynamics Tether System

The Tether Retrieval System provides a means to drag a satellite probe through the atmosphere as in Fig. 10 down to ~100 km altitude without losing the satellite due to atmospheric drag. In this case the tether would provide mechanical support of the atmospheric satellite with a length of ~100 km.[14] This technique provides an important and unique tool for probing the thermospheric region.

For magnetospheric work, a conducting tether wire restraining a large conducting body can produce large motional potentials along the tether of kilovolt magnitudes. An electron accelerator on the Orbiter can emit electrons into the plasma to cause current flow in the tether which may establish electrodynamic effects such as low-frequency wave emissions and field-aligned current systems. Wake, current, and wave effects can be studied by subsatellite probes tethered along the tether wire and by subsatellite probes in the vicinity as depicted in Fig. 11. Combined with the WISP transmitter, the conducting tether can serve as a very efficient vlf transmitting antenna.[14]

On-Orbit Operations

Whatever the subsatellite system in use as part of the Space Plasma Lab Facility, the general operational features are planned as follows:

1) The subsatellites are deployed just after reaching orbit and recovered just before deorbit (if appropriate); the class 2 and class 3 systems may have a capability to stay on orbit between Spacelab missions to serve as a low-altitude spacecraft.

2) The Orbiter or S-TSS must be maneuvered to obtain the appropriate Orbiter-subsatellite geometry along the orbital track or along a magnetic flux tube.

3) Commands are issued simultaneously by the Orbiter crew or the Payload Operations Control Center (POCC) to all of the Spacelab instruments and the subsatellite instruments as to mode and time of the next experiment.

4) Data are transmitted back to the Orbiter and displayed

to the crew so that critical instrument parameters can be changed in order to optimize the experiment conditions.

Summary

Subsatellites are an essential part of the evolving Space Plasma Lab Facility. A simple throw-away subsatellite—the Plasma Diagnostics Package—has flown in 1982 attached to the RMS and will fly as a subsatellite in 1984. A system of Magnetospheric Multiprobes and a Recoverable Plasma Diagnostics Package is undergoing initial design for a 1987 launch opportunity as enhancements to the Space Plasma Lab capability. By 1990 a fully maneuverable Solar-Terrestrial Subsatellite may be available. These subsatellite systems measure fields, waves, particles, and optical emissions associated with natural magnetospheric processes and with active injections of waves, plasma beams, and chemical tracers.

Acknowledgments

This work was supported through NASA Contract NAS8-33770 with the Marshall Space Flight Center.

References

[1]Shawhan, S.D., "A Spacelab Principal Investigator's Guidance for Planning Scientific Experiments Using the Shuttle," AIAA Paper 81-0272, Jan. 1981, *Journal of Spacecraft and Rockets*, to be published.

[2]"NASA Workshop on Solar-Terrestrial Studies From a Manned Space Station," NASA CP-2024, Feb. 1977.

[3]"Spacelab Sub-Satellites for Atmosphere, Magnetosphere and Plasmas-In-Space," *Detached Subsatellites*, Vol. II, European Space Agency, TF/GD-DD/CS/5063, Oct. 1976.

[4]Chappell, C.R., Garriott, O.K., and Bauer, S.J., "Science Objectives of the Atmospheric, Magnetospheric and Plasmas-In-Space (AMPS) Payload for the Spacelab/Shuttle," NASA Marshall Space Flight Center, 1977.

[5]Johnson, F.S., ed., "Final Report, Scientific Definition Panel for AMPS Spacelab Payload," Universities Space Research Association, Sept. 1976.

[6]"Interm Report of the Subsatellite Definition Team," J.L. Burch, Chairman, Southwest Research Institute, Jan. 1978.

[7]"AMPS Subsatellite Facility Plan," AMPS Subsatellite Facility Definition Team, J.L. Burch, Chairman, Southwest Research Institute, March 1978.

[8]"Solar-Terrestrial Subsatellite (S-TSS) Study Report," J.L. Burch, Chairman, NASA Goddard Space Flight Center, Oct. 1980.

[9]Neupert, W.M., ed., "Office of Space Sciences-1 Experiment Investigation Descriptions," NASA Goddard Space Flight Center, Sept. 1979.

[10]Raitt, W.J., Banks, P.M., Burch, J.L., Williamson, P.R., Baker, K.D., and Obayashi, T., "Early Experiments in Charged Particle Beams from the Space Shuttle," AIAA Paper 82-0083, Jan. 1982.

[11]Clifton, K.S., "Spacelab Mission 2 Experiment Descriptions," NASA TM-78198, Sept. 1978.

[12]Mendillo, M. and Bernhardt, P., "The Space Shuttle as an Ionspheric Modification Experiment," AIAA Paper 82-0084, Jan. 1982.

[13]Roberts, W.T., ed., "Space Plasma Physics Active Experiments," NASA CP-2165, Oct. 1980.

[14]"The Tethered Satellite System," Facility Requirements Definition Team, P.M. Banks, Chairman, Utah State University, May 1980.

A Spacelab Principal Investigator's Guidance for Planning Scientific Experiments Using the Shuttle

S.D. Shawhan

Reprinted from
Journal of Spacecraft and Rockets
Volume 20, Number 5, September-October 1983, Page 477
AMERICAN INSTITUTE OF AERONAUTICS AND ASTRONAUTICS • 1633 BROADWAY • NEW YORK, N.Y. 10019

A Spacelab Principal Investigator's Guidance for Planning Scientific Experiments Using the Shuttle

Stanley D. Shawhan*
The University of Iowa, Iowa City, Iowa

Experience gained in defining and developing the payload and the mission timeline for the OSS-1, Spacelab-1, and Spacelab-2 missions suggests several areas which require careful planning to carry out a Shuttle scientific experiment. During the experiment definition phase early attention should be given to the thermal design, the analysis of potential safety hazards, and contamination since these areas can escalate the instrument design. In completing the Experiment Requirements Document it is important to be realistic in specifying the requirements and desires for mass, energy, data, orbit and attitude, and crew time but to be flexible in how these requirements are satisfied. Examples of resource allocations for Spacelab-1 and Spacelab-2 are given. To optimize the scientific return from a mission it is suggested that joint operations of complementary and compatible experiments be planned from the beginning to maximize the use of the limited resources. Crew members should be given primarily tasks of essential commanding and data interpretation; the experiment computer use should be limited to servicing the dedicated experiment processors and providing essential onboard commands and displays. It may be desirable to rely on experiment ground support equipment for essential data capture and processing rather than on the Payload Operations Control Center data services.

Introduction

THE advent of the Space Transportation System (STS) offers the first possibility to deploy and return scientific instrumentation from the near Earth orbit.[1] Instrumentation is placed above the obscuring lower atmosphere and into a high vacuum, low acceleration environment at the lower edge of geospace in the midst of a variety of solar-terrestrial processes within a region suitable for active plasma-particle-wave-photon experimentation.

Instrumentation can be accommodated in small standard containers of the "Get-Away Special" (GAS) program, housed in the crew storage lockers, rack-mounted at the aft-flight-deck or hard-mounted to the Orbiter structure within the payload bay. Items within the bay can be detached and articulated to distances of 50 ft using the Remote Manipulator System (RMS). Large or complex instrumentation and facilities can be most conveniently accommodated by the European Space Agency's (ESA) Spacelab system[1,2] with components including a manned module, pallets, and an Instrument Pointing System (IPS) along with associated remote acquisition units (RAUs), experiment computer (EC), cold plates and freon cooling loop, power distribution unit, and data display unit (DDU).

A unique feature of the STS is that crew space is available to carry not only the members required to position the Orbiter in orbit and attitude but also mission specialists and payload specialists who have the skills to operate the instrumentation and associated flight support equipment in order to maximize the results from a particular mission. The command and data systems on the Orbiter allow for man-in-the-loop operation and the high rate data link to the Payload Operations Control Center (POCC) allows for the investigation team to also be included in the loop in nearly real time. With the possibility of several missions to carry out a scientific program the hardware, software, and techniques can evolve based on on-orbit performance as well as on careful analysis of data between missions.

Presented as Paper 81-0272 at the AIAA 19th Aerospace Sciences Meeting, St. Louis, Mo., Jan. 12-15, 1981; submitted June 17, 1981; revision received Aug. 19, 1982.

*Professor of Physics, Department of Physics and Astronomy.

Although the prospects for experimentation on the Orbiter look bright, the experience being gained during the definition and development of instruments and timelines for the OSS-1,[3] Spacelab-1,[4] and Spacelab-2[5] missions indicates that some design areas and resource constraints need careful consideration in order to accomplish the scientific objectives. The point of this paper is to identify these design areas and limited resources and to suggest schemes by which scientific experiments can be planned and executed to obtain the desired data within these constraints.

For the discussion that follows, the Spacelab-1 and Spacelab-2 missions are used as representative of science-dedicated missions. They are important models because they do utilize the selection, funding, management, development, mission operations, and data analysis philosophies and procedures that are intended for Spacelab missions of the future. The Spacelab-1 mission[4,6] utilizes the Spacelab manned-module and a pallet of instruments to accommodate 38 instruments from ESA and NASA investigators. Spacelab-2[5,7] uses the Instrument Pointing System, three instrument pallets, and a special support structure. The remote Manipulator System is used to deploy a subsatellite. Both missions are to carry out investigations in the areas of physics, life sciences, astrophysics, and applications sciences.

Spacelab Experiment Allocations

The Spacelab system allows for the accommodation of a large variety of scientific instrumentation with a minimum of interface complexity and, consequently, for the rapid interchange of instrumentation between Spacelab missions.[1,2] Also, the command and data handling systems are particularly designed to accommodate the crew in the loop for nominal or contingency operations. However, the resources available to the payload for science must also support this Spacelab system.

Some of the primary resources which are allocated to the Spacelab payload in general and the percent of the allocation which is dedicated to the Spacelab-1 and Spacelab-2 experiments themselves are listed in Table 1. The total payload mass is limited by the maximum landing weight. Experiments on Spacelab-2 are allocated a larger portion—32%—compared to Spacelab-1 because of the additional Spacelab-1 weight for the module and support equipment. Both the

power and the energy allocations are determined by the capability of a single fuel cell. In the case of Spacelab-2, most of the experiments could be run simultaneously for the entire mission from a power and energy standpoint. The Spacelab overhead is ~80% of the energy. For Spacelab-1 the module increases the overhead to ~90%. Instruments on Spacelab-1 must have a lower duty cycle because the peak experiment power exceeds the available power (119%), not including the overhead. One of the big uncertainties in the power usage and energy budget is the instrument heater requirements. Several Orbiter flights are required to test the thermal models to establish the heater duty cycles.

Low digital data rates can be handled through the Spacelab RAUs by the experiment computer.[1,2] However, the bulk of the digital data is handled through the high rate multiplexer (HRM).[1,2] Neither the Spacelab-1 nor Spacelab-2 peak data rates approach the 32 Mbps capability of this channel. As the maximum rate is approached the data recording onboard and on the ground as well as the downlink scheduling become significant problems. Experiment commanding and onboard data displays as well as servicing of dedicated experiment processors (DEP) can be handled by the experiment computer operations software (ECOS) which requires ~44 kbytes of the 65 kbytes EC memory. Any special DEP or analysis or control programs are routines in the 20 kbytes experiment computer applications software (ECAS) of which 60% and 70% are allocated to Spacelab-1 and Spacelab-2, respectively. The balance of ECAS is for crew use.

Propellant is required to create or negate "g" loads, to change orbit, and to track specific targets. In order to accomplish objectives requiring orbit or attitude adjustment, approximately 50% of the propellant is available for experiment use including attitude maneuvering for data dumps to the Tracking and Data Relay Satellite System (TDRSS). The balance is used for orbit insertion and for deorbit. Given the energy and propellant constraints and the occurrence of appropriate observing conditions, the prime observing time for an experiment can be determined. For a seven-day mission approximately 152 h are available. For Spacelab-2, 567 h are allocated as prime time or 371% of that available—meaning that almost four experiments can be conducted simultaneously through a mixture of crew and POCC control. Spacelab-1 has many more experiments and most of these operate for the duration of the mission with very little crew attention so nearly 15 experiments can operate simultaneously. Since two scientific crews are available each shift—8 h for the mission specialists and 10 h for the payload specialists—252 h of dedicated crew time is possible. For Spacelab-1 and Spacelab-2, ~65% is assigned to specific experiments with the balance used to monitor other experiments and to carry out other payload duties. Even if energy and propellant were available, the dedicated crew time limits the optimization of results from the man-in-the-loop operations.

A listing of the Spacelab-2 experiments and a detailed breakdown of the resources are given in Table 2. Mass values range up to 2000 kg for the experiment 6 cosmic ray telescope, which is a specialized structure instead of a pallet. Power

Table 1 Spacelab resource allocation to experiments

	Spacelab allocation	Spacelab-1 experiments[6]	Spacelab-2 experiments[7]
Mass	14,515 kg	2784 (19%)	4637 (32%)
Power	Average 7 kW	0.7 (10%)	1.3 (19%)
	Peak 12 kW	14.3 (119%)	2.6 (32%)
Energy	~900 kWh	100 (11%)	199 (22%)
HRM data	Peak 32 Mbps	4.7 (15%)	2.5 (8%)
Experiment computer memory for ECAS	~20 kbytes	12 (60%)	14 (70%)
On-orbit propellant	~7400 lb	3457 (47%)	3957 (53%)
Prime observing time	152 h	2248 (1479%)	567 (371%)
Dedicated crew time	252 h	177 (70%)	150 (60%)

Table 2 Spacelab-2 experiment resources utilization[7]

Experiment No.		Mass, kg	Average power, W	Energy, kWh	Maximum HRM data rate, Kbps	ECAS memory, kbytes	Prime time, h	Dedicated crew time, h
1	Vitamin D. Metabolites and bone demineralization	32	0	0	0	0	9	12
2	The interaction of oxygen and gravity influenced lignification	24	52	9	0	0	166	3
3	Ejectable plasma diagnostics package	372	34	5	333	0	19	48
4	Plasma holes for ionospheric and radio astronomy studies	0	0	0	0	0	7	7
5	Small helium-cooled i.r. telescope	770	101	15	614	2.0	27	Monitor
6	Elemental composition and energy spectra of cosmic ray nuclei	1968	232	33	102	1.25	137	Monitor
7	Hard X-ray imaging of clusters of galaxies and other extended X-ray sources	570	179	25	64	2.2	103	Monitor
8	Solar magnetic and velocity field measurements system	198	150	22	1365 (video)	1.9	18	
9	Solar coronal helium abundance Spacelab experiment (chase)	100	74	12	8 (RAU)	2.0	15	79
10	Solar u.v. high resolution telescope and spectrograph	256	325	47	(video)	2.6	16	
11	Solar u.v. spectral irradiance monitor	83	95	14	(RAU)	1.5	4	
12	In-orbit calibration of mesa low g accelerometer	15	20	3	(RAU)	0.2	23	Monitor
13	Properties of superfluid helium in zero g	250	93	14	20	0.35	23	Monitor
	Total	4637	1355	199	2506	14.0	567	150
	"Average" experiment	357	104	15	193	1.1	44	12

values range up to 325 W with an energy allocation of 47 kWh for experiment 10 on the IPS. Maximum HRM data rates of 1365 kbps occur for experiment 8 in addition to the use of the 4.5 MHz video downlink. Experiment 10 utilizes 2.6 kbytes of the 14 kbytes of ECAS memory. Both experiment 2 and experiment 6 are allocated prime observing time for nearly the entire mission since very little crew intervention is required. However, experiment 3 and the solar experiments on the IPS (experiments 8-11) require more than one crew member to support the allocated prime time; for example, experiment 3 has 48 h of dedicated crew for 19 h of prime time indicating ~2.5 crews for the subsatellite deployment and fly-around operations. Values for an "average" Spacelab-2 experiment are given at the bottom of Table 2. These values may be representative of the future discipline-dedicated Spacelab payloads.

Experiment/Instrument Definition

Joint Operations

Experiments for the current OSS-1, Spacelab-1, -2, and -3 missions and the 38 experiments for possible future spacelabs were selected from proposals submitted in response to NASA Announcements of Opportunity. These experiments were proposed largely as stand-alone investigations without regard for other proposed complementary investigations. Joint experiment scenarios have subsequently been developed between investigation teams. For example, the vehicle charging and potential experiment and the plasma diagnostics package on OSS-1, the four solar experiments (experiments 8-11) on Spacelab-2, and the plasma holes (experiment 4) and plasma diagnostics package (experiment 3) on Spacelab-2 have defined joint functional objectives. These joint operations are particularly significant because they enhance the overall scientific output for the mission by providing complementary measurements and they minimize the various resources required to obtain these results. It is therefore important for the possibility of joint operations to be identified early in the experiment definition phase.

Experiment Requirements Document

Experiments are assigned for definition and development to any of the NASA Centers usually along discipline lines. Marshall Space Flight Center (MSFC) has the responsibility to accommodate the experiment into a spacelab once the investigation has been assigned to a particular mission. During the definition and development phase an Experiment Requirements Document[8] (ERD or equivalent) is prepared which specifies the requirements in terms of resources, pointing accuracy, orbit, special tests, ground operations, software, safety, POCC services, etc., that are necessary to complete the investigation. MSFC then carries out a physical and timeline accommodation study including all the experiments for that mission to maximize the number of requirements that can be satisfied, and this information is collected in the Integrated Payload Requirements Document (IPRD).[6,7] After some iteration the Instrument Interface Agreement (IIA)[9] is created.

In preparing and iterating the ERD it is important to establish requirements that are consistent with the original proposal, in line with the resources available as indicated in Tables 1 and 2, commensurate with the Orbiter performance characteristics, and include scenarios for joint operations. Firm requirements must be clearly distinguished from desired performance. Suggestions for meeting a particular requirement are appropriate but the suggestions should be written so they are not interpreted as the requirements themselves.

Design Analyses

Three areas related to the instrument design have required particular attention for instruments developed for OSS-1, Spacelab-1, and Spacelab-2: thermal control, safety hazard analysis, and contamination control. Thermal control is a particular problem because the Orbiter bay can be oriented toward or away from the sun for extended periods of time which allows the pallet-mounted equipment to become very hot or very cold. On pallets, instrumentation can be mounted on cold plates connected to a freon loop with a large heat capacity and a radiator system. However, in the hot case the radiator system is the least efficient. Within the module, equipment is forced air cooled. Also, the equipment should be able to survive the hot and cold extremes of a contingency situation if the freon loop or forced air were to fail. The thermal design has been particularly difficult for the Spacelab-2 experiment 3 plasma diagnostics package which has to operate in the bay without a cold plate, on the RMS, and as a satellite. Also, instruments mounted on the IPS must maintain thermal control without cold plates. To date thermal design parameters have been changing as the payload thermal analyses evolve.[1,6,7] After several STS flights, the thermal modeling should be more realistic so that thermal control techniques can be more readily specified.

Rigid safety criteria have been established to protect the ground crews during payload integration and the flight crew during the mission.[10] Of particular concern have been the stress on mechanical structures and the flammability and outgassing of nonmetallic materials. Stress due to launch and landing loads and stress corrosion have been addressed in detail in Sec. 14.0 of the IPRD,[6,7] for example. Flammability during ground operations and toxic outgassing are stringently controlled through the selection of materials.[11] Another criteria is that the experiment ground support equipment (EGSE) must undergo both a mechanical and an electrical safety analysis to protect both the flight hardware and the ground crews, particularly at the Kennedy Space Center (KSC). Consideration of these safety issues has meant that techniques and materials that have been acceptable in other space programs are not necessarily acceptable for STS hardware. Obviously, these issues must be identified early in order to comply with the safety criteria and to keep the instrument cost reasonable.

Finally, the area of contamination due to gaseous and particulate matter is of particular concern to instruments with optical surfaces. These restrictions have been imposed by the Investigator Working Group itself for Spacelab-2 as appropriate for the particular complement of instruments. As a result of these contamination limits, additional restrictions on materials, thermal control surfaces, and instrument purges may be applied.

Mission Timeline

The mission timeline for 84-96 h mission elapsed time (MET) for Spacelab-2 is shown in Fig. 1 to give an overall feel for the many factors that must be taken into account in the timeline accommodations. During this 12 h crew timeline period the blue crew, consisting of a payload specialist (PS2) and a mission specialist (MS2), is active although there is a handover to the red crew at −94 MET. For the active crew, the specific tasks fall into blocks of time from as short as 10 min to well over 1 h. The notation in each time block refers to a particular task (SPC1 = solar physics, MS2LU/PS2LU = lunch, PS2PSA/MS2PSA = sleep). A typical crew function flowchart is given in Fig. 2 to indicate the types of steps to be performed in a task and the interactions required with the DEP through the EC and with the investigator team in the POCC.

In defining the extent of crew involvement one must assess if the involvement is essential to the conduct of the experiment in terms of issuing critical commands or in terms of interpreting data displayed onboard in order to issue a sequence of commands to optimize the experiment or to take advantage of a "target-of-opportunity." Could the data be interpreted and commands issued just as easily from the POCC? A

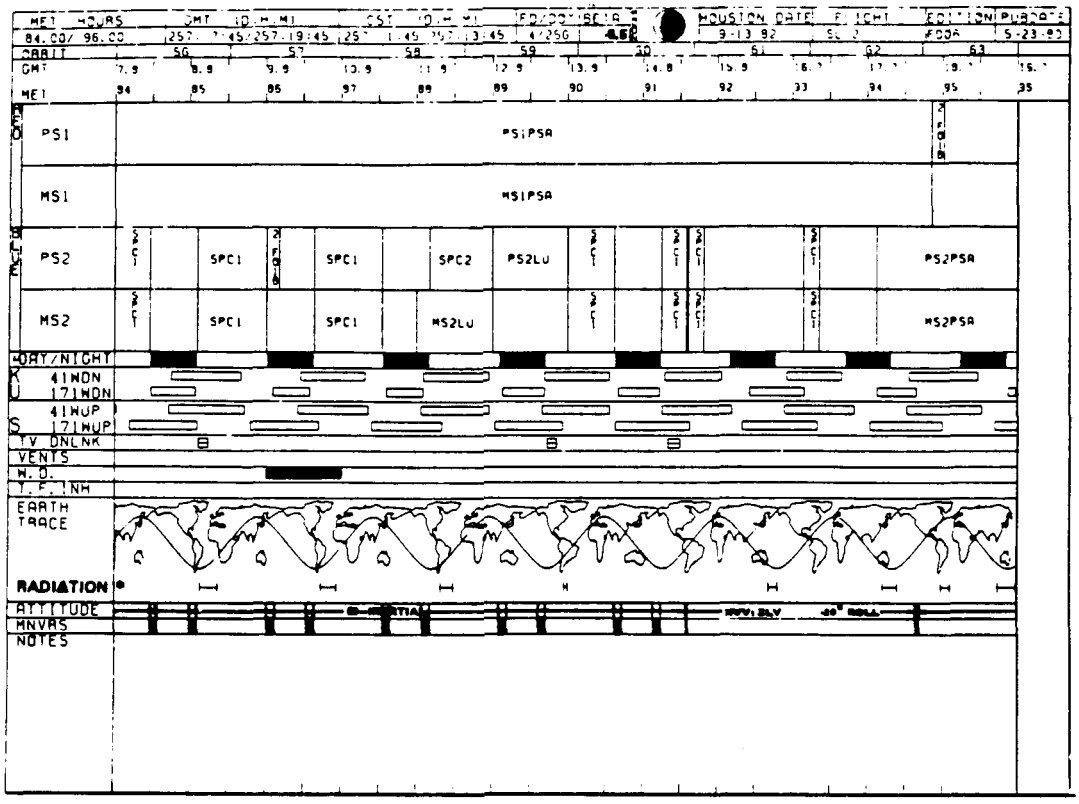

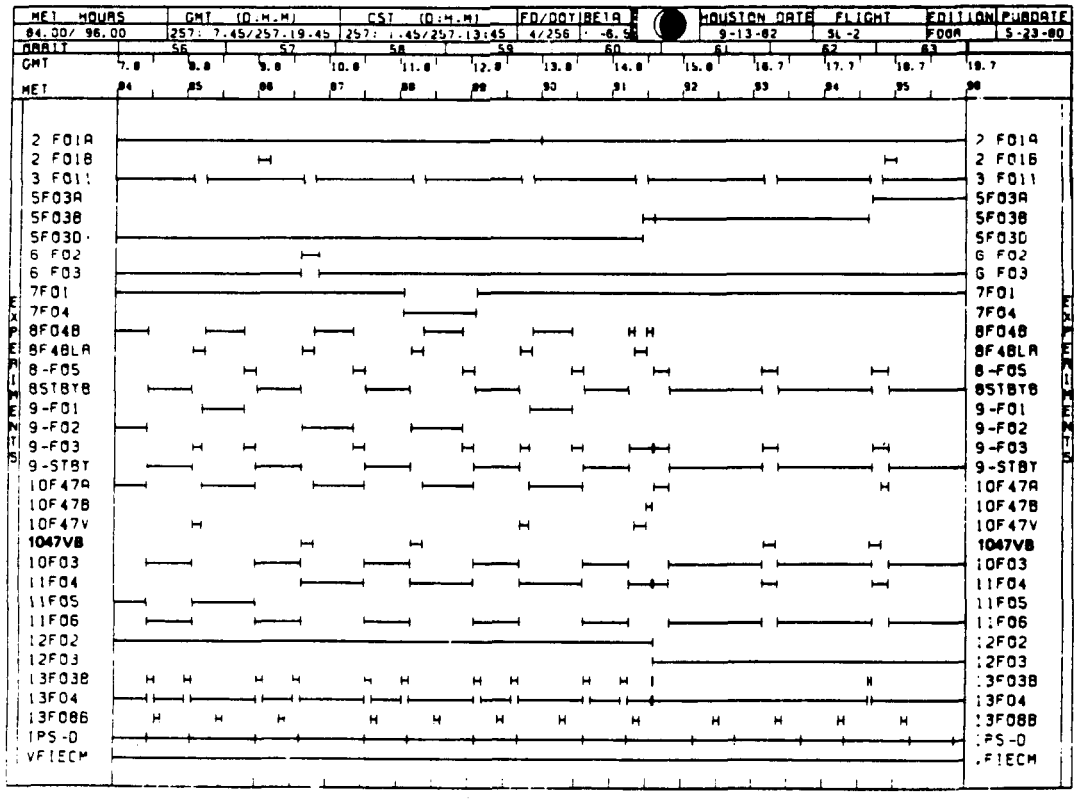

Fig. 1 Sample mission timeline from Spacelab-2 (Ref. 12).

significant crew involvement means that one or more crew members on each shift need to have the skills required to interpret the results from the instrument which in turn implies an extensive crew training program.

Data Link Timeline

Most of the science data comes via the Ku-band (KU) downlink. At the time of Spacelab-2 there will be only two TDRSS satellites so that the real-time coverage is limited to about 70%. For future Spacelab flights, three satellites will provide ~90% coverage so that the POCC can be considered in the loop.

Attitude Timeline

In order to satisfy a variety of attitude requirements for a number of instruments over the mission duration, the Spacelab-2 Orbiter is required to make a series of attitude maneuvers each orbit. A representative bi-inertial and +30 deg roll attitude is depicted in Fig. 3. Although it may be possible to develop an attitude timeline to obtain the required duration of specified look directions, the propellant budget indicated in Table 1 may be an overriding constraint. On Spacelab-2 there are engine firings to deposit large clouds of burn products to study the ionospheric effects (experiment 4), and there are orbit change maneuvers to fly around the subsatellite (experiment 3) and to gain altitude (experiment 7) in addition to attitude maneuvers.

Instrument Operation Timeline

During the period covered in Fig. 1, the crew is dedicated primarily to the operation of the four solar instruments on the IPS with some time available to take data for the plant growth units (experiment 2) at ~86 and ~95 MET (task 2F01B). This is an interesting time period in that all the onboard instrumentation (lead number identifies instrument) are operating simultaneously although most of them are undergoing automatic sequencing. The energy constraint does not allow simultaneous operation for the entire mission.

Timeline Replanning

It is unreasonable to think that the "final" mission timeline that is developed nearly a year before flight will be executed perfectly for the entire mission. Launch holds or delays, space motion sickness, instrument failure, inadequate task descriptions, etc., could all contribute to the modification of the timeline during the mission. For Spacelab-1 and Spacelab-2, MSFC has proposed a 12-h, replanning cycle which occurs continuously. Every 12 h, mission operations personnel meet to assess the status of the Orbiter and crew and to establish any mission constraints for the 12-h period in question. The investigators meet with the payload personnel to assess the status of the payload and the instruments. Any modifications to the planned timeline are proposed and the impacts are evaluated. The crew is then informed of the procedural changes. For any 12-h period, the goal is always to return to the nominal timeline.

In order to support this replanning activity, the investigator team must have enough personnel to staff at least two shifts each day. Also, contingency schemes should be planned including the command sequences that would be needed to be uploaded to the DEP from the POCC.

Command and Data Handling

Experiment Computer

The experiment computer is coupled to 1) the remote acquisition units to obtain data from instruments and to provide commands, 2) a digital display unit with a keyboard for initiating commands onboard and displaying processed RAU data, 3) a mass memory unit for memory/program exchange, and 4) the data link with the POCC.[1,2] A sample

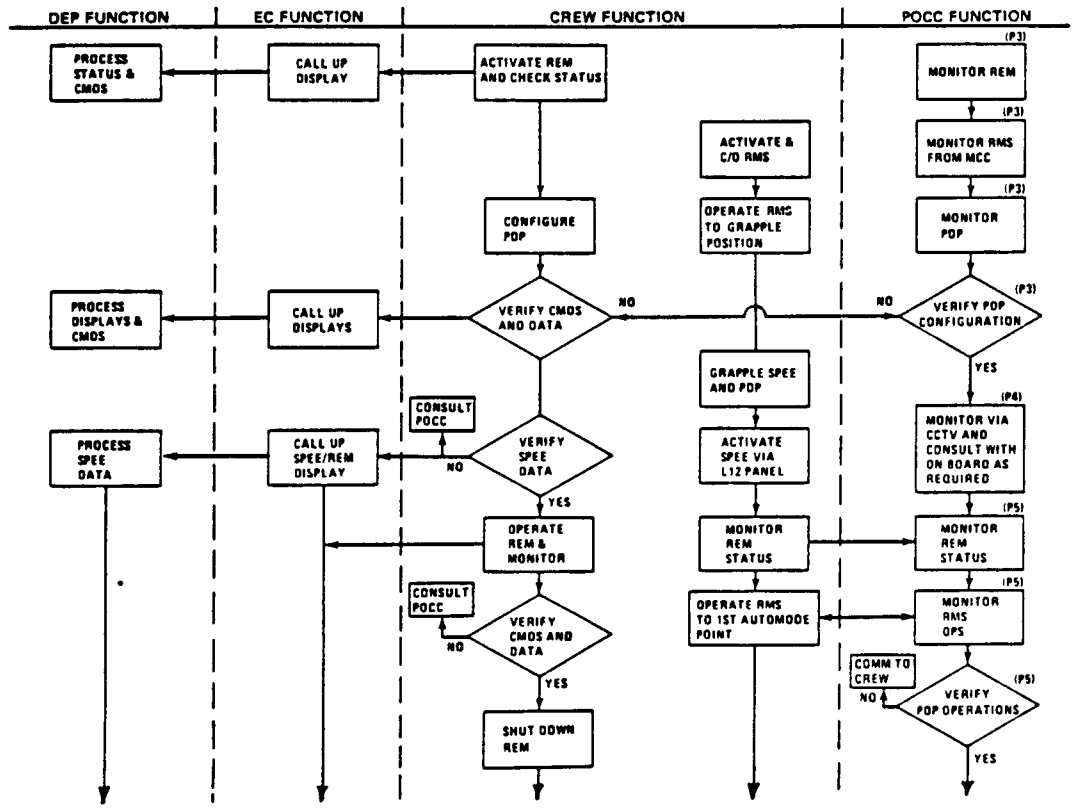

Fig. 2 Typical crew function flowchart.

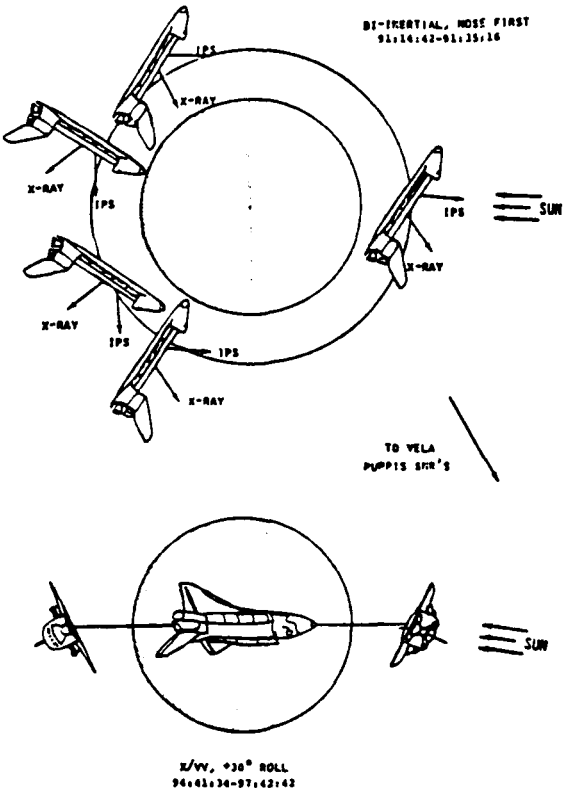

Fig. 3 Typical attitude maneuvers.

display from Spacelab-2 experiment 3 is shown in Fig. 4. This display contains item entry commands (items 1-24) which can be sent by two keystrokes since these commands are active only when the display is up and the commands are predefined. The remainder of the display contains housekeeping data for experiment 3. On Spacelab-2 there are ~500 item entries and ~50 displays which are supported by ECOS.

To build a discrete command at the keyboard it takes six keystrokes and to build a serial command it takes 13-20 keystrokes. Once a command is entered it takes ~1 s to execute. For commands issued from the POCC it takes 1-2 s for a single stage command (not checked on receipt) and ~12 s for a two-stage (checked) command if the uplink is established.

In controlling an instrument it is important to decide on the prime command scheme. Neither commands from the keyboard nor from the POCC can be counted on for quick reaction to a contingency situation. Keyboard item entry commands are the most efficient from the crew standpoint since they are predefined. Routine commanding from the POCC relieves the crew from having to call up a display and to send item entry commands, or from having to compose commands if they are not in response to some newly interpreted data or to a target-of-opportunity. A scheme which would minimize the crew time and ECOS/ECAS overhead is to store command sequences in the DEP. These sequences could be time-tagged or initiated by item entry. The item entry could also be used to fill limited data fields (to set parameter limits) within the DEP commands. All DEP command sequence updates could be handled from the POCC. The flexibility of rebuilding the instrument sequences is particularly important if the timeline is replanned during the mission.

Use of the mass memory unit (MMU) can expand the very limited EC core space in support of ECAS. However, the

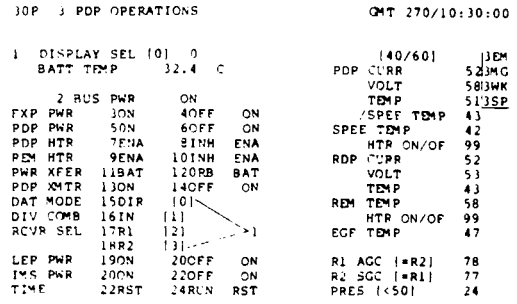

Fig. 4 Sample Spacelab-2 display.

MMU has an access time of 2-30 S. Use of ECAS to handle DEP protocol, instrument control logic, and special processing of data to be displayed may be justified. However, one implementation problem lies in the inability to completely check the software before actual integration into the Orbiter just before launch, although simulators are available. It seems that unless the EC is upgraded, instruments should contain DEPs to handle any instrument-unique tasks such as instrument control logic and specialized displays not handled by ECOS. Also, the degree of data processing and display handled by ECOS should be kept to the minimum that the crew can reasonably use in order to minimize the number of loads from the MMU.

Analog Data

Some types of experiments produce moderate bandwidth analog data that are not really efficiently handled by an analog-digital conversion and the HRM digital link or by the 4.5 MHz CCTV downlink (when it is available). Two such services are slow-scan TV images from optical experiments and electromagnetic wave data from space plasma wave instruments (~50 kHz). Future developments of Spacelab should accommodate these types of data.

POCC Operations

Each experiment is provided with a user area in the POCC which includes a console for initiating commands to the user's instrument and for displaying and capturing any parameters from the Orbiter instrumentation (OI) or experiment computer input/output (ECIO) data stream. HRM data are delivered as they are inputted to the Spacelab. All of the downlinked data including the OI, ECIO, HRM, and CCTV (analog) are captured for nearly realtime playback and for later processing onto computer compatible tapes as may be specified.[1] The POCC provides very limited capability, however, for processing the HRM data. The trend seems to be to provide EGSE in the POCC which is adequate for capturing and processing HRM instrument data. These EGSE data systems almost have to exist anyway in order to conduct instrument-level tests before and after integration into the Spacelab.

Summary

Through development of instruments for the OSS-1 and Spacelab-2 missions, various opinions have been developed about the capabilities and the limitations of the STS for the conduct of scientific experiments. Implications of the STS design requirements and resource allocations have been discussed as they apply to the experiment/instrument definition, to the mission timeline, and to command and data handling. For these areas, approaches have been suggested to maximize the capability to meet the scientific objects which should be considered as a scientific experiment is being planned and as the Spacelab is upgraded for future missions.

References

[1]"Mission Integration Guidelines for Development of STS Attached Payloads," Spacelab Payloads Project Office, NASA Marshall Space Flight Center, Huntsville, Ala., June 1980.

[2]"Spacelab Payload Accommodations Handbook (SPAH)," European Space Agency, ESA SLP/2104, July 31, 1978.

[3]Neupert, W.M., "Office of Space Sciences-1 Experiment Investigation Descriptions," NASA Goddard Space Flight Center, Greenbelt, Md., Sept. 1979.

[4]Craven, P.D., "Spacelab Mission 1 Experiment Descriptions," NASA TM-78173, May 1978.

[5]Clifton, K.S., "Spacelab Mission 2 Experiment Descriptions," NASA TM-78198, Sept. 1978.

[6]"Spacelab Mission 1 Integrated Payload Requirements Document," NASA Marshall Space Flight Center, Huntsville, Ala., JA-010 Rev. C., April 1980.

[7]"Spacelab Mission 2 Integrated Payload Requirements Document," NASA Marshall Space Flight Center, Huntsville, Ala., JA-017 Rev. B, May 1980.

[8]"Experiment Requirements Document," NASA Marshall Space Flight Center, Huntsville, Ala., MSFC Form 3591, Dec. 1978.

[9]"Instrument Interface Agreement for Spacelab 2," NASA Marshall Space Flight Center, Huntsville, Ala., JA-030, Jan. 1980.

[10]"Space Transportation System Payload Safety Guidelines Handbook," NASA Johnson Space Center, Houston, Tex., JSC-11123, July 1979.

[11]"Material Selection Guide for MSFC Spacelab Payloads," NASA Marshall Space Flight Center, Huntsville, Ala., MSFC-HDBK-527B, Dec. 9, 1978.

[12]"Spacelab Two Flight Definition Document FDD," NASA Marshall Space Flight Center, Huntsville, Ala., JA-037, June 1980.

GEOPHYSICAL RESEARCH LETTERS, VOL. 10, NO. 12, PAGES 1215-1218, DECEMBER 1983

MULTIPLE ION STREAMS IN THE NEAR VICINITY OF THE SPACE SHUTTLE

N. H. Stone,[1] U. Samir,[2,5] K. H. Wright, Jr.,[3]
D. L. Reasoner,[1] and S. D. Shawhan[4]

Abstract. Differential measurements of ion flow direction and energy during the third Space Shuttle mission (STS-3) have revealed the existence of ion streams in the near vicinity of the Orbiter at angles of attack as great as 50° with respect to the ram direction and typically with 10% of the ram current intensity. Neither the source nor the mechanism by which these secondary ion streams were created are known at present; however, it is reasonably certain that they are not of geophysical origin, but result from the interaction of the Orbiter with its environmental ionospheric plasma. The energy of the secondary streams was observed to be very close to the ion ram energy and they were, therefore, not detected by a standard planar Retarding Potential Analyzer (RPA) instrument. This leaves open the question as to their existence in the vicinity of orbiting spacecraft in general. Possible connections between secondary ion streams and phenomena previously observed in the vicinity of ionospheric spacecraft are mentioned.

Introduction

The STS-3 mission offered the first opportunity to measure the plasma and field environment of the Space Shuttle Orbiter. This was accomplished by the Plasma Diagnostics Package (PDP) experiment which is a self-contained, deployable satellite that carries an ensemble of fourteen instruments. During the 7-day mission, the PDP was deployed up to 15 m above the Orbiter bay with the Remote Manipulator System (RMS) on mission days three and four. The effects reported herein were observed on both of these days with one of the PDP instruments, the Differential Ion Flux Probe (DIFP).

The DIFP was developed at the Marshall Space Flight Center for use in laboratory investigations of the electrodynamic interaction of rarefied plasma flows with test bodies [Stone, 1977]. Its unique feature is the ability to deconvolve and measure the characteristics of multiple ion streams, differing in flow direction and/or energy at a single point in space. The DIFP has been used extensively in laboratory investigations and, in addition to the STS-3 mission, has flown on two sounding rocket missions (Project Centaur Multiple Auroral Probe missions, MAP-1 and MAP-2, launched in December 1981).

The existence of ion streams in the disturbed region of ionospheric satellites was inferred by Henderson and Samir [1967] and has been studied extensively in the laboratory; e.g., Hester and Sonin [1970a,b], Stone et al. [1972], Samir et al. [1974], Fournier and Pigache [1975], and Stone [1981a,b,c]. In all of the above cases, the ion streams were associated with the downstream wake region and, in fact, one of the PDP science objectives was to study the wake of the Orbiter. However, the secondary ion streams observed during the STS-3 mission were totally unexpected in that they were measured when the PDP was not in the wake of the Orbiter and, in some cases, when extended upstream from the Orbiter.

Experimental Data from STS-3

The geometry of the PDP and the field-of-view of the DIFP are shown in Figure 1a. The DIFP scan discerns the ion flux angle of incidence only in the plane containing the PDP axis of symmetry. The azimuthal angle must be determined from spin phase modulation. Since the PDP did not spin during the STS-3 mission, there is no straightforward measurement of the azimuthal dependence. (This should be measured on the Spacelab 2 mission when the PDP will be free-flying.) Figure 1b shows the PDP position and orientation at the point in the example maneuver (described below) when the ram current passed through normal incidence. Note that the location of the secondary ion streams in the plane of the velocity vector-PDP axis may not be as shown due to the azimuthal ambiguity discussed above.

Figure 2 gives a spectrogram presentation of data obtained over a period of several minutes during which the PDP underwent a maneuver that changed the angle between its axis of symmetry and the ram direction, beginning with a negative angle of attack, then rotating through normal incidence to a smaller positive angle of attack, which was approximately maintained for the duration of the maneuver. The spectrogram shows the time variation (horizontal axis) of the current collected as a function of the deflection voltage (vertical axis) which produces the electronic sweep and is, therefore, related to the ion flux angle of attack relative to the instrument normal. Normal incidence occurs at 0 volts (center) while positive and negative angles of incidence are indicated by positive and negative voltages (above and below the center line), respectively. The current levels indicated beside the color scale are powers of ten.

The most intense (red) ion stream in Figure 2 is the ram ion flux which is seen to change direction, following the PDP orientation changes

[1]Space Science Laboratory, NASA/Marshall Space Flight Center, Huntsville, AL 35812

[2]NRC Senior Associate, Space Science Laboratory, NASA/MSFC, Huntsville, AL 35812

[3]Physics Department, The University of Alabama in Huntsville, Huntsville, AL 35899

[4]Department of Physics & Astronomy, The University of Iowa, Iowa City, IA 52242

[5]On leave from Dept. Geophys. & Planet. Science, Tel-Aviv Univ., Israel and Space Sci. Laboratory, The University of Michigan, Ann Arbor, MI 48109.

Paper number 3L1623.

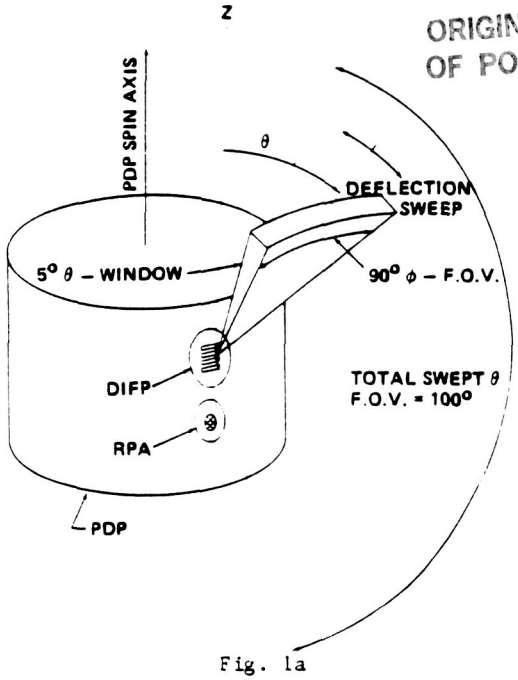

Fig. 1a

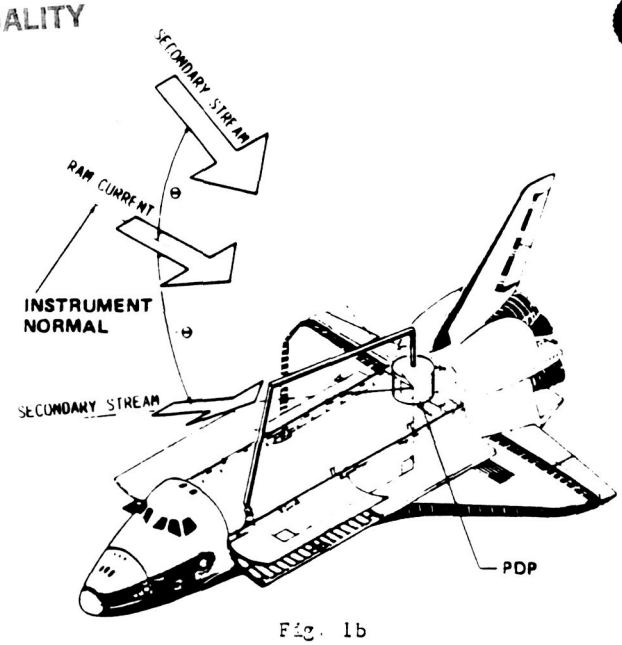

Fig. 1b

Fig. 1. a) Geometry of the Plasma Diagnostics Package (PDP) and the field of view of the Differential Ion Flux Probe (DIFP). b) Position and orientation of the PDP and the ram and secondary ion streams with respect to the Space Shuttle Orbiter at 21:14:30 UT (the point of normal ram current incidence).

during the maneuver. In addition, secondary, less intense (green) ion streams occur at high angles of incidence. These secondary streams also follow the PDP orientation changes.

The energy of the ram and the secondary ion streams were determined by retarding potential analysis to be approximately 10 eV, which indicates the PDP to be negatively charged to approximately -5 volts. (The ram energy of atomic oxygen at 240 km altitude is about 5 eV.) This is in agreement with the expected emf generated between the main engine nozzles (the only significant conducting surface on the Orbiter) and the PDP location by the geomagnetic field [Shawhan and Murphy, 1983].

A plot of current intensity as a function of the angle of attack, measured at 21:14:30 UT, is shown in Figure 3. Notice that there are two distinct ion streams, the ram ions at +10 degrees and the secondary ion stream at -54 degrees. The ratio of the secondary to ram current intensities is 0.08. The DIFP obtained data while deployed on the RMS during a total of 17 periods. Of these, secondary ion streams similar to those shown in Figure 3 were clearly observed during 12 periods (or 71% of the periods). The ratio of

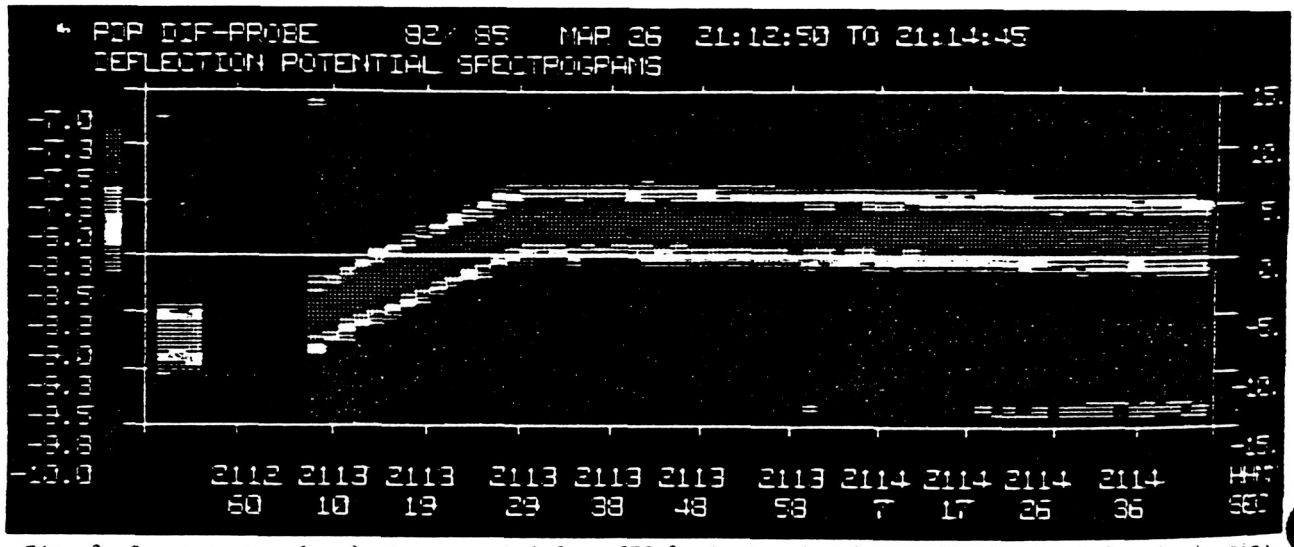

Fig. 2. Spectrogram of a 2-minute period from STS-3 mission day four. The horizontal axis is time (hr:min:sec), the vertical axis is deflection potential (volts), and the ion current is color coded in powers of ten (amps).

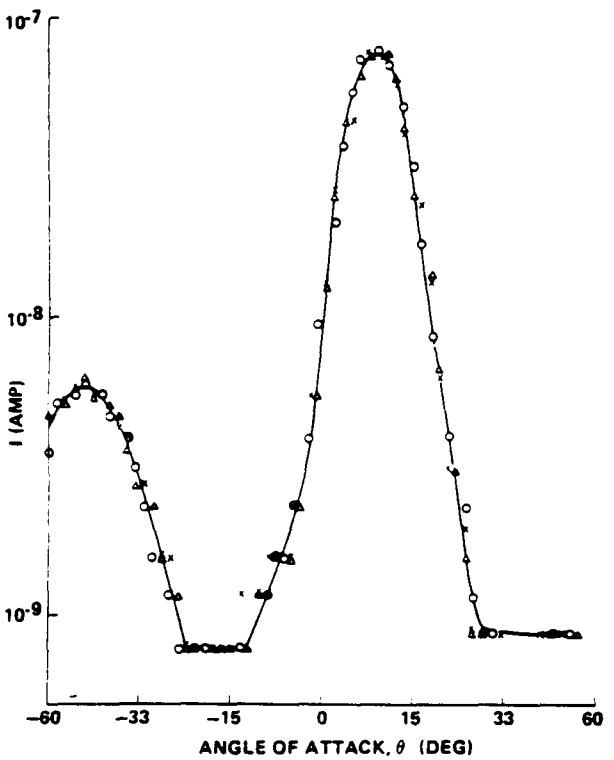

Fig. 3. Ion current versus angle of attack at 21:14:30 UT.

secondary stream intensity to the ram current intensity ranged from 3% to 20%. All observations were made when the Orbiter was in sunlight.

Data obtained from a PDP-mounted planar RPA at 21:14:30 UT gave values of the O^+ density and temperature typical of the ambient ionosphere. Moreover, there was no indication in the RPA data of the secondary ion streams observed by the DIFP during the same period.

Discussion

The DIFP has been used extensively in the laboratory, and the flight instrument underwent rigorous functional testing and calibration, before and after flight, in a synthesized, collisionless plasma stream with properties similar to those of the ionospheric plasma at the Orbiter. While its ability to deconvolve multiple streams has been well proven by deliberately creating such test conditions, in no case has the instrument ever spuriously indicated the existence of secondary streams when none existed. The complete PDP underwent testing in a plasma environment at the Johnson Space Center where no secondary ion streams should have occurred--and none were found in the DIFP data. Furthermore, no secondary ion streams were observed by the DIFP on the Project Centar sounding rocket flights. Therefore, there is no reason to interpret the STS-3 data as an instrumental effect. Even though the secondary ion streams were found in an unexpected region, the DIFP data clearly indicates their presence just as it has in previous laboratory studies where multiple streams were expected and are well understood [Stone, 1981a,c].

The observation of secondary ion streams numerous times, at several positions with respect to the Orbiter, and for several different plasma conditions suggests that this may be a rather general phenomenon. The fact that all measurements were obtained in sunlight does not preclude the existence of secondary ion streams when the Orbiter is in the Earth's shadow since, for this condition, no data was obtained with the DIFP--possibly the result of the Orbiter/PDP attitude [Shawhan and Murphy, 1983] or lower ionospheric densities coupled with limited instrument sensitivity. The relative intensity of 3% to 20% of the ambient ram current may be indicative only of values within the limited range of the measurements. The PDP was placed at relatively few positions and distances from the Orbiter during the STS-3 mission. Finally, in all cases, it appears that the PDP was negatively charged, and the effect of the electric potential on this phenomenon is unknown. It will, therefore, be of interest to investigate the possible influence of body potential on future missions.

The RPA provides scalar measurements of the ion flux intensity and energy. Since the secondary ion streams and ram ion current differ significantly only in flow direction and intensity while having essentially the same energies, it is not surprising that the RPA was unable to observe the secondary streams. However, because of this lack of sensitivity to vector-related effects, one naturally wonders if secondary ion streams may occur for all orbiting spacecraft, but have simply gone undetected in the absence of differential vector ion flux measurements.

This speculation is supported by previous observations of anomalous effects in the near vicinity of orbiting spacecraft which appear to be associated with the interaction of the spacecraft with the terrestrial magnetoplasma. For example, Henderson and Samir [1967] observed significant variations of the electron flux within $\pm$ 30° of the ram direction of the Ariel I satellite, and an enhancement of the electron temperature in the wake region of the Explorer 31 satellite was reported by Samir and Wrenn [1972] and by Troy et al. [1975]. Indications of plasma oscillations generated in the wake region of spacecraft have been reported by Samir and Willmore [1965], based on data from Ariel 1, and by Raitt et al. [1983], based on data from the STS-3 mission. Additionally, Shawhan and Murphy [1983] and Shawhan et al. [1983] report direct observations of electrostatic noise on the STS-3 mission, which is assumed to result from an interaction between the Orbiter and the ionosphere on the basis of an attitude dependence.

It is highly probable that all of the above anomalous effects are products of the electrodynamic interaction between spacecraft and the ionospheric plasma. If so, it may be possible that they are interrelated; i.e., secondary ion streams may generate oscillations which heat the electrons and/or produce electrostatic noise via a two-stream type instability; or, the secondary streams may be involved in setting up plasma instabilities of the type suggested by Papadopoulos and Ko [1983]. However, without further delineation of the specific effects of plasma parameters, spacecraft potential and attitude, measurement location with respect to the Orbiter, and

sunlight, it is difficult to determine the source or the governing mechanisms of the secondary ion streams, or their relationship to other plasma-electrodynamic interaction effects. It is possible that much of the required information may be forthcoming from the Spacelab 2 mission.

Acknowledgments. U. Samir is indebted to the National Academy of Sciences/National Research Council for its support during his tenure at the Space Science Laboratory, NASA/MSFC. K. Wright acknowledges support from NASA under contract NAS8-33982.

References

Fournier, G., and Pigache, D., Wakes in collisionless plasma, Phys. Fluids, 18, 1443, 1975.

Henderson, C. L., and Samir, U., Observations of the disturbed region around ionospheric spacecraft, Planet. Space Sci., 15, 1499, 1967.

Hester, S. D., and Sonin, A. A., A laboratory study of the wakes of small cylinders under ionospheric conditions, Phys. Fluids, 13, 641, 1970a.

Hester, S. D., and Sonin A. A., A laboratory study of the wakes of ionospheric satellites, AIAA J., 8, 1090, 1970b.

Papadopoulos, K., and Ko, K., Beam plasma discharge phenomena under ionospheric conditions, in Radio Science: Emissions from Particle Beams in Space, 1983.

Raitt, W. J., Siskind, D. E., Banks, P. M., and Williamson, P. R., Measurements of the thermal plasma environment of the Space Shuttle, in press, Planet. Space Sci., 1983.

Samir, U., and Willmore, A. P., The distribution of charged particles near a moving spacecraft, Planet. Space Sci., 13, 285, 1965.

Samir, U., and Wrenn, G. L., Experimental evidence of an electron temperature enhancement in the wake of an ionospheric satellite, Planet. Space Sci., 20, 899, 1972.

Samir, U., Stone, N. H., and Oran, W. A., Does a 'two-stream' flow model apply to wakes of large bodies in space?, Astrophys. and Space Sci., 31, L1, 1974.

Shawhan, S. D., and Murphy, G., Plasma Diagnostics Package assessments of the STS-3 Orbiter plasma environment, in press, J. Spacecraft & Rockets, 1983.

Shawhan, S. D., Murphy, G. B., and Fortna, D. L., Measurement of STS-3 electromagnetic interference by the OSS-1 Plasma Diagnostics Package, in press, J. Spacecraft & Rockets, 1983.

Stone, N. H., Technique for measuring the differential ion flux vector, Rev. Sci. Instruments, 48, 1458, 1977.

Stone, N. H., The plasma wake of mesosonic conducting bodies: Part 1 - An experimental parametric study of ion focusing by the plasma sheath, J. Plasma Phys., 25, 351, 1981a.

Stone, N. H., The plasma wake of mesosonic conducting bodies: Part 2 - An experimental parametric study of the mid-wake ion density peak, J. Plasma Phys., 26, 385, 1981b.

Stone, N. H., The aerodynamics of bodies in a rarefied ionized gas with applications to spacecraft environmental dynamics, NASA Technical Paper 1933, Nov. 1981c.

Stone, N. H., Oran, W. A., and Samir, U., Collisionless plasma flow over a conducting sphere, Planet. Space Sci., 20, 1787, 1972.

Troy, Jr., B. E., Maier, E. J., and Samir, U., Electron temperature in the wake of an ionospheric satellite, J. Geophys. Res., 80, 993, 1975.

(Received September 16, 1983;
accepted October 4, 1983.)

Plasma Diagnostics Package Initial Assessment of the Shuttle Orbiter Plasma Environment

S.D. Shawhan, G.B. Murphy, J.S. Pickett

Reprinted from

Journal of Spacecraft and Rockets

Volume 21, Number 4, July-August 1984, Page 387

AMERICAN INSTITUTE OF AERONAUTICS AND ASTRONAUTICS • 1633 BROADWAY • NEW YORK, N.Y. 10019

Plasma Diagnostics Package Initial Assessment of the Shuttle Orbiter Plasma Environment

Stanley D. Shawhan,* Gerald B. Murphy,† and Jolene S. Pickett†
University of Iowa, Iowa City, Iowa

A primary objective of the Plasma Diagonostics Package (PDP) on the third Space Shuttle flight (STS-3) was to assess aspects of the Orbiter's induced gaseous, plasma and electrical environment with respect to the conduct of scientific investigations. Instrumentation temperatures were found to be within predicted limits, payload bay pressure varied from ambient (10^{-7} Torr) up to almost 10^{-3} Torr with thruster firings, electromagnetic interference (EMI) levels were found to be below worst-case estimates but included Orbiter-induced electrostatic noise, and Orbiter potential was consistent to first order with $V \times B$ motional potentials varying ± 5 V with respect to the plasma. Electrostatic noise, neutral pressure and potential all exhibited orbit-period modulation. Payload bay plasma varied in density and composition from ambient to a rarefied mixture with Orbiter-produced H_2O^+. Energetic electrons and ions with energies up to 10's of electron volts were observed occasionally. Primary and vernier thrusters typically induce a momentary perturbation to the electron density, to the pressure, and to the electric field and spacecraft potential with low-energy ions and electrons occasionally observed. With the PDP on the remote manipulator system (RMS), both automode and manual modes were used to seek sources of EMI, to characterize the Orbiter's plasma wake, and to measure beam-plasma phenomena.

Introduction

DURING March 22-30, 1982, PDP was flown on STS-3 as part of the Office of Space Science first science payload (OSS-1).[1] A photograph taken of the OSS-1 pallet configuration during the STS-3 mission can be found in Ref. 8 also in this issue.

The purpose of this paper is to report the initial results of one of the principal technical objectives of the PDP which was to measure the thermal, pressure, electromagnetic, and plasma environment found on-orbit both in and near the Orbiter bay. A summary of results from the science objectives can be found in Ref. 2.

Sensors for measurement of these environmental parameters are identified on the PDP in Fig. 1. Detailed measurement parameters and measurement ranges for the various PDP instruments are listed in Table 1. Most of these instruments and sensors were either flight spare units from previous NASA programs such as IMP, HELIOS, and ISEE or were built from spare parts with modified designs from earlier sounding rocket programs, ISEE and SCATHA.

Thermal Environment

The STS-3 flight test mission was designed as a mission of thermal extremes in order to evaluate the operation of the Orbiter. A 23-h tail-to-sun and an 80-h nose-to-sun attitude exposed the payload bay to continuous dark conditions and cold extremes. The hottest possible conditions were obtained from the top-to-sun attitude which was sustained for 26 h.

Since the PDP unit was not coupled to a coldplate, part of the freon cooling loop, it responded to these temperature extremes in a manner representative of a large payload element. Thermal control of the PDP was carried out with internal thermostatically controlled heaters, external multilayer thermal blankets, and external radiating (taped and painted) surfaces.[3]

Even with the thermal environment extremes, the minimum and maximum temperature values stayed within the desired operating limits. Operating limits and observed temperature values for a few monitoring points, including an interface electronics box which was on a coldplate, are given in Table 2. The release/engagement mechanism (REM) allows the PDP to be separated from the pallet.

Pressure Environment

Included as part of the PDP instrument complement is a colimated and baffled cold cathode ionization pressure gage with a dynamic range of 10^{-3} to 10^{-7} Torr. The pressure gage operated any time the PDP was activated so that the pressure environment was monitored during most of the STS-3 mission. At OSS-1 pallet turn-on at MET 00:04:45 (days: hours:minutes) the pressure was 10^{-5} Torr; it took nearly 24 h to outgas to the ambient level for 240 km altitude of 10^{-7} Torr.

On MET days 2, 3, 4, and part of 5, the most prominent feature is the modulation of the apparent pressure between the ambient level for 240 km altitude of 10^{-7} Torr up to 10^{-5} Torr. This distinct modulation which is shown in Fig. 2 for part of MET days 2 and 3, occurs during the nose-to-sun attitude with the Orbiter rolling at two rolls per one orbit ($2\times$ orb rate). However, the modulation is at the orbit rate and not at the roll rate. A sketch of the STS-3 nose-to-sun orbit configuration is given in Fig. 3. The ascending node occurs when the Orbiter crosses the equator going toward the north. At this point, the Orbiter attitude is such that the atmospheric gases are ramming into the Orbiter bay. As the Orbiter continues to high latitude and then toward the descending node at night, the Orbiter completely blocks the flow into the bay and a wake attitude predominates. This ram-to-wake-to-ram sequence is cyclic at the orbit period. Note in Fig. 2 that the maximum apparent pressures occur at the ascending node under maximum ram conditions. Even during the periods when the PDP is deployed on the RMS (see periods of "periodic FPEG emissions" on day 03) the pressure modulation trend persists. Perturbations are caused by the fast pulse electron generator (FPEG) electron beam

Presented as Paper 83-0253 at the AIAA 21st Aerospace Sciences meeting, Reno, Nev., Jan. 10-13, 1983. Received June 3, 1983; revision received Nov. 8, 1983.

*Professor of Physics, Department of Physics and Astronomy; presently, Branch Chief, Space Plasma Physics and the Earth Science and Applications Division, NASA Headquarters, Washington, D.C.

†Staff Research Assistant, Department of Physics and Astronomy.

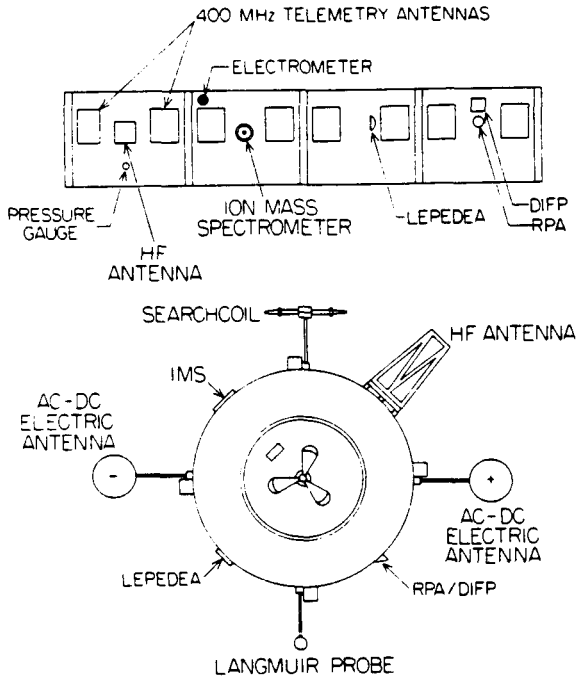

Fig. 1 Identification of the various sensors and instruments carried by the PDP.

Table 1 OSS-1 PDP instrumentation and measurements

Low-energy proton and electron differential energy analyzer (LEPEDEA)
Nonthermal electron and ion energy spectra and pitch angle distributions for particle energies between 2 and 50 36 keV.
ac magnetic wave searchcoil sensor
Magnetic fields with a frequency range of 10 Hz to 178 kHz.
Total energetic electron fluxemeter
Electron flux 10^9-10^{14} electrons/cm^2 s.
ac electric and electrostatic wave analyzers
Spectra with a frequency range of 10 Hz to 1 GHz.
Electric field strength at S-band, 2.2 GHz.
Wideband receiver
Analog electric and magnetic fields in three 10 kHz bands to 30 kHz.
dc electrostatic double probe with spherical sensors
Electric fields in one axis from 4 mV/m to 4 V/m.
Spacecraft potential ±8 V.
dc triaxial fluxgate magnetometer
Vector magnetic fields from 12-mG to 1.5 G.
Langmuir probe
Thermal electron densities between 10^3 and 10^7 cm^{-3}.
Density irregularities with frequencies of 1 Hz to 178 kHz.
Retarding potential analyzer/differential ion flux probe
Ion number density from 10^2 to 10^7 cm^{-3}.
Energy distribution function below 16 eV.
Directed ion velocities up to 15 km/s.
Ion mass spectrometer
Mass ranges of 1-64 amu.
Ion densities from 20 to 2×10^7 ions cm^{-3}.
Pressure gage
Ambient pressure from 10^{-3} to 10^{-7} Torr.

operations and by attitude changes of the PDP by the RMS. Figure 2 also illustrates that attitude control thruster firings produce short-duration pressure increases of typically an order of magnitude.

More detailed pressure plots for selected hours are shown in Fig. 4. For Figs. 4a and 4b the PDP is deployed on the RMS and is being rotated through 360 deg so that the pressure gage is alternatively directed close to the incoming gas flow (ram

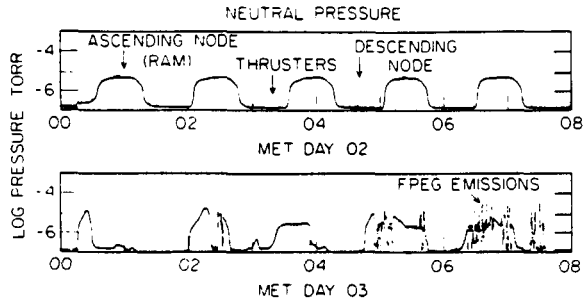

Fig. 2 Sample pressure data for the STS-3 mission both in bay (day 02) and on RMS (day 03).

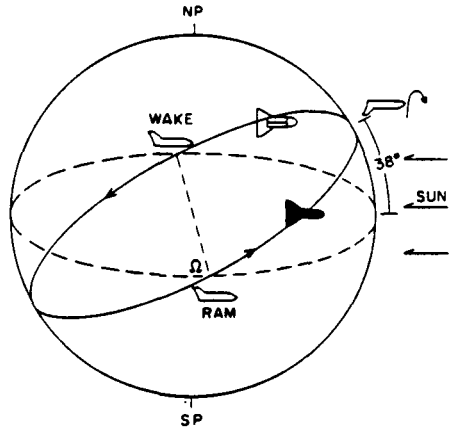

Fig. 3 STS-3 nose-to-sun attitude with the Orbiter roll at 2× orbit rate.

Table 2 Operating limits vs observed temperature values

Location	Desired limits low/high, °C	Observed low/high, °C
PDP instrument deck	−30/+50	−2[a]/+51
EGF connector housing	−65/+135	−38[a]/+53
REM structure	−75/+150	−13/+40
Electronics box on coldplate	−30/+40	+7/+15

[a] Low values controlled by thermostatic heaters in the −32 to −37°C range.

condition) and away from the flow (wake condition). A general increase in pressure is seen near the ascending node point but the pressure is modulated by the gage rotation. Consequently, the 10^{-5} Torr value cannot be due to a pervasive bay pressure of 10^{-5} Torr. The gage is baffled so that it is not subject directly to ram effects of neutrals or ions. In a ram condition, it is possible for the dynamic pressure near the gage surface on the PDP to be a factor of 20 to 50 above the ambient value,[4] but a factor of up to 200 is observed (see Fig. 4a or 4b).

It is believed that the measured pressure must be indicative of a surface chemical effect due to atomic oxygen reacting at the spacecraft surface near the pressure gage, thus causing a higher density gas layer. When the PDP is pointed away from the ram direction or when the Orbiter blocks the oxygen flow to the surface near the gage, the gas layer is not formed and ambient pressure is measured. This hypothesis is supported by the TV and photographs taken during dark periods. Surfaces of the Orbiter subject to the atmospheric ram are observed to glow. This resultant glow layer appears to be 20-50 cm thick.[5-10] Papadopoulos[6] theorizes that this thickness will be approximately 10-20 cm, which is fairly consistent with the

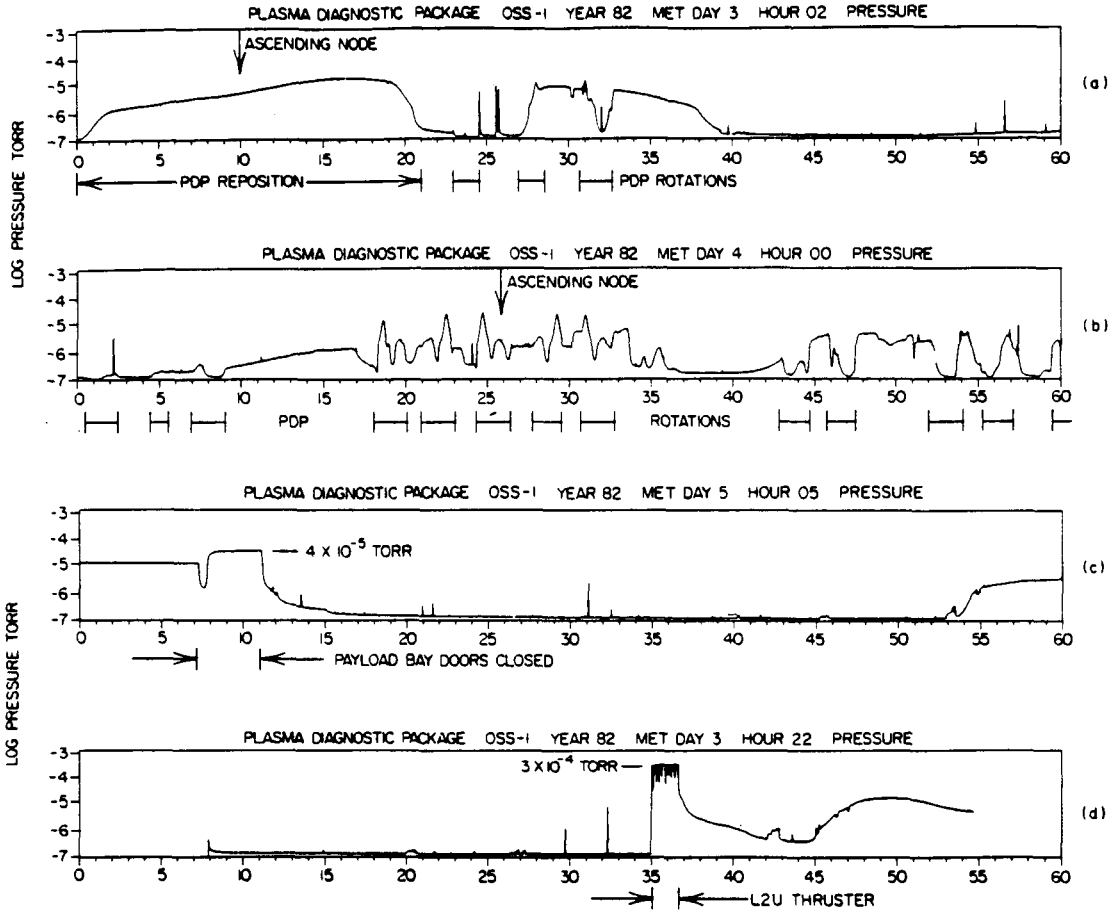

Fig. 4 Detailed 1-h pressure plots: a) and b) PDP deployed and rotated near ascending node: c) payload bay doors closed; d) L2U PRCS thruster firing.

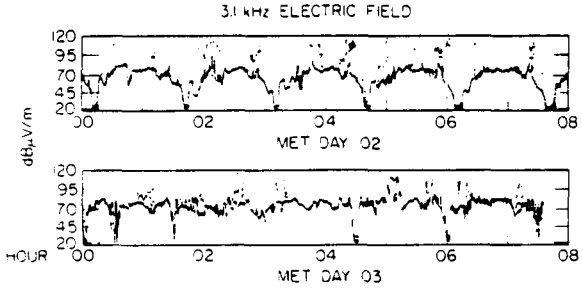

Fig. 5 Intensity of 3.1 KHz broadband electrostatic noise both in bay (day 02) and on RMS (day 03).

observations. Also, the electron beam from the FPEG is not distinctly visible except within about 50 cm of the FPEG aperture—again suggesting a low ambient bay pressure but an enhanced pressure (gas layer) near the surface at the FPEG aperture.

Atomic oxygen ram surface effects are definitely not the cause of the pressure increases shown in Figs. 4c and 4d. Figure 4c includes a period on MET day 5 at 05:08 h when the bay doors are completely closed. In this case, the bay pressure rises to 4×10^{-5} Torr probably due to outgassing of the payload elements and gas leaks into the bay itself. This value is consistent with that measured by the neutral mass spectrometer which was included in the induced environment contamination monitor (IECM). During a sustained test firing of primary reaction control system (PRCS) thrusters, Fig. 4d shows a pressure rise to 3×10^{-4} Torr for the 1.5-min firing period. Evidence of the short vernier thruster control system (VRCS) firings are also seen at 22:30 and 22:32. Additional effects of thruster firings are discussed in the section on thruster perturbations and Ref. 7.

Orbiter Electromagnetic Wave Environment

The PDP is equipped with wave receivers which measure electric field emissions from a few hertz through S-Band and magnetic field emissions from a few hertz to 200 kHz. Emissions are due to Orbiter and payload subsystems, Orbiter-induced plasma perturbations, natural ionospheric plasma waves, and operation of the FPEG electron beam.

Details of the performance characteristics for the PDP receiver systems are given in two companion papers.[8,9] Measurements of the Orbiter and payload background EMI levels indicated that the upper Orbiter limits were not exceeded at any frequency for the broadband electric field or narrowband magnetic field.

A ubiquitous electrostatic background noise dominates the electric field spectrum from 30 Hz to 178 kHz with a peak in the spectrum at 300-500 Hz of 130 dB μV/m/MHz. The noise is thought to be Orbiter-induced due to the motion of the Orbiter through the ionospheric plasma since the noise variability exhibits a marked orbit periodicity. Figure 5 illustrates this variability at a frequency of 3.1 kHz chosen because of its representative nature. The brief dropouts of the noise occurred when the payload bay was most nearly in the wake attitude near the descending node of the orbit. This noise is observed to be enhanced by ~20 dB during thruster

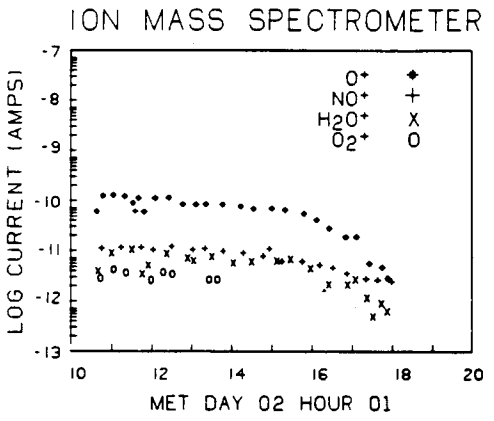

Fig. 6a Ion currents collected while the PDP was in the Orbiter cargo bay.

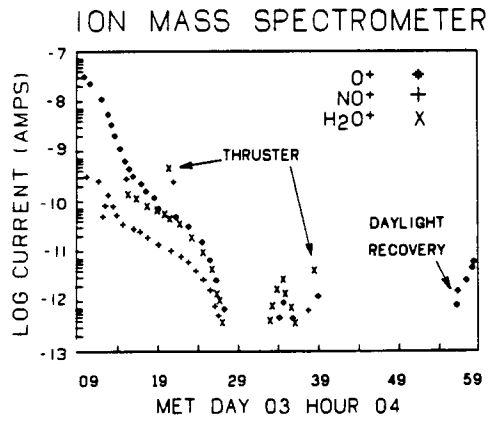

Fig. 6b Ion currents collected while the PDP was on the extended RMS.

firings and by ~40 dB during operation of the FPEG and to be increased by water dumps at night. No theory for the source of this noise has yet been confirmed. More details of the electromagnetic environment are found in Refs. 8 and 9.

Plasma Environment

The plasma environment of the Orbiter is monitored using three instruments—the ion mass spectrometer (IMS) which gives the thermal ion composition and density, the combined retarding potential analyzer/differential ion flux probe (RPA/DIFP) which measures ion energy and analyzes directional ion flow, and the low-energy proton and electron differential energy analyzer (LEPEDEA) which detects the pitch angle and flux of energetic suprathermal electrons and ions.[2]

Measurements of the thermal ion composition are given in Figs. 6a and 6b for the cases of the PDP in the payload bay and on the RMS, respectively. The log current scale is directly proportional to density. In both cases the expected ambient ionospheric components of O^+, NO^+ are observed. However, the H_2O^+ must be produced by the Orbiter since it is not naturally present in the ionosphere. It could be that H_2O^+ is ionized H_2O from water dumps and flash evaporator operations, that it comes from water absorbed by the Orbiter's surface tiles, or that it is produced with the atomic oxygen surface reaction. There is some evidence of increased H_2O^+ concentrations after the flash evaporators have been operating for some extended period of time or during water dumps on the dark side of the orbit. Although NO^+ is expected as a natural ionospheric constituent, it appears to be

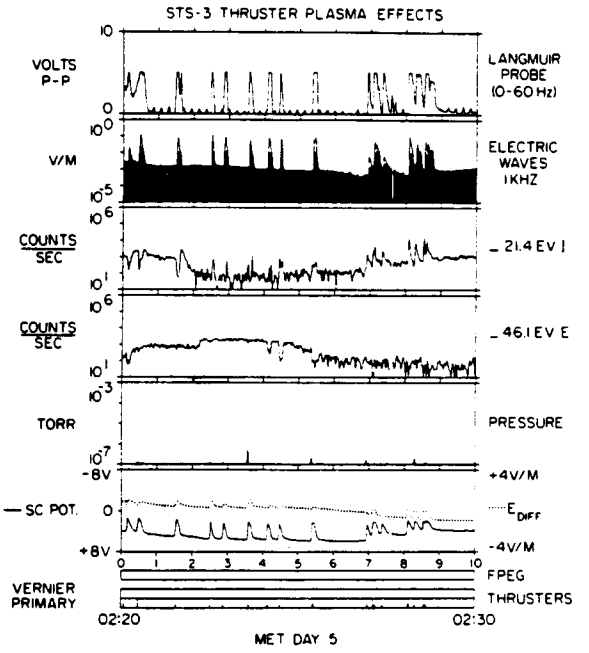

Fig. 7 Sample of PDP measurements indicating the pressure and plasma effects of thruster firings.

enhanced during and just after thruster firings (Fig. 6b). This is expected since NO^+ is a primary ion constituent of the plume.[7]

The marked decrease in density seen in Fig. 6b (greater than or equal to five orders of magnitude) occurs as the Orbiter moves into darkness and into the wake condition. Measurements with the RPA and Langmuir probe on the PDP and the spherical retarding potential analyzer and Langmuir probe of the vehicle charging and potential (VCAP) investigation confirm this marked decrease in plasma density within the payload bay.[10] Since the Orbiter is large compared to a thermal ion or electron gyroradius and is moving at a speed of Mach 5 to 7, a very significant plasma wake is expected behind the Orbiter.

When the PDP is deployed on the RMS, the direction of ion flows are detected by the DIFP instrument. In some cases the DIFP detects two flows of ions coming from different directions.[12] One beam seems to come from the velocity vector as expected, the other, at an angle of typically 30 deg to the first, is as yet unexplained. The RPA observes mean energies of the bserves mean energies of the ions of 10 eV. Assuming that the predominant ion is O^+ as seen by the IMS, only 5 eV of the 10 eV would be due to the kinetic energy of the O^+ ion as it flows into the Orbiter; the other 5 eV gives further evidence that the PDP and Orbiter are charged negatively with respect to the ambient plasma by at least 5 V (see next section).

On occasion energetic plasma is observed with the LEPEDEA (without electron gun operation). Ions are observed with energies up to 30 eV which are sometimes concurrent with the ion beams. More frequently, energized electrons are observed with energies up to 80 eV on the dayside of the orbit. The energetic electrons may be photoelectrons emitted from the Orbiter and PDP surfaces since they are observed predominately on the sunlit parts of the orbit. However, the energy spectrum is not that expected for photoelectrons and is not yet explained. Current work seeks evidence for a significant plasma sheath or evidence to support a beam-plasma interaction.

Orbiter Potential

On the PDP a measurement is made between the average potential of the two 20-cm-diam spheres and the PDP circuit common which is the same as the Orbiter circuit common. This potential is found to vary up to ±5 V with the orbit period.[11] This potential variation is observed even when the presence of energetic plasma (see previous sections) suggests that the Orbiter may be surrounded by a large potential sheath. Therefore the variation must be caused locally.

All of the Orbiter is covered primarily with thermal insulating tiles or other nonconducting material except for 30 m^2 conducting area on the main engine farings. Therefore, the potential variation has been compared with $V \times B \cdot L$ motional potential due to the Orbiter velocity V (modeled from the Fig. 3 orbit geometry) through the Earth's magnetic field B. The distance L is taken to be from the engine farings to the PDP. This simplistic model explains to first order the potential variation observed. Significant deviations from this model occur duing electron gun operations (causing a positive potential) and during thruster firings.

Thruster Perturbations

Thruster firings are necessary to change the Orbiter attitude as well as to maintain a specified attitude within a deadband. On the STS-3 mission there were more than 40,000 thruster firings. Thirty-eight 870-lb thrusters make up the PRCS and six 25-lb thrusters make up the VRCS. Effects of the thruster firings can be seen with several of the PDP detectors. A sample of these effects is given in Fig. 7 for a 10-min period during which time several PRCS thrusters fired. Note that the PDP provides a resolution of 1.6 s for most measurements which is longer than the typical 80 ms thruster firing period.

The Langmuir probe, which responds to variations in the electron density in the vicinity of the PDP, sees a significant perturbation with frequency components in the 0-40 Hz range when thrusters fire. Coincident with the thruster firing is an increase in the intensity of the electric field from 30 Hz to above 10 kHz—the 1 kHz response is representative in Fig. 7. Increases by two orders of magnitude up to 0.1 V/m are observed. Frequently low-energy ions or electrons or both are observed to change fluxes with the LEPEDEA. For example, in Fig. 7 both decreases and increases in the 21 eV ion flux are observed although the 46 eV electron flux shows only occasional decreases. Pressure spikes with peak values up to 10^{-4} Torr are occasionally observed associated with some of the thruster firings (see also Figs. 2 and 4). The spacecraft potential (SC POT) shows a 2-V change with each thruster sequence and the electric field in the vicinity of the PDP indicates perturbation up to 1 V/m. Similar effects are associated with some of the VRCS thruster operations.

The mechanism or mechanisms which produce these effects have not yet been determined. A more detailed investigation of thruster effects and an examination of their causes are presented in Ref. 7.

Summary

Operation of the PDP at its pallet location and on the RMS provides a reasonably comprehensive set of measurements on the thermal, pressure, electromagnetic, and plasma environment that is experienced by a payload element on the Orbiter. Thermal extremes are moderate. The payload bay reaches the 10^{-7} Torr ambient pressure of the atmosphere only with the payload bay in wake condition. A gas layer of pressure up to 10^{-5} Torr seems to be associated with surfaces that are bombarded with the atmospheric gases. Pressure increases well above ambient are observed with the payload bay doors closed and during thruster operations. Orbiter-generated EMI is below the Orbiter specification limits. However, an intense electrostatic broadband noise is observed which may be the result of an Orbiter-plasma interaction. Orbiter-produced H_2O^+ ions are observed with densities comparable to the ambient ions. Energetic ions and electrons with energies up to 10's of electron volts are seen occasionally; it is suggested that under some conditions the Orbiter is surrounded by a plasma sheath. With or without the sheath, the Orbiter exhibits a motional potential which varies ±5 V over an orbit. Thruster firings perturb the electron density, electrical, and energetic particle environment of the Orbiter but the mechanisms for these effects have not yet been determined.

In general, the Orbiter provides a friendly platform from which to carry out plasma-related experiments and in fact its motion through the ionosphere is itself an interesting plasma experiment. To minimize some perturbing effects during sensitive experiments the attitude and orbit location needs to be specified and the thruster system disabled. Awareness of the operation of the flash evaporator system and/or water dump cycles may also be important for some experiments.

Acknowledgments

This research is supported by NASA Marshall Space Flight Center Contract NAS8-32807. The authors wish to thank the PDP Coinvestigators N. D'Angelo, L.A. Frank, D.A. Gurnett, D. Odem, and H. Owens from the University of Iowa; H. Brinton, J. Grebowsky, M. Pharo III, H. A. Taylor, and D. L. Fortna from Goddard Space Flight Center; and D. L. Reasoner and N. Stone from Marshall Space Flight Center for their contributions to this work. The OSS-1 pallet was managed by K. Kissin and his staff at the Goddard Space Flight Center. We appreciate their technical expertise and long hours of work.

References

[1] Neupert, W. M. et al., "Science on the Space Shuttle," *Nature*, Vol. 296, No. 5854, March 18, 1982, pp. 193-197.

[2] Shawhan, S.D. and Murphy, G.B., "STS-3/OSS-1 Plasma Diagnostics Package (PDP) 90-Day Science Report," University of Iowa, Iowa City, Iowa, Rept. OSS-1/PDP 82-07, July 1982.

[3] Kerl, M.E., Clark, T.W., and Shawhan, S.D., "STS-3/PDP Thermal History and Time Constants," University of Iowa, Iowa City, Iowa, Rept. OSS-1/PDP 82-09, Sept. 1982.

[4] Carrigan, G., Private communication, University of Michigan, Ann Arbor, Mich., Oct. 1982.

[5] Banks, P.M., Williamson, P.R., and Raitt, W.J., "Space Shuttle Glow Observations," *Geophysics Research Letters*, Vol. 10, No. 2, Feb. 1983, pp. 118-121.

[6] Papadopoulos, K., "On the Shuttle Glow (The Plasma Alternative)," *Radio Science*, Vol. 19, No. 2, March-April 1984, pp. 571-577.

[7] Murphy, G.B., Shawhan, S.D., and Pickett, J.S., "Perturbations to the Plasma Environment Induced by the Orbiter's Maneuvering Thrusters," AIAA Paper 83-2599, Oct. 1983.

[8] Shawhan, S.D., Murphy, G.B., and Fortna, D.L., "Measurements of Electromagnetic Interference on OV102 Columbia Using the Plasma Diagnostics Package," *Journal of Spacecraft and Rockets*, Vol. 21, July-Aug. 1984, pp. 392-397.

[9] Murphy, G.B. and Shawhan, S.D., "Radio Frequency Fields Generated by the S-Band Communication Link on OV102," *Journal of Spacecraft and Rockets*, Vol. 21, July-Aug. 1984, pp. 398-399.

[10] Murphy, G.B. et al., "Interaction of the Space Shuttle Orbiter with the Ionospheric Plasma," *Proceedings of the 17th ESLAB Symposium*, Noordwijk, The Netherlands, 1983, pp. 73-78.

[11] Shawhan, S.D. and Murphy, G.B., "STS-3/OSS-1 Plasma Diagnostics Package (PDP) Measurements of Orbiter-Generated $V \times B$ Potentials and Electrostatic Noise," *Proceedings: Workshop on Charging of Large Space Structures in Near Earth Polar Orbit*, Sept. 14-15, 1982, pp. 119-123.

[12] Stone, N.H. et al., "Multiple Ion Streams in the Near Vicinity of the Space Shuttle," *Geophysics Research Letters*, Vol. 10, Dec. 1983, pp. 1215-1218.

Measurements of Electromagnetic Interference on OV102 Columbia Using the Plasma Diagnostics Package

S.D. Shawhan, G.B. Murphy, D.L. Fortna

Reprinted from

Journal of Spacecraft and Rockets

Volume 21, Number 4, July-August 1984, Page 392

AMERICAN INSTITUTE OF AERONAUTICS AND ASTRONAUTICS • 1633 BROADWAY • NEW YORK, N.Y. 10019

Measurements of Electromagnetic Interference on OV102 Columbia Using the Plasma Diagnostics Package

Stanley D. Shawhan* and Gerald B. Murphy†
University of Iowa, Iowa City, Iowa
and
Dwight L. Fortna‡
NASA Goddard Space Flight Center, Greenbelt, Maryland

The Plasma Diagnostics Package (PDP) of the Office of Space Science-1 (OSS-1) payload included a complement of receivers covering the frequency range of 30 Hz to 800 MHz and S-band at 2200 ± 150 MHz to assess the intentional (transmitter) and unintentional (subsystem) electromagnetic interference (EMI) levels on the Space Shuttle Columbia's STS-3 mission. The following results were noted: at the pallet location, the uhf voice downlink transmitter field strengths did not exceed 0.1 V/m; on the remote manipulator system (RMS) arm the PDP measured less than 0.5 V/m; above 300 kHz Orbiter subsystem noise was not detected at the receiver noise levels (80 dBμV/m/MHz) which was well below the Interface Control Document (ICD) specification limits for the Shuttle; below 300 kHz the magnetic field noise was 30 dB pT ±20 db (due to power converters and clocklines) also below the worst-case specifications; below 300 kHz the electric field noise was broadband and variable over at least 60 dB depending on thruster firings and Orbiter attitude. This noise may have been generated by the Orbiter interaction with the ambient plasma; emissions stimulated by the OSS-1 fast pulse electron generator electron beam were ~20 dB above Orbiter associated levels at all frequencies <60 MHz.

Introduction

USERS of the STS Space Shuttle are concerned about the possible high levels of electromagnetic interference produced by the Orbiter subsystems. Interface Control Document curves for the worst-case electric field and magnetic field emissions are available in Ref. 1. Especially for space plasma investigations, which make use of sensitive plasma wave receivers,[2] emissions at the ICD specification limits would limit the dynamic range of the potential experiments. Because of these concerns, early measurements of the OV101 (Enterprise) EMI levels were carried out during the Orbiter's hardware development phase. Although the measurements were not complete in frequency range and did not include all on-orbit operating subsystems, the levels detected in the 10 MHz to 10 GHz range were significantly less than the proposed ICD worst-case specifications.[3] Consequently, the ICD specifications were revised downward in this frequency range.[1]

One of the primary objectives of the Office of Space Science-1 (OSS-1) Plasma Diagnostics Package on the third Shuttle mission was to measure the radiated EMI of the Orbiter Columbia on orbit, to interpret these measurements in terms of possible sources, and to compare these levels with the ICD worst-case specifications.[4] This report presents the results of an initial analysis of the PDP measurements from the STS-3 mission in March 1982. Some additional aspects of the Columbia EMI environment are available in other references.[5,6]

Received June 3, 1983; revision received Nov. 8, 1983.

*Professor of Physics, Department of Physics and Astronomy; presently, Branch Chief, Space Plasma Physics and the Earth Science and Applications Division, NASA Headquarters, Washington, D.C.

†Staff Research Assistant, Department of Physics and Astronomy.

‡Standard Engineer, Code 302, Assurance Management and Test Policy Office.

Description of PDP Receiver Systems

Sensors for the detection of magnetic and electric wave fields are identified in Fig. 1 which is an on-orbit picture of the OSS-1 pallet. Two spheres of 20 cm diameter, separated by 1.6 m, make up the electric dipole antenna which is utilized from dc to 20 MHz. For frequencies in the range 20-2300 MHz, a broadband single polarization horn antenna is used. The searchcoil sensor is used to detect the magnetic field component of electromagnetic waves from 30 Hz to 178 kHz. The Langmuir probe is sensitive to fluctuations in the electron density (plasma oscillations) over a frequency ranging from dc to 178 kHz.

A block diagram of the PDP sensors and associated receivers is shown in Fig. 2. One very low frequency (VLF) range spectrum analyzer from the NASA/IMP program is switched between the electric dipole, the searchcoil and the Langmuir probe sensors every 51.2 s to provide 16 channels of VLF spectra—30 Hz to 178 kHz. In addition, the waveform is preserved in the wideband receiver (WBR) and these analog data are included in the PDP data stream. The WBR switches 10 kHz bands sequentially covering 0-10, 10-20, and 20-30 kHz for each sensor. A second VLF receiver from the HELIOS spacecraft program (VLF-HELIOS) is always connected to the electric dipole giving a redundant peak and an average spectrum of the electric field every 1.6 s. Both spectrum analyzers have channels spaced logarithmically in frequency at four/decade with a 3.1, 5.6, 10, 17.8 center frequency sequence and a ±15% bandwidth.

The electric dipole also drives the medium frequency receiver (MFR) which covers 316 kHz to 17.8 MHz in eight channels also spaced logarithmically in frequency at four/decade with a ±30% bandwidth. This MFR shares a log detector video amplifier with the high frequency receiver (HFR) which has four broadband channels spanning the range 20-800 MHz. Both peak and average spectra are obtained from the MFR and HFR every 1.6 s. The HFR as well as the S-band receiver makes use of the horn antenna. This horn antenna is a broadband, folded, tapered dipole which was designed by the U.S. National Bureau of Standards in Boulder, Colorado. For redundancy purposes, S-band field

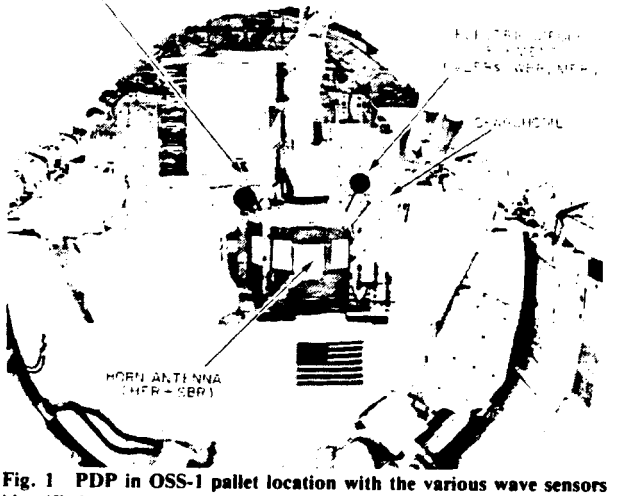

Fig. 1 PDP in OSS-1 pallet location with the various wave sensors identified.

strengths are also measured by a linear detector covering the range 1-72 V/m in a frequency band of 2200±150 MHz. Details of the S-band receiver and results are given by Murphy and Shawhan.[7]

Overview of Orbiter ac Electric Field Environment

Figure 3 depicts in one 30-min time interval an example of the different types of electric field noise typically seen by the PDP. The 16 channels of the VLF spectrum analyzers are shown (VLFR-HELIOS), eight channels of the MFR, and four of the HFR. S-band results are discussed in detail in Ref. 7 and are not shown here. Note the scale is logarithmic in amplitude with 100 dB dynamic range for the VLFR and 80 dB for the MFR and HFR. Details such as minimum sensitivity level of each channel are given in Table 1 and are useful for getting an order of magnitude estimate of the field strength from the figure.

Several phenomena are evident in Fig. 3. The short bursts of noise at 04:37 and 04:39 result from attitude control thruster firings. The general decrease in noise at all VLF frequencies between 04:36 and 04:40 is a result of the PDP being situated in the Orbiter wake. The increase in noise at all VLF frequencies and the bursts of noise in the MFR between 04:40 and 04:51 illustrate the effect of firing the 100 W

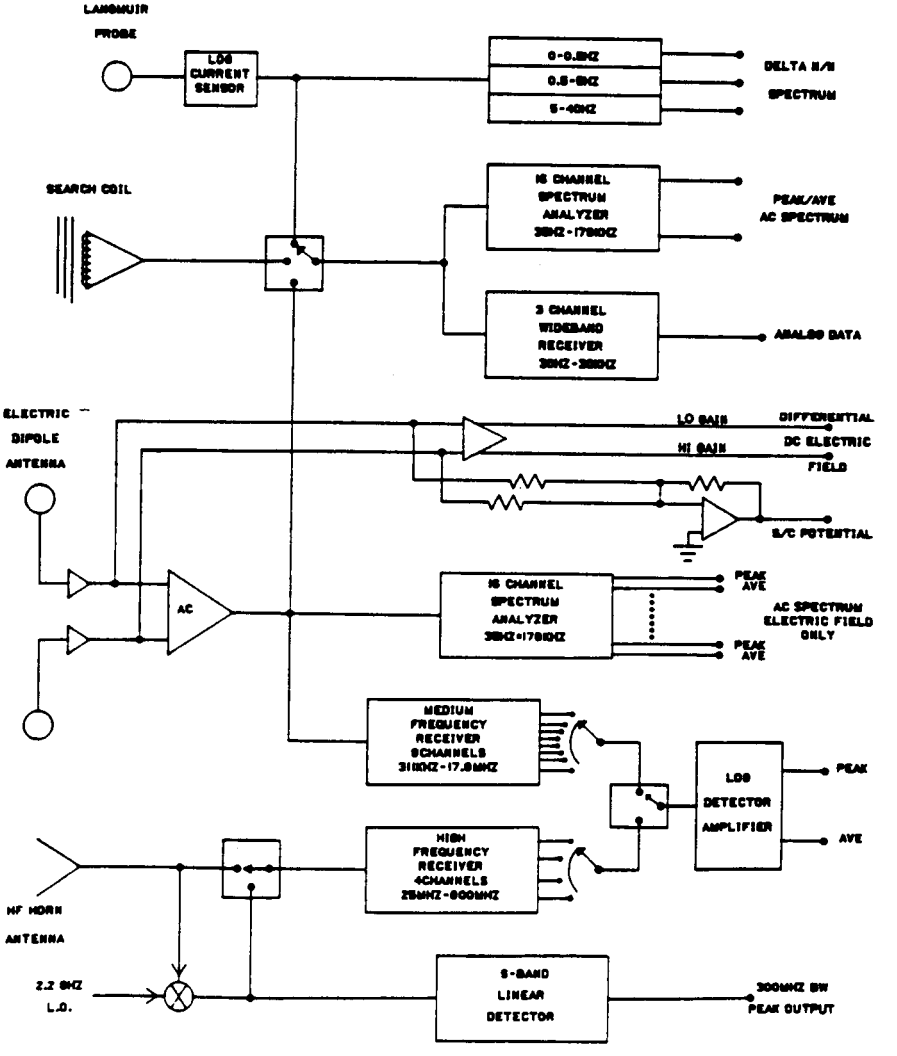

Fig. 2 Block diagram of the PDP wave sensors and receivers.

electron gun (FPEG) which was part of the vehicle charging and potential (VCAP) experiment. The PDP rotation which is evident by the change in magnitude of one magnetic field component plotted along the top of the figure shows that there is a certain degree of polarization to the waves in the MFR but less in the VLFR.

The uhf transmitter is detected when keyed on and registers in the 271 MHz channel. Only this uhf transmitter and an occasional ground transmitter are observed above the plasma frequency which is approximately 10 MHz for the ambient ionospheric plasma density at the Orbiter's altitude. The next figures and text section examine some of these observations in more detail.

Electric Field Details

Figure 4 illustrates further that the broadband electrostatic noise is extremely variable in amplitude. There is a 60-80 dB variation in intensity over a period of approximately 10 min. The noise seems most certain to be generated by the Orbiter as it flies through the plasma[9] and is strong, but variable as long as the PDP is not in the Orbiter's wake. When in the deep wake, the noise disappears entirely and it is encouraging to note that at this time no Orbiter subsystems, whose EMI may previously have been masked, are evident at any frequency.

Figure 5 presents data taken during a time when the payload bay doors were closed for several minutes. Note that the broadband electrostatic noise is gone and only very low level signals are seen, which is further evidence of the relative cleanliness of the vehicle from an EMI standpoint, and that the broadband electrostatic noise is generated externally.

Another important phenomenon in Fig. 5 is the high frequency of thruster firings. Figure 3 leads one to believe that attitude thruster events are infrequent; however, Fig. 5 presents data which is much more typical. These noise spikes actually last for several seconds and in a typical 10-min interval will occur from 1 to 10 times depending on the deadband setting of the autopilot. A detailed discussion of thruster plasma effects is available in Ref. 10.

In summary, electric field spectral characteristics are always dominated by noise from an Orbiter-plasma interaction or attitude control system thruster firings.

Magnetic Field Observations

Figure 6 is a reproduction of the WBR data from dc to 30 kHz. Note again evidence that a typical pallet measurement of electric field noise is "white" even with the payload bay doors closed. Only at very low frequencies is there any spectral content evident and then only when the automatic gain control has turned on maximum receiver gain. The magnetic component however indicates the "line spectra" nature of emissions detected by the searchcoil. Some, but not all lines have been identified and are invariably associated with instrument power converters or the 400 Hz ac Orbiter bus. The frequencies that are present change as instruments and

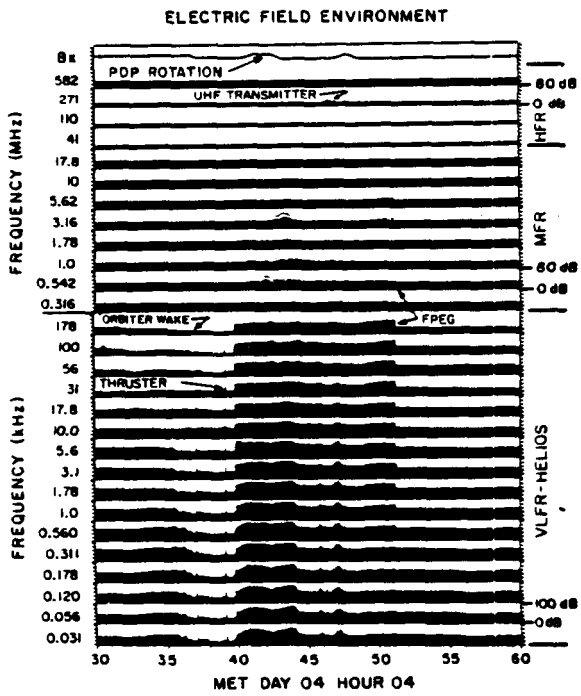

Fig. 3 Overview of the STS-3 Orbiter electric field environment as detected with the PDP.

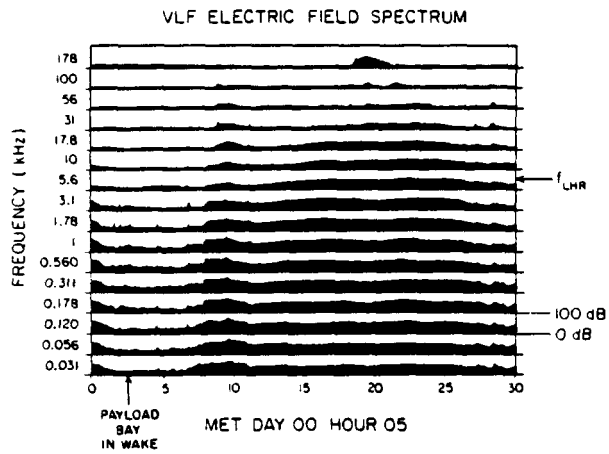

Fig. 4 Variability of electrostatic noise with plasma wake associated decrease.

Table 1 PDP wave receiver characteristics

Receiver	Center frequency	Bandwidth	Saturation level, dB μV/m (at 5 V out)	Sensitivity, dB/V
VLFR	1, 1.78, 3.1, 5.6 in log sequence from 31 Hz to 178 kHz	±15%	120	20
MFR	1, 1.78, 3.1, 5.6 in log sequence from 311 kHz to 17.8 MHz	±30%	150	16
HFR	40 MHz	25-65 MHz	172	16
	100 MHz	65-165 MHz	161	
	250 MHz	165-400 MHz	153	
	600 MHz	400-800 MHz	152	

systems cycle on and off. The next section discusses the amplitude of these emissions.

Comparison to ICD Specifications

By searching the periods of time while the PDP was stowed on the pallet, values for the minimum (solid circles) and the maximum electric field (open circles) noise levels have been obtained and are displayed in Fig. 7. These values are calibrated in microvolts per meter and normalized to a 1 MHz bandwidth. The receiver channels and dynamic ranges are also indicated by the vertical boxes. Also plotted for comparison are the broadband electric field limits for the Shuttle itself and for a payload. Extrapolations are shown below the 14 kHz spec limit. When the FPEG is not operating, the maximum level (open circles) does not exceed the payload limit above 14 kHz. When the FPEG operates with the PDP manipulated by the RMS to be in the beam, the levels are increased by −20 dB in the VLF range as indicated by the triangles. This situation of course would not occur in a typical mission.

Narrowband magnetic field strengths are much less variable (±10 dB) from the minimum (solid circles) to maximum (open circles) observed levels as seen in Fig. 8. These levels are not Orbiter-attitude dependent and unlike the electric field emissions, the levels were higher with the payload bay doors closed. It is surmised that the magnetic field levels are due to Orbiter subsystems which should be slightly time dependent as systems turn "on/off." All subsystem and payload levels fall well below the Orbiter specifications limit up to 50 kHz.

When the FPEG operated, the magnetic levels did increase by as much as 30 dB in the frequency range 1-100 kHz. However, these emissions were due primarily to the wave stimulation which produced induction fields in the kHz range and at harmonics. Only at 30 kHz and above did these fields exceed the specification limits.

One filter channel of the PDP HFR covered the band of 165-400 MHz which included the 295 MHz frequency of the uhf voice downlink transmitter. As discussed previously, when this transmitter was keyed "on" and connected to the Orbiter upper antenna, a signal was detected by the PDP (Fig. 3). These measured peak field strengths were always below 0.5 V/m with the PDP on the RMS at 8 m from the radiating antenna and below 0.1 V/m at the PDP pallet location which was 13 m from the radiating antenna. These levels are well below the 2 V/m radiated susceptibility field strengths anticipated in this frequency range.

At S-band, the 150 W data downlink transmitter (2287.5 MHz) can produce fields which are modeled to be 49.6 V/m/R (with R distance in meters) in the beam of the selected "quad" antenna.[7] Even at many meters, these fields could be at damage level for payload instruments or for satellites being manipulated by the RMS. The SBR was especially designed to measure the field strengths in and around the payload bay. A detailed report on these measurements and models is given by Murphy and Shawhan.[7]

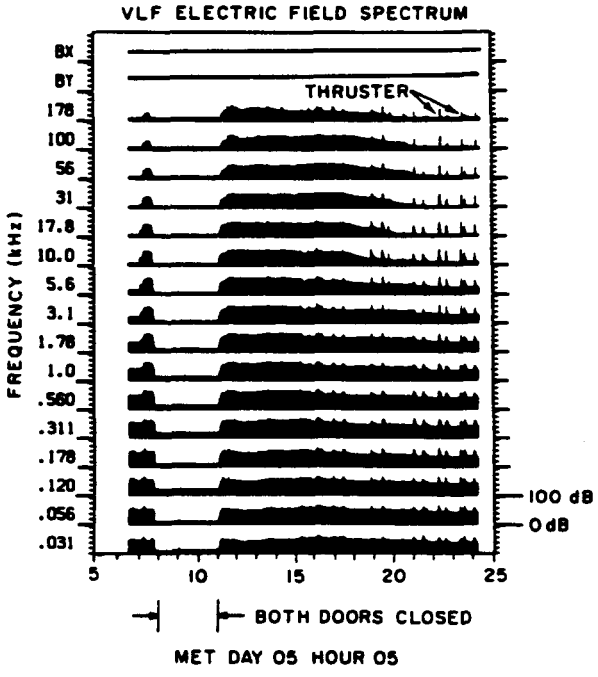

Fig. 5 Electrostatic noise disappears when the payload bay doors are closed and is more intense during thruster firings.

Summary

Receivers on the Plasma Diagonostics Package covering the frequency range from a few hertz to 2 GHz for electric fields and from a few hertz to 200 kHz for magnetic fields monitored the Orbiter Columbia and the OSS-1 payload on

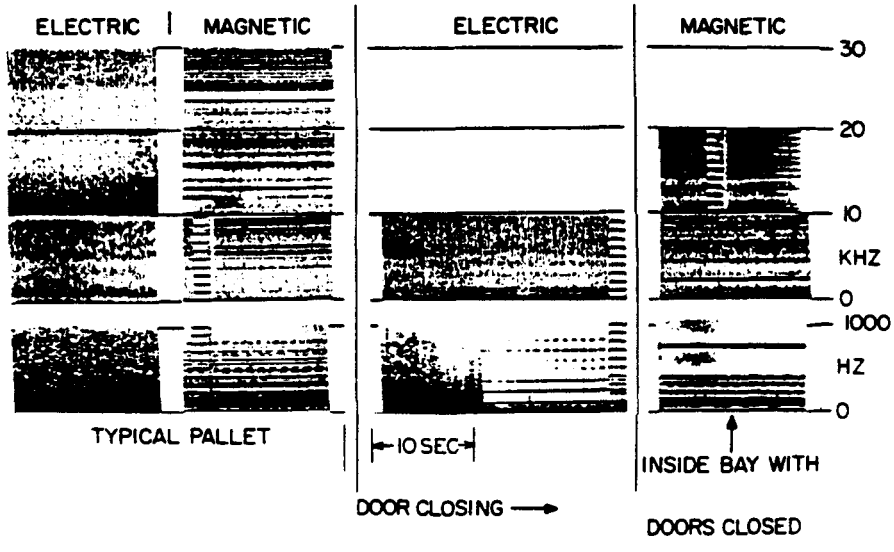

Fig. 6 Detailed spectra of electric and magnetic field noise in the frequency range of 0-30 kHz.

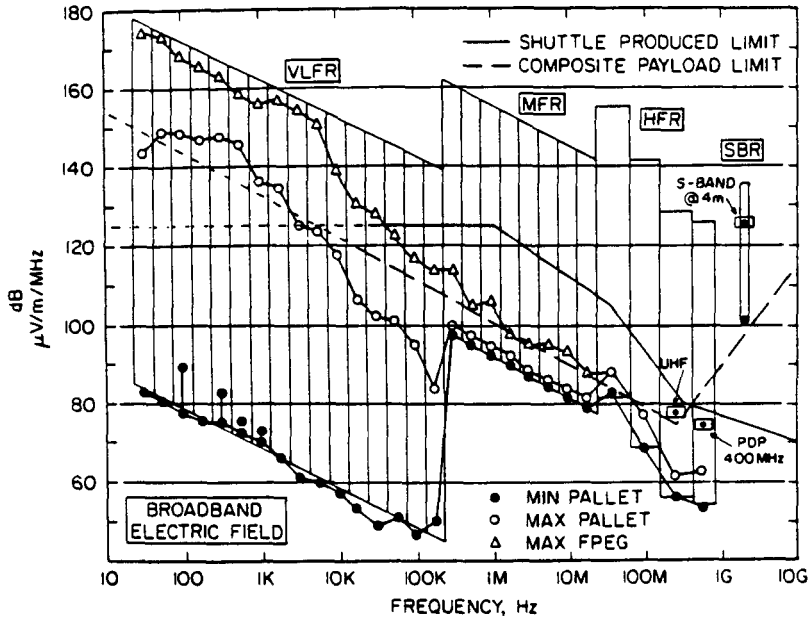

Fig. 7 Minimum and maximum electric field noise levels for PDP at pallet location.

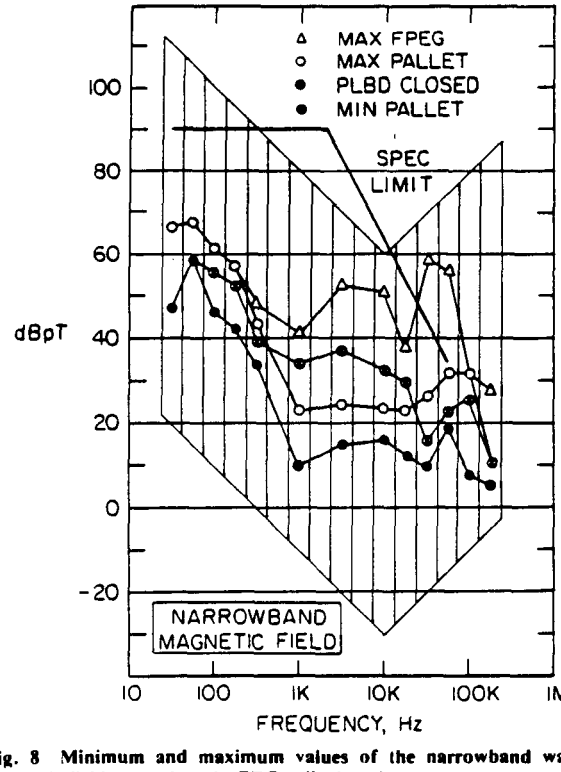

Fig. 8 Minimum and maximum values of the narrowband wave magnetic field strength at the PDP pallet location.

the STS-3 Shuttle mission. Under nominal operating conditions, the Orbiter and payload systems emissions did not exceed the ICD worst-case specification limits. When the 100 W fast pulse electron generator was operated, emission levels increased by 20-30 dB probably due to induction fields from the electron beam. Even these intentional emissions were within acceptable limits.

A broadband electrostatic noise with fields up to 10 dB V/m/MHz in the range from 30 Hz to 100 kHz was discovered to be generated by the Orbiter's motion through the ambient ionospheric plasma and dominated electric field spectra.

The Plasma Diagnostics Package is scheduled for a reflight in 1985 as part of the Spacelab-2 mission on STS-24. It will make measurements at its pallet location, on the RMS, and as a free-flying satellite. Several upgrades are being implemented. A Ku-band has been added to measure the field strength in and around the payload bay at ranges of 100 m to 2 km from the Orbiter. Within the Ku-band transmitting antenna beam fields up to 275 V/m are predicted. The S-band receiver is to have a dedicated horn antenna and a wider dynamic range receiver. The high frequency receiver is to be eliminated in order to improve the time resolution and the sensitivity of the medium frequency receiver. Both the MFR and the two VLF receivers will have improved sensitivities since the dipole antenna will have a tip-to-tip length of approximately 4 m when the PDP is in the free-flyer configuration. The MFR will also have a 20 dB gain preamp which will increase its sensitivity further.

Many of the STS-3 measurements will be repeated to verify the general results, to determine differences in EMI levels with the Spacelab payload, and to explore hypotheses about the noise sources. In addition, more comprehensive measurements of emission from the FPEG electron beam will be made out to a range of 2 km from the Orbiter.

Acknowledgments

The authors wish to thank our co-investigator, Dr. Donald Gurnett, for providing the flight spare VLF receivers from the HELIOS and IMP spacecraft programs. We also thank our engineers Daniel Odem, Allen Huneke, Michael Miller, Miles Bailey, and Kerry Neal for carrying out the necessary receiver design and refurbishment. Receiver calibration was carried out at NASA Goddard Space Flight Center by Gerry Taylor. Thanks to Arthur Reubens of NASA Johnson Space Center and Theodore Pumphrey of Rockewell International for their advice on the interpretation of the measurements.

Support for the PDP on the STS-3/OSS-1 mission was provided through NASA Marshall Space Flight Center Contract NAS8-32807. OSS-1 mission management was provided by NASA Goddard Space Flight Center.

References

[1]Interface Control Document (ICD) 2-19001, "Shuttle Orbiter/Cargo Standard Interfaces," Johnson Space Center, Doc. 07700, Vol. XIV, Att. 1 (Sec. 10), Rev. F, Sept. 22, 1978.

[2]Shawhan, S.D., Burch, J.L., and Fredricks, R.W., "Subsatellite Studies of Wave, Plasma and Chemical Injections from Spacelab," *Journal of Spacecraft and Rockets*, Vol. 20, May-June 1983, pp. 238-244.

[3]Fortna, D.L., "Report on Analysis of EMI Data and Measurement Program on the Space Shuttle Orbiter Vehicle 101," NASA Goddard Space Flight Center, Code 302, June 27, 1977.

[4]Neupert, W.M. et al., "Science on the Space Shuttle," *Nature*, Vol. 296, March 18, 1982, pp. 193-197.

[5]Colonna, R.A., "STS Payload Bay Environment" in *The Shuttle Environment Workshop*, edited by J. Lehmann, S.G. Tanner, and T. Wilkerson, Systematics General Corp., NAS5-27362, Feb. 1983, pp. A-15 to A-30.

[6]Giffin, B.L. and Blount, R.L., "The Electromagnetic Environment for the Space Shuttle Orbiter," AIAA Paper 83-0332, Jan. 1983.

[7]Murphy, G.B. and Shawhan, S.D., "Radio Frequency Fields Generated by the S-Band Communications Link on OV102," *Journal of Spacecraft and Rockets*, Vol. 21, July-Aug. 1984, pp. 398-399.

[8]Shawhan, S.D., Murphy, G.B., and Pickett, J.S., "Plasma Diagnostics Package Initial Assessment of the Shuttle Orbiter Plasma Environment," *Journal of Spacecraft and Rockets*, Vol. 21, July-Aug. 1984, pp. 387-391.

[9]Murphy, G.B. et al, "Interaction of the Space Shuttle Orbiter with the Ionospheric Plasma," *Proceedings of the 17th ESLAB Symposium*, Noordwijk, the Netherlands, 1983, pp. 73-78.

[10]Murphy, G.B., Shawhan, S.D., and Pickett, J.S., "Perturbations to the Plasma Environment Induced by the Orbiter's Maneuvering Thrusters," AIAA Paper 83-2599, Oct. 1983.

Radio Frequency Fields Generated by the S-Band Communication Link on OV102

G.B. Murphy and S.D. Shawhan

Reprinted from

Journal of Spacecraft and Rockets

Volume 21, Number 4 July-August 1984 Page 398

AMERICAN INSTITUTE OF AERONAUTICS AND ASTRONAUTICS • 1633 BROADWAY • NEW YORK, N.Y. 10019

Radio Frequency Fields Generated by the S-Band Communication Link on OV102

Gerald B. Murphy* and Stanley D. Shawhan†
University of Iowa, Iowa City, Iowa

Abstract

THE Plasma Diagnostics Package (PDP) flew as part of the Office of Space Science (OSS-1) mission aboard the Columbia on STS-3 in March 1982. The PDP had as part of its instrumentation an S-band antenna and detector. By utilizing the remote manipulator system (RMS) arm, the PDP was maneuvered through a predetermined computer-controlled sequence in the Orbiter X-Z plane above the upper quad and hemi S-band communications antennas. Measurements of the field strength of these antennas during high-power modes of the transmitters were made and compared to ground full-scale measurements and predictions. Results indicated a field strength approximately 4.8 ± 3 dB higher than measurements predicted. This rf field is due primarily to the quad PM transmitter which had a power output of approximately 115 W compared to 15 W for the hemi.

Contents

Instrumentation

A description of the detailed instrumentation of the PDP can be found in Ref. 1, and a detailed block diagram of the S-band field measurement system is available in Ref. 2. The system employs a broadband folded dipole antenna developed at the National Bureau of Standards for hf and uhf frequencies and parallel linear and log detector systems. Due to an rf relay failure, only data obtained from the linear detector are used in this analysis. The dynamic range of this linear detector configuration at the quad pm frequency of 2287.5 MHz is approximately 35 dB. The minimum detectable field along boresight is 1 V/m. The sensitivity at 2250 MHz (hemi transmitter frequency) is 4 dB greater.

Operation

Since the PDP was designed as an RMS probe for this flight, a special automated sequence was created to measure the S-band field strength above the cabin and Orbiter bay. This sequence is illustrated in Fig. 1. The PDP is shown on the end of the arm with the structure pointing downward being the S-band antenna. At each of the locations shown, the PDP was rotated about an axis parallel to the Orbiter Y axis (see Fig. 1). The rotation enabled the data taken to reproduce the PDP receiver antenna pattern, which had been measured in the lab, and thus to sort out that part of the data that was not reliable. This technique was useful since the Columbia's quad transmitter power was intermittent at times on this flight. The RMS sequence in Fig. 1 was run several times under different transmitter configurations. However, the data taken when the upper starboard quad and upper hemi antennas were selected at high power provided the highest field strength and thus are used in this report.

Data Analysis

Data reduction involved first sorting out those data which, by reproduction of the antenna pattern, appeared reliable. Next, an average electric field at the RMS position was calculated by correcting for the receiver antenna gain $G(\theta,\phi)$ to an equivalent field measured at boresight with gain $G(0,0)$.

Although the hemi and quad antennas were both active, the reduced power of the transmitter at 2250 MHz (15.5 W at 2250 MHz vs 114 W at 2287.5 MHz), plus the position of the PDP with respect to the hemi resulted in the primary response of the detector being due to the 2287.5 MHz quad signal in the first two cases listed in Table 1. However, for positions 2 and 3 some correction to received power was made due to received hemi power. Table 1 lists the four measurement positions that were illustrated in Fig. 1 relative to the starboard quad antenna.

Both sources of predicted field strengths, 49 V/m/R (Ref. 3) and 75 V/m/R (Ref. 2), assumed a measurement boresight with the transmitting quad antenna. Since none of the PDP data was at boresight, a correction for pattern of the tra

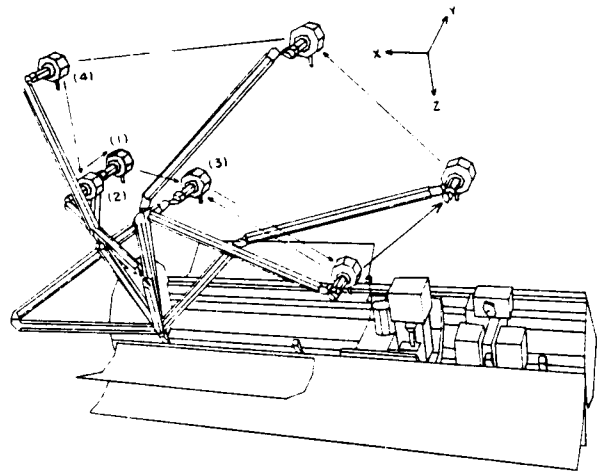

Fig. 1 Automode sequence 4: measurement points highlighted.

Table 1 PDP locations for starboard quad measurements

Position no.[a]	RMS position[b] X	Y	Z	ψ,[c] deg	R, m
1	−550	110	−650	52	4.3
2	−550	10	−650	83	4.4
3	−750	10	−650	86	6.
4	−550	10	−850	74	9.

[a] Position number corresponds to Fig. 1. [b] RMS position (in inches) in Orbiter body axis system (origin at nose of external tank). [c] ψ is angle from boresight of transmitting quad antenna.

Received May 23, 1983; revision received Nov. 8, 1983.

*Staff Research Assistant, Department of Physics and Astronomy.

†Professor of Physics, Department of Physics and Astronomy; presently, Branch Chief, Space Plasma Physics and the Earth Science and Applications Division, NASA Headquarters, Washington, D.C.

Table 2 Measured field intensity compared to predictions

Position no.	Measured field,[a] V/m	Predicted field[c] 75/R	Predicted field[c] 50/R	Prediction error[d]
1	22.8 ± 2.4 dB[b]	13.8	9.2	±1 dB
2	19.2 ± 3.5 dB	8.5	5.8	±2 dB
3	8.5 ± 3.4 dB	5.1	3.4	±2 dB
4	7.8 ± 2.6 dB	5.4	3.6	±1 dB

[a]Corrected for receiving antenna gain and response to the lower power hemi transmitter. [b]Error includes measurement uncertainty plus calibration uncertainty. [c]Corrected for $G_t(\theta,\phi)$. [d]Only the error in correcting for $G_t(\theta,\phi)$ is included.

mitting antenna must be made. Utilizing measurements of the antenna pattern made on a full-scale half-model of the starboard quads[2] a normalization to boresight can be made. The angle of the PDP from boresight of the upper starboard quad is shown in Table 1 and the required correction in Table 2. By dividing by the distance of the PDP measurements (Table 1), an electromagnetic field normalized to the same units of these two models is obtained for comparison.

Table 2 summarizes the results of the four measurements along with their associated errors and compares the measured values with the predicted field at that distance and angle from the antenna.

Assumptions and Sources of Error

Calibration errors are most easily accountable and are estimated to total ±2 dB.[2] Other sources of error involve uncertainty in correction of data for $G_r(\theta,\phi)$ the receiving antenna gain, and $G_t(\theta,\phi)$ the transmitting antenna gain. The PDP receiving antenna gain function is not smooth and errors can be as great as ±2 dB. Since detailed patterns of the transmitting quad given in Ref. 2 were a superposition of all quad antennas, correction factors for $G_t(\theta,\phi)$ at large θ and ϕ can be in error. The actual angle between transmitter boresight and the PDP is large in all cases (see Table 1), therefore, the correction for $G_t(\theta,\phi)$ could result in an error of ±2 dB.

Summary

The average measured electric field at a given point (Table 2) is 4.8 dB higher than the Ref. 2 prediction corrected for distance and measurement position. Considering the calibration accuracy of the PDP receiver, assumptions about antenna gain, and the resulting magnitude of uncertainty in this measurement, the guideline driving design criteria for payloads manipulated by the RMS should be on the high side of prediction with a several decibel safety margin. It must also be noted that at no time during measurements made in the cargo bay did the S-band electric fields exceed 1 V/m.[4] More information about other sources of electromagnetic interference is available in Ref. 4.

Acknowledgments

This research was supported by NASA MSFC Contract NAS8-32807. Special thanks by the authors to Arthur Reubens, Johnson Space Flight Center, and Theodore Pumphrey, Rockwell International, for their cooperation in providing the necessary ancillary data for this report, and to Dwight Fortna, Goddard Space Flight Center, for providing the calibration facility. Additional measurements of S-band as well as Ku-band fields are planned for a flight in early 1985, probably aboard Discovery. A different Orbiter antenna configuration necessitates these additional measurements, and changes in the PDP receivers will provide improved accuracy.

References

[1]Shawhan, S.D., Murphy, G.B., and Pickett, J.S., "Plasma Diagnostics Package Initial Assessment of the Shuttle Orbiter Plasma Environment," *Journal of Spacecraft and Rockets*, Vol. 21, July-Aug. 1984, pp. 387-391.

[2]Murphy, G.B. and Shawhan, S.D., "Report on S-Band Field Strength Due to Transmitters of the Columbia as Measured on STS-3," Department of Physics and Astronomy, University of Iowa, Iowa City, Iowa, Rept. 82-10, Rev. 1, May 1983.

[3]Reubens, A., "'Orbiter's Intentionally Generated RF Environment," NASA Johnson Space Flight Center, Houston, Tex., Internal Rept. Oct. 1980.

[4]Shawhan, S.D., Murphy, G.B., and Fortna, D.L., "Measurements of Electromagnetic Interference on OV102 Columbia Using the Plasma Diagnostics Packge," *Journal of Spacecraft and Rockets*, Vol. 21, July-Aug. 1984, pp. 392-397.

Radio Science, Volume 19, Number 2, Pages 471–486, March–April 1984

Wave emissions from dc and modulated electron beams on STS 3

Stanley D. Shawhan and Gerald B. Murphy

Department of Physics and Astronomy, University of Iowa

Peter M. Banks and P. Roger Williamson

Space, Telecommunications and Radio Science Laboratory, Stanford Electronics Laboratory, Stanford University

W. John Raitt

Center for Atmospheric and Space Sciences, Utah State University

(Received March 25, 1983; revised August 18, 1983; accepted August 26, 1983.)

The first active beam-plasma experiments utilizing the space shuttle were carried out in March 1982 as part of the NASA Office of Space Science mission on the third space shuttle flight. A fast pulse electron generator emitted a 1-keV, 100-mA electron beam in either a continuous (dc) mode or an on/off modulated mode in the ELF to HF frequency range. Stimulated electrostatic and electromagnetic waves and associated plasma effects were measured with the plasma diagnostics package as it was maneuvered through and near the beam by the remote manipulator system. For the dc beam the wave spectrum was electrostatic, was peaked in the 300- to 500-Hz range with a spectral density of 4×10^{-3} V^2 m^{-2} Hz^{-1}, and was unpolarized. Above the nominal lower hybrid resonance frequency the intensity decreased but was polarized. Strong emissions near the electron gyrofrequency and the plasma frequency were occasionally detected. The background spectrum was similar to the dc case for VLF and ELF modulations, but the emissions at the modulation frequency were more electromagnetic and more intense with field strengths of up to 1 V m^{-1}.

INTRODUCTION

Experiments involving the emission of an electron beam into a plasma have been carried out in space simulation chambers and in space utilizing both rockets and satellites to carry the electron emitter and diagnostic instruments. These experiments have been designed for a variety of purposes, for example, to investigate the charge neutralization processes in the plasma medium near the beam emitter, to probe the nature of electric fields along remote sectors of the geomagnetic field lines, to determine field line lengths and conjugate locations, to study electron scattering and diffusion, to create artificial aurora under controlled conditions, and to stimulate beam-plasma interactions for investigation of wave emissions and particle acceleration. Papers addressing this wide range of experiments include those of *Winckler* [1980], *Annales de Geophysique* [1980], *Grandal* [1982], P. M. Banks and P. R. Williamson (unpublished manuscript, 1983), and this issue of *Radio Science*.

During March 22–29, 1982, the third space shuttle *Columbia* flight (STS 3) carried the first scientific payload from the NASA Office of Space Science (OSS 1) into a 240-km circular orbit inclined at 38.4°. The instrumentation and the scientific objectives of the OSS 1 payload are described by *Neupert et al.* [1982]. Two OSS 1 investigations were coordinated to assess the electrical, electromagnetic, and plasma environment of the orbiter and to diagnose wave emissions and related plasma effects due to the injection of an electron beam into the surrounding ionosphere. Reports on the passive environmental measurements have been given by *Banks et al.* [1983] and by *Shawhan et al.* [1984*a*]. This paper and the paper by P. M. Banks and P. R. Williamson (unpublished manuscript, 1983) report on wave emissions and related plasma processes which were stimulated by the first electron beam emissions from the space shuttle. These on-orbit measurements are compared to measurements made in the NASA Johnson Space Center (JSC) space simulation chamber (chamber A)

Paper number 3S1436.
0048-6604/84/003S-1436508.00

TABLE 1. Fast Pulse Electron Generator Characteristics

Characteristic	Value
Beam energy	1 keV
Beam current	
FPEG1	100 mA
FPEG2	50 mA
Beam divergence	5°
Pulse rise and fall time	100 ns
Minimum pulse duration	600 ns
Maximum pulse duration	107 s
Maximum number of pulses in one sequence	32,768

FPEG is fast pulse electron generator.

in March 1981, using similar instrumentation. The space simulation results have been reported by *Banks et al.* [1982], *Raitt et al.* [1982], and *Shawhan* [1982]. Both the STS 3 and JSC plasma chamber measurements are compared to other similar rocket experiments and to other space chamber measurements.

DESCRIPTION OF INSTRUMENTATION AND OPERATIONS

During the STS 3 mission, active beam-plasma experiments were conducted using the fast pulse electron generator (FPEG) of the vehicle charging and potential investigation (VCAP). Pertinent characteristics of this 1-keV, 100-mA electron accelerator are given in Table 1. Diagnostics of the plasma response, the orbiter electrical state, and emitted waves were carried out with pallet-mounted VCAP instrumentation and with instrumentation in the detachable plasma diagnostics package (PDP) [*Shawhan*, 1982]. The PDP includes a variety of instruments which measure the relevant plasma parameters. These parameters are listed in Table 2. The PDP was operated in the payload bay and was grappled by the 15-m remote manipulator system (RMS). Attached to the RMS, it was maneuvered over the FPEG and around the orbiter. A view from the aft flight deck toward the tail of the orbiter is shown in Plate 1. The PDP is being held over the location of the FPEG by the RMS. During this period the orbiter is in a nose-to-sun attitude so that the payload bay is in shadow. During the experiments reported here, the orbiter is rolling about its long axis at two rolls per orbit.

Joint VCAP-PDP operations were carried out by the STS 3 crew members: J. Lousma (commander) and G. Fullerton (pilot). There were seven prime operational periods each lasting about 20 min. For five of these periods the crew initiated the RMS preprogramed search pattern and the FPEG for a 15-min firing of an unmodulated (dc) electron beam while looking for maximum readings of selected on-board parameters. For two other periods the pilot manipulated the PDP under manual RMS control to find the center of the electron beam using on-board parameters. During other intervals, when the PDP was stationary on the RMS, latched into the payload bay, or maneuvered on the RMS for other objectives, the FPEG was operated in many other modulated modes. These modes included short bursts to change the charge state of the orbiter and square wave modulation in the HF, VLF, and ELF frequency ranges (P. M. Banks and P. R. Williamson, unpublished manuscript, 1983). The plasma effects and wave emissions associated with both the dc and the modulated operations are reported in the following sections.

PLASMA EFFECTS OF BEAM EMISSIONS

A 10-min survey plot of PDP measurements for 1982, day 85, 2038–2048 UT is presented in Plate 2. These measurements were made during a joint VCAP-PDP dc beam search period. Other survey plots are presented in Plates 3 and 4 for the FPEG modulated at VLF and ELF, respectively. Fifteen panels are identified on the survey plots [*Shawhan et al.*, 1983*a*]. These panels are associated with specific PDP measurements as identified in Table 2. Panels 1–6 give density irregularity and wave spectral information. The neutral gas pressure on a log scale from 10^{-7} to 10^{-3} torr is given in panel 7. Energetic electrons and ions from 2.5 eV to 50 keV on a log energy scale are presented in panels 8 and 9. The ion mass composition, energy distribution, and flow direction are displayed in panels 10, 11, and 12 which result from measurements by the ion mass spectrometer, the ion retarding potential analyzer, and the differential ion flux probe, respectively. In panel 13 the yellow curve indicates the potential of the PDP with respect to the orbiter ground over a ± 8 V range (negative at the top of the panel). The green curve gives the electric field over a ± 4.8 V m^{-1} range (the red curve is 30 times more sensitive). Total flux of energetic electrons is displayed in panel 14; the scale is logarithmic downward covering the range of 3×10^{10} to 5×10^{17} (red curve) and 5×10^{8} to 5×10^{15} (green curve) electrons cm^{-2} s^{-1}. Three orthogonal axes of the magnetic field for a range of ± 0.6 G are given in panel 15.

Many of the plasma effects related to the operation of the FPEG can be seen in Plate 2. Beam turn-on

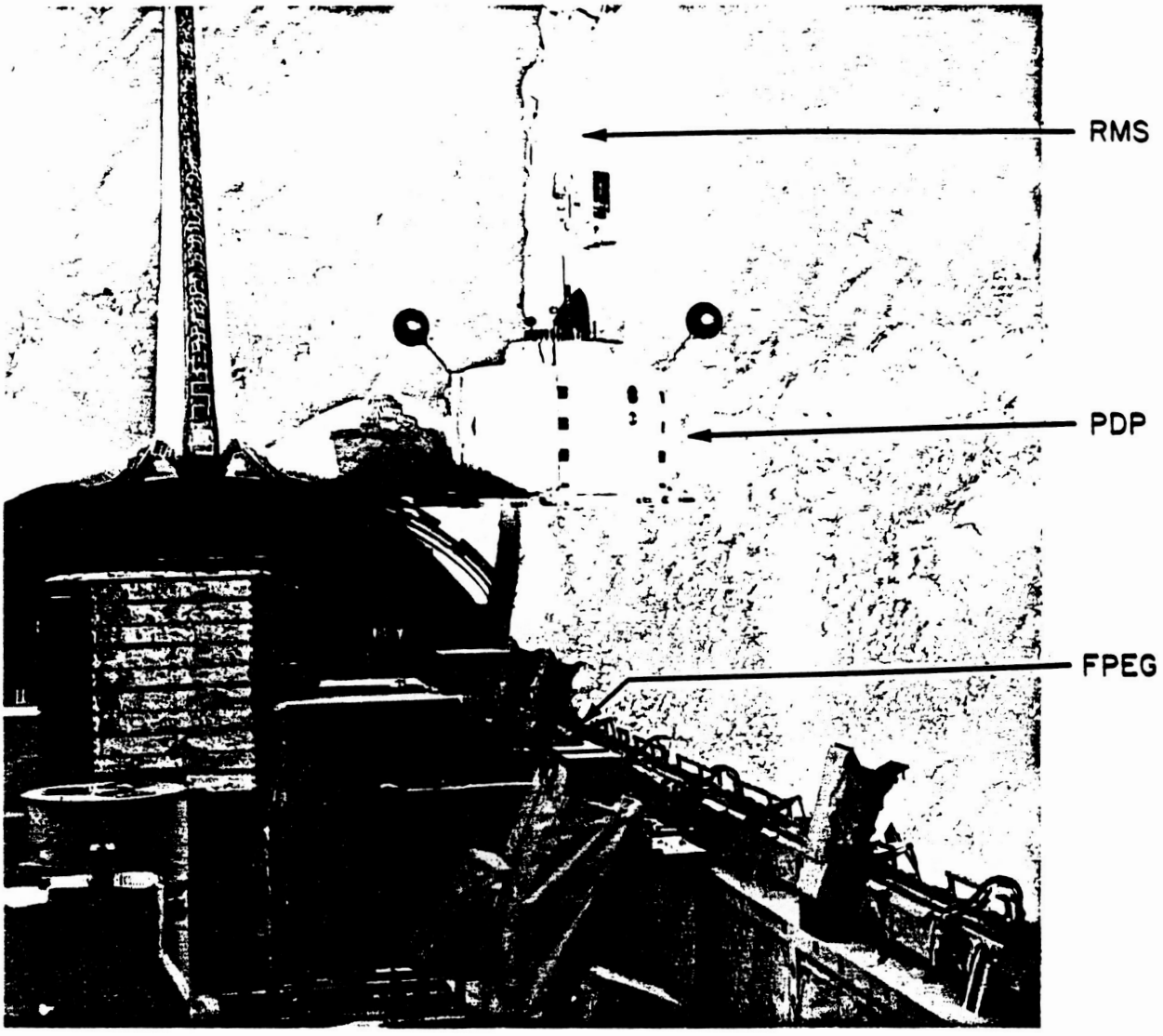

Plate 1. Photograph of the plasma diagnostics package on the remote manipulator system over the fast pulse electron generator location in March 1982 on STS 3.

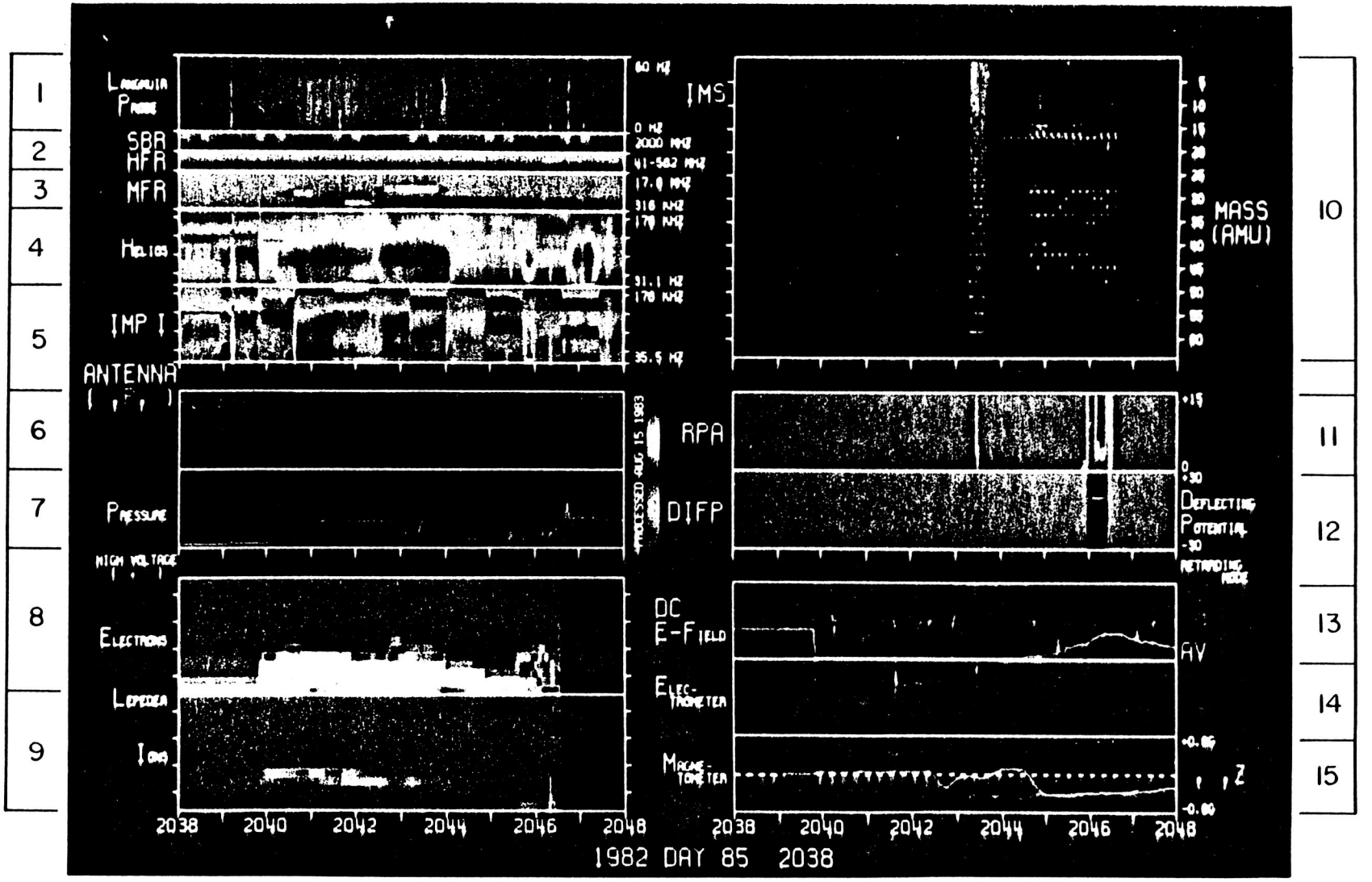

Plate 2. Survey plot of PDP measurements during search around an FPEG dc beam. Energetic electrons (panel 8) and enhanced electrostatic wave emissions (panel 4) are observed. See text for explanation of measurements.

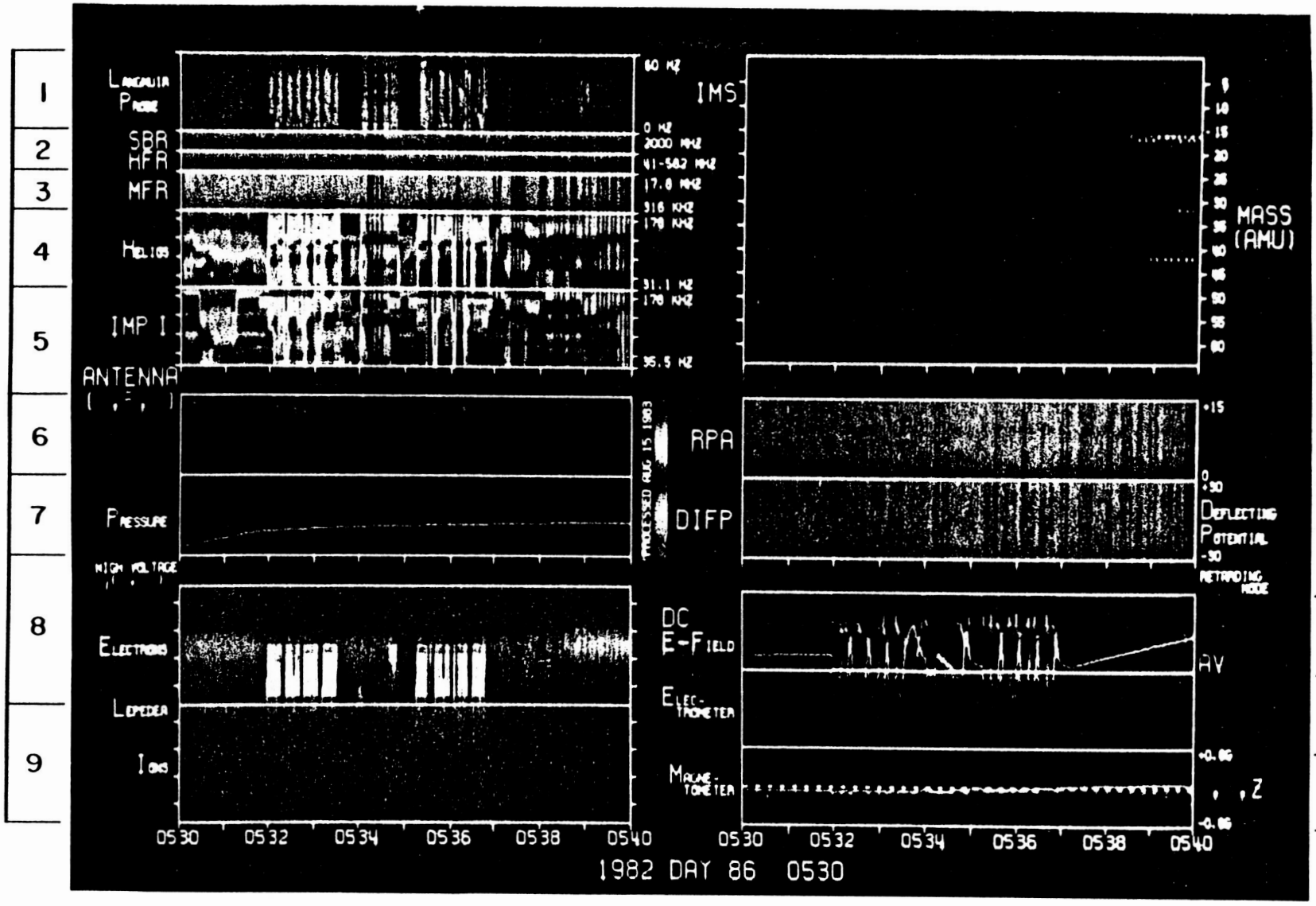

ORIGINAL PAGE
BLACK AND WHITE PHOTOGRAPH

Plate 3. Survey plot similar to Plate 2. FPEG electron beam is modulated alternately at 3-kHz and 5-kHz rates, which produces electromagnetic VLF emissions and a background electrostatic spectrum (panels 4 and 5).

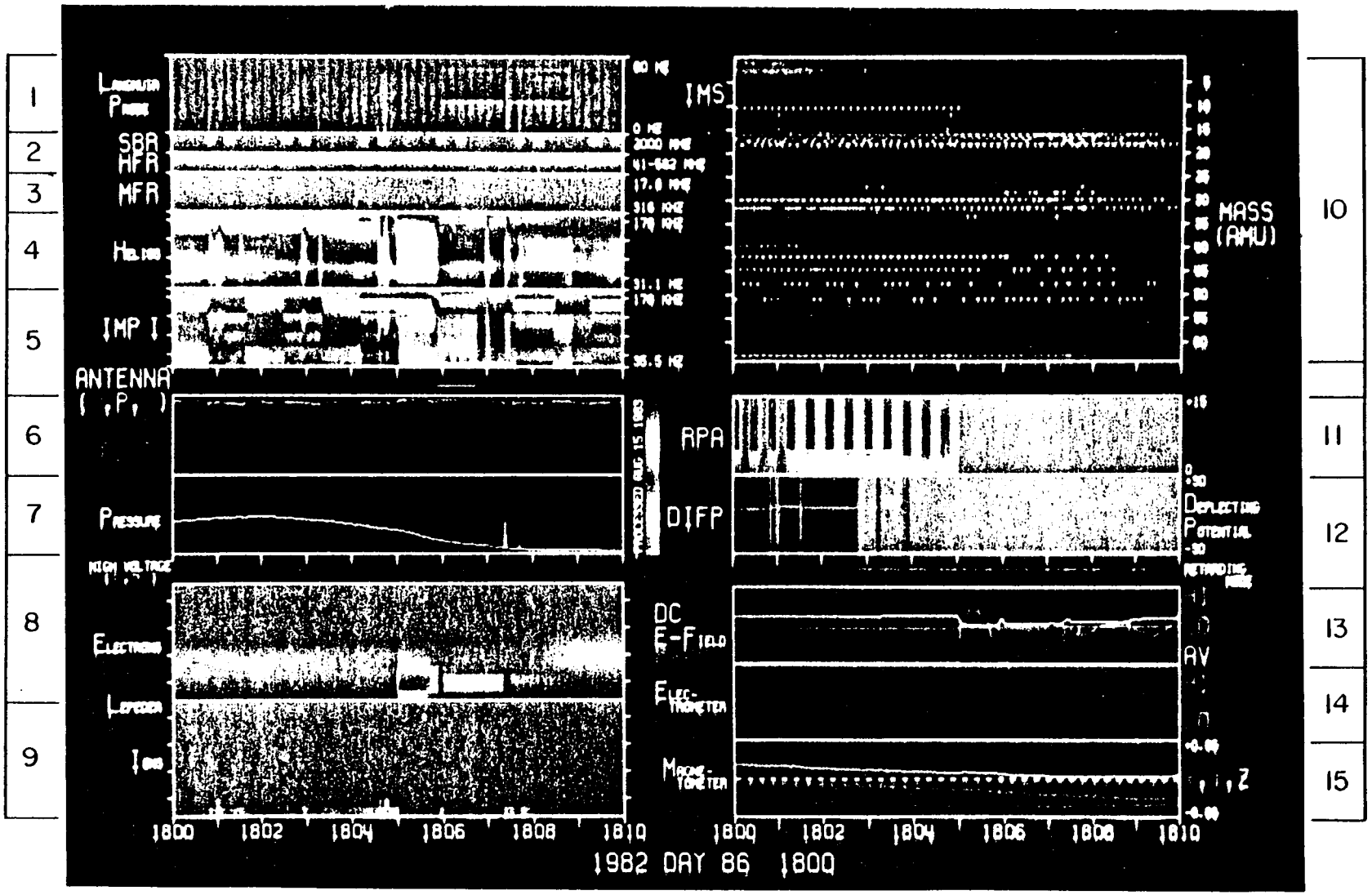

Plate 4. Survey plot similar to Plate 2. FPEG electron beam is modulated at 25 Hz but with different on/off duty cycles. Variations of 25 and 50 Hz in the Langmuir probe current are observed (panel 1).

TABLE 2. PDP Measurements

Panel*	Measurement	Color Bar (Dark Blue to Red)
1	Langmuir probe spectrum of density fluctuations, $\Delta N/N$, from 4 to 50 Hz	0% to 0.75% linear
2	*S band field strength monitor* (2200 MHz)	not functional
	High-frequency receiver (HFR); four bands 25 to 800 MHz	-48 to $+32$ dBV m^{-1}
3	Medium-frequency receiver (MFR); eight bands log spaced 316 kHz to 17.8 MHz (f_{ge} ranges 0.9 to 1.3 MHz; f_{pe} 1–10 MHz)	-68 to $+28$ dBV m^{-1}
4	VLF electric field receiver from Helios program; 16 bands, log spaced 31 Hz to 178 kHz	-96 to $+4$ dBV m^{-1}
5	VLF receiver from IMP program; 16 bands, log spaced 35 Hz to 178 kHz switched:	
	Magnetic search coil (red)	-10 to $+80$ dBpT at 1 kHz
	Langmuir probe $\Delta N/N$ (yellow)	2.5×10^{-4}% to 2.5% log
	Electric dipole (green)	-96 to $+4$ dBV m^{-1}
6	Wide-band receiver automatic gain control switches sensor every 51.2 s (see panel 5)	
	AGC1 (red); 0–10 kHz, 20–10 kHz, 20–30 kHz; 100-dB range; quasi-log	N/A
	AGC2 (green); 0–1 kHz; 100-dB range; quasi-log	N/A
7	Pressure gauge; 10^{-7} to 10^{-3} torr, logarithmic	N/A
8	Low-energy electrons (LEPEDEA); 2 eV to 50 keV, logarithmic	3×10^{1} to 1×10^{7} electrons cm^{-2} s^{-1} sr^{-1} eV^{-1} logarithmic
9	Low-energy protons (LEPEDEA); 2 eV to 50 keV, logarithmic	6×10^{0} to 2×10^{8} protons cm^{-2} s^{-1} sr^{-1} eV^{-1} logarithmic
10	Ion mass spectrometer (IMS); 1–64 amu	10^{-13} to 10^{-8} A logarithmic
11	Retarding potential analyzer (RPA)	10^{-10} to 10^{-6} A logarithmic
	Scanning mode 0–15 V (12.8 s)	
	Fixed mode 0 V (12.8 s)	
12	Differential ion flux probe (DIFP); deflection angle $-50°$ to $+50°$	10^{-9} to 10^{-7} A logarithmic
13	dc electric field	
	High gain (red); -0.15 V to $+0.15$ V m^{-1}	N/A
	Low gain (green); -4.8 to $+4.8$ V m^{-1}	N/A
	Spacecraft potential (yellow); -8.2 to $+8.2$ V	N/A
14	Electrometer (Faraday cup)	
	High range/low sensitivity (red); 5×10^{17} to 3×10^{10} electrons cm^{-2} s^{-1}	N/A
	Low range/high sensitivity (green); 5×10^{15} to 6×10^{8} electrons cm^{-2} s^{-1}	N/A
15	Magnetometer; -0.6 to $+0.6$ G; X (red), Y (green), Z (yellow) components	N/A

AGC is automatic gain control.
*Refer to Plates 2, 3, and 4.

happens during the min 2039. At turn-on, energetic electrons (panel 14) with energies up to 100 eV (panel 8) are immediately observed. The electric wave noise is also significantly enhanced in panel 4. A positive PDP potential in excess of +8 V is indicated in panel 13 although the electric field does not change significantly. After turn-on, the PDP is manipulated around the beam region, and the various detectors are rotated. The movements and rotations are apparent in the changing magnetic vector components in panel 15. This motion and rotation result in a variation of the observed maximum electron energy, electron flux, intensity and spectrum of the wave emissions, and magnitude and polarity of the electric field. These variations are due to the localization of the electron beam column and to the accessibility of

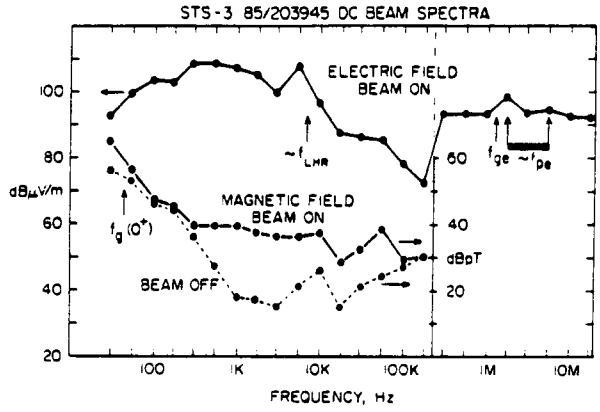

Fig. 1. Electric and magnetic wave fields during dc beam operation with characteristic plasma frequencies noted.

energetic particles with specific energies and pitch angles to the detector and to the polarization of the stimulated waves. Note that wave emissions in the range of the electron gyrofrequency ($f_{ge} \sim 1$ MHz) and plasma frequency ($f_{pe} \sim 1$–10 MHz) are also observed in panel 3. These same qualitative plasma responses are seen in Plates 3 and 4 when the FPEG is modulated at VLF and ELF.

WAVE EMISSIONS FROM dc BEAMS

Electric and magnetic wave field spectra during the dc beam emission period presented in Plate 2 are shown in Figure 1. The wave field strengths are given on a decibel scale (in decibels above 1 μV m^{-1}, ± 3 dB) for three measurements: the electric field with the beam on, the magnetic field with the beam on, and the magnetic field noise level with the beam off. Measurements are made over the frequency range of 30 Hz to 178 kHz in 16 bands each with a bandwidth of 15% spaced logarithmically in frequency at four bands per decade in a 1.0, 1.78, 3.11, and 5.62 sequence. Another, less sensitive receiver extends the scheme with eight more bands to 17.8 MHz for the electric fields only.

Although the spectra in Figure 1 are presented in terms of electric field strength in decibels, the noise does not appear to be narrow band in nature. When observed on a separate 10-kHz wide-band receiver (not shown in Plate 2) over the frequency range of 10 Hz to 30 kHz, the noise appears nearly "white" [see *Shawhan et al.*, 1984*a*]. The background magnetic field noise is cluttered with discrete emission lines from various power converters on the orbiter. However, the beam-generated magnetic noise also appears to be white. Consequently, the spectra should be plotted in terms of voltage spectral density, V^2 m^{-2} Hz^{-1}, and magnetic spectral density, T^2 Hz^{-1}, to make the bandwidth conversion for the electric field spectral density, for example,

$$\mathrm{dB(V^2\ m^{-2}\ Hz^{-1})} = \mathrm{dB(\mu V\ m^{-1})} - 10 \log (0.15f) - 120\ \mathrm{dB} \quad (1)$$

where f is the center frequency of the filter.

The electric field spectrum has a broad peak in the 300- to 500-Hz range, a sharper peak at 5 kHz near the lower hybrid resonance frequency ($f_{LHR} = f_{ge}/172$ for $f_{pe} > f_{ge}$ and O^+ ions) with a significant falloff toward higher frequencies. Some emissions occur near the electron gyrofrequency and plasma frequency at 1.2 MHz and 10 MHz, respectively. In the 1-kHz to 100-kHz range there is a significant magnetic field component given in Figure 1 in decibels above 1 pT (± 5 dB). Although the measurements are made in the near field of the beam, the relative electromagnetic nature of this noise can be judged by comparing the apparent index of refraction from the ratio of the measured fields, "n" $= cB_y/E_x$ where c is the speed of light, to the index of refraction expected for a cold plasma and parallel wave propagation (in the far field of the source), $n^2 = f_{pe}^2/(ff_{ge})$ where $f_{pe} \gg f_{ge}$ is assumed [*Stix*, 1962]. From the measured field values the apparent index of refraction, "n", can be derived as follows:

$$\text{"}n\text{"} = 316B\ (\mathrm{pT})/E\ (\mu \mathrm{V\ m^{-1}}) \quad (2)$$

For example, at 562 Hz, B is 79 pT (38 dBpT), and E is 2.5×10^5 μV m^{-1} (108 dBμV m^{-1}) so that "n" is

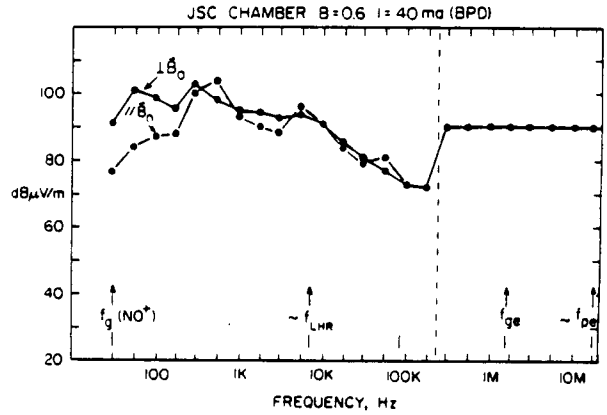

Fig. 2. Electric wave field spectrum from Johnson Space Center space simulation chamber under BPD conditions. Note similarity to STS 3 spectrum in Figure 1.

0.1. For electromagnetic waves far from the source, the lowest possible value is 1.0. For a wave frequency of 5 kHz and for a plasma frequency range of 2 to 6 MHz (derived from the PDP Langmuir probe) and a gyrofrequency $f_{ge} = 1.2$ MHz (obtained from a model), the expected index ranges from 25 to 75. Apparently, the wave field is electrostatic in nature but with a small magnetic component.

It must be noted that all of these measurements are probably made in the near field of the local beam "antenna." Even for an index of refraction of 50, the wavelength is 1200 m at 5 kHz, so that the PDP would need to be ~12 km away (10 wavelengths) to be in the far field; the PDP is at most 15 m from the local beam. However, the beam itself extends many tens of kilometers along the magnetic field line away from the orbiter, and according to *Harker and Banks* [this issue], the beam may emit primarily from its leading edge. Consequently, the far-field approximations may be marginally valid, but there is no good test to judge the validity. On future shuttle flights the PDP will make wave measurements out to ranges of hundreds of kilometers from the electron beam and from radiating antennas [*Shawhan et al.*, 1983*b*].

One important objective of the VCAP and PDP joint operations was to compare the phenomena observed in the JSC space simulation chamber with those observed in space. The experimental setup in the JSC chamber, the experiments, and the results are described by *Banks et al.* [1982], *Raitt et al.* [1982], and *Shawhan* [1982]. An electric wave field spectrum taken at JSC under similar conditions to those on orbit is shown in Figure 2. The spectrum looks very similar in intensity and shape to that of Figure 1, although in the chamber the magnetic fields are terminated by the conducting top and bottom of the chamber and the width of the chamber is smaller than an energetic ion gyroradius. Additionally, in the chamber the electron beam continuously loads the same magnetic flux tube, whereas on orbit the orbiter moves the beam across an energetic electron gyrodiameter in 1 ms. Since the spectra are very similar, however, one could conclude that the generation mechanisms depend primarily on electrons and that the generation volume is relatively local.

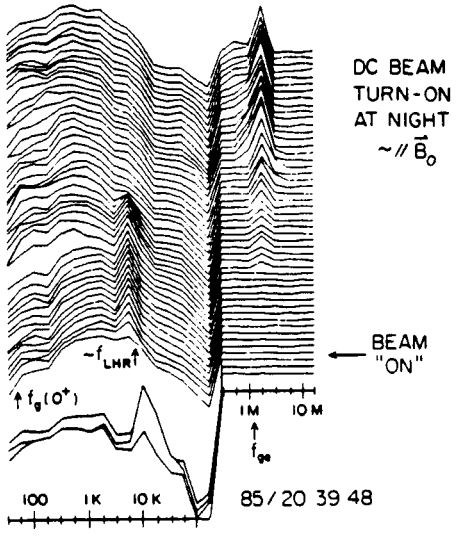

Fig. 3. Electric wave spectrum development with time over 1.4-min period on dark side of orbit.

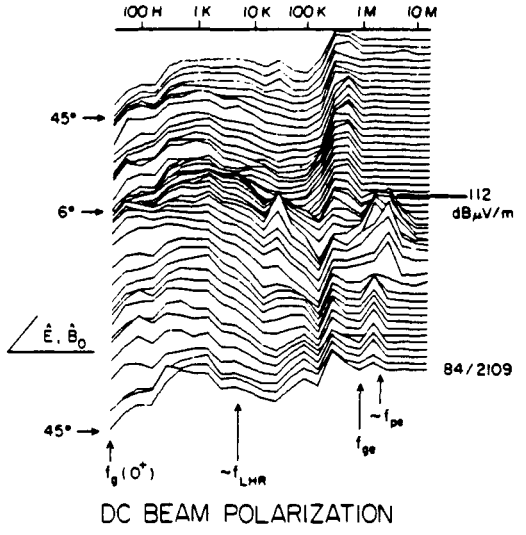

Fig. 4. Electric wave spectrum as a function of the angle between the electric antenna $\hat{E}$ and the geomagnetic field $\hat{B}_0$.

Figure 3 shows the time development of the wave electric spectrum at and just after the beam turn-on for the period in Plate 2. Each spectral trace covers the frequency range of 30 Hz to 17.8 MHz with a trace separation of 1.6 s. The increase in noise level at the beam turn-on is 40 dB. Just after turn-on a prominent emission near the lower hybrid resonance frequency is apparent, but this emission fades out as an emission above the electron gyrofrequency (at the plasma frequency?) becomes prominent. From the PDP Langmuir probe the plasma frequency is estimated to be between 3 and 10 MHz. This change in spectrum occurs near 30 s and is probably related to the rotation of the PDP electric field antenna with respect to the magnetic field (see panel 15 in Plate 2).

With the PDP on the RMS, it was possible to

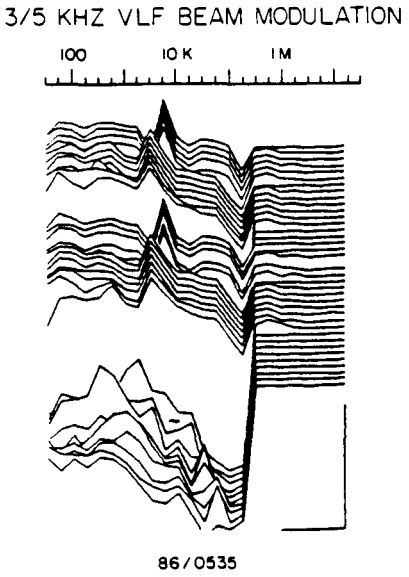

Fig. 5. Electric wave spectrum as a function of FPEG beam modulation alternating between 3 kHz and 5 kHz.

rotate the PDP so that the electric field antenna could measure the polarization of the electric field emissions with respect to the geomagnetic field direction. An example of the polarization measurements is shown in Figure 4. Angles between the electric dipole antenna and the geomagnetic field, 6° to 45°, are included for the full spectral range of 30 Hz to 17.8 MHz. Near 45° the spectra are similar to those in Figures 1 and 2. Below the lower hybrid frequency (f_{LHR}) there is very little variation with angle. Above the f_{LHR} there is some variation especially when the antenna is nearly aligned with the magnetic field. At this alignment the intensity is increased overall, and very prominent emissions appear at or near the electron plasma frequency. The amplitude reaches 0.4 V m^{-1} (112 dBμV m^{-1}). This polarization near f_{pe} is consistent with these waves being Langmuir plasma waves [*Stix*, 1962].

WAVE EMISSIONS FROM VLF-MODULATED BEAMS

A unique characteristic of the FPEG is that it could be square wave modulated up to the HF frequency range. An example of a VLF modulation period is shown in Plate 3. In panel 4, centered at 0533 and 0536, are VLF emission sequences. The modulation is alternated between 3 kHz and 5 kHz. Alternating red intensities are apparent in these two bands. As with the dc beam emissions, the energetic electrons (panel 8), the PDP potential shift (panel 13), and the intensified background wave emissions (panels 4 and 5) are observed. The time sequences of electric field wave spectra are shown in Figure 5. At the start of the sequence the intensity increases by 40 dB in the VLF range, and emission just below the electron gyrofrequency ($f_{ge} \sim 1.2$ MHz) is initiated. Further enhancement at the 3-kHz and 5-kHz fundamental modulation frequencies is apparent.

In Figure 6 a representative electric and magnetic spectrum is given. The background electric spectrum produced by the beam is very similar to that of the dc beam shown in Figure 1. The magnetic field background is also similar in level except that the orbiter-associated and payload-associated magnetic noise levels are higher. At the 3-kHz fundamental frequency there is a 10- to 15-dB enhancement in the magnetic field. Using equation (2), the background beam noise is found to have "n" < 1 and is interpreted to be electrostatic, whereas the noise at the modulation frequency tends to be electromagnetic: the apparent index of refraction, "n", is 4, which is greater than 1.0. The calculated value of the index is again in the range of 25 to 75. Although the index of refraction is not strictly valid in the near field, it is seen that these VLF waves are relatively more electromagnetic (by a factor of 4/0.1 = 40) than the "electrostatic" waves from the dc beam under nearly identical beam geometry and diagnostic conditions.

These VLF emission sequences were utilized in about 60 different periods during the mission with the PDP on the RMS and also latched to the pallet. Emissions occurred under varying day/night, electron density, and beam pitch angle conditions with generally the same result as that depicted in Figure 6.

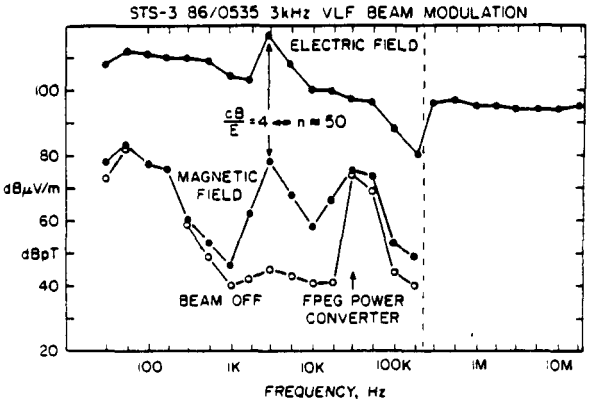

Fig. 6. Electric and magnetic wave field spectrum at the time of a 3-kHz FPEG beam modulation. A significant magnetic component is observed at 3 kHz.

WAVE EMISSIONS FROM ELF-MODULATED BEAMS

With the PDP on the pallet, the FPEG was modulated at 25 Hz in the ELF range with a low on-off duty cycle of 1:2 and high on-off duty cycle of 2:1. Emissions at ELF frequencies appear most predominantly in the Langmuir probe electron density irregularity spectrum ($\Delta N/N$). Emissions at 25 Hz and the first harmonic are seen in panel 1 of Plate 4. These emissions are centered on 1807 and 1808 UT. Both emissions have associated low fluxes of energetic electrons in panel 8 and a small PDP potential shift in panel 13. However, the total electron flux is not detectable in panel 14, probably because the PDP is in the cargo bay. Significant wave emissions are not seen in the VLF receivers (panels 4 and 5), since the 25-Hz fundamental is just below the lowest-frequency filter center.

Although the on-to-off duty cycles are different, the emission frequencies for the two emission periods are the same. Note that the electron flux and energy spread in panel 8 is higher for the first period in Plate 4, which is expected for the higher duty cycles. Detailed electric field spectra are given in Figure 7 for both cases. Very near the fundamental frequency the higher duty cycle emission has a higher intensity, as might be expected since more power is available. In the low duty cycle case, the intensity is lower at the fundamental and higher at higher frequencies. Since the low duty cycle spectrum is equal to or greater than the high duty cycle intensity above the fundamental, the total power emitted appears to be higher: the lower duty cycle beam appears to be more efficient at producing electric fields in the near-field regime.

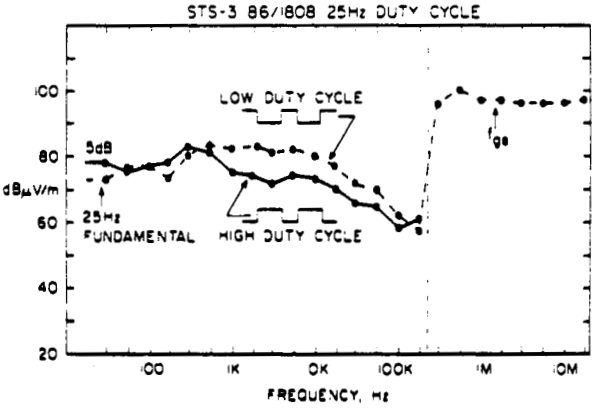

Fig. 7. Spectra of electric field emissions for the FPEG modulated at 25 Hz for cases of low and high duty cycle. At high duty cycle the fundamental is enhanced, but the total power is less in comparison to the low duty cycle.

DISCUSSION

Instrumentation on the PDP is limited in its time resolution and its frequency resolution. All wave, particle, and field measurements have a 1.6-s resolution, so that effects that occur on time scales of tens of milliseconds cannot be resolved. In the VLF frequency range (5 Hz to 30 kHz) the wide-band waveform receiver (not shown in Plates 2–4) provides high time (40 ms) and frequency (20 Hz) resolution. At higher frequencies, however, the multiple channel spectrum analyzer provides peak and average amplitude measurements at four frequencies, each decade of frequency at 15–30% bandwidth every 1.6 s. Consequently, the harmonics of the electron gyrofrequency cannot be distinguished from each other or from the electron plasma frequency in the 1- to 10-MHz range. However, since the PDP could be rotated and moved across the electron beam from the FPEG, a unique set of wave, particle, and field measurements have been obtained on the steady state wave spectra, the wave polarization, the beam spectra after wave-particle interactions, and the associated electric and magnetic field strength for both dc and modulated operations of the FPEG.

Results from the PDP measurements on the dc beam operations are summarized in Table 3 by frequency range: near the plasma frequency ($f_{pe} \sim 1$–10 MHz), near the gyrofrequency ($f_{ge} \sim 1$ MHz), above the lower hybrid frequency (6 kHz $> f < f_{ge}$), and below the lower hybrid frequency ($f < 6$ kHz). Also listed are conclusions reached from experiments performed both in space simulation chambers and on sounding rockets. These experiments were chosen because of the similarity in observing conditions to those of the FPEG/PDP on STS 3, but the listed results are representative of many experiments [see *Winckler*, 1980; *Annales de Geophysique*, 1980; *Grandal*, 1982]. The summarized results were extracted under the conditions that a keV electron beam of ≥ 50 mA was being injected into a plasma and the beam plasma discharge (BPD; see, for example, *Bernstein et al.* [1975, 1979, 1982]) was thought to be occurring.

A Langmuir probe on the PDP (results not shown in Plates 2–4) gives an estimate of the local electron density N_e from which the plasma frequency can be determined:

$$f_{pe} = 9[(N_e\ (\mathrm{cm}^{-3})]^{1/2} \quad \mathrm{kHz} \qquad (3)$$

TABLE 3. Comparison of Beam Wave Emissions

PDP Results	Space Simulation Chamber and Space Rockets Results
Near Plasma Frequency ($f_{pe} \sim 1$–10 MHz)	
Fields up to 0.5 V m^{-1} observed	VCAP/PDP in JSC chamber
Polarized parallel to geomagnetic field	Fields up to several volts per meter[a]
Predominant within one gyroradius of electron beam; not always stimulated	Polarized parallel to magnetic field[b]
	Predominant within one gyroradius of electron beam[a]
	Plasma frequency increases up to 32 MHz in ~10-ms time with 80-mA beam[b]
	Emissions at the upper hybrid frequency are enhanced for large pitch angles[c]
	Other space chamber experiments
	Emissions at the plasma or upper hybrid frequency observed under BPD or non-BPD conditions; non-BPD emissions are weaker[d]
	Field strengths up to 10 V m^{-1} are observed inside the beam[e]
	Echo rocket experiments
	Amplitude of ~1 mV m^{-1} observed at 100-m range for 70-mA beam (Echo I)[f]
	Emissions deduced to be electrostatic (Echo I)[f]
	Polar 5 rocket experiment
	Enhanced emission near plasma frequency 2–5 MHz delayed 20 ms after beam turn-on[f]
	Polarized parallel to magnetic field[g]
	f_{pe} emissions may be related to natural auroral particles[g]
	ARAKS rocket experiments (500-mA beam current)
	Emissions observed between the plasma and the upper hybrid frequencies[h]
	Emissions occur for 0°–70° pitch angles (down) but not for 140° pitch angle (up)[h]
	Even though beam current was 10 times Echo, field strength was comparable[h]
	Possible emission is by incoherent Cerenkov radiation[h]
	E//B rocket experiment
	Beam-associated emissions sometimes observed at local plasma frequency
Near Gyrofrequency ($f_{ge} \sim 1$ MHz)	
Noise band often just below f_{ge}	VCAP/PDP in JSC chamber
Noise amplitude up to 0.1 V m^{-1}	Similar PDP results to STS 3[a]
Occasional noise in $1f_{ge}$ to $3f_{ge}$ range below f_{pe} but no good f resolution	Detailed spectra indicate transient emissions at $2f_{ge}$ and $3f_{ge}$ (Bernstein mode?)[b]
Noise band not strongly polarized or localized to vicinity of beam	Emissions at the gyrofrequency are enhanced for small pitch angles[c]
	Other space chamber experiments
	Emissions at $(n + \frac{1}{2})f_{ge}$ occur in presence of return beam[i] but return beam requirement is not confirmed[d]
	Amplitude of f_{ge} harmonics depends exponentially on the beam current[d]
	Echo rocket experiments
	Amplitude up to 200 μV m^{-1} at 1-km range from 70-mA beam at $2f_{ge}$ frequency (Echo I)[f]
	Emissions up to $5f_{ge}$ observed (Echo I)[f]
	Emissions observed on ground at ~200-km range at $2f_{ge}$ for 100-mA 40-kV beam; emission only for downward beam (Echo IV)[j]

TABLE 3. (continued)

PDP Results	Space Simulation Chamber and Space Rockets Results
Above Lower Hybrid Frequency ($6\ kHz < f < f_{ge}$)	
Falling spectrum toward the electron gyrofrequency	VCAP/PDP in JSC chamber
Significant polarization with maximum amplitude neither parallel nor perpendicular to the geomagnetic field direction	Similar PDP results to STS 3[a]
No significant enhancement at the lower hybrid frequency	Other space chamber experiments
Noise appears to be electrostatic and enhanced in and near the beam	Significant emissions < 100 kHz are observed under BPD and non-BPD conditions[d]
	Emissions < 100 kHz are very impulsive[d]
	Echo rocket experiments
	Amplitude up to 1 mV m^{-1} observed at 1-km range from 70-mA beam (Echo I)[f]
	For downward emitted beam, emission spectrum was broad and cutoff at 0.6 MHz (Echo II)[k]
	The whistler mode emission appears to be emitted at the leading edge of the electron beam (Echo II)[k]
	The whistler mode emission appears to be emitted at the leading edge of the electron beam (Echo II)[k]
	ARAKS rocket experiments
	Noise in 7- to 100-kHz range is electrostatic[l]
	Amplitude reached 1 mV m^{-1}; spectrum decreases with frequency[l]
	Emissions are created by any beam pitch angle[l]
	Noise intensity drops exponentially with distance from beam[l]
Below Lower Hybrid Frequency ($f < 6\ kHz$)	
Nearly flat spectrum with roll-off at the low-frequency end below the O^+ gyrofrequency and about the lower hybrid frequency at the high-frequency end	VCAP/PDP in JSC chamber
	Similar PDP spectrum to that observed on STS 3[a]
	Peak of spectrum at ~1 kHz with 1 V m^{-1} [a]
	Some polarization just above ion gyrofrequency[a]
Peak situation in the 0.3- to 1-kHz range	Spiky VLF emission (flickering) with ~10-Hz periodicity emphasized at large pitch angles; harmonic spectrum. Emission enhanced in some frequency ranges $< f_{LHR}$ [c]
Peak amplitude of ~0.3 V m^{-1}	Other space chamber experiments
No significant polarization with respect to the geomagnetic field direction	Peak frequency of VLF spectrum depends on beam current; amplitudes up to 0.1 V m^{-1} detected at 50-mA beam; bursts up to 10 V m^{-1} [m]
Noise appears to be electrostatic	Echo rocket experiments
No spiky VLF emission (flickering) observed	Amplitude up to 2 mV m^{-1} at range of 100–1000 m from 70-mA beam with peak in 50- to 200-Hz range (Echo I)[f]
	Polar 5 rocket experiment
	Enhanced VLF emission ~5 kHz delayed 30–40 ms after beam turn-on[g]
	No preferred polarization observed[g]
	Discrete emissions are observed at 1–3 kHz[g]
	ARAKS rocket experiments
	Broadband electrostatic emissions at 1–10 kHz[n]
	E//B rocket experiment
	Emission with spectral peaks in the 5- to 6-kHz range[o]

[a] *Shawhan* [1982].
[b] *Raitt et al.* [1982].
[c] *Banks et al.* [1982].
[d] *Bernstein et al.* [1979].
[e] *Jost et al.* [1982].
[f] *Cartwright and Kellogg* [1974].
[g] *Grandal et al.* [1980].
[h] *Dechambre et al.* [1980a].
[i] *Bernstein et al.* [1975].
[j] *Monson and Kellogg* [1978].
[k] *Monson et al.* [1976].
[l] *Dechambre et al.* [1980b].
[m] *Holzworth et al.* [1982].
[n] *Dechambre et al.* [1980c].
[o] *Bernstein et al.* [1982].

Usually, the frequency falls into the range of 1–10 MHz. Under some conditions, with the PDP in or near the FPEG beam, emissions in the vicinity of f_{pe} are observed with up to 0.5 V m^{-1} amplitudes and polarized parallel to the geomagnetic field. These general features are consistent with earlier experiments both in space chambers and with rockets. It is surmised that the emission is at the upper hybrid frequency f_{UH} rather than the plasma frequency:

$$f_{UH} = f_{ge}[1 + (f_{pe}/f_{ge})^2]^{1/2} \quad (4)$$

For $f_{ge} \ll f_{pe}$ the upper hybrid and plasma frequencies are nearly the same. Chamber measurements by *Jost et al.* [1982] suggest amplitudes in the beam column of 10 V m^{-1} which dropped off rapidly outside; rocket measurements indicated ~1 mV m^{-1} at 100 m range from the beam [*Cartwright and Kellogg*, 1974]. Measurements of these emissions with rockets seem to be consistent with an incoherent Cerenkov mechanism due to the primary beam itself [*Dechambre et al.*, 1980*a*].

During FPEG operations, emissions are often observed which have a high-freqency cutoff at the electron gyrofrequency:

$$f_{ge} = 2800B\,(\mathrm{G}) \quad \mathrm{kHz} \quad (5)$$

Another emission band is observed above f_{ge} at $1-3f_{ge}$ but below the plasma frequency. These emissions range up to 0.1 V m^{-1} in amplitude, are nonpolarized, and seem not to be localized to the vicinity of the electron beam. In plasma chambers and from rockets it has been found that the waves below f_{ge} are probably electromagnetic waves in the whistler mode, which is consistent with the PDP observed characteristics. Above f_{ge}, high-resolution spectrum analyzers show transient bursts at harmonics of f_{ge} up to $5f_{ge}$ [*Cartwright and Kellogg*, 1974]. During the Echo IV experiment, emissions at $2f_{ge}$ were observed at a ground receiving station, consistent with the propagating electromagnetic nature of the waves [*Monson and Kellogg*, 1978].

Below the electron gyrofrequency the slope of the noise spectrum increases down to the lower hybrid frequency, becomes polarized oblique to the geomagnetic field direction, and tends to be electrostatic. These PDP findings are generally consistent with those of chamber and rocket experiments. Because of the pronounced polarization and relatively low amplitude at the higher-frequency end (hundreds of kilohertz), we suggest that these emissions are generated by the Cerenkov process for resonant beam particles since the index of refraction tends toward infinity for the oblique resonance at frequencies between the lower hybrid frequency and the electron gyrofrequency.

Although the lower hybrid frequency f_{LHR} [*Stix*, 1962] may not be physically defined if the PDP is measuring in the near field of the wave source region, the spectral observations seem to indicate a significant change in characteristics below the f_{LHR} as compared to those above. On STS 3 the PDP consistently observed an electrostatic noise with a broad peak in the 0.3- to 1-kHz range having amplitudes up to 0.3 V m^{-1}. This noise masked out natural VLF emissions in the ionosphere as well as possible orbiter electromagnetic interference. No significant polarization was found below the lower hybid frequency. These characteristics of the VLF noise were consistent with the JSC plasma chamber results except that the on-orbit noise did not flicker in amplitude as it did in the chamber [*Banks et al.*, 1982; *Holzworth et al.*, 1982]. Although the PDP observed momentary spectra with peaks of ~6 kHz (see Figure 1), the spectra did not consistently peak in the kilohertz range as was observed in several rocket experiments [*Grandal et al.*, 1980; *Dechambre et al.*, 1980*c*; *Bernstein et al.*, 1982].

This background electrostatic noise appears to be ubiquitous; spectra for the dc and the modulated electron beams are very similar, as can be seen by comparing Figures 1, 2, 6, and 7. There is another comparable electrostatic noise spectrum due just to the orbiter moving through the ionospheric plasma. This orbiter-generated noise is seen in Figures 3 and 5 before the electron beam is initiated. Some characteristics of this noise are described by *Shawhan et al.* [1984*b*]. This noise is generally of lower intensity than the beam-associated noise by about 20–40 dB but has the same general spectral shape. It is assumed to be orbiter-associated because the amplitude is modulated at the orbit period, with minima occurring when the orbiter bottom and tail block the plasma flow past the PDP. *Papadopoulos* [this issue] argues that the noise results from a lower hybrid drift instability which is driven by the steep electron density gradients at the orbiter surfaces and at the electron beam column boundary. Many other mechanisms may also fit the observations as reviewed by *Grandal* [1982] and *Harker and Banks* [this issue].

In contrast to the "n" $= cB/E = 0.1$ for the broadband electrostatic noise at VLF, the near-field emissions caused by modulating the beam at 3 and 5 kHz

had an apparent index of refraction, "n", of 4. Although the calculation of "n" is not strictly correct in the near field, the relative values indicate that the modulated emissions are more electromagnetic. Whether propagating electromagnetic waves are generated is an open question. On a sounding rocket, *Holzworth and Koons* [1981] modulated a beam of 80 mA at 3 kHz. Signals were received at a distance of 1.4 km, but the time delay for the receipt of the signals ranged up to 0.2 s, much too long for electromagnetic waves. It is thought that the time delay is related to the time for onset of BPD which causes a "disturbance" to reach the receiver. During the STS 3 flight, VLF ground stations and satellite wave receivers were operated in hopes of receiving the modulated signals. *Inan et al.* [this issue] report a negative detection from the DE 1 spacecraft during periods of magnetic conjunctions with the orbiter. However, in most cases the 100-W FPEG beam impacted the orbiter and did not escape.

At 3 kHz in the VLF range, *Holzworth and Koons* [1981] suggested that the modulated beam was driving the plasma in and out of the BPD condition. *Denig* [1982] discusses results from a JSC plasma chamber test at 68 Hz. With a short on time and long off time the pulsing spectrum exhibits harmonics to high frequencies. With a long on time and short off time the spectrum is concentrated at low frequency around the fundamental; the onset of BPD may destroy the beam as it propagates away if the beam on time exceeds the onset time for BPD. According to *Bernstein et al.* [1982] the BPD should not really occur at the STS 3 altitude because the neutral pressure is low at $\sim 10^{-7}$ torr. However, the PDP measurements at 25 Hz exhibit the same characteristics as those reported by Denig for the 68-Hz modulation when BPD was possible. These low-frequency observations may provide a good data base with which to test theories of beam emissions. *Harker and Banks* [this issue], for example, consider both coherent and incoherent processes. The most efficient emission seems to be a coherent Cerenkov and cyclotron mode at the leading edge of the beam. An optimum duty cycle would be 50%; any shorter has less power, and any longer provides more time for the coherency to be destroyed.

Further shuttle experiments are planned for the Spacelab 1 mission through use of the Space Experiments With Particle Accelerators (SEPAC) [*Obayashi et al.*, 1982] 40-keV, 1.6-A accelerator and of the Phenomena Induced by Charged Particle Beams (PICPAB) [*Beghin*, 1979] 10-keV, 100-mA accelerator and associated diagnostics. On Spacelab 2 the FPEG and PDP will be flown together with the PDP at a range of up to 1 km from the FPEG.

CONCLUSIONS

Measurements by the plasma diagnostics package of waves stimulated by the operation of the FPEG 50- to 100-mA, 1-keV electron beam have yielded characteristics which largely agree with results from space simulation chamber and sounding rocket measurements under the beam plasma discharge conditions. Electrostatic waves in the frequency range between the electron plasma and upper hybrid freqency are infrequently observed; these waves appear to be confined to the beam cylinder, which is not often explored with the PDP. Emissions are found in the range including harmonics of the electron gyrofrequency, and a spectrum of electromagnetic whistler mode waves extend below the electron gyrofrequency. At lower frequencies these waves become electrostatic with a peak at 0.3 to 1 kHz below the lower hybrid frequency. Electrostatic emissions are observed in this VLF frequency range without the beam being emitted, probably because of the orbiter's motion through the plasma. When the beam is on, the noise is enhanced by ~ 40 dB. Some rocket and plasma chamber measurements have exhibited peaks and/or discrete emissions of ~ 5 kHz, but these are not persistently seen on STS 3. Modulation of the beam at VLF and ELF yields ac fields that are more electromagnetic in character. The beam modulation may be significantly altered as the beam propagates by beam-plasma (BPD?) interactions.

Acknowledgments. The authors wish to thank the PDP and VCAP coinvestigators and other colleagues for their contributions to the instrumentations, mission operations, and data interpretation: L. Frank, D. Gurnett, N. D'Angelo, N. Stone, D. Reasoner, H. Brinton, H. Owens, D. Odem, T. Fraser-Smith, and N. Kawashima. This research is supported at the University of Iowa by NASA contract NAS8-32807, at Stanford University by NASA grant NAGW-235, and at Utah State University by NASA contract NAS5-24455.

REFERENCES

Annales de Geophysique. Special issue on the results of the active French-Soviet Araks experiments, *36*, 271–445, 1980.

Banks, P. M., W. J. Raitt, and W. F. Denig, Studies of beam-plasma interactions in a space simulation chamber using prototype space shuttle instruments, in *Artificial Particle Beams in Space Plasma Studies*, edited by B. Grandal, p. 393–404, Plenum, New York, 1982.

Banks, P. M., P. R. Williamson, and W. J. Raitt, Space shuttle glow observations, *Geophys. Res. Lett.*, *10*, 118–121, 1983.

Beghin, C., Plasma physics investigations on the first spacelab payload, *ESA J.*, *3*, 123, 1979.

Bernstein, W., H. Leinbach, H. Cohen, P. S. Wilson, T. N. Davis, T. Hallinan, B. Baker, J. Martz, R. Zeimke, and W. Huber, Laboratory observations of RF emissions at ω_{pe} and $(n + \frac{1}{2})\omega_{ce}$ in electron beam-plasma and beam-beam interactions, *J. Geophys. Res.*, *80*, 4375–4379, 1975.

Bernstein, W., H. Leinbach, P. J. Kellogg, S. J. Monson, and T. Hallinan, Further laboratory measurements of the beam plasma discharge, *J. Geophys. Res.*, *84*, 7271–7278, 1979.

Bernstein, W., P. J. Kellogg, S. J. Monson, R. H. Holzworth, and B. A. Whalen, Recent observations of beam plasma interactions in the ionosphere and a comparison with laboratory studies of the beam plasma discharge, in *Artificial Particle Beams in Space Plasma Studies*, edited by B. Grandal, pp. 35–64, Plenum, New York, 1982.

Cartwright, D. G., and P. J. Kellogg, Observations of radiation from an electron beam artifically injected into the ionosphere, *J. Geophys. Res.*, *79*, 1439–1457, 1974.

Dechambre, M., G. A. Gusev, Yu. V. Kushnerevsky, J. Lavergnat, R. Pellat, S. A. Pulinets, V. V. Selegel, and I. A. Zhulin, High frequency waves during the Araks experiments, *Ann. Geophys.*, *36*, 333–340, 1980*a*.

Dechambre, M., Yu. V. Kushnerevsky, J. Lavergnat, R. Pellat, S. A. Pulinets, and V. V. Selegel, Waves observed by the Araks experiments: The whistler mode, *Ann. Geophys.*, *36*, 341–350, 1980*b*.

Dechambre, M., J. Lavergnat, and R. Pellat, Waves observed by the Araks experiments: The VLF range, *Ann. Geophys.*, *36*, 351–359, 1980*c*.

Denig, W. F., Wave and particle observations associated with the beam plasma discharge in a space simulation chamber, Ph.D. thesis, Utah State Univ., Logan, 1982.

Grandal, B. (Ed.), *Artificial Particle Beams In Space Plasma Studies*, Plenum, New York, 1982.

Grandal, B., J. A. Holtet, J. Trim, B. Maehlum, and B. Pran, Observations of waves artificially stimulated by an electron beam inside a region with auroral precipitation, *Planet Space Sci.*, *28*, 1131–1145, 1980.

Harker, K. J., and P. M. Banks, Radiation from pulsed electron beams in space plasmas, *Radio Sci.*, this issue.

Holzworth, R. H., and H. C. Koons, VLF emissions from a modulated electron beam in the auroral ionosphere, *J. Geophys. Res.*, *86*, 853–857, 1981.

Holzworth, R. H., W. B. Harbridge, and H. C. Koons, Plasma waves stimulated by electron beams in the lab and in the auroral ionosphere, in *Artificial Particle Beams in Space Plasma Studies*, edited by B. Grandal, pp. 381–391, Plenum, New York, 1982.

Inan, U. S., M. Pon, P. M. Banks, P. R. Williamson, W. J. Raitt, and S. D. Shawhan, Modulated beam injection from the space shuttle during magnetic conjunctions of STS 3 with the DE 1 satellite, *Radio Sci.*, this issue.

Jost, R. J., H. R. Anderson, W. Bernstein, and P. J. Kellogg, Radial dependence of HF wave field strength in the BPD column, in *Artificial Particle Beams in Space Plasma Studies*, edited by B. Grandal, pp. 431–437, Plenum, New York, 1982.

Kellogg, P. J., and S. J. Monson, Further studies of auroral roar, *Radio Sci.*, this issue.

Monson, S. J., and P. J. Kellogg, Ground observations of waves at 2.96 MHz generated by an 8- to 40-keV electron beam in the ionosphere, *J. Geophys. Res.*, *83*, 121–131, 1978.

Monson, S. J., P. J. Kellogg, and D. G. Cartwright, Whistler mode plasma waves observed on Electron Echo 2, *J. Geophys. Res.*, *81*, 2193–2199, 1976.

Neupert, W. M., et al., Science on the space shuttle, *Nature*, *296*(5854), 193–197, 1982.

Obayashi, T., et al., Space experiments with particle accelerators (SEPAC), in *Artificial Particle Beams in Space Plasma Studies*, edited by B. Grandal, pp. 659–671, Plenum, New York, 1982.

Papadopoulos, K., On the shuttle glow (the plasma alternative), *Radio Sci.*, this issue.

Raitt, W. J., P. M. Banks, W. F. Denig, and H. R. Anderson, Transient effects in beam-plasma interactions in a space simulation chamber stimulated by a fast pulse electron gun, in *Artificial Particle Beams In Space Plasma Studies*, edited by B. Grandal, pp. 405–418, Plenum, New York, 1982.

Shawhan, S. D., Description of the plasma diagnostics package (PDP) for the OSS-1 shuttle mission and JSC chamber test in conjunction with the fast pulse electron gun (FPEG), in *Artificial Particle Beams In Space Plasma Studies*, edited by B. Grandal, pp. 419–430, Plenum, New York, 1982.

Shawhan, S. D., G. B. Murphy, and J. S. Pickett, Data users guide to plasma diagnostics package survey slides, *Rep. ID 82-022A-01A*, U.S. Natl. Space Sci. Data Center, Goddard Space Flight Center, Greenbelt, Md., 1983*a*.

Shawhan, S. D., J. L. Burch, and R. W. Fredricks, Subsatellite studies of wave, plasma and chemical injections from Spacelab, *J. Spacecr. Rockets*, *20*, 238–244, 1983*b*.

Shawhan, S. D., G. B. Murphy, and J. S. Pickett, Plasma diagnostics package initial assessment of the shuttle orbiter plasma environment, *J. Spacecr. Rockets*, in press, 1984*a*.

Shawhan, S. D., G. B. Murphy, and D. L. Fortna, Measurements of electromagnetic interference on OV102 Columbia by the plasma diagnostics package, *J. Spacecr. Rockets*, in press, 1984*b*.

Stix, T. H., *Theory of Plasma Waves*, McGraw-Hill, New York, 1962.

Winckler, J. R., The application of artificial electron beams to magnetospheric research, *Rev. Geophys. Space Phys.*, *18*, 659–682, 1980.

P. M. Banks and P. R. Williamson, STAR Laboratory, Stanford Electronics Laboratory, Stanford University, Stanford, CA 94305.

G. B. Murphy and S. D. Shawhan, Department of Physics and Astronomy, University of Iowa, Iowa City, IA 52242.

W. J. Raitt, Center for Atmospheric and Space Sciences, Utah State University, Logan, UT 84322.

Radio Science, Volume 19, Number 2, Pages 487–495, March–April 1984

Modulated beam injection from the space shuttle during magnetic conjunctions of STS 3 with the DE 1 satellite

U. S. Inan, M. Pon, P. M. Banks, and P. R. Williamson

Space, Telecommunications and Radioscience Laboratory, Stanford University

W. J. Raitt

Center for Atmospheric and Space Sciences, Utah State University

S. D. Shawhan

Department of Physics and Astronomy, University of Iowa

(Received May 4, 1983; accepted September 13, 1983.)

An electron beam emitted from the Office of Space Sciences 1 pallet on STS 3 was pulsed with specially designed very low frequency (VLF) formats in an attempt to generate whistler mode waves. Modulated operations of the beam emitted by a fast pulse electron generator (FPEG) were initiated during times of magnetic conjunctions between STS 3 and the high-altitude DE 1 satellite equipped with broadband VLF receivers. Coordinated FPEG/VLF modulation and DE 1 wideband data acquisition were achieved in 12 different cases. No evidence of any waves generated by FPEG were detected on the DE 1 analog wideband data. However, it is shown that in all of the cases, either the STS 3 attitude was such that the emitted electrons struck the main body of the vehicle, or it was not possible for whistler mode waves to propagate from the STS 3 location up to the vicinity of the DE 1 satellite.

1. INTRODUCTION

In the last 14 years there have been more than 20 experiments involving the emission of particle beams from rockets and satellites. In addition there have been supporting experiments in large vacuum chambers (Bernstein et al., 1975, 1978, 1979; Banks et al., 1982; Raitt et al., 1982).

The space-borne particle beam experiments have been mainly directed at studies to produce artificial aurorae such as the Precede and Excede programs (O'Neil et al., 1978, 1982); to study magnetic and electric reflection such as the Echo program (Winckler, 1975, 1980, 1982) and Polar program (Maehlum et al., 1980); and a combination of the two studies in the Artificial Radiation and Auroras Between Kerguelen and the Soviet Union (ARAKS) (Cambou et al., 1980) and Kaui (Davis et al., 1980) programs.

Paper number 3S1515.
0048-6604/84/003S-1515$08.00

Experiments on wave stimulation have been mainly limited to excitation of electrostatic waves due to the beam plasma interaction. These experiments on satellites include EXOS-B (Kawashima et al., 1982), SCATHA (Koons and Cohen, 1982) and ISEE-1 (Lebreton et al., 1982). Some experiments on sounding rockets have included beam modulation in the VLF range (Bernstein et al., 1982; Holzworth et al., 1982).

In this paper we report on modulated beam experiments performed on a recent flight of the space shuttle when attempts were made to detect waves propagating from the space shuttle to a magnetically linked satellite as a result of pulsing an electron gun at frequencies in the VLF range. The experiments were carried out successfully, but positive results were not obtained in the sense that no evidence of any beam-generated signals was observed on the satellite receivers. Although in this sense our results do not advance the state of knowledge, we have found it valuable to publish them as a primer for future efforts.

As part of the Vehicle Charging and Potential (VCAP) Experiment, the oFfice of Space Sciences (OSS 1) pallet on the third flight of the space shuttle (i.e.,

Space Transportation System (STS) 3) included a fast pulse electron generator (FPEG) [Neupert et al., 1982; Banks et al., 1983]. This instrument was capable of emitting a 100-mA beam of nearly monoenergetic 1-keV electrons. The pulse duration of the beam was adjustable from 600 ns (1.6 MHz) to 109 s ($\sim$0.01 Hz) under programmable microprocessor control. While the primary functional objective of the FPEG instrument was to change the electrical potential of the orbiter for vehicle charging experiments, the capability of pulsing the beam over a wide range of frequencies presented an opportunity for investigating the effectiveness of a pulsed electron beam in generating electromagnetic radiation . For this purpose a number of modulation sequences were preprogramed for pulsing the beam at frequencies up to 1 MHz. The primary instrument for detecting the possible radiation from the beam was the plasma diagnostic package (PDP) on the OSS 1 pallet [Neupert et al., 1983; Shawhan et al., this issue]. Even though the PDP instrument was on occasion moved away from the pallet using the remote manipulator system, it was at all times within $\sim$20 m of the electron generator. Thus, in most cases, the PDP sensors were well within the "near" field in terms of any electromagnetic radiation that would be generated by the electron beam.

In order to assess the feasibility of using electron beams for generating electromagnetic waves that would propagate away from the orbiter, a coordinated experiment attempting to detect the beam-generated radiation at ground-based sites and on existing free-flying satellites was conceived. Of particular interest for these experiments was the possibility of using the beam for radiating waves in the ELF/VLF frequency range. Several ground-based observatories with broadband VLF receivers were used for this purpose. While no obvious evidence of beam-induced radiation was observed, detailed analysis of the ground site overpasses of STS 3 is not complete and will be reported separately.

In terms of free-flying satellites, the Dynamics Explorer 1 (DE 1) satellite launched in 1981 [Hoffman, 1981] equipped with a broadband VLF receiver (Shawhan et al., 1981) presented a suitable platform for space observations. Thus, during the flight of STS 3 in March 1982, coordinated FPEG modulation and DE 1 observations were arranged during times of magnetic conjunctions of the two spacecraft. In this paper we report on the results of these experiments. To our knowledge they represent the first coordinated experiment of this type involving two spacecraft with independent orbits. In addition to the obvious constraint involving the spacecraft orbits and the geometry of the geomagnetic field, the experiments were further complicated by the fact that the DE 1 broadband VLF data could only be acquired with real-time telemetry by NASA ground stations around the globe, the same stations that were heavily involved in tracking and commanding the space shuttle (STS 3). In addition, the commands for the initiation of FPEG operation during magnetic conjunctions with DE 1 had to be uplinked to STS 3 in real time since, due to the uncertainty of the launch time of STS 3, the conjunctions could not be determined until after launch.

Since none of the preprogramed FPEG modulation sequences of the VCAP experiments was suitable for the STS 3/DE 1 experiments, special VLF beam modulation formats were designed and uplinked to the VCAP control microprocessor after launch. On DE 1, the wideband analog receiver operating in the 3 to 6-kHz range was used due to the need for high time resolution as well as for identification of any beam-induced radiation in the midst of a highly variable natural VLF background.

Coordinated FPEG VLF operations were also attempted during magnetic conjunctions of STS 3 with other satellites, namely the International Sun-Earth Explorer 1, 2 (ISEE 1, 2) and the ISIS 1, 2 satellites. Due to the orbital configuration of these spacecraft, very few conjunctions with STS 3 were physically possible. Also due to various operational constraints the acquisition of the satellite data in the desired modes was not possible in most of these conjunctions. For this reason, we limit our discussion in this paper to the STS 3/DE 1 experiments.

In the following we first describe the modulation formats and criteria used for determining the magnetic conjunctions of the two spacecraft. We then present the results of the experiments and ray-tracing computations to determine whether any waves generated at the location of STS 3 would be expected to reach the satellite. Finally, we present our conclusions and discuss the implications of the results for future experiments.

2. DESCRIPTION OF THE EXPERIMENT

In this section we discuss the DE 1 satellite instrumentation, the VLF modulation format for FPEG, and the criteria used for magnetic conjunctions of the two spacecraft. The FPEG instrumentation is described elsewhere [Banks et al., 1983] and is not repeated here.

DE 1 wave receiver description

The Stanford University linear wideband receiver (LWR) is integrated into the plasma wave instrument (PWI) on DE 1 [Shawhan et al., 1981; Inan and Helliwell, 1982]. The receiver measures the wave magnetic or electric field intensity and spectra selectively over the range of frequencies 1.5-3, 3-6, and 10-16 kHz. The LWR can be connected to a magnetic loop or a long electric dipole or it can be commanded to cycle between the two. For the STS 3/DE 1 experiments reported in this paper, the 3 to 6-kHz wide-band channel connected to the primary magnetic loop antenna with a threshold sensitivity of 6×10^{-7} $\gamma/\mathrm{Hz}^{1/2}$ at 6 kHz was used. The gain of the LWR can be set at 10-dB steps over a 70-dB range and can be varied automatically or can be commanded to remain at a fixed level. In the automatic mode that was used for the STS 3/DE 1 experiments, the gain is updated every 8 s. The receiver response is linear over a 30-dB dynamic range at any gain setting, thus facilitating accurate measurements of

signal intensity and temporal growth rate. Also, the fact that the gain level remains fixed for 8 s enables the identification of relatively weaker signals in a background of much stronger but short-duration natural signals such as lightning-generated whistlers and emissions.

The plasma wave instrument on DE 1 is also equipped with a wide-band receiver with automatic gain control over the frequency range 650 Hz to 10 kHz or 40 kHz. This receiver was not used in the present experiments since weaker signals would be suppressed by the relatively intense plasmaspheric hiss that is usually observed below 1 kHz. DE 1 wave data were also acquired using the digital output sweep frequency receiver (SFR), also part of PWI. The SFR has a 32 s time resolution and is thus not expected to be useful in detecting the VLF modulation format used for pulsing FPEG.

FPEG VLF modulation format

The VLF modulation format that was used to pulse FPEG during its magnetic conjunctions with DE 1 is shown in Figure 1. The format consists of frequency shift keying between two frequencies, 3.25 and 4.873 kHz, both within the 3 to 6 kHz band of the LWR on DE 1. Due to the fact that a fixed number of pulses (32K) was used for FPEG at any pulsing frequency, the duration of the modulation at the two frequencies is different. The main cycle of the FPEG/VLF format typically lasted ~ 92 s.

Magnetic conjunctions

A "magnetic" conjunction between the two spacecraft was assumed to occur when either of the two conjugate magnetic "footprints" of DE 1 was within 1500 km of an STS 3 footprint. In order to estimate the footprint, the orbital parameters of the spacecraft were used in conjunction with an Olson-Pfitzer model of the earth's magnetic field [Olson and Pfitzer, 1974]. With the criterion adopted here a typical STS 3/DE 1 conjunction lasted 4-5 min.

A computer code that computes the magnetic conjunctions of any two earth- orbiting spacecraft was developed at Stanford University for the purpose of the STS 3/DE 1 experiments. The inputs to the code are the state vectors (i.e., spatial and velocity components at a given time) of the two spacecraft and the distance criteria for defining a conjunction (in this case 1500 km). The output is a listing of the possible conjunctions in the specified time period and the orbital parameters of the two vehicles at the time of conjunction. Since the STS 3 orbit was not precisely known until after launch, the determination of the conjunctions was done after the launch of STS 3. Furthermore, the conjunction estimates were periodically updated as STS 3 orbit parameters changed slightly due to attitude maneuvers.

In the next section we present the results of the experiments and ray-tracing analysis to determine whether any FPEG-induced waves would be expected to propagate up to the location of the DE 1 satellite.

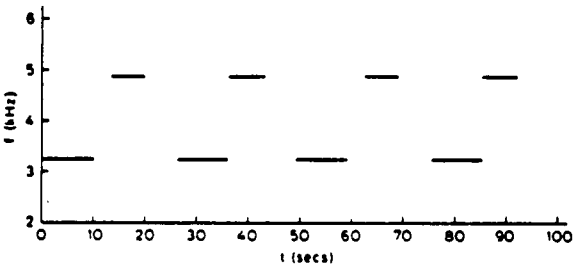

Fig. 1. The FPEG/VLF modulation format used in the STS 3/DE 1 experiments. The format consists of frequency shift keying between 3.25 and 4.873 kHz.

3. RESULTS

With the 1500-km criterion that was adopted for determining the magnetic conjunctions, in all there were 43 possible conjunctions during the flight of STS 3. Of these, the FPEG/VLF modulation sequences were utilized for 17 cases, whereas DE 1 wide-band data were acquired in 24 of the 43 possible conjunctions. The number of cases where both FPEG/VLF format was used and DE 1 data were acquired was 12. The various parameters of these cases are listed in Table 1. Shown in this table are the locations of STS 3 and DE 1 at the time of closest approach during the conjunction, the beam pitch angle and whether or not the beam escaped the vehicle (see below).

Beam pitch angle and PDP observations

In order to assess the effectiveness of the emitted electron beam for radiating whistler mode waves, it is first necessary to determine the beam voltage and pitch angle, modulation frequency and polar angle of observation with respect to the geomagnetic field [Harker and Banks, this issue]. Since the size of the STS 3 vehicle is comparable to the gyroradius of the ~ 1-keV electron beam, the emitted electron beam can collide with the vehicle for certain pitch angle ranges.

A computer code was developed at Utah State University that uses the in-orbit attitude information for STS 3 in a model of the earth's magnetic field to determine not only the pitch angle of the beam at any given time but also whether or not the beam collided back onto the vehicle [Sojka et al., 1980]. For the case in hand, it was determined that in 11 of the 13 cases the emitted electron beam collided with the vehicle within one gyroradius and thus did not move away from the vehicle. This was confirmed with the measurement of the termination of the ~ 1-keV electron flux observed by the PDP [Shawhan et al., this issue].

While the radiation characteristics of a pulsed electron beam are not well known, the radiated electromagnetic field intensity is proportional to the physical length of the nondispersed portion of the beam [Harker and Banks, this issue]. Thus, it is expected that the fields radiated by a beam that does not leave

TABLE 1. Magnetic Conjunctions of STS 3 and DE 1 Satellites

Number	GMT dd/hhmm:ss	STS 3 Dipole Latitude	STS 3 Dipole Longitude	DE Dipole Latitude	Closest Footprint Distance	Pitch	Beam Escape
2	083/1630:59	-47.54	2.27	20.74	803.00	70.65	no
4	083/2059:08	-40.73	1.80	-13.97	879.50	71.06	no
5	083/2225:59	-32.76	1.46	-19.00	1177.60	66.20	no
17	085/1308:27	-43.94	2.00	-65.74	1141.10	76.43	no
20	085/1732:57	-46.89	2.22	40.18	875.40	68.70	no
22	085/2203:59	-38.14	1.68	13.05	1033.40	85.36	no
25	086/1117:31	-40.53	1.79	2.80	821.40	55.39	no
26	086/1252:54	-46.51	2.19	19.73	703.90	77.75	no
27	086/1425:45	-47.04	2.23	-48.00	818.80	76.60	no
29	086/1849:58	43.50	1.97	8.11	792.80	69.21	no
32	087/0939:30	-39.96	1.76	30.84	1402.30	149.27	possible
33	087/1109:30	-43.94	2.00	57.79	1178.40	149.68	possible

the immediate vicinity of the vehicle will be lower in intensity than those that would be radiated by a beam that propagates away. Data from the plasma diagnostic package (PDP) on the OSS 1 pallet for 4 of the 12 cases in Table 1 showed that both electric and magnetic fields were associated with the FPEG operation times discussed here. While these exhibited signatures of the FPEG-induced VLF modulation, such observations in the close vicinity of the beam cannot easily be used to determine whether or not any propagating waves were generated by the electron beam [Shawhan et al., this issue].

Ray-tracing analysis

Since the physical distance between DE 1 and STS 3 varied greatly during the magnetic conjunctions, ray-tracing analysis has been done to determine whether any VLF waves that might be generated at the location

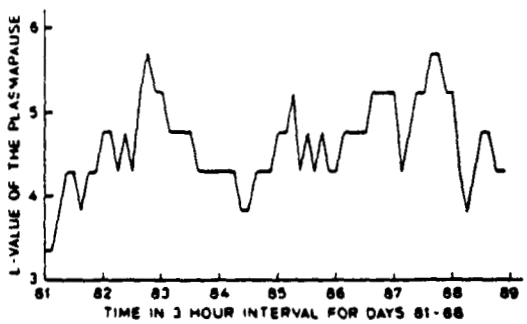

Fig. 2. The approximate L value of the plasmapause during the STS 3 mission estimated using the criteria, $L_p \simeq 5.7 - 0.47Kp$ where Kp is the maximum value of the Kp index in the preceding 12 hours [Carpenter and Park, 1973].

of STS 3 could propagate to DE 1. Here we present sample ray-tracing analyses representative of the conditions for the 12 cases listed in Table 1.

Theoretical analysis of modulated electron beam-induced radiation shows that the beam is expected to radiate waves over a broad frequency range, but with maxima at the modulation frequency and at the condition where the derivative of the ray angle with frequency is zero [Harker and Banks, this issue]. In our ray-tracing calculations, we have used initial wave normals $\psi < \pm\psi_r$, where ψ_r is the local resonance cone angle and where the wave propagation direction for $\psi = 0$ is the direction opposite to the motion of the electron beam.

Propagation paths of whistler mode waves in the magnetosphere are governed by the gradients of the static magnetic field and the cold plasma density in the anisotropic medium within which the rays are refracted. As the density model we have assumed a diffusive equilibrium model of the cold plasma density inside the plasmasphere and an r^{-4} model outside the plasmapause [Angerami and Carpenter, 1966]. For the static magnetic field a centered dipole approximation is used [*Helliwell*, 1965]. To determine the location of the plasmapause we have used an approximate criterion given by Carpenter and Park, [1973], i.e., that the L value of the inner edge of the plasmapause is given by $L_p \simeq 5.7 - 0.47Kp$ where Kp is the maximum Kp in the preceding 12 hours. Figure 2 shows a plot of L_p as a function of time during the STS 3 mission. According to this plot, the plasmapause during this period was in the range L_p=4 to 5.

To compute the ray paths, we have used the Stanford University VLF ray-tracing program described by Burtis, [1974]; and Inan and Bell, [1977]. Figure 3 shows the equatorial cold plasma density profile for

which the ray paths were determined. The plasmapause location was taken to be $L_p = 4.5$.

Figure 4 shows typical ray trajectories in a magnetic meridional plane for a wave frequency $f = 4$ kHz propagating inside the plasmasphere. We have chosen 4 kHz since it is roughly the average of the two discrete frequencies used in the FPEG/VLF format. As the injection latitude we have taken $\lambda_m = -45°$, again representative of the average λ_m for the STS 3 locations during the conjunctions listed in Table 1. Also shown in Figure 4 are the locations of the DE 1 satellite during the same 12 conjunctions as identified by the conjunction numbers. The trajectories shown are for rays with wave normals $\psi < \pm\psi_r$ and spaced at 10° intervals injected at the STS 3 altitude ($\sim$240km). The dashed lines indicates the $L = 4.5$ field line.

The ray paths shown in Figure 4 indicate that in 10 of the 12 cases listed in Table 1, it was not possible for any VLF waves generated in the vicinity of STS 3 to reach the location of the DE 1 satellite. In these cases, the DE 1 satellite was typically outside the plasmapause and at too high a latitude or altitude to be intercepting waves generated at the STS 3 location with any initial wave normal. For example, in the two cases where the electron beam did leave the vehicle (conjunctions 32 and 33) the satellite was too far north at latitudes $\lambda_m >$ 30°. In the cases of conjunctions 4 and 25, the satellite position was within reach of any FPEG-generated waves with initial wave normals in the range. However, as seen in Table 1, in both cases the FPEG-generated electrons collided with the main body of the STS 3 vehicle within one gyroradius.

DE 1 linear wideband receiver data

In this section we show sample wave data acquired on DE 1 using the LWR during conjunction 4, one of the two conjunctions when the DE 1 satellite is believed to have been within the plasmasphere. Figure 5 shows frequency-time spectra in the 2 to 7-kHz range (the nominal receiver bandwidth in the mode used was 3 to 6-kHz) at two different times, both within a minute of the time of closest "magnetic" approach of STS 3 and DE 1 at 2059:08 UT on March 24, 1982. The top panel shows lightning-generated whistlers that may have arrived at the satellite through direct or reflected paths [Edgar, 1976], much like those shown in Figure 4. In this case, however, the lightning-generated impulses must have entered the magnetosphere at magnetic latitudes higher than the $\lambda_m = \pm 45°$ used to represent the injection point of any FPEG-induced waves. The presence of whistlers with distinctly different dispersion indicates that they arrive at the satellite on at least two different paths. Also, the whistlers may be generated by different lightning flashes in the two hemispheres.

The second panel shows similar spectra except for a noise burst that is observed beginning at $\sim$2059:52 UT. The "bullet shaped" front end of the noise burst is consistent with a distant generation region and dispersion

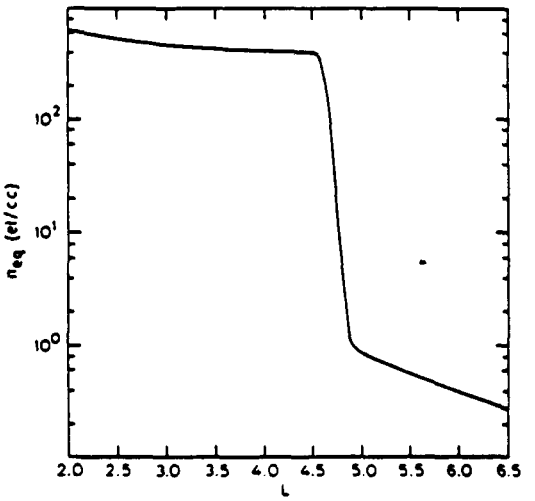

Fig. 3. The equatorial cold plasma density profile used for the ray-tracing calculations.

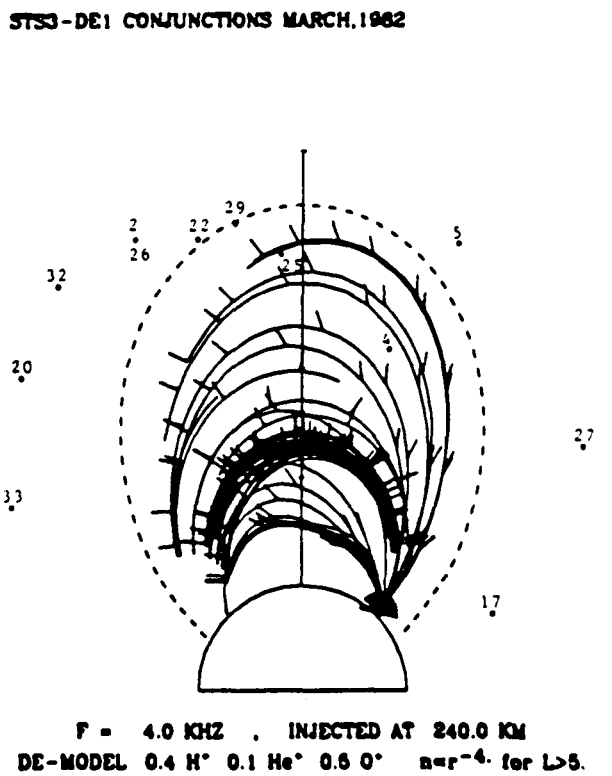

Fig. 4. Ray paths for $f = 4$ kHz rays injected at a geomagnetic latitude of $\lambda_m \simeq -45°$ with the cold plasma model being as shown in Figure 3. Rays with initial wave normals between $-\psi_r$ and $+\psi_r$ at 10° spacings are shown. Also shown are the locations of the DE 1 satellite during the 12 conjunctions of Table 1.

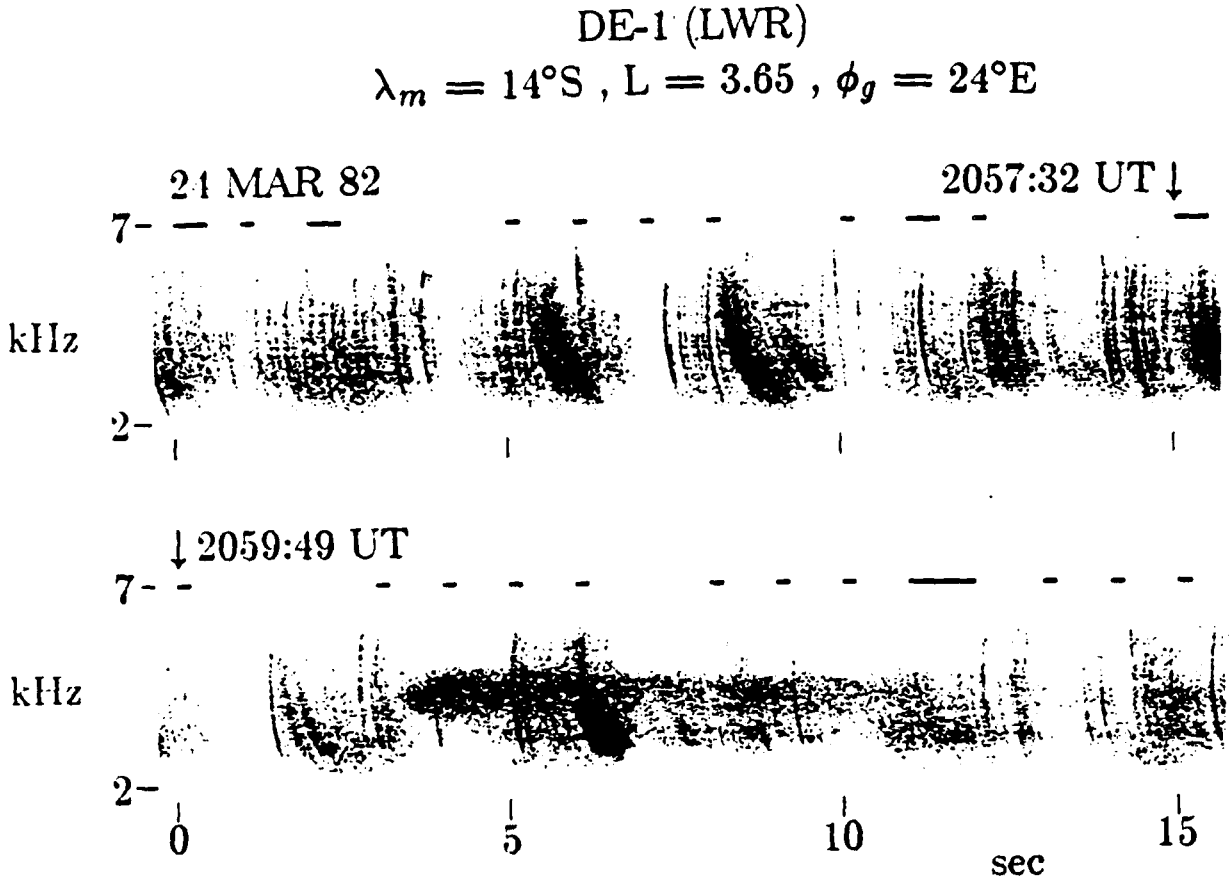

Fig. 5. Example of DE 1 LWR data acquired during conjunction 4 on March 24, 1982. The upper panel shows lighting generated whistlers with distinctly different dispersion. The lower panel shows the same plus a noise burst observed at 2059:52 UT. The tail end of this noise burst lasted until 2100:15 UT.

along the path of propagation from there to the satellite. The characteristics and the frequency range (~ 3-5 kHz) of this event warrant consideration for possible generation by FPEG/VLF modulation. However, the timing of the burst observation seems to rule out this possibility. According to the STS 3/OSS 1 data, the FPEG was pulsed with a VLF format between 2059:08 to 2059:40 UT, and no electrons were emitted from 2059:40 to 2100:10 UT. Since the one-hop whistler mode time delay on the field lines $L < 4$ inside the plasmasphere is typically 2-5 s, it does not seem possible that a noise burst like the one shown, observed over times that are 12 to 24 s after the time at which the FPEG was turned off, could be induced by the emitted electron beam. In fact, the tail end of the noise burst lasted up to 2100:15 UT, well beyond the time corresponding to the rightmost edge of the bottom panel of Figure 5. Also, observation of natural noise bursts of the kind shown in Figure 5 is not uncommon [Dingle and Carpenter, 1981].

Thus, there seems to be no conclusive evidence that any FPEG-induced waves were observed by the DE 1/LWR during conjunction 4, consistent with the fact that, as shown in Table 1, the emitted electron beam did not leave the immediate vicinity of the STS 3 vehicle during this magnetic encounter. While we have not shown DE 1 LWR data acquired during the rest of the 12 conjunctions of Table 1, we note here that no significant wave activity was observed in the 3 to 6-kHz band during most of these remaining 11 conjunctions. Since the satellite was outside the plasmapause during these times, no significant whistler activity was observed as would be expected [Carpenter et al, 1969]. Observations of chorus emissions during some of these conjunctions were also consistent with earlier satellite observations outside the plasmapause [Burtis and Helliwell, 1975].

During most of the 12 conjunctions the 3 to 6-kHz spectra were very quiet and uniform with no detectable wave activity.

4. SUMMARY AND DISCUSSION

In summary, we conclude that no detectable evidence of any FPEG-induced waves were observed on the DE 1 satellite. However, it should be noted *there were no cases where the* STS 3/DE 1 experiments were optimally carried out in the sense of emitting an electron beam that propagates away from the vehicle during a conjunction where it is possible for beam-induced waves to propagate up to the satellite location. Thus, the results from the STS 3/DE 1 experiments are essentially inconclusive; in other words, we cannot, on the basis of these experiments, determine whether or not an electron beam with the characteristics of FPEG (in terms of current level and modulation frequencies) can generate electromagnetic radiation in the form of propagating whistler mode waves at a level detectable by presently available satellite based wave receivers. This determination would be an important goal of future experiments involving space-based electron generators such as those planned for Spacelab 1 and 2 and ground- or satellite-based wave receivers.

In the immediate future, there exist at least two opportunities for carrying out experiments similar to those reported in this paper. The flight of Spacelab 1 (STS 9) in September 1983 will carry the Space Experiments with Particle Accelerators (SEPAC) package, involving an electron generator that can emit a 1.7-A beam of ~7-keV electrons, thus operating at >50 times higher power level than the FPEG. While the modulation capability of SEPAC is limited, a 5-kHz pulsing frequency is planned to be used in an attempt to generate electromagnetic waves. In addition, the OSS 1 VCAP experiment is scheduled to be flown again on Spacelab 2 in March 1985 with the plasma diagnostic package (PDP). In this flight the PDP will be released from the orbiter, permitting it to measure any FPEG-generated radiation at distances of many wavelengths from the vehicle.

In both the Spacelab 1 and 2 experiments, the potential also exists for coordinated experiments with existing free-flying satellites as well as ground stations equipped with wave receivers. The criteria used for defining a magnetic conjunction in such experiments should be chosen in the light of the ray-tracing result given in Figure 4. While the criterion outlined in section 2 above was utilized for STS 3/DE 1 experiments in order to reduce the number of conjunctions in the limited time available, other criteria may also be used. For example, while it is important for the two satellites to be close in geomagnetic longitude, the nonducted ray paths of Figure 4 indicate that closeness in latitude is not that critical. In fact, almost any latitude to the north of the STS 3 location in Figure 4 would have been satisfactory for the case shown.

Acknowledgments. The STS 3/DE 1 experiments, representing the first active coordinated experiment of its kind involving two spacecraft with independent orbits, could not have been carried out without the help and cooperation of many people. These experiments were conceived of only a few months prior to the STS 3 mission, and the fact that data were successfully acquired is a tribute to the many people involved and especially the project personnel at Goddard Space Flight Center and the payload support team at the Johnson Space Center who made it possible to carry out active real-time scientific experiments in space. In addition, we would like to acknowledge the major effort made by C. Gustafson of the Dynamics Explorer project for his help in acquiring the DE 1 wide-band analog data. The support provided by the personnel in the Orbiting Satellites Division of the Goddard Space Flight Center in providing up-to-date state vectors for the DE 1 and ISEE 1 satellites is also appreciated. For their help in carrying out the FPEG experiments we acknowledge the support we have received from Jack Sevier and other personnel of the Universities Space Research Associations' Lunar and Planetary Laboratory in Houston, Texas. For developing, building and testing the FPEG we acknowledge the contributions of A. B. White of Utah State University. We also acknowledge discussions we have held with our colleagues in the STAR Laboratory. The STS 3/DE 1 experiments were supported by the National Aeronautics and Space Administration under contract NAS-25688 for DE 1 data acquisition and analysis (U. S. I.), under contracts NAS5-24455 at Utah State University and NAGW-225 at Stanford University for VCAP experiments and data analysis (M. P., P. M. B., P. R. W., W. J. R.) and under contract NAS8-32807 for PDP operations and data analysis (S. D. S.).

REFERENCES

Angerami, J. J., and D. L. Carpenter, Whistler studies of the plasmapause in the magnetosphere, 2, Equatorial density and total tube electron content near the knee in magnetospheric ionization, *J. Geophys. Res.*, *71(9)*, 711, 1966.

Banks, P. M., W. J. Raitt, and W. F. Denig, Studies of beam-plasma interactions in a space simulation chamber using prototype space shuttle instruments, in *Artificial Particle Beams in Space Plasma Studies*, edited by B. Grandal, Plenum, New York, 393, 1983.

Bernstein, W., et al., Laboratory observations of RF emissions at ω_{pe} and $(n + 1/2)\omega_{ce}$ in electron- beam-plasma and beam-beam interactions, *J. Geophys. Res.*, *80*, 4375, 1975.

Bernstein, W., et al., Electron beam experiments: The beam plasma discharge at low pressures and magnetic field strengths, *Geophys. Res. Lett.*, *5*, 127, 1978.

Bernstein, W., H. Leinbach, P. J. Kellogg, S. J. Monson, and T. Hallinan, Further laboratory measurements of

the beam plasma discharge, *J. Geophys. Res., 84*, 7271, 1979.

Bernstein, W., P. J. Kellogg, S. J. Monson, R. H. Holzworth, and B. A. Whalen, Recent observations of beam plasma interactions in the ionosphere and a comparison with laboratory studies of the beam plasma discharge, in *Artificial Particle Beams in Space Plasma Studies*, edited by B. Grandal, 35-64, Plenum, New York, 1982.

Burtis, W. J. *User's Guide to the Stanford VLF Ray Tracing Program*, Radioscience Laboratory, Stanford Electronics Laboratories, Stanford University, Stanford, Calif., 1974.

Burtis, W. J., and R. A. Helliwell, Magnetospheric chorus: Amplitude and growth rate, *J. Geophys. Res., 80*(22), 3265, 1975.

Cambou, F., V. S. Dokoukine, J. Lavergnat, R. Pellat, H. Reme, A. Saint-Marc, R. A. Sagdeev, and I. A. Zhuline, General description of the ARAKS experiments, *Ann. Geophys., 36*, 271, 1980.

Carpenter, D. L., and C. G. Park, On what ionospheric workers should know about the plasmapause-plasmasphere, *Rev. Geophys. Space Phys., 11*, 133, 1973.

Carpenter, D. L., C. G. Park, H. A. Taylor, Jr., and H. C. Brinton, Multi-experiment detection of the plasmapause from EOGO satellites and Antarctic ground stations, *J. Geophys. Res., 74*(7), 1848, 1969.

Davis, T. N., W. N. Hess, M. C. Trickel, E. M. Wescott, T. J. Hallinan, H. C. Steinbaek-Nielsen, and E. J. R. Maier, Artificial aurora conjugate to a rocket-borne electron accelerator, *J. Geophys. Res., 85*, 1722, 1980.

Dingle, B., and D. L. Carpenter, Electron precipitation induced by VLF noise bursts at the plasmapause and detected at conjugate ground stations, *J. Geophys. Res., 86*, 2286, 1981.

Edgar, B. C., The upper and lower frequency cutoffs of magnetospherically reflected whistlers, *J. Geophys. Res., 81(1)*, 205, 1976.

Harker, K. J., and P. M. Banks, Radiation from pulsed electron beams in space plasmas, submitted to *Radio Sci.*, this issue.

Helliwell, R. A. *Whistlers and Related Ionospheric Phenomena*, Stanford University Press, Stanford, Calif., 1965.

Hoffman, R. A. (Ed., Dynamics Explorer, *Space Sci. Instrum. 5(4)*, 1981.

Holzworth, R. H., W. B. Harbridge, and H. C. Koons, Plasma waves stimulated by electron beams in the lab and in the auroral ionosphere, in *Artificial Particle Beams in Space Plasma Studies*, edited by B. Grandal, p. 381, Plenum, New York, 1982.

Inan, U. S., and T. F. Bell, The plasmapause as a VLF waveguide, *J. Geophys. Res., 82(19)*, 2819, 1977.

Inan, U. S., and R. A. Helliwell, DE 1 observations of VLF transmitter signals and wave-particle interactions in the magnetosphere, *Geophys. Res. Lett., 9*, 563, 1982.

Kawashima, N., et al., Wave excitation in electron beam experiment on Japanese satellite "JIKIKEN (EXOS-B)", in *Artificial Particle Beams in Space Plasma Studies*, edited by B. Grandal, Plenum, New York, 101, 1982.

Koons, H. C., and H. A. Cohen, Plasma waves and electrical discharges stimulated by beam operations on a high altitude satellite, in *Artificial Particle Beams in Space Plasma Studies*, edited by B. Grandal, Plenum, New York, 1982.

Lebreton, J. P., R. Torbert, R. Anderson, and C. Harvey, Stimulation of plasma waves by electron guns on the ISEE-1 satellite, in *Artificial Particle Beams in Space Plasma Studies*, edited by B. Grandal, Plenum, New York, 1982.

Maehlum, B. N., et al., Polar-5 an electron accelerator experiment within an aurora. 1. Instrumentation and geophysical conditions, in *Planetary Space Science, 28* 259, 1980.

Neupert, W. M., et al., OSS-1: A pathfinder mission for space science science on the space shuttle, *Nature, 296*(5854), 193-197, 1982.

Olson, W. P., and K. A. Pfitzer, A quantitative model of the magnetospheric magnetic field, *J. Geophys. Res., 79*, 3739, 1974.

O'Neil, R. R., F. Bien, D. Burt, J. A. Sandock, and A. T. Stair, Jr., Summarized results of the artificial auroral experiment, PRECEDE, *J. Geophys. Res., 83*, 3273, 1978.

O'Neil, R. R., A. T. Stair, Jr., W. R. Pendleton, Jr., and D. A. Burt, The EXCEDE spectral artificial auroral experiment: An overview, in *Artificial Particle Beams in Space Plasma Studies*, edited by B. Grandal, Plenum, New York, 1982.

Raitt, W. J., P. M. Banks, W. F. Denig, and H. R. Anderson, Transient effects in beam-plasma interactions in a space simulation chamber stimulated by a fast electron gun, in *Artificial Particle Beams in Space Plasma Studies*, edited by B. Grandal, Plenum, New York, 1982.

Shawhan, S. D., D. A. Gurnett, D. L. Odem, R. A. Helliwell, and C. G. Park, The plasma wave and quasi-static electric field instrument (PWI) for Dynamics Explorer-A, *Space Sci. Instrum., 5*, 535, 1981.

Shawhan, S. D., G. B. Murphy, P. M. Banks, P. R. Williamson, and W. J. Raitt, Wave emissions from DC and modulated electron beams on STS 3, *Radio Sci.*, this issue.

Sojka, J. J., W. J. Raitt, and K. D. Hunt, Calculation of escape trajectories for particle beams emitted from spacecraft, report, Center for Atmospheric and Space Sciences, Utah State Univ. Logan, 1980.

Winckler, J. R., The application of artificial electron beams to magnetospheric research, *Rev. Geophys. Space Phys., 18*, 659, 1980.

Winckler, J. R., The use of artificial electron beams as probes of the distant magnetosphere, in *Artificial Particle Beams in Space Plasma Studies*, edited by

B. Grandal, Plenum, New York, 1982.
Winckler, J. R., R. L. Arnoldy, and R. A. Hendrickson, Echo #2: A study of electron beams injected into the high-latitude ionosphere from a large sounding rocket, *J. Geophys. Res., 80,* 2083, 1975.

P. M. Banks, U. S. Inan, M. Pon, and P. R. Williamson, Space, Telecommunications and Radioscience Laboratory, Stanford University, Stanford, CA 94305.

R. J. Raitt, Center for Atmospheric and Space Sciences, Utah State University, Logan, UT 84322.

S. D. Shawhan, Department of Physics and Astronomy, University of Iowa, Iowa City, IA 52242.

JOURNAL OF GEOPHYSICAL RESEARCH, VOL. 90, NO. A4, PAGES 3487-3497, APRIL 1, 1985

Effects of Chemical Releases by the STS 3 Orbiter on the Ionosphere

JOLENE S. PICKETT, GERALD B. MURPHY, WILLIAM S. KURTH, AND CHRISTOPH K. GOERTZ

Department of Physics and Astronomy, University of Iowa, Iowa City

STANLEY D. SHAWHAN

NASA Headquarters, Washington, D. C.

The Plasma Diagnostics Package, which was flown aboard STS 3 as part of the Office of Space Science first shuttle payload (OSS 1), recorded the effects of various chemical releases from the orbiter. Changes in the plasma environment were observed to occur during flash evaporator system releases, water dumps, and maneuvering thruster operations. During flash evaporator operations, broadband orbiter-generated electrostatic noise was enhanced, and plasma density irregularities ($\Delta N/N$) were observed to increase by 3–30 times with a spectrum which rose steeply and peaked below 6 Hz. Ions with energies up to several hundred eV were also observed during one flash evaporator operation. In the case of water dumps, background electrostatic noise was enhanced at frequencies below about 3 kHz and suppressed at frequencies above 3 kHz during the dump, and $\Delta N/N$ was also seen to increase by 5–6 times. Various changes in the plasma environment were effected by primary and vernier thruster operations, including increases in electron density by as much as 3 orders of magnitude, neutral pressure increases to as high as 10^{-4} torr from the nominal 10^{-7} torr, and perturbations in the spacecraft potential by several volts, particularly when measured in relation to the plasma potential in the wake. Thruster activity also stimulated electrostatic noise with a spectrum which peaked at approximately 0.5 kHz. In addition, ions with energies up to 1 keV were seen during some thruster events.

1. INTRODUCTION

Since the first space shuttle launch, in April of 1981, considerable interest has been generated in ionospheric modifications effected by the shuttle, both during launch and during orbital operations. The effects of rocket exhaust on the ionosphere have been studied and recorded in considerable detail since *Booker* [1961] first reported a local diminution in ionization density forming a hole through the *F* region associated with the firing of Vanguard II in 1959. A review of the findings to date, particularly with regard to large space systems, was given by *Rote* [1980] and included such environmental effects as plasma depletion, temperature change, and airglow excitation. A brief history of rocket-induced perturbations upon the upper atmosphere was also given by *Mendillo* [1980]. In addition, he described a method for assessing how the space shuttle's engines would affect the ionosphere in the vicinity of the engine burns. A review of the effects on the ionosphere due to the deliberate release of known quantities of highly reactive chemicals such as H_2O and CO_2 was given by *Pongratz* [1981]. The environmental impact on the *D* and *E* regions of the ionosphere of chronic discharges of water vapor from large rockets was investigated by *Forbes* [1980]. While most of the previously mentioned papers deal with large-scale chemical releases, whether planned releases for scientific study or whether released as a result of rocket transit through the ionosphere, shuttle-produced chemical releases, although much smaller by comparison, do perturb the environment near the shuttle. These perturbations tend to be more localized than the large-scale releases; however, they do affect the ambient ionosphere and therefore help us understand the effects of larger releases. On the other hand, it is important to understand the distinction between these two types of releases. The foregoing discussion of large-scale releases provides the impetus and background for studying the smaller shuttle-produced releases.

The purpose of this paper is to present observational evidence of ionospheric modification by using data taken by the Plasma Diagnostics Package (PDP) [*Neupert et al.*, 1982] during Space Shuttle orbiter chemical releases. The space shuttle is an ideal vehicle for experiments involving ionospheric modification. Not only does it initiate chemical releases, but it also provides the platform from which to monitor the effect of those releases. While not intended to be scientific ventures, the orbiter water dumps, flash evaporator system (FES) releases and thruster operations are, in effect, chemical releases. It is to be understood that the study of these effects is limited to the near vicinity of the orbiter and indeed to the gaseous and plasma envelope of the shuttle itself. However, the measurements of the effects should not be ignored simply because they cannot tell us what the end result of the release will be. The first few seconds of any release are very important in that many of the critical chemical reactions and kinetic effects happen during that time. By being in the bay of the shuttle near the point of release, the first few seconds of these releases can be studied in detail giving us a clue to the early chemistry that takes place in larger releases. An underlying theme of this paper is that orbiter operations produce effects which are measurable by a wide range of instruments. Hence, it is obvious that a potential shuttle experimenter should be aware of the nonambient nature of the ionosphere in close proximity to his or her detectors.

An outline of the paper is as follows: Section 2 contains STS 3 mission and operational considerations, including an overview of orbit and ionospheric characteristics, shuttle operations, and PDP instrumentation. The observations of the effects of flash evaporator system releases, water dumps, and thruster operations are presented in Section 3. Finally, some concluding remarks and possible explanations for the physical processes involved are offered in Section 4.

Paper number 4A1380.
0148-0227/85/004A-1380$05.00

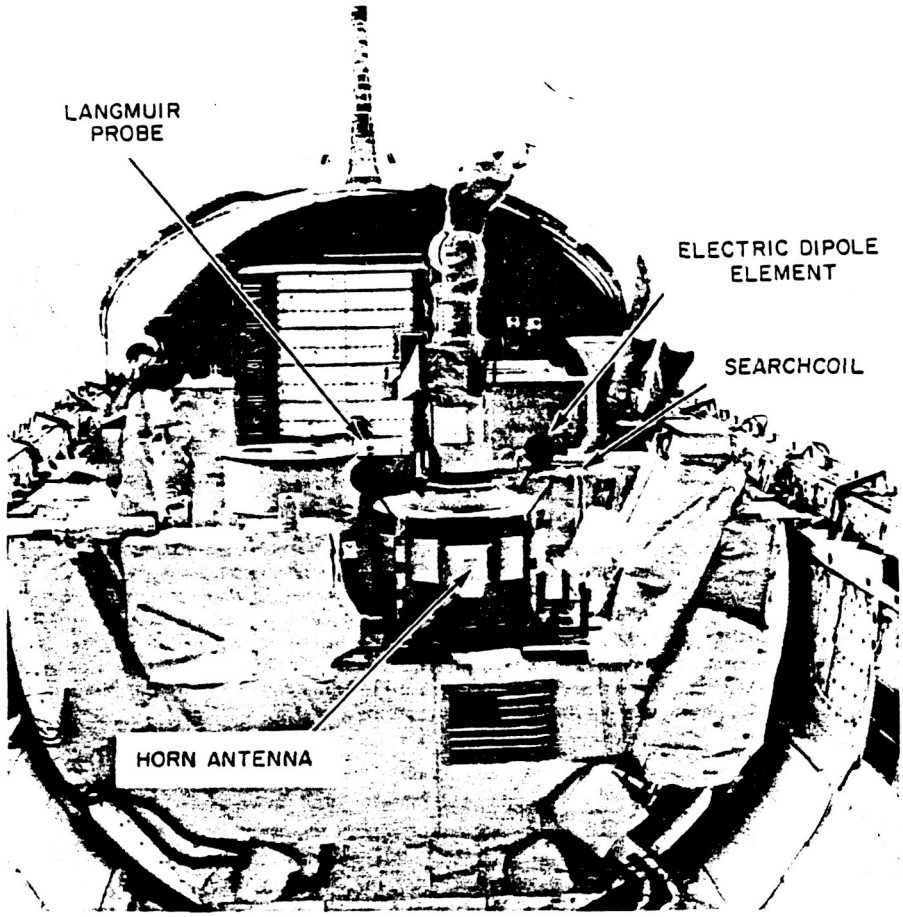

Fig. 1. Plasma Diagnostics Package in pallet location as part of the Office of Space Science first shuttle payload. The various wave sensors are identified on the Plasma Diagnostics Package.

2. Mission and Operational Considerations

2.1. *STS-3 Mission*

During March 22–30, 1982, the Plasma Diagnostics Package was flown on the third space shuttle mission (STS 3) as part of the Office of Space Science (OSS 1) first shuttle payload [*Neupert et al.*, 1982]. Figure 1 shows the OSS 1 instruments as they were mounted on the aft pallet and points out the external sensors on the PDP. The orbiter was placed in a circular orbit at an altitude of 241 km and an inclination of 38°, which resulted in an orbit period of approximately 1½ h. The STS 3 mission's primary objective was to analyze the orbiter's operation over a wide range of thermal extremes; thus many different orbiter attitudes were achieved. Eighty hours out of approximately 192 were spent in a nose-to-sun attitude to cause low temperature extremes in the engine compartments, with a roll rate which was twice the orbit rate (see Figure 2); this attitude interval was when most of the PDP data were taken. At the ascending node (equator crossing moving northward), the orbiter attitude was such that atmospheric gases were ramming into the bay. As the orbiter headed toward descending node and night, it completely blocked the flow of gases into the bay, and a wake condition prevailed in and just above the bay.

2.2. *Ionospheric Characteristics*

Using satellite measurements as well as numerical models, the *F2* region of the ionosphere can be characterized as follows: It extends from approximately 225 to 400 km with a neutral component of $\leq 10^9$ cm^{-3} and an average plasma density of 10^5–10^6 cm^{-3}. The dominant ion of this region is O^+, which is created by ionizing UV, and the dominant neutral is O. In addition, N_2 and O_2 are important constituents since they are believed to play an important role in the principal loss process of the O^+ ion [*Banks and Kockarts*, 1973].

2.3. *Shuttle Operations*

During orbital operations the flash evaporator may discharge water to supplement heat rejection when the orbiter attitude is thermally unfavorable. A secondary function of the evaporator is to expend excess potable water produced by the fuel cells that has accumulated in the potable water tanks. The vaporized water produced by the FES during these two processes is discharged through two thrust-balancing sonic nozzles, one on each side of the aft fuselage, which are known as topping FES vents (see Figure 3). An FES plume study was conducted in June of 1978 at Johnson Space Center (S. Jacobs, personal communication, 1984). The results of this study were inconclusive owing to some of the equipment malfunctioning and the fact that the tests took place in a large chamber with many exposed cold surfaces. However, these tests did suggest that 100% water vapor (no particulates) was released by the FES during topping releases. In fact, the FES topping system was specifically designed to be 100% efficient at releasing steam. No crews of any shuttle flights to date have reported seeing any particulates released through the FES toping vents

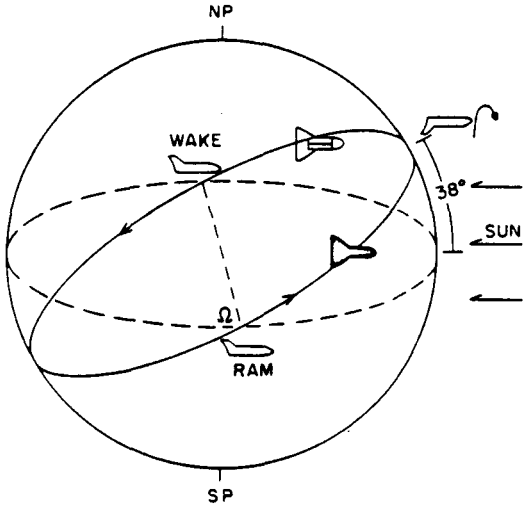

Fig. 2. Sketch of the orbit of the third space shuttle flight during the nose-to-sun attitude with the Orbiter roll at 2 times the orbit rate leading to a ram condition near the ascending node and a wake condition at the descending node.

(S. Jacobs, personal communication, 1984). The water vapor is discharged in pulses with a variable pulse rate and a pulse width equal to 200 ± 30 ms. The maximum pulse rate is 4 Hz at 22.7 kg/h [*Hamilton Standard Engineering*, 1982]. For example, for an average FES release of 2.3 kg/hr., the pulse rate is 0.4 Hz, which means every 2½ s there is a 0.2-s pulse of water vapor and a 2.3-s gap. It should be noted that a plot of mass flow rate versus pulse rate is not linear since mass flow rate also depends on feedwater pressure. Therefore if the mass flow rate is known, only an estimate of the pulse rate can be obtained. The plume expands along the $\pm Y_0$ axes of the orbiter and in some cases is reflected by the wings [*European Space Agency (ESA)*, 1982]. A high-load FES vent is also pointed out on Figure 3 which was used primarily at the beginning and end of the mission when the payload bay doors were closed. During the STS 3 mission there were 20 FES releases of varying lengths from a minute to more than 2 h. The PDP was turned on during four of these FES releases, all of which were topping FES releases. Table 1 lists these releases and the location of the PDP.

Water management on the orbiter includes storing, distributing, and disposing of excess water generated by the fuel cells. This excess water is dumped overboard in a nonpropulsive fashion at predetermined times [*ESA*, 1982]. The water relief vent for water dumps is located on the port side, rearward of the forward bulkhead and about 1.5 m down from the door hinge (see Figure 3). A total of nine water dumps were made during the mission, each of which lasted for approximately 45 min to an hour. The average dump rate was 64 kg/h, with the amount of water being dumped varying from 41 to 93 kg. Most of the water dumps began around sunset and ended shortly after sunrise. The water dumped at night turned to ice upon release. The ice sublimated as the Orbiter passed into sunlight.

The Reaction Control System (RCS) is used on the orbiter to control attitude. The system consists of 38 primary (395 kg) thrusters and 6 vernier (11 kg) thrusters. Figure 3 shows the location of these thrusters from a side view. Both verniers and primaries are located in the front and rear of the orbiter. In this view the circular designation means the thrust is directed sideways, and the oval means the thrust is directed down. The other side of the orbiter has a matching set of these thrusters. In addition, there are a set of primaries which thrust up and forward in the front of the orbiter and a set of primaries which thrust up and back in the rear of the orbiter. Because of the location and direction of thrust of some of the RCS thrusters, a certain number of the thruster plume molecules are reflected off orbiter surfaces [*ESA*, 1982] as well as returned to payload instruments, resulting in contamination [*Ehlers*, 1984].

Table 2 shows thruster plume characteristics for both the vernier and primary thrusters, including composition of the exhaust and numbers of ions and neutrals ejected in a typical firing (while maintaining orbit) and in a long firing event (while maneuvering to a new orbit attitude). It should be noted that the stated composition of the exhaust plume, both neutral and ionic, is based on thermodynamic equilibrium calculations since actual measurements are very difficult to make. These predictions are the result of a thermodynamic one-dimensional model program called CONTAM III, which was

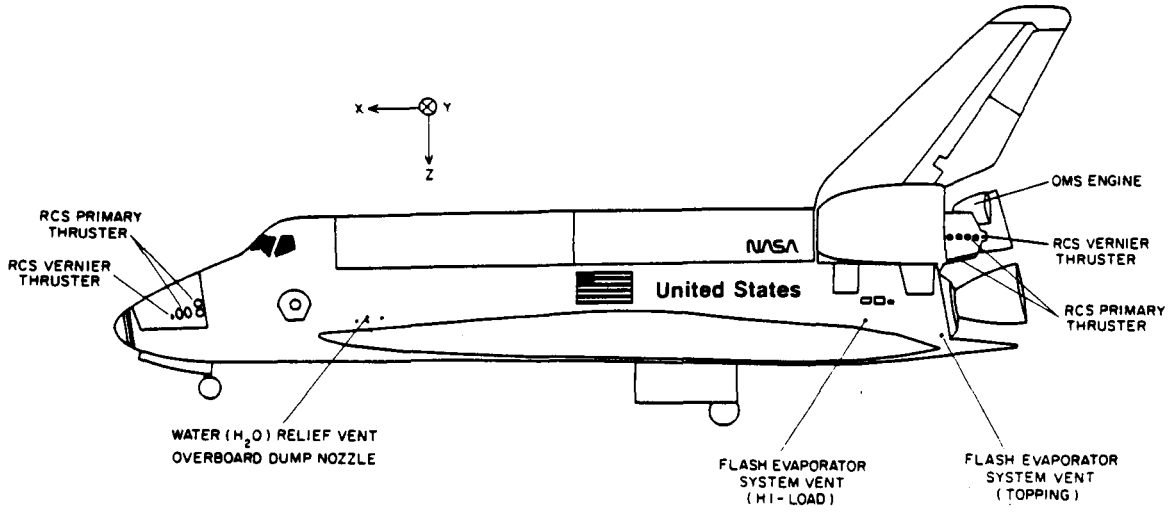

Fig. 3. Identification of the flash evaporator system vents which release water vapor, the water relief vent which releases liquid water, and the maneuvering thrusters (primary and vernier) which release many neutrals and ions as shown in Table 2.

TABLE 1. STS 3 FES Water Usage

Start Time		Duration,		Location	Usage,
Day	UT	h:min	Type	of PDP	kg
82	0117:58	0:02	Topping	Pallet	<.45
85	1230:00	2:32	Topping	RMS*	26
85	1501:44	1:30	Topping	RMS	15
86	2010:00	0:01	Topping	Pallet	<.45

*Remote Manipulator System Arm

developed for the purpose of predicting plume contamination effects [*Hoffman and Hetrick*, 1982]. The model does not take into account kinetic effects, chemical reactions, or charge interchanges that may occur immediately after a thruster firing. Thus, although such ions as CO_2^- are unstable and predicted to be a part of the thruster exhaust, these ions most likely undergo immediate chemical reactions with other components of the exhaust or even neutrals and ions present in the ionosphere. We would also like to point out the following regarding Table 2: (1) MMH-No_3 is only a suspected constituent of the plume and is believed to be a condensable, and (2) Only the most dominant ions (mole fraction $>10^{-10}$) are listed in the table. The model actually predicts several other ions to be present, such as OH^+ and NO_2^-; however, the maximum mole fraction of each of these ions is predicted to be $\leq 10^{-10}$, and thus we have not included them in the table. The velocity of the exhaust gases at all points in the plume after all energy has been converted is predicted to be 3.5 km/s based on a given temperature of approximately 3000° K (using the CONTAM III model). During the mission, there were over 40,000 thruster firings of varying lengths from 0.08 s to tens of seconds. When the PDP was turned on and taking data, nearly all of these firings as well as every FES release and water dump were evident in the data through one or more measured parameters.

2.4. *PDP Instrumentation*

A primary objective of the PDP was to measure aspects of the orbiter's induced environment both in the payload bay at the pallet level and above the bay to a 15-m height through use of the Remote Manipulator System (RMS). The PDP carried a complement of 14 instruments that measured electrostatic and electromagnetic waves, dc magnetic and electric fields, ion composition and flow, ion and electron energy distribution functions, plasma temperature and density, and neutral pressure. Some of the instruments which showed effects during chemical releases are briefly described below. A more detailed description of the instrument complement, the associated receiver systems, and the range of measurements possible can be found in works by *Shawhan et al.* [1984*a*, *b*].

A 5-cm-diameter, gold-plated spherical Langmuir Probe measured electron density and temperature and electron density irregularities ($\Delta N/N$) in the frequency range 0–40 Hz. Two spectrum analyzers were used to look at electrostatic and electromagnetic waves and $\Delta N/N$ irregularities in the frequency range 31 Hz to 178 kHz. One of the spectrum analyzers was dedicated to observing the electric component of waves using a double probe with two 20-cm-diameter black spherical sensors separated by 1.6 m. The other analyzer was periodically switched between the electric dipole antenna, the magnetic search coil, and the Langmuir Probe (see Figure 1 for location of these sensors on the PDP). The dc electric fields in the range ±4.8 V/m were measured using the electric dipole antenna, and spacecraft potential with range ±8.2 V was measured by taking the average potential between the two spheres with respect to the PDP ground, which was the same as the orbiter ground. A cold cathode ionization gauge measured ambient pressures from 10^{-7} to 10^{-3} torr. Finally, pitch angle and flux of energetic electrons and ions with energies 2 eV to 36 keV were detected with a low-energy proton and electron differential energy analyzer.

3. OBSERVATIONS

3.1. *Flash Evaporator System Releases*

Figure 4 provides Langmuir Probe and plasma wave data taken during the 2-min FES release on day 82 (UT) under daytime conditions. The top panel shows that for every 1.6-s sample plotted during the release the Langmuir Probe saw peak to peak voltage outputs which covered the full dynamic range of the instrument. By applying a fast Fourier transform (FFT) algorithm to these data, the $\Delta N/N$ plasma turbulence spectrum shown at the top of Figure 5 was obtained. This spectrum shows that the turbulence was increased by as much as 30 times over background below 10 Hz and increased by approximately 3 times at frequencies 10–40 Hz. The FES release spectrum was seen to rise steeply below 6 Hz and peak at approximately 0.5 Hz, which was, in all probability, the pulse rate of the FES release at this time. The basis for this assumption will be discussed at the end of this subsection.

TABLE 2. Thruster Plume Characteristics

Primary Thruster (PRCS)	Vernier Thruster (VRCS)	
$\dot{m}$ = 1419.8 g/s/engine	$\dot{m}$ = 40.8 g/s/engine	
Species	Molecular Weight	Mole Fraction
	Composition, Neutrals	
H_2O	18	0.328
N_2	28	0.306
CO_2	44	0.036
O_2	32	0.0004
CO	28	0.134
H_2	2	0.17
H	1	0.015
MMH-NO_3	108	0.002
	Composition, Dominant Ions	
NO^+	30	1.7×10^{-8}
CO_2^-	44	2.7×10^{-10}
OH^-	17	4.3×10^{-10}
Electrons	—	2.4×10^{-9}

	Total Number of Neutrals and Ions Ejected	
	Number of Neutrals	Number of Ions (Electrons)
	VRCS	
Typical*	1.3×10^{25}	3.1×10^{17}
Longest†	1.7×10^{26}	3.8×10^{18}
	PRCS	
Typical‡	9.2×10^{24}	2.1×10^{17}
Longest§	5.5×10^{25}	1.2×10^{18}

*Based on 2 firings ejecting 163 g over 2 s.
†Based on 14 firings ejecting 2100 g over 30 s.
‡Based on 1 firing ejecting 114 g over 80 ms.
§Based on 5 firings ejecting 682 g over 720 ms.

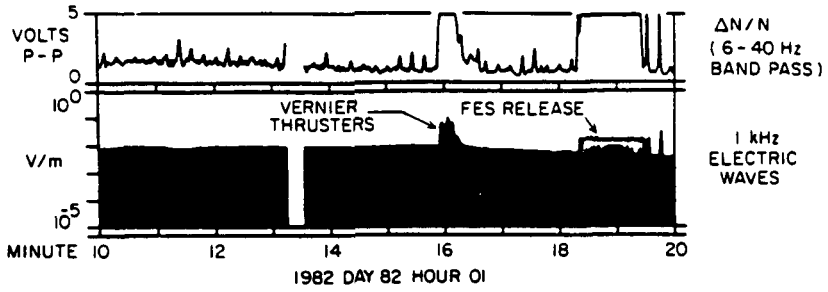

Fig. 4. Effects of a flash evaporator system release at 0118. The top panel shows that the Langmuir Probe registered peak-to-peak voltage outputs covering the full dynamic range of the instrument. The bottom panel shows that the peak intensity of 1-kHz electric waves rose substantially over the background during the release while the average did not. A vernier thruster firing is also pointed out at 0116.

Associated with the $\Delta N/N$ increase was an enhancement in the background orbiter-generated electrostatic noise [*Shawhan et al.*, 1984*b*], which in panel 2 of Figure 4 was shown to be 10^{-2} V/m at 1 kHz before the release. The average value of the 1-kHz electric field (based on the average seen during each 1.6-s sample) during the release rose only slightly while the peak value (the maximum encountered during each 1.6-s sample) was at least half an order of magnitude greater than before the release. An effect in the electric field during FES releases was seen at all frequencies from 31 Hz to 31 kHz and sometimes as great as 100 kHz, depending on Orbiter attitude and on day/night and ram/wake conditions. The bottom half of Figure 5 shows electric field spectral density for the FES release on day 82. It can be seen here that electric field spectral density was clearly enhanced by as much as 20 dB up to 31 kHz. Other data available show there were no obvious effects on the wave magnetic field, spacecraft potential, dc electric field, or neutral pressure.

The FES release discussed above took place during the nose-to-sun attritude. It is apparent from Figure 1 that the PDP sensors, i.e., Langmuir Probe and electric field sensors, were located well inside the bay and were shielded by other instrument packages from flow in some directions. Since the plume of water vapor expands along the $\pm Y_0$ axes of the orbiter, a more ideal location for the PDP would be on the RMS near the back of the orbiter. Of the two releases that took place while the PDP was on the RMS, essentially the same effects as noted above were seen. In addition, a pulsing effect was seen in the fluxes of low-energy electrons and ions. This was particularly obvious in the ion data when the PDP was on the RMS near the back of the orbiter as seen in Figure 6*a*. At this time, which was shortly after noon, we saw a pulsing effect in the ion fluxes up to about 1 keV. A line plot of counts versus time for 92.1-eV ions, shown at the bottom of this figure, clearly shows the variation.

A careful analysis of the data, which showed a cycle of about 5/min, the sweep time of the particle detector (1.4 s plus 0.2 s rest), and the pulse rate of the flash evaporator system (which we know to be less than 4 Hz) indicated that the pulsing effect was due to a beat frequency between the sweep of the particle detector and the FES pulse rate. In fact, computer modeling has shown that a FES pulse rate of 1.8 Hz would give a spectrum similar to that shown at the top of Figure 6*a*. In addition, output amplitude versus time from the Langmuir Probe clearly showed a periodic variation at 1.8 Hz for this release (see Figure 6*b*), and the $\Delta N/N$ plasma turbulence spectrum peaked between $1\frac{1}{2}$ and 2 Hz. A pulse rate of 1.8 Hz for the FES at this time is consistent with what engineering models from Hamilton Standard predict (A. Decrisantis, personal communication, 1984). The production of hot ions up to 1 keV is not yet fully understood; however, a few remarks concerning a mechanism which could possibly explain this phenomenon are given in Section 4.

3.2. *Water Dumps*

Figure 7 is a plot which shows Langmuir Probe and plasma wave measurements as a water dumping operation ended. The water dump had begun 35 min prior to the beginning of this plot. The end of the dump was characterized by an abrupt decrease in $\Delta N/N$ turbulence at 1654 UT on day 83. A total of 42 kg of water was dumped at an average dump rate of 65 kg/hr. Panel 1 shows that during the water dump the Langmuir Probe recorded peak to peak voltage outputs which covered the full dynamic range of the instrument. At water shutoff the voltage output dropped to background level almost immediately, which was the case with FES releases. However,

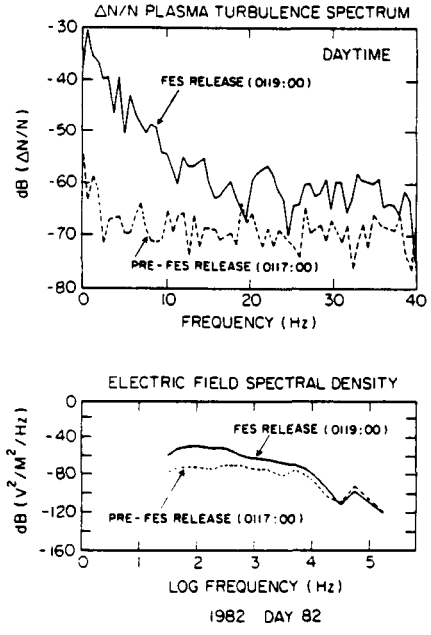

Fig. 5. $\Delta N/N$ plasma turbulence spectrum and electric field spectral density for the flash evaporator system release shown in Figure 4. The $\Delta N/N$ spectrum rose steeply below 6 Hz and peaked at about 0.5 Hz, which was the pulse rate of the flash evaporator at this time. The bottom plot shows that background electrostatic noise was enhanced at all frequencies up to about 31 kHz. Zero dB corresponds to 1 $V^2/M^2/Hz$.

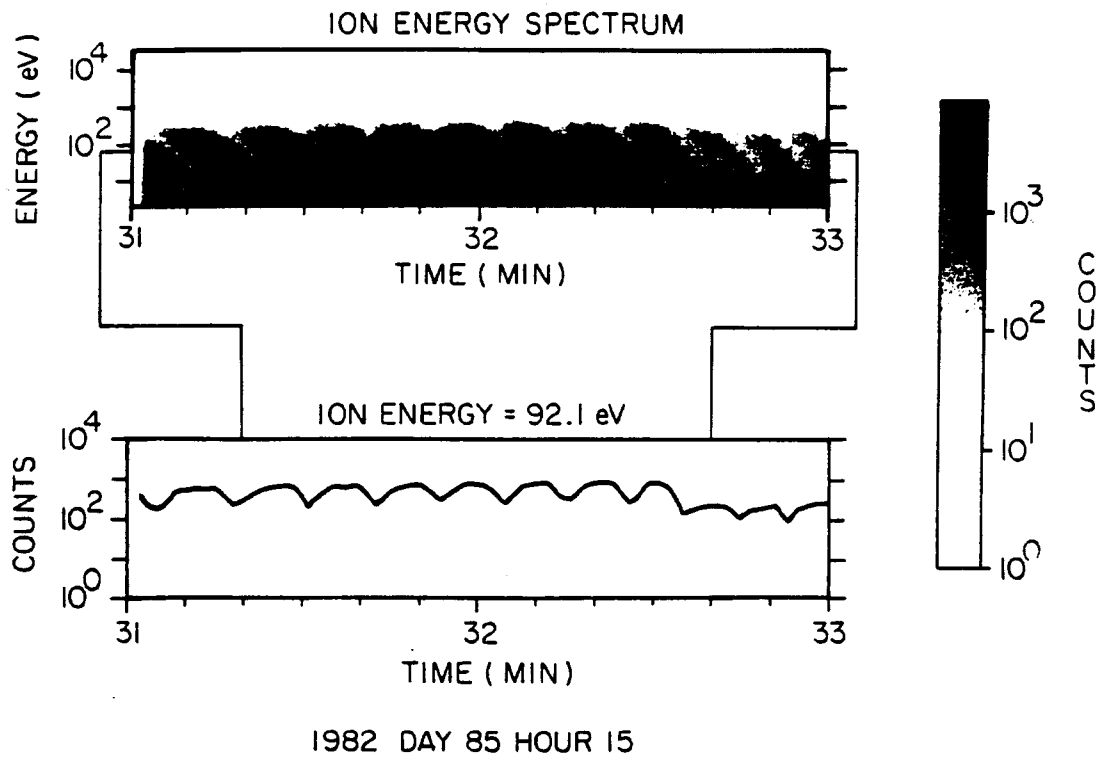

Fig. 6*a*. Ion energy spectrum during a flash evaporator system release while the Plasma Diagnostics Package was on the Remote Manipulator System. The spectrum shows a beat frequency between the sweep time of the ion detector and the pulse rate of the flash evaporator. Ions with energies up to about 1 keV are seen at this time (see discussion in 4.1). The bottom panel shows the 92.1-eV energy channel plotted to show the flux variation with time.

the turbulence spectrum was much broader and extended to higher frequencies than that observed during FES operations as shown at the top of Figure 8. Plasma turbulence appeared to be increased 5 to 6 times over background at all frequencies 0-40 Hz.

Panel 2 of Figure 7 shows that the background noise at 0.178 kHz had been elevated slightly during the water dump. Figure 8 shows that in fact, amplitudes at all frequencies up to about 3 kHz were elevated during the dump and amplitudes at all frequencies from 3 to 100 kHz were suppressed. However, this spectrum depression was not seen in the FES releases as shown at the bottom of Figure 5. It should be noted that sunrise occurred at approximately 1651 UT on day 83 in Figure 7, which is also a near-ram condition. Even though the water dump had begun during nighttime conditions, peak to peak voltage outputs covering the full dynamic range from the Langmuir Probe were seen during most of the dump. A water dump that occurred on day 84 also showed similar effects. As seen in Figure 9, the beginning of this water dump at 0111 was evident only at the low frequencies, possibly because the bay was in a wake condition at this time and the orbiter-generated noise was almost absent. The near lack of effects seen when the electrostatic noise was absent might imply that the effect of the water dump was not to generate the noise but merely to amplify it if it was already present. Wave magnetic field, spacecraft potential, and dc electric field were not affected by the water dumps, as was the case with FES releases. However, neutral pressure appeared to be affected only during that part of the orbit in which density was lowest, i.e., in wake. During this part of the orbit, neutral pressure readings were slightly greater with water being dumped than without it.

Smiddy et al. [1983] reported that on another shuttle mission during a water dump there was a $\Delta N/N$ increase at frequencies between 30 and 503 Hz, an enhancement of electrostatic noise, a decrease in the spacecraft potential, and an unchanged dc field. With the exception of a decrease in spacecraft potential the results seem to be similar to those of the PDP.

3.3. *Thruster Operations*

Most of the plasma effects observed by the PDP during thruster firings are shown in Figure 10. This plot covers a 10-min time period during the daytime (sunset occurred at 1540) with the payload bay in a near-wake condition up to 1536 and during which several primary thrusters were fired. The PDP was in the bay at this time, but the effects were similar when the PDP was on the RMS. Note that the PDP provided a resolution of 1.6 s for most of these measurements, which was considerably longer than the typical 80-ms firing of

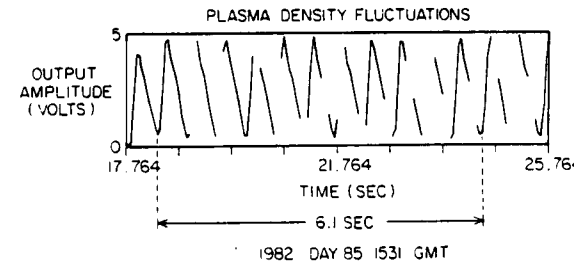

Fig. 6*b*. Plasma density fluctuations during an FES release while the PDP was on the remote manipulator system (see Figure 6*a*). The data show 11 cycles in 6.1 s for a periodic variation at 1.8 Hz, which other data and modeling show to be the pulse rate of the flash evaporator at this time.

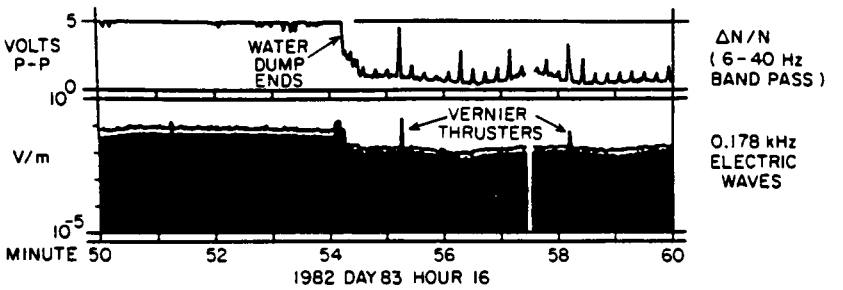

Fig. 7. Effects of a water dump that ended at 1654. The top panel shows that the Langmuir Probe registered peak-to-peak voltage outputs covering the full dynamic range of the instrument during most of the dump. The bottom panel shows that 1-kHz electric waves were elevated over background during the dump. Vernier thruster firings are also pointed out at 1655 and 1658.

a primary thruster. When thrusters fired, the Langmuir Probe, which responded to variations in the electron density near the PDP, typically saw peak to peak voltage outputs which covered the full dynamic range of the instrument with frequency components in the 0- to 40-Hz range (see Panel 1 of Figure 10). In addition, the Langmuir Probe measured electron density. As shown in Panel 2, the density was seen to increase by 2–3 orders of magnitude every time a thruster fired. Please note that the absolute density scale as labeled is still subject to revision at this time. However, the relative change seen in density with every thruster firing will be unchanged should the scale be revised. At the same time the electric field at frequencies from 30 Hz to $\gtrsim$10 kHz was seen to increase by almost 2 orders of magnitude to 0.1 V/m. The 1-kHz channel, which is representative, is shown in Panel 3. In the fourth and fifth panels, low-energy ions (58.9 eV) and electrons (2.56 eV) are displayed which showed increases in flux with nearly every thruster firing up to 1536. Ions with energies up to 1 keV were seen with some thruster firings during the mission. Pressure spikes (Panel 6) were seen for several firings, with some producing increases up to 2×10^{-6} torr. Pressure spikes up to 10^{-4} torr were observed during certain thruster firings tests [*Shawhan et al.*, 1984*b*]. The resolution of the pressure gauge is 1.6 s, which explains why many of the thruster firings showed no effect on pressure. In Panel 7 the potential of the PDP spacecraft and orbiter with respect to the plasma (SC POT.) shows a 2-V change with each firing up to 1536. The electric field in the vicinity of the PDP (E_{DIFF}) was occasionally perturbed by as much a 1 V/m. Finally, Panel 8 shows that only primary thrusters were fired during this 10-min time period. The firing of one thruster is indicated by a half line, with a full line indicating the firing of two or more thrusters at approximately the same time.

As mentioned in the preceding paragraph, electron density was seen to increase by 2–3 orders of magntiude during a thruster firing. This effect was most pronounced, however, when the orbiter was in a wake condition, i.e., low initial density ($< 10^3$ cm^{-3}). At higher electron density ($> 10^5$ cm^{-3}) and thus at a different attitude a thruster firing tended to reduce the density. In addition, the ion mass spectrometer which was flown on the PDP [*Grebowsky et al.*, 1983] saw order of magnitude enhancements in H_2O^+ and NO^+ during thruster firings. Although NO^+ is a constituent of the exhaust

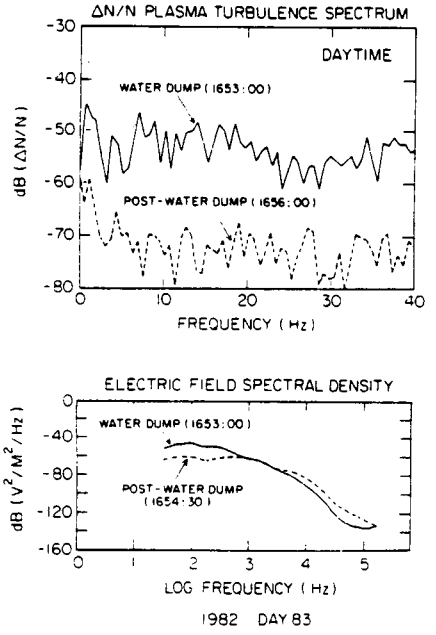

Fig. 8. $\Delta N/N$ plasma turbulence spectrum and electric field spectral density for the water dump shown in Figure 7. The $\Delta N/N$ spectrum was elevated over background at all frequencies from 0 to 40 Hz. The bottom plot shows that background electrostatic noise was enhanced at all frequencies up to about 3 kHz and suppressed at all frequencies above that. Zero dB corresponds to 1 V^2/M^2/Hz.

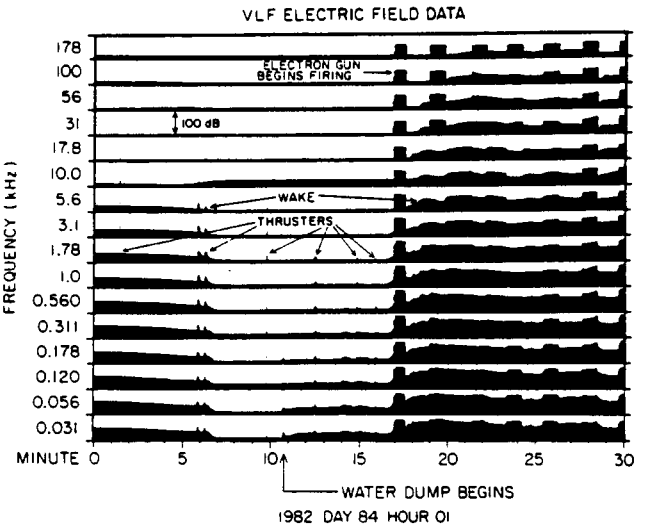

Fig. 9. A 30-min plot of VLF electric field data which shows that a water dump began at about 0111. Effects are noticed only at low frequencies since the bay of the orbiter was in a wake condition. Vernier thruster firings are also pointed out.

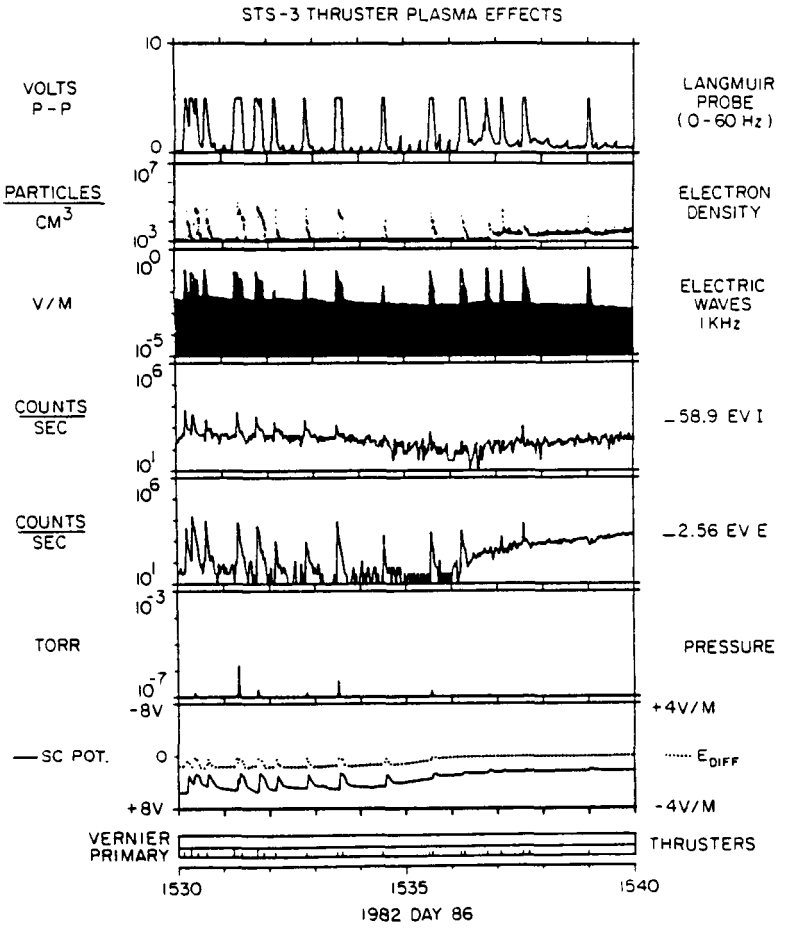

Fig. 10. A 10-min sample plot of measurements made by the PDP indicating the pressure and plasma effects of primary thruster firings. Some of the effects disappeared as the bay came out of a near-wake condition at about 1536.

plume (see Table 2), these momentary enhancements of NO^+ are most likely due to the reaction $O^+ + N_2 \rightarrow NO^+ + N$, which takes place at the rate of 1.3×10^{-12} cm^3/s [*Ferguson*, 1973]. Thus, it is the dominant neutral N_2 constituent of the plume which reacts with the ambient O^+ to produce the enhanced NO^+. Likewise, the H_2O^+ must be produced by charge exchange between ambient O^+ and neutral water, which is a dominant constituent of the plume. It should be noted that the lack of effects in the ion and electron data and in the electric field and spacecraft potential after 1536 was certainly a result of the payload bay coming out of wake and/or approaching the day/night terminator.

Vernier thruster firings produced the same effects as noted above, although in many cases the effects were minimized owing to the smaller amount of gas being ejected. Some vernier thruster firings are noted on Figures 4, 7, and 9. The spikes seen in the $\Delta N/N$ data (panel 1) in Figures 4 and 7 and not noted as thruster firings are an instrumental effect and are in no way related to thruster firings. In addition, the turbulence spectrum and electric field spectral density spectrum for a vernier thruster firing are shown in Figure 11. These plots show that $\Delta N/N$ electron density irregularities during thruster firings were increased over background by as much as 10 times at all frequencies 0–40 Hz and background electrostatic noise stimulated by the thruster firing was most intense at frequencies below 10 kHz and peaked around 0.5 kHz. For more details on the effects of thruster firings during STS 3, see *Murphy et al.* [1983]. Similar effects to the ones mentioned above have been reported on other shuttle flights [*Smiddy et al.*, 1983; *McMahon et al.*, 1983; and *Narcisi et al.*, 1983].

4. Discussion and Conclusions

The Space Shuttle perturbs the ambient ionosphere in many ways as it carries out its planned missions. A foreknowledge of these perturbations will aid all researchers who wish to use the shuttle as a platform from which to conduct their experiments, whether they be astronomy-related or physics-related experiments. The results of the PDP on STS 3, as presented in this paper, show clearly the early effects on the ionosphere of shuttle-produced chemical releases. These results are valuable in helping to understand the early effects on the ambient ionosphere of the larger releases from rockets for which measurements close to the release are nearly impossible. A summary of the effects observed by the PDP and possible explanations for them are as follows.

4.1. *Flash Evaporator System Releases*

The flash evaporator system released vaporized water at a variable pulse rate. During this time the plasma density irregularities ($\Delta N/N$) were increased by 3–30 times. In addition, the fast Fourier transform of the Langmuir Probe data showed a spectrum that rose steeply and peaked below 6 Hz, in agreement with the possible pulse rates, and extended to 40 Hz, which was the limit of the detector. At the same time the plasma wave data (Figure 4) showed an enhancement in the background orbiter-generated electrostatic noise at fre-

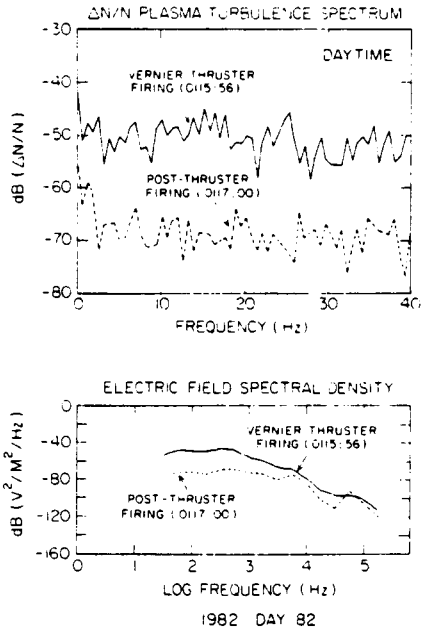

Fig. 11. $\Delta N/N$ plasma turbulence spectrum and electric field spectral density for the vernier thruster firings shown in Figure 4. The $\Delta N/N$ spectrum was elevated over background at frequencies from 0 to 40 Hz. The bottom plot shows that electrostatic noise was stimulated at all frequencies up to about 10 kHz. The spectrum peaked at about 0.5 kHz. Zero dB corresponds to 1 $V^2/M^2/Hz$.

quencies 30 Hz to 31 kHz and as high as 100 kHz depending on the orbit and attitude characteristics. Figure 6*a* illustrates the periodic variation in energetic ion particle flux which was consistent with an FES pulse rate of 1.8 Hz. The fact that this variation exists is evidence that the time scale of the onset of plasma modification by the water vapor was fast. For releases of only a few grams of water vapor per pulse the plume dispersed rapidly (within a few seconds), which reasonably explains the decay time of any plasma effect. The fast (< 1 s) onset time is consistent with the O^+/H_2O charge exchange reaction which occurs at the kinetic rate (2.4×10^{-9} cm^3/s) [*Ferguson*, 1973]. The fact that this charge exchange reaction occurs 1000 times faster than the dominant *F* region O^+ loss process [*Mendillo et al.*, 1975] causes it to dominate the local ionospheric chemistry.

Additional evidence of the rapidity of the plasma/H_2O interaction is provided by the Lagopedo ionospheric depletion experiments conducted in September 1977 [*Pongratz et al.*, 1978; *Sjolander and Szuszczewicz*, 1979] which involved releasing water vapor into the *F* region of the ionosphere. These experiments confirmed that charge exchange and dissociative recombination took place shortly after the releases and persisted for nearly a half hour. The hole was nearly isotropic and Gaussian in profile, with a thickness at half depletion of 60 km.

Day versus night effects are summarized by *Bernhardt* [1976] when he states that water vapor is acceptable as a daytime release from the Shuttle but loses efficiency at creating a hole in the plasma at night owing to its condensation into ice crystals upon release. *Zinn and Sutherland* [1980] pointed out that such ice crystals have an evaporative lifetime of about 5 min, which is long enough for them to traverse a great distance (kilometers) before they evaporate. This would seem to indicate that the PDP should see little or no change in electron or ion flux during night releases. This prediction can neither be confirmed nor denied for the case of FES operation since not enough data were taken under appropriate conditions.

During the time the PDP was on the RMS (see Figures 6*a* and 6*b*) the flash evaporator was releasing an average of 0.6 g of water vapor each time it pulsed. This means that approximately 4×10^{22} water vapor molecules were being released every second. Because this release is pulsed and occurs in vapor form, the FES should be very efficient at creating a plasma hole at *F* region altitudes. The PDP data taken during the daytime support this. Section 4.4 further examines the plasma/H_2O physics, seeking to understand the phenomenon which would take place after the charge exchange reaction occurs.

4.2. *Water Dumps*

Plasma effects noted during water dumps include increased pressure in the shuttle wake, plasma turbulence increases at all frequencies up to 40 Hz, and enhancement of the background orbiter-generated electrostatic noise at frequencies from 30 Hz to approximately 3 kHz and a suppression at frequencies above 3 kHz. This observation is consistent with a theory proposed by *Papadopoulos* [1984], which attributes the broadband electrostatic noise and glow phenomena to lower hybrid drift instabilities driven by plasma density gradients. When the bay is in ram and thus the density is very high ($\sim 10^6$ cm^{-3}), there appears to be a critical frequency which determines whether the background orbiter-generated electrostatic noise is enhanced or suppressed. PDP data show this critical frequency to be approximately 3–4 kHz, which is near the lower hybrid resonance frequency. Electromagnetic noise was recorded during the large liquid water release at 105 km on the second flight test of the Saturn booster in 1962 [*Debus et al.*, 1964]. Signal strength measurements during that release at frequencies ranging from 10 kHz to 230 MHz indicated that radio frequency waves generated by electrical discharge were associated with the cloud that developed after the release.

It is expected that liquid water would be less efficient at creating a plasma hole in the ionosphere than vaporized water since at release, only a small amount would be vaporized and the remainder would become ice particles, as was the case with the Saturn booster experiment [*Debus et al.*, 1964]. In view of the PDP measurements and the releases which were recorded during STS 3 it is not possible to state whether or not liquid water was less efficient at creating a hole than vaporized water.

4.3. *Thruster Operations*

Finally, a summary of the effects of thruster firings includes the following: an increase in plasma turbulence over the 0- to 40-Hz spectrum, increases or decreases in electron density which were orbit dependent, enhancement of the background electrostatic noise from 30 Hz to above 10 kHz, neutral pressure spikes up to 10^{-4} torr, perturbations to the spacecraft potential by as much as 2 V and to the dc electric field by as much as 1 V/m primarily under wake conditions, and occasional changes in the low-energy ion and/or electron fluxes. It is likely that the enhancement in electron density during thruster firings, which was seen primarily during the times when the orbiter was in a wake condition, was due to ion scattering into the wake as a result of the high pressure gas cloud which surrounded the shuttle and to other chemical reactions. With regard to the high-energy ions and electrons which were seen during some thruster firings, it is not possible,

with the data available, to absolutely determine whether these ions and electrons were due to neutral or ionic effluents of the thruster exhaust. Most of the other effects noted during thruster firings, including enhancement of the background electrostatic noise and perturbation to the spacecraft potential and dc electric field, could have an explanation rooted in the qualitative description of plasma/H_2O physics contained in the next section.

4.4. *Physics in a Cloud of Water*

Further examination of the physics which could take place in a cloud of water (from FES releases, water dumps, or thruster operation) released into the ionosphere hints at some possible explanations for the observed phenomena.

Charge exchange between the ambient O^+ ions moving at 8 km/s relative to the H_2O molecules in a plume produces stationary H_2O^+ ions (in the reference frame of the plume) and fast O atoms which are rapidly lost from the plume. Since in this moving frame there is a motional electric field ($\mathbf{E} = -\mathbf{V} \times \mathbf{B} \simeq 2$ mV/m), the newly created ions experience a force $\mathbf{F} \propto \mathbf{E} + \mathbf{V} \times \mathbf{B}$. The subsequent motion is cycloidal, thus the guiding centers of the H_2O^+ ions are displaced in the direction of the electric field. This displacement contributes a current, the so-called pickup current [*Goertz*, 1980], which will lead to a buildup of charge at the end of the plume. These charges will partially screen the motional electric field from the inside of the magnetic flux tube connected to the plume. The electric field in the plume must then be calculated by balancing the pickup current with field aligned currents carried by Alfvén waves [*Goertz*, 1980].

It can be shown that if the plume is fairly dense, $N_{H_2O} \gtrsim 10^{14}$ cm^{-3}, (which would occur during the first few tenths of a second after an FES release) the electric field in the plume flux tube (PFT) is significantly reduced.

Ambient ions overtaken by the Alfvén wave will be accelerated perpendicularly to the magnetic field and form a ring distribution in velocity space. In addition, ambient O atoms entering this nearly field-free region are photoionized and also form a ring distribution in velocity space which is unstable to electrostatic waves [*Harris*, 1959]. It is known that such a ring distribution will quasilinearly diffuse in velocity space with a rapid formation of a high-energy tail [*Kulygin et al.*, 1971].

It needs to be investigated quantitatively what the plasma density and composition is in the PFT and whether the O^+ ions stay in the plume long enough to be affected by charge exchange with the H_2O molecules. If charge exchange occurs before the O^+ ions leave the plume along magnetic field lines, the ring distribution may not be strong enough to cause rapid growth of electrostatic waves and heating.

In addition to the foregoing, we would like to point out that it has been suggested that the observed spacecraft potential changes, electrostatic noise, and plasma turbulence during FES releases may be due to nozzle spray electrification (triboelectric effects). While this is an interesting suggestion, its investigation is beyond the scope of this paper. The paper's main purpose is to present observational evidence of effects noted during shuttle-produced chemical releases and to suggest possible explanations for the effects observed. In light of this, a thorough study of all of the suggested explanations contained in this paper needs to be undertaken.

Further measurements by the Plasma Diagnostics Package coordinated with ground-based observations, both of which are investigations of the Spacelab 2 mission scheduled for a July 1985 launch, will provide an opportunity to further study the plasma/H_2O interactions through orbiter chemical releases. In situ measurements by the PDP will be extended to the regime around the orbiter far beyond the reaches of the RMS (the PDP will be released as a free-flying satellite) and coordinated with simultaneous ground observations to provide much more extensive input to theory. Further, it is hoped that the measurements obtained by the PDP on Spacelab 2 will aid other experimenters who plan to use the space shuttle as an experimental platform.

Acknowledgments. The authors wish to thank the PDP coinvestigators, Nicola D'Angelo, Louis A. Frank, and Donald A. Gurnett, for use of their data; Steve Jacobs and Lubert Leger of Johnson Space Center, Paul Campbell of Rockwell International, and Angelo Decrisantis of Hamilton Standard for their assistance in obtaining the necessary Orbiter data and information; and Christine Joyner for her patient typing. Helpful discussions with R. A. Smith are gratefully acknowledged. Credit for the suggestion of triboelectric effects goes to one of the referees. This research was supported by NASA through contract NAS8-32807 with Marshall Space Flight Center and through grant NAG3-449 from Lewis Research Center.

The Editor thanks R. S. Narcisi and J. M. Forbes for their assistance in evaluating this paper.

REFERENCES

Banks, P. M., and G. Kockarts, *Aeronomy, Part B*, pp. 175–186, Academic, Orlando, Fla., 1973.

Bernhardt, P. A., The response of the ionosphere to the injection of chemically reactive vapors, *Tech. Rep. 17*, pp. 1–247, Stanford University, Stanford, Calif., 1976.

Booker, H. G., A local reduction of F region ionization due to missile transit, *J. Geophys. Res., 66*, 1073–1079, 1961.

Debus, K. H., W. G. Johnson, R. V. Hembree, and C. A. Lundquist, A preliminary review of the upper atmosphere observations made during the Saturn high water experiment, in *Proceedings of the XIIIth International Astronautical Congress*, pp. 182–196, Springer-Verlag, New York, 1964.

Ehlers, H. K. F., An analysis of return flux from the space shuttle orbiter RCS engines, paper presented at the AIAA 22nd Aerospace Sciences Meeting, Am. Inst. of Aeronaut. and Astronautics, Reno, Nev., January 9–12, 1984.

Eur. Space Agency, Spacelab Payload Accommodation Handbook, *Doc. SLP/2104*, Neuilly, France, 1982.

Ferguson, E. E., Rate constants of thermal energy binary ion-molecule reactions of aeronomic interest, *At. Data Nucl. Data Tables, 12*, 159–178, 1973.

Forbes, J. M., Upper atmosphere modifications due to chronic discharges of water vapor from space launch vehicle exhausts, in *Space Systems and Their Interactions With Earth's Space Environment*, edited by H. B. Garrett and C. P. Pike, pp. 78–98, American Institute of Aeronautics and Astronautics, New York, 1980.

Goertz, C. K., Io's interaction with the plasma torus, *J. Geophys. Res., 85*, 2949–2956, 1980.

Grebowsky, J. M., M. W. Pharo III, H. A. Taylor, Jr., and I. J. Eberstein, Measured thermal ion environment of STS-3, paper presented at the Shuttle Environment and Operations Meeting, Am. Inst. of Aeronaut. and Astronautics, Washington, D. C., October 31, 1983.

Hamilton Standard Engineering, Flash evaporator controller operation, *Memo. SEM 62408*, Windsor Locks, Conn., January 25, 1982.

Harris, E. G., Unstable plasma oscillations in a magnetic field, *Phys. Rev. Lett., 2*, 34, 1959.

Hoffman, R. J., and M. A. Hetrick, Jr., Plume contamination effects prediction: CONTAM III Computer Program, *Tech. Rep. AFRPL TR82-033*, Air Force Rocket Propul. Lab., Edwards AFB, Calif., 1982.

Kulygin, V. M., A. B. Mikhailovskii, and E. S. Tsapelkin, Quasi-linear relaxation of fast ions moving transverse to a magnetic field, *Plasma Phys., 13*, 1111–1116, 1971.

McMahon, W., R. Salter, R. Hills, and D. Delorey, Measured electron contribution to shuttle plasma environment, paper presented at the Shuttle Environment and Operations Meeting, Am. Inst. of Aeronaut. and Astronautics, Washington, D. C., October 31, 1983.

Mendillo, M., Modification of the ionosphere by large space vehicles,

C-2

in *Space Systems and Their Interactions With Earth's Space Environment*, edited by H. B. Garrett and C. P. Pike, pp. 99–117, American Institute of Aeronautics and Astronautics, New York, 1980.

Mendillo, M., G. S. Hawkins, and J. A. Klobuchar, A sudden vanishing of the ionospheric F region due to the launch of Skylab, *J. Geophys. Res.*, *80*, 2217–2228, 1975.

Murphy, G. B., S. D. Shawhan, and J. S. Pickett, Perturbations to the plasma environment induced by the orbiter's manuevering thrusters, paper presented at the Shuttle Environment and Operations Meeting, Am. Inst. of Aeronaut. and Astronautics, Washington, D. C., October 31, 1983.

Narcisi, R., E. Trzcinski, G. Frederico, L. Wlodyka, and D. Delorey, The gaseous and plasma environment around space shuttle, paper presented at the Shuttle Environment and Operations Meeting, Am. Inst. of Aeronaut. and Astronautics, Washington, D. C., November 2, 1983.

Neupert, W. M., et al., Science on the space shuttle, *Nature*, *296*, 193–197, 1982.

Papadopoulos, K., On the shuttle glow (The plasma alternative), *Radio Science*, *19*, 571–577, 1984.

Pongratz, M. B., Large scientific releases, *Adv. Space Res.*, *1*, 253–273, 1981.

Pongratz, M. B., G. M. Smith, C. D. Sutherland, and J. Zinn, Lagopedo-F-region ionospheric depletion experiments, in *Effect of the Ionosphere on Space and Terrestrial Systems*, edited by J. M. Goodman, pp. 438–441, U.S. Government Printing Office, Washington, D. C., 1978.

Rote, D. M., Environmental effects of space systems: A review, in *Space Systems and Their Interactions With Earth's Space Environment*, edited by H. B. Garrett and C. P. Pike, pp. 3–53, American Institute of Aeronautics and Astronautics, New York, 1980.

Shawhan, S. D., G. B. Murphy, and D. L. Fortna, Measurements of electromagnetic interference on OV102 Columbia using the Plasma Diagnostics Package, *J. Spacecraft and Rockets*, *21*, 392–397, 1984*a*.

Shawhan, S. D., G. B. Murphy, and J. S. Pickett, Plasma Diagnostics Package initial assessment of the shuttle orbiter plasma environment, *J. Spacecr. Rockets*, *21*, 387–391, 1984*b*.

Sjolander, G. W., and E. P. Szuszczewicz, Chemically depleted F_2 ion composition: measurements and theory, *J. Geophys. Res.*, *84*, 4393–4399, 1979.

Smiddy, M., W. Sullivan, D. Girouad, and P. Anderson, Shuttle electrical environment, paper presented at the Spacecraft Environmental Interactions Technology Conference, U.S. Air Force/Nat. Aeronaut. and Space Admin., Colorado Springs, Colorado, October 4, 1983.

Zinn, J. and C. D. Sutherland, Effects of rocket exhaust products in the thermosphere and ionosphere, *Space Sol. Power Rev.*, *1*, pp. 109–132, 1980.

C. K. Goertz, W. S. Kurth, G. B. Murphy, and J. S. Pickett, Department of Physics and Astronomy, University of Iowa, Iowa City, IA 52242.

S. D. Shawhan, Code EE, NASA Headquarters, Washington, D. C., 20546.

(Received February 27, 1984;
revised November 11, 1984;
accepted November 13, 1984.)

GEOPHYSICAL RESEARCH LETTERS, VOL. 13, NO. 3, PAGES 217-220, MARCH 1986

FURTHER OBSERVATIONS OF SPACE SHUTTLE PLASMA-ELECTRODYNAMIC EFFECTS FROM OSS-1/STS-3

N. H. Stone,[1] K. H. Wright, Jr.,[2] K. S. Hwang,[1,3]
U. Samir,[4] G. B. Murphy,[5] and S. D. Shawhan[5,6]

Abstract. Recent analyses of ion measurements obtained from the Differential Ion Flux Probe (DIFP) on the deployed Plasma Diagnostics Package (PDP) during the OSS-1/STS-3 mission have provided an additional insight into the plasma-electrodynamics of the Space Shuttle Orbiter: (1) Measured ion flow directions and energies suggest that the disturbance created in the ionospheric plasma by the Shuttle Orbiter may be confined to an interaction region that extends on the order of 10 m in the forward direction and has a boundary thickness of about 2 m. (2) A correlation between the DIFP and pressure gauge measurements indicates a direct, local proportionality between the neutral gas and ion densities. (3) Preliminary results from a theoretical model of the possible interaction between measured secondary, high inclination ion streams and the ambient plasma indicate the generation of broad-band electrostatic noise such as that observed by wave instruments on the PDP.

Introduction

The OSS-1 payload, carried on the third Space Shuttle flight (STS-3), included the Plasma Diagnostics Package (PDP) experiment. The PDP is a self-contained, deployable satellite that carries an ensemble of 14 scientific instruments [Shawhan et al., 1984]. During the 9-day STS-3 mission, the PDP was deployed up to 15 m above the Orbiter payload bay with the Remote Manipulator System (RMS) on mission days three and four. As a result, the PDP performed a partial mapping of the Orbiter's near environment. Some of the initial observations (specifically, the existence of secondary, high inclination ion streams) were reported in Stone et al. [1983]. In this paper, we discuss three additional aspects of the Orbiter's plasma environment based on ion measurements obtained from the deployed PDP: (1) the spatial extent of the interaction region in the forward direction; (2) a correlation between the neutral pressure (i.e., neutral particle density) and the primary and secondary ion stream intensities [Stone et al., 1983]; and (3) a possible connection between the secondary ion streams and broad-band electrostatic noise observed in the frequency range of 30 Hz to 178 kHz [Shawhan et al., 1984].

The Differential Ion Flux Probe (DIFP), used for the ion measurements, has been described in Stone [1977] and Stone et al. [1985]. Briefly, this instrument has the capability to deconvolve and measure the characteristics of multiple ion streams differing in flow direction and/or energy.

Differential Ion Flow and Energy Measurements from OSS-1/STS-3

The mounting arrangement and field-of-view of the DIFP on the PDP are discussed in Stone et al. [1983]. Figure 1 shows the track and orientation of the PDP during an RMS maneuver on Julian day 85, 1982 for the period 16:48:40 to 16:51:05 UT. During this period, the Orbiter traveled so that the orbital velocity vector was nearly aligned with the Orbiter Y-axis. Since the Shuttle made two rolls per orbit, Orbiter attitude changes represent only a small correction factor. The main source of attitude change was, therefore, the PDP/RMS maneuver. Notice that while being translated, the PDP also performed a positive roll, followed by a negative roll which rotated the DIFP from a

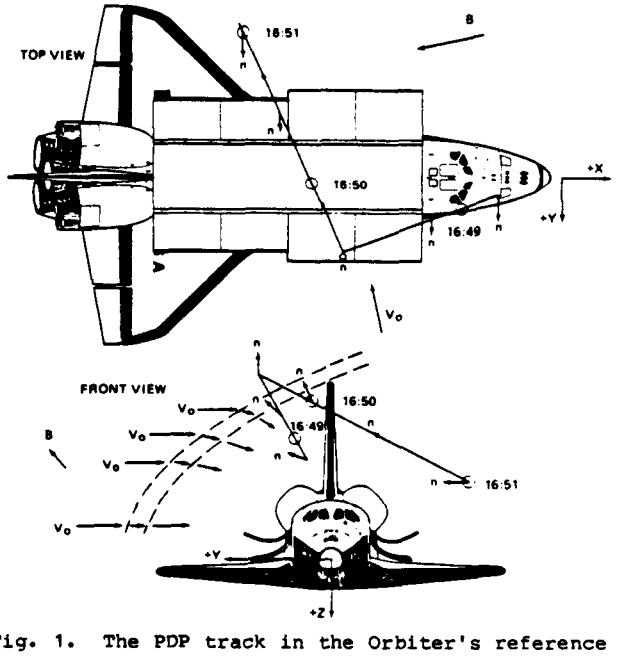

Fig. 1. The PDP track in the Orbiter's reference frame on Julian day 85 for the period 16:48:40 to 16:51:05. DIFP normal is indicated by n, while the dashed lines indicate the inferred position, shape, and thickness of the boundary of the interaction region. The indicated deflection of the ram ion stream lines is obtained from the data of Figure 3. The geomagnetic field and orbital velocity are indicated by B_o and V_o, respectively.

[1]Space Science Laboratory, NASA Marshall Space Flight Center, Huntsville, AL 35812
[2]Physics Department, The University of Alabama in Huntsville, Huntsville, AL 35899
[3]NRC Associate
[4]Tel-Aviv University, Israel and Space Phys. Res. Lab., University of Michigan, Ann Arbor, MI 48109
[5]Department of Physics and Astronomy, The University of Iowa, Iowa City, IA 52242
[6]Code E, NASA Headquarters, Washington, DC 20402

Paper number 5L6689.
0094-8276/86/005L-6689$03.00

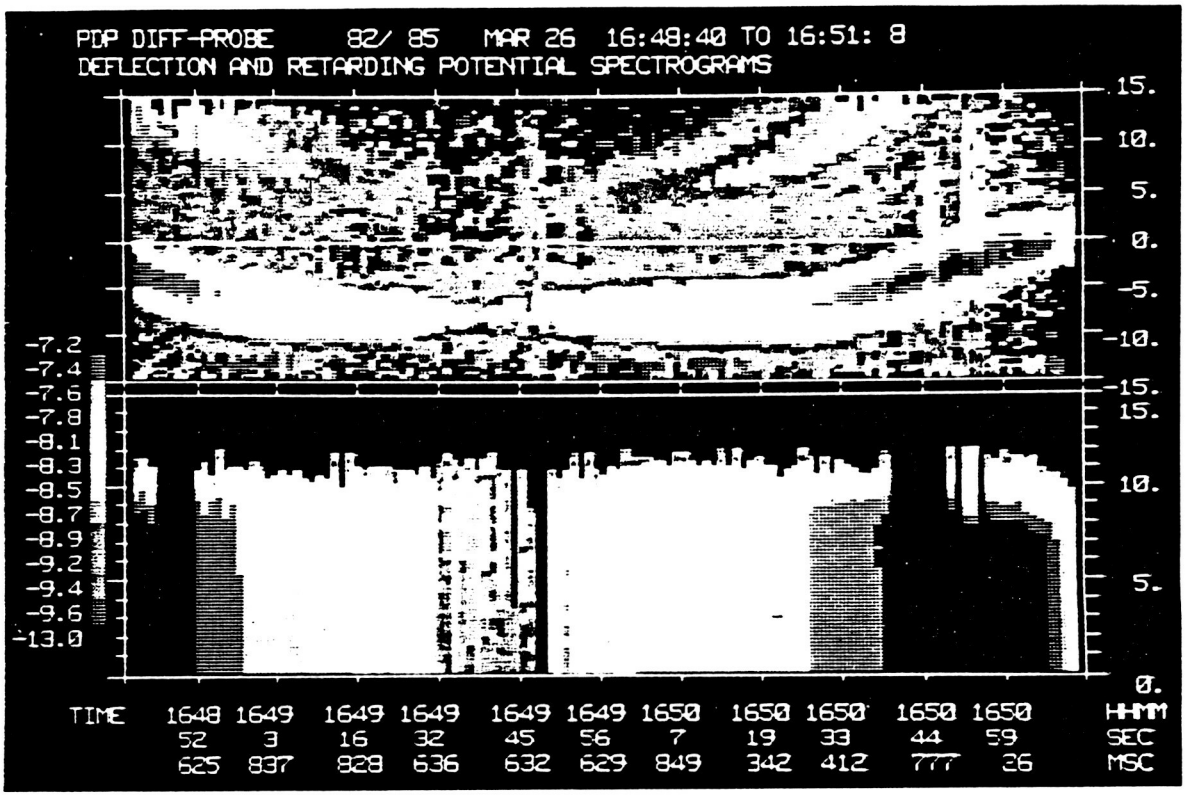

Fig. 2. Deflection voltage (ϕ_d)-time (top) and retarding potential (ϕ_r)-time (bottom) spectrograms of DIFP data for the period 16:48:40 to 16:51:05 on Julian day 85 (ϕ_d ~ angle of attack and ϕ_r ~ ion energy). Ion current is color coded in powers of ten (amps).

ram-facing attitude to an almost normal attitude and back into the ram again. At all times during the maneuver, the PDP/DIFP had an unobstructed view of the plasma, with the exception of the end of the period near 16:51 when it came near the wake of the starboard payload bay door, which is of no consequence in the present analysis. Ignoring the effect of the translation for the moment, the attitude change can be seen in the angle-time spectrogram given in Figure 2. Note that the peak ram current at the beginning of the maneuver occurs at approximately zero deflection voltage (corresponding to an almost normal incidence of the ion stream to the instrument face). However, as the PDP rolled and the instrument normal rotated upward, the peak ion current occurred at increasingly negative deflection voltages (indicating that the ion stream arrived at an increasingly negative angle). As the PDP was rolled back to its original orientation with the DIFP facing into the ram, the current peak moved back up toward zero voltage. Note that, although the angle determination depends on both the deflection and retarding voltages [Stone, 1977], the energy-time spectrogram in Figure 2 shows the ion energy to be approximately constant over this period so that angle is directly proportional to the deflection voltage. The reduced angles corrected for PDP potential [see Stone et al., 1985] are shown in Figure 3 as a function of time.

In addition to the primary ram ion stream, a secondary stream is clearly visible in the angle-time spectrogram of Figure 2. This stream, with about 65 percent of the current density of the primary stream, arrived at a high positive angle with respect to the Y-axis and (initially) the DIFP normal. As the DIFP rotated upward, the secondary stream moved toward zero deflection voltage, as expected; i.e., the roll maneuver moved the instrument normal into alignment with the high inclination secondary stream. The reduced angle

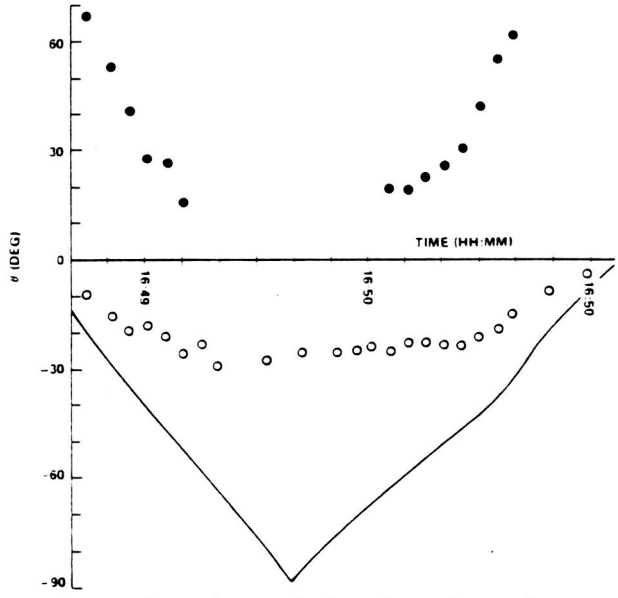

Fig. 3. Angles-of-attack for the primary (open circles) and secondary (closed circles) ion stream for the period 16:48:40 to 16:51:05 on Julian day 85. The solid line is the angle between the DIFP normal and the orbital velocity vector.

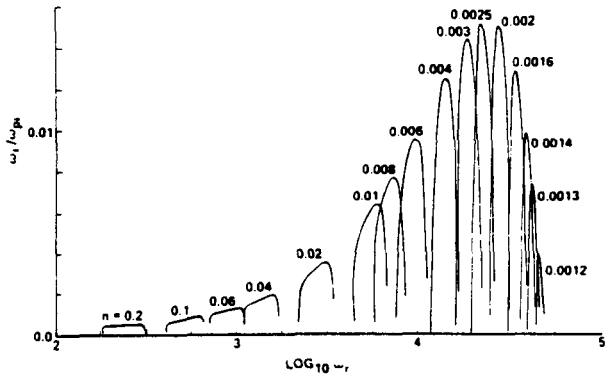

Fig. 5. Theoretical calculation of the normalized growth rate for ion stream-plasma interaction produced ion acoustic waves over a broad frequency range for various propagation angles.

the exception of a pressure burst that occurred as the PDP passed over the port payload bay door. (The pressure gauge was baffled and oriented perpendicular to the ram flow throughout the maneuver.) The ion current density measured by the DIFP also followed a 1/r dependence and increased simultaneously with the pressure burst. The direct proportionality of the ion and neutral particle densities is shown in Figure 4. Although it is possible for neutral gas injections to either reduce or increase ionization locally, this suggests that the neutral gas emitted from the Orbiter is rapidly ionized and contributes significantly to the Orbiter's total plasma environment. This conclusion is in accord with the high plasma density measurements reported by Raitt et al. [1984] and Siskind et al. [1984]. The linear dependence shown in Figure 4 is in agreement with theoretical ionization rate predictions (e.g., Papadopoulos, 1984).

A Possible Connection Between Secondary Ion Streams and Other Shuttle-Induced Phenomena

To date, the OSS-1 experiments have revealed the existence of several phenomena peculiar to the near-Orbiter environment, including high inclination secondary ion streams [Stone et al., 1983], broad-band noise measured from 30 Hz to 178 kHz [Shawhan et al., 1984], elevated electron temperatures, and higher than normal plasma densities [Raitt et al., 1984; Siskind et al., 1984].

Intuitively, one would suspect that these phenomena might be linked. In principle, ion streams moving through the ambient plasma should generate instabilities, which may take the form of broad-band noise, and could heat the electron population which could, in turn, ionize the neutral gas cloud. The first step of this process, i.e., secondary ion streams providing the free energy required to generate broad-band noise, has similarities to the mechanism discussed by Kintner et al. [1980]. This is being investigated in the present context (see Figure 1) by inserting the appropriate charged particle distribution functions into the linearized collisionless Vlasov equation to obtain a general dispersion relation for electrostatic ion acoustic waves. Preliminary computations were made for the conditions encountered by the PDP, using $T_e/T_i = 7.5$, in accord with Siskind et al. [1984]. The results, shown in Figure 5, predict the generation of electrostatic ion waves over a wide range of frequencies, in agreement with the OSS-1 broad-band noise obervations reported by Shawhan et al. [1984]. However, it is not claimed, at present, that these preliminary computations account for all of the observed properties of the broad-band noise. This work is continuing and the results, along with mathematical details, will be published elsewhere. Evaluation of the possible connections between the broad-band noise, electron heating, and neutral particle ionization will require careful consideration of wave growth rates and the efficiency of coupling with the electrons.

Acknowledgments. The authors acknowledge the computational assistence of Wayne Thompson of Boeing Computer Support Services. U.S. and K.H.W. acknowledge support under NASA grant NGR 23-005-320 and NASA contact NAS8-33982, respectively.

References

Kintner, P. M., M. C. Kelley, G. Holmgren, and R. Bostrom, The observation and production of ion acoustic waves during the Trigger experiment, J. Geophys. Res., 85, 5071, 1980.

Papadopoulos, K., On the shuttle glow (the plasma alternative), Radio Sci., 19, 571, 1984.

Pickett, J. S., G. B. Murphy, W. S. Kurth, C. K. Goertz, and S. D. Shawhan, Effects of chemical releases by the STS-3 Orbiter on the ionosphere, J. Geophys. Res., 90, 3487, 1985.

Raitt, W. J., D. E. Siskind, P. M. Banks, and P. R. Williamson, Measurements of the thermal plasma environment of the Space Shuttle, Planet. Space Sci., 32, 457, 1984.

Samir, U., N. H. Stone, and K. H. Wright, Jr., On plasma disturbances caused by the motion of the Space Shuttle and small satellites--A comparison of in situ observations, J. Geophys. Res., 91, 277, 1986.

Shawhan, S. D., G. B. Murphy, and J. S. Pickett, Plasma Diagnostics Package initial assessment of the Orbiter plasma environment, J. Spacecr. Rockets, 21, 387, 1984.

Siskind, D. E., W. J. Raitt, P. M. Banks, and P. R. Williamson, Interactions between the orbiting Space Shuttle and the ionosphere, Planet. Space Sci., 32, 881, 1984.

Stone, N. H., Technique for measuring the differential ion flux vector, Rev. Sci. Instrum., 48, 351, 1977.

Stone, N. H., U. Samir, K. H. Wright, Jr., D. L. Reasoner, and S. D. Shawhan, Multiple ion streams in the near vicinity of the Space Shuttle, Geophys. Res. Lett., 10, 1215, 1983.

Stone, N. H., B. J. Lewter, W. L. Chisholm, and K. H. Wright, Jr., Instrument for differential ion flux vector measurements on Spacelab 2, Rev. Sci. Instrum., 56, 1897, 1985.

(Received September 3, 1985;
accepted January 6, 1986.)

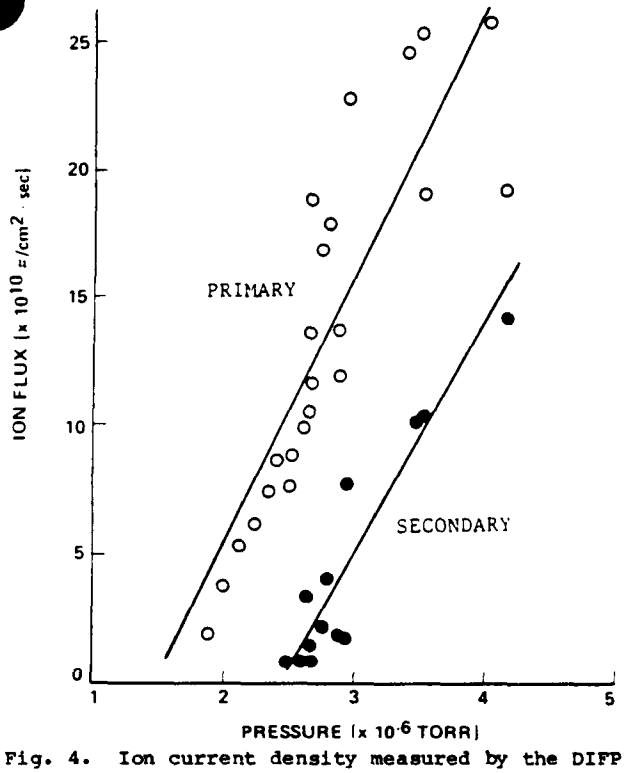

Fig. 4. Ion current density measured by the DIFP vs. pressure (neutral particle density) measured by the University of Iowa PDP pressure gauge. Solid lines are least squares fits of the primary and secondary ion stream data points. The data have been corrected for the variation of DIFP sensitivity with angle.

data for the secondary stream are also shown in Figure 3. This appears to be the same type of secondary ion stream phenomenon reported by Stone et al. [1983] for a different period of time.

Discussion

Evidence for an Interaction Envelope

The important characteristics of the present data are the behavior of the ram and secondary ion stream current densities and the angle-of-attack of the ram ion stream. The DIFP sensitivity decreases with increasing angle-of-incidence as a result of the collimator; i.e., a given stream at 0° would appear more intense than the same stream at 40° [Stone, 1977]. This is indeed the behavior followed by the ram current. It is maximum at zero deflection voltage and diminishes as its angle of incidence increases and the current peak moves away from the zero voltage line. However, this does not hold for the secondary ion stream.

The secondary ion stream initially arrived at a high angle-of-attack to the ram current; i.e., at 16:48:40 UT the secondary stream entered the DIFP at 52°. At this angle the DIFP sensitivity is reduced by 92 percent and the measured ion current is low, as expected. As the DIFP rotated into alignment with the secondary stream, its sensitivity to this stream increased and there should have been a corresponding increase in the measured current. However, this did not happen. To the contrary, as shown in Figure 2, the secondary ion stream vanished. Since this cannot be the result of instrument sensitivity, nor can it be the effect of geometric shadowing since the PDP/DIFP had an unobstructed view upstream, it must indicate that the secondary stream was no longer present. At this point on the track, the PDP had translated to a radial distance of about 8.8 m from the Orbiter's X-axis (the axis normal to the velocity vector) and was located 65° above the XY-plane (see Figure 1). If the secondary ion stream was an ionospheric drift, atomic oxygen ions would be required to drift normal to the XY-plane at speeds in excess of the orbital velocity, i.e., about 10 km/s. Since ionic drifts of this magnitude are not known in the undisturbed mid-latitude ionosphere, it is reasonable to conclude that the secondary ion stream is generated within the interaction region surrounding the Orbiter and, that the PDP was extended beyond this region during the period 16:49:20 to 16:50:00. Once the PDP moved beyond the boundary of the source region for the secondary ion population, the secondary streams could no longer be detected by the outward facing DIFP; i.e., there would be no incoming secondary ions beyond the source region and outward traveling ion streams would not be in the field-of-view of the instrument.

Notice that the secondary ion stream current density, shown in Figure 2, diminished gradually as the PDP moved farther out from the Orbiter at 16:49:20 and increased gradually as it moved back in at 16:50:00. These transitions occurred over a 2-m change in radial distance from the Orbiter X-axis. We conclude, therefore, that the boundary of the interaction region (at least for secondary ion production) is approximately 2 m thick.

It is also apparent in Figure 3 that the primary ion stream does not follow the angle-of-attack of the orbital velocity vector as the ram current should. This behavior is consistent with the existence of an electric field within the boundary of the interaction region. If the electric field is everywhere normal to the boundary, then any deflection of the ionospheric ions will be proportional to the angle between the normal of the boundary surface and the velocity vector. Referring to Figure 3, this implies that the boundary was normal to the ram direction at 16:48:40 but became increasingly skewed with distance from the XY-plane, suggesting the general parabolic shape shown by the dashed lines in Figure 1. This shape is generally consistent with a gas source moving through a stationary medium--regardless of the interaction mechanism. (It is recognized that some distortion may be produced by the action of the geomagnetic field.)

Coupling Between Ion and Netural Densities

Since the ionosphere is collisionless on the scale size of the Orbiter, the existence of an interaction region that extends upstream suggests that the Orbiter emits particles and/or fields that can interact with the oncoming ionosphere several meters ahead of its leading surface. It is well known that the Orbiter is the source of a significant gas cloud that moves along with it [Shawhan et al., 1984; Pickett et al., 1985; Samir et al., 1986]. In the present maneuver, the PDP traveled 10 m radially out from the Orbiter and back. The pressure gauge data (which correspond to neutral density) follow a 1/r dependence with

Planet. Space Sci., Vol. 34, No. 10, pp. 993–1004, 1986
Printed in Great Britain.

0032-0633/86 $3.00 + 0.00

MEASUREMENTS OF PLASMA PARAMETERS IN THE VICINITY OF THE SPACE SHUTTLE

G. MURPHY, J. PICKETT, N. D'ANGELO and W. S. KURTH
Department of Physics and Astronomy, The University of Iowa, Iowa City, IA 52242, U.S.A.

(*Received* 29 *April* 1986)

Abstract—A Langmuir probe flown as part of the Plasma Diagnostics Package aboard the third space shuttle flight was used to determine electron densities, temperatures and plasma potential in the vicinity of the shuttle orbiter. Measurements taken both in the cargo bay and 10 m above the cargo bay on the Remote Manipulator System arm are consistent with small satellite and laboratory results in that reduced densities and elevated temperatures are observed in the shuttle wake. The primary difference in the shuttle measurements is one of magnitude, i.e. orders of magnitude density decreases and factor of five temperature enhancements.

Analysis of data taken in $\Delta N/N$ mode (used to measure plasma density fluctuations) reveals large plasma fluctuations with a significant spectral component up through the lower-hybrid frequency. The peak amplitude of this $\Delta N/N$ turbulence can be as high as a few percent, and the most intense turbulence seems to occur near regions with a steep gradient in plasma pressure.

1. INTRODUCTION

Measurements of temperature and densities behind a body immersed in a flowing plasma which have thus far been reported in the literature can be divided into three categories: (1) those obtained in the laboratory under controlled conditions, (2) those obtained in the wake of small scientific satellites, and (3) those recently reported from experiments aboard the space shuttle (Raitt *et al.*, 1984; Siskine *et al.*, 1984). This paper will discuss the plasma parameter measurements made by the Plasma Diagnostics Package (PDP) which flew as part of the third shuttle payload.

Subdividing plasma measurements in this way is quite natural, since these categories correspond to an ever-increasing ratio of object size to Debye length. Laboratory measurements have typically achieved scaling in the range of 1–50 λ_D (Stone, 1981). Measurements from small satellites (e.g. Samir and Willmore, 1965) and the *Gemini-Agena* (Troy *et al.*, 1970) rocket experiment have been in a range of up to $\sim 100\ \lambda_D$, while the space shuttle has typical dimensions on the order of 1000 λ_D. For the *F*-region in which the orbiter typically flies, densities of 10^6 cm^{-3} and temperatures of 1000 K are common. There are some other variables which complicate the picture and make comparisons between the small satellite and shuttle cases more difficult; namely, the small satellites are typically conducting bodies, whereas the shuttle is primarily an insulator on surfaces exposed to the plasma; also, there is evidence to indicate that the shuttle outgassing products constitute a large portion of the neutral atmosphere (Shawhan *et al.*, 1984) near the vehicle. This neutral gas may be enough to alter details of the wake structure. Despite these difficulties, measurements by the PDP Langmuir probe indicate an overall consistency with the information provided by data from small satellites and laboratory experiments.

This paper will discuss in detail the methodology of the shuttle observations and then summarize the results within the framework of previous experiments.

2. INSTRUMENTATION

The PDP Langmuir probe is a relatively simple instrument which has two operational modes, the first as an electron density/temperature measurement tool, the second as a diagnostic for $\Delta N/N$ fluctuations in electron density over the frequency range 0.5–40 Hz. The instrument uses a 6 cm diameter gold-plated spherical sensor mounted on a fixed boom approximately 30 cm from the body of the PDP. The location of the probe is illustrated in Fig. 1. The electronics operates in two modes, alternated by a timing signal generated by the PDP spacecraft encoder. The total cycle lasts for approximately 13 s and consists of a 12-s "lock" period where the probe is held at +10 V relative to the PDP chassis, followed by a 1-s 120-sample sweep from +10 to −5 V. Figure 2 illustrates this cycle. During the lock cycle, the probe is in the $\Delta N/N$ mode and the output current fluctuations are sensed by a logarithmic sensor and sampled through

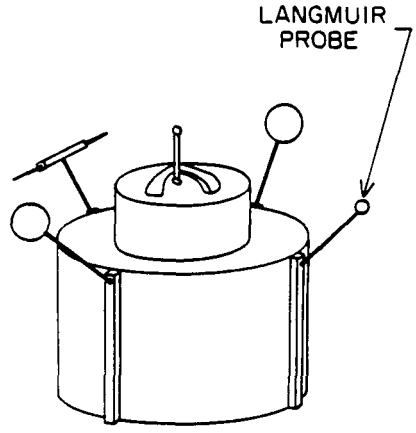

FIG. 1. A SIMPLIFIED DIAGRAM OF THE PDP STRUCTURE SHOWS THE LOCATION OF THE LANGMUIR PROBE ON A BOOM APPROXIMATELY 30 cm IN LENGTH.

three filters: 1 Hz low pass, 1–6 Hz bandpass, and 6–40 Hz bandpass. A fourth filter (30 Hz high pass) routes the output to a wide-band receiver and spectrum analyzer which, when in the Langmuir probe mode (51.2 s out of a total sensor switching cycle of 409.6 s), can look at details of the current fluctuations up to a frequency of 178 kHz. The sample rates of the filters were adjusted such that the Nyquist criterion was satisfied, that is 5, 20 and 120 Hz, respectively, for the first three filters. The 30 Hz high-pass filter which was sampled by the spectrum analyzer was peak detected and each of the 16 channels sampled once each 1.6 s.

The voltage sweep cycle of the probe had a step size of 0.125 V, which is relatively coarse for a plasma with ambient temperatures of 1000 K and presented some difficulties which will be discussed later. The probe was sampled once each voltage step. Since the probe steps from +10 to −5 V and then jumps back to +10 V, it was not possible to check for possible hysteresis effects on the probe. The output of this mode is a voltage, proportional to log of the current, vs sweep voltage. Unlike the probe described by Raitt *et al.* (1984), no differentiation takes place; the probe, in fact, works much like manually swept probes used in the laboratory giving the *I–V* (current–voltage) curve directly.

A word is in order about the reference potential for the Langmuir probe. The voltage on the probe is referenced to the PDP chassis. The PDP chassis is grounded to the orbiter both while in the payload bay and on the Remote Manipulator System (RMS) arm.

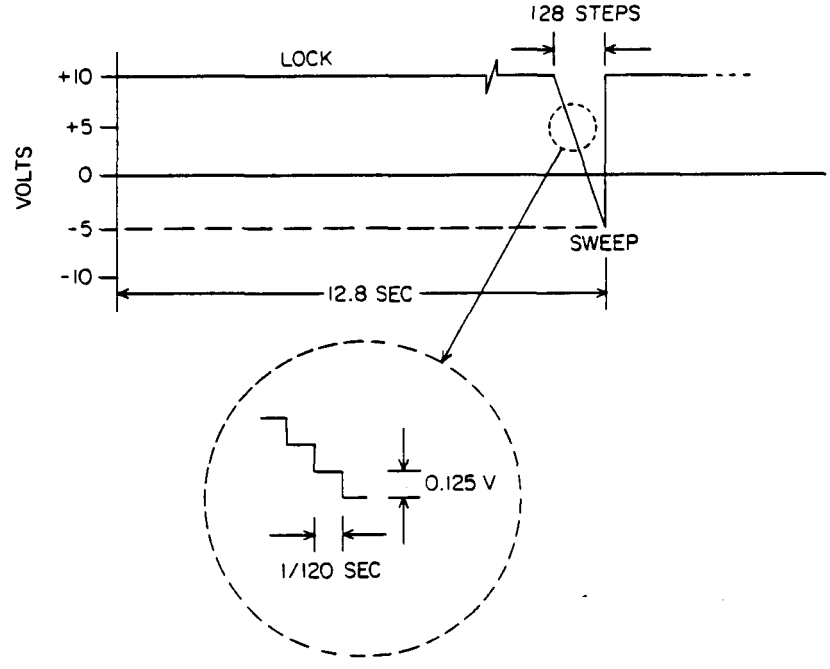

FIG. 2. THE LANGMUIR PROBE INSTRUMENT CYCLE HAD A PERIOD OF 12.8 s (EIGHT MAJOR DATA FRAMES). At the end of the cycle, a sweep consisting of a series of 0.125 V steps is driven by a 120 Hz clock. The wide sweep range accommodates swings in the PDP potential due to charging effects.

TABLE 1. LANGMUIR PROBE PERFORMANCE PARAMETERS

Current sensor	0.1 μA–1 mA
T_e	(800–5000 K)
n_e	(10^3–10^7 cm^{-3})
$\Delta N/N$	
< 1 Hz	1.8–460%
1–6 Hz	0.12–30%
6–40 Hz	0.012–3%
> 30 Hz (spectrum analyzer)	−30 to −80 db $\Delta N/N$

Thus the probe is swept with respect to orbiter chassis ground and a measurement of the potential of the vehicle with respect to the plasma is possible. This is relevant considering that the orbiter is primarily an insulating body and its principal conducting surfaces are the engine nozzles at the rear of the vehicle.

The sensitivities and dynamic ranges of the two modes of the Langmuir probe are summarized in Table 1. It should be noted that it is difficult to state an absolute temperature measurement range since that range is density dependent. For that reason, the current sensitivity of the log current sensor is given as the primary specification, with temperature and density dynamic ranges in parentheses.

3. DATA ANALYSIS

The process of deriving electron temperature, density and plasma potential from a Langmuir I–V characteristic is straightforward in the ideal case but has several limitations in practice that the reader needs to be aware of in order to fairly judge the results of this research.

As noted previously, the Langmuir probe is stepped from +10 to −5 V in 0.125 V increments with its current sampled at each step. Even though this voltage range extends well below the floating potential, the electronics uses a transistor's base-emitter junction to detect directly the log of the current and therefore cannot measure negative (ion) current. Thus, we see two fundamental limitations in the probe design which were engineering compromises necessary for operation in the uncertain shuttle environment.

The relatively large step size (0.125 V) implies there will not be very many samples of current in the retardation region for typical ionospheric electron temperatures of ~0.1 eV. For example, at a density of $\sim 10^6$ cm^{-3}, the electron current at plasma potential for our probe would be $I_p \cong 10^{-3}$ A. Considering that the minimum detectable current for the electronics is 10^{-7} A approximately six points would lie on the electron retardation region of the characteristic. Clearly at densities $< 10^3$ cm^{-3} it would not be possible to accurately determine temperatures. The software used to calculate temperature and density thus uses a number of first and second derivative tests to determine if a statistically significant number of points lie beyond the "knee" of the curve and in the retardation region of the characteristic. If statistically good fits are not possible, the analysis of that sweep is halted and the data are written to a "bad record" file where records are examined further by hand. Comparison of machine calculations to those done by hand for a large number of sweeps over the full range of these data were used to refine the "intelligence" of the software to a point where high confidence can be placed in the results.

The second limitation, the fact that the probe does not measure ion current, results in an underestimate of temperature and overestimate of density at high ambient densities. To see why this is so we look at two sample sweeps in detail.

Figure 3 illustrates a log-I vs V curve taken at 21:47:38 U.T. yielding electron "density" of $\sim 1 \times 10^4$ and "temperature" of ~2600 K. In this particular case, the dotted lines are fit by the computer routine and the plasma density (proportional to saturation current), temperature and plasma potential determined accordingly. What is the effect of the unmeasured ion current? Once the measured current falls below a certain threshold, the ion current may become a significant portion of it. Since the ion current subtracts from the electron current, the measured current is less than it would be if only electron current were present, thus increasing the slope of the curve and causing the computed temperature to be too low. An upper bound for the ion current can be calculated as $I_i = A \cdot q \cdot n_i \cdot v_s$, where A is the projected area of the probe, n_i the ion density, q the elementary charge and v_s the shuttle velocity through the plasma. For the case in Fig. 3, the ion current would be $3.6 \times 10^{-12} \cdot n_i$ or $\sim 3.6 \times 10^{-8}$ A, a correction which is below the instrument sensitivity. As one can see from Fig. 3, the corrected and uncorrected slopes are indistinguishable.

Since the ion current is variable—it depends on ram-wake conditions, detailed geometry in the payload bay, etc.—it was found that no consistently accurate correction could be calculated and implemented under all conditions. Therefore, the decision was made to let the software fit the data uncorrected for ion current, and determine instead what worst-case effect this has on the calculated "temperature" and "density". In these data, presented in the next section, the reader will find that, under ram conditions, densities are high by about a factor of two

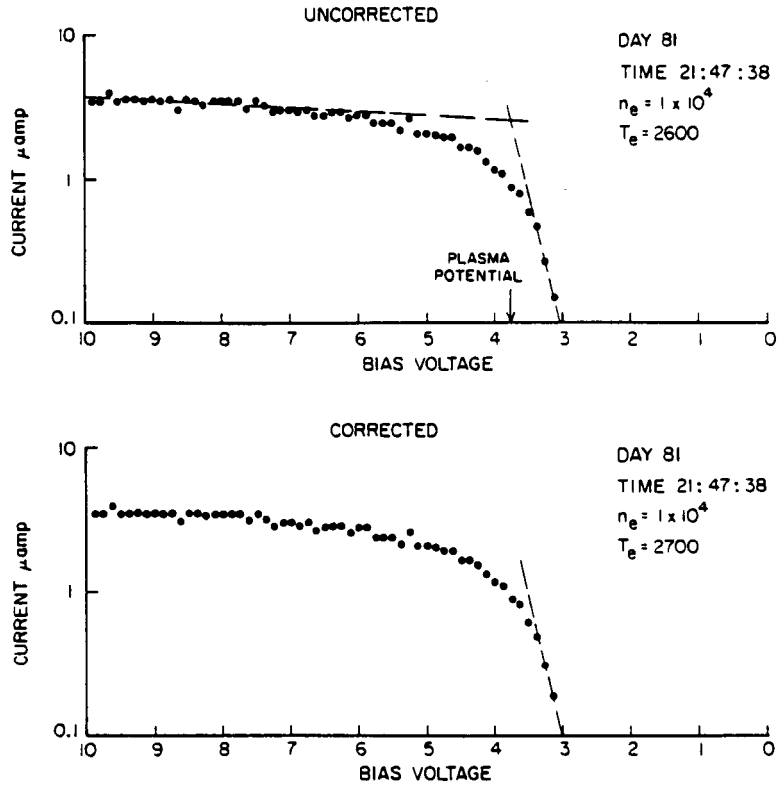

FIG. 3. A TYPICAL LANGMUIR CHARACTERISTIC IS GIVEN FOR A DENSITY OF 1×10^4. Note how density, temperature and plasma potential are determined by using two straight-line fits. This method slightly overestimates plasma potential but does so fairly consistently by a few KT_{ev}. In this case, the lower curve corrected for ion current is not significantly different from the uncorrected version.

and temperatures correspondingly low by ambient daytime ionosphere standards. It is important to realize that no elaborate physics need be invoked to explain these results; it is simply an ion current effect. The above formula can be used to calculate ion current, but one must keep in mind that due to lower ion densities in wake and semi-wake conditions and the fact that ions impacting the probe under these conditions must have a velocity less than v_s, the calculation gives an upper limit valid only in undisturbed plasma flow regions (ram).

Figure 4 illustrates data taken in these ram conditions and shows the effect of correcting for ion current which is not negligible in this case ($I_i \sim 1.4 \times 10^{-5}$ A. A look at the effect under various conditions gives the following general rule for the underestimate of temperature as a function of actual ambient electron density:

$$10^6 \text{ cm}^{-3} \rightarrow 100\%; \quad 10^5 \text{ cm}^{-3} \rightarrow 50\%; \quad \text{and } 10^4 \text{ cm}^{-3} \rightarrow \text{negligible.}$$

These effects are accounted for in the plots of the next section by the dashed lines which illustrate the best mean solution for density and temperature consistent with the above rule.

Fortunately, although extremely low densities cannot be accurately measured and high densities have ion current corrections, the range for most of the interesting physics of the wake region discussed here remains free of instrumental limitations.

4. OBSERVATIONS

We will first present a summary of a representative sample of our observations and then discuss each in detail. Details of the *STS*-3 flight, where these measurements were made, can be found in Shawhan *et al.* (1984). The important aspects from the point of view of this paper are that the orbiter flew just below the peak in the *F*-region in a 240 km circular orbit at an inclination of 37°. Measurements presented here

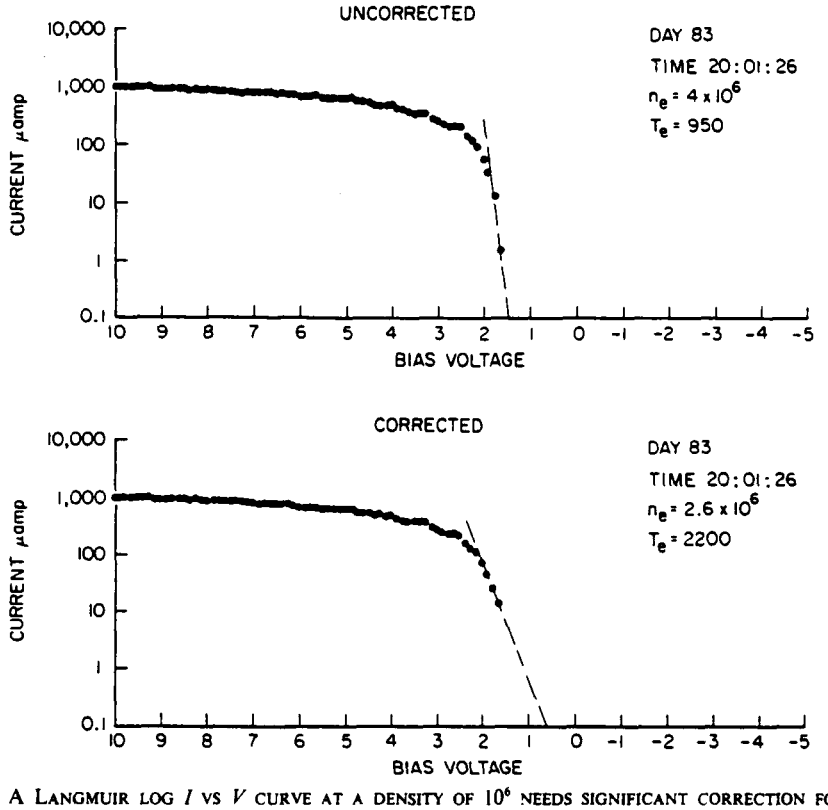

FIG. 4. A LANGMUIR LOG I VS V CURVE AT A DENSITY OF 10^6 NEEDS SIGNIFICANT CORRECTION FOR ION CURRENT.
In this case, the value of ion current is $\sim 1.4 \times 10^{-5}$ A so no data points are available below that value in the corrected curve. The correction of slightly more than a factor of two in temperature implies a corresponding decrease in the estimate of density since $n_e \propto 1/\sqrt{T_e}$.

were taken either while the PDP was stowed in the cargo bay or while it was deployed on the RMS arm 5–10 m above the bay. The location of the PDP in these two cases is illustrated in Figs 5 and 6.

Electron temperature and density are shown as a function of universal time (U.T.) in Fig. 7 for the case of the PDP in the cargo bay. The obvious periodic structure which repeats four times across the plot is due to the "ram-wake cycle" which resulted from a slow orbiter roll about its x-axis (nose-to-tail axis). In order to relate the observed density and temperature variations to the vehicle attitude, we need to set up a coordinate system to describe the direction of plasma flow. This coordinate system is illustrated at the bottom of Fig. 8, which is the attitude plot for the same time period as Fig. 7. The "pitch" angle of plasma flow is θ_1. When $\theta_1 = 0°$, the plasma flows at the orbiter from its underside; when $\theta_1 = 180°$, the plasma is streaming directly down into the cargo bay. The immediate correlation between plasma density and θ_1 is evident when comparing Figs 7 and 8. The azimuth angle of the plasma flow is θ_2 and is measured counterclockwise from the nose (as viewed from above the orbiter). Sensitivity to θ_2 is evident only when the angle θ_1 is near 90°. This is primarily due to the vertical stabilizer and other large structures in the cargo bay near the PDP.

The magnitude of the density depletions in Fig. 7, which is greater than three orders of magnitude, is striking. It should be recalled that the computational method used to determine density and temperature is halted when too little of the I–V curve is available for unambiguous interpretation (see Section 3). The probe current is usually at least one order of magnitude above the probe threshold of detectability at this point but continues to fall rapidly until no current is detected at any sweep voltage. Thus, the three orders of magnitude depletion is a conservative estimate of the density change and in reality the $\alpha = N_{wake}/N_{ambient}$ probably extends into the 10^{-4} or 10^{-5} range. It should

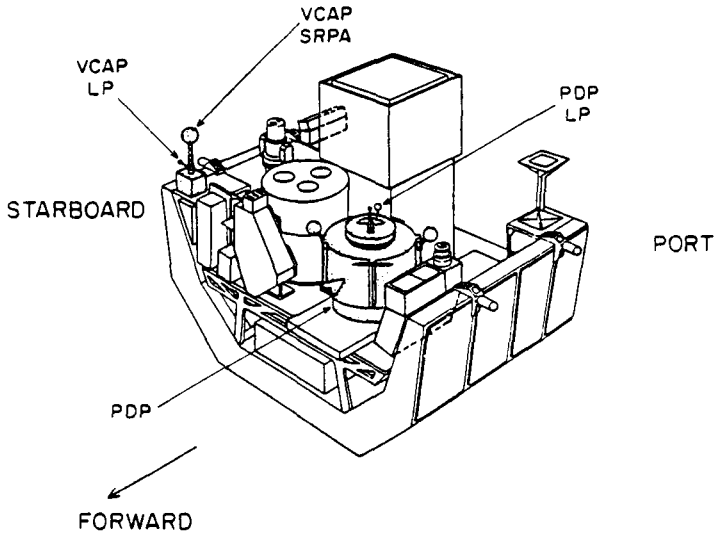

FIG. 5. THE *OSS*-1 PAYLOAD FOR THE THIRD SHUTTLE FLIGHT HAD THE PDP POSITIONED SUCH THAT THE LANGMUIR PROBE WAS APPROXIMATELY AT STILL LEVEL IN THE CARGO BAY.
The VCAP instrumentation is also highlighted. Note that large structures such as the Thermal Cannister Experiment, only inches from the Langmuir probe, complicate geometry in the analysis of plasma flow in the payload bay.

be noted in Fig. 7 that the dotted lines represent a correction for ram ion current to the probe and no real density enhancement or temperature depression in ram is believed to be present, compared to standard ionospheric conditions.

The next and perhaps more interesting result is the remarkable temperature enhancement seen as the probe enters the wake region. The fact that the temperature shows no evidence of "leveling off" at a stable value before calculations are stopped (refer to the gaps in the data at ~21:30 and 22:08 U.T.) implies that temperature may rise considerably higher in the extreme rarefaction region. Since the probe voltage has a step size of 0.125 V, it is inherently less accurate at determining low temperatures in the range of 1000 K (0.1 eV) (see Section 3), but that accuracy improves as the temperature rises and statistical fits to the straight line portion of the I–V curve are very good. In summary, although the absolute accuracy of the probe in measurements of temperature is probably no better than 50%, and the low end temperatures are underestimated, the trend in Fig. 7 is apparent and cannot be attributed to instrumental effects.

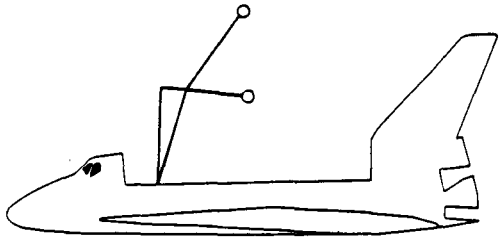

FIG. 6. THE LOCATION OF THE PDP ABOVE THE CARGO BAY FOR THE "RMS" DATA ILLUSTRATED IN THIS PAPER PLACES IT WELL OUT OF THE WAY OF STRUCTURES IN THE BAY ITSELF, MAKING THE ORBITER BODY THE DOMINANT OBJECT IN ALL WAKE ANALYSIS.
(The RMS is 50 ft long when fully extended.)

To determine the variation of the density depletion in the wake region as a function of distance behind the vehicle, it is useful to compare the above results obtained while the PDP was in the payload bay with those obtained while on the RMS at a distance of 10 m above the payload bay. This is, of course, equivalent to having a probe further behind the obscuring plate in the laboratory experiments or mounting a sensor on the boom of a small satellite.

Figure 9 shows data from one orbit while the PDP is on the RMS arm. Figure 10 is the corresponding orbiter attitude. Note that the density rarefaction from ~17:00 to 17:20 U.T. is not nearly as pronounced as those in Fig. 7 and that the temperature enhancement is also less dramatic. The fine structure in the plot (sharp peaks of a few minutes duration) correlates well with the predicted wake of the PDP

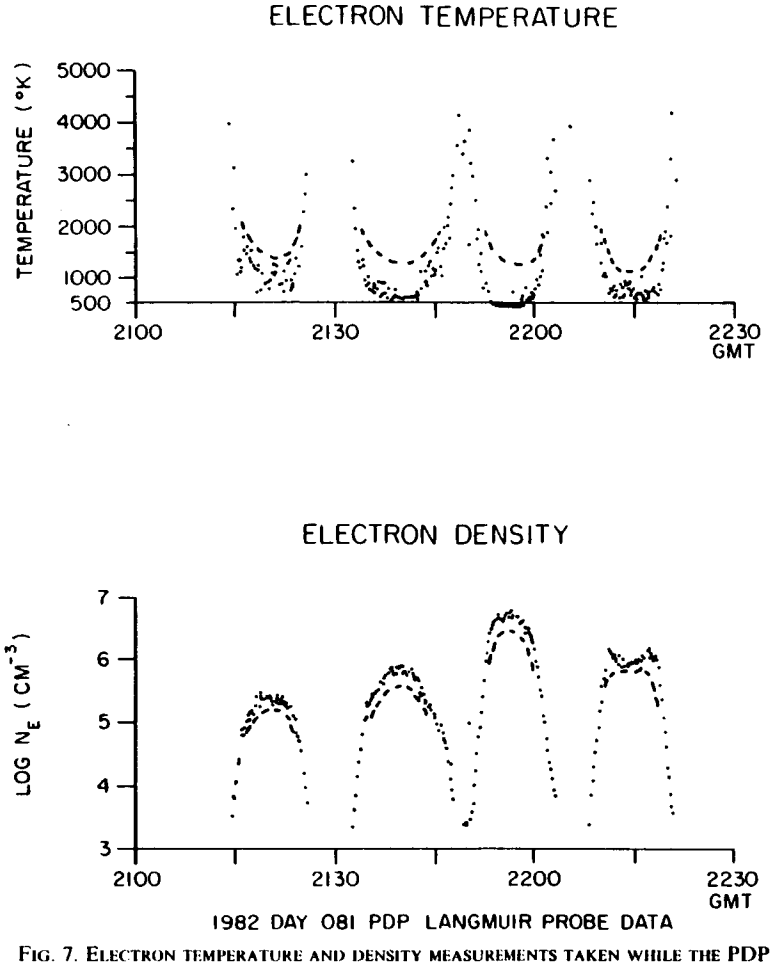

FIG. 7. ELECTRON TEMPERATURE AND DENSITY MEASUREMENTS TAKEN WHILE THE PDP IS IN THE ORBITER BAY ARE DOMINATED BY THE WAKE STRUCTURE RESULTING FROM A PASSIVE THERMAL CONTROL (PTC) ATTITUDE, WHICH ROLLS THE ORBITER ABOUT AN AXIS THROUGH ITS NOSE AT A RATE OF 24° min^{-1}.

The low-end temperatures are underestimated by approximately a factor of two by processing software (see Section 3 for details). Dotted lines represent ion current corrections.

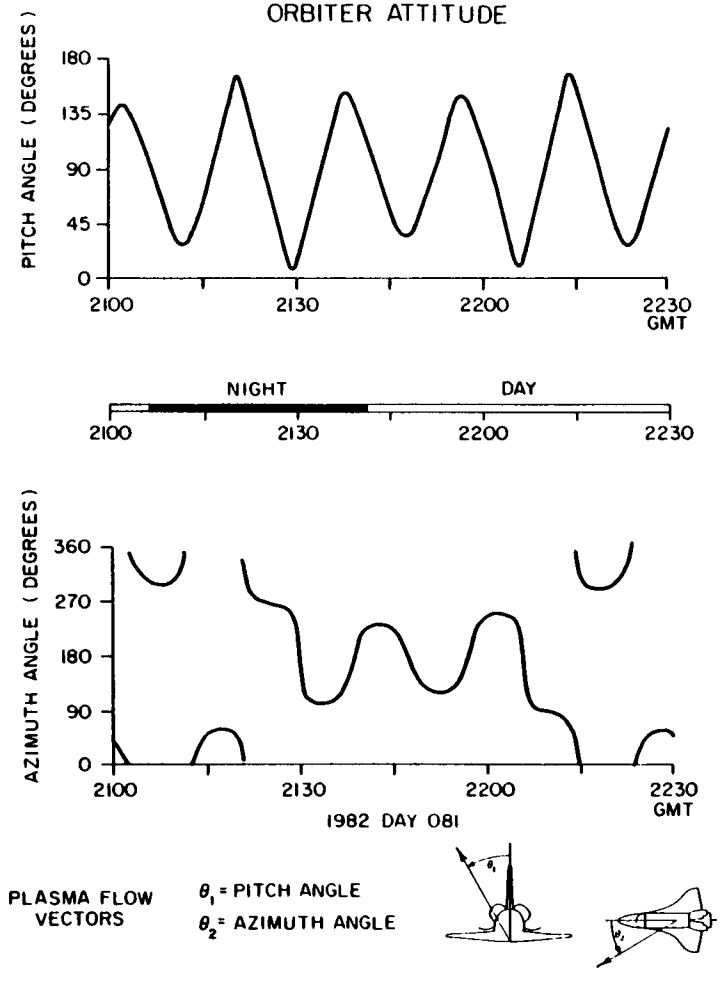

FIG. 8. θ_1 AND θ_2 INDICATE THE PLASMA FLOW VECTORS FOR THE TIME PERIOD ILLUSTRATED IN FIG. 7.

The ram-wake effect is dominated by θ_1, the "pitch" angle or co-elevation of the flow. When θ_1 is less than 90°, the flow is from underneath the orbiter and the PDP is in the plasma wake. θ_2 has little effect except when θ_1 is near 90°.

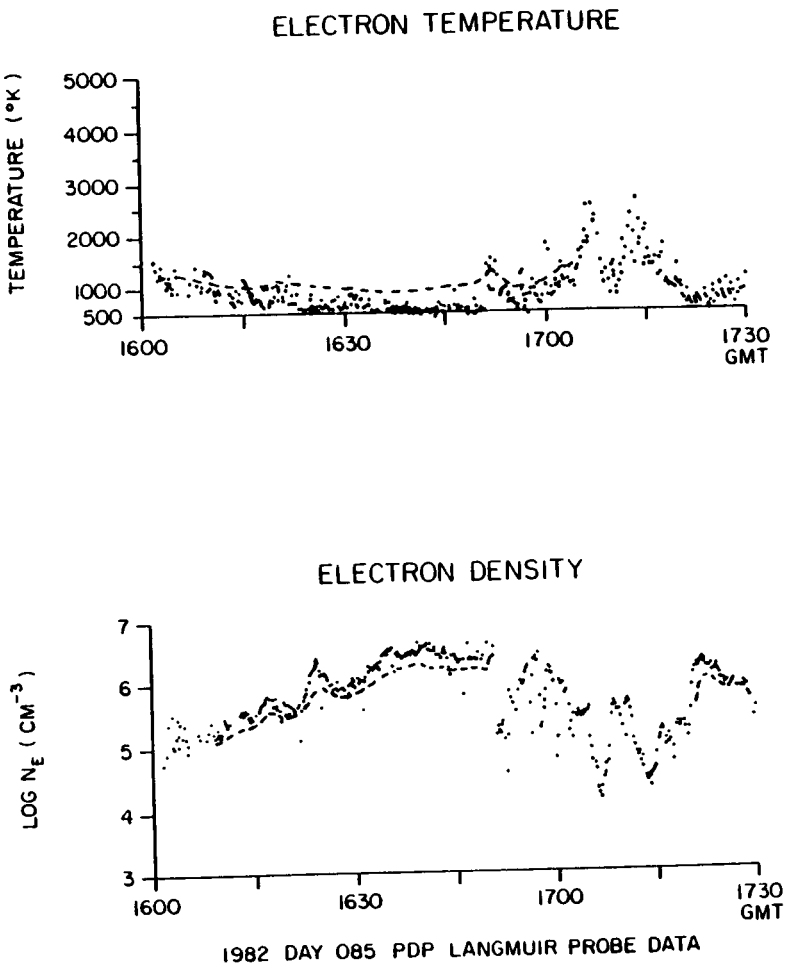

FIG. 9. ELECTRON TEMPERATURE AND DENSITY MEASUREMENTS ON THE RMS DO NOT SHOW THE DEEP WAKE OBSERVED IN THE PAYLOAD BAY, BUT INDICATE THE SUPERPOSITION OF A SHALLOWER ORBITER WAKE COMBINED WITH A WAKE DUE TO THE PDP ITSELF AS IT IS ROTATED ON THE RMS.
Note that low end temperatures are underestimated (see Section 3 for details). Dotted lines represent corrections due to ion current.

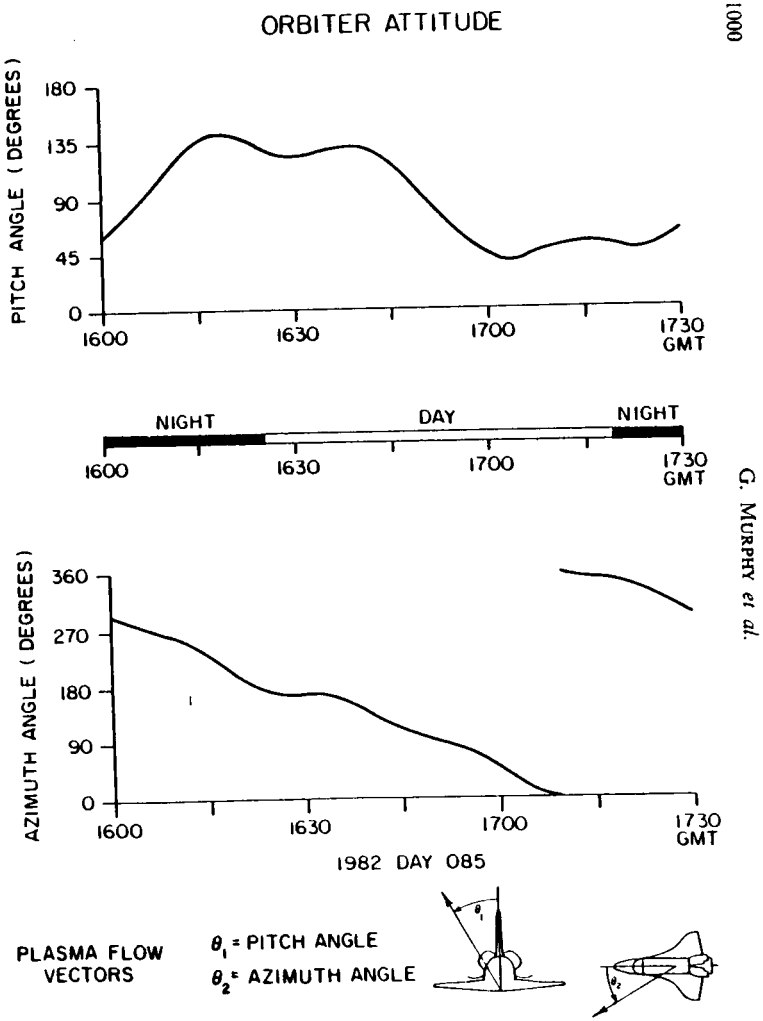

FIG. 10. THE ORBITER ATTITUDE DURING THE TIME INTERVAL FOR DATA SHOWN IN FIG. 9 WAS "NOSE-TO-SUN" WITH AN 8° min $^{-1}$ ROLL.
This resulted in a once-per-orbit "ram wake" cycle as illustrated by the θ_1 and θ_2 plasma flow vectors.

and RMS. Since the PDP was being rotated while on the RMS, the orientation of the Langmuir probe with respect to plasma flow around the PDP and RMS (angle of attack) varies, producing this fine structure variation. It would be useful to compare these data to those from the small satellite category since the PDP is approximately 1 m in diameter and the RMS is approximately 0.3 m in diameter. Again, as with Fig. 7, the dotted line represents temperature and density measurements corrected for worse-case ion current.

The third set of raw data which this paper will address is the $\Delta N/N$ output. The plasma turbulence (Raitt *et al.*, 1984) present in the vicinity of the shuttle has received some attention, and understanding its nature can give us greater insight into the special problems associated with large vehicles interacting with the ionospheric plasma. Figure 11(a) is a plot of the RMS value (averaged over 1.6 s) of $\Delta N/N$ in the 6–40 Hz region. This plot covers the same time period as Figs 7 and 8 and was taken while the PDP was in the orbiter's payload bay. The turbulence in this

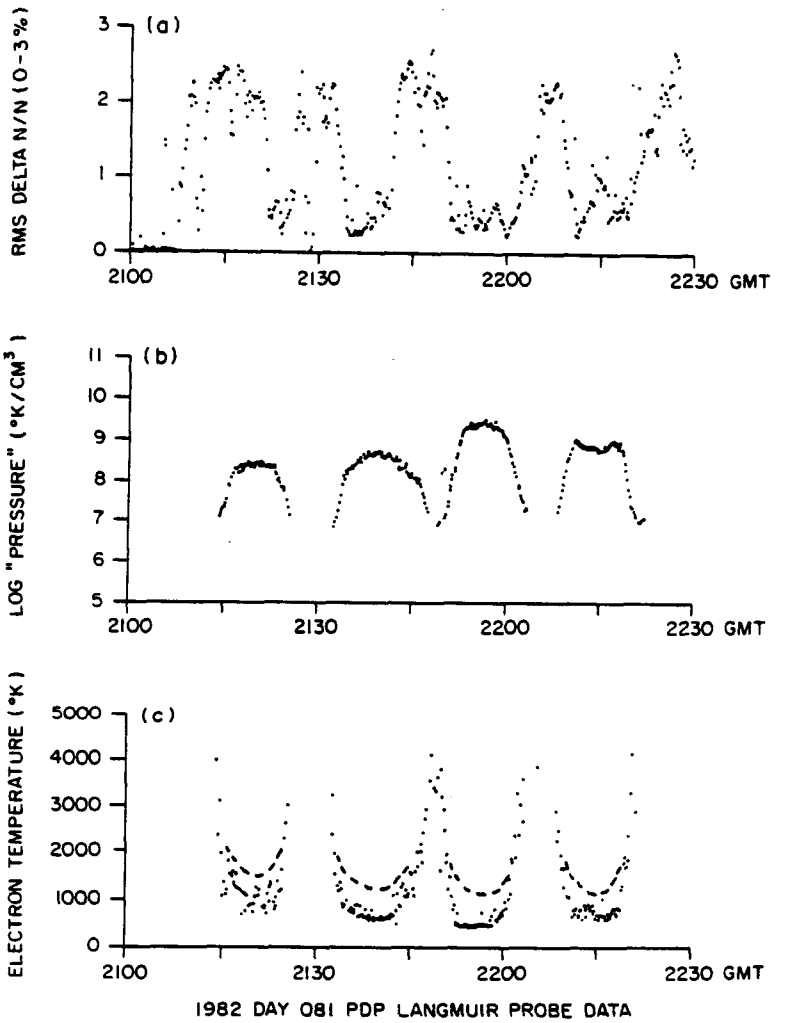

FIG. 11. (a) THE RMS VALUE OF THE PERCENTAGE OF DENSITY FLUCTUATIONS ($\Delta N/N$) IN THE FREQUENCY RANGE 6–40 HZ IS PLOTTED FOR THE SAME TIME PERIOD AS THE FIG. 7 DATA.
Note the peaks have a "double-humped" character with maxima at rising and falling edges of the electron temperature curve.
(b) DENSITY AND TEMPERATURE IN THE PLASMA YIELDS A VALUE PROPORTIONAL TO ELECTRON PRESSURE.
Note that maxima in (a) correlate well with the steepest pressure gradients.
(c) THE TEMPERATURE DATA FROM FIG. 7 HAVE BEEN REPLOTTED FOR EASE OF COMPARISON TO (a).

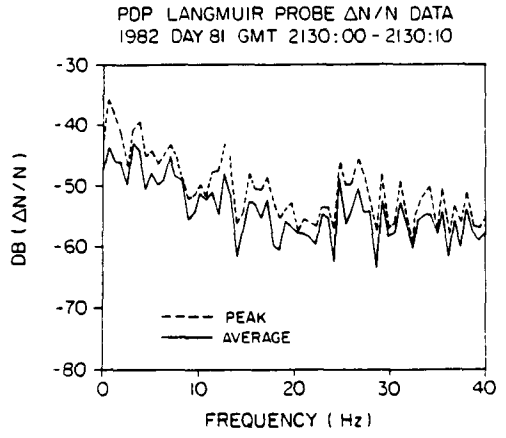

FIG. 12. A FFT OF THE $\Delta N/N$ DATA FOR THE FREQUENCY RANGE 1–40 Hz SHOWS NO PARTICULAR STRUCTURE. This plot is typical of data taken during a time of moderate turbulence.

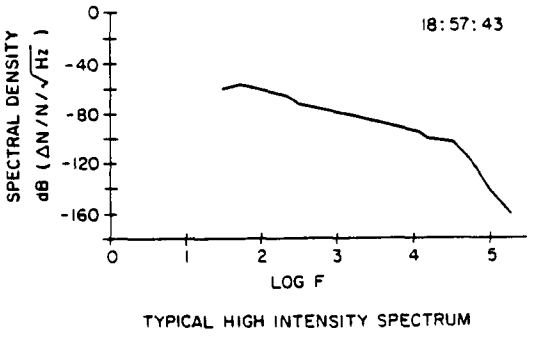

FIG. 13. EXTENDED FREQUENCY ANALYSIS OF THE $\Delta N/N$ SPECTRUM FOR A TYPICAL SAMPLE OF THE NOISE SHOWS A RELATIVELY FLAT SPECTRUM UP TO APPROXIMATELY 30 kHz. This data was taken in the payload bay (D.O.Y. = 083).

frequency range is not observed to be highest in ram as reported by Raitt *et al.* (1984) but highest, generally, in a transition zone between ram and wake. For ease of comparison, the temperature and pressure are also shown in Fig. 11, and one can see a "double-humped" character to the noise, the two peaks appearing more or less at the beginning and end of the wake boundary.

In order to understand the nature of this turbulence, its frequency spectrum needs to be examined as well. Figure 12 is a plot of the Fast Fourier Transform (FFT) of the turbulence from 1 to 40 Hz. The spectrum shows little structure and a typical magnitude of $\Delta N/N$ at any given frequency is less than 1%. Extended frequency analysis up to 178 kHz has been done by using the special Langmuir probe mode on the spectrum analyzer. The noise shows a relatively flat spectral response up through the lower hybrid resonance frequency. This extended analysis has been combined with that at low frequency and a typical spectrum shown in Fig. 13.

5. DISCUSSION AND COMPARISON WITH PREVIOUS RESULTS

Since measurements of the wake characteristics of very large objects are quite new, an assessment needs to be made of how these observations stand against the following: (1) instrumental or systematic problems, (2) other measurements, and (3) predictions from theory and the scaling of observations made in a regime where the object is much smaller.

The Langmuir probe instrument itself seems to perform well. The probe is believed to be quite clean due to atomic oxygen bombardment. It is also relevant that there seemed to be no significant shift in data over the time frame of the mission, leading one to believe the probe condition is a constant. Although absolute accuracy is difficult to achieve, the probe gives (after correcting for ion current) temperatures and densities within approximately 50% of the expected values at peak F-region altitudes and since it is the change in density and temperature which is significant here, the absolute accuracy is not at issue. Further evidence that the probe is measuring plasma characteristics correctly is given in Fig. 14. Here we have plotted the plasma potential as measured by the Langmuir probe, the floating potential as measured by dual-floating probes on the PDP and the difference between plasma and floating potential (ΔV) for the same time interval as the data plotted in Fig. 7. Note that the "cusps" or increases in ΔV correspond to the wake region and are consistent with the increasing plasma temperature observed there. These regions of increasingly negative plasma potential have been observed in the laboratory and are a principal mechanism driving the self-similar ion expansion that has been studied by several investigators (Raychaudhuri *et al.*, 1986). Thus, even without actually measuring the slope of the log I vs V curve to determine temperature, we can independently verify that temperature must, in fact, be increasing at these times.

Comparison with other measurements must first take place where spacecraft scales are similar. The *Gemini/Agena*, *Explorer* 31 and *AE-C* spacecraft (Medved, 1969; Samir and Wrenn, 1972; Samir and Fontheim, 1981) were similar in size to the PDP and sampled regions of similar plasma density at comparable Mach number. The temperature and density data shown in Fig. 9 while the PDP is on the RMS arm show small-scale depletions in density ($\sim 50\%$)

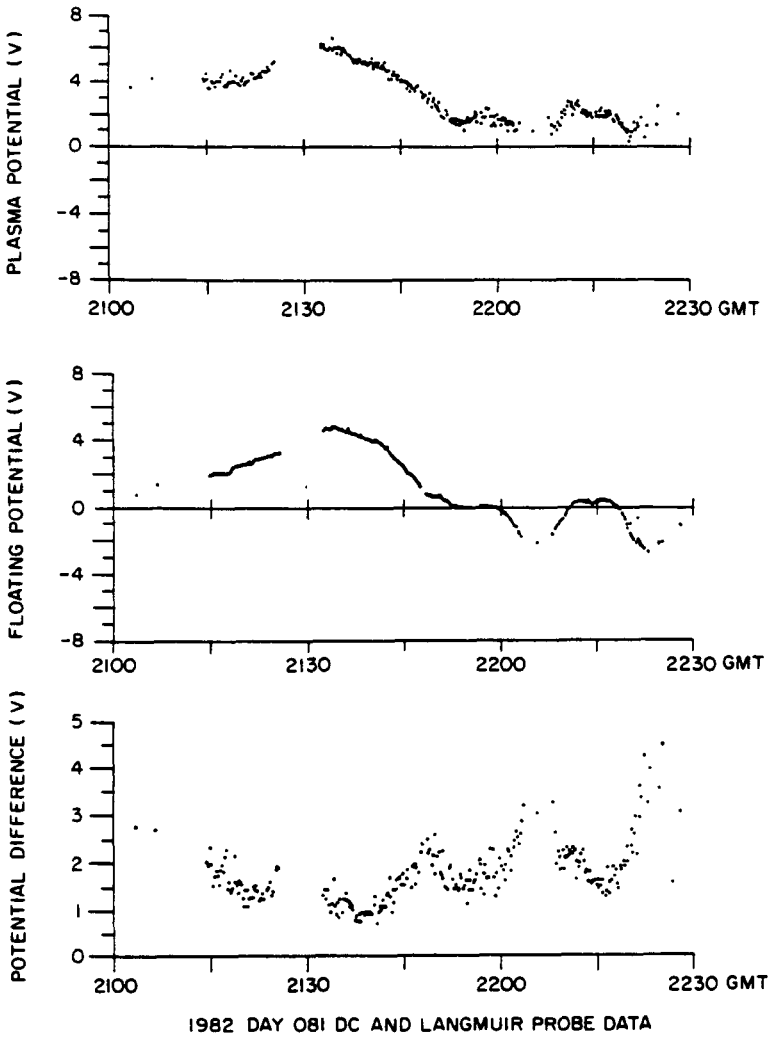

FIG. 14. THE TOP TWO PANELS ARE A COMPARISON OF THE PLASMA POTENTIAL DATA MEASURED BY THE LANGMUIR PROBE WITH THE FLOATING POTENTIAL MEASURED BY THE SPHERICAL FLOATING PROBES. The third panel is a plot of plasma potential minus floating potential and should be proportional to the plasma temperature. Note the 1–2 V offset is consistent with that expected in this temperature density regime but is periodically enhanced during wake encounters.

and increases in temperature (50–100%), which are entirely consistent with the previous results on small spacecraft.

Comparison of our results to those of Siskind *et al.* (1984), which were also made on the *STS*-3, shows both experiments agree on the magnitude of electron density depletions. However, while the PDP Langmuir probe indicates an elevated temperature in wake, Siskind *et al.* (1984) interpret the VCAP Langmuir probe data to indicate an elevated temperature in ram. Although the PDP and VCAP instruments were not always operating simultaneously, data were taken under similar circumstances and general agreement would be expected. Samir *et al.* (1986) have systematically compared the results of laboratory and small satellite experiments, as well as the predictions of several theories, to the Siskind *et al.* (1984) data. They state that "No electron temperature enhancement, known to the authors, has been found for ram conditions on small satellites. Therefore, we submit that the results of Siskind *et al.* (1984) and Siskind (1983) are in contrast with all earlier results." While the PDP Langmuir probe temperature measurements are contrary to the Siskind *et al.* (1984) measurements.

they do agree with the majority of other experimental results.

It is difficult to scale measurements from bodies of the 50–100 λ_D size range to those of the orbiter, but the enhancement in T_e has been seen to be a function of body size up through the *Gemini-Agena* experiment. Plasma chamber experiments performed by Oran *et al.* (1975), Illiano and Storey (1974) and Stone (1981) all indicate temperature enhancement in the near wake. In particular, Stone (1981) carried the measurements further downstream and supports the result that the temperature enhancement is a near-wake phenomenon, extending spatially downstream only to about $z = SR_0$, where S = Mach number and R_0 = body size. This is consistent with the comparison made between our pallet and RMS data. At a distance of $\lesssim R_0$ downstream, the density depletion was only two orders of magnitude and the temperature enhancement was only $\sim 100\%$, compared to more than three orders of magnitude density depletions and factors of five temperature enhancement seen in the near wake during pallet measurements. This suggests that a rough scaling law may indeed work for objects the size of the shuttle orbiter, at least for the gross wake structure.

An explanation for the elevated electron temperature observed in the wake of orbiting spacecraft has been addressed by various authors (e.g. Samir and Wrenn, 1972; Troy, 1975; Gurevich *et al.*, 1973). It has been speculated that the hot electrons may result: (1) from a selection effect by the negative potential generally found in the spacecraft wake, or (2) from energization of the electrons by wave–particle interactions in the plasma turbulence present in or near the wake. A third and alternative explanation, which does not involve turbulence, may be along the lines indicated by Fried and Wong (1966) to explain ion cooling when ions from a high potential expand into a low-potential region in a laboratory double-plasma device. In the case of an orbiting spacecraft, electrons reaching the spacecraft within the wake would be nearly adiabatically compressed (and heated) as they enter the low-potential region attached, at the wake, to the spacecraft. Simple estimates indicate that this effect may account for the observed heating.

The final observation to discuss is that of the plasma turbulence. Turbulence similar to that reported herein has been observed in the wake region of other satellites, e.g. *Ariel* 1 (Samir and Wilmore, 1965). The PDP Langmuir probe results again seem inconsistent with those of Siskind *et al.* (1984) in that Siskind *et al.* report this turbulence to be greatest in ram, whereas the PDP results show that the turbulence is generally greatest in the transition region between ram and wake. The key difference in the observations may be due to the spectral content of the noise. Components between 2 and 3 kHz which is the frequency range observed by Siskind *et al.* with the VCAP instrumentation region may show a different ram–wake dependence than those in the 6–40 Hz frequency range plotted in Fig. 12. Since the whole spectrum of turbulence is only available when the 16-channel spectrum analyzer is in Langmuir probe mode (approximately 1 min out of every 8), a study of the spectral dependence vs angle of attack has not been possible.

Acknowledgements—The authors wish to thank Professor D. Gurnett for the use of his potential data and Fahad Jalawi for his hard work in developing a very "smart" code for automation of the Langmuir probe data analysis. Special thanks are extended to Uri Samir for his interest and advice and to Nobie Stone and Ken Wright for helpful discussions in relation to laboratory work. The hard work and special help from the reviewer in calling attention to the ion-current effect has enhanced understanding of the data and added to the strength of the work. This help was greatly appreciated.

This paper was supported by NASA Lewis Research Center Grant NAG3-449. The hardware and flight of the PDP on *OSS*-1 was supported by MSFC Contract No. NAS8-32807.

REFERENCES

Fried, B. D. and Wong, A. Y. (1966) *Physics Fluids* **9**, 1084.
Gurevich, A. V., Pariiskaya, L. V. and Pitaevskii, L. P. (1973) *Sov. Phys. JETP* **36**, 274.
Illiano, J. M. and Storey, L. R. O. (1974) *Planet. Space Sci.* **22**, 873.
Medved, D. B. (1969) Rarefied gas dynamics, *Sixth Int. Symp. Proc.* p. 1525.
Oran, W. A., Samir, U., Stone, N. H. and Fonrhwim, E. G. (1975) *Planet. Space Sci.* **23**, 1081.
Raitt, W. J., Siskind, D. E., Banks, P. M. and Williamson, P. R. (1984) *Planet. Space Sci.* **32**, 457.
Raychaudhuri, S., Hill, J., Chang, H. Y., Tsikis, E. K. and Lonngren, K. E. (1986) *Physics Fluids* **29**, 289.
Samir, U. and Fontheim, E. G. (1981) *Planet. Space Sci.* **29**, 975.
Samir, U., Stone, N. H. and Wright, K. H., Jr. (1986) *J. geophys. Res.* **91**, 277.
Samir, U. and Willmore, A. P. (1965) *Planet. Space Sci.* **13**, 285.
Samir, U. and Wrenn, G. L. (1972) *Planet. Space Sci.* **20**, 899.
Shawhan, S. D., Murphy, G. B. and Pickett, J. S. (1984) *J. Spacecraft Rockets* **21**, 387.
Siskind, D. E. (1983) Ph.D. Thesis, Utah State University.
Siskind, D. E., Raitt, W. J., Banks, P. M. and Williamson, P. R. (1984) *Planet. Space Sci.* **32**, 881.
Stone, N. H. (1981) The aerodynamics of bodies in a rarefied ionized gas with applications to spacecraft environmental dynamics, NASA Technical Publication 1933.
Troy, B. E., Jr., Medred, D. B. and Samir, U. (1970) *J. astronautical Sci.* **18**, 173.
Troy, B. E., Jr., Maier, E. J. and Samir, U. (1975) *J. geophys. Res.* **80**, 993.

JOURNAL OF GEOPHYSICAL RESEARCH, VOL. 91, NO. A12, PAGES 13,463–13,471, DECEMBER 1, 1986

Plasma Diagnostics Package Measurements of Ionospheric Ions and Shuttle-Induced Perturbations

DAVID L. REASONER

Space Science Laboratory, NASA Marshall Space Flight Center, Huntsville, Alabama

STANLEY D. SHAWHAN[1] AND GERALD MURPHY

Department of Physics and Astronomy, University of Iowa, Iowa City

The plasma diagnostics package (PDP) on the space shuttle STS-3 mission in March 1982 carried among its instrument complement a retarding potential analyzer. This instrument measured both the ambient ion plasma density and temperature, and perturbations to the plasma produced by shuttle orbiter effects. Whenever the plasma flow streamline at the instrument was more than a distance of the order of thermal ion gyroradii away from any orbiter surface, the measurements were characteristic of the ambient ionosphere. In several situations, the PDP was positioned so as to scan the wake in the plasma flow produced by orbiter surfaces. The density profile of the major species O^+ was consistent with a classic Mach cone. However, strong perturbations extended for several meters outside the Mach cone which resulted in failure of flowing Maxwellian distributions to represent the data. Configurations where the plasma flow impacted orbiter surfaces downstream of the PDP resulted in generation of a suprathermal ion component. The observations are discussed in terms of a recent model of the mechanism for generation of shuttle glow.

1. INTRODUCTION

The flight of the STS-3 shuttle mission during March 22–30, 1982, carried a pallet of science investigations (OSS-1) sponsored by the NASA Office of Space Science [*Neupert et al.*, 1982]. Among the experiments on the mission was the University of Iowa's plasma diagnostics package (PDP) [*Murphy et al.*, 1983]. The instrument complement of the PDP included a retarding potential analyzer (RPA). The RPA was designed to measure the density and temperature of the major thermal ion species, both the ambient ionospheric plasma and perturbations to the ambient plasma produced by the presence of the shuttle orbiter. Other scientific objectives of the PDP included measurement of the electromagnetic environment around the orbiter, the neutral gas pressure in the orbiter cargo bay, and the effects of the electron beam of the vehicle charging and potential (VCAP) experiment [*Banks et al.*, 1983*a*]. Preliminary results from the PDP and from the electron beam experiments have been reported in the papers referenced above. More comprehensive studies, including the effects of water dumps and thruster firings, have been reported by *Shawhan et al.* [1984] and *Pickett et al.* [1985]. In this paper we concentrate upon measurements made by the RPA. The objectives of this experiment were to study interactions between the ambient ionospheric plasma and the orbiter, to determine under what conditions the RPA, in proximity to the orbiter, could make a valid measurement of ambient thermal ion parameters, and how the presence of the large orbiter body may have affected the measurements. The orbiter was large in the sense that its dimensions (37 m in length; 24 m wing span) exceeded the Debye length and the thermal ion and electron gyroradii. For typical ionospheric density and temperature parameters (see, for example, *Sharp* [1966] and *Benson et al.* [1977]), the Debye length is less than 1 cm. The gyroradii for ions in the range m = 16 to 30 and T = 1000° to 1500°K ranges from 5 to 10 m for B = 0.3 G. The ion sound speed $V_{is} = k\bar{T}_e/m_i$, is 0.72–1.0 km/s for T_e = 1000°–2000°K, and therefore the orbiter with a velocity of 7.85 km/s was highly supersonic with Mach numbers ($M = V_{orb}/V_{is}$) in the range 7.8–11.

The STS-3 mission was launched March 22, 1982 (day 81), into a near-circular orbit with apogee of 237.1 km, perigee of 228.3 km, and inclination of 38°. For the data period of interest reported here, the local time of the ascending node varied from 5.53 to 6.24 hours.

The retarding potential analyzer was a conventional four-grid instrument with a planar grid structure. All grids were fabricated from electroformed mesh with 90% transmission. The entrance grid was 1.6 cm diameter, or 2.0 cm^2 in area. The retarding grid, shield grid biased at ground potential, and suppressor grid biased at -40 V completed the grid system. A guarded collector with a diameter of 4.0 cm was connected to the electrometer input. The shield grid served to isolate the retarding region from the relatively high suppressor potential, as well as to reduce capacitive coupling between the retarding grid and the collector. The intergrid spacing was 0.3 cm, and the geometry was arranged such that the angular acceptance range of 45° half-angle was defined by the projection of the entrance aperture onto the collector.

The collector current from positive ions was measured and conditioned for telemetry by a four-decade range-switching electrometer. The most sensitive range was 1.0×10^{-9} A full scale with eight-bit (0–255) resolution. The electrometer noise level was about 2×10^{-12} A.

The retarding potential program was a stairstep sequence from 0.0 to 15.0 V in 0.5-V increments. The 0.0-V step was repeated in order to allow the electrometer to settle when transitioning from the 15.0-V step with minimum current to the 0.0-V step with maximum current.

In order to perform a series of scientific experiments, the PDP was lifted out of the orbiter bay by the remote maneuvering system (RMS) and moved according to a set of preprogrammed sequences. At other times, the PDP was manually positioned by the orbiter

[1]Now at Space Plasma Physics, Office of Space Science and Applications, NASA Headquarters, Washington, D.C.

Paper number 5A8301.
0148-0227/86/005A-8301$05.00

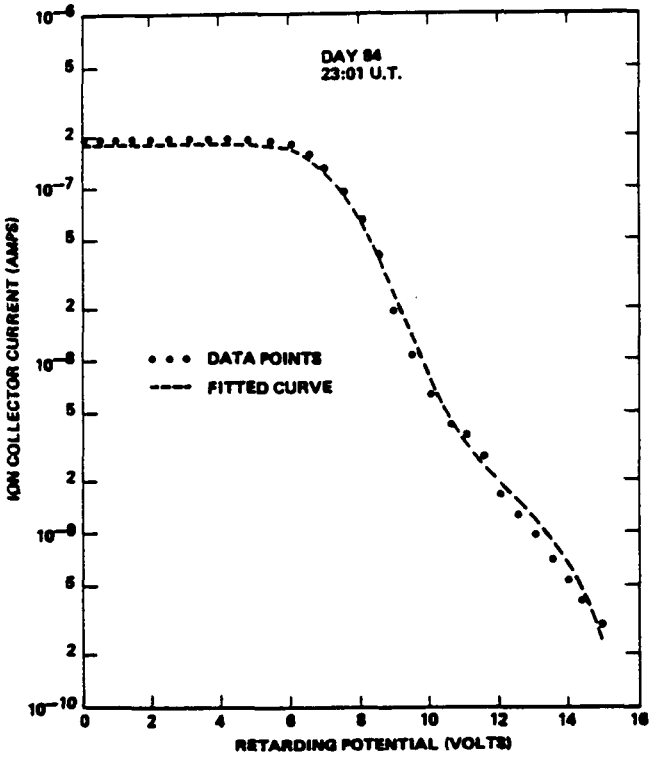

Fig. 1. A typical plot of the RPA collector current as a function of retarding voltage, for day 84, 2301 UT in the daytime ionosphere. The method for reduction of these data to physical units is discussed in the text.

crew in order to place the PDP in a favorable position to diagnose the VCAP electron beam. The PDP could be positioned in X, Y, and Z coordinates relative to the orbiter and oriented in pitch, yaw, and roll by the RMS.

2. Data Analysis Methodology

The initial goal of the RPA data analysis was to determine the density and temperature of the major ion species and to see what effect, if any, the presence of the orbiter had upon these determinations. As we shall see, it was also necessary to consider the potential of the PDP relative to the ambient plasma. In the flight situation the PDP was attached to the orbiter by the RMS and the $\vec{V} \times \vec{B}$ electric field of approximately 0.2 V/m created significant potentials over the length of the orbiter. The amount of conducting area of the orbiter in contact with the plasma ($\approx$50 m^2) was an order of magnitude larger than that of the PDP ($\approx$3 m^2). Hence the electromotive force ($\pm$5 V) was able to drive and sustain the PDP potential to values significantly different than the thermal energies of the ambient plasma. As well, the PDP potential could be a significant fraction of the ram energy of the plasma flow relative to the orbiter.

An example of a plot of the collector current versus retarding potential from the RPA is shown in Figure 1. At the time these data were taken the orbiter latitude and east longitude were 34.62° and 224.07°, respectively, the local time was 1357, and the solar zenith angle was 42°. The solid circles are the data points, and the dashed curve is a fit to the data points by a method discussed in detail below. At low retarding potentials the curve is typical of that produced by a single component ion plasma with a high Mach number. However, at higher retarding potentials the departure of the retarding portion of the curve from a straight line indicates that one or more higher mass ion components had a significant presence. The RPA equation found, for example, by *Hanson et al.* [1970] was fit to the data with a multiparameter least squares fitting procedure based on the routine CURFIT from *Bevington* [1969]. The fitting procedure was first attempted with a seven-parameter fit. The parameters were the density and temperature of O^+, NO^+, and O_2^+ and the PDP potential. However, the 0.5-V resolution of the RPA was only slightly less than the difference in ram energy between NO^+ and O_2^+ at orbital velocity. It was found that the fitting procedure was highly unstable and did not converge well. Tests of the fitting program with simulated data plus random noise showed that the fitted values would be in error by a factor of 2 or more and were not invariant under choice of differing random number seeds. Therefore the fitting technique chosen was to assume a two-ion flowing Maxwellian distribution composed of O^+ and NO^+. Admittedly, the choice of NO^+ as opposed to O_2^+ was somewhat arbitrary, but data from an ion mass spectrometer on the same spacecraft (J. M. Grebowsky, private communication; OSS-1/STS-3 Post Mission Interim Science Report, 1982) show that in most cases the NO^+ density exceeded the O_2^+ density by a factor of 2 or more. Unfortunately, the ion mass spectrometer and the RPA were on opposite sides of the spacecraft, and since the spacecraft was not spinning, near-simultaneous data from the two instruments were not possible. The fitting program had five free parameters, specifically the density and temperature of O^+ and NO^+ and the PDP potential. The ram angle (angle between the instrument normal and the flow velocity) of the RPA and the orbiter velocity were known from the orbiter and RMS ancillary attitude data. The normal component of the ion velocity relative to the RPA was an input to the fitting procedure. The fitting procedure applied to the data of Figure 1 resulted in the following parameters: O^+ density = 1.1 $\times$ 10^6, O^+ temperature = 1450°K, NO^+ density = 2.5 $\times$ 10^4, NO^+ temperature = 2640°K, and PDP potential = –2.6 V.

The RPA grid design was such that there was no internal shadowing of the RPA collector by the grid structure until the ion angle of the incidence reached 45°. That is, up to 45° the effective area followed a cos θ dependence but fell more rapidly at higher angles. Fitting at higher angles would have involved a complex iterative convolution procedure with questionable accuracy. Therefore the fitting procedure was only done if the ram angle was 45° or less. This was a significant restriction in terms of the amount of data available for analysis. The PDP was out of the orbiter bay attached to the RMS for the periods day 84, 1620–2330 UT and day 85, 1500–2200 UT, or a total of 14.1 hours. Of this, only 154 min of data met the criterion that the ram angle was 45° or less.

The effects upon the plasma environment from STS-3 emissions of water and water vapor from the holding tanks and the flash evaporator system have been discussed by *Pickett et al.* [1985]. The effects of these chemical releases were seen in plasma wave data and in observations of enhanced plasma turbulence. None of the periods of available RPA data overlapped water release periods except for a short interval on day 85, 1622-1630 UT. No obvious effects could be seen in this segment, and any conclusions based on this one short period of overlap could hardly be justified. Therefore this study was limited to periods that were free of long-duration perturbations due to water releases but includes periods of thruster operations. These periods have also been shown to cause plasma perturbations [*Pickett et al.*, 1985]. However, thruster operations were of brief duration, typically tens to hundreds of milliseconds, and the time resolution of the RPA data plus the method of data analysis emphasized long-term trends and obscured short-term effects.

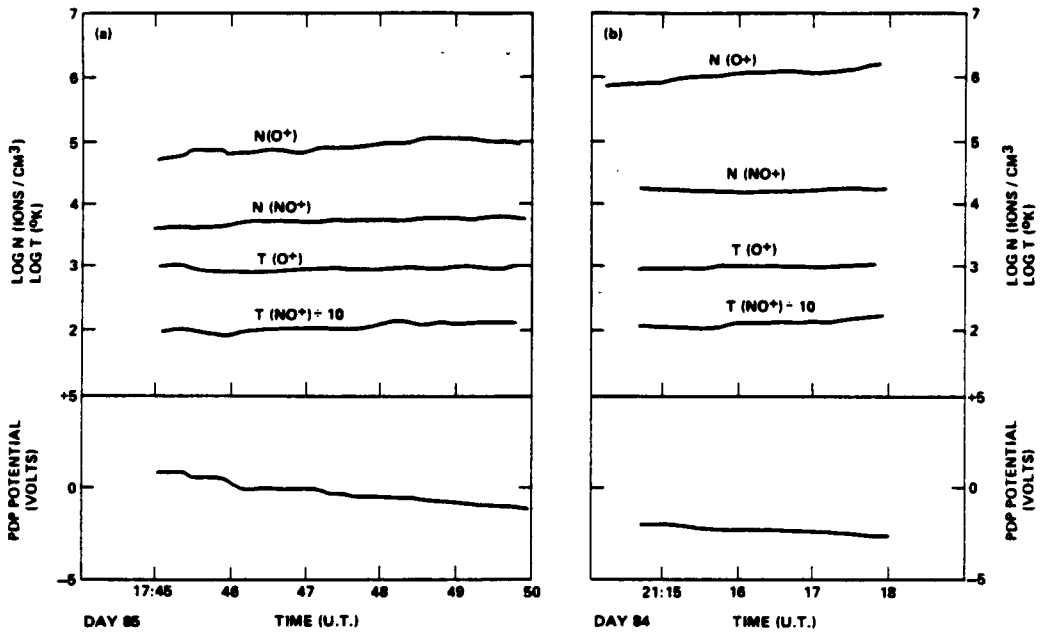

Fig. 2. Examples of data from (*a*) the night ionosphere and (*b*) the daytime ionosphere. The data presentation shows the density and temperature of O^+ and NO^+ and the value of the PDP potential relative to the plasma. The NO^+ temperature has been shifted one decade for the sake of clarity. Figure 2*a* is from the period day 85, 1745-1750 UT, and Figure 2*b* is from the period day 84, 2115-2118 UT.

3. Coordinate System

A word about the coordinate system used as the orbiter/PDP reference is in order. The shuttle coordinate system is Cartesian with the X axis along the fore-aft direction and $+X$ toward the nose. $X = 0$ is arbitrarily located in the plane containing the nose of the external tank. The Z axis is the yaw axis with $-Z$ being upward out of the cargo bay, and $Z = 0$ being along the centerline. Y completes the system, and $+Y$ is toward the starboard (right) wing. The location of the orbiter velocity vector and the $\vec{B}$ vector was given in a modified polar coordinate system of coelevation and azimuth, with coelevation being measured from the $-Z$ axis and azimuth being measured clockwise looking from above from the $-X$ axis. The ancillary ephemeris and attitude data gave the X, Y, and Z position of the PDP and the pitch, yaw, and roll angles of the PDP in the orbiter system. These data allowed determination of the geometry of the plasma flow and $\vec{B}$ vectors relative to the orbiter/PDP system.

4. Data

The PDP was first deployed on the RMS on day 84 at 1610 UT. For all of the periods that the PDP was deployed on the RMS, the orbiter was oriented with the $+X$ axis toward the sun (nose to sun), and rolling twice per orbit such that at the ascending and descending nodes the $-Z$ axis, upward out of the bay, was perpendicular to the ecliptic plane.

An example of plasma data in the local night ionosphere is shown in Figure 2*a* for the period day 85, 1745–1750 UT. The plot shows the density and temperature of O^+ and NO^+ and the value of the PDP potential. The orbiter latitude ranged from -28° to -18° during this period. The O^+ and NO^+ densities were near 10^5 and 5×10^3 ions/cm^3, respectively, and the ion temperatures were near 1000°K. Note that during this period the PDP potential ranged from +1 to -2 V, a consequence of the changing value of the $\vec{V} \times \vec{B}$ electric field with changing orientation of the $\vec{B}$ field relative to the orbiter. Figure 2*b* shows an example of data for the sunlit ionosphere for the period day 84, 2115–2118 UT. The orbiter latitude ranged from 26° to 31°. Here the O^+ density was $0.9–1.5 \times 10^6$ ions/cm^3, the NO^+ density was 2×10^4 ions/cm^3, and the ion temperatures ranged between 1100° and 1500°K.

The geometry of the PDP and the orbiter is illustrated in Figure 3 for the data periods discussed above. The PDP was positioned 20.5 m above the level of the payload bay doors and 1.8 m right of the centerline as viewed from the front of the orbiter. The directions of the instrument normal and the range of directions of the plasma ram flow vectors are shown. It is particularly important to note that the PDP-orbiter separation exceeded all of the plasma scale sizes discussed earlier (Debye length and ion and electron gyroradii). Furthermore, the distance between the plasma streamlines upstream of the PDP and any orbiter surface exceeded the plasma scale sizes.

These two examples of data from the dark and sunlit ionosphere gave computed values of the ion densities and temperatures which were certainly reasonable [*Sharp*, 1966; *Benson et al.*, 1977], and we consider this as a proof of the instrument and of the data analysis methodology. These examples show as well that under certain conditions, examined in greater detail later in this paper, an instrument attached to the orbiter is able to make valid measurements of the characteristics of the ambient ionosphere. This is particularly important to future space plasma missions where active experiments injecting particle beams, electromagnetic waves, and chemicals will require measurements of the ambient medium and perturbations of the medium in order to understand fully the plasma physics involved.

The roll of the orbiter twice per orbit meant that the plasma velocity vector was constantly changing in the orbiter coordinate system, and therefore there should be periods when the plasma flow at the RPA should have been shadowed by some portion of the orbiter structure. Two clear examples were found in the data. These are shown in Figures 4*a* and 4*b* for the time periods day 84, 1835–1840 UT, and day 85, 1650–1653 UT. Both of these periods are characterized by fluctuations in the computed values of the NO^+

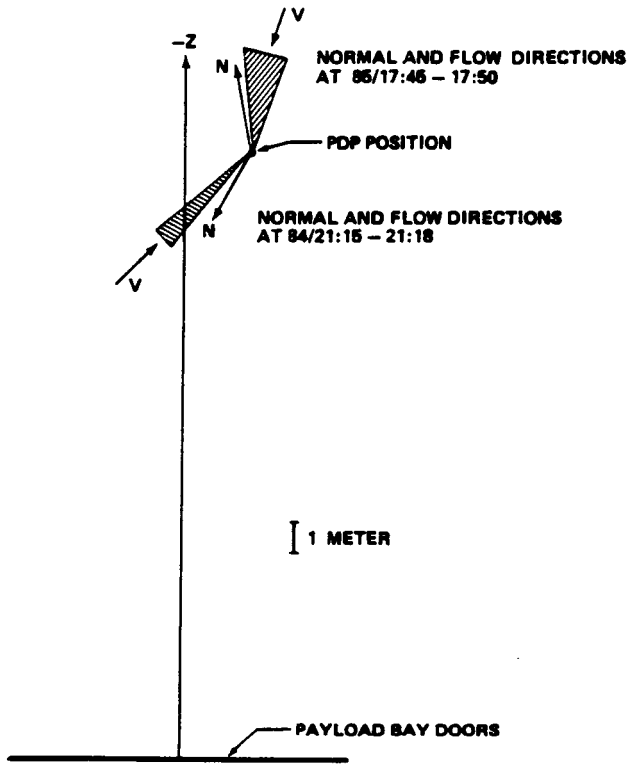

Fig. 3. The geometry of the orbiter-PDP system applicable to the data of Figure 2. The envelope of the payload bay doors, shown as the horizontal line, was the critical surface for both examples. The figure shows the PDP position, the direction of the instrument normal, and the range of directions of the plasma flow vectors for the two periods shown in Figure 2.

density and of the ion temperatures. We do not claim that the computed values of the ion temperatures and the NO^+ density represent the actual state of the plasma. The value of the χ^2 goodness-of-fit parameter was >5 in most cases which indicated that the two-ion flowing Maxwellian model failed to fit the data. This explains as well the erratic behavior of the computed value of the PDP potential. These traces are shown primarily to illustrate that the plasma was highly disturbed, and the subsequent discussion will consider this in greater detail. Contrast these data with those shown inn Figures 2*a* and 2*b* where the PDP was in a region of undisturbed flow and the computed plasma parameters displayed smooth variations.

The computed O^+ density continued to give reasonable values. This is understandable since O^+ is the major ion in terms of number density by at least one order of magnitude and the flow is highly supersonic. Therefore the collector current at zero retarding voltage continued to be an accurate measurement of the O^+ density even in the presence of significant perturbations of the thermal distribution. The O^+ density shows a marked decrease in the first case at day 84, 1839, and in the second at day 85, 1650:30. The solar zenith angles were 53° and 37°, respectively, for these two cases, and hence these density decreases were not a result of solar ultraviolet terminator crossings. Rather, the explanation is found in an examination of the geometry of the plasma flow relative to the orbiter during these periods.

Figures 5*a* and 5*b* show sketches of the geometry relevant to these events. The origin of the coordinate system is the centerline of the payload bay ($Y = 0, Z = 0$), and the horizontal line at $Z = 0.75$ m represents the payload bay doors, which is the critical surface for shadowing of plasma flows from the PDP in this situation. At 1833 on day 84 (Figure 5*a*) the ram angle in the PDP *Y-Z* plane was +20° and decreased over the period 1833–1840 UT to -15°. The PDP was oriented with the instrument normal collinear with the orbiter $+Y$ direction, and hence the plasma flow was initially from above the orbiter *X-Y* plane and during this period moved to a direction from below the *X-Y* plane. The plasma flow streamline approached the edge of the payload bay door, and the plasma stream was more and more under the influence of the perturbing effect of this surface. The sudden decrease in the measured density at 1839 UT was correlated with a movement of the PDP in the $-Y$ direction which carried the instrument farther into the wake created by the payload bay door.

The second example of such a wake effect (Figures 4*b* and 5*b*) occurred over a relatively brief interval (1 min) when the PDP was moved from a position over the center of the payload bay to over the port (left) wing. The PDP was initially positioned over the center of the payload bay, moved rearward (in the $-X$ direction) between 1648 and 1650 UT, and then from 1650 to 1651 UT moved as shown in Figure 5*b*. The PDP was held stationary from 1651 to 1654 UT. However, the maneuver included rotations of the PDP and the ram angle was less than 45° only for the interval 1650–1653 UT. In the course of the maneuver the PDP entered the wake created in the plasma flow by the starboard payload bay door.

We have also examined the data from a Langmuir probe on the PDP. The data for the first period (day 84, 1835–1840 UT) were not available but were for the second period (day 85, 1650–1654 UT). These data are shown in Figure 6. The panels show the electron density, temperature, and the RMS value of $\Delta n/n$ in two frequency ranges, 1–6 Hz and 6–40 Hz. It is seen that prior to entry into the wake (1645), the inferred electron density was $\sim 3 \times 10^6$, in good agreement with the ion density, and the electron temperature was indicated as ~600°K.

The electron temperature measurements are subject to large errors in the range of 1000°K since the voltage step size was 0.125 V. The accuracy improves at higher temperatures, and the trends displayed in the figure cannot be due to instrumental effects [*Murphy et al.*, 1986].

At 1650 UT the electron density decreased by a factor of 10, and the electron temperature rose sharply to 2100°K. Furthermore, the $\Delta n/n$ value increased markedly during this interval, indicating that significant levels of plasma turbulence were being generated.

Assuming a daytime ionosphere electron temperature of 1200°K, the ion sound speed was 0.79 km/s, and therefore the Mach cone angle was 5.7° for the orbital velocity of 7.85 km/s. For a PDP location 10 m downstream of the wake-generating surface we would expect to encounter plasma density decreases when the PDP was within 1 m of the geometric shadow line. Examination of the geometry shown in Figures 5*a* and 5*b* shows this to be the case. However, the data also show that the concept of a fluid dynamic Mach cone is not strictly valid, for it is clear that prior to entering the Mach cone the PDP was not in a region of undisturbed flow, but rather there were significant perturbations to the plasma distribution function which resulted in failure of the assumed two-ion flowing Maxwellian distribution to fit the data, even when the PDP was outside of the Mach cone. Compare the distance scales shown in Figures 3 and 5. In the former case the PDP-orbiter separation was larger than the plasma scale sizes. In the latter it was not, and the disturbances to the plasma are evident.

The data examples discussed thus far represent cases when the RPA was either in a region of undisturbed plasma flow or when a known disturbance source, in particular, wake effects from orbiter surfaces, was perturbing the ambient plasma distributions. There are several instances, however, when the computed density and

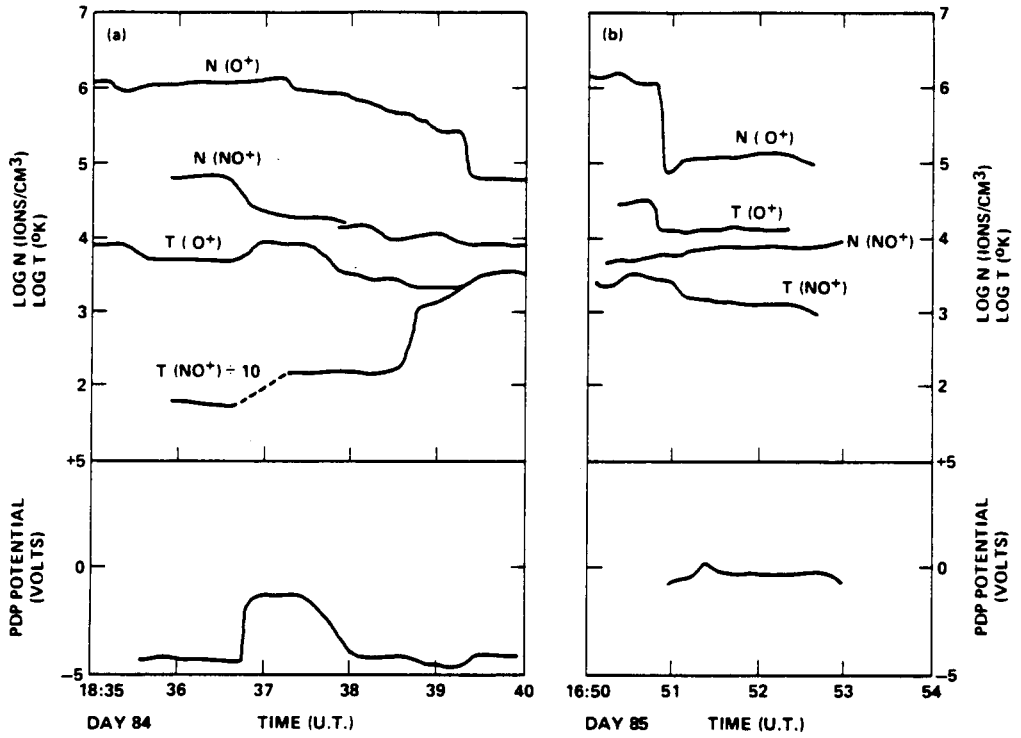

Fig. 4. Examples of daytime ionosphere data when the PDP moved into the downstream wake created by the orbiter payload bay door. Figure 4*a* is for the period day 84, 1835–1840 UT, and Figure 4*b* is for the period day 85, 1650–1653 UT. In Figure 4*a* the NO^+ temperature has been shifted one decade.

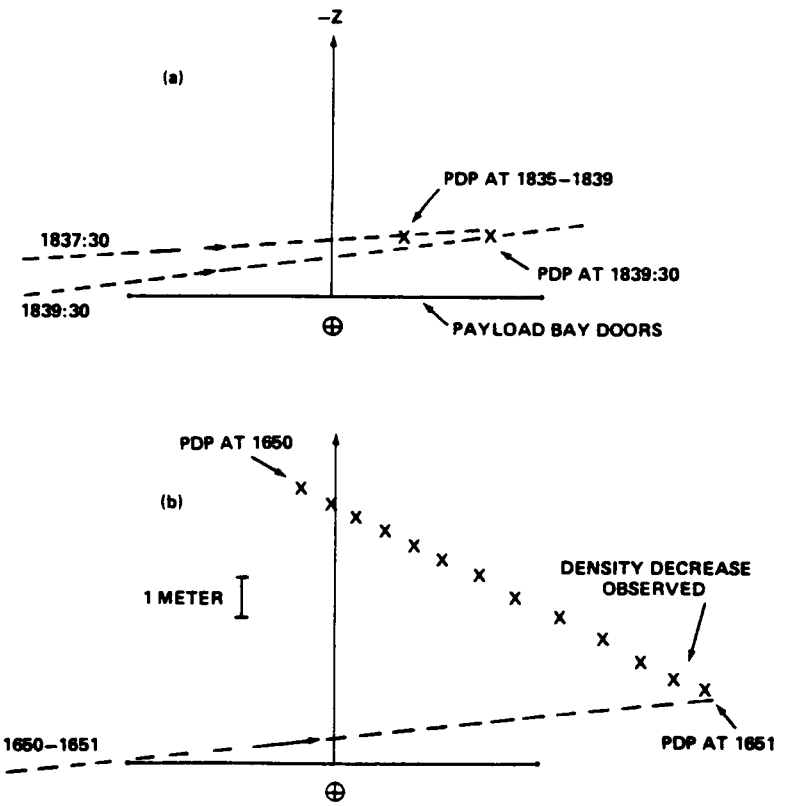

Fig. 5. The geometry of the orbiter-PDP system applicable to the data shown in Figure 4 above. The horizontal line is the envelope of the payload bay doors. The PDP positions are denoted by crosses. Plasma flow vectors are depicted as dashed lines.

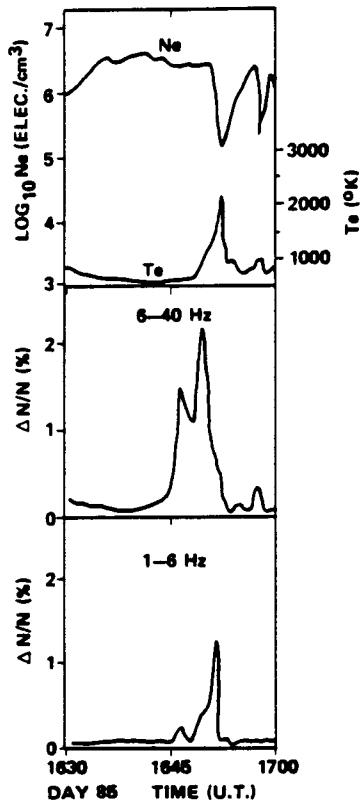

Fig. 6. Electron density, temperature, and density fluctuation data from the Langmuir Probe on the PDP. The time period shown, day 85, 1630–1700 UT, includes the period of the entry of the PDP into the wake at 1650:30 depicted in Figures 4*b* and 5*b*.

temperature of the major ion and the density of the minor ion were reasonable, yet the minor ion temperature displayed abnormally high values. An example of this behavior is shown in Figure 7. The major and minor ion temperatures are approximately equal at the beginning of the segment, as would be expected at an altitude of 250 km. The minor ion temperature then began to increase and reached an apparent value of over 10,000°K. The behavior shows a smooth trend, and as well, the χ^2 goodness-of-fit values were small. This is in marked contrast to the situations discussed earlier when the plasma was disturbed by wake effects and the fitted values of the plasma parameters were erratic.

It is difficult to accept that such high temperatures of the minor ion reflect the true state of the ambient distribution. We assume, therefore, that this is an effect either of the data analysis procedure or of orbiter-plasma interactions. Both possibilities are now examined.

The possibility exists that the seemingly abnormally high temperatures seen in the NO^+ ion were a consequence of a change in the ionospheric composition such that the minor ions were O_2^+ rather than NO^+. It would seem logical that if the fitting program assumed that the minor ions were NO^+ (m = 30), and in fact there were a significant population of O_2^+ (m = 32), then the curve fitting program would converge to a higher temperature than was actually the case.

To test this assumption, the fitting program was run for simulated data input. As was done for the flight data, the fitting assumed that the ions were O^+ and NO^+, but the simulated data generation routine allowed specification of satellite potential and the densities and temperatures of O^+, NO^+, and O_2^+. Various test plasmas consisting of mixtures of O^+, NO^+, and O_2^+ were tried, but it was not possible to concoct a distribution that resulted in an artificially high value of the NO^+ temperature. Thus we are led to conclude that there was a suprathermal ion component present, and we now examine the conditions that resulted in these observations.

There were four periods in the data set that displayed these high NO^+ ion temperatures, and there were three aspects of the geometry that were common to all. The first was that the PDP was parked over the centerline of the orbiter bay. The second was that the plasma flow vector was at low coelevation angles (<55°) and the azimuth ranged from 180° to 270°, or from generally above the orbiter, over the cabin. Under these conditions the plasma flow upstream of the PDP was well clear of any orbiter surface, but the flow downstream of the PDP impacted the larger surface area presented by the payload bay and doors, the wings, and the engine pods. The third condition was that the ram angle between the instrument normal and the flow vector was larger than about 20°, as illustrated in Figure 8. Here are plotted the inferred density and temperature of the O^+ and NO^+ ions, along with the ram angle. During this period the coelevation ranged between 40° and 25°, and the azimuth ranged between 160° and 270°. Beginning at day 84, 2244 UT, the O^+ and NO^+ temperatures were nearly equal. However, it is seen that as the ram angle increased between 2247 and 2253 UT, the inferred NO^+ ion temperature increased as well. Between 2253:20 and 2255:00 UT the ram angle decreased from 45° to 15°, and this was accompanied by a decrease in the indicated NO^+ temperature.

The data would indicate that an interaction with the orbiter produced a heating of the NO^+ ion or, possibly, created hot NO^+ ions. This hot population was masked by the colder ram plasma when the RPA instrument normal was at small angles to the flow but became ever more apparent as the detector viewed away from the ram direction. With the limited angular resolution of the RPA, it was not possible to measure the angular distribution of this suprathermal component.

A companion instrument to the RPA was the differential ion flux probe (DIFP) mounted in the same package with a view direction colinear with that of the RPA. This instrument and data therefrom are discussed in detail by *Stone et al.* [1983]. The DIFP had a fan-shaped field of view of 5° by 90° which was electronically swept in the PDP *Y-Z* plane. (See *Stone et al.* [1983] for a detailed description of the geometry.) A significant result was that on many occasions the instrument detected a primary ion stream aligned with the bulk flow velocity and, simultaneously, secondary streams with angles up to 60° from the ram direction. The intensity of these secondary streams ranged from 3 to 20% of the primary stream intensity. Stone et al. showed a specific example for day 85, 2112–2114 UT, where the secondary stream was 64° away from the primary stream with an intensity ratio of 8%. RPA data for this same period, where the ram angle for the RPA was near the 45° limit, showed O^+ densities near 2×10^6 ions/cm^3, but with erratic values of the other three ion parameters and a large value of the goodness-of-fit parameter χ^2.

Recall that the fitting procedure assumes a two-ion flowing Maxwellian plasma. Departures from this model, such as the presence of a secondary stream component, would produce such a behavior in the computed parameters.

5. Discussion and Conclusions

At the outset, measurements of ambient plasma parameters with an instrument in close proximity to the shuttle orbiter may seem an impossible task. The orbiter is by no means a passive vehicle but

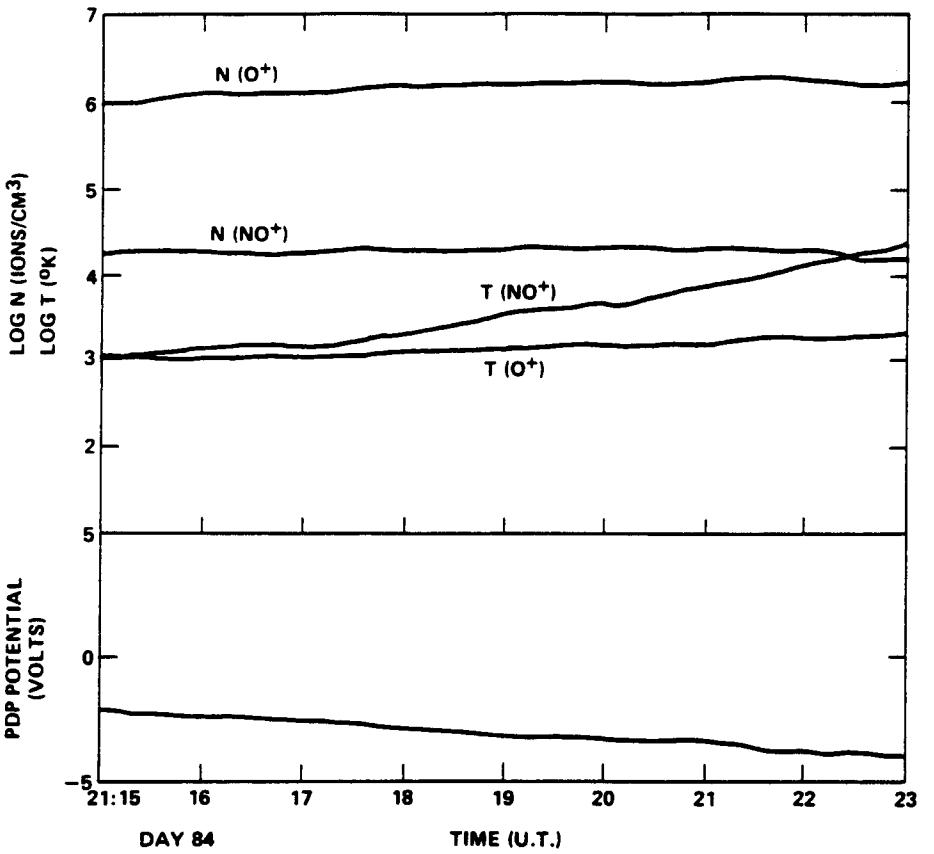

Fig. 7. An example of anomalously high temperatures observed for the NO^+ ion. The data format is identical to that in Figures 2 and 4, except that here the O^+ and NO^+ temperatures are plotted to the same baseline to facilitate comparison.

rather, as has been shown, creates significant perturbations in the local medium with water and water vapor ejections and with firings of thrusters. It creates as well significant levels of electrostatic wave activity as it moves at a high Mach number through the background plasma [*Murphy et al.*, 1983].

However, the data presented here have shown that valid measurements of the ambient ion parameters can be made if the instrument is positioned such that the separation between the instrument and the orbiter and the separation between the plasma flow streamline and the orbiter, especially upstream, is greater than the plasma scale sizes. Here the limit was set by the thermal ion gyroradii of approximately 10 m. The instrument, therefore, must be positioned on a boom or the RMS. However, this extension from the orbiter has the effect of driving the instrument to a nonequilibrium potential of a few volts by the $\vec{V} \times \vec{B}$ electric field. This potential, which can easily be significantly higher than the ambient plasma thermal energies of ~0.1 eV, must be taken into account in the data analysis procedures. Other conditions which should be met to insure a valid measurement are the requirements that the instrument have a narrow acceptance angle, less than about 40° full angle and that the instrument normal be aligned parallel to the plasma velocity vector.

The examples of shadowing of plasma flows by the orbiter surfaces have shown (Figures 4*a* and 4*b*) that the density profile of the major ion varied as would be expected according to a fluid dynamic Mach cone. However, the plasma is strongly perturbed so that the model of a flowing Maxwellian fails to match the data, as evidenced by the erratic values of the fitted temperatures and the large values of the χ^2 fit parameter. *Shawhan et al.* [1984] have reported PDP observations of a persistent electrostatic background noise which dominated the electric field spectrum at frequencies between 30 Hz and 178 kHz with a maximum intensity of 130 dB μV/m/MHz in the range 300–500 Hz. The frequency range of these waves encompasses the ion gyrofrequency, ion plasma frequency, and lower hybrid resonance frequency. We suggest that these electrostatic wave modes, whatever their generation mechanism, do in fact interact with the ambient ion distributions and perturb the plasma thermal distributions in the manner indicated above. However, the ion data from periods when the plasma flow streamlines are more than an ion gyroradius away from any orbiter surfaces, as illustrated in Figures 2*a* and 2*b*, show that these perturbations are localized and do not extend to large distances in the plasma.

Perhaps the most significant finding of this study is the observations of high-temperature components of the NO^+ ions and to lesser extent the O^+ ions. These high-temperature components were seen under a special set of conditions in the sunlit ionosphere. The PDP was in a position such that the plasma flow downstream of the PDP impacted on orbiter surfaces, and the detector normal was at a sufficiently large angle to the flow direction so that the high-temperature distribution was not masked by the ambient cold ion plasma flow.

Hanson and Cragin [1981] have reported observations of irregularities in retarding potential analyzer derivative curves (dI/dV) on the Atmospheric Explorer C and D satellites. They interpreted these as due to irregularities in the major ion density, with $\Delta N/N \approx$ 2% and wavelengths of approximately 2.2 m. They argued that a two-stream instability driven by reflected ions with twice the satellite velocity in the ambient plasma frame was responsible. The dis-

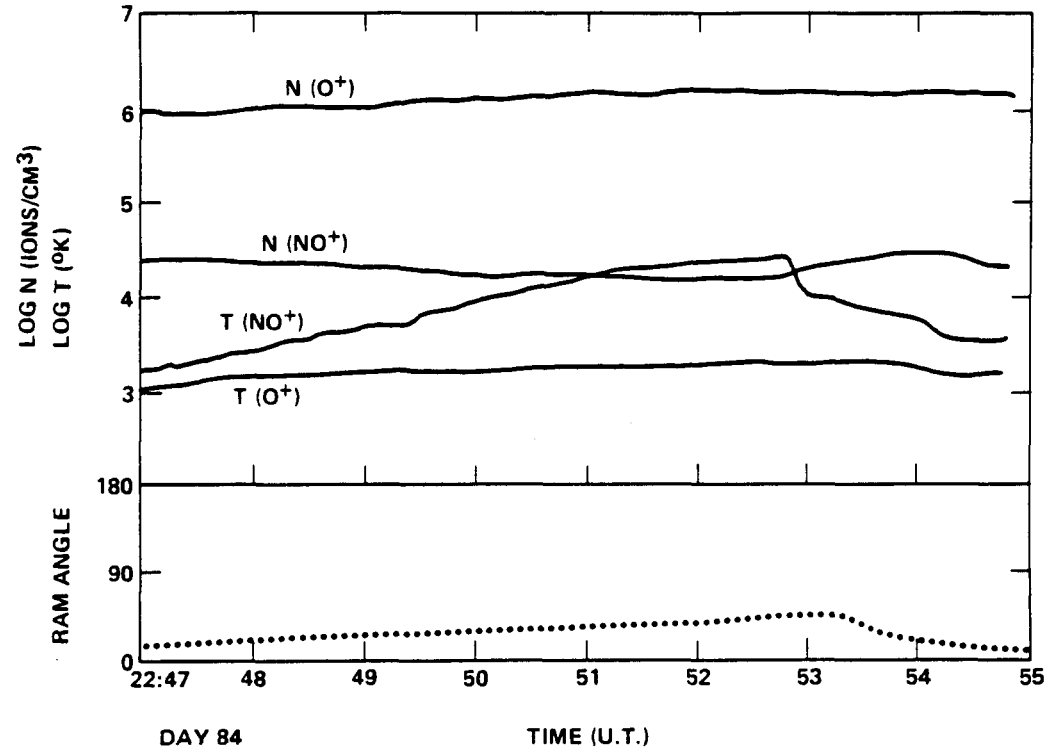

Fig. 8. A second example of anomalously high NO^+ temperatures. The ram angle of the plasma flow relative to the instrument is displayed in the lower panel. This illustrates that given certain other conditions discussed in the text, the high NO^+ temperatures are correlated with increasing ram angle. Note particularly the decreases of NO^+ temperature and ram angle near 2253 UT.

persion relation for electrostatic lower-hybrid waves was calculated, and growth rates of the order of a few milliseconds were computed. They predicted as well that the effects would probably be more obvious in the vicinity of larger spacecraft.

Optical instruments on various shuttle missions have detected a glow adjacent to orbiter surfaces with estimates of intensities at optical wavelengths ranging from a few hundred Rayleighs to 10 kR [*Banks et al.*, 1983*b*; *Mende et al.*, 1983]. *Papadopolous* [1984] has proposed a mechanism for the generation of seed ionization in the neutral gas cloud surrounding the orbiter by ionospheric ions reflecting from the surfaces with relative velocities exceeding the critical velocity [*Alfvén*, 1954]. The newly created ions form an unstable distribution which leads to growth of electrostatic wave modes. The mechanism is similar to that proposed earlier by *Hanson and Cragin* [1981], although the former work did not specifically involve the critical velocity hypothesis and obviously did not include a neutral gas cloud traveling with the satellite. These waves in turn heat electrons which close the chain in a positive feedback sense by creating new ions by impact ionization. The model predicts creation of ion distributions with temperatures up to 110 eV, beams of ions with energies of 5–10 eV, and an electrostatic wave spectrum with frequencies in the orbiter frame of reference up to 20 kHz.

The observations reported here and elsewhere (see references) from the PDP instrumentation of plasmas and waves support, at least qualitatively, the predictions of the model of *Papadopolous* [1984]. The secondary ion streams observed by the DIFP [*Stone et al.*, 1983], the electrostatic wave modes which intensify with water ejections and thruster firings [*Murphy et al.*, 1983; *Pickett et al.*, 1985], and the hot ion distributions reported here all are in agreement with various aspects of this model. It is interesting to note that according to the analysis given in the model, the wavelengths of unstable waves in the plasma near the ion plasma frequency and ion cyclotron frequency are of the order of tens of meters, that is, of the order of the orbiter dimensions.

In summary, this experimental effort has shown that strong perturbations to the ambient ion plasma can occur in the presence of the orbiter. In the case of geometrical shadowing by a surface or edge, the density variation of the major ion (with distance from the streamline) behaves as would be expected from a fluid dynamic Mach cone geometry. However, orbiter-plasma interaction effects extend to a few meters outside of the Mach cone and cause significant departures from a flowing Maxwellian distribution. The impact of the plasma flow with the orbiter creates high-temperature components of the ion distributions which are observed when the ion collector is looking away from the ram direction. However, we have also shown that valid measurements of ambient ion parameters can be made with an instrument attached to the orbiter on the RMS or a boom if the geometry is arranged such that the instrument and the plasma flow streamline are greater than about 10 m from any orbiter surface and the instrument is collimated around the plasma flow vector.

The next investigation with this RPA instrument on the PDP has occurred on the Spacelab 2 mission in July–August 1985. The PDP was released from the orbiter and functioned as a free-flying spinning subsatellite. By means of a series of orbiter maneuvers, the PDP "flew around" the orbiter and thus allowed detailed and systemmatic measurements of the structure of the plasma wake and perturbation regions both upstream and downstream.

Acknowledgments. This research was supported by the Marshall Space Flight Center contract NAS8-32807 and by the MSFC Spacelab Payloads Project Office. We are indebted to William A. Chisholm and William J. Lewter for the mechanical and electrical design of the retarding potential

alyzer and to Luann Lusk for development of the data analysis software. The Editor thanks W. J. Raitt and two other referees for their assistance in evaluating this paper.

REFERENCES

Alfvén, H., *On the Origin of the Solar System*. Oxford at the Clarendon Press, London, 1954.

Banks, P. M., P. R. Williamson, W. J. Raitt, S. D. Shawhan, and G. Murphy, Electron beam experiments aboard the space shuttle, Proceedings on Active Experiments in Space, *Eur. Space Agency Spec. Publ., ESA SP-195*, 171, 1983*a*.

Banks, P. M., P. R. Williamson, and W. S. Raitt, Space shuttle glow observations, *Geophys. Res. Lett., 10*, 118, 1983*b*.

Benson, R. F., P. Bauer, L. H. Brace, H. C. Carlson, J. Hagen, W. B. Hanson, W. R. Hoegy, M. R. Torr, R. H. Wand, and V. B. Wickwar, Electron and ion temperatures—A comparison of ground-based incoherent scatter and AE-C satellite measurements, *J. Geophys. Res., 82*, 36, 1977.

Bevington, P. R., *Data Reduction and Error Analysis for the Physical Sciences*, Chapter 11, McGraw-Hill, New York, 1969.

Hanson, W. B., and B. L. Cragin, The case of the noisy derivatives—Evidence for a spacecraft-plasma interaction, *J. Geophys. Res., 86*, 10,022, 1981.

Hanson, W. B., S. Sanatani, D. Zuccaro, and T. W. Flowerday, Plasma measurements with the retarding potential analyzer on OGO 6, *J. Geophys. Res., 75*, 5483, 1970.

Mende, S. B., O. K. Garriott, and P. M. Banks, Observations of optical emissions on STS-4, *Geophys. Res. Lett., 10*, 122, 1983.

Murphy, G. B., S. D. Shawhan, L. A. Frank, N. D'Angelo, D. A. Gurnett, J. M. Grebowsky, D. L. Reasoner, and N. H. Stone, Interaction of the space shuttle orbiter with the ionospheric plasma, Proceedings of the 17th ESLAB Symposium on Spacecraft/Plasma Interactions and Their Influence on Field and Particle Measurements, *Eur. Space Agency Spec. Publ., ESA SP-178*, 73, 1983.

Murphy, G., J. Pickett, N. D'Angelo, and W. S. Kurth, Measurements of plasma parameters in the vicinity of the space shuttle, *Planet. Space Sci.*, in press, 1986.

Neupert, W. M., P. M. Banks, G. E. Brueckner, E. G. Chipman, J. Cowles, J. A. M. McDonnell, R. Novick, S. Ollendorf, S. D. Shawhan, J. J. Triolo, and J. L. Wronberg, Science on the space shuttle, *Nature, 296*, 193, 1982.

Papadopolous, K., On the shuttle glow (the plasma alternative), *Radio Sci., 19*, 571, 1984.

Pickett, J. S., G. B. Murphy, W. S. Kurth, C. K. Goertz, and S. D. Shawhan, Effects of chemical releases by the STS-3 orbiter on the ionosphere, *J. Geophys. Res., 90*, 3487, 1985.

Sharp, G. W., Mid-latitude trough in the night ionosphere, *J. Geophys. Res., 71*, 1345, 1966.

Shawhan, S. D., G. B. Murphy, and J. S. Pickett, Plasma diagnostic package initial assessment of the shuttle orbiter plasma environment, *J. Spacecr. Rockets, 21*, 387, 1984.

Stone, N. H., U. Samir, K. H. Wright, Jr., D. L. Reasoner, and S. D. Shawhan, Multiple ion streams in the near vicinity of the space shuttle, *Geophys. Res. Lett., 10*, 1215, 1983.

G. Murphy, Department of Physics and Astronomy, University of Iowa, Iowa City, IA 52242.

D. L. Reasoner, NASA Marshall Space Flight Center, Code ES53, Huntsville, AL 35812.

S. D. Shawhan, Space Plasma Physics, Office of Space Science and Applications, NASA Headquarters, Washington, D.C. 20546.

(Received November 12, 1985;
revised June 13, 1986;
accepted July 2, 1986.)

JOURNAL OF GEOPHYSICAL RESEARCH, VOL. 92, NO. A10, PAGES 11,262–11,268, OCTOBER 1, 1987

The Space Shuttle as a Platform for Observations of Ground-Based Transmitter Signals and Whistlers

T. NEUBERT, T. F. BELL, AND L. R. O. STOREY

STAR Laboratory, Stanford University, Stanford, California

D. A. GURNETT

Department of Physics and Astronomy, The University of Iowa, Iowa City

Recent experimental and theoretical studies indicate that coherent VLF waves, such as lightning-generated whistlers and signals from ground-based VLF transmitters, can often produce significant pitch angle scattering in energetic particles in the magnetosphere. However, the relative importance of these waves in controlling the lifetimes of energetic particles is only partially understood due to limited knowledge of the global distribution of the coherent waves throughout the magnetosphere. The present paper presents a preliminary global study of VLF transmitter signals and low-latitude whistlers received at 245 km altitude on the space shuttle. The observations were made in a 5-day period during the STS 3 mission of the space shuttle in March 1982. The threshold sensitivity of the wave receiver when mounted in the shuttle bay was 0.3 pT ± 10 dB (set by the shuttle electromagnetic interference), which was sufficient to detect the whistler mode signals in large regions of the ionosphere. We find that the direct signals from a 10-kW transmitter located at 28°S magnetic latitude were received in a roughly circular region with a diameter of 6000 km centered around the transmitter. The signals propagating through the magnetosphere from a 500-kW magnetically conjugate transmitter at 40°N magnetic latitude were received inside a region extending 5000 km in longitude and 2000 km in latitude. Finally, the direct signals from a 1 MW-transmitter at 31°S magnetic latitude were received in a region extending 22,000 km in longitude, while the latitudinal extent (5000 km) was limited by the shuttle orbit and the day/night terminator. Except for one case, signals were received only during nighttime. Extremely small dispersion whistlers were detected on L-shells between 1.04 and 1.11, suggesting that the lack of ducted whistlers on magnetic field lines in this range is not due to transmission loss across the D region boundary or to high ionospheric absorption loss, but most likely to a lack of ducts.

1. INTRODUCTION

The dynamics and lifetime of energetic electrons in the magnetosphere depend in large measure on the VLF wave activity both generated spontaneously in the medium and arising from ground-based VLF transmitters and from lightning-generated whistlers. Estimations of whistler wave-electron interactions are usually done with either of two assumptions: (1) that the waves propagate in a ducted mode parallel to the earth's magnetic field; or (2) that the waves are nonducted but their ray paths can be described by two-dimensional ray tracing calculations in which transmeridional propagation is neglected. The ionosphere is often the boundary in these calculations, from which rays are "launched" into the magnetosphere. The actual field amplitudes in the ionosphere are dependent on D region absorption, coupling into ducts, and coupling between the two wave polarizations, and thus they are complicated functions of local time, geographic location of the transmitter, geomagnetic activity, and signal frequency. However, both for lightning-induced whistlers and for VLF transmitter signals, in situ measurements of the global distribution of field intensities in the ionosphere (a boundary condition) are rare. With this pilot study, we want to draw attention to the opportunity provided by the space shuttle to resolve this problem.

The STS 3 mission of the space shuttle was carried out in March 1982. The shuttle was launched into an almost circular orbit with an altitude of 240 to 250 km and an inclination of 37°. The nighttime passes were in the southern hemisphere, and the daytime passes in the northern hemisphere, the shuttle crossing the day/night terminator within a few degrees of the geographic equator at local times of roughly 0600 or 1800 LT. The range of L shells [*McIlwain*, 1961] covered by the shuttle was from 0.95 to 2.63.

The transmitters we have selected for this study are the USSR Alpha stations in Komsomolskamur and Krasnodar, the Omega stations in Japan, Hawaii, La Réunion, and Argentina, and the NWC transmitter in Australia. The geographic latitude, longitude, radiated power, and frequency range of each of these transmitters are listed in Table 1.

Signals from these VLF stations were most often received during nighttime when the shuttle was in the southern hemisphere. From the distribution in latitude and longitude and the time delays of the Omega and Alpha station signals, we infer that signals from the northern hemisphere stations propagated through the magnetosphere along the earth's magnetic field before reaching the shuttle, while signals propagated directly through the ionosphere up to the shuttle from southern hemisphere transmitters.

The measurements presented here were performed by a wideband analog receiver system, which was part of a plasma

Paper number 7A8922.
0148-0227/87/007A-8922$02.00

TABLE 1. List of Transmitters

Transmitters	Latitude, deg	Longitude, deg	Radiated Power, kW	Frequency, kHz
NWC (Australia)	21°49′S	114°10′E	1000	22.3
Alpha				
Komsomolskamur	50°34′N	136°58′E	10–500	11.9–15.6
Krasnodar	45°02′N	38°39′E	10–500	11.9–15.6
Omega				
Japan	34°36′N	129°27′E	10	10.2–13.6
Hawaii	21°24′N	157°49′W	10	10.2–13.6
La Réunion	20°58′S	55°17′E	10	10.2–13.6
Argentina	43°03′S	65°11′W	10	10.2–13.6

Data are from Inan et al. [1984].

diagnostics package (PDP) [*Shawhan et al.*, 1984*a*]. During the mission the PDP was housed in the shuttle payload bay. An electric dipole antenna with two 20-cm-diameter spheres separated by 1.6 m was used to monitor the electric wave field, while the magnetic field was probed by a search coil sensor. A wideband receiver was connected to the electric antenna (51.2 s) alternating with the magnetic antenna (51.2 s). Every eighth 51.2-s format, a Langmuir probe was substituted for a magnetic sensor.

The receiver had a 10-kHz bandwidth, selecting nominally 0–10 kHz (25.6 s), 10–20 kHz (12.8 s), and 20–30 kHz (12.8 s). The frequency format was synchronized with the antenna format. The 10- to 20- and 20- to 30-kHz range were heterodyned down to 0–10 kHz. In the process, the 10- to 20-kHz band was inverted, so that an assumed 20-kHz signal appears as a 0-kHz signal.

Signals from ground-based stations were most commonly seen in the magnetic field data, and thus the data presented here are primarily based on measurements from the search coil. The wideband receiver was designed to give high frequency and time resolution in the VLF frequency range, but not to give accurate field intensities. However, the search coil sensor was also connected to a 30-Hz to 178-kHz receiver with 16 logarithmically spaced channels. This receiver has been calibrated. It has been found that the magnetic fields in the range 10.0–17.8 kHz and 17.8–31.0 kHz have amplitudes of 7 pT ± 10 dB in each of the two bands and that the noise primarily consists of a number of narrow-band emissions from power converters, etc. [*Shawhan and Murphy*, 1984*b*]. This noise level is independent of the orbiter attitude and only slightly time dependent as systems in the payload bay are turned on or off. To estimate an approximate threshold field amplitude for detection of the transmitters in gray scale spectrograms, scans of amplitude versus frequency at selected times have been inspected. Comparing the amplitudes on these scans, of a transmitter signal and the most dominant interference lines, we estimate that the threshold amplitude is about 0.3 pT ± 10 dB.

The wideband data base consists of about 24 hours of observations which were acquired over a total of roughly 16 orbits. In the following sections the data are presented and discussed. We also provide brief comments on the advantages of the space shuttle and its orbit for future wave experiments.

2. OBSERVATIONS

Typical examples of VLF transmitter signals and whistlers detected by the wideband receiver are shown in Figure 1*a* and 1*b*. Figures 1*a* shows 51.2 s of data from the magnetic antenna followed by 51.2 s of data from the electric antenna. Each 51.2-s section is divided into three parts, marked I, II, and III. Part I represents data in the 0 to 10-kHz range; part II represents data in the 10 to 20-kHz range which has been heterodyned down to the 0 to 10-kHz range and inverted so that the base corresponds to 20 kHz, while the top part of the spectrogram corresponds to 10 kHz. Part III represents data in the 20 to 30-kHz range which has been heterodyned down to 0–10 kHz. In this part the base corresponds to 20 kHz, while the top part of the spectrogram corresponds to 30 kHz.

Figure 1*a* contains signals from two VLF transmitters, Komsomolskamur and NWC. The transmission format of the Alpha station Komsomolskamur consists of a sequence of 400-ms CW pulses, each at one of the three frequencies 11.905, 12.649, and 14.881 kHz, while the NWC Australia transmissions consist of a continuous stream of 5-ms pulses at either of the two closely spaced frequencies 22.3 kHz ± 50 Hz. From Figure 1*a*, we note that the signals appear to be relatively stronger on the magnetic antenna. This is at least partly due to the strong broadband electrostatic noise level presumably generated by the shuttle interacting with the ambient plasma [*Shawhan et al.*, 1984*b*], which imposes a higher threshold for detection of the electric component of the signals.

Figure 1*b* shows an echoing whistler train observed at $L \sim 2.3$. This type of whistler train has been observed on other spacecraft in the past (for example, see *Bell et al.* [1983]). The echoing components are believed to consist of whistler mode waves which have leaked from ducts and have subsequently scattered to the spacecraft position. Although numerous whistlers were observed during the STS 3 mission, their occurrence rate was generally low compared with the rates of 1 to 10 per minute commonly measured at mid-latitude on other low-altitude spacecraft [*Carpenter et*

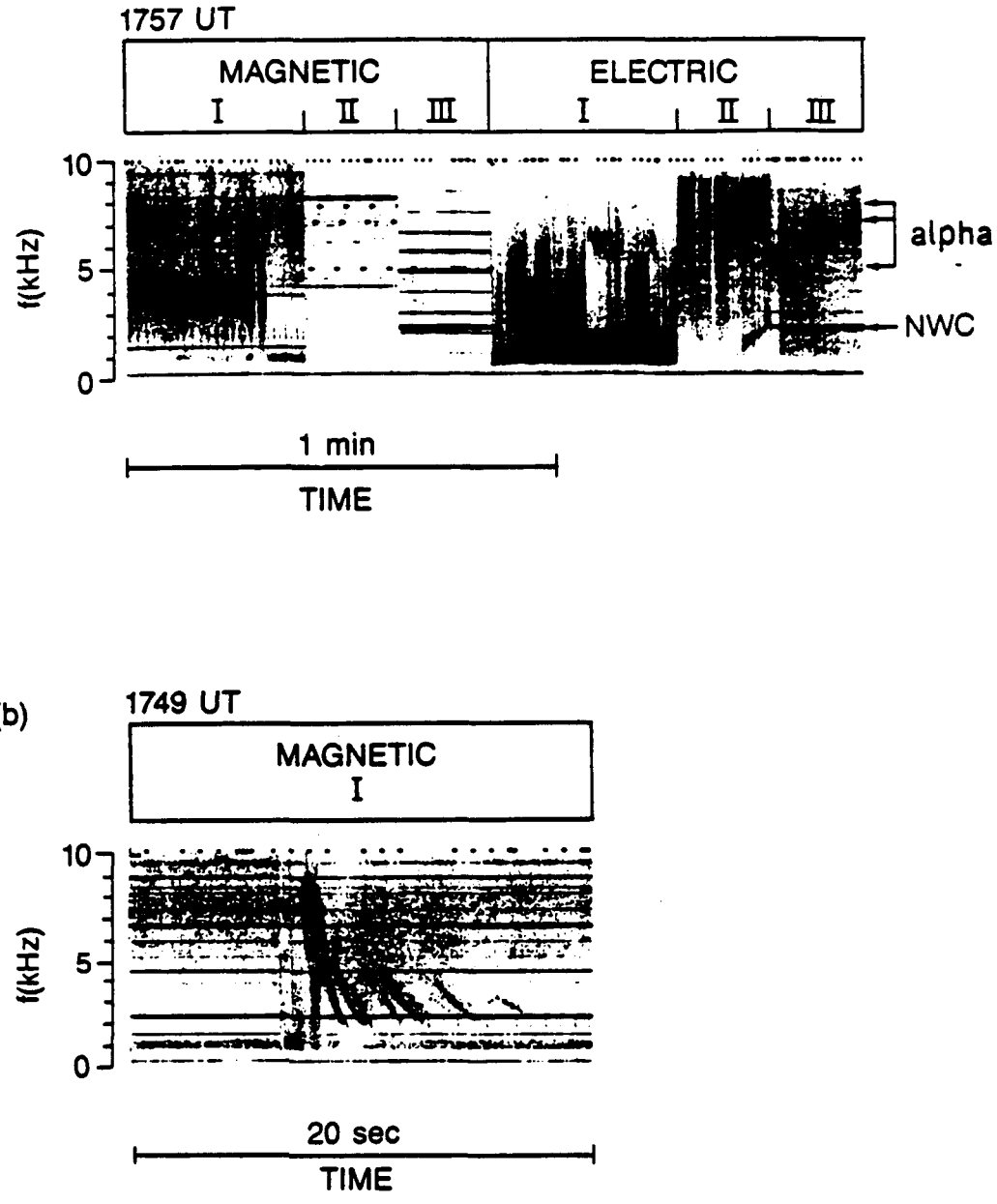

Fig. 1. Gray scale spectrograms showing (a) the reception of signals from the Alpha station Komsomolskamur (KO) seen as a dot pattern and the NWC Australia station seen as a constant frequency line, and (b) the reception of whistlers. Also indicated is the antenna format and the frequency format; I: 0–10 kHz, II: 20–10 kHz, and III: 20–30 kHz.

al., 1968; *Smith and Angerami*, 1968; *Walter and Angerami*, 1969]. This low rate cannot be attributed to a lack of sources since the shuttle often passed over Indonesia, a well-known area of thunderstorm activity [*Lewis*, 1982]. Instead we believe that the low rate can be attributed to the relatively high level of electromagnetic interference (EMI) which existed in the payload bay.

The time resolution of the measurements is limited by the antenna and frequency format. Any of the bands at 10–20 kHz and 20–30 kHz are monitored by a particular antenna for 12.8 s every 102.4 s. In the 89.6-s time interval that a frequency band is not monitored by for instance the magnetic antenna the shuttle moves about 700 km with a velocity of 7.8 km/s.

Assuming that the signals from the ground-based VLF transmitters largely propagate along the earth's magnetic

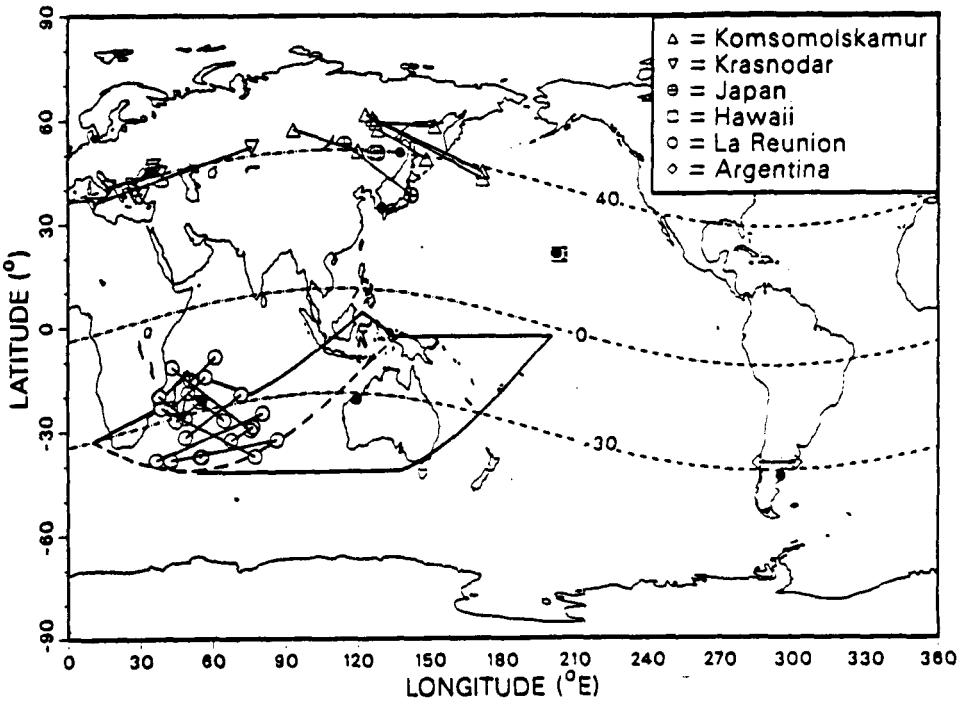

Fig. 2. The global reception of VLF transmitter signals. The magnetic footprint of the shuttle is shown when signals from the Alpha and Omega transmitters were first received and when they later disappeared. The orbit during reception is approximated by straight lines. The contour limiting the reception of the NWC Australia transmitter is also shown. The location of the transmitters is indicated by solid circles and the 40°, 0°, and -30° magnetic latitude contours by dashed lines. One orbit during reception of the NWC station is also shown.

field lines, for instance in a ducted mode when propagating from a transmitter located in the opposite hemisphere of the shuttle, the global reception of ground-based VLF transmitter signals during the shuttle mission can be summarized as in Figure 2. This figure shows the location of the shuttle when projected along the earth's magnetic field to the surface of the earth during times when ground-based transmitters were received. The projection has been done by approximating the earth's magnetic field with a dipole field centered at the earth's center and the magnetic pole at 11.435° colatitude and -69.761° east longitude. The shuttle location is projected toward the hemisphere where the transmitters are located. Since the transmitters are received almost exclusively at nighttime, the shuttle itself was in the southern hemisphere. For the Alpha and Omega stations are shown the magnetic footprint of the shuttle when the signals are first received and when they disappear, and the orbit during reception is approximated with straight lines. For the NWC Australia station, the contour limiting the region of reception and one projected orbit are shown. Also indicated are the location of the transmitters (solid circles) and the 40°, 0° and -30° magnetic latitude lines (dashed lines). Note that the Omega station in Australia was not in operation at the time of the STS 3 flight.

Signals from the NWC transmitter were observed during six orbits, and receptions were confined solely to the nighttime sector. In fact, from 120° to 200° longitude the northern boundary of reception was aligned with the geographic equator, the approximate latitude at which the spacecraft crossed the day/night terminator. Signals disappeared here within 20 min of 0600 LT, the time of terminator crossing. The eastern boundary is determined by limitations in the wideband data set, and the southern boundary by the shuttle orbit. The western boundary, however, is a true boundary of reception.

Figure 3 gives an oveview of the data base containing the Alpha and Omega stations ordered in local time. It is based on visual inspection of gray scale spectrograms and includes only these stations because they have an easily recognizable frequency format distinct from the shuttle interference lines. The abscissa is the local time divided into 1-hour bins. The top panel shows the number of times the orbiter passed through a LT bin while receiving one of the stations. The bottom panel shows the number of times when the magnetic footprint of the shuttle (both direct and conjugate projection) was within 10° latitude and longitude of a transmitter without receiving the signal from this station. Figure 3 shows that the stations almost exclusively were received during nighttime, althought opportunities were also present during the daytime as defined by the 10° latitude and longitude criterion. While the limited data base and the uncalibrated wideband receiving system do not allow us to perform any deeper statistical analysis, the results shown in Figure 3 suggest that the reception of the signals has a strong dependence on LT, in that the signals were rarely observed during the daytime. This is not surprising as the higher D region plasma density is expected to increase the absorption by about 20 dB at 10 kHz and 30 dB at 30 kHz [*Helliwell*, 1965].

During nighttime when the shuttle was either magnetically conjugate to a transmitter or in the same hemisphere within 1000 km, the signals from this transmitter were usu-

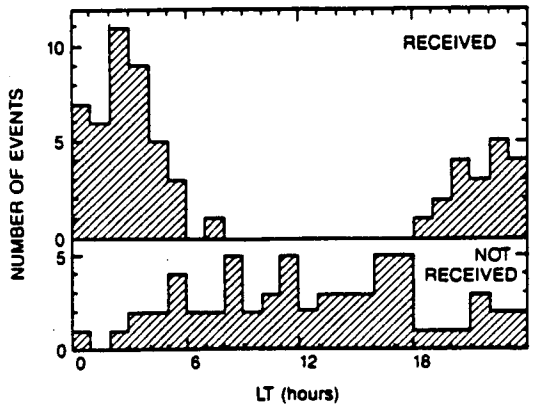

Fig. 3. Local time (LT) is divided into 1-hour bins. Top panel shows the number of times the shuttle passed through a LT bin and received signals from one of the stations. Bottom panel shows the number of times signals were not received when the footprint of the orbiter passed a transmitter within 10° in latitude and longitude.

ally received on the magnetic antenna. The only exception is the Argentina transmitter whose signals occasionally were not received during the nighttime. This transmitter is also comparatively rarely observed on satellites (*T. F. Bell*, personal communication, 1987). The coverage of this transmitter is unfortunately poor in the present data set, with data from only four orbits passing within 10° in latitude and longitude of the transmitter. Out of the four opportunities, the signals were missing in three. The lack of reception could be influenced by the increased ionospheric electron density expected near the South Atlantic anomaly [*Vampola and Gorney*, 1983], which would increase the absorption losses.

3. Discussion

The detailed analysis of magnetospheric interactions between energetic electrons and coherent signals from ground-based transmitters requires knowledge of both the input and output signals as well as information concerning the energetic particle distribution function. In past experiments, measureents of these parameters have been made on both rockets and high- and low-altitude satellites, and important advances in knowledge have resulted from the analysis of these data [*Inan et al.*, 1978; *Bell et al.*, 1981, 1983; *Neubert et al.*, 1983; *Kintner et al.*, 1983; *Imhof et al.*, 1974, 1976, 1983*a*,*b*]. However, most past work has involved case studies in limited regions of the magnetosphere and little has been published concerning the global distribution of wave energy from ground-based VLF transmitters. This is a quantity that must be known in order to understand the details of wave injection experiments, as well as to assess the importance of VLF transmitters, vis a vis the ambient wave background in determining the lifetimes of energetic electrons in the magnetosphere [*Imhof et al.*, 1974, 1976, 1983*a*,*b*].

In principle, the radiation fields in the ionosphere from ground-based transmitters could be calculated from a full-wave solution of Maxwell's equations extending from the earth-ionosphere waveguide through the ionosphere. However, important properties of the ionosphere, such as collision frequencies and plasma density distributions, are not well known near the locations of most ground-based transmitters. Consequently measurements of input wave properties in the ionosphere will be necessary to calibrate future theoretical models. From this point of view, wave measurements made at shuttle altitudes can play an important part in understanding wave-particle interactions in the ionosphere and magnetosphere.

An example of ionospheric wave magnetic field data as observed on STS 3 is shown in Figure 4. The signals were transmitted from the NWC transmitter at 22.3 kHz and received during the pass shown as a dashed line in Figure 2. The figure shows the wave magnetic field amplitude as a function of the distance between the transmitter and the foot of the magnetic field line on which the shuttle was located (we define the "foot" of the magnetic field line as the point of intersection of the field line with the earth's surface in the hemisphere of the transmitter). The amplitude is given in relative units and is compared to a very simple model proposed by *Inan et al.* [1984], which predicts the relative amplitude variation with distance from a transmitter. It can be seen that the fit between theory and observations is reasonably good, insofar as the relative amplitude variation is concerned. The absolute value of the wave amplitude cannot be predicted from the simple theory. Note however, that with the current assumption of 0.3 pT ± 10 dB for the threshold field sensitivity, the maximum field strength received during this pass reaches 15 pT ± 10 dB, which is consistent with previously reported magnetic field amplitudes of waves from ground based VLF stations measured from satellites [*Heyborne*, 1966; *Inan et al.*, 1984].

Recent theories predict enhanced energetic electron precipitation above LF and MF transmitters through a cyclotron resonance interaction between the electrons and the wave field in the topside ionosphere above the transmitters [*Neubert et al.*, 1987]. However, in situ measurements of wave fields in this frequency range are rather scarce. The shuttle could provide, with a wave experiment flown on consecutive launches, a global map of LF and MF field intensities in the ionosphere.

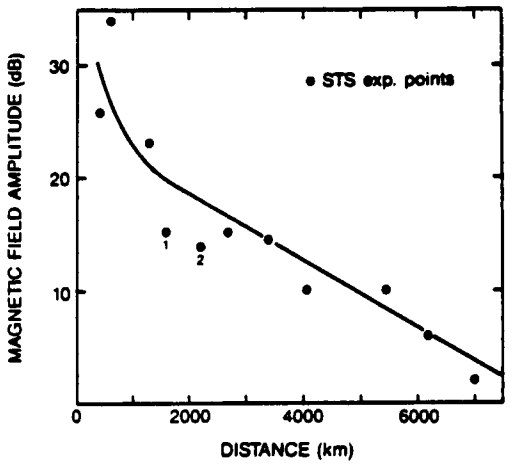

Fig. 4. Amplitude of the NWC transmitter signals as a function of distance from the transmitter of the Shuttle magnetic footprint for the orbit indicated on Figure 2. The 0-dB level corresponds to 0.3 pT ± 10 dB. Also shown is the relative amplitude variation predicted from a simple model [*Inan et al., 1984*]. The experimental points marked 1 and 2 are from the pass north of the transmitter when the distance was increasing.

VLF wave amplitude measurements in the topside ionosphere would be important for understanding the propagation characteristics of low-latitude whistlers by complementing ground based measurements [*Tsuruda and Hayashi*, 1975; *Okada et al.*, 1977, 1981; *Hayakawa et al.*, 1981]. It has been proposed to use low-latitude whistlers as a diagnostic tool to determine the distribution of cold plasma within the inner radiation belts ($L < 2$). However, a number of unsolved problems remain concerning the mode of propagation of whistler mode waves on low-latitude paths and the efficiency of whistler duct excitation at low latitude [*Hayakawa and Tanaka*, 1978; *Ohta et al.*, 1984; *Hayakawa et al.*, 1985]. Wave magnetic and electric field measurements of whistlers and signals from ground-based transmitters at shuttle altitudes (245–400 km) would be very useful in attempting to answer these questions.

In the present study, extremely small dispersion whistlers were detected on days 84, 85, and 86 as the spacecraft crossed magnetic shells in the range $1.04 \leq L \leq 1.11$. Examples were obtained at local times of both $\sim$ 0600 and $\sim$ 1700 LT. The dispersions of the whistlers lay in the range $D = 1.5\text{–}2.5$ s$^{1/2}$, which is within the expected range for short-fractional hop whistlers (direct propagation from the ground through the ionosphere).

These observations give direct evidence that VLF waves can be transmitted across the D region boundary at these low latitudes and can propagate through the ionosphere to altitudes near the F region plasma density peak. Past work on low-latitude whistlers has indicated that ducted whistlers are generally not observed at geomagnetic latitudes less than 15° ($L < 1.13$), and the smallest measured values of dispersion are roughly $D \sim 10$ s$^{1/2}$ [*Hayakawa and Tanaka*, 1978]. The present observations suggest that the lack of ducted whistlers at $L < 1.13$ is more likely due to a lack of whistler mode ducts on these L shells, rather than to high ionospheric absorption or high transmission loss across the D region boundary. Since the dispersion is closely proportional to the integral of the electron plasma frequency along the ray path, it can in principle be used as a diagnostic tool to determine plasma density variations below the spacecraft.

The STS 3 VLF wave data show that even though the shuttle EMI imposes limits on the threshold sensitivity of the wave receivers, valuable measurements of VLF wave activity can be performed even when the antennas are housed in the shuttle bay. Thus, with calibrated receivers, global studies of VLF magnetic field intensities may be performed accurately at shuttle altitudes close to the F peak region of the ionosphere. It is clear, however, that the electric field measurements are significantly disturbed by shuttle-generated noise. For such measurements the wave experiment must be free flying at some distance from the shuttle, say 100–300 m, as was done during the Spacelab 2 mission [*Gurnett et al.*, 1986].

Acknowledgments. The authors thank J. P. Katsufrakis and J. W. Yarbrough for their help with the spectral analysis. K. Fletcher, G. Walker and K. Faes Avery helped prepare the manuscript. The work done at Stanford was sponsored by NASA under contracts NAS8-35350, NGL-05-020-008, and NGR-235, and by the Danish Natural Science Research Council under contract 11-4839. The Space Physics Analysis Network (SPAN) was used in the preparation of this report.

The Editor thanks E. E. Gaines and T. Okada for their assistance in evaluating this paper.

REFERENCES

Bell, T. F., U. S. Inan, and R. A. Helliwell, Nonducted coherent VLF waves and associated triggered emissions observed on the ISEE 1 satellite, *J. Geophys. Res.*, *86*, 4649, 1981.

Bell, T. F., U. S. Inan, I. Kimure, H. Matsumoto, T. Mukai, and K. Hashimoto, EXOS-B/Siple VLF wave-particle interaction experiments, 2, Transmitter signals and associated emissions, *J. Geophys. Res.*, *88*, 295, 1983.

Carpenter, D. L., F. Walter, R. E. Barrington, and D. J. McEwen, Alouette 1 and 2 observations of abrupt changes in whistler rate and of VLF noise variations at the plasmapause: A satellite-ground study, *J. Geophys. Res.*, *73*, 2929, 1968.

Gurnett, D. A., W. S. Kurth, J. T. Steinberg, P. M. Banks, R. I. Bush, and W. J. Riatt, Whistler-mode radiation from the Spacelab 2 electron beam, *Geophys. Res. Lett.*, *13*, 225, 1986.

Hayakawa, M., and Y. Tanaka, On the propagation of low-latitude whistlers, *Rev. Geophys.*, *16*, 111, 1978.

Hayakawa, M., T. Okada, and A. Iwai, Direction findings of medium-latitude whistlers and their propagation characteristics, *J. Geophys. Res.*, *86*, 6939, 1981.

Hayakawa, M., K. Ohta, T. Okada, and Y. Tanaka, Absolute intensities of low-latitude whistlers as deduced from the direction-finding measurement, *Radio Sci.*, *20*, 985, 1985.

Helliwell, R. A., *Whistlers and Related Ionospheric Phenomena*, Stanford University Press, Stanford, Calif., 1965.

Heyborne, R. L., Observation of whistler-mode signals in the OGO satellites from VLF ground station transmitters, Tech. Rep. 3415/3418-1, STAR Lab., Stanford Univ., Stanford, Calif., 1966.

Imhof, W. L., E. E. Gaines, and J. B. Reagan, Evidence for the resonance precipitation of energetic electrons from the slot region of the radiation belts, *J. Geophys. Res.*, *79*, 3141, 1974.

Imhof, W. L., E. E. Gaines, and J. B. Reagan, Local time dependence of the loss of energetic electrons from the slot region of the radiation belts, *J. Geophys. Res.*, *81*, 291, 1976.

Imhof, W. L., J. B. Reagan, H. D. Voss, E. E. Gaines, D. W. Datlowe, J. Mobila, R. A. Helliwell, U. S. Inan, and J. P. Katsufrakis, The modulated precipitaton of radiation belt electrons by controlled signals from VLF transmitters, *Geophys. Res. Lett.*, *10*, 615, 1983*a*.

Imhof, W. L., J. B. Reagan, H. D. Voss, E. E. Gaines, D. W. Datlowe, J. Mobila, R. A. Helliwell, U. S. Inan, and J. P. Katsufrakis, Direct observation of radiation belt electrons precipitated by the controlled injection of VLF signals from a ground-based transmitter, *Geophys. Res. Lett.*, *10*, 361, 1983*b*.

Inan, U. S., T. F. Bell, and R. A. Helliwell, Nonlinear pitch angle scattering of energetic electrons by coherent VLF waves in the magnetosphere, *J. Geophys. Res.*, *83*, 3235, 1978.

Inan, U. S., H. C. Chang, and R. A. Helliwell, Electron precipitation zones around major ground-based VLF signal sources, *J. Geophys. Res.*, *89*, 2891, 1984.

Kintner, P. M., R. Brittain, M. C. Kelley, D. L. Carpenter, and M. J. Rycroft, In situ measurements of transionospheric VLF wave injection, *J. Geophys. Res.*, *88*, 7065, 1983.

Lewis, E. A., High frequency radio noise, in *Handbook of Atmospherics*, vol. 1, p. 251, edited by H. Volland, CRC Press, Boca Raton, Fla., 1982.

McIlwain, C. E., Coordinates for mapping the distribution of magnetically trapped particles, *J. Geophys. Res.*, *66*, 3681, 1961.

Neubert, T., F. Lefeuvre, M. Parrot, and N. Cornilleau-Wehrlin, Observations on GEOS-1 of whistler mode turbulence generated by a ground-based VLF transmitter, *Geophys. Res. Lett.*, *10*, 623, 1983.

Neubert, T., T. F. Bell, and L. R. O. Storey, Resonance between coherent whistler mode waves and electrons in the topside ionosphere, *J. Geophys. Res.*, *92*, 255, 1987.

Ohta, K., M. Hayakawa, and Y. Tanaka, Ducted propagation of daytime whistlers at low latitudes as deduced from ground-based direction findings, *J. Geophys. Res.*, *89*, 7557, 1984.

Okada, T., A. Iwai, and M. Hayakawa, The measurement of incident and azimuthal angles and the polarization of whistlers at low latitudes, *Planet. Space Sci.*, *25*, 233, 1977.

Okada, T., A. Iwai, and M. Hayakawa, A new whistler direction finder, *J. Atmos. Terr. Phys.*, *43*, 679, 1981.

Shawhan, S. D., G. B. Murphy, and D. L. Fortna, Measurements of electromagnetic interference on OV102 Columbia using the plasma diagnostics package, *J. Spacecr. Rockets, 21*, 392, 1984.

Shawhan, S. D., G. B. Murphy, P. M. Banks, P. R. Williamson, and W. J. Raitt, Wave emissions from dc and modulated electron beams on STS-3, *Radio Sci, 19*, 471, 1984a.

Smith, R. L., and J. J. Angerami, Magnetospheric properties deduced from OGO 1 observations of ducted and nonducted whistlers, *J. Geophys. Res., 73*, 1, 1968.

Tsuruda, K., and K. Hayashi, Direction finding technique for elliptically polarized VLF electromagnetic waves and its application to low-latitude whistlers, *J. Atmos. Terr. Phys., 37*, 1193, 1975.

Vampola, A. L., and D. J. Gorney, Electron energy deposition in the middle atmosphere, *J. Geophys. Res., 88*, 6267, 1983.

Walter, F., and J. J. Angerami, Nonducted mode of VLF propagation between conjugate hemispheres; observations on OGO's 2 and 4 of the '"walking-trace" whistler and Doppler shifts in fixed frequency transmissions, *J. Geophys. Res., 74*, 6352, 1969.

T. F. Bell, T. Neubert, and L. R. O. Storey, STAR Laboratory, Durand 337, Stanford University, Stanford, CA 94305.

D. A. Gurnett, Department of Physics and Astronomy, University of Iowa, Iowa City, IA 52242.

(Received January 27, 1987;
revised April 27, 1987;
accepted April 16, 1987.)

JOURNAL OF GEOPHYSICAL RESEARCH, VOL. 93, NO. A5, PAGES 4143–4147, MAY 1, 1988

Comment on "Ram Ion Scattering Caused by Space Shuttle v × B Induced Differential Charging" by I. Katz and V. A. Davis

N. H. STONE,[1] U. SAMIR,[2,3] K. H. WRIGHT, JR.,[4] AND K. S. HWANG[5]

INTRODUCTION

During the third space shuttle flight (STS 3) the plasma gnostic probe (PDP) experiment, a self-contained deploye satellite, provided the first measurements of the plasma l field environment of the space shuttle orbiter. The asurements from this and the subsequent Spacelab 2 mis n still represent our primary source of information regard the plasma environment of the orbiter. In their paper, *tz and Davis* [1987] claim that the design of the PDP ther l blanket, which included a conducting wire mesh covering, ulted in the scattering of ionospheric ions from the PDP ien it was biased several volts negative by the v × B emf nerated between the orbiters' main engine bells (the ground g point of the orbiter) and the PDP located on the remote anipulator system (RMS). Moreover, they claim that these attered ions are responsible for the high-inclination second y ion streams reported in the near environment of the or ter by *Stone et al.* [1983, 1986].

Considering the details of the design, it could be expected at under certain conditions, ions may be reflected from the DP's surface. With a negative potential on the conducting ire mesh covering the nonconducting beta cloth, the poten al structure that develops is like that of a classical retarding otential analyzer (RPA). However, *Katz and Davis* [1987] so claim that the reflected ions are scattered. Moreover, in riving at their conclusions as to whether this actually hap ened in the case of the PDP and, if so, what effect such flections may have had on the measurements, *Katz and avis* [1987], by their own admission, have considered only ery limited portions of the STS 3 data and have ignored ther measurements that their computations are unable to plain. Here we point out that even the STS 3 data con dered by *Katz and Davis* [1987] are not properly represented their model and, moreover, that their results are inconsis nt with laboratory experiments in which a section of the DP thermal blanket, together with its wire mesh covering, as placed in the flight configuration with the flight model of e RPA/differential ion flux probe (DIFP) and exposed to a asma with ionospheric characteristics (i.e., values of the asma density, temperature, and drift velocity approximating ose of the lower ionosphere).

MEASUREMENTS FROM THE STS 3 MISSION

Stone et al. [1983, 1986] pointed out that two distinct ion streams had been observed upstream in the near-orbiter plasma environment, i.e., the expected ram ion flux (approximately coincident with the angle of attack) and a second, less intense stream at a large angle to the ram. In considering whether the scattering mechanism suggested by *Katz and Davis* [1987] can explain these observations, it should be noted that the angles of the ram and secondary ion streams have opposite signs. In other words, they arrive from opposite directions with respect to the normal to the PDP surface. The mechanism suggested by *Katz and Davis* [1987] would result in the secondary and ram ions always arriving from the same side of the surface normal [*Katz and Davis*, 1987, Figure 3]. We take exception to the claim made by *Katz and Davis* [1987] that a small strip of exposed beta cloth around the RPA DIFP sensor heads could have repelled ions. This strip was only 0.5 cm (approximately one Debye length) wide and located on the surface of the PDP while the sensor heads protruded 1.3 cm above the surface and the entrance slits of the DIFP were located almost 4 cm from the edge of the sensor head (or more than 8 Debye lengths from the strip). Moreover, the results published by *Katz and Davis* [1987] do not show any repulsion of ions—only a slight (1°) deviation in direction (see their Figures 7 and 9). It does not appear, therefore, that a scattering mechanism can explain a case, such as that reported by *Stone et al.* [1983, 1986], where a secondary stream arrives from the opposite side of the surface normal from the ram ion current and, moreover, where no secondary stream arrives from the same side of the surface normal.

Stone et al. [1986] also pointed out that (1) the high-inclination secondary ion stream vanished when the PDP was translated 8.8 m from the X axis and 65° above the XY plane of the orbiter, (2) the intensity of the secondary stream (and the ram ions) was directly proportional to the measured neutral density, (3) the density of ionized and neutral particles decreased as $1/r$ with distance from the orbiter, and (4) the ram ions were not precisely aligned with the ram direction derived from orbiter and PDP attitude data. It should also be noted, as was pointed out by *Stone et al.* [1986], that all reported measurements were corrected for PDP potential and the variation of DIFP sensitivity with angle, as reported by *Stone et al.* [1985].

Once again, it seems doubtful that a scattering mechanism explains the observed characteristics of the high-inclination secondary ion streams. First, when the secondary streams vanished, the PDP was still located fully in the unobstructed ionospheric plasma, and although the DIFP was tilted to a high angle of attack, some ram ion current was still measured. If the secondary stream had resulted from scattered ram ions, it should have continued to exist at this point.

Second, if the conclusions of *Katz and Davis* [1987] concerning the role of a scattering mechanism in producing this phenomenon were correct, the secondary ion stream should have vanished when the PDP potential became less than a few

[1]Space Science Laboratory, NASA Marshall Space Flight Center, untsville, Alabama.
[2]Tel Aviv University, Tel Aviv, Israel.
[3]Also at Space Physics Research Laboratory, University of Michi n, Ann Arbor.
[4]Department of Physics, University of Alabama in Huntsville.
[5]Mechanical Engineering Department, University of Alabama in untsville.

aper number 7A9352.
148-0227/88/007A-9352$02.00

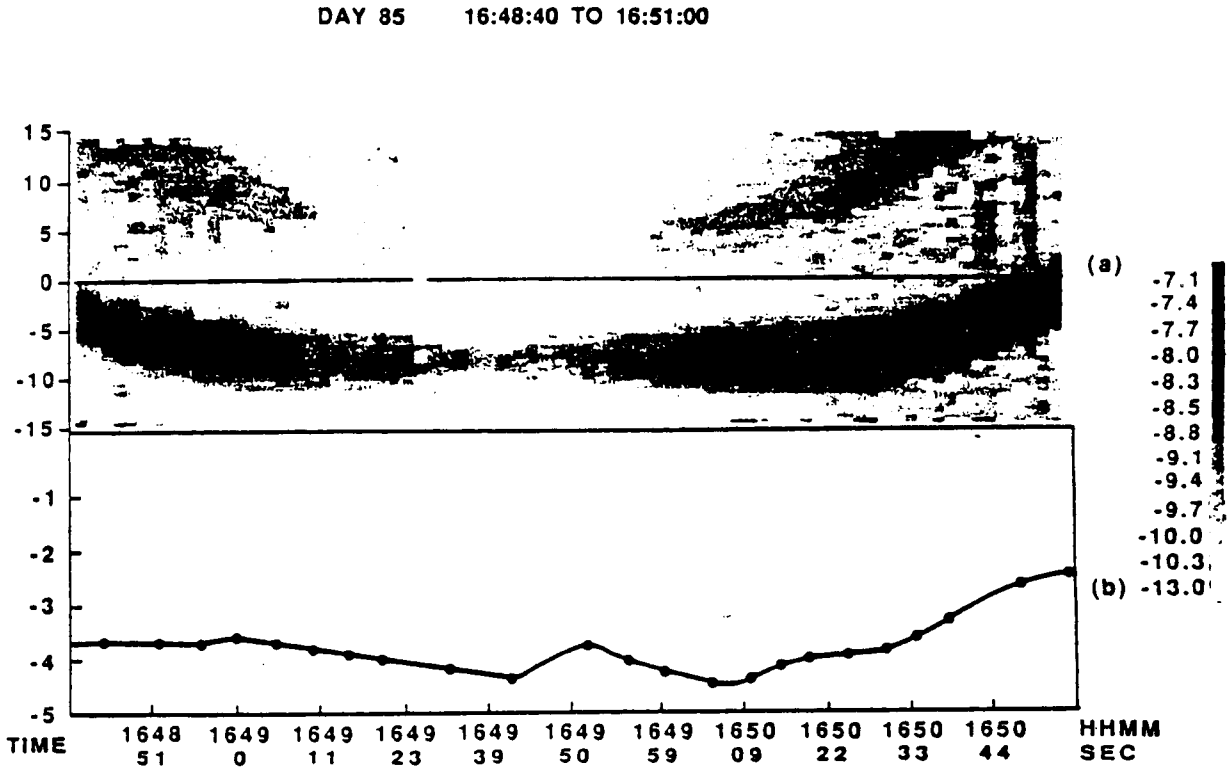

Fig. 1. Vector ion current measurements and PDP potential profile for the STS 3 period 1648:40 to 1651:05 UT on Julian day 85. Note that ϕ_d is proportional to angle, ϕ_p is the PDP potential, and the gray scale is $\log_{10}(I/I_0)$.

s negative and could not exist as the potential approached . In fact, as shown in Figure 1*b*, the potential of the PDP :d over the time period reported from approximately 5 V at 1648:45 UT (which may meet the requirements of computations made by Katz and Davis) to −2.5 V at :00 UT (which is outside the potential range for which the : and Davis computations apply). Note that the secondary :tream does not vanish at this point. To the contrary, as /n in Figure 1*a*, between approximately 1650:00 and :45 the secondary ion stream increases in intensity even gh the PDP potential is becoming more positive and ap- ches zero just beyond this period. The secondary stream ıt observed beyond 1650:45 UT simply because it has :d out of the instruments' field of view.

fore leaving the STS 3 measurements, two further points ld be made clear. First, as stated by *Stone et al.* [1983],)IFP performs an angle scan in only one plane. We were ıware of the possible effects of the unknown, out-of-plane ponent of the ion velocity (which was intended to be de- ned by the PDP spin phase but was unavailable from the)inning PDP on the orbiter's RMS) and therefore delib- y chose data for which the out-of-plane component of rbital velocity remained small. In the case reported by *et al.* [1986], for example, the out-of-plane angle never ded 15° and therefore was not a significant factor in zing the ram ion current. Since scattered ions can be ted to be most intense in the flow direction (i.e., down- ı of the impact point, which is what Figure 2 of *Katz 'avis* [1987] suggests), the out-of-plane effect should be ıal for any possible reflected ions as well.

ɔnd, the inference by *Katz and Davis* [1987] that the of the secondary ion streams exceed the critical angle erefore originated at the PDP's surface is incorrect. For the case of negative spacecraft potentials, there does exist a critical angle above which the ions must have come from within the spacecraft sheath. However, *Katz and Davis* [1987] have incorrectly defined the angle. The tangent of the critical angle is the ratio of the initial ion velocity, parallel to the surface, to the component normal to the surface that results from ion acceleration within the sheath, i.e.,

$$\theta_{crit} = \tan^{-1}\left[V_0/(2e\phi/m)^{1/2}\right] \quad (1)$$

where V_0 is the parallel component of velocity, ϕ is the potential drop across the sheath, and e and m are the ionic charge and mass, respectively. (Note that θ_{crit} is the measured angle, uncorrected for sheath effects.)

In a particular case, the value of the critical angle depends on the mass and initial speed of the ions and the potential drop across the spacecraft sheath. If we assume the ions to be atomic oxygen initially traveling parallel to the PDP's surface at the orbital velocity of 7.7 km/s and use, as an example, the varying PDP potential for the time period reported by *Stone et al.* [1986] and shown here in Figure 1*b*, the results, given in Figure 2, show that the calculated critical angle is always greater than the measured angle of incidence for the ions. Therefore it is not necessary to invoke an ion source on the surface of the PDP to explain the high inclination of the secondary ion streams. They can originate from outside the sheath, beyond the influence of the PDP.

Results From Laboratory Experiments

In order to test for possible effects produced by the interaction between the PDP and its environmental plasma, two experiments were conducted in the space plasma research facilities at the Marshall Space Flight Center. These experi-

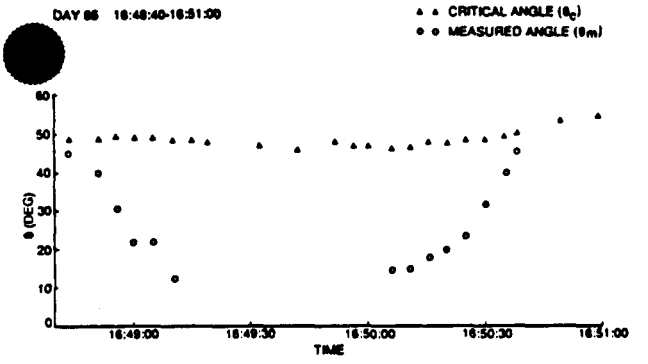

Fig. 2. Comparison of secondary ion stream angles of attack with the calculated "critical" angle for the period shown in Figure 1.

ments, which used sections of the PDP's thermal blanket, complete with its wire mesh covering, and the flight model of the RPA/DIFP instrument, are shown schematically in Figure 3. In both cases, the wire mesh covering was connected to a power supply and biased over a wide range of voltages. Experiment 1, shown in Figure 3*a*, was designed to determine if particles can be reflected from the surface of the PDP. In this case, a laboratory model of the DIFP was placed so that it could detect particles coming off a section of the PDP thermal blanket but would not be able to see the ambient plasma stream. The thermal blanket sample could be rotated out of the plasma stream to allow a second, control instrument to measure the ambient stream characteristics. In experiment 2, shown in Figure 3*b*, the flight model of the RPA/DIFP was mounted in the PDP flight configuration with a section of the PDP thermal blanket; i.e., the blanket section was formed to the PDP radius, and the RPA/DIFP viewed the plasma through the same penetrations in the blanket and with the same view angle as during the STS 3 and Spacelab 2 missions. In this case, the ambient plasma stream was measured directly

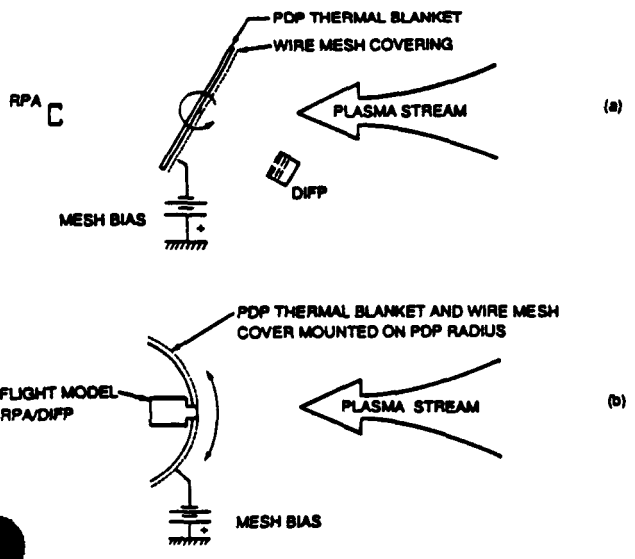

Fig. 3. PDP surface-plasma interaction effects experiments. (*a*) Schematic of experiment 1: investigation of reflected ions. (*b*) Schematic of experiment 2: investigation of return current to the PDP surface.

by the DIFP, and ions reflected from the surrounding surface of the thermal blanket were searched for.

Experiment 1 revealed that with sufficiently negative potentials on the wire mesh, ions can be reflected from the surface of the PDP. Figure 4 shows the intensity of the reflected ions, normalized to the free stream value, as a function of their flow angle with respect to the normal to the surface of the thermal blanket. Several values of the bias voltage were applied to the wire mesh covering on the thermal blanket as indicated in the figure. (In all cases shown here, the angle of the incident plasma stream was $-30°$.) Notice that the current density of the reflected ions peaks sharply at an angle of $+30°$ and has a full width at half maximum (FWHM) value of about 9°. As shown by the geometry of the flow directions given in Figure 5, this is indicative of specular reflection and parallel flow rather than scattering, or diffuse reflection. In Figure 6 the normalized current density of the reflected ions is shown as a function of the bias applied to the wire mesh cover on the thermal blanket. Notice that there is a sharp cutoff as the potential approaches zero. In the case where the electron thermal energy was several electron volts, the cutoff occurred at approximately -10 V, whereas in the case where the electron thermal energy was only a few tenths of an electron volt, the cutoff occurred very near zero. When corrected for the positive plasma potential in the synthesized plasma stream, this is equivalent to a few volts negative.

From the results of experiment 1 we conclude, then, that the PDP surface could have reflected ions when its potential with respect to the surrounding plasma was more than a few volts negative. This is not surprising, since the potential structure is

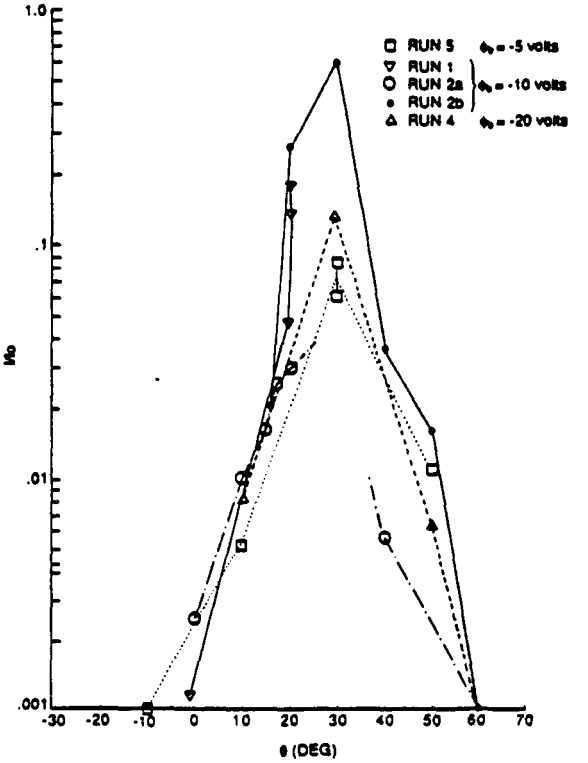

Fig. 4. Normalized reflected ion current density as a function of angle to the surface normal. I_0 is the ambient plasma stream current density.

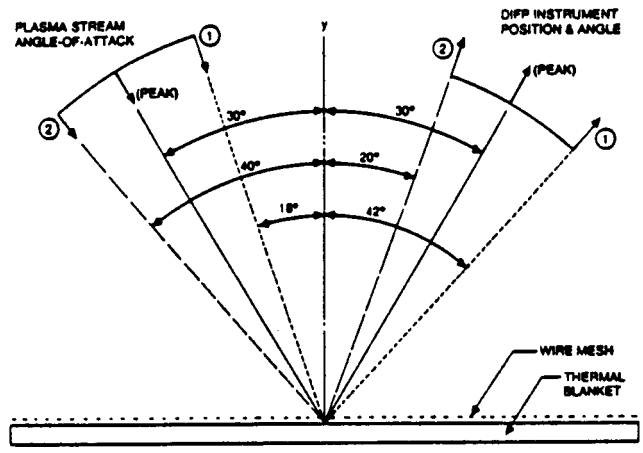

Fig. 5. Schematic of incident and reflected ion trajectories. Angles are measured with respect to the surface normal of the thermal blanket sample. The trajectories 1 and 2 indicate the angles of the FWHM positions of the distribution shown in Figure 4.

similar to that of an RPA. However, experiment 1 also shows that the ions coming off the surface would have been specularly reflected rather than scattered and would have approximated parallel flow. The predictions of *Katz and Davis* [1987] are inconsistent with this result.

During experiment 2, repeated attempts were made to observe secondary ion streams. After an initial null result for conditions approximating those of experiment 1, the current density of the incident plasma stream was increased so that it exceeded that of the rammed ionospheric plasma, the angle of attack of the DIFP to the stream was varied over a wide range (±60°), and the potential applied to the wire mesh covering on the sample was varied from zero to −50 V. In no case were any reflected, secondary ions measured—only the incident ion stream. Since this range of conditions exceeds those for the flight measurements, we can conclude that if any reflection of ions did, in fact, occur at the PDP, it would not have been possible for them to be detected by the RPA/DIFP instrument as it was configured for the STS 3 and Spacelab 2 missions. It is apparent from geometric considerations that this would be the case if ions were specularly reflected as suggested by experiment 1.

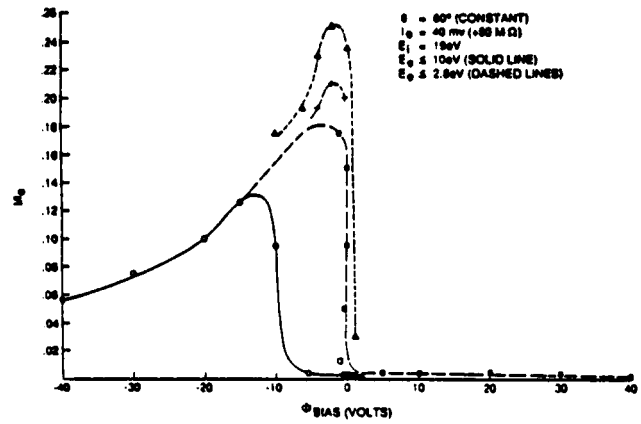

Fig. 6. Reflected ion current as a function of potential on the wire mesh covering of the PDP thermal blanket. Angle of incidence was fixed at −30° to the surface normal.

CONCLUSIONS

While the results of *Katz and Davis* [1987] may correctly predict the possibility that ions could have been reflected from the PDP's surface during the STS 3 and Spacelab 2 missions, they are incorrect in their more specific claim that the ions were scattered from the PDP's surface, and in their application of this mechanism to the STS 3 results. While the superficial agreement makes such an application tempting, a more thorough look reveals that the conditions for which the computations are valid agree only sporadically with the much wider range of conditions under which the measurements were made. In short, the conditions on, and predictions of, the computations simply do not agree with the measurements and the conditions under which they were made. Specifically, this is shown by the fact that (1) the secondary stream intensity was independent of the value of the PDP potential and the streams existed when the PDP potential was near zero and much less negative than required by the computations of *Katz and Davis* [1987], (2) typically two secondary ion streams were found to exist—one on either side of the rammed ion stream, (3) when only one stream was observed, it was always on the opposite side of the instrument normal from the ram current, (4) the secondary ion stream intensity varied with distance from the orbiter and vanished at one point when the PDP was in the unobstructed rammed ionospheric plasma, and (5) the secondary ion streams exhibited a direct dependence on the density of neutral particles.

Laboratory experiments conducted with the PDP thermal blanket material and the flight RPA/DIFP instrument sho that ions can only be reflected when a negative potential o several volts or greater exists between the thermal blankets' wire mesh covering and the plasma, and that when any reflection does occur, it is specular in nature and results in a nearly parallel outflow. Without scattering, the application of a surface reflection mechanism to explain the previously reported high-inclination secondary ion streams observed during the STS 3 mission seems highly doubtful. Moreover, the laboratory experiments discussed above indicate that the specularly reflected ions are unable to be observed by the DIFP instrument as configured for the STS 3 and Spacelab 2 missions.

In summary, we conclude that the scattering mechanism proposed by Katz and Davis does not explain the STS 3 measurements. It is contrary to the example cases reported to date and does not explain a number of cases that occurred under more complex conditions. Moreover, it is contrary to the results of detailed laboratory experiments designed to determine the effects of the PDP surface on the surrounding plasma. When all aspects of the STS 3 measurements (including the observation of broadband radiation and elevated plasma densities and temperatures as well as the secondary ion streams) are considered in the context of the large extent of outgasing by the orbiter, the complex interaction between a hypersonic neutral gas cloud and a magnetoplasma as suggested in the work by *Stone et al.* [1986] still seems to be the most consistent explanation.

Acknowledgments. U.S. acknowledges support under NASA gran NGR-23-005-320, K.H.W. acknowledges support under NASA gra NAG8-058, and K.S.H. acknowledges support under NASA contrac NAS8-37107.

REFERENCES

Katz, I., and V. A. Davis, Ram ion scattering caused by space shuttle $v \times B$ induced differential charging, *J. Geophys. Res.*, *92*, 8787, 1987.

Stone, N. H., U. Samir, K. H. Wright, Jr., D. L. Reasoner, and S. D. Shawhan, Multiple ion streams in the near vicinity of the space shuttle, *Geophys. Res. Lett.*, *10*, 1215, 1983.

Stone, N. H., B. J. Lewter, W. L. Chisholm, and K. H. Wright, Jr., Instrument for differential ion flux vector measurements on Spacelab 2, *Rev. Sci. Instrum.*, *56*, 1897, 1985.

Stone, N. H., K. H. Wright, Jr., K. S. Hwang, U. Samir, G. B. Murphy, and S. D. Shawhan, Further observations of space shuttle plasma-electrodynamic effects from OSS-1/STS-3, *Geophys. Res. Lett.*, *13*, 217, 1986.

K. S. Hwang, Mechanical Engineering Department, University of Alabama in Huntsville, Huntsville, AL 35899.

U. Samir, Space Physics Research Laboratory, University of Michigan, Ann Arbor, MI 48109.

N. H. Stone, Space Science Laboratory, NASA Marshall Space Flight Center, MS ES53, Huntsville, AL 35812.

K. H. Wright, Jr., Department of Physics, University of Alabama in Huntsville, Huntsville, AL 35899.

(Received October 19, 1987;
revised December 23, 1987;
accepted December 31, 1987.)

JOURNAL OF GEOPHYSICAL RESEARCH, VOL. 93, NO. A1, PAGES 162-174, JANUARY 1, 1988

VLF Wave Stimulation by Pulsed Electron Beams Injected From the Space Shuttle

G. D. REEVES, P. M. BANKS, A.C. FRASER-SMITH, T. NEUBERT, AND R. I. BUSH

Space Telecommunications and Radioscience Laboratory, Stanford University, Stanford, California

D. A. GURNETT

Department of Physics and Astronomy, University of Iowa, Iowa City

W. J. RAITT

Center for Atmospheric and Space Science, Utah State University, Logan

Among the investigations conducted on the space shuttle flight STS 3 of March 1982 was an experiment in which a 1-keV, 100-mA electron gun was pulsed at 3.25 and 4.87 kHz. The resultant waves were measured with a broadband plasma wave receiver. At the time of flight the experimental setup was unique in that the electron beam was square wave modulated and that the shuttle offered relatively long times for in situ measurements of the ionospheric plasma response to the VLF pulsing sequences. In addition to electromagnetic response at the pulsing frequencies the waves exhibited various spectral harmonics as well as the unexpected occurrence of "satellite lines" around those harmonics. Both phenomena occurred with a variety of different characteristics for different pulsing sequences.

1. INTRODUCTION

Many different electron beam experiments have been undertaken with rockets and spacecraft in recent years for a variety of purposes. The pioneering work of Hess [1969], for example, demonstrated that it was possible to create an artificial aurora in the upper atmosphere with a relatively low-power electron beam. Later work by Winckler and his colleagues [*Winckler*, 1980] showed that it was possible to use rocket-borne electron beams to probe successfully the structure of the magnetosphere. Other rocket-borne electron beam experiments have investigated electrical charging phenomena [e.g., *Maehlum et al.* 1980], made measurements of ambient electric fields at geosynchronous orbit [*Melzner et al.*, 1978], and been studied as sources for ELF and VLF radiation arising from modulated beam operation [*Gendrin*, 1974; *Holzworth and Koons*, 1981; *Winckler et al.*, 1984 1985].

The present paper reports the results from low-frequency electron beam pulsing experiments made on the space shuttle flight STS 3. The objective of this work was to increase knowledge of the way a pulsed 1-keV, 100-W electron beam would interact with the ambient ionosphere to produce plasma waves. From a fundamental point of view, the present experiments also investigate the various mechanisms operative in converting the kinetic energy of the electron beam into various types of low-frequency plasma waves, including electromagnetic radiation. In comparison with previous rocket experiments, the shuttle offered a much more extended time period for such operations and, at the same time, permitted observations in a much wider range of ambient plasma conditions. The penalty for using this platform, however, is also important to understand: the shuttle plasma environment is very complex, and the different modes of interaction of the beam with the surface of the shuttle and its surrounding disturbed plasma environment are not well known [*Shawhan et al.*, 1984a, *Banks et al.*, 1987].

The present experiment was flown on the space shuttle on March 22-30, 1982 on the Columbia orbiter as part of the Office of Space Science 1 (OSS 1) mission. Through combined use of the Fast Pulsed Electron Generator (FPEG), which was part of the Vehicle Charging And Potential (VCAP) experiment, and the varied instruments of the Plasma Diagnostics Package (PDP) experiment, approximately 1 hour of data was acquired showing the plasma response to FPEG pulsing at VLF frequencies. These data are the topic of the present paper and are described in detail below. The objectives and results of the later Space Experiment with Particle Accelerators (SEPAC) beam-plasma experiments, which were flown on Spacelab 1, were considerably different and have been described by *Obayashi et al.* [1982], *Akai* [1984], *Sasaki et al.* [1986], and *Neubert et al.* [1986].

The FPEG was fully tested, prior to the OSS 1 mission, in the Johnson Spaceflight Center vacuum chamber. The chamber and experimental setup are described in detail by *Denig* [1982], *Banks et al.* [1982], *Raitt et al.* [1982], and *Shawhan* [1982]. The conditions in the chamber simulated the conditions found at shuttle altitudes with two major exceptions. The neutral gas pressure was 1-2 orders of magnitude higher than the 4.3×10^{-7} torr of the STS 3 ex-

Paper number 7A9097.
0148-0227/88/007A-9097$05.00

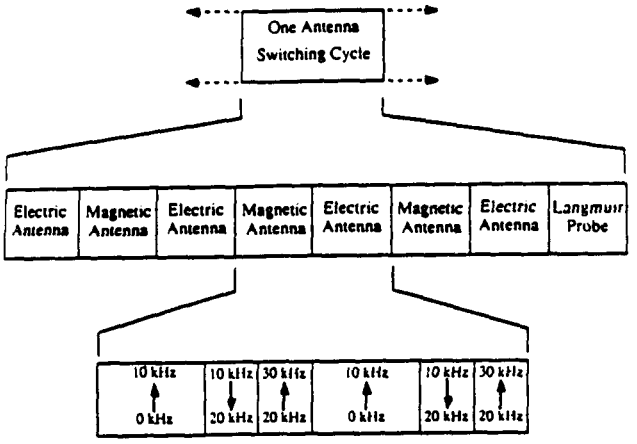

Fig. 1. A schematic representation of the antenna and frequency range switching pattern.

periments. In addition, the chamber was terminated on both ends with a grounded conductor. On the shuttle, of course, the beam was frequently unbounded on one end, and since the shuttle's thermal insulating tiles are also electrically insulating, even when the beam hit a shuttle surface, the boundary conditions were quite different.

One of the primary results of the chamber experiments was the observation of beam plasma discharge (BPD), which was found to occur under almost all chamber conditions, provided the beam current was large enough [*Denig*, 1982; *Banks et al.*, 1982; *Raitt et al.*, 1982]. On STS 3, however, BPD may not have occurred at all and certainly was not a primary effect in the FPEG sequences with short (<0.2 ms) beam emission times [*Banks et al.*, 1987]. This is in agreement with the predictions of *Bernstein et al.* [1982], which suggested that BPD should not occur at the relatively low neutral gas pressures encountered by the orbiter.

2. Experimental Consideration

The Fast Pulsed Electron Generator is a versatile square-pulsed electron beam generator. It was normally operated with a beam energy of 1 keV and a current of 100 mA for a total beam power of 100 W. On a few occasions, however, it was also operated at 50 mA to produce a 50-W beam. The beam half-angle divergence at the FPEG exit is approximately 7.5°. The gun direction is fixed with respect to the orbiter, pointing perpendicularly outward from the payload bay. Both the beam on and off times for the pulses were command controllable. The minimum on or off times were 600 ns, and the maximum on times were 107 s. The beam current had a nominal rise time of 100 ns. Each gun firing, or pulsing period, could contain up to 32,768 pulses. Thus a wide variety of modulation patterns were possible.

The primary diagnostic tool for studying the beam plasma interaction was the University of Iowa Plasma Diagnostics Package (PDP) which contained an array of sensors which are described by *Shawhan* [1984a, Table 1]. The three instruments of principal interest to this investigation were an electric field antenna, a magnetic field search coil and a Low-Energy Proton and Electron Differential Energy Analyzer (LEPEDEA). The ac electric field analyzer and magnetic field search coil were alternately connected to a wideband receiver which was sensitive in the range 10 Hz to 30 kHz. The LEPEDEA is sensative to electrons and positive ions with energies from 2 to 50 eV. During most of the flight the PDP was attached to a pallet in the orbiter cargo bay but during two intervals it was grappled with the Remote Manipulator System (RMS) and moved to selected locations outside the payload bay to distances of 15 m.

Most instruments on the PDP were sampled every 1.6 s. For the electric and magnetic field antennas, however, a continuous recording scheme was used to obtain wideband spectrographic records. The high-resolution spectrum analyzer records two sets of data simultaneously in the ranges 10 Hz to 1 kHz (ELF) and 400 Hz to 10 kHz (VLF). The ELF band recorder switches between the electric and magnetic antennas. The VLF data recording scheme is more complicated. It also follows the electric/magnetic switching pattern, but within each antenna period, three frequency ranges are recorded as follows: 400 Hz to 10 kHz for 25.6 s; then through frequency shifting and inversion, 19.6 to 10 kHz is recorded for 12.8 s; and finally 20.4 to 30 kHz is recorded for 12.8 s. To complicate matters slightly more, every fourth magnetic antenna recording is replaced by a Langmuir probe

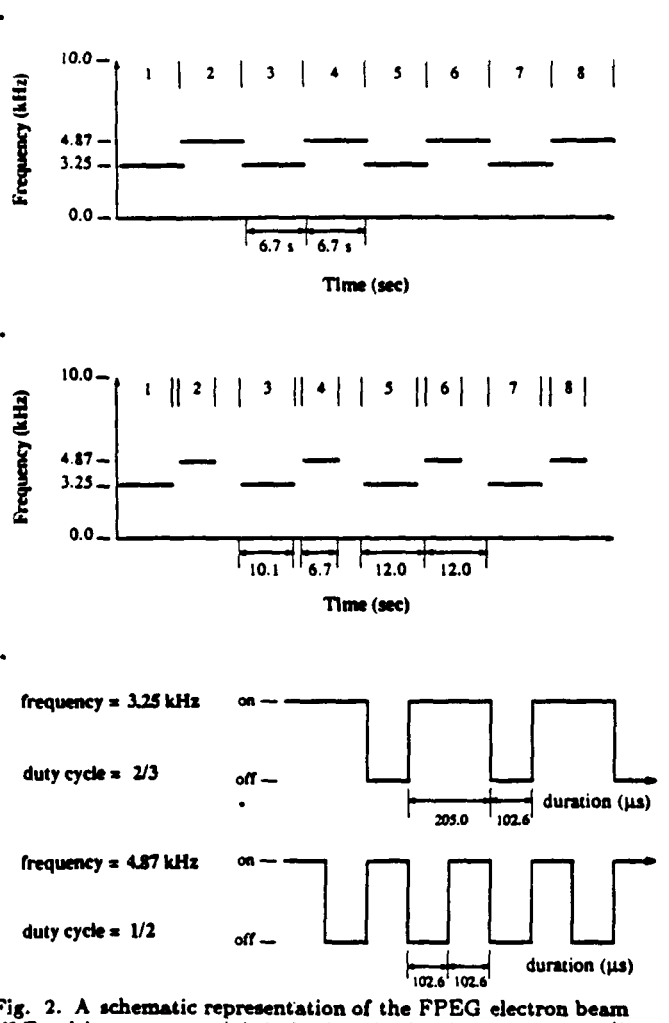

Fig. 2. A schematic representation of the FPEG electron beam VLF pulsing sequence: (*a*) the back-to-back pulsing mode and (*b*) the spaced pulsing mode; (*c*) the waveforms of the two primary pulsing frequencies.

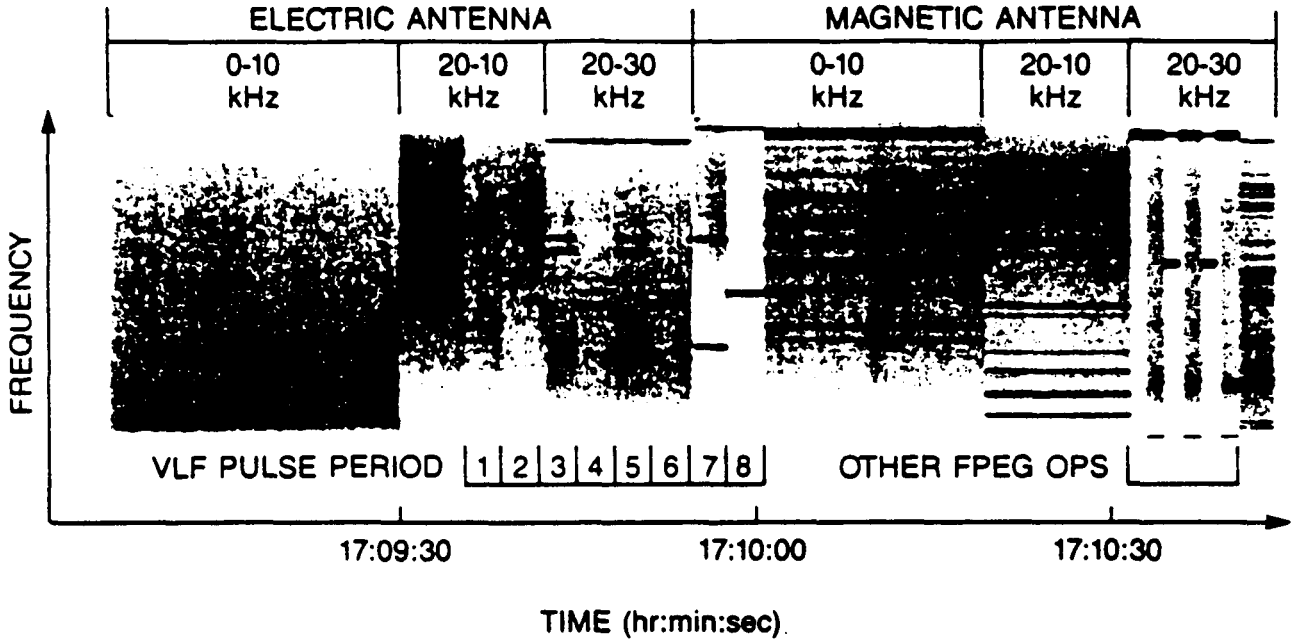

Fig. 3. Wideband data showing wave response to a VLF pulsing sequence superimposed on the antenna switching pattern. Response at the FPEG pulsing frequencies and at harmonics of those frequencies is seen. Other emission features called "satellite lines" are seen associated with some of the harmonic emissions in the 20-10 kHz and 20-30 kHz frequency ranges. FPEG pulsing periods with 3.25 kHz pulsing frequency are even numbered, 4.87 kHz are odd.

recording. (Figure 1 illustrates these sequences.) In the VLF range (0-30 kHz), data were processed into spectrograms made up of sweeps occurring every 25 ms, each consisting of 250 steps of 40 Hz bandwidth and 30 dB of dynamic range.

The antenna switching pattern is persistent in the data and it is important to note that although the data are taken continuously, while one antenna and frequency range is being recorded, the data from the other antenna or the other frequency ranges are lost. Thus there are no continuous electric and magnetic field data for the entire 400 Hz to 30 kHz range.

It is also relevant that the wideband receiver has an Automatic Gain Control (AGC) which operated independently on the ELF and VLF data ranges. The AGC had a 100-dB dynamic range and a response time of about 0.5 s. Values are read out every 1.6 s. It is set according to the integrated wave intensity in the frequency range being recorded at the time. The AGC levels provide information about the total wave intensity as well as allowing comparison of the intensity of emissions in different frequency ranges.

3. Observations

The FPEG was operated in several distinct modulation patterns during the VCAP experiment on STS 3. The modulation patterns are described in detail by *Fraser-Smith et al.* [1985]. The sequences we consider here are the VLF electron beam pulsing sequences. For these, the beam current was set at 100 mA and the gun was pulsed at two primary frequencies: 3.25 and 4.87 kHz. The former had a duty cycle (the ratio of pulse on time to total pulse period) of $\frac{2}{3}$ while the latter had a $\frac{1}{2}$ duty cycle. A typical VLF sequence consisted of eight pulsing periods which alternated between the two frequencies starting with the 3.25 kHz. The details of these sequences are given in Figure 2.

Periods of VLF beam pulsing produced an electromagnetic response which is markedly different from the characteristic background signals during passive conditions. A typical spectrum obtained during passive conditions is dominated by broadband electrostatic noise and discrete spacecraft-generated electromagnetic interference (EMI). During periods of VLF pulsing, relatively strong beam-generated signals are detected at levels of up to 30 dB above the background. [*Shawhan et al.*, 1984b] Both narrowband and broadband signals are generated. The broadband signals are similar to those reported by *Gurnett et al.* [1986]. In this paper we will concentrate on the narrowband signals produced by pulsed electron beam emission. A short time ($\approx$ 0.5 s) after the beam pulsing begins, the AGC reduces the overall gain, thus suppressing the background noise. As Figure 3 illustrates, what is then observed in intensity spectrograms is reduced background noise with eight pulsing periods in which the fundamental firing frequencies and some of their harmonics appear as distinct spectral lines. Which lines are detectable depends, in part, on which parts of the antenna switching pattern the VLF sequence spans.

During the STS 3 mission, broadband spectral data were obtained for 48 VLF sequences producing approximately 1 hour of VLF wave stimulation data. For each of these 48 sequences, discrete emissions were detected at both fundamental pulsing frequencies and at harmonics of those frequencies. This is in agreement with the theory that an electron beam square wave pulsed at VLF frequencies will produce discrete emissions at the pulsing frequency and its harmonics which can propagate in the whistler and the slow and fast Alfvén modes [*Harker and Banks*, 1983, 1985] How-

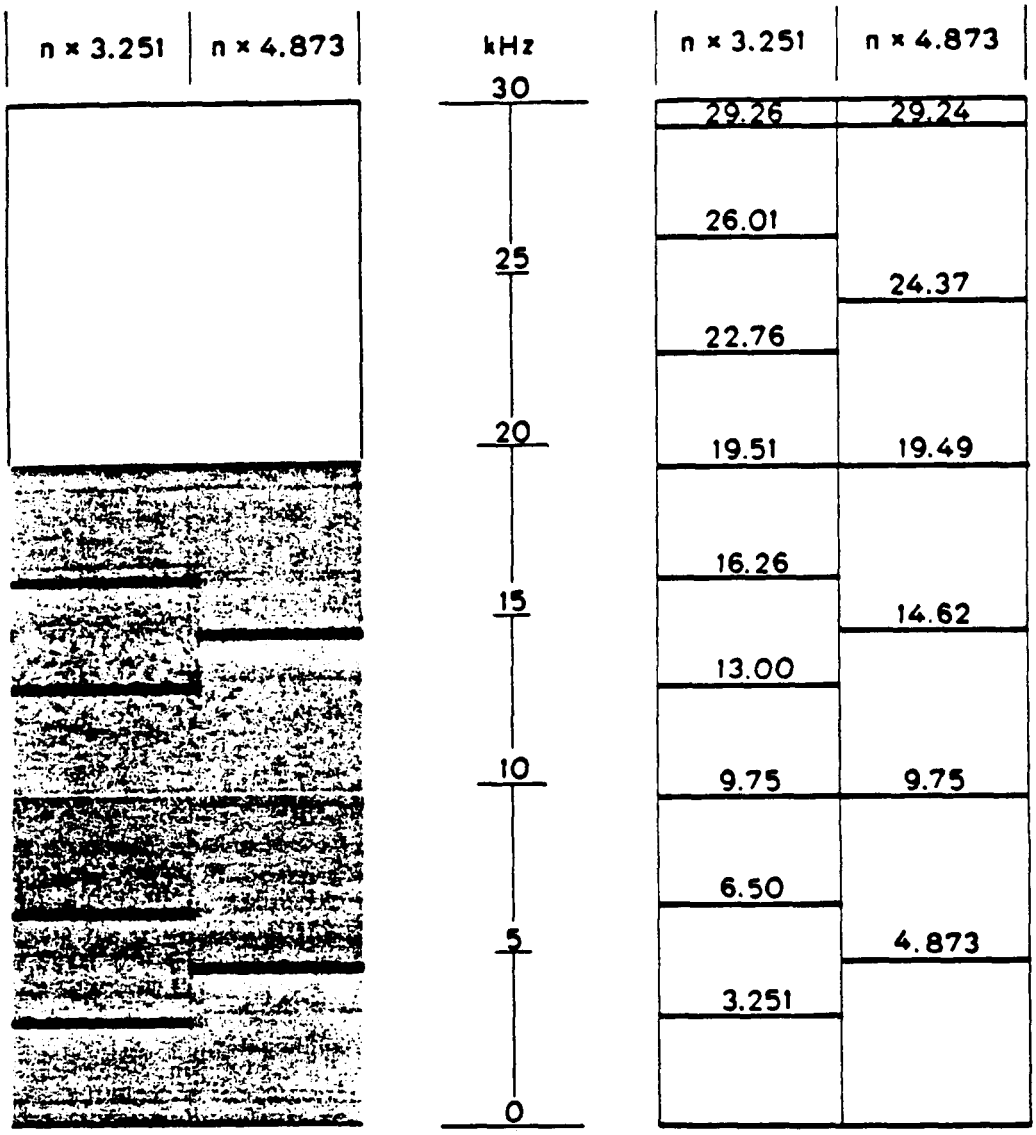

Fig. 4. A spectrogram which agrees well with theory. Narrow-band emissions are seen at the gun pulsing frequencies and at harmonics of those frequencies. Lines with integral $n(b/d)$, called "forbidden frequencies," are not observed.

ever, it cannot be determined if the emissions produced by the VLF sequences are propagating waves using the wide-band wave receiver on the PDP because the PDP was at all times within 15 m of the FPEG and therefore well within the near-field region. No qualitative difference was seen between the VLF pulsing sequences for which the PDP was in the payload bay and sequences for which it was attached to the manipulator arm. In addition, attempts to detect whistler mode emissions during magnetic conjunctions from the Dynamics Explorer 1 (DE 1) satellite, at distances of up to several thousand kilometers, did not produce conclusive results. (Magnetic conjunction during FPEG operations was achieved for 12 cases, but in all but two of those, the DE satellite was outside the region of whistler mode propagation as determined through ray-tracing techniques. For the two other cases the electron beam was known to have hit the STS 3 orbiter within one gyroperiod [*Inan et al.*, 1984].)

During the VLF sequences many other phenomena can be seen in addition to the discrete emissions at the pulsing frequencies. A variety of interesting results can be broadly classified under the two categories "harmonic structure" and "satellite lines." A third category, which may be related to the second, can be called "subharmonics." These will be examined in detail below and analyzed in the following section.

Harmonic Structure

The VLF wave stimulation experiment produced wave response at the gun pulsing frequencies of 3.25 and 4.87 kHz and at integral multiples of those frequencies. The amplitudes of these harmonic spectral lines varied from one sequence to another, but they were present in every pulsing sequence at frequencies up to the 30-kHz limit of the PDP wave receiver. The 3.25-kHz firings have nine harmonics which fall in the 0-30 kHz range and the 4.87-kHz firings

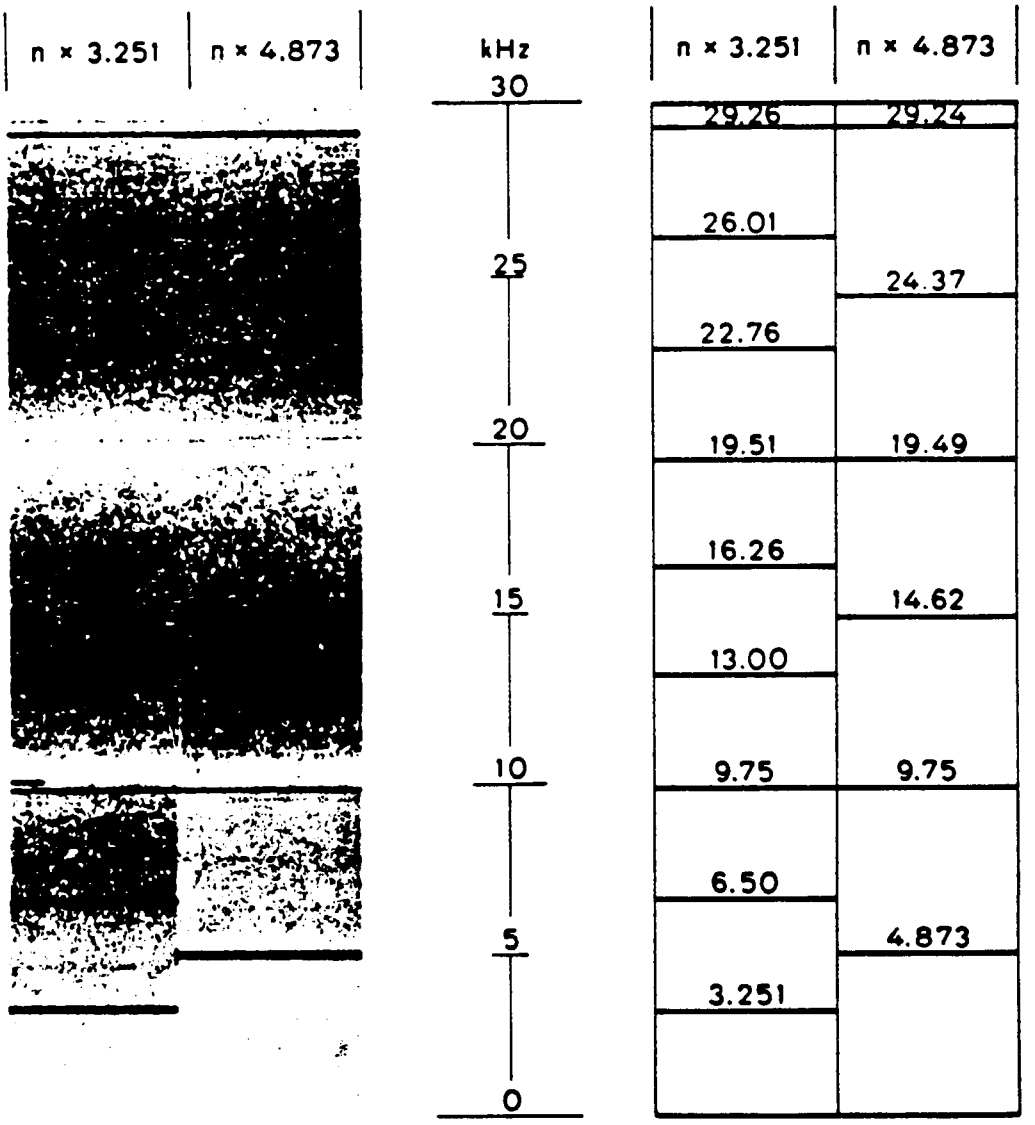

Fig. 5. A spectrogram showing the presence of lines at "forbidden frequencies" as well as "satellite lines" associated with the harmonic spectral lines at the higher frequencies.

have six. These frequencies have particularly simple duty cycles (ratio of beam on time to total period) of $\frac{2}{3}$ and $\frac{1}{2}$, respectively. The choice of these frequencies gives common harmonics at nearly 9.75, 19.75, and 27.24 kHz. For a pulsed electron beam with the given choices of duty cycle, power spectrum theory also predicts that these frequencies (the so-called "forbidden frequencies") should not appear for either pulsing frequency.

Figure 4 illustrates a spectrum with a normal harmonic structure. It was constructed by taking the broadband data (as in Figure 3) and ordering it to remove the complexity of the antenna switching pattern. Although the 20-30 kHz data were not available for this sequence, we see that there are strong emissions at the fundamental pulsing frequencies and their harmonics and no appreciable signals at the "forbidden frequencies."

In contrast to the predictions of theory, our experimental results indicate that in a surprising number of cases, the harmonic spectral lines include the "forbidden frequencies." Figure 5 shows such a situation. In fact, in approximately 60% of the VLF sequences, the 9.75-kHz line was present with an amplitude which ranged from as low as 30 dB below the amplitude of the fundamental to cases in which it was actually more intense. Cases of spectra which generally include the "forbidden frequencies" and cases which do not are seen with both the electric and magnetic antennas, and there seems to be little difference in the morphology of the response of the two fields.

Unfortunately, instrumental limitations complicated the complete analysis of the presence of the "forbidden frequencies." Sensitivity roll-off at the lower end of the recorded frequency range makes it impossible to measure signals near 19.75 kHz which corresponds to the sixth harmonic of the $\frac{2}{3}$ duty cycle pulsings and the fourth harmonic of the $\frac{1}{2}$ duty cycle pulsings. (Recall that the 10-20 kHz band is inverted for recording.) The signals near 9.75 and 27.24 kHz have no such difficulty since the instrument was sensitive to within a few hertz of 10 kHz. The lines at 27.24 kHz, which are the

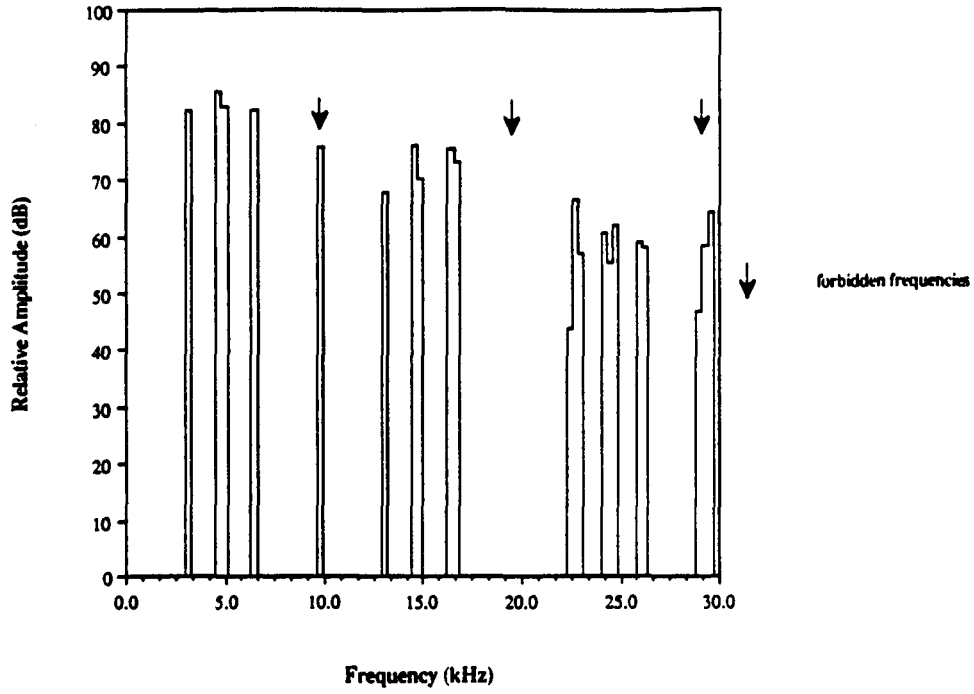

Fig. 6a. Relative amplitude of the spectral lines as measured by the electric antenna.

ninth harmonic of the $\frac{2}{3}$ pulsings and the sixth harmonic of the $\frac{1}{2}$ pulsings, are, however, obscured by an interfering signal probably produced by the FPEG power converter. This EMI is detectable with both the electric and magnetic antennas when the PDP is stowed on the OSS 1 pallet and is detectable primarily with the magnetic antenna when the PDP is deployed on the manipulator arm. The principal effect of this line is to make it difficult to determine if the harmonics at 27.24 are present or not. Thus we are limited in our studies of "forbidden frequencies" to the signals at 9.75 kHz.

Figure 6 shows the relative amplitude of the spectral components observed with the electric and magnetic antennas. The plots were constructed by splitting the 30-kHz band

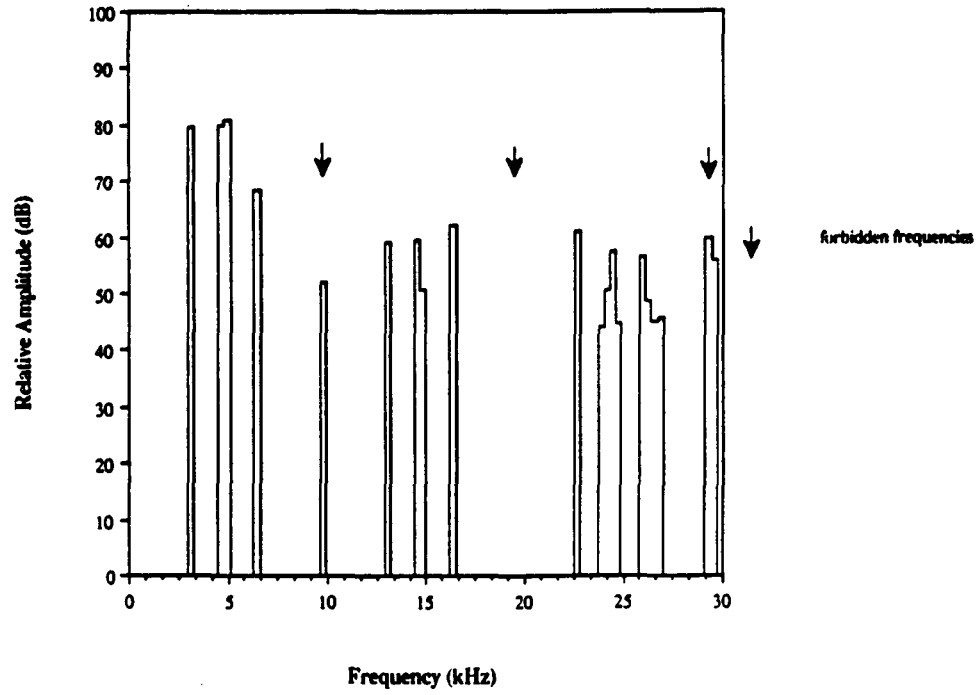

Fig. 6b. Relative amplitude of the spectral lines as measured by the magnetic antenna.

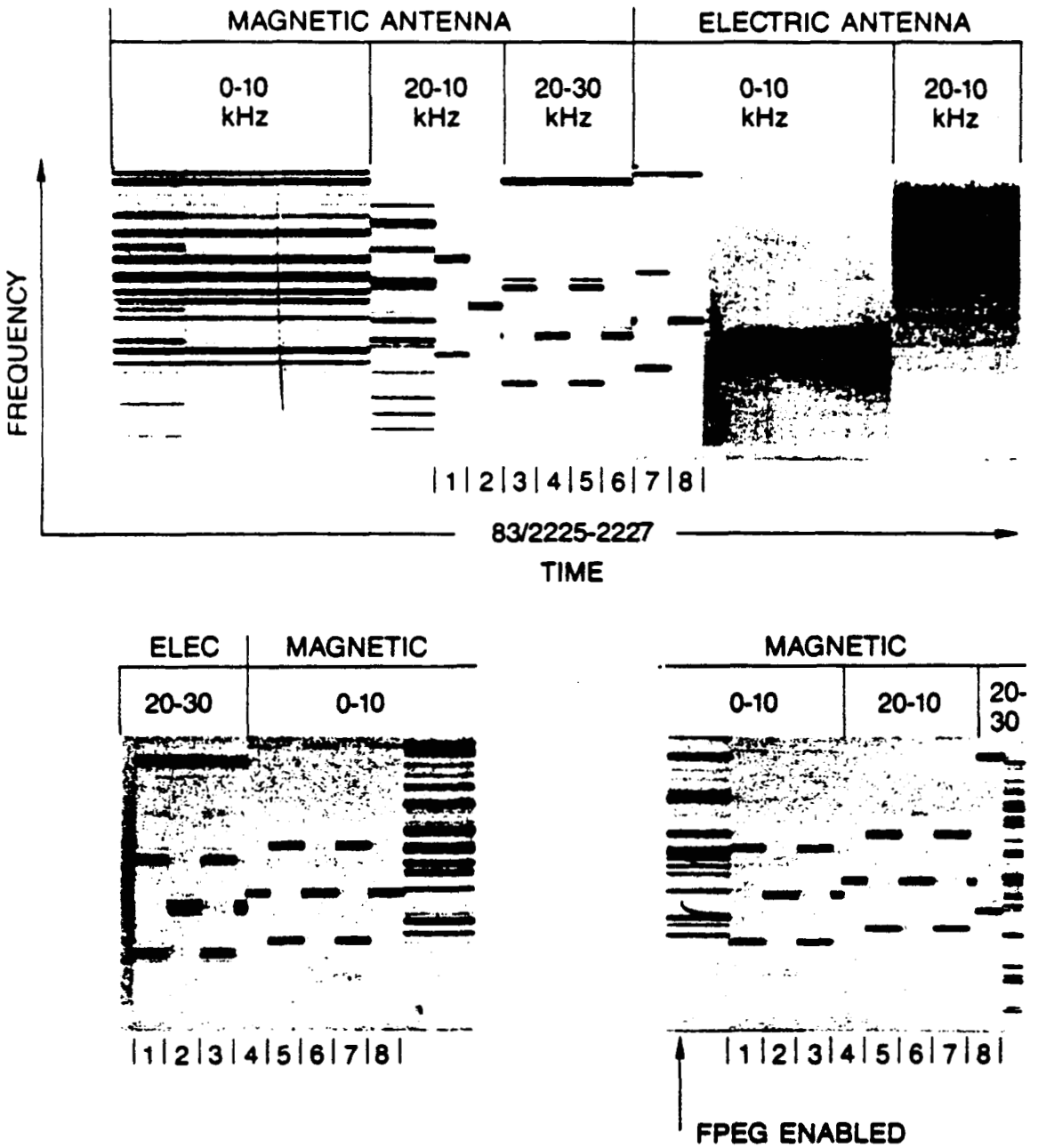

Fig. 7a. Spectrograms, with antenna switching pattern included, showing a variety of manifestations of satellite lines and including single satellite lines of higher frequency as seen in the first spectrogram in pulsing periods 3-6, satellite lines of both higher and lower frequency as in the second spectrogram in the lower harmonics of pulsing periods 1-4, and broadened line emissions as seen in the second and third spectrograms at various harmonics.

into one hundred 300-Hz bands and averaging the contributions from seven typical sequences. Many of these sequences had satellite lines (described later), which accounts for the apparent broadening of the lines. We also note that the broadband receiver provides only relative amplitudes between similar antennas: the electric and magnetic relative amplitudes cannot be compared with each other, although one electric or magnetic spectrum can be compared with another like spectrum. Further, the amplitudes at 27.24 kHz must be considered an estimate because of the presence of EMI. Within these limits of interpretation we see that the averaged amplitude of the spectral components generally decreases slowly with increasing frequency and that there is significant decrease in amplitude at the "forbidden frequencies." The fact that there is a response at those frequencies indicates the presence of VLF sequences which have lines at the "forbidden frequencies."

Satellite Lines

Another interesting and unexpected phenomenon observed in the STS 3 broadband VLF data obtained during

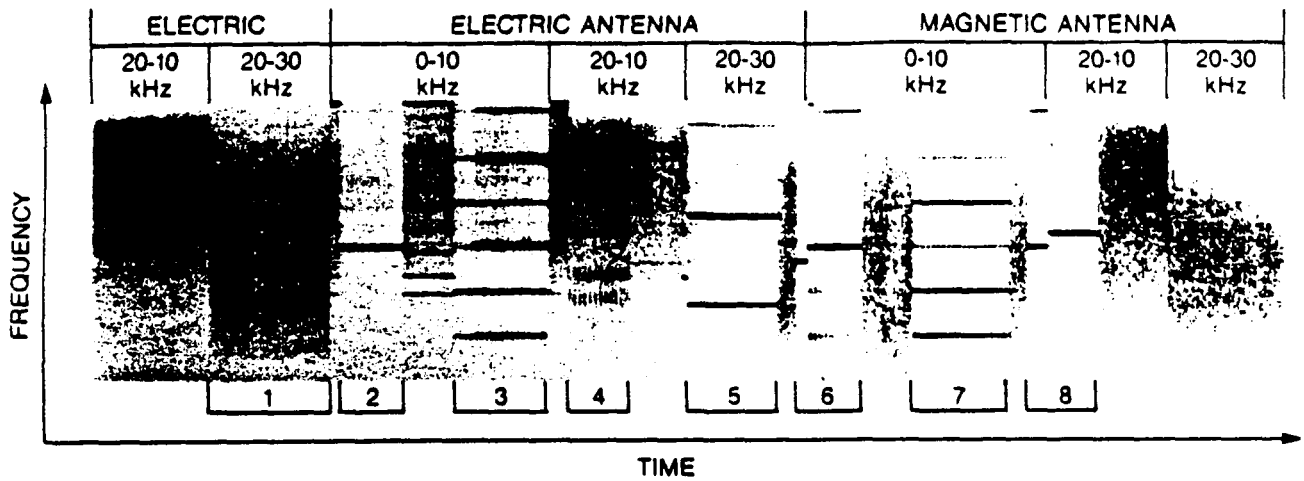

Fig. 7b. A spectrogram, with antenna switching pattern included, showing emissions at half integral multiples of the pulsing frequency which occur during pulsing periods 3 and 7.

FPEG pulsing sequences was the presence of "satellite lines" situated near the various harmonic spectral lines. To our knowledge, this is a previously unobserved effect. It is characterized by one or more emissions separated in frequency from the harmonic spectral lines produced by the pulsed electron beam. The separation can range from 100 Hz to over 1 kHz. satellite lines were detected in 26 out of 48 sequences. In seven of those 48 cases, measurements in the 20–30 kHz frequency range were not obtained. Since satellite lines are most frequently observed in the 20–30 kHz range, no conclusions can be drawn for these seven cases.

The most common type of satellite line is a single subsidiary line which is higher in frequency than its primary. Figure 5 shows a typical spectrum with a single satellite line of higher frequency associated with some of the harmonic spectral lines. Of the 26 sequences with satellite lines, 10 were of this type. They occur mainly in the 20–30 kHz range but are also seen between 10 and 20 kHz and, rarely, in the 0–10 kHz range. In general, all satellite lines in a given observational period have the same frequency separation from their associated harmonic lines for each harmonic. There are, however, notable exceptions. The strength of the satellite lines is also highly variable. It is intriguing to note that the satellite lines occur as soon as the firing is detected, which is instantaneous within measurement limitations: no buildup is detected. The satellite lines also disappear, with the primary lines, when the gun is turned off.

Figure 7 shows some of the other varieties of satellite lines. Of these, the most common are satellite lines of both higher and lower frequency. Sometimes several pairs of satellite lines will surround a given harmonic. Another variation is the presence of a narrow noise band around the primary spectral lines. Intensity maxima and minima may indicate the development of satellite lines but the lack of sufficient cases makes this uncertain. It is also possible to have narrow bands and distinct lines around the same primary line.

An even more unusual case of the presence of spurious emissions is seen in Figure 7b during the pulsing periods labeled 3 and 7. At those times, Figure 7b shows one of two sequences in which "half integral harmonics" were seen. It is not thought that these are satellite lines with large frequency separation in part because these lines change in intensity during a firing.

In passing we note that a variable frequency emission associated with enabling high voltage to the FPEG is also seen prior to electron emission. This emission is seen, for example, in Figure 7 at the point marked "FPEG enabled" and between 800 and 900 Hz in Figure 9 prior to the appearance of subharmonics. It is fairly common and is associated with enabling of the FPEG filament high voltage before a pulsing sequence begins. It generally appears in the magnetic antenna. Since these emissions are clearly instrumental in origin and do not appear to be related to any of the other observed features, they have not been the subject of extensive investigation.

Figure 8 shows the distribution of the frequency separation (Δf) between a satellite line and its primary. Several features are evident. First, cases which have satellite lines at higher frequencies ($\Delta f > 0$) are more common (particularly at 400 Hz). The most common separations have $70 \text{ Hz} \leq |\Delta f| \leq 160$ Hz. Separations this small do not appear as distinct lines on the spectrographic films but, rather, as broadened dark lines. Amplitude scans of the data obtained from analysis of the original magnetic tapes do reveal signals at these frequency separations. We note also that for those separations, there is almost always a pair of lines with one higher and one lower in frequency than the primary.

Subharmonics

A third type of emission feature has been identified in the 0-1 kHz (ELF) broadband data which was recorded simultaneously with the 0-30 kHz (VLF) data. For want of a better name, we have termed these "subharmonics". They are illustrated in Figure 9 along with the same sequences seen in the 0-30 kHz range. The subharmonics, like the harmonic spectral lines, are narrowband, begin and end with the pulsing period, and have reasonably constant amplitude during a pulsing period. Several features are striking. First, we note that the frequency of the subharmonics decreases with time. The rate of decrease is of the order of 1-2 Hz/s. (No correlation was found with the fractional change per unit time of the subharmonic frequency and the STS 3 orbital environ-

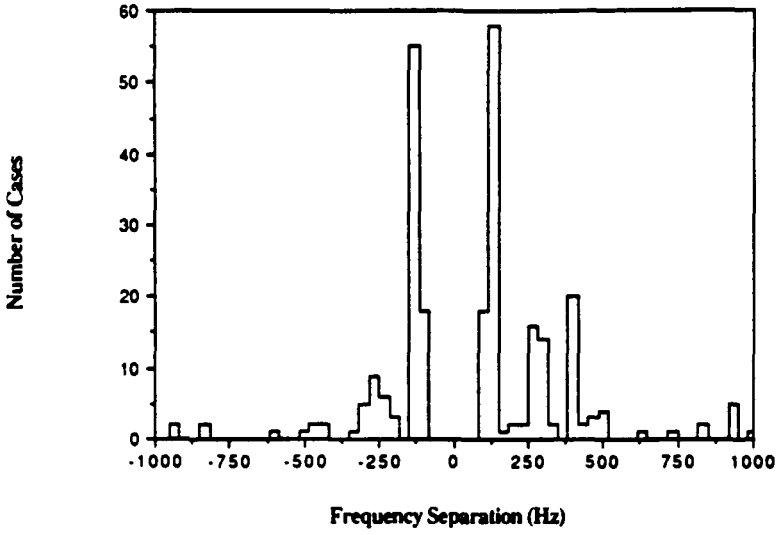

Fig. 8. The distribution of frequency separation, Δf , between a primary spectral line and its satellite line is shown. The number of cases refers to the total number of lines with such a separation, not the number of pulsing periods.

ment parameters, however.) At least six sequences, including two of those of Figure 9, clearly display pairs of subharmonics. Regardless of the frequency of the subharmonic or the frequency of the fundamental, the higher-frequency subharmonic spectral line is twice the frequency of the lower. This leads us to conclude that the higher frequency lines are the second harmonic of the lower. A third harmonic or higher was never observed. Since spectral lines at the pulsing frequencies are not observed to drift in frequency, the ratio of pulsing frequency to subharmonic frequency is nonintegral and time varying. Further, the ratio of the pulsing frequency to the subharmonic ELF frequency is different for the 3.25- and 4.87-kHz firings.

4. DISCUSSION

Harmonic Structure

Harker and Banks [1983, 1985] presented a simple model for the far-field radiation expected from a pulsed electron beam in a magnetized plasma. This theory predicts that the beam will radiate at the pulsing frequency and at harmonics of that frequency in the whistler and the slow and fast Alfvén modes. *Harker and Banks, [1986]* later expanded that work to include contributions from the near field as well. In both cases, the power in the fields for each harmonic n was found to be proportional to the term $sin^2(n\pi(b/d))$ where b/d is

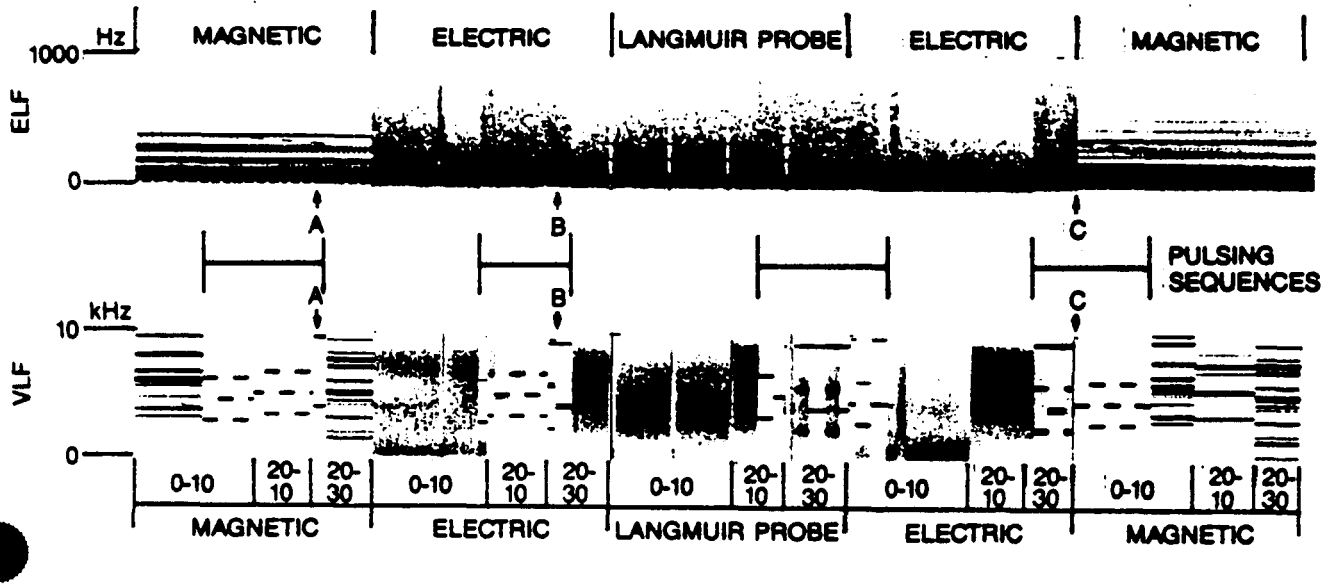

Fig. 9. Spectrograms, with antenna switching pattern included, are shown in (*a*) the ELF (0-10 kHz) and (*b*) the VLF (0-30 kHz) ranges. Good correlation between the frequency of the subharmonics in Figure 9a and the frequency separation of the satellite lines in Figure 9b is illustrated. At the points marked A, B, and C the subharmonic frequencies are 330, 250, and 163 Hz, respectively. The frequency separation of the satellite lines from the harmonics of the pulsing frequencies at those points are 330, 267, and 150 Hz.

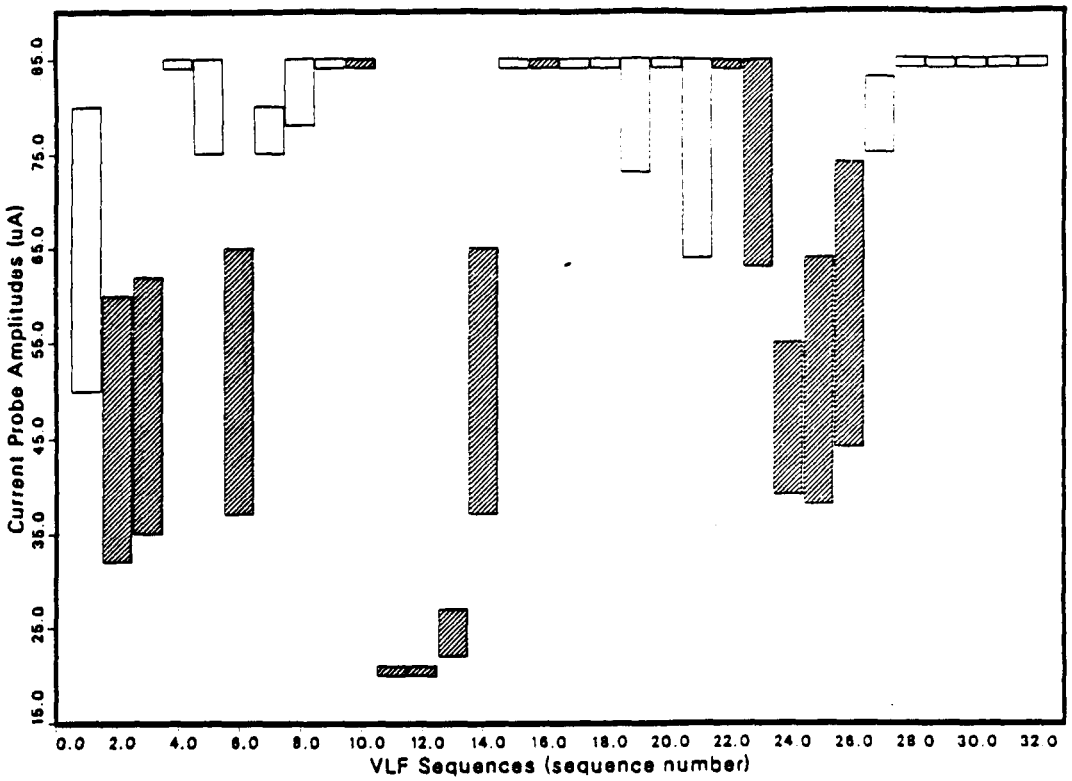

Fig. 10a. The range of return current collected by the CP1 instrument is shown for each sequence which had wideband data in the 20-30 kHz frequency range of the electric antenna. Sequence number is as they occurred in time during the mission and should be considered schematic.

the duty cycle of the pulse. The expected amplitude of the harmonics is considerably more complicated and the reader is referred to their papers, but one feature is quite striking. For integral $n(b/d)$, the amplitudes go to zero. Thus, as in Figure 3, for the $\frac{2}{3}$ duty cycle firings (3.25 kHz) the third, sixth, and ninth harmonics should be missing, and for the $\frac{1}{2}$ duty cycle (4.87 kHz) all the even harmonics should vanish.

For both fundamental pulsing frequencies, the vanishing harmonics correspond to 9.75, 19.75 and 27.24 kHz, hence the term "forbidden frequencies." These frequencies are, of course, forbidden only for our particular choice of pulsing parameters and are a result, in part, of the Fourier decomposition of the given waveform. As Figures 4-6 indicate, our data conformed with theory in many cases but deviated from that theory for the majority of VLF sequences.

Efforts have been made to isolate the physical factors which give rise to the presence of unexpected harmonics. However, no correlation was found between the amplitude of the harmonics and the best estimated trajectory (BET) environmental parameters, which include the magnetic field vector, the ram (or antivelocity) vector, altitude, latitude, longitude, L shell, and a day/night parameter. In addition, there were the calculated variables such as electron beam column radius (electron gyroradius), the electron beam column center to detector distance, the V×B vector, and a shuttle hit/miss parameter. Two-variable scatter plots were made for each pair of parameters and sequences with particular spectral characteristics given different symbols to determine if there was a preferred region of, or trajectory in, parameter space which contained the sequences which conformed to theory and another region, or trajectory, which contained those which did not. Due, in part, to the fact that many parameters covered only a small part of their total possible range, the results were ambiguous, and no correlations could be found for any of the above mentioned parameters. We can conclude, then, that the factor controlling the presence of lines at the "forbidden frequencies" is variable but is not a simple function of the orbiter environment.

We have also investigated the possibility that the variation in harmonic structure arises from an instrumental effect. However, the lack of any correlation between primary signal intensity and presence of the forbidden harmonics argues strongly against this possibility. A more likely possibility is a degradation of the electron beam radiation condition such that the assumption of beam coherence used by *Harker and Banks*, [1983, 1985, 1986] is violated. If, for example, each pulse radiated only at the leading or trailing ends, the spectrum obtained would contain uniform harmonics of equal amplitude. Work is now proceeding to extract the phase information from the spectrogram in an attempt to reconstruct the effective radiating portion of the pulse and to determine what parameters would change the effective pulse shape.

Satellite Lines and Subharmonics

We have grouped satellite lines and subharmonics under the same section at this point because we have reason to believe that the presence of subharmonics and the presence of satellite lines are related to the same physical phenomenon,

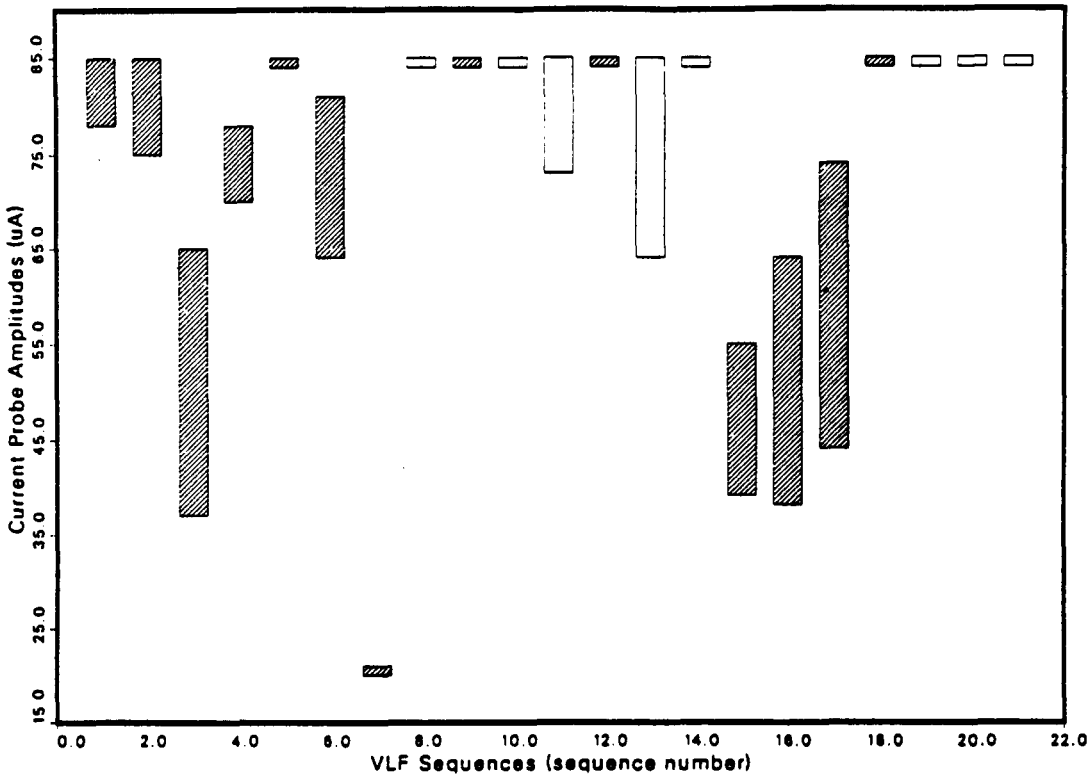

Fig. 10b. The same as Figure 10a but for sequences which had wideband data in the 20-30 kHz frequency range of the magnetic antenna.

and it becomes redundant to discuss them separately. Out of 43 VLF sequences with complete (ELF and VLF) data, 19 sequences had neither satellite lines nor subharmonics while 18 had both satellite lines and subharmonics and only six had either satellite lines or subharmonics but not both. Of the 18 sequences with satellite lines and subharmonics, 13 had subharmonics with frequencies comparable to one or more frequency separations for the satellite lines ($\Delta f \approx f_{sub}$). It should be noted that of that 13, nine had additional satellite lines or subharmonics with no counterpart. To complete the inventory, five sequences had satellite lines and subharmonics but $\Delta f \neq f_{sub}$. Further evidence of the relationship between satellite lines and subharmonics is seen in Figure 9. Comparing three points in the series of firings (labeled A,B, and C in Figure 9) we find subharmonic frequencies of 330, 250, and 163 Hz, respectively. (All with an error of ±10 Hz.) For the satellite lines, we find that the difference frequencies (Δf) at the same points are 330, 267, and 150 Hz (all ±33 Hz). The agreement is quite good but can not be compared for all sequences because of complications arising from the VLF antenna switching pattern. The ELF wave data are continuously displayed for 0-1 kHz, but the VLF antenna switching provides data in the 20-30 kHz range, where satellite lines are most commonly observed, only for one quarter of the time. Thus the full temporal development of the satellite lines cannot be observed.

Examination of data from the VCAP current probes and the LEPEDEA indicates that the orbiter electrical return current is involved in the interaction. Figure 10 shows the data from the current probe 1 (CP1). The ordinate is the peak current measured in each sampling period of 17 ms. The area of the detector is 0.05 m^2 and the current is measured in microamperes. The saturation value for the detector was 85 μA. The CP1 values shown here indicate the peak flux of electrons minus ions collected on the detector surface. The bars in Figure 10 indicate the range of peak currents detected during one pulsing sequence with shaded bars indicating sequences with satellite lines. We see that for times when the pulsing sequence overlaps the times when the 20-30 kHz range is monitored, satellite lines tend to occur for relatively low values of the return flux of electrons measured by CP1, which is located next to the FPEG. There is no correlation with the current collected by CP2, which is located several meters away from the FPEG on the opposite side of the OSS 1 pallet. (See Figure 11.) The current collected at this probe appears to be controlled by ambient plasma flow which is, in turn, controlled by the attitude of the orbiter, the orbiter plasma environment, and the orbiter-plasma potential. Figure 11 shows the relative positions of the FPEG, PDP, and the CCP 1 and CCP 2 instruments. The projection of the beam column onto the plane of the payload bay is also shown shaded for a typical magnetic field configuration.

In contrast to the current probes, the LEPEDEA tended to measure larger fluxes of hot electrons at times when satellite lines were observed. The PDP was located 1.55 m away from the FPEG on the forward part of the OSS 1 pallet, and electrons did not reach it by following unperturbed helical trajectories. If the electrons spread along the magnetic field direction, the helix becomes a cylindrical shell with its axis along the magnetic field. We were surprised to find that our analysis indicates that the PDP was outside this beam column for all the VLF sequences for which the PDP was mounted in the payload bay. (When the PDP was on the manipulator arm, its position was not known.)

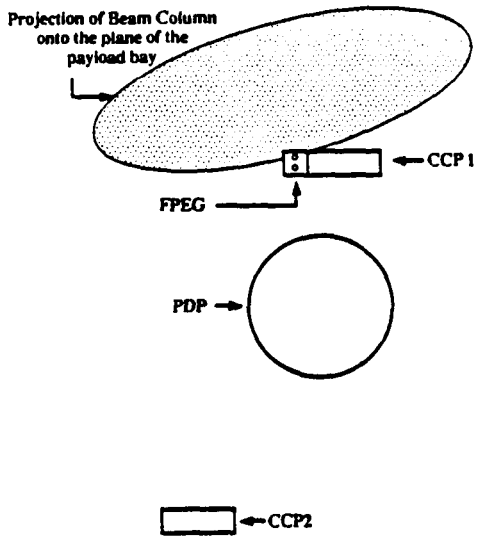

Fig. 11. The relative positions of the Fast Pulsed Electron Generator, the Plasma Diagnostics Package, and the charge and current probes. Also shown as a shaded ellipse is the column formed by the gyromotion of the electron beam projected onto the plane of the payload bay for a typical magnetic field strength and direction.

There does not appear to be any correlation between distance to the beam column and the presence or strength of satellite lines. We conclude then that the LEPEDEA does not measure freely escaping beam electrons but rather energetic electrons coming from collisions, coulombic expansion of the beam, or some undetermined instability which drives electrons perpendicular to the magnetic field. This occurs at the same time that the number of electrons traveling toward the FPEG, as measured by CCP 1, is reduced. Hence we are led to suspect a process which reduces the number of electrons scattered back along the field lines and scatters them, instead, perpendicular to the field lines. These results indicate a strong beam plasma interaction.

We have taken care to avoid calling the satellite lines "sidebands," which would imply conventional mechanisms such as amplitude or frequency modulation, linear beating with an undetected frequency, or some aliasing mechanism. We have considered these mechanisms but have found that none can explain the complexities in the data. The electron beam was modulated in a simple pulsed mode producing a square wave modulated current source. If there is any coherent amplitude or frequency modulation of the source, it would necessarily imply a beam plasma interaction. Both the linear beating and the aliasing possibilities are unlikely because the VLF and ELF wave receiver channels are independent and have separate cutoff filters. We believe that the correlation between the frequency separation of the satellite lines and the frequency of the subharmonics rules out those processes. Further, aliasing would not account for the gradual drift in frequency of the satellite lines and subharmonics. We rule out Doppler shift for the simple reason that the source and the receiver are comoving. If any additional argument was needed, one could note that Doppler shifting would not produce subharmonics through any linear mechanism. The possibility of problems caused by the heterodyning of the signal was also considered because the satellite lines occur most often in the 10-20 and 20-30 kHz bands which are heterodyned by the broadband receiver down to the 0-10 kHz range. The fact that the subharmonics appear for the duration of a pulsing sequence argues against this possibility. The ELF channels are not heterodyned and are subject to only the electric/magnetic switching pattern. Further, aliasing would not account for the gradual drift in frequency of the satellite lines and subharmonics. We have been unable to determine any other instrumental effect which could satisfactorily explain the presence of these emission features.

A possible explanation may be that under certain conditions, the electron beam creates a hot plasma environment in the payload bay and any one of the many orbiter instruments could induce a periodic disturbance in that plasma which could then interact, in an undetermined manner, with the beam-generated signals. This possibility is given added weight when one notices the presence of satellite lines with $\Delta f = 400 \pm 33$ Hz in three VLF sequences around a total of 20 individual primary lines and that the AC power available on the orbiter was at 400 Hz. It should be noted that although a subharmonic at approximately 400 Hz was detected for each of those three VLF sequences, no subharmonic near 400 Hz was detected in any of the 40 other sequences.

5. CONCLUSIONS

In summary, our primary observation was the existence of a narrowband electromagnetic response detected at the pulsing frequencies of 3.25 and 4.87 kHz. In addition, narrowband lines were seen at harmonics of those frequencies. The harmonic structure often deviated from predictions, but the causes for those deviations are, as yet, unknown. Another prominent feature which was frequently observed in the spectra was the presence of "satellite lines" which appear to be related to the presence of energetic electrons around the PDP as measured by the LEPEDEA and a corresponding decrease in current flow to the orbiter near the FPEG. "subharmonics" were observed during VLF sequences at frequencies far below the fundamental pulsing frequencies. There is statistical evidence that they are part of the same phenomenon which produces the "satellite lines." The exact nature of that phenomenon and the cause of the deviation of the primary harmonic structure from theory are areas of ongoing research.

Acknowledgments. The authors would like to acknowledge the contribution of D. Gurnett and L. Frank of the University of Iowa in providing data from the Plasma Diagnostics Package instruments and the valuable assistance of K. Harker and J. Yarbrough of Stanford University. This work was supported under grants NAGW-235 and RADC F19628-84-K-0014 at Stanford University.

The Editor thanks K.N. Erickson and D.N. Walker for their assistance in evaluating this paper.

REFERENCES

Akai, K., Electron beam-plasma interaction experiment in space, ISAS Res. Note 285, Inst. of Space and Astronaut. Sci., Tokyo, 1984

Banks, P.M., W.J. Raitt, and W.F. Denig, Studies of beam-plasma interactions in a space simulation chamber using prototype space shuttle instruments, in *Artificial Particle Beams in Space Plasma Studies*, edited by B. Grandal p.393, Plenum, New York, 1982.

ks, P.M., W.J. Raitt, A.B. White, R.I. Bush, and P.R. Williamson, Preliminary results from the Vehicle Charging and Potential experiment on STS 3, *J. Spacecr. Rockets*, in press 1987.

Bernstein W., P.J. Kellog, S.J. Monson, R.H. Holzworth, and B.A. Whalen, Recent observations of beam-plasma interactions in the ionosphere and a comparison with laboratory studies of the beam plasma discharge., in *Artificial Particle Beams in Space Plasma Studies*, edited by B. Grandal, p.35, Plenum, New York, 1982. Plenum Press, NY, 1982.

Denig, W.F., Wave and particle observations associated with the beam plasma discharge in a space simulation chamber., PhD. thesis, Utah State Univ., Logan, 1982.

Fraser-Smith, A.C., P.M. Banks, and G.D. Reeves, Observations of sub-LF electromagnetic field phenomena associated with modulated electron beams on STS 3, *Final Tech. Rep. RADC-TR-85-152*, Rome Air Force Dev. Cent., Griffiss AFB, New York, Aug. 1985.

Gendrin, R., The French-Soviet ARAKS experiment, *Space Sci. Rev., 15*, 905, 1974.

Gurnett, D.A., W.S. Kurth, J.T. Steinberg, P.M. Banks, R.I. Bush, and W.J. Raitt, Whistler-mode radiation from the spacelab-2 electron beam, *Geophys. Res. Lett., 13*, 225, 1986.

Harker, K.J., and P.M. Banks, Radiation from pulsed electron beams in space plasmas, *Radio Sci., 19*,(2), 454, 1983.

Harker, K.J., and P.M. Banks, Radiation from long pulse train electron beams in space plasmas, *Planet. Space Sci., 33*, 953, 1985.

Harker, K.J., and P.M. Banks, Near fields in the vicinity of pulsed electron beams in space, *Planet. Space Sci., 35*, 11, 1986.

Hess, W.N., Generation of artificial aurora, *Science, 164*, 1512, 1969.

Holzworth, R.H., and H.C. Koons, VLF Emissions from a modulated electron beam in the auroral ionosphere., *J. Geophys. Res., 86*, 853, 1981.

n, U.S., M. Pon, P.M. Banks, P.R. Wiliamson, W.J. Raitt, and S.D. Shawhan, Modulated beam injection from the space shuttle during magnetic conjunctions of STS 3 with the DE 1 satellite, *Radio Science, 19*(2), 487, 1984.

Maehlum, B.N., K. Maseide, K. Aarsnes, A. Egeland, B. Grandal, J. Holtet, T.A. Jacobsen, N.C. Maynards, F. Soraas, J. Stadsnes, E.V. Thrane, and J. Troim, Polar 5–An electron accelerator experiment within an aurora, 1-4, *Planet. Space Sci., 28*, 259, 1980.

Melzner, F., G. Metzner, and D. Antrack, The GEOS electron beam experiment S 329, *Space Sci. Instrum., 4*, 45, 1978.

Neubert, T., W.W.L. Taylor, L.R.O. Storey, N. Kawashima, W.T. Roberts, D.L. Reasoner, P.M. Banks, D.A. Gurnett, R.L. Williams, and J. Burch, Waves generated during electron beam emissions from the space shuttle., *J. Geophys. Res., 91*, 11,321 1986.

Obayashi, T., N. Kawashima, K. Kuriki, N. Nagatomo, K. Ninomiya, S. Sasaki, A. Ushirokawa, I. Kudo, M. Ejiri, W.T. Roberts, R. Chappell, J. Burch, and P.M. Banks, Space experiments with particle accelerators (SEPAC), in *Artificial Particle Beams in Space Plasma Studies*, edited by B. Grandal, p659, Plenum, New York, 1982.

Raitt, W.J., P.M. Banks, W.F., Denig, and H.R. Anderson, Transient effects in beam-plasma interactions in a space simulation chamber stimulated by a Fast Pulse Electron Generator., in *Artificial Particle Beams in Space Plasma Studies*, edited by B. Grandal, p405, Plenum, New York, 1982.

Sasaki, S., N. Kawashima, K. Kuriki, M. Yanagisawa, and T. Obayashi, Vehicle charging observed in SEPAC spacelab-1 experiment., *J. Spacecr. Rockets*, 23, 194, 1986.

Shawhan, S.D., Description of the Plasma Diagnostics Package (PDP) for the OSS–1 shuttle mission and JSC chamber test in conjunction with the Fast Pulse Electron Generator (FPEG), in *Artificial Particle Beams in Space Plasma Studies*, edited by B. Grandal, p419, Plenum, New York, 1982.

Shawhan, S.D., G.B Murphy, and J.S. Picket, Plasma Diagnostics Package initial assessment of the STS 3 orbiter plasma environment, *J. Spacer. Rockets, 21*, 387, 1984a.

Shawhan, S.D., G.B. Murphy, and D.L. Fortna, Measurements of electromagnetic interference on OV102 *Columbia* using the Plasma Diagnostics Package, *J. Spacer. Rockets, 21*, 392, 1984b.

Winckler, J.R., J.E. Steffen, P.R. Malcolm, K.N. Erickson, Y. Abe, and R.L. Swanson, Ion resonances and ELF wave production by an electron beam injected into the ionosphere: Echo 6, *J. Geophys. Res., 89*, 7565, 1984.

Winckler, J.R., The application of artificial electron beams to magnetospheric research, *Rev. Geophys., 19*, 659, 1980.

Winckler, J.R., K.E. Erickson, Y. Abe, J.E. Steffen, and P.R. Malcolm, ELF Wave production by an electron beam emitting rocket system and its suppression on auroral field lines, *Geophys. Res. Lett., 12*, 457, 1985.

P.M. Banks, R.I. Bush, A.C. Fraser-Smith, T. Neubert, and G.D. Reeves, STAR Laboratory, Durand 202, Stanford University, Stanford CA 94305.

D.A. Gurnett, Department of Physics and Astronomy, University of Iowa, Iowa City, IA 52242.

W.J. Raitt, Center for Atmospheric and Space Science, Utah State University, Logan, UT 84322

(received May 4, 1987;
revised August 31, 1987;
accepted September 2, 1987.)

From: Proceedings of the Twelfth Space Simulation Conference "Shuttle Plus One-A View of Space," NASA Conference Publication 2229, Institute of Environmental Sciences, Pasadena, CA, May 17-19, 1982.

MEASUREMENTS BY THE PLASMA DIAGNOSTICS PACKAGE ON STS-3

Stanley D. Shawhan
Gerald B. Murphy

University of Iowa

ABSTRACT

The Plasma Diagnostics Package provides a comprehensive set of measurements about the Orbiter environment by providing information about ion and electron particle densities, energies, and spatial distribution functions; about ion mass for identification of particular molecular ion species; and about magnetic fields, electric fields and electromagnetic waves over a broad frequency range. Shuttle environmental measurements will be made both on the pallet and, by use of the Remote Manipulator System (RMS), the PDP will be maneuvered in and external to the bay area to continue environmental measurements and to carry on a joint plasma experiment with the Utah State University Fast-Pulsed Electron Generator (FPEG).

Results of Orbiter environment EMI measurements and S-band field strengths as well as preliminary results from wake search operations indicating wake boundary identifiers will be reported. An evaluation of the use of the RMS and PDP latch down and grapple mechanism will be discussed.

Comparisons of results with the FPEG experiments conducted on this flight will be made with results from a similar electron beam experiment conducted during March 1981 in the large vacuum chamber at Johnson Space Center.

THE PDP INSTRUMENT

On the OSS-1 payload, the Plasma Diagnostics Package (PDP) is a first generation set of instruments to assess the plasma environment and the plasma wake created by the Orbiter, to test the capabilities of the Remote Manipulator System (RMS) and to carry out an active beam-plasma experiment in conjunction with the Fast Pulse Electron Generator (FPEG) of the Vehicle Charging and Potential Experiment. These objectives are illustrated in Figure 1. The PDP instrumentation and measurement ranges are listed in Table 1. These measurements include electric and magnetic fields, plasma waves, energetic ions and electrons and plasma parameters--density, composition, temperature and directed velocity.

INDUCED ENVIRONMENT MEASUREMENTS

The PDP is operated both latched onto the OSS-1 pallet and attached to the RMS. On the RMS, the PDP is positioned and rotated through sets of

preplanned "automode" trajectories. As the PDP is moved in and around the Orbiter bay, measurements are made of the ambient pressure and of the spectrum of electromagnetic interference (EMI) generated by the Orbiter subsystems. These pressure profiles in time and in distance from the Orbiter are of interest for instruments sensitive to gaseous contamination and for instruments with high voltage power supplies. Upper limits to the levels of EMI expected from the Orbiter are shown in Figure 2 in comparison to the PDP receiver ranges and to the OSS-1 pallet noise. The sensitivity of wave receivers and of plasma sounders to be flown on future Spacelabs will be determined by these Orbiter EMI levels.

ORBITER WAKE

In the ionosphere, the Orbiter moves at supersonic velocity compared to the characteristic plasma (ion acoustic) sound speed. The Mach number is about 6 (2). Consequently, the Orbiter creates a plasma wake which may be identified by plasma depletion, energization of particles and the creation of Alfven waves behind the Orbiter. These processes are thought to be important as bodies move through plasmas. Evidence exists that Alfven waves behind the Jovian moon Io accelerate particles which cause the decametric radio noise bursts (3). RMS trajectories have been designed to move the PDP through the wake boundary at preferred points in the orbit. The Ion Mass Spectrometer, Retarding Potential Analyzer and AC/DC electric field probes aboard the PDP will be used to help identify characteristics of the wake depletion region, wake boundary and the shock. When the PDP flies again on the Spacelab-2 mission as a subsatellite, the wake will be examined out to 20 km behind the Orbiter (4).

PDP/VCAP JOINT ELECTRON BEAM EXPERIMENT

The active experiment of firing an electron beam into a plasma has been carried out in a number of laboratory and sounding rocket experiments (5). These experiments have made use of the electron beam to create artificial aurora, to excite plasma waves, to sound magnetic field lines for electric fields and to examine the charging, light emission and other plasma properties in the vicinity of the electron source. In planetary and astrophysical situations, it is thought that energetic particle streams lead to a variety of radio, light and x-ray emissions which is our only source of information about these distant entities. With OSS-1, the Fast Pulse Electron Generator (FPEG) of the VCAP experiment provides the electron beam; effects in the plasma are measured with the Plasma Diagnostics Package (PDP).

A perspective view of the OSS-1 beam-plasma experiment is shown in Figure 3. The FPEG fires a beam of electrons at an angle to the earth's magnetic field line determined by the Orbiter position and attitude. Attached to the RMS, the PDP is moved back and forth through the beam region to measure fields, waves, energetic particles and plasma characteristics in the beam and remote from it.

Similar experiments have been conducted in laboratory space simulation chambers (5). Under certain conditions a phenomenon called the beam-plasma discharge (BPD) occurs in which the electron beam is destroyed and the plasma column is energized to emit intense light and radio waves.

The BPD condition is a plasma instability which, when studied in vacuum chambers, is found to depend on the value of beam current and energy, ambient pressure, magnetic field strength and injection angle of the electron beam with respect to the magnetic field. BPD is characterized by a diffuse beam, with orders of magnitude higher light intensity than the electron beam in a pre-BPD configuration, as well as certain electric field and electrostatic wave modes. Particle distribution functions show electrons with a significant suprathermal tail which are believed to be the prime source of ionization.

Considerable controversy exists over whether BPD can take place in this Orbiter beam experiment and whether BPD can be significant factor in neutralizing the vehicle as it emits electrons. Since the PDP has been used in ground-based vacuum chamber studies it will be able to help answer these and other questions which are of interest to plasma studies done on the Orbiter in the future (6).

The OSS-1 PDP/VCAP experiments will investigate other interactions as well. The charge condition of the Orbiter is to be assessed through electric field and particle measurements with the PDP. Wave stimulation over a wide frequency range will be studied by pulsing the electron beam and measuring the emitted wave spectra with the PDP. The PDP will also be used as an in situ probe for natural plasma processes occurring at the Orbiter's attitude.

REFERENCES

1. Active Experiments Working Group, Solar-Terrestrial Science in Earthspace: A Strategy for Shuttle-Spacelab Missions, Essex Corporation, 1981.

2. Samir, U. and Stone, N. H., "Shuttle-Era Experiments in the Area of Plasma Flow Interactions with Bodies in Space," Acta Astronautica, 1, 1901-1141, 1980.

3. Gurnett, D. A. and Goertz, C. K., "Multiple Alfven Wave Reflections Excited by Io: Origin of the Jovian Decametric Arcs," J. Geophys. Res., 8b, A2, 717, 1981.

4. Shawhan, S. D., Burch, J. L. and Fredricks, R. W., "Subsatellite Studies of Wave, Plasma and Chemical Injections from Spacelab," AIAA Paper 82-0085, Orlando, Florida, January 1982.

5. Grandal, B. (ed.), Artificial Particle Beams Utilized in Space Plasma Physics, Plenum Press, 1982.

6. Raitt, W. J., P. M. Banks, Burch, J. L., Williamson, P. R., Baker, K. D. and Obayashi, T., "Early Experiments in Charged Particle Beams from the Space Shuttle," AIAA Paper 82-0083, Orlando, Florida, January 1982.

TABLE 1: OSS-1 PDP INSTRUMENTATION AND MEASUREMENTS

- LOW ENERGY PROTON AND ELECTRON DIFFERENTIAL ENERGY ANALYZER
  - Nonthermal electron and ion energy spectra and pitch angle distributions for particle energies between 2 eV and 50 keV
- AC MAGNETIC WAVE SEARCH COIL SENSOR
  - Magnetic fields with a frequency range of 10 Hz to 30 kHz
- TOTAL ENERGETIC ELECTRON FLUXMETER
  - Electron flux 10^9 - 10^{14} electrons/cm^2sec
- AC ELECTRIC AND ELECTROSTATIC WAVE ANALYZERS
  - Electric fields with a frequency range of 10 Hz to 1 GHz
  - S-band field strength meter
- DC ELECTROSTATIC DOUBLE PROBE WITH SPHERICAL SENSORS
  - Electric fields in one axis from 2 mV/m to 2 V/m
- DC TRIAXIAL FLUXGATE MAGNETOMETER
  - Magnetic fields from 12 milligauss to 1.5 gauss
- LANGMUIR PROBE
  - Thermal electron densities between 10^4 and 10^7 cm^{-3}
  - Density irregularities with 10 m to 10 km scale size
- RETARDING POTENTIAL ANALYZER/DIFFERENTIAL VELOCITY PROBE
  - Ion number density from 10^2 to 10^7 cm^{-3}
  - Energy distribution finction below 16 eV
  - Directed ion velocities up to 15 km/sec
- ION MASS SPECTROMETER
  - Mass ranges of 1 to 64 atomic mass units
  - Ion densities from 20 to 2 x 10^7 ions cm^{-3}
- PRESSURE GAUGE
  - Ambient pressure from 10^{-3} to 10^{-7} torr

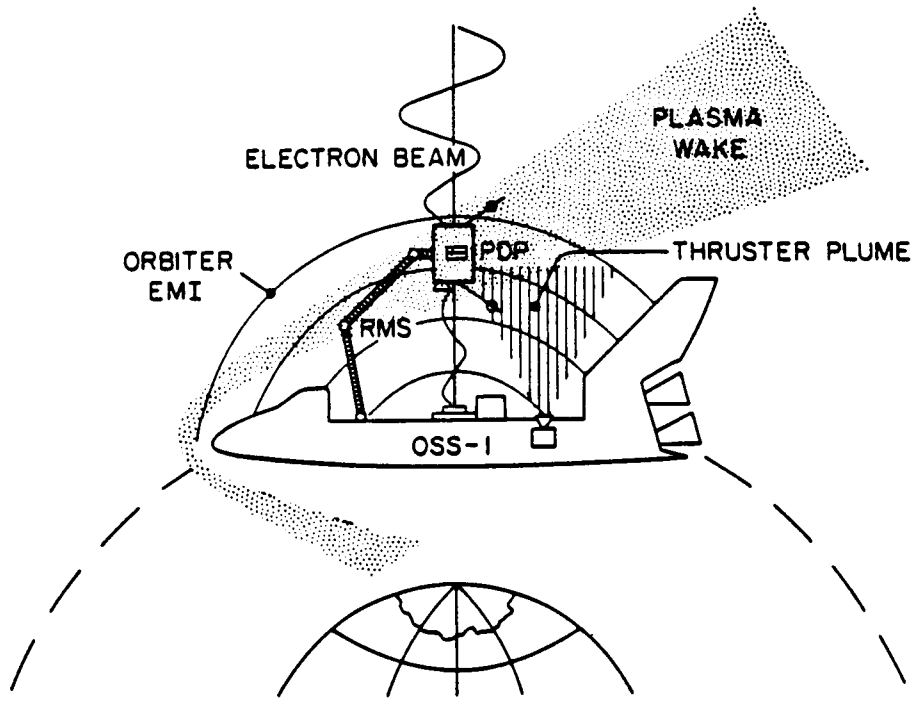

Figure 1. Illustration indicating the principal science objectives for the Plasma Diagnostics Package (PDP). The PDP contains instruments for measuring plasma fields, waves, composition, temperature and distribution functions. The Remote Manipulator System (RMS) moves the PDP about the Orbiter in pre-planned trajectories to measure electromagnetic interference (EMI) levels, the pressure profile, properties of the plasma wake formed behind the Orbiter and effects due to firing an electron beam into the plasma.

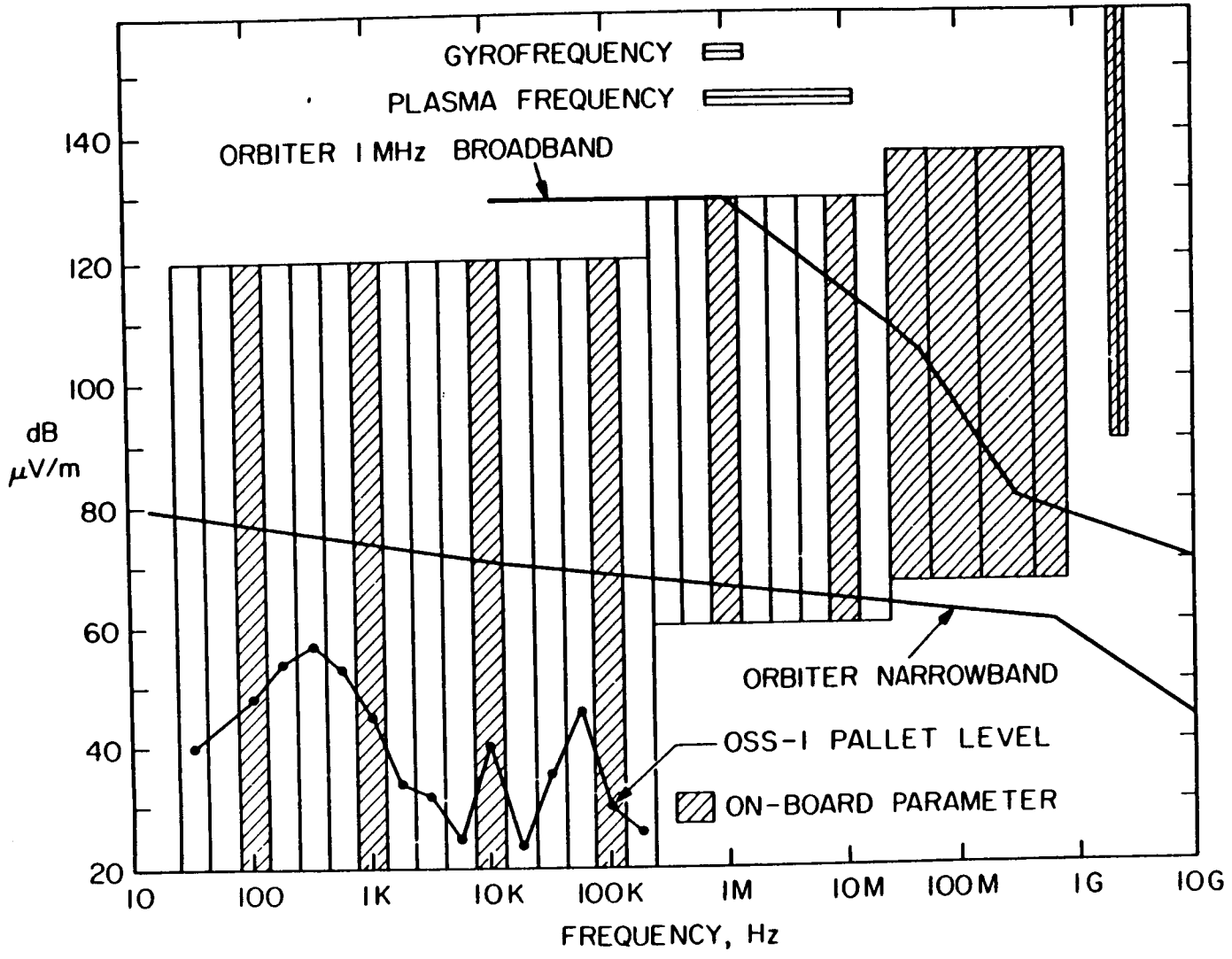

Figure 2. Plot of the expected upper limits of Orbiter electromagnetic wave emissions (EMI), the PDP wave receiver ranges and the EMI emission levels measured from the OSS-1 pallet itself. Natural and stimulated wave emissions occur at the lower levels.

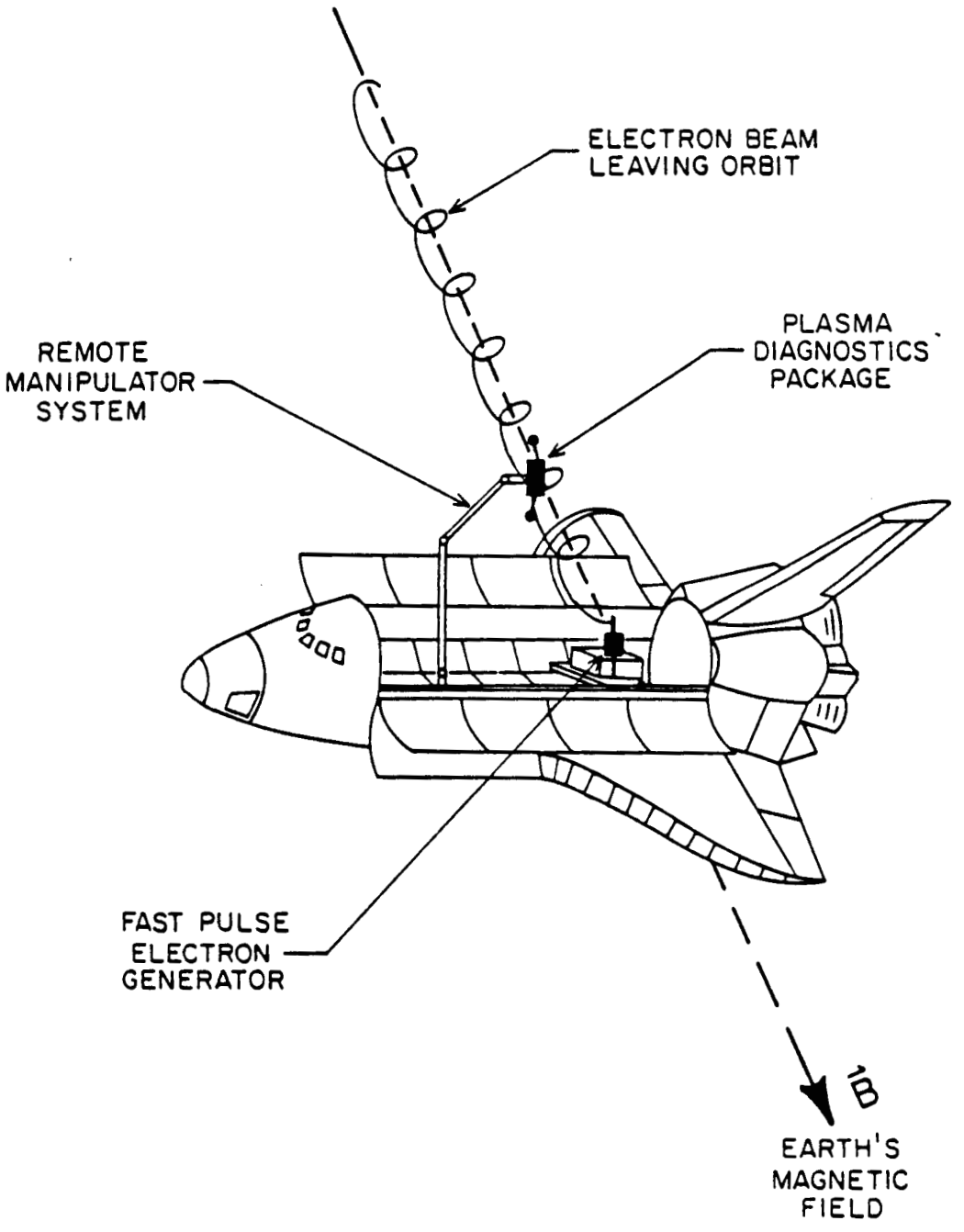

Figure 3

Scheme for the joint PDP and FPEG operations. As the electron beam is fired along some angle to the earth's magnetic field, the RMS sweeps the PDP back and forth across the beam region to make measurements of plasma fields and waves and of the energy distributions for electrons and ions.

From: Proceedings of the Air Force Geophysics Laboratory Workshop on Natural Charging of Large Space Structures in Near Earth Polar Orbit, AFGL-TR-0046, Hanscom AFB, MA, January 25, 1983.

6. STS-3/OSS-1 Plasma Diagnostics Package (PDP) Measurements of Orbiter-Generated $\underline{V} \times \underline{B}$ Potentials and Electrostatic Noise

by

S. D. Shawhan
G. B. Murphy
Department of Physics and Astronomy
The University of Iowa
Iowa City, Iowa 52242

The Plasma Diagnostics Package (PDP) was flown as part of the OSS-1 pallet on the Space Shuttle flight STS-3 in March 1982. During this eight-day mission, the PDP was operated in its pallet position and on the Remote Manipulator System (RMS). PDP measurements included dc electric and magnetic fields; ac magnetic fields to 100 kHz; ac electric fields to 800 MHz and at S-band; energetic ions and electrons from 2.5 eV to 50 keV; total electron flux; the ion mass spectrum, energy distribution, and streaming direction; the electron density and temperature, and the neutral pressure. A detailed list of the measurement parameters is shown in Table 1.

The STS-3 attitude was chosen to meet the thermal flight test objectives. It was discovered that charging characteristics and the intensity of observed electrostatic noise, both of which are discussed below, were Orbiter-attitude dependent. Figure 1 illustrates the approximate geometry of the nose-to-sun twice-orbital rate roll attitude--the condition under which the following observations were made.

Table 1. OSS-1 PDP Instrumentation and Measurements

- Low Energy Proton and Electron Differential Energy Analyzer (LEPEDEA)
  - Nonthermal electron and ion energy spectra and pitch angle distributions for particle energies between 2 eV and 50 keV
- AC Magnetic Wave Search Coil Sensor
  - Magnetic fields with a frequency range of 10 Hz to 30 kHz
- Total Energetic Electron Fluxmeter
  - Electron flux 10^9-10^{14} electrons/cm^2 sec
- AC Electric and Electrostatic Wave Analyzers
  - Electric fields with a frequency range of 10 Hz to 1 GHz
- DC Electrostatic Double Probe With Spherical Sensors
  - Electric fields in one axis from 2 mV/m to 2 V/m
- DC Triaxial Fluxgate Magnetometer
  - Magnetic fields from 12 milligauss to 1.5 gauss
- Langmuir Probe
  - Thermal electron densities between 10^4 and 10^7 cm^{-3}
  - Density irregularities with 10-m to 10-km scale size
- Retarding Potential Analyzer/Differential Velocity Probe
  - Ion number density from 10^2 to 10^7 cm^{-3}
  - Energy distribution function below 16 eV
  - Directed ion velocities up to 15 km/sec
- Ion Mass Spectrometer
  - Mass ranges of 1 to 64 atomic mass units
  - Ion densities from 20 to 2×10^7 ions cm^{-3}
- Pressure Gauge
  - Ambient pressure from 10^{-3} to 10^{-7} torr

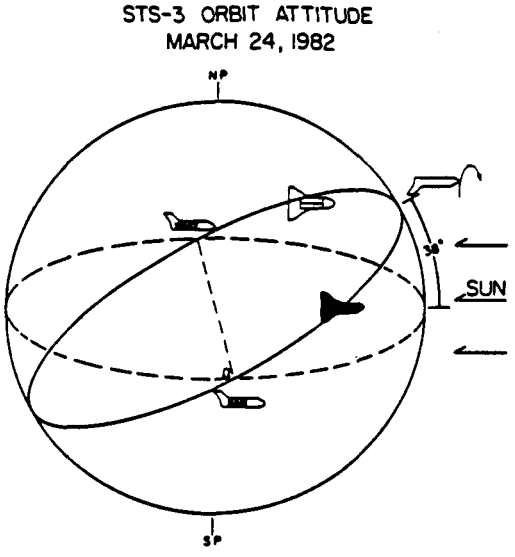

Figure 1. Approximate Geometry of the Nose-to-Sun Roll Attitude

The PDP measured the common-mode potential between two spherical probes mounted on 0.5-m booms and Orbiter ground. This potential difference is consistent with the motional potential $\underline{V} \times \underline{B} \cdot \underline{L}$, where $\underline{L}$ is the distance between the Orbiter conducting engine fairings and the PDP on the pallet or on the RMS. On STS-3, the most positive potential was ~ 4 V near sunset with the PDP in the velocity wake direction; the most negative potential was ~ 3 V near sunrise with the PDP in the velocity ram direction. Figure 2 shows a comparison between this measured potential and a crude $\underline{V} \times \underline{B} \cdot \underline{L}$ model as described in the caption. Firing the 1 kV 100 mA electron gun*, significantly enhances spacecraft positive potential to levels beyond the instrumentation range (> 8V). Preliminary indications are that thruster firings also enhance the Orbiter potential.

Additional measurements indicate, however, that at a time when the PDP electric field sensors may indicate fairly low $\underline{V} \times \underline{B} \cdot \underline{L}$ potentials (close to zero V), the PDP electron energy analyzer indicates a significant flux of 10 to 30 eV electrons. These energized electrons are also orbit-periodic and seem to depend on the Orbiter's attitude. These particle detectors may be the only way of accurately measuring the potential of the Orbiter and its sheath with respect to the ambient plasma.

*The FPEG was designed and built by Dr. John Raitt of Utah State University and Dr. Peter Banks of Stanford University.

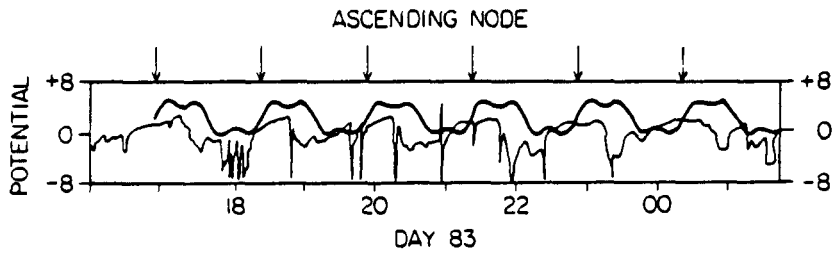

Figure 2. Potential as Measured by the PDP (light line) vs V × B · L Model (heavy line). B is modeled as a simple dipole; V is modeled from the Figure 1 orbit geometry and L is the vector from the SME fairings to the PDP. The model is offset upward by 2 V for easier comparison. Note relative amplitude and periodicity agree well but detailed structure does not. The large excursions in the data can always be associated with FPEG operation or thruster firings

Ac electric fields from 30 Hz to 178 kHz are also observed and vary by ~ 70 dB over an orbit with field strengths up to 0.1 V/m at the spectral peak of ~ 0.3 kHz with the PDP in the velocity ram direction. Figure 3 shows the relevant geometry and samples of the data. At thruster firing periods, the higher frequencies in the 10^3 to 10^5 kHz range are significantly attentuated, whereas the 10^1 to 10^3 range is enhanced; when the payload bay doors were closed, the electric field noise was attentuated to receiver noise levels at all frequencies. It is thought that this electrostatic noise is generated in the Orbiter wake at frequencies near the ion plasma frequency (~ 50 kHz) and below in the ion acoustic mode. The highest frequencies ~ 200 kHz are Doppler-shifted short wavelengths (~ 0.1 m); the lowest frequencies are probably characteristic of several thermal ion Larmor radii (~ tens of meters). In the ram direction, all frequencies can reach the PDP. In the wake orientation, the high frequencies may be attenuated across the wake region so that only the longer wavelength lower frequencies are detected. With thruster firings, the ion density may be significantly lower, which lowers the ion plasma frequency and thus lowers the upper Doppler-shifted frequency. This electrostatic noise generation may cause significant drag on large space structures.

Work in progress includes a detailed look at correlation between short-term potential variations and thruster firings, evaluation of more data from the particle analyzer and correlation of results with the FPEG/VCAP experiment. The PDP will fly again on Spacelab-2 (November 1984 launch) and a number of experiments are being designed to investigate further the phenomena discovered on this mission.

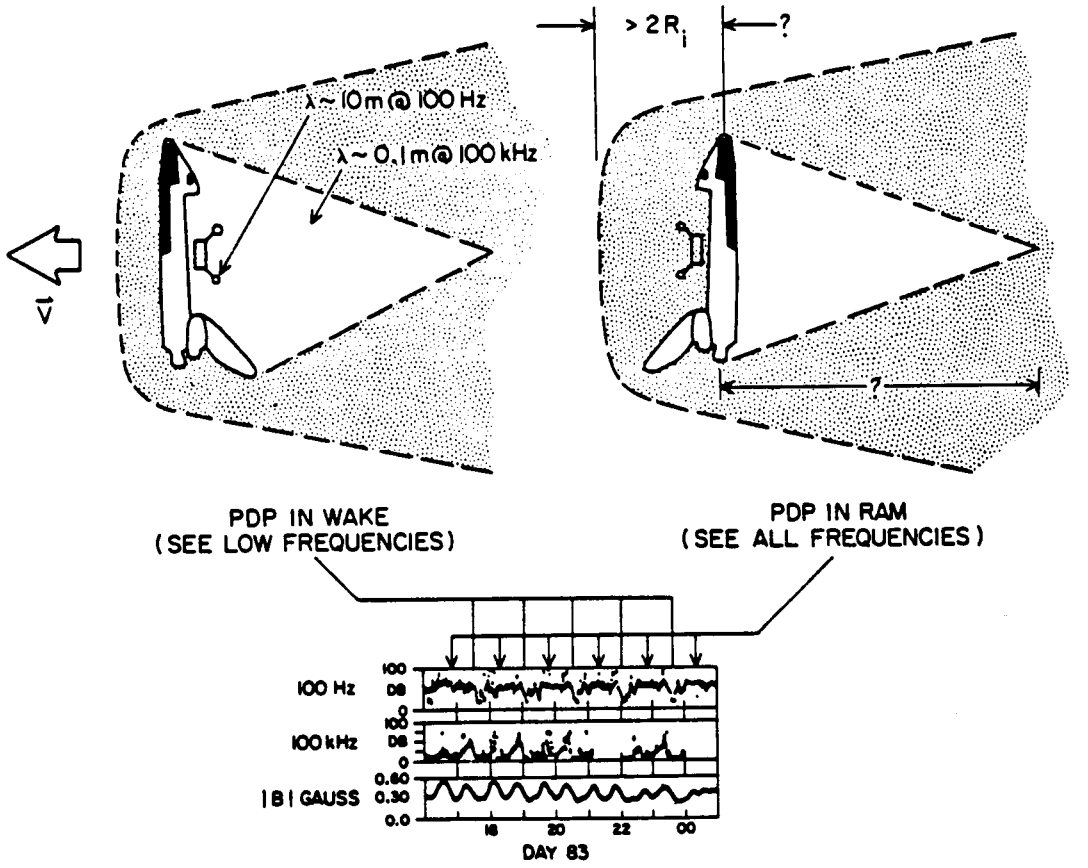

Figure 3. Relevant Plasma Diagnostics Package Geometry and Samples of Data

Acknowledgment

This work was performed under NASA contract with Marshall Space Flight Center NAS8-32807.

STS-3/OSS-1 PLASMA DIAGNOSTICS PACKAGE (PDP) MEASUREMENTS OF THE TEMPERATURE PRESSURE, AND PLASMA

S. D. Shawhan and G. Murphy
University of Iowa

From: Proceedings of the Shuttle Environment Workshop,
NASA Office of Space Science and Applications,
Calverton, MD, Oct. 5-9, 1982.

STS-3/OSS-1

PLASMA DIAGNOSTICS PACKAGE (PDP)
90-DAY SUMMARY SCIENCE REPORT

by

Stanley D. Shawhan
PDP Principal Investigator

and

Gerald B. Murphy
PDP Data Processing Manager

Contributors:

Roger D. Anderson
Roger R. Anderson
Terry Averkamp
Bob Brechwald
Henry Brinton/NASA-HQ
Tim Clark
Terry Clausen
Ann Dresselhaus
Don Enemark
Dwight Fortna/GSFC
Lou Frank
Joe Grebowsky/GSFC
Don Gurnett
Marty Karl
Rich Kroeger
Maja Lorkovic
Kerry Neal
Harry Owens
Merritt Pharo/GSFC
Dave Reasoner/MSFC
Joel Score
Nobie Stone/MSFC
Harry Taylor/GSFC
Lisa Vodra
Ev Williams

Contract NAS8-32807

Marshall Space Flight Center, Huntsville, Alabama 35812

July 1982

Department of Physics and Astronomy
The University of Iowa
Iowa City, Iowa 52242
319/353-3294

1.0 INTRODUCTION

This 90-day summary science report for the STS-3/OSS-1 PDP is submitted as required by the "OSS-1/Plasma Diagnostics Package Data Management Plan" dated January 1982 (Report OSS-1/PDP 82-01, University of Iowa) in accordance with the letter from A. Martin Eiband, dated 22 December 1982, Code 420, GSFC File 03496 "OSS-1, Phase III, Data Analysis." Mission operations and data analysis is supported through Marshall Space Flight Center Contract NAS8-32807 for the OSS-1 and Spacelab-2 PDP effort.

Data utilized for this report has included hard copy data from the POCC, PDP data received directly at the North Liberty (Iowa) Radio Observatory, processed flight data tapes (57 hours), and PDP data from the OSS-1/IUE data tapes (116 hours). In addition, ancillary data on the RMS coordinates in hard copy form has been utilized. Ancillary data not yet available include the best-estimate-trajectory and attitude, the operations status of key orbiter subsystems such as thrusters and flash evaporators, and the catalog of VCAP/FPEG operations. Of the PDP flight data, 28 hours have been displayed in ten minute summary plot format on 35mm color slides. All of the IUE data (16 selectable parameters) has been plotted against time at 30 minutes per plot.

For the STS-3/OSS-1 mission, the PDP was to carry out the following technical and scientific objectives:

1.1 Flight Test of Systems and Procedures

Flight test the systems and procedures and associated with the Spacelab-2 PDP experiment with particular emphasis on the RMS operations, on unlatching and relatching the PDP unit, and on evaluating the RF telemetry link.

1.2 Orbiter EMI and Plasma Contamination

Measure and locate the sources of fields, Electromagnetic Interference (EMI) and plasma contamination in the environment of the Orbiter out to 15 meters.

1.3 Orbiter Wakes and Shocks

Study the orbiter-magnetoplasma interactions within 15 meters of the orbiter through measurement of electric and magnetic fields, ionized particle wakes and generated waves.

1.4 Electron Gun Beam Diagnostics and Plasma Effects

Ascertain the characteristics of the electron beam emitted from the orbiter out to a range of 15 meters; measure the results of beam-plasma interactions in terms of fields, waves and particle distribution functions.

The technical objective 1.1 was discussed in the "STS-3/OSS-1 Plasma Diagnostics Package (PDP) 30-Day Engineering Report", dated 30 April 1982. Progress-to-date on the thermal and pressure environment of the PDP and on the science objectives 1.2, 1.3 and 1.4 is presented in this report in Sections 2.0 through 6.0 and is summarized in Section 7.0. In Section 8.0, the plan for continued data analysis is briefly described.

2.0 THERMAL AND PRESSURE HISTORY

With the availability of the complete PDP flight tape recorded data and the OSS-1/IUE PDP data parameters, it has been possible to extract the PDP thermal and pressure history.

2.1 PDP Thermal History

The PDP was designed to withstand the thermal extremes of the STS-3 mission through the use of heaters and of thermal blankets. The PDP sat on the Release/Engagement Mechanism (REM) on the OSS-1 pallet without a coldplate and was attached to the RMS for two extended periods.

Figure 2.1 gives a plot of temperature vs. mission elapsed time MET for two temperative sensors. The solid curve labeled "PDP" is a thermistor internal to the PDP on the instrument deck. This point is seen to reach a minimum of -25°C after the extensive tail-to sun cold period near MET 1/0900. At this point, the PDP deck heater was activated and holding the -25°C setpoint. This same sensor showed a maximum of 52°C near MET 6/1000 at the end of the extensive hot top-to-sun period; model calculations predicted 50°C. Note that during the PDP deployment periods early on MET Day 3 and Day 4, the PDP warmed up slowly to -5°C.

The dotted curve in Figure 2.1 labeled "EGF" is a thermistor on the electrical grapple fixture connector which is external to the PDP. This point has a very much shorter thermal time constant. Variations are more rapid with a minimum of -35°C at MET 1/0600 and a maximum of 56°C near MET 6/0400. Still this point remains between the heater trip point of -32°C and a desired upper limit of 60°C. Consequently, the PDP thermal design is considered suitable for Spacelab-2. Similar designs should work for other spacelab pallet-mounted instruments without coldplates.

2.2 Pressure Profile

Pressure in the range of 10^{-3} to 10^{-7} torr, measured 3 inches from the skin of the PDP, is plotted in Figure 2.2 against GMT during the mission (0/0000 MET = 81/1600 GMT). Just after pallet activation, the pressure decreased to ~ 10^{-6} torr and then slowly decreased over the day to as low as 10^{-7} torr which is near ambient level for 240 km altitude.

The most distinctive feature of the pressure profile is the modulation at the orbit period. This variation of between 10^{-5} torr and 10^{-7} torr has a 90 minute orbit period even though the Orbiter is

rolling at two-times the orbit rate (2 rolls/orbit). From interpretation of the attitude information, it is found that the pressure peaks when the atmospheric gas is rammed into the payload bay; the curve in Figure 2.2 can be fit with a log-sine function. This modulation is seen also when the PDP is on the RMS during the FPEG operations periods. Note that on GMT Day 81 near 2200, there is a 6x orbit rate modulation when the Orbiter was rolling at 6x orbit rate during PTC.

Ancillary data giving the status of Orbiter systems that might affect the pressure are not completely available. However, the primary thrustor L2U burn at GMT 85/1430, increases the pressure to 3×10^{-4} torr. During the three minutes of closed payload bay doors, the pressure increased to 3×10^{-5} torr. Little data were taken during the top-to-sun attitude but pressure values as high as 2×10^{-5} were recorded--presumably due to increased outgassing of the Orbiter bay.

Instruments sensitive to pressure variations or to pressure levels above 10^{-4} torr--in the corona region if high voltages are involved--may need a pressure sensor to provide protection.

Figure 2-1

PDP THERMAL HISTORY STS-3 MARCH, 1982

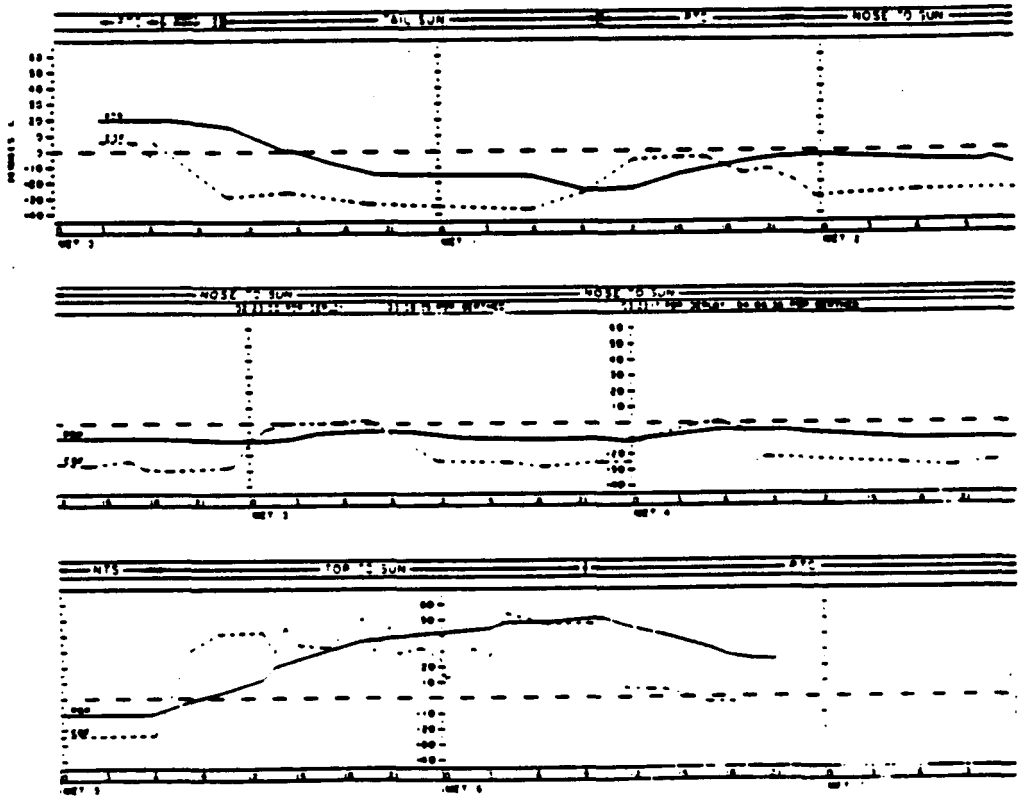

Figure 2-2

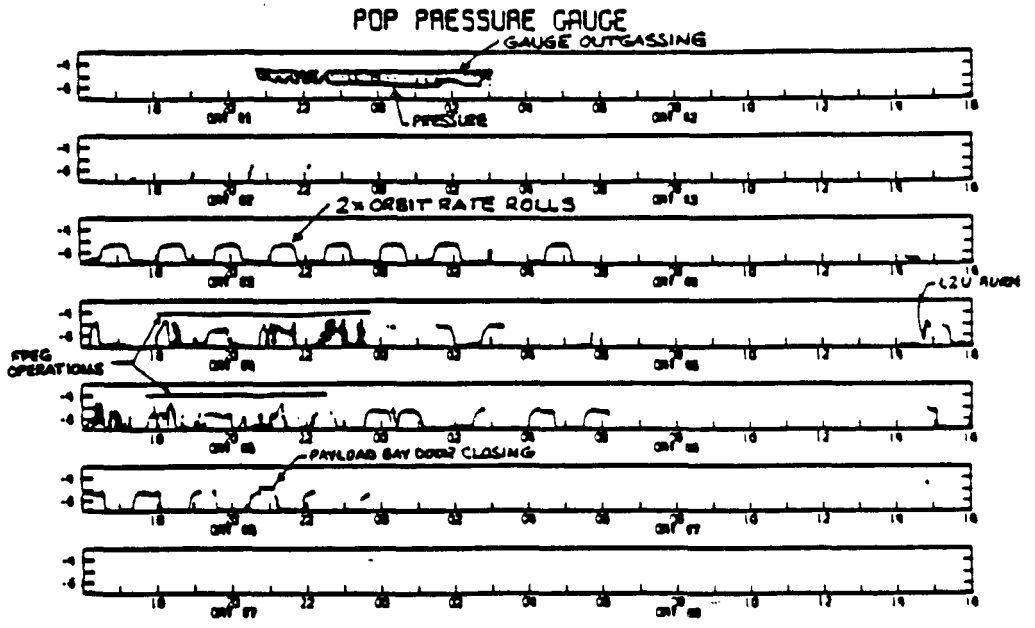

3.0 ORBITER RADIATED ELECTROMAGNETIC FIELDS

An extensive set of wave field receivers covering the frequency range of 30 Hz to 800 MHz and S-Band (2200 MHz) was included on the PDP. These receivers provided a capability to characterize the Orbiter's unitentional radiated spectrum and its time variability and intentional communication transmitter's field strength.

3.1 Pallet EMI Levels and Time Variations

One of the prime PDP measurements was to determine the electric and magnetic noise spectrum and time variability due to the Orbiter systems. It was found that the magnetic field was composed of discrete frequencies and harmonics. These emissions are probably due to power converters and clocklines. The characteristic amplitude of 60 dBpT ± 20dB did not vary significantly over the mission.

Measurements of the electric field emissions showed a broadband spectrum which varied by at least 60 dB over time. An example of the time variability is shown in Figure 3.1 for the 16 VLF channels. Note that changes occur on the time scale of seconds—probably due to thruster firings. Also there is a large variation on the time scale of tens of minutes which is found to be correlated with the Orbiter orbit period. The intensity is usually maximum when the Orbiter is in a ram attitude—bay in the velocity vector direction. This modulation is similar to that of the pressure gauge.

The range of observed electric field levels is plotted in Figure 3.2. Orbiter-associated noise was as low as the receiver noise levels. At frequencies above 300 kHz, the receivers were not sensitive enough to detect the noise at all. When the FPEG was operated, the fields exceeded the Orbiter-induced noise at all frequencies.

In general, it is found that the Orbiter unitensional emissions are at the spec level or below and that the electric field noise is not due to Orbiter subsystems, but rather to the Orbiter's interaction with the plasma in the ionosphere. Work is continuing on this investigation.

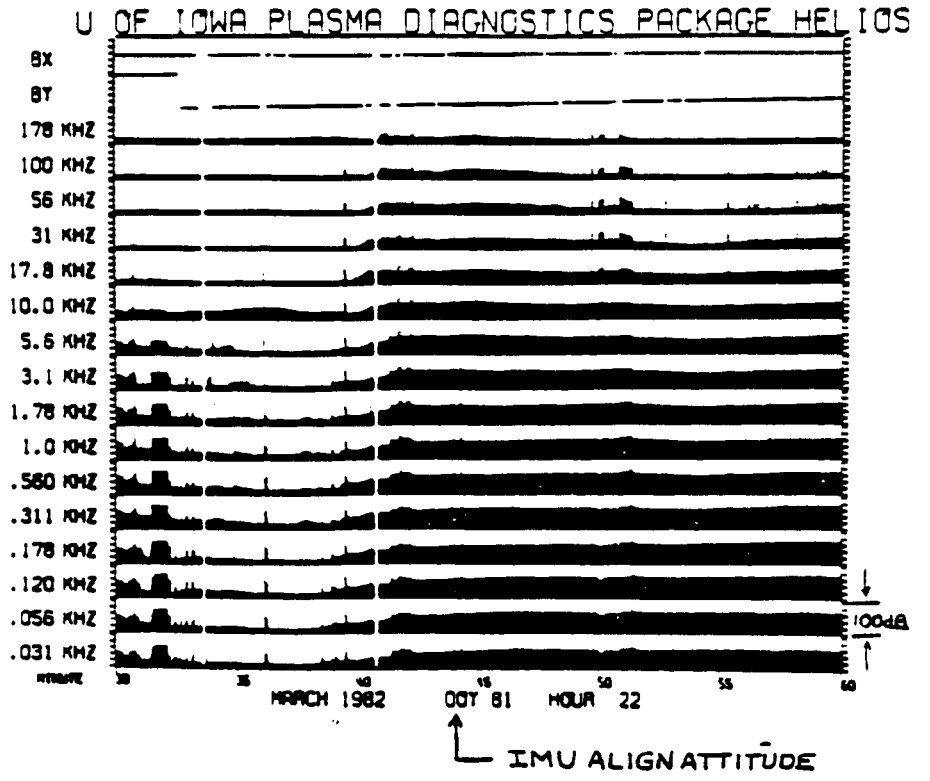

NOISE TIME VARIABILITY WITH THRUSTERS BUT NO FPEG

Figure 3-1

3.2 UHF and S-Band Transmitter Field Strengths

One filter channel of the PDP High Frequency Receiver covered the band of 165-400 MHz which includes the 295 MHz frequency of the UHF voice downlink transmitter. When this transmitter was keyed on and connected to the upper antenna, a signal was detected by the PDP. These measured field strengths were always below 0.5 V/m with the PDP on the RMS and below 0.1 V/m at the PDP pallet location. Average and peak field strengths are given in the following table:

Location/Field Strengths ± 2dB	Average	Peak
PDP on Pallet at 13 meters from Antenna	.05 V/m	0.08 V/m
PDP on RMS at 8 meters from Antenna	.23	.44

These levels are well below the suggested radiated susceptibility field strengths.

At S-Band, the 150 watt data downlink transmitter (2287.5 MHz) can produce fields which are modeled to be 49.6 V/m/R (meters) in the beam of the selected "quad" antenna. Even at many meters, these fields could be at damage level for payload instruments or for satellites being manipulated by the RMS. The PDP carried a receiver especially designed to measure the field strengths in and around the payload bay. These measured levels were about 5 dB ± 2 dB higher than the modeled values but comparable to a crude theoretically calculated value as follows:

	Field Strength Relation (V/m)
Modeled @ 150 Watts	49.6 /R (meters)
Measured with PDP (± 2dB)	90.3 /R (meters)
Calculated @ 150 Watts	94.9 /R (meters)

The calculated value assumes that all of the power is emitted into a hemisphere with 100% efficiency.

In the antenna beam, the fields exceed 20 V/m inside of 5 meters. However, with the PDP on the pallet at a range of 13 meters off the edge of the beam, the fields were not observed at the threshold of 2 V/m whereas the in-beam prediction would be 7V/m. Consequently, payload bay instrumentation is not subjected to damage levels.

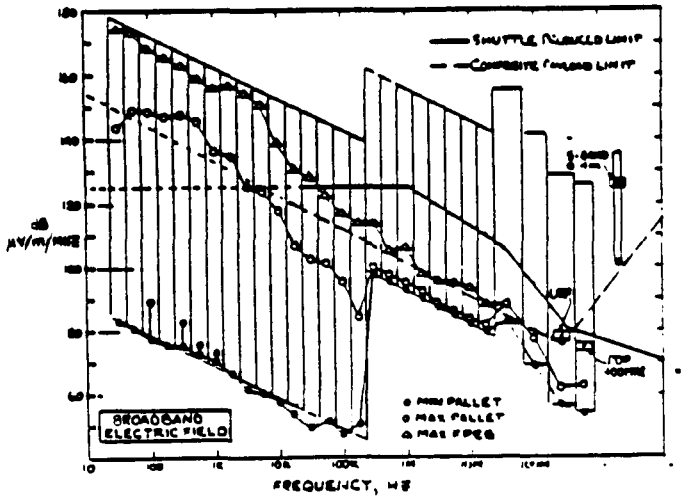

Figure 3-2

4.0 ORBITER ION PLASMA ENVIRONMENT

(Henry C. Brinton, Joseph M. Grebowsky, Merritt W. Pharo III, Harry A. Taylor, Jr./GSFC)

The Bennett RF Ion Mass Spectrometer on the STS-3/OSS-1 Plasma Diagnostics Package (PDP) performed nominally throughout the mission. Measurements of ion spectra were obtained both in the cargo bay and during experiment periods in which the PDP was operated on the extended Remote Manipulator System (RMS) arm. Real time data obtained from several orbit passes over the North Liberty (Iowa) Radio Observatory ground station and playback data obtained while the PDP was operated on the extended RMS arm have been examined. Ion currents observed covered the entire dynamic range (2×10^5) of the ion mass spectrometer system demonstrated response to the extremes of ambient and perturbed plasma conditions. Data tapes provided were of sufficient quality to enable use of the GSFC developed software on the DEC 11/70 computer for initial data reduction activities.

Initial data processing was concerned with positively identifying the atomic mass numbers of the detected ion species. As anticipated, the effects of electrical charge buildup and/or the plasma ram velocity altered the calibrated direct relationship between the atomic mass number of an ion and the applied spectrometer voltage required for its detection. The net of such effects upon the spectrometer range from -3 to -8 volts on the various data samples studied. A detailed examination of a number of individual mass scans was therefore undertaken which considered apparent potential shifts in the fundamental current peaks due to spacecraft charging as well as the shifts in the locations of the harmonic derivatives of the fundamental peaks. This analysis provided a scheme for identifying the atomic mass number of the detectable ions. A more complete analysis will be made once the orbit-attitude data are available.

Since detailed event timeline and aspect information for determining the orientation of the spectrometer orifice with respect to the plasma flow, are not yet available, it was not possible to determine the exact magnitude of the ion concentrations sampled, nor to interpret the source of strong fluctuations. However, the collected ion currents provide the basis for a rough estimate of the relative abundance of each ions species, and of course, the variations of the ion currents with time reflect similar variations in the concentrations. Hence the preliminary evaluation of the data considered the ion currents only while one of the immediate future goals will be to convert these currents to concentrations.

Some examples of the ion currents collected during the flight of STS-3/OSS-1 are shown in Figures. Three distinctive phases of the PDP operations are depicted. Figure 4.1 corresponds to early measurements when the PDP was still in the shuttle bay while Figures 4.2 and 4.3 show measurements made on the extended RMS arm. In the event shown in Figure 4.3, the electron beam created abrupt disturbance of all the ion currents. As these figures show, the most dominant ion species observed correspond to atomic mass numbers of 16, 18, 30, and 32. The existence

of mass numbers 16, 30 and 32 were expected since the shuttle is operating at F-region altitudes where there are substantial ambient plasma O^+ (16 amu), and NO^+ (30 amu) and O_2^+ (32 amu) plasma densities. The existence of mass 18, assumed to correspond to H_2O^+ ions, demonstrates that the shuttle not only dynamically perturbs the ambient plasma as it moves through it, but apparently has its own inherent atmosphere environment to interact with the ambient medium.

Further analysis of the ion spectrometer measurements will proceed, given operations and aspect data. From a merging of the orbit and attitude data with the ion measurements, it is expected that geophysical variations in the ion concentrations may be separated from shuttle induced perturbations - for example - the noticeable decreases in current seen in Figures 1 and 2 may be of either source. A further study will be made of the identification of ambient and contaminant ions and of composition changes due to electron gun and thruster firings.

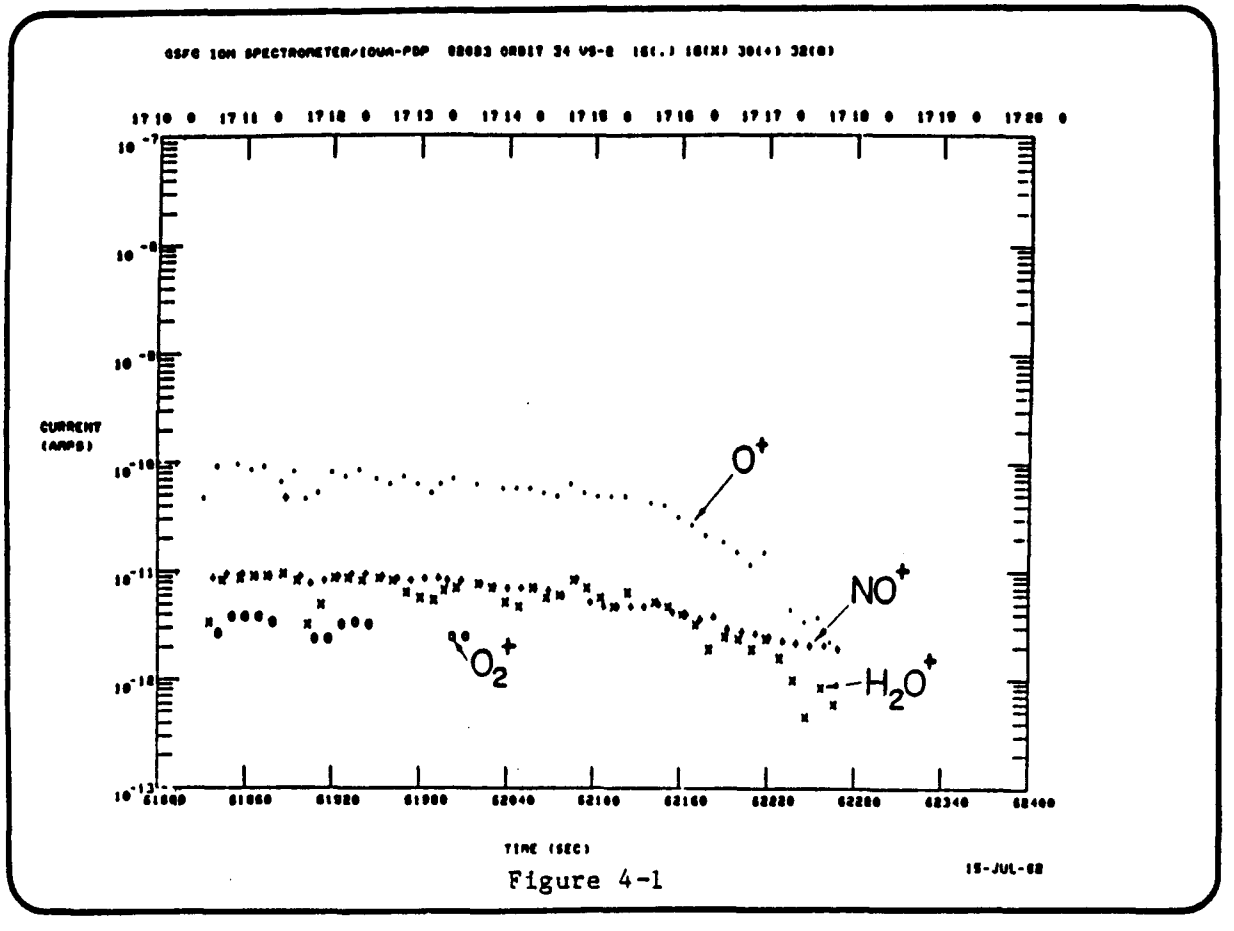

Figure 4-1

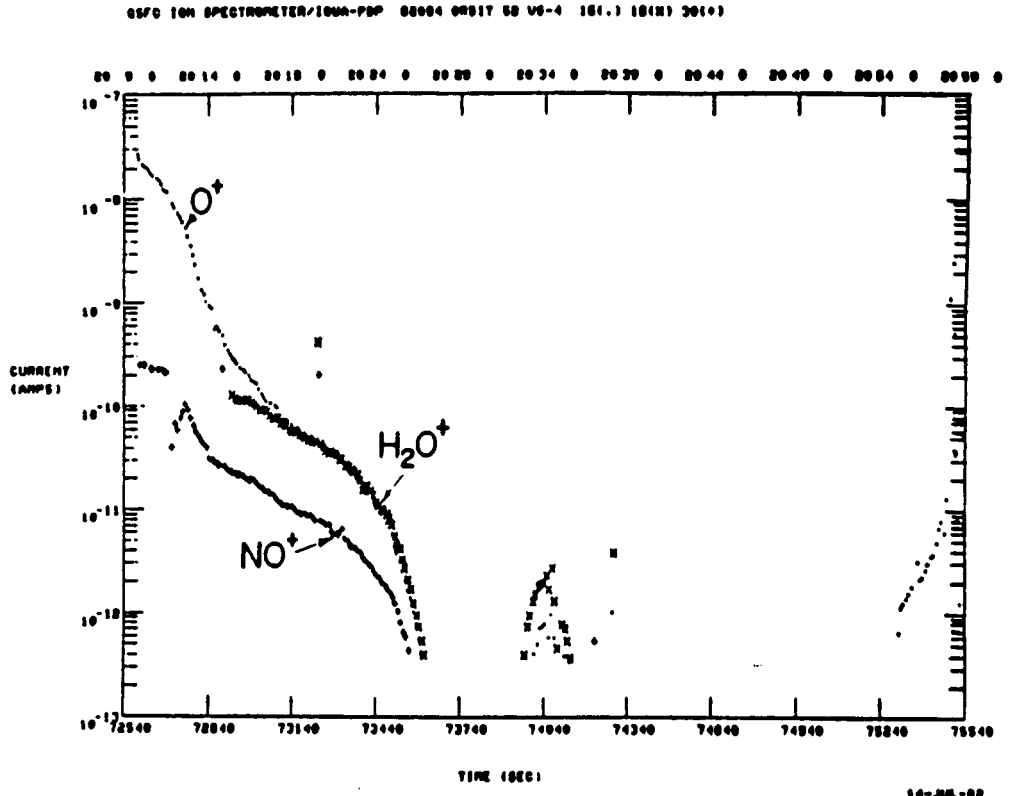

Figure 4-2

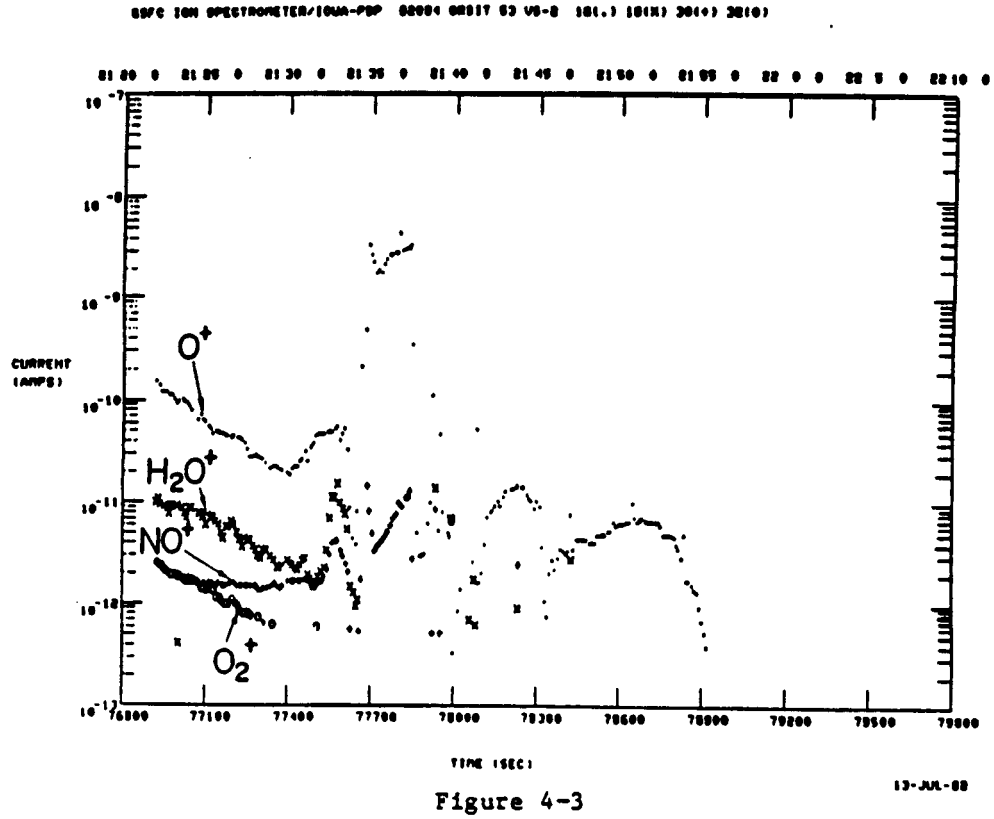

Figure 4-3

5.0 ORBITER-INDUCED PLASMA WAKE
(Nobie H. Stone and David L. Reasoner/MSFC)

The RPA/DIFP instrument is designed to provide the total ion current density, energy and temperature (RPA) and the ion flow direction (even for multiple streams) and the associated current density, drift energy and temperature of each stream (DIFP).

Figure 5.1 is a color survey plot which includes the RPA/DIFP data showing; (1) an attitude change of the PDP with respect to the orbital velocity vector and (2), two distinct ion streams; i.e., the intense ram ion stream which flows parallel to the velocity vector (lower crescent) and a fainter stream inclined upward at 45° -50° above the orbital velocity vector (upper crescent) in the time interval of GMT 85/1648-1652.

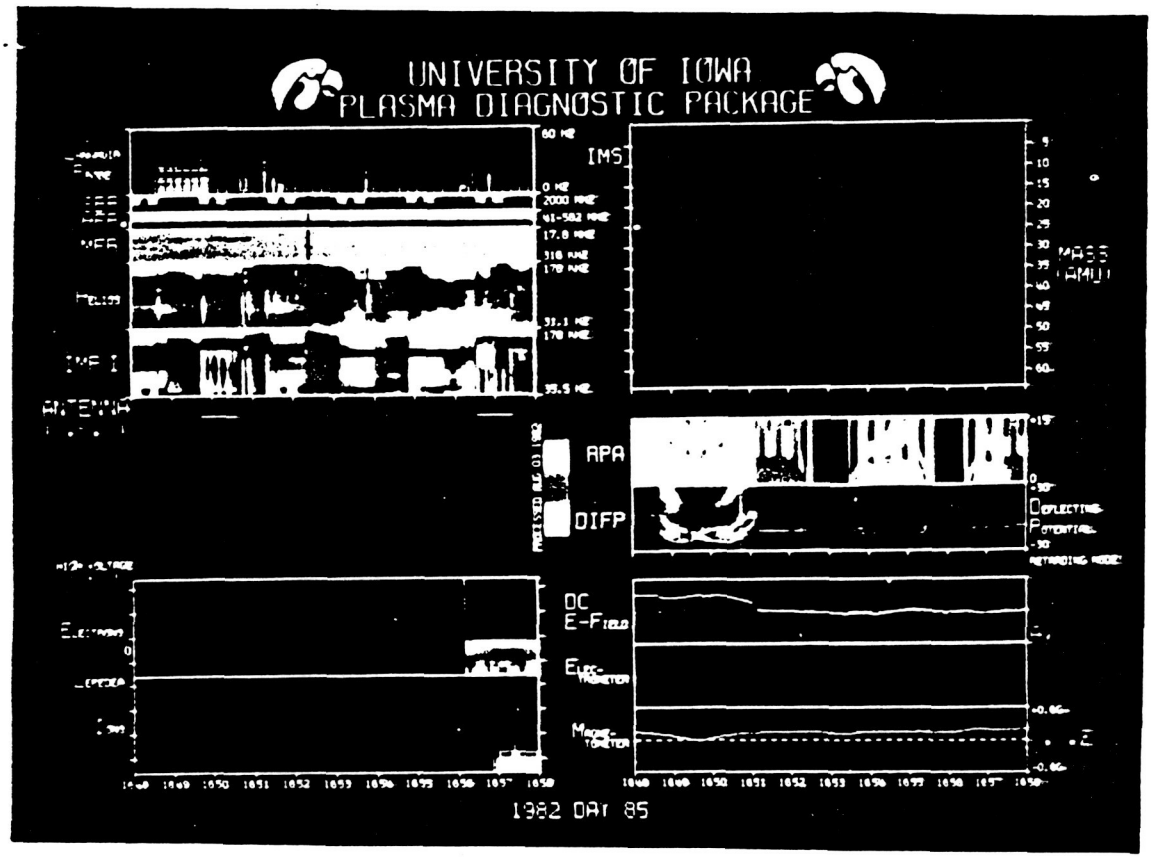

Figure 5-1

Figure 5.2 shows, schematically, the orientation of the Orbiter with respect to the velocity vector, V_o, during the period in which the data were obtained. As the PDP was moved through the indicated path, its orientation changed, as indicated, at points 1, 2 and 3. It is the change in orientation of the PDP along the path that produces the crescent effect in the spectrogram. At point 1, the RPA/DIFP looked directly into the ram direction. It became perpendicular to the flow at point 2, but looked into the ram again at point 3. The deflection voltage on the DIFP, which is proportional to angle of attack, follows this maneuver precisely, being near zero when the PDP was at points 1 and 3 and highly negative at point 2.

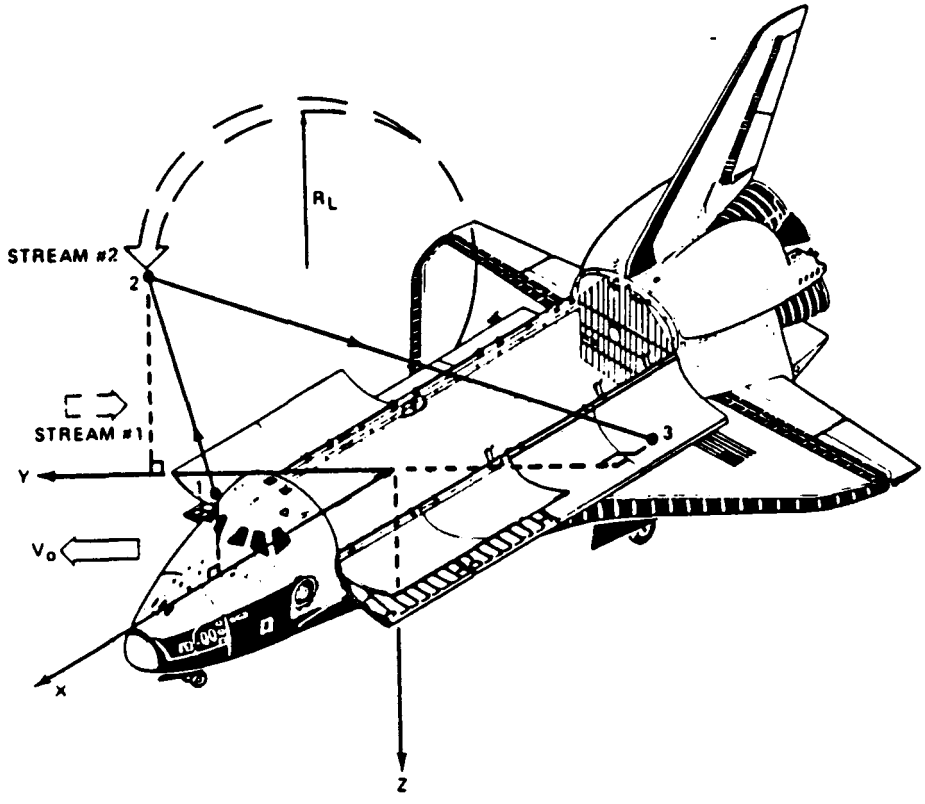

SHUTTLE ORIENTATION & PDP TRACK
Figure 5-2

A plot of the DIFP current as a function of deflection voltage during one sweep, made at time 16:49:01.7, is given in Figure 5.3 and shows two distinct peaks. These peaks arrive at -16 and +26°. We assume that the PDP was inclined upward at 16° and that Peak No. 1 represents the ram current. The second ion stream, therefore, arrived at an angle of 42° to the velocity vector. This stream appears to result from ions that were accelerated by the interaction with the Orbiter and have reached the RPA/DIFP by traveling over an arc of a Larmor radius as indicated in Figure 4.3.

The streams were analyzed by a retarding potential and both have an energy of ~ 10 ev. (The RPA indicates an energy of 9 ev when most closely aligned with the velocity vector. The difference in energy may be due to the remaining angle of attack). Since the ram energy of O^+ is 5 ev, the observed energies suggest a potential -4 to -5 volts on the PDP. In fact, the average potential of the spheres with respect to the PDP is given by the yellow "AV" curve in the "DC E-Field" panel as +6 volts during the ion beam. This value means that the PDP was -6 volts with respect to the plasma in agreement with the RPA analysis.

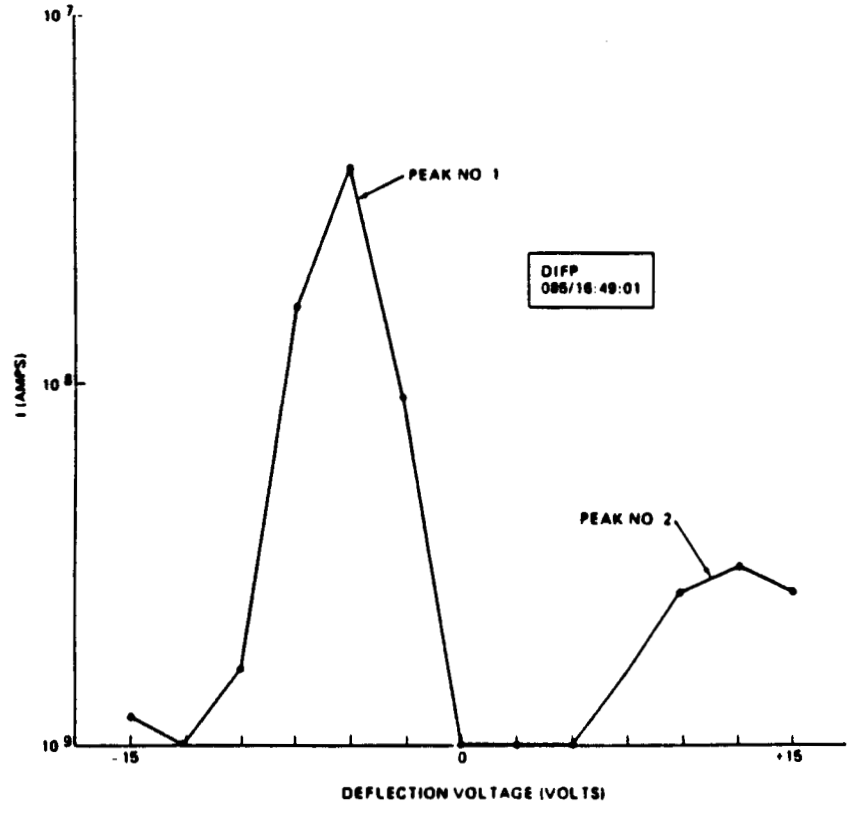

Figure 5-3

6.0 ELECTRON BEAM--PLASMA INTERACTIONS

Work on the FPEG beam and its interaction with the plasma has not progressed significantly. To effectively carry out this investigation, certain ancillary data are required. These required data and the status are listed below:

RMS Coordinates	Provided by JSC as Printout
Orbiter-Attitude Timeline	State Vectors Available on Paper; Awaiting BET Tape
Orbiter Magnetic Alignments	Requires Orbiter-Attitude Timeline
FPEG Firing Catalog	Just Received from Utah State

Consequently, the major holdup is the Orbiter-attitude data. Once this information is received and interpreted, the separate data sets can be collated into a common timeline.

Addition VCAP/PDP Joint Beam Search data have processed into survey plots. An example is given in Figure 6.1 for 1982 Day 85 at 1750 GMT. During this period, the PDP on the RMS being maneuvered to search for the FPEG beam. Electrons are observed up to 1 keV in energy; low fluxes of ions are observed up to 250 eV. VLF emissions peak in the 0.5 -2 kHz range. Emission in the several MHz range are probably associated with the gyrofrequency (~ MHz) and the plasma frequency (~ 10 MHz). Electric fields in excess of 10V/m and the PDP potential of greater than + 12V with respect to the plasma are also encountered.

Many of the beam-plasma characteristics observed on-orbit were also observed in the JSC Plasma Chamber Tests of March 1981. In parallel, the Chamber Test data are being processed through the same analysis and display programs so that detailed comparisons can be made.

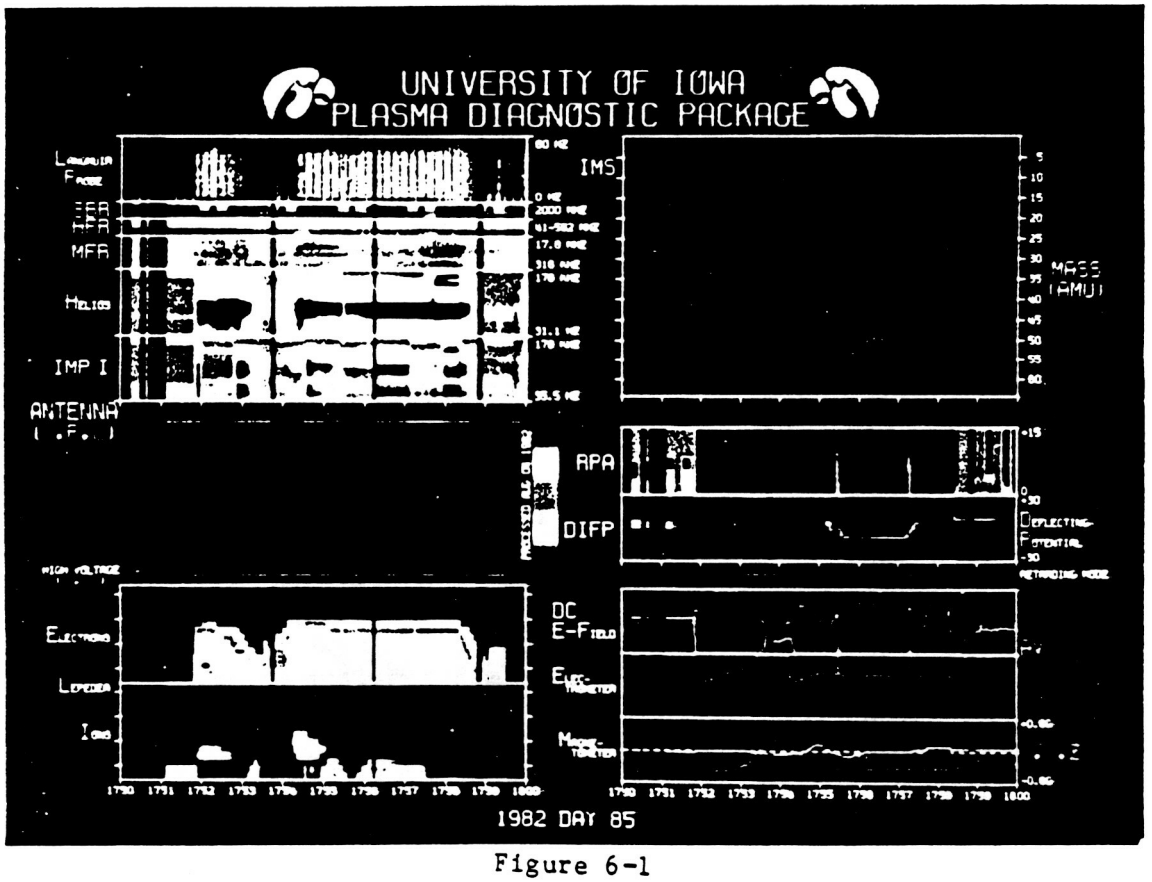

Figure 6-1

7.0 SUMMARY OF PDP

An overall summary of the environmental and science results to date is as follows:

- Orbiter related EMI levels are signficantly low so that natural noise phenomena, FPEG stimulated waves and Orbiter-induced wake noise are detectable
  - With the bay doors closed, the PDP-detected noise levels dropped to the receiver threshold values for frequencies from 30 Hz to 800 MHz except for magnetic field discrete line emissions at 25 Hz, 1 kHz, 25 kHz and harmonics
  - Field strength measurements of the S-Band communication system are approximately a factor of two higher than the modeled values
  - Stimulated FPEG waves in the Hz to MHz ranges were clearly detectable
  - Natural noise emissions including spherics, whistlers, chorus and hiss were detected above the background noise levels
  - Based on the observed decrease of EMI noise levels with the bay doors closed and on the amplitude variation of the noise depending on Orbiter attitude, it is hypothesized that a broad spectrum of electrostatic noise is being generated by the Orbiter's motion in the plasma--probably in the wake. This noise is a maximum with the bay in the ram direction
  - Due to natural charging effects, the Orbiter can reach a few volts potential with respect to the plasma
  - Orbiter-caused magnetic field perturbations are typically less than .05 gauss

- The presence of the Orbiter and the Orbiter gaseous environment produces a plasma environment in and near the plasma bay which is significantly different than the ambient ionospheric plasma
  - Plasma density and temperature at the PDP pallet location can vary by at least 3 orders of magnitude in the time scale of minutes and by a larger factor depending on the Orbiter attitude
  - Time variations in pressure of about two orders of magnitude are observed with some correlation to Orbiter RAM/wake attitude and thruster operations; on the scale of minutes, the pressure reaches 10^{-5} torr with the bay in the ram direction whereas the pressure exceeded 10^{-4} for a PRCS jet operation.
  - Dominant ions include O^+, N_2^+ and O_2^+ from the ambient ionosphere and H_2O^+ from the Orbiter itself.
  - Measured plasma energy depends on PDP charging which is controlled by day/night and RAM/wake effects

- On the RMS, directed ion streams are detected which are probably due to refilling of the Orbiter wake cavity. Modulation of the energy is associated with the charge state of the PDP

- The FPEG electron beam undergoes a strong interaction with the ambient ionospheric plasma and perhaps with the Orbiter gas cloud and local plasma

  - Electrons and energized ions reach the PDP in its pallet location below the FPEG

  - Waves are stimulated, ions energized and electrons deenergized and scattered along the electron beam column

  - Electrons of 1 keV and below are found within a column of approximately 6 meters diameter--the electron gyrodiameter--with a nearly uniform distribution in flux

  - Ions with energies up to 250 eV are associated with the beam--plasma interaction.

  - Significantly intense VLF and LF waves are stimulated by pulsing the FPEG beam

  - Potentials up several 10's of volts and electric fields in excess of 10V/m are measured during FPEG operations

8.0 DATA ANALYSIS PLAN

Within the limited resources to carry out the OSS-1/PDP data analysis, work is progressing to prepare reports and publications on the following topics:

- Potentials and Electric Fields of the Orbiter
- Nature of the Orbiter-Induced Plasma Wakes
- The Orbiter Plasma Environment
- Effects of the Beam-Plasma Interaction
- Characteristics of the Electrostatic Noise Generated by the Orbiter-Plasma Interaction
- Description of the OSS-1/PDP System
- Orbiter EMI Levels
- S-Band and UHF Communications Radiated Field Strengths
- Power Buss and Microprocessor Performance History
- Pressure Measurements by PDP on STS-3
- Thermal History of the PDP on STS-3

These reports and papers are to be the basis for presentations at a number of meetings in the near future:

- European Geophysical Society, Leeds, England 23-27 August
- Activate Experiments Working Group and Spacelab-1 IWG, MSFC, 30-31 August
- Workshop on Charging of Large Space Structures in Polar Orbit, AFGL, 14-15 September
- NASA/Spacelab Workshop on Orbiter Environment, Calverton, Maryland, 5-7 October
- Fall AGU Meeting, San Francisco, 7-12 December
- AIAA Meeting, Reno, 10-14 January
- URSI Meeting, Boulder, 17-21 January
- Spring AGU Meeting, Baltimore, 30 May - 3 June

ADDITIONS TO
DR. S. SHAWHAN
PRESENTATION

TABLE 6

SUMMARY OF PDP ORBITER ENVIRONMENT MEASUREMENTS

ORBITER POTENTIAL

- POTENTIAL WITH RESPECT TO PLASMA VARIED UP TO ± 5V WITH PDP ON RMS
- POTENTIAL VARIATION CONSISTENT WITH $\underline{V} \times \underline{B} \cdot \underline{L}$ WHERE $\underline{L}$ = DISTANCE FROM ENGINES TO PDP
- ORBITER ALWAYS DRIVEN POSITIVE DURING FPEG OPERATIONS

EMC/EMI

- NO MICROPROCESSOR (2 UNITS) MALFUNCTIONS [WATCH-DOG TIMER UTILIZED]
- 28V PDP POWER BUSS RANGE: 27.0-31.0 VOLTS
- 28V PDP POWER BUSS STEPS: < 1.0V IN 1.6 SECONDS
  < 1.5V IN 5 MINUTES
- ELECTRIC AND MAGNETIC FIELD RADIATED EMISSIONS WITHIN SPECIFICATIONS
- ORBITER-PLASMA INTERACTION GENERATES ELECTROSTATIC NOISE UP TO ~ 1 V/M
- UHF TRANSMITTER: < 0.1 V/M IN BAY; < 0.5 V/M ON RMS
- S-BAND TRANSMITTER: < 2 V/M IN BAY; < 20 V/M ON RMS > 5 M

TABLE 6

SUMMARY OF PDP ORBITER ENVIRONMENT MEASUREMENTS

THERMAL PERFORMANCE

- FLIGHT HARDWARE MOUNTED ON COLD PLATE, PALLET AND RMS
- THERMAL CONTROL BY HEATERS, THERMAL BLANKETS AND RADIATING SURFACES
- ALL TEMPERATURES STAYED WITHIN DESIGN LIMITS

PRESSURE MEASUREMENTS

- APPARENT PRESSURE VARIES 10^{-7} TO 10^{-5} TORR AT ORBIT PERIOD WITH MAXIMA AT ASCENDING NODE (RAM IN NOSE-TO-SUN ATTITUDE)
- PRESSURE INCREASED TO 3 X 10^{-4} TORR DURING L2U BURN
- PRESSURE INCREASED TO 4 X 10^{-5} TORR DURING PAYLOAD BAY DOOR CLOSING (86/21:10)
- APPARENT PRESSURE IS MODULATED BY PDP ROTATION

PLASMA COMPOSITION AND ENERGY

- VERY SIGNIFICANT DENSITY VARIATION FOR DAY/NIGHT AND RAM/WAKE
- H_2O+ ORBITER-PRODUCED ION ALWAYS PRESENT
- DIRECTED ION BEAMS OBSERVED IN WAKE AND WHEN ORBITER IS NEGATIVELY CHARGED
- INSTANCES OF 100 eV IONS AND ELECTRONS IN PAYLOAD BAY

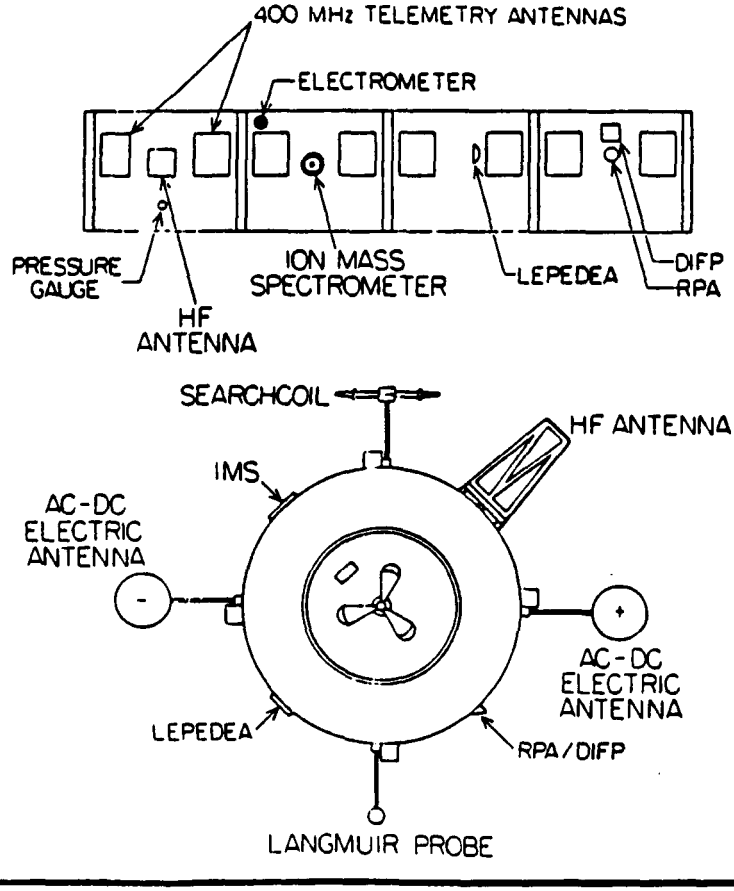

STS-3 ORBIT ATTITUDE
MARCH 24, 1982

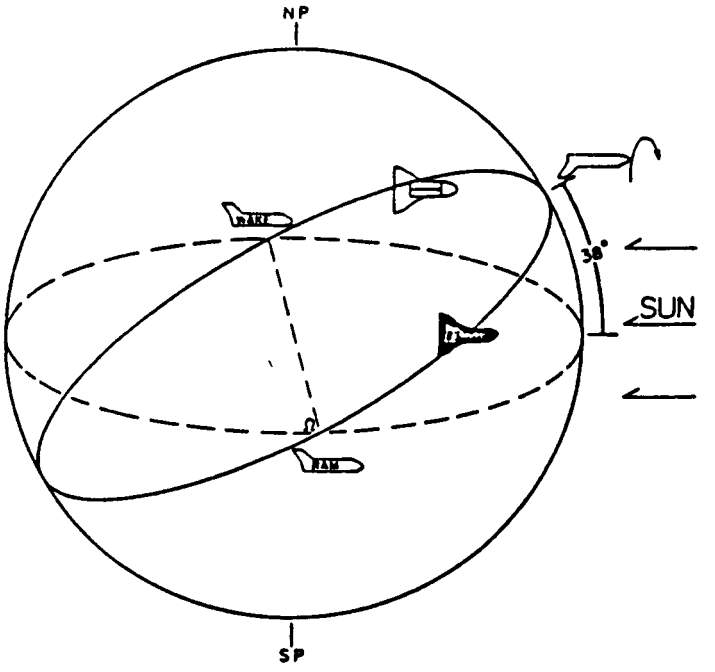

NOSE TO SUN 2x ORB RATE ROLL

PDP PRESSURE GAUGE

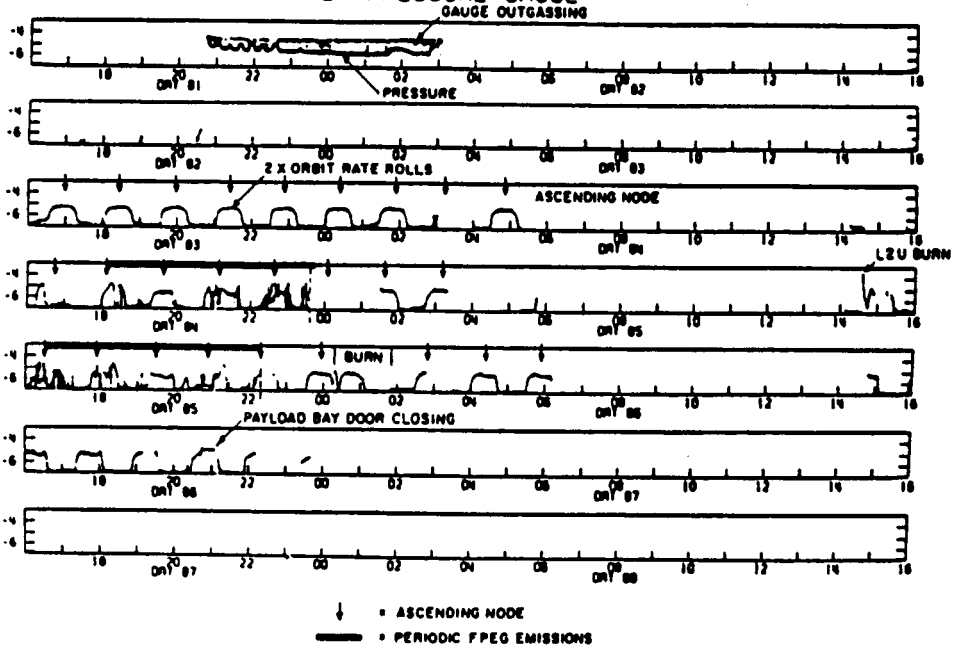

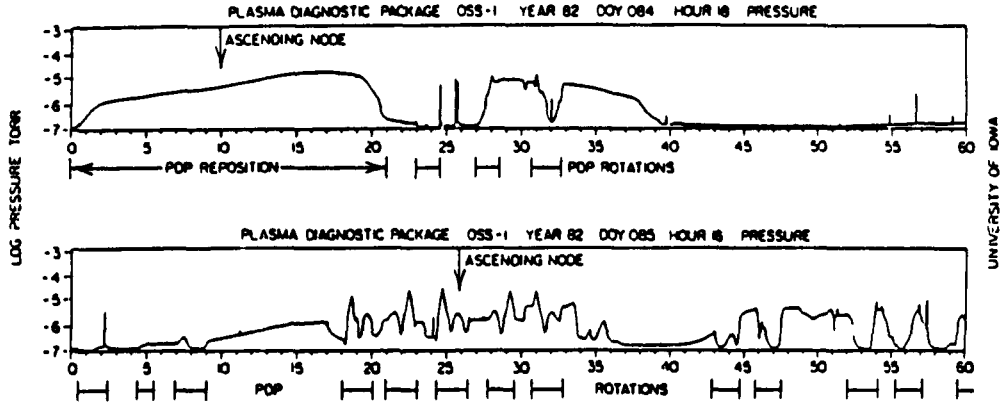
PLASMA DIAGNOSTIC PACKAGE OSS-1 YEAR 82 DOY 084 HOUR 18 PRESSURE
ASCENDING NODE
POP REPOSITION
POP ROTATIONS
PLASMA DIAGNOSTIC PACKAGE OSS-1 YEAR 82 DOY 085 HOUR 16 PRESSURE
ASCENDING NODE
POP
ROTATIONS
LOG PRESSURE TORR
UNIVERSITY OF IOWA

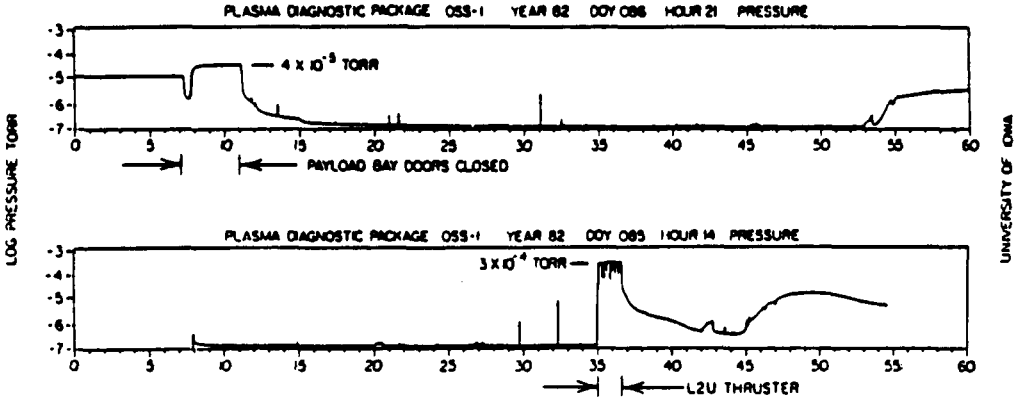
PLASMA DIAGNOSTIC PACKAGE OSS-1 YEAR 82 DOY 086 HOUR 21 PRESSURE
4 x 10⁻⁵ TORR
PAYLOAD BAY DOORS CLOSED
PLASMA DIAGNOSTIC PACKAGE OSS-1 YEAR 82 DOY 085 HOUR 14 PRESSURE
3 x 10⁻⁴ TORR
L2U THRUSTER
LOG PRESSURE TORR
UNIVERSITY OF IOWA

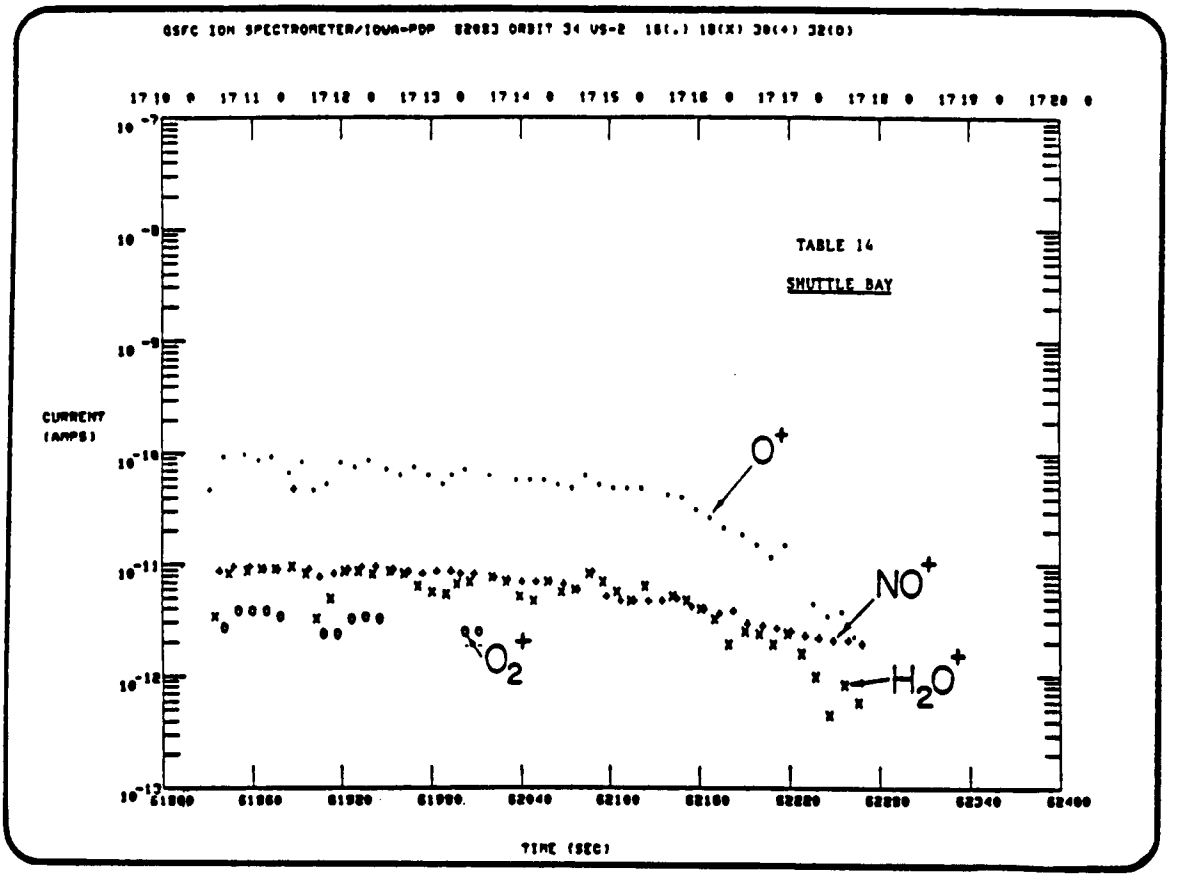
GSFC ION SPECTROMETER/IOUA-PDP 82083 ORBIT 34 VS-2 16(.) 18(X) 30(+) 32(0)
TABLE 14
SHUTTLE BAY
CURRENT (AMPS)
O+
NO+
O2+
H2O+
TIME (SEC)

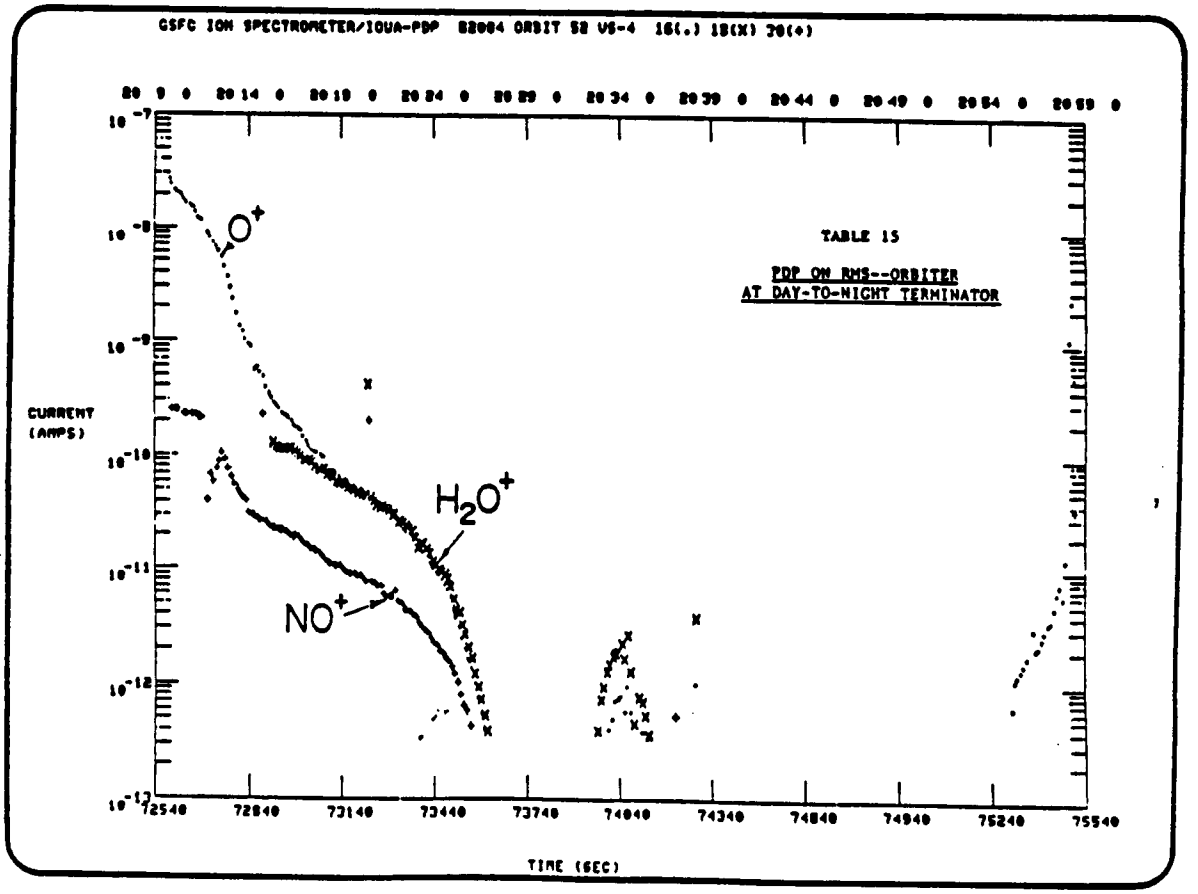
GSFC ION SPECTROMETER/IOUA-PDP 82084 ORBIT 58 VS-4 16(.) 18(X) 30(+)
TABLE 15
PDP ON RMS--ORBITER
AT DAY-TO-NIGHT TERMINATOR
CURRENT (AMPS)
O+
H2O+
NO+
TIME (SEC)

TABLE 18

ORBITER DC POTENTIAL

- DAY 83 HAD THE PDP MOUNTED TO THE PALLET (AND GROUNDED TO ORBITER)
  - PDP MEASURES THE AVERAGE POTENTIAL OF ITS TWIN CARBON COATED SPHERES WITH RESPECT TO THE SPACECRAFT GROUND AND OBTAINS A MAXIMUM POSITIVE POTENTIAL OF 3-4 VOLTS (NOT COUNTING ELECTRON GUN EMISSION TIMES) AND A MAXIMUM NEGATIVE POTENTIAL OF - 2-3 V
  - PEAK POSITIVE POTENTIALS OCCURRED CLOSE TO SUNSET (DURING PAYLOAD BAY WAKE)
  - THE ELECTRON GUN ALWAYS DROVE THE POTENTIAL OFFSCALE POSITIVE (> 8V) WITH A RECOVERY TIME VARIABLE FROM SECONDS TO MINUTES
  - PEAK NEGATIVE POTENTIALS OCCURRED APPROXIMATELY 1/2 ORBIT LATER AT ASCENDING NODE (DURING PAYLOAD BAY RAM)
- DAY 84 HAD THE PDP ON THE RMS (STILL GROUNDED TO ORBITER)
  - HOURS 16:30 TO 18:30 HAD THE PDP IN A FIXED POSITION ABOVE THE PAYLOAD BAY AND ARE SUITABLE FOR COMPARISON TO PREVIOUS DAYS RESULTS
  - ONE ORBIT PERIODICITY STILL EXISTS WITH ~ ±5V VARIATION

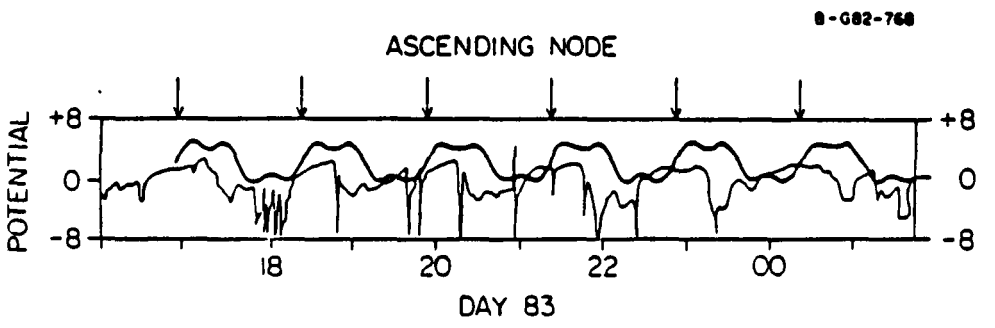

STS-3/OSS-1 PLASMA DIAGNOSTICS PACKAGE (PDP) MEASUREMENTS OF ORBITER TRANSMITTER AND SUBSYSTEM ELECTROMAGNETIC INTERFERENCE

S. D. Shawhan and G. Murphy
University of Iowa

From: Proceedings of the Shuttle Environment Workshop, NASA Office of Space Science and Applications, Calverton, MD, Oct. 5-9, 1982.

1.0 INTRODUCTION

This report is intended to present a quick-look analysis of the Plasma Diagnostics Package (PDP) electromagnetic spectral measurements on the STS-3/OSS-1 mission from March 1982. Further interpretation of the data is awaiting ancillary information on the operation of Orbiter subsystems, such as thrusters and on the detailed trajectory and attitude.

The PDP receiver system is described to identify the various antennas and to characterize the complement of receivers which cover the frequency range of 30 Hz to 800 MHz and S-Band at 2200 ± 300 MHz. Sample results are presented to show the variety of electromagnetic effects associated with the Orbiter and the time variability of these effects. The electric field and magnetic field maximum and minimum field strength spectra observed during the mission at the pallet location are plotted. Values are also derived for the maximum UHF transmitter and S-band transmitter field strengths. Finally, calibration data to convert from the survey plots to actual narrowband and broadband field strengths are listed.

Support for the PDP on the STS-3/OSS-1 Mission was provided through NASA/MSFC Contract NAS8-32807. OSS-1 Mission management was provided by NASA/GSFC.

2.0 DESCRIPTION OF RECEIVER SYSTEM

Sensors for the detection of magnetic and electric wave fields are identified in Figure 1. Two spheres of 8 inch diameter, separated by 1.2 meters make up the electric dipole antenna which is utilized from DC to 20 MHz in frequency. Calibration measurements at NASA/GSFC before flight indicated that the effective electrical length of this dipole was only 0.22 meters because of the proximity to the PDP. For higher frequency electric fields, a broadband single polarization horn antenna is utilized. It covers the range of 20 MHz through S-band at 2200 MHz. In addition, the searchcoil sensor is used to detect the magnetic field component of electromagnetic waves from 30 Hz to 178 kHz. The Langmuir Probe is sensitive to electrostatic plasma waves over the same VLF range of 30 Hz to 178 kHz.

A block diagram of the PDP sensors and associated receivers is shown in Figure 2. One VLF range receiver from the IMP program VLFR-IMP is switched between the electric dipole, the searchcoil and the Lagnmuir Probe sensors every 51.2 seconds to provide 16 channels of VLF spectra--30 Hz to 178 kHz. In addition, the waveform is preserved in the Wideband Receiver (WBR) and this analog data is included in the PDP data stream. Every 12.8 seconds the WBR switches 10 kHz bands sequentially covering 0-10 kHz, 20-10 kHz and 20-30 kHz for each sensor. The VLFR-HELIOS always is connected to the electric dipole antenna to give a peak and average spectrum every 1.6 seconds.

The electric dipole also drives the Medium Frequency Receiver (MFR) which covers 316 kHz to 17.8 MHz in 8 channels. This MFR shares a logarithmic detector with the High Frequency Receiver (HFR) which has four broadband channels spanning the range of 20 MHz to 800 MHz. Bandwidths for the VLFR and MFR are narrower at ± 15% and ± 30%, respectively. By mixing the S-band signal down to the HFR frequency range, the same log detector is used for the SBR by time multiplexing. Both peak and average spectra are obtainined each 1.6 seconds.

A summary of the receiver characteristics is given in Table 1. Detailed performance specifications for the receivers and the other PDP instrument are given in Table 2. Note that the stated field strength ranges are only approximate.

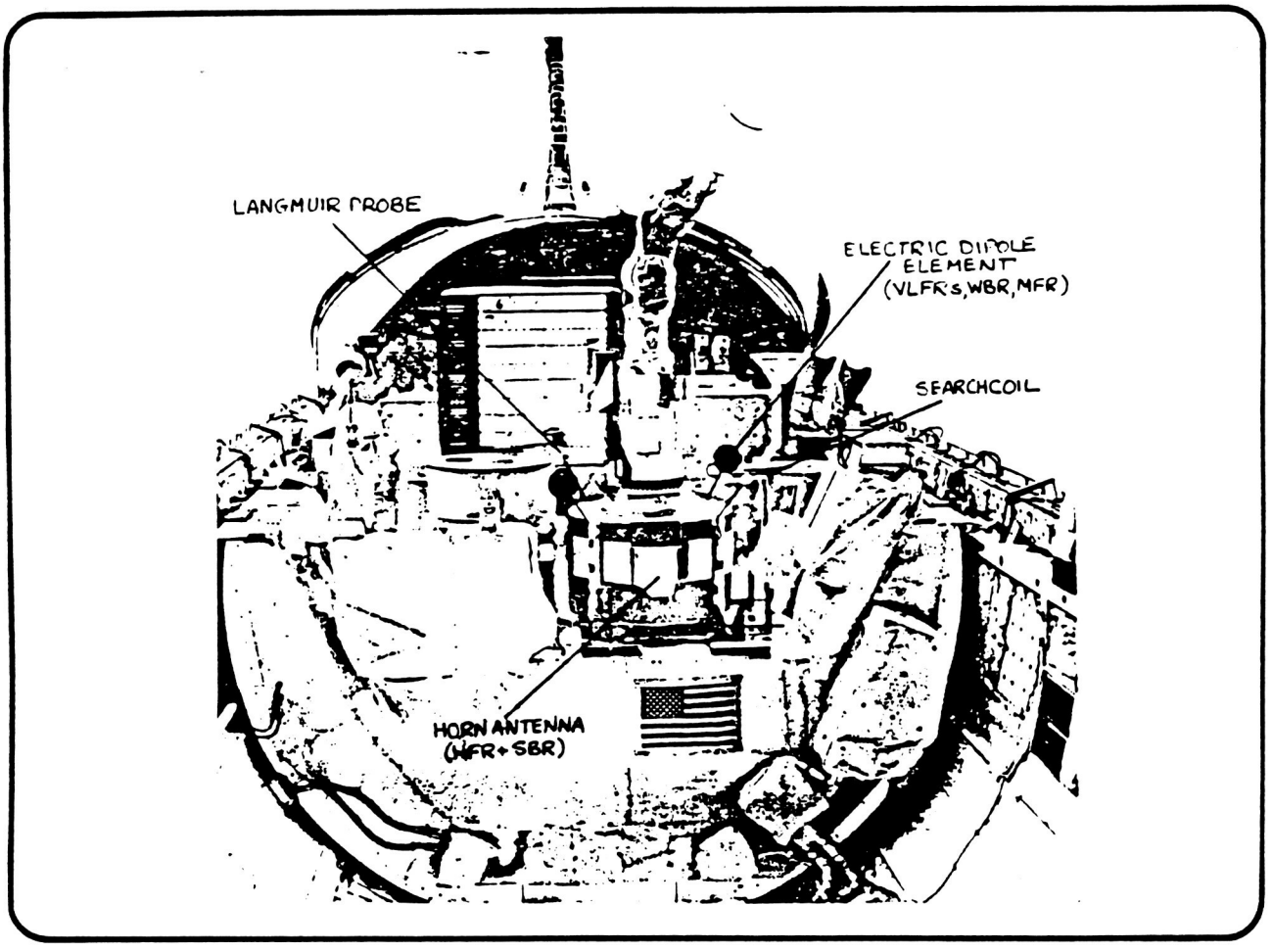

PDP on Pallet: Antennas Identified

Figure 1

Figure 2

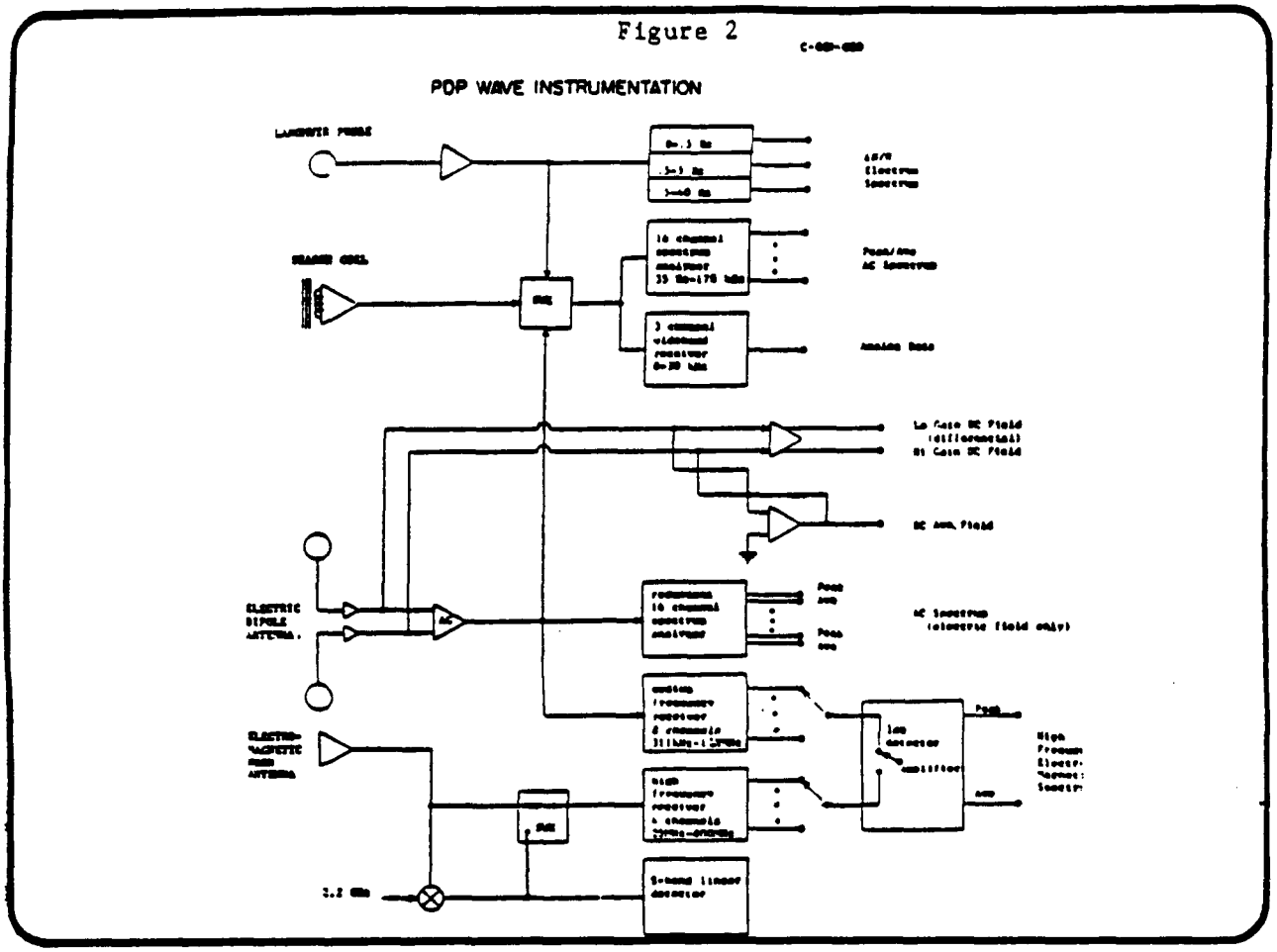

Table 1

STP-3/POP RECEIVER CHARACTERISTICS

VERY LOW FREQUENCY (VLFR)

- 16 CHANNELS
- 30 HZ TO 178 KHZ

MEDIUM FREQUENCY RECEIVER (MFR)

- 8 CHANNELS
- 311 KHZ TO 17.8 MHZ
- 65 DB DYNAMIC RANGE

HIGH FREQUENCY RECEIVER (HFR)

- 4 CHANNELS
- 20 MHZ TO 800 MHZ

S-BAND RECEIVER (SBR)

- 4 CHANNELS WITH LOG DETECTOR
- 1 CHANNEL WITH LINEAR DETECTOR
- ~ 2200 MHZ ± 300 MHZ

Table 2

PDP SCIENTIFIC INSTRUMENTS PERFORMANCE SPECIFICATIONS

MEASUREMENT	TECHNIQUE	PARAMETERS	VALUE/RANGE
DC Magnetic Field	Triaxial Fluxgate Magnetometer	Dynamic Range	±12 milligauss to ±1.5 gauss each axis
		Temporal Resolution	10 samples/second each axis
DC Electric Field	1m Double Probe with Spherical Sensors	Dynamic Range	±2 mV/m to ±2 V/m (average and differential
		Temporal Resolution	20 samples/second
AC Magnetic Waves	Searchcoil Sensor; Wideband Receiver	Frequency Range	5Hz-1kHz & 0.65-10, 10-20, 20-30kHz
		Amplitude Range	100db @ 0.4db resolution; 3nγ-300γ
		Duty Cycle	12.8 seconds out of 51.2 sec.
	Searchcoil Sensor; VLF Spectrum Analyzer (IMP) VLFR-IMP	Frequency Range	16 channels 35.5 Hz to 178kHz
		Frequency Resolution	±15% bandwidth
		Amplitude Resolution	100db @ 0.4dB resolution; $3x10^{-5}$ - $3\gamma Hz^{-1/2}$ (peak and average)
		Temporal Resolution	0.6 sample/second each channel
		Duty Cycle	12.8 seconds out of 51.2 sec.
AC Electric and Electrostatic Waves	1m Dipole Antenna Wideband Receiver WBR	Frequency Range	5Hz-1kHz, 0.65-10kHz, 10-20kHz & 20-30kHz
		Amplitude Range	100db @ 0.4db resolution; 3μV/m - 300 mV/m
		Duty Cycle	38.4 seconds out of 51.2 sec.
	1m Dipole Antenna VLF Spectrum Analyzer (Helios) VLFR-HELIOS	Frequency Range	16 channels-31.2Hz to 178kHz
		Frequency Resolution	±15% bandwidth
		Amplitude Resolution	100db @ 0.4dB resolution; $3x10^{-8}$ - $3x10^{-3}Vm^{-1}Hz^{-1/2}$ (peak and average)
		Temporal Resolution	0.6 sample/second each channel
		Duty Cycle	100%
	1m Dipole Antenna, Mid Frequency Receiver MFR	Frequency Range	8 channels-31.6Hz to 17.8 MHz
		Frequency Resolution	±30% bandwidth
		Amplitude Resolution	70db @ 1dB resolution; $3x10^{-3}$ - 10 V/m (peak and average)
		Temporal Resolution	1.6 second/scan
VHF/UHF EMI Levels	Horn Antenna VHF/UHF Receiver HFR	Frequency Range	4 channels-25-65, 65-160, 160-400, 400-800 MHz
		Frequency Resolution	±50%
		Amplitude Resolution	70db @ 1db resolution; 10^{-2} - 30 V/m; (peak and average)
		Temporal Resolution	1.6 sec/scan
S-Band Field Strength Monitor SBR	Horn Antenna VHF/UHF Receiver + Mixer and L.O.	Frequency Range	2000-2330 MHz
		Amplitude Range	.01 to 30 V/m (peak & average)
		Temporal Resolution	1.6 sec.
Suprathermal Particles	Low Energy Proton & Electron Differential Energy Analyzer (LEPEDEA)	Energy Range	2eV-50keV in 42 steps: electrons and ions
		Energy Resolution	34%
		Field of View	6^o x 162^o (7 detectors)
		Flux: Electrons	30-$1x10^7$, electrons/cm^2 sec sr eV
		Protons	6-$2x10^8$ protons/cm^2 sec sr eV
		Temporal Resolution	1.6 sec for spectrum
	Electrometer	Flux Range	10^9 -10^{14} elect cm^{-2} sec^{-1}
		Temporal Resolution	10 samples/second
	Retarding Potential Analyzer/Differential Ion Flux Probe	Density Range	$2x10^1$ -$1x10^7$ ions cm^{-3}
		Energy Range	0-16 eV
		Velocity Range	0-15km sec^{-1}
		Temporal Resolution	0.8 sec/scan; 51.2 sec/analysis
Thermal Electrons	Langmuir Probe, Density	Dynamic Range	10^3 -10^7 electrons cm^{-3}
		Temporal Resolution	1 second sweep every 12.8 sec.
	Langmuir Probe, Density Irregularities	Scale Sizes	10 meters to 100 km
		Dynamic Range	80db @ 5db resolution; 10^2 - 10^8 cm^{-3}
Thermal Ions	Ion Mass Spectrometer	Dynamic Range	20-$2x10^8$ ions cm^{-3}
		Mass Range	1-64 AMU @ < 1% overlap
		Temporal Resolution	1.6 seconds for mass scan
Ambient Pressure	Ionization Gauge	Pressure Range	10^{-7} to 10^{-3} torr

3.0 OVERVIEW OF ORBITER AC ELECTRIC FIELD ENVIRONMENT

In Figure 3 is presented a 30 minute summary plot of the PDP measured electric fields from 30 Hz to S-band for GMT DAY 85 20:30 to 21:00. Noted in the figure are the variety of phenomena which have been detected during the mission. Note that for each frequency, the vertical scale represents approximately 100 dB of dynamic range.

Very short bursts in the VLF range near 20:37 and 20:39 are assumed to be due to thruster firings. The changing VLF field strength from 20:30 to 20:37 has been identified as a broadband electrostatic noise which is Orbiter-attitude dependent--it peaks when the plasma is rammed into the payload bay (-Z axis parallel to velocity vector). Also very obvious in the VLF range is the increased intensity as the Fast Pulse Electron Generator (FPEG) emitts a 50 ma beam of 1 keV electrons. As the PDP is moved in and near the beam by the RMS (Remote Manipulator System), the noise is seen in the channels of the MFR. Probably these emissions occur near the electron gyrofrequency (~ 1 MHz) and the plasma frequency (3-10 MHz).

These FPEG generated plasma waves do not extend up into the HFR range, typically. At 271 MHz (165-400 MHz channel of the HFR) is seen the UHF downlink transmitter. Since the PDP is being rotated and positioned at various points just above the payload bay, it sees different S-band field strength levels as indicated.

Some of these effects are depicted in more detail in the next section.

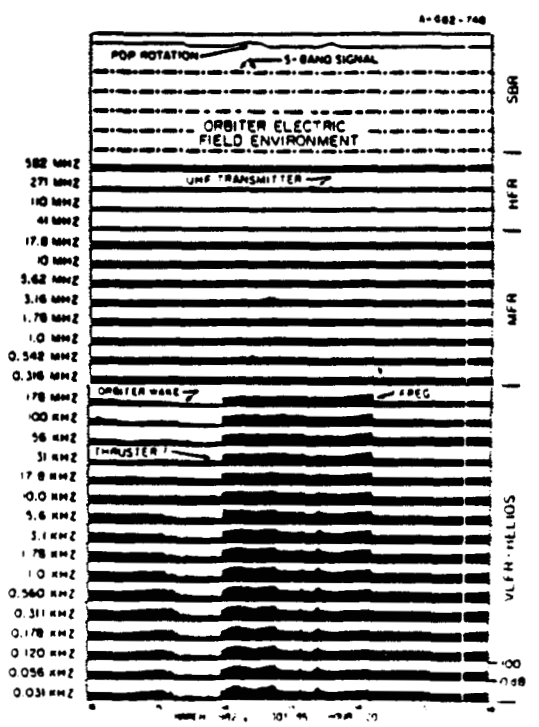

Figure 3

4.0 TIME VARIABILITY OF OBSERVED NOISE

The following series of figures illustrate the time variability of the VLF electric field noise from time scales of seconds to tens of minutes. Typically only the UHF and S-band transmitters are observed above 178 kHz because the receivers are less sensitive and plasma-related waves do not extend to frequency above 10 MHz. Thus waves at frequencies of a few hundred kilohertz to 20 MHz are not seen unless the FPEG is operating.

In Figure 4 is seen a ~ 60 dB overall amplitude change in the matter 10 minutes with short bursts of only seconds in duration. The overall trend is attributed to the Orbiter-attitude related electrostatic noise. Short bursts are most likely thrusters. For Figure 4, the PDP is stowed on the pallet whereas for Figure 5 the PDP is on the RMS. The overall levels are not much different but the levels do change with PDP rotation. This change indicates that the noise sources are either strongly polarized or what is more likely, localized on the Orbiter. Note that BX is a component of the earth's magnetic field which indicates the PDP rotation.

Experiment and Orbiter systems can definitely affect the signal strengths. When the FPEG operates, levels increase by ~ 20 dB. In the one case of a Primary Reaction Control System (PRCS) jet firing at GMT DAY 85 14:36, the noise actually decreases at the higher frequencies. The momentary gas output may moderate the Orbiter interaction with the plasma which produces the broadband electrostatic noise.

Evidence that the broadband electrostatic noise is not due to an Orbiter subsystem or instrument is presented in Figure 7 at the time of a payload bay door closing. During this three minute interval, the noise dropped below the receiver noise levels at all frequencies. Consequently, the noise does not originate inside the bay; it is shielded by the doors. When the doors are opened, the noise returns. If this noise is a significant problem to payload instrumentation, it can be minimzed by directing the bay away from the velocity vector.

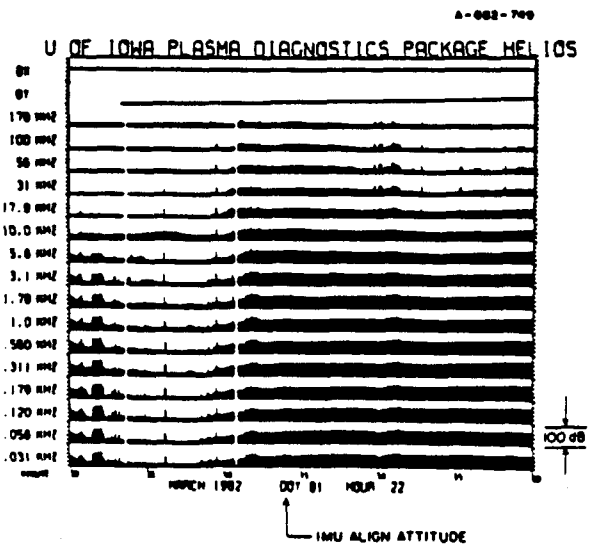

NOISE TIME VARIABILITY WITH THRUSTERS

Figure 4

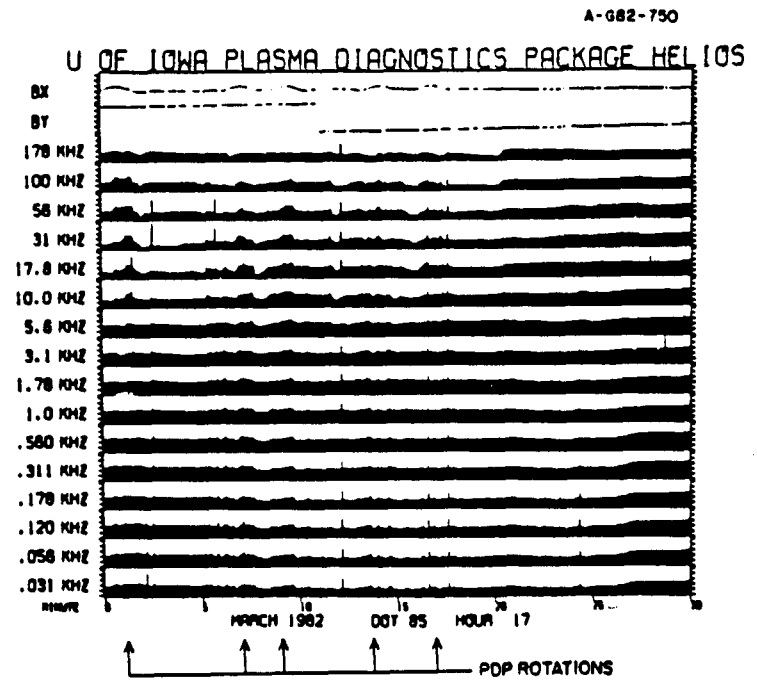

SIGNAL STRENGTH VS PDP ROTATION

Figure 5

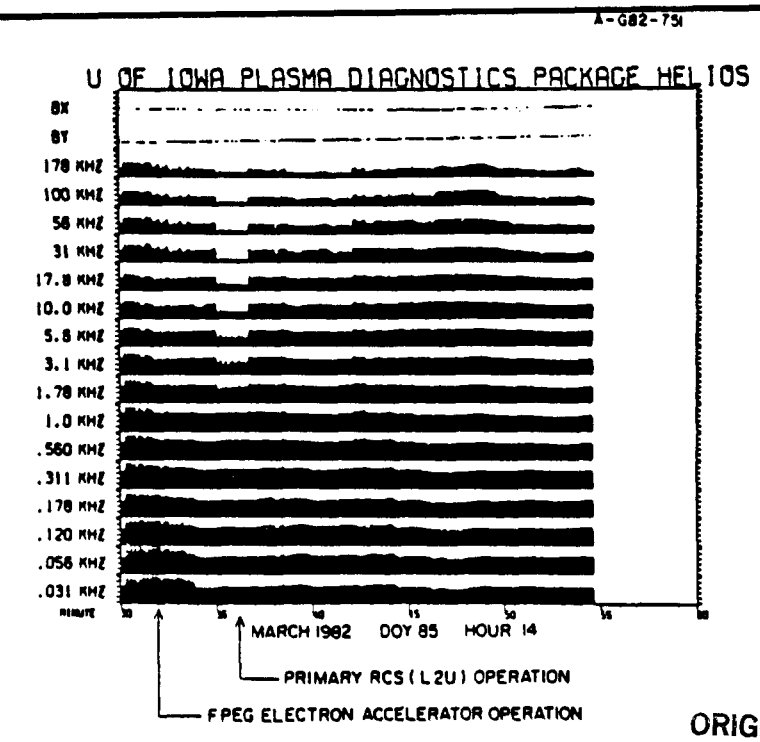

BACKGROUND NOISE MODULATION

Figure 6

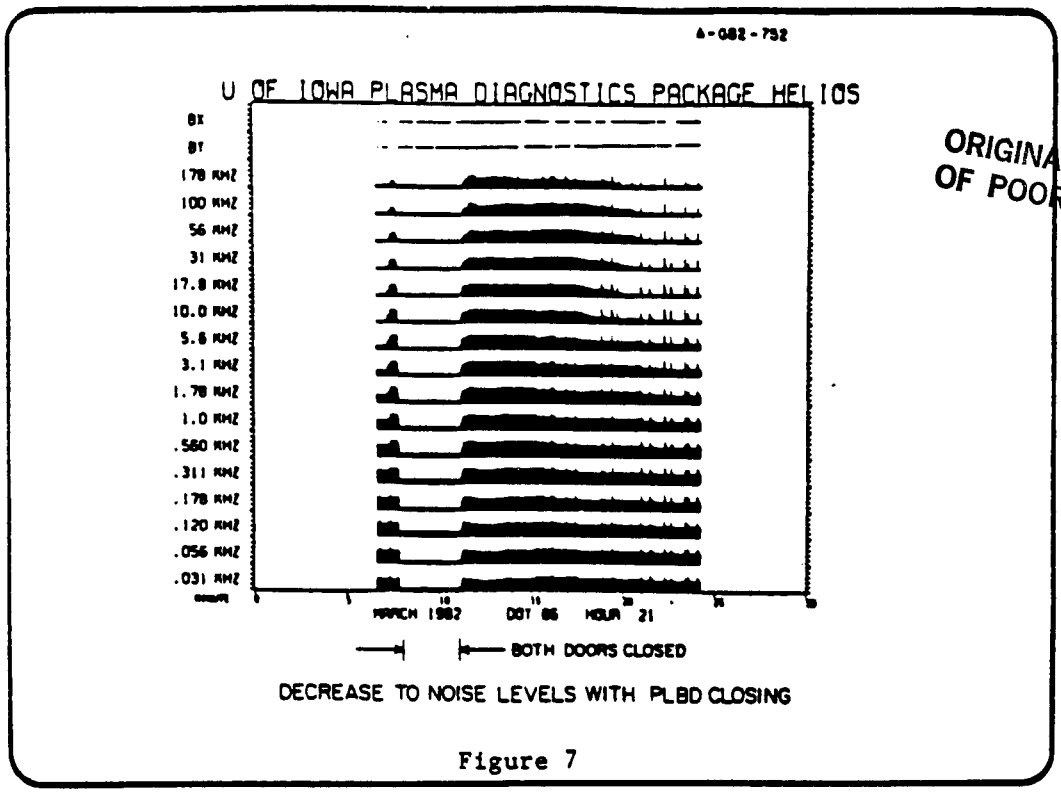

Figure 7

5.0 SPECTRUM OF ELECTROMAGNETIC NOISE

Use has been made of the Wideband Analog Receiver (WBR) to determine the spectral nature of the electric field and magnetic field noise. Spectra covering 0 to 30 kHz for several minutes of time are shown in Figure 8. The magnetic field noise shows intense lines with spacings of Hz, kHz, 10's kHz, and harmonics. Further work is in progress to identify the exact frequencies and their change with time. It is surmized that these lines are associated with data clocks and power converters.

On the other hand, the electric field spectra show a "white noise" characteristic which does not change much with time. During the payload bay door closing, weak spectral lines were evident since the external broadband noise was screened out. Note that the WBR has an automatic gain control so that the amplitude variations of Figure 4, for example, are not evident.

By searching over extended periods while the PDP was stowed on the pallet, values for the minimum and the maximum noise levels have been obtained and displayed in Figure 9. These values are calibrated in volts per meter and normalized to a 1 MHz bandwidth. The electric scales as 20 log (electric field), whereas, the bandwidth scales as 10 log (bandwidth) as the data are presented. Also plotted for comparison are the broadband electric field limits for the Shuttle itself and for a payload. When the FPEG is not operating, above the 14 kHz cutoff, the maximum level (open circles) does not exceed the payload limit. When the FPEG operates with the PDP in the beam, the levels are increased by ~ 20 dB in the VLF range.

Narrowband magnetic field strengths are much less variable ($< \pm$ 10 dB) from the minimum to maximum observed levels. These levels are not Orbiter-attitude dependent and in fact, the levels were above the maximum door-opened levels with the payload bay doors closed. It is surmized that these levels are due to Orbiter subsystems which should be slightly time dependent as systems turn ON/OFF. During FPEG operations, levels in the 1-100 kHz range are increased.

ORIGINAL PAGE IS
OF POOR QUALITY

A-G82-747

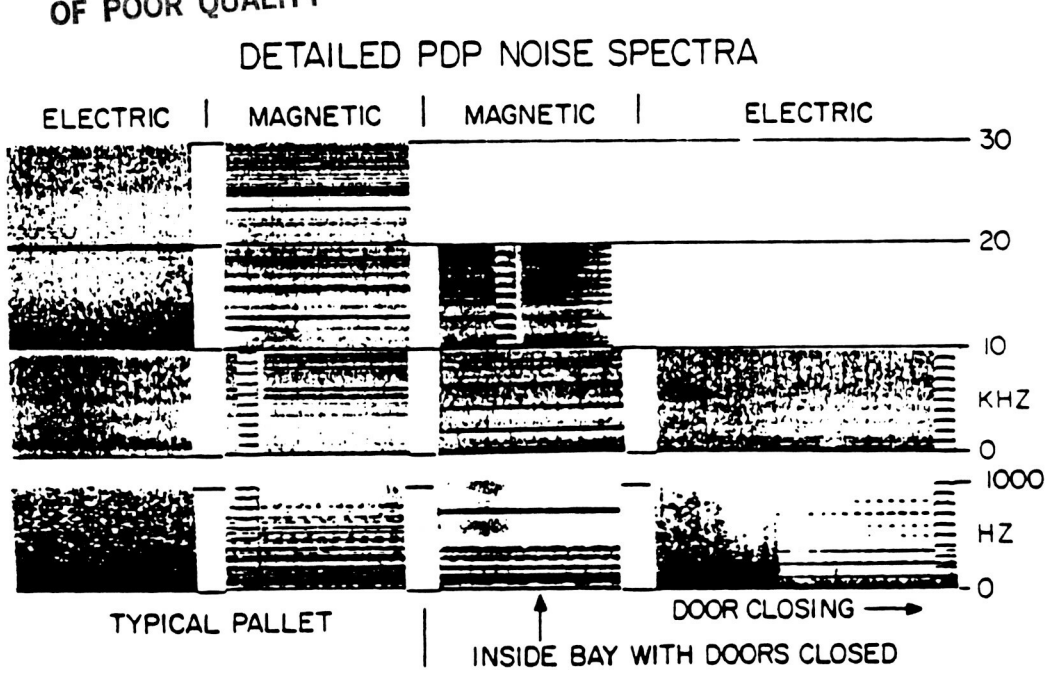

Figure 8

A-G82-746

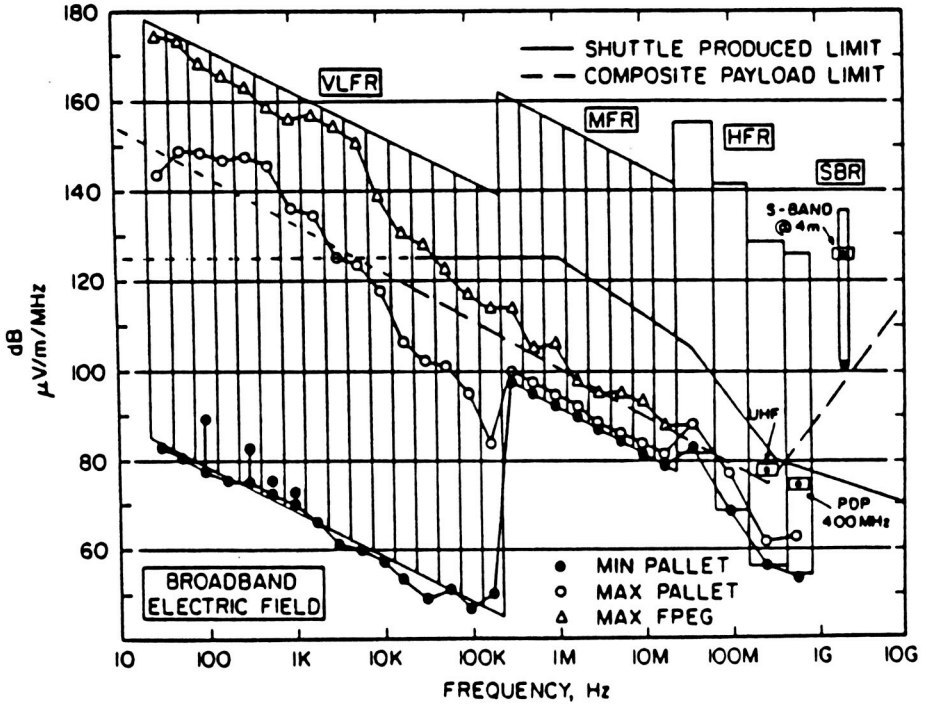

Figure 9

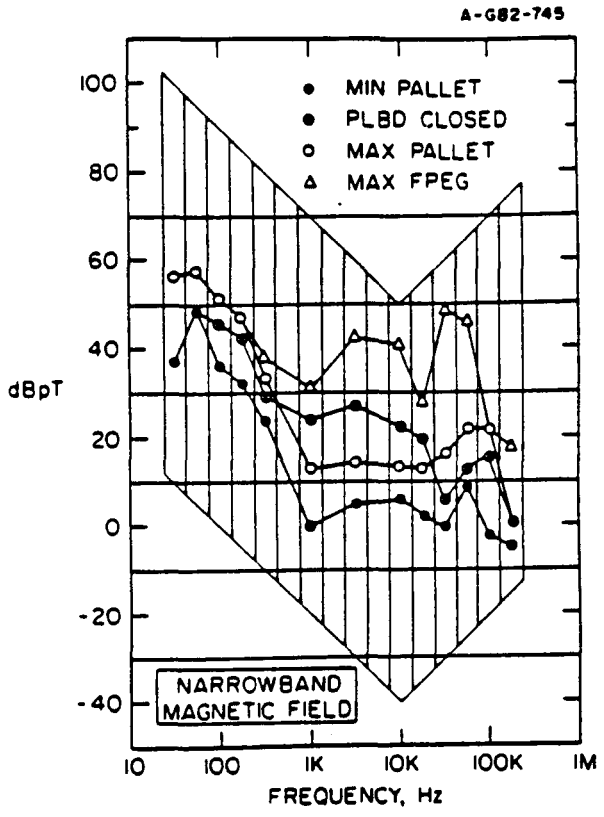

Figure 10

6.0 UHF AND S-BAND TRANSMITTER FIELD STRENGTHS

One filter channel of the PDP HFR covered the band of 165-400 MHz which includes the 295 MHz frequency of the UHF voice downlink transmitter. When this transmitter was keyed ON and connected to the upper antenna, a signal was detected by the PDP as shown in Figure 3. These measured field strengths were always below 0.5 V/m with the PDP on the RMS and below 0.1 V/m at the PDP pallet location. Average and peak field strengths are given in the following table:

Location/Field Strengths ± 2dB	Average	Peak
PDP on Pallet at 13 meters from Antenna	.05 V/m	0.08 V/m
PDP on RMS at 8 meters from Antenna	.23	.44

These levels are well known below the suggested radiated susceptibility field strengths.

At S-band, the 150 watt data downlink transmitter (2287.5 MHz) can produce fields which are modeled to be 49.6 V/mR (meters) in the beam of the selected "quad" antenna. Even at many meters, these fields could be at damage level for payload instruments or for satellites being manipulated by the RMS. The SBR was especially designed to measure the field strengths in and around the payload bay as shown in Figure 3. These measured levels were about 5 dB ± 2 dB higher than the modeled values but comparable to a crude theoretically calculated value as follows:

	Field Strengths Relations (V/m)
Predicted Field Strengths	49.6 /R (meters)
Measured with PDP (± 2 dB)	90.3 /R (meters)
Calculated @ (150 Watts)	94.9 /R (meters)

The calculated value assumes that all of the power is emitted into a hemisphere (2 π steradians) with 100% efficiency.

In the antenna beam, the fields exceed 20 V/m inside of 5 meters. However, with the PDP on the pallet at a range of 13 meters off the edge of the beam, the fields were not observed at the threshold of 2 V/m whereas the in-beam prediction would be 7V/m. Consequently, payload bay instrumentation is not subjected to damage levels.

7.3 HFR

Because of the variety of bandwidths, the dynamic range is listed in the following table:

Center Freqency	Bandwidth	Minimum	Maximum	Slope
40 MHz	20 - 65 MHz	-40 dBV/m	+32 dBV/m	16 dB/V
100	65 - 165	-40	+32	16
250	165 - 400	-31	+41	16
600	400 - 800	-22	+52	16

dBV/m ~ Maximum dB + 16 dB V/m * Output Voltage -80 dB

7.4 SBR

Only the linear detector on the S-band system operated. An RF relay failure prevented the S-band signal from getting to the log-detector. Using calibrations at GSFC and Iowa before flight and re-calibration after flight, it is determined that the linear response is

V/m = 5.7 * Output Voltage at 2287.5 MHz Boresight

giving a fit to the field with range of about

$$V/m = \frac{90\ V/m}{R\ (meters)}$$

where R is the distance from the S-band quad antenna in the nominal beam.

8.0 COMMENTS

Comprehensive sets of Orbiter noise spectrum measurements have been obtained. It is found that the noise levels do not exceed the worst case predictions for the Orbiter. Consequently, the receivers really need to be more sensitive to obtain the science and the EMI data on Spacelab-2 especially since the PDP measures the Orbiter at 100 meters range. It is hoped that these improvements in sensitivity can be made for Spacelab-2.

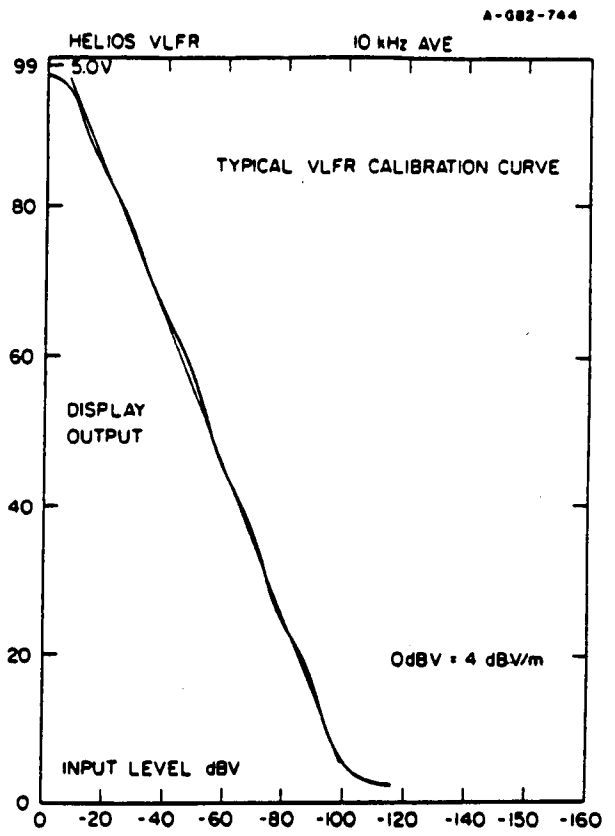
A-082-744
HELIOS VLFR
10 kHz AVE
5.0V
TYPICAL VLFR CALIBRATION CURVE
99
80
60
40
20
0
DISPLAY
OUTPUT
0dBV = 4 dBV/m
INPUT LEVEL dBV
0
-20
-40
-60
-80
-100
-120
-140
-150
-160

Figure 11

ADDITIONS TO
DR. S. SHAWHAN
PRESENTATION

TABLE 4

STS-3/POP RECEIVER CHARACTERISTICS

VERY LOW FREQUENCY (VLFR)

- DOUBLE SPHERE ANTENNA FOR ELECTRIC FIELD
- SEARCH COIL ANTENNA FOR MAGNETIC FIELD
- 16 CHANNELS (x2 SYSTEMS)
- 30 HZ TO 178 KHZ
- WIDEBAND RECEIVER 30 HZ TO 30 KHZ

MEDIUM FREQUENCY RECEIVER (MFR)

- 8 CHANNELS
- 311 KHZ TO 17.8 MHZ
- 65 DB DYNAMIC RANGE

HIGH FREQUENCY RECEIVER (HFR)

- 4 CHANNELS
- 20 MHZ TO 800 MHZ

S-BAND RECEIVER (SBR)

- 4 CHANNELS WITH LOG DETECTOR (FAILED)
- 1 CHANNEL WITH LINEAR DETECTOR
- ~ 2200 MHZ ± 300 MHZ

ORIGINAL PAGE IS
OF POOR QUALITY

P D P WAVE INSTRUMENTATION ON STS-3 / OSS-1

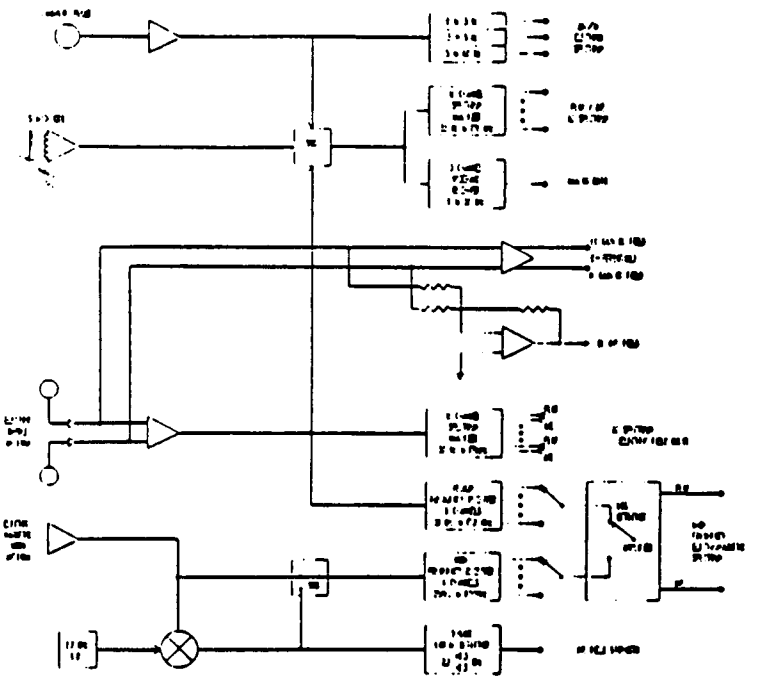

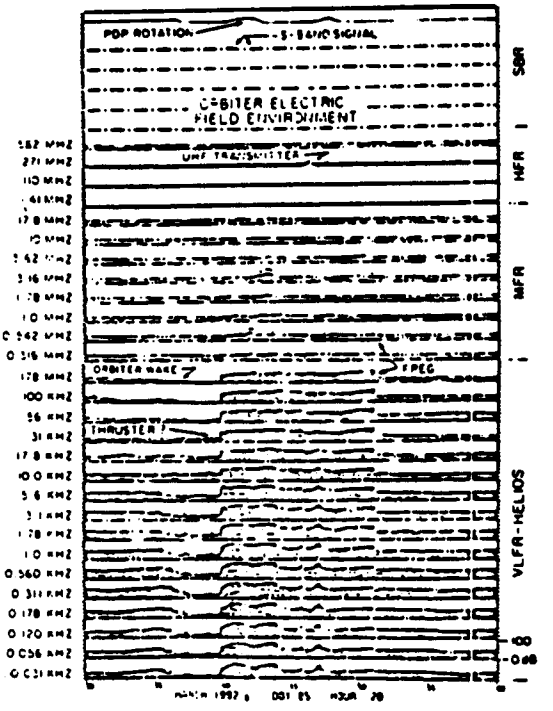

TABLE 17

ORBITER-GENERATED ELECTROSTATIC NOISE

- OBSERVED CHARACTERISTICS
  - SPECTRAL EXTENT - 30 HZ TO 178 KHZ
  - SPECTRAL PEAK - 0.1 V/M @ 0.3 KHZ
  - VARIABILITY - 70 DB OVER ORBIT
  - MAGNETIC COMPONENT - NONE DETECTABLE OVER ORBITER MAGNETIC FIELD EMI
  - LOCATION - COMPLETELY DISAPPEARS WITH PAYLOAD BAY DOOR CLOSED; IMPLIES EXTERNAL TO ORBITER
    - NO SIGNIFICANT DIFFERENCE WITH PDP ON RMS; IMPLIES GENERATED IN LARGE VOLUME
  - THRUSTER RESPONSE - HIGH FREQUENCIES (> 10^4 KHZ) ARE ATTENUATED DURING FIRINGS
    - LOW FREQUENCIES ENHANCED IF NOT ALREADY PRESENT
  - ORBITER ATTITUDE DEPENDENCE - MAX INTENSITY - RAM
    - MIN INTENSITY - WAKE
    - SEE LOW FREQUENCY AT ALL ATTITUDES EXCEPT EXACTLY WAKE
    - SEE HIGH FREQUENCY ONLY - RAM

- TENTATIVE INTERPRETATION
  - WAVE MODE: ION ACOUSTIC
  - PHASE/GROUP VELOCITY: $V \sim 2 \times \times 10^3$ M/SEC
  - MINIMUM WAVELENGTH: λ (MIN) $\sim 2\pi\lambda$ (DEBYE)
    λ (MIN) $\sim$ 0.02 METERS
  - MAXIMUM DOPPLER SHIFT FREQUENCY: F (MAX) $\sim V/\lambda$ (MIN) $\sim$ 100 KHZ
  - MAXIMUM WAVELENGTH: λ (MAX) $\sim$ 10 LARMOR RADII
  - MINIMUM FREQUENCY: F (MIN) $\sim V/\lambda$ (MAX) $\sim$ 30 HZ

- POSSIBLE ORBIT ENERGY DISSIPATION
  - ENERGY DENSITY (STIX): $W = \frac{\epsilon_1^2}{\omega^2} \cdot \left\{\frac{1}{2} \cdot \epsilon_0 \cdot E^2\right\}$ (MKS)

    $W \sim \left(\frac{50\ \text{kHz}}{300\ \text{Hz}}\right)^2 \cdot \frac{1}{2} \cdot 9 \times 10^{-12} \cdot (0.1\ \text{V/M})^2$

    $W \sim 1 \times 10^{-9}$ Joules/m^3
  - VOLUME ESTIMATE: $V \sim (10\ \text{LARMOR RADII})^3 \sim (R_i)^3$

    $V \sim 2.2 \times 10^5\ m^3$
  - TOTAL ENERGY/VOLUME: $W.V \sim 3 \times 10^{-4}$ Joules
  - POWER: $P \sim \frac{W.V}{10R_i} \cdot$ Velocity

    $P \sim 4 \times 10^{-2}$ WATTS

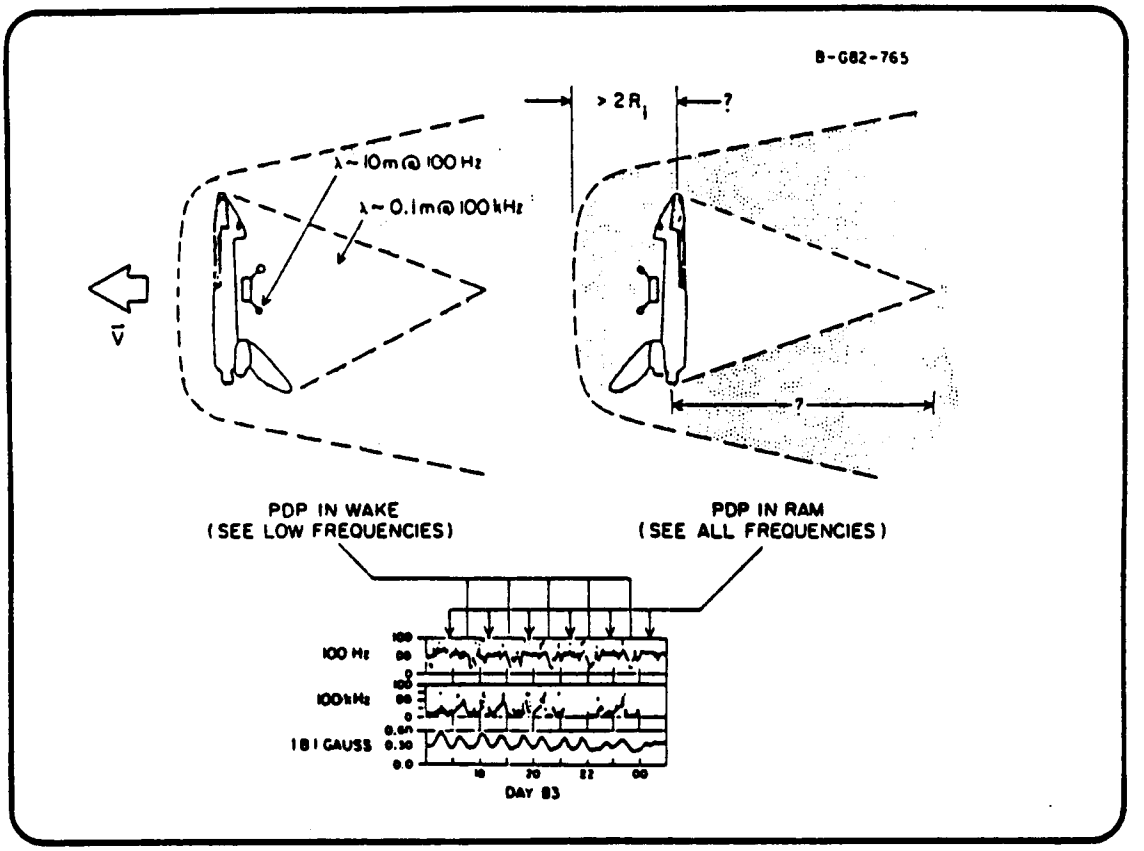

TABLE 9A

UHF/S-BAND TRANSMITTER FIELD STRENGTHS

UHF VOICE LINK (165-400 MHZ)

- PALLET LOCATION: < 0.1 V/METER
- RMS SCANS: < 0.5 V/METER

S-BAND COMMUNICATIONS LINK (2200 ± 300 MHZ)

	V/M @ 1M
• MEASURED WITH PDP (± 2 DB)	90.3
• EXPECTED @ 150W	49.6
• CALCULATED @ 150W (100% INTO HEMISPHERE)	94.9

INTERACTION OF THE SPACE SHUTTLE ORBITER WITH THE IONOSPHERIC PLASMA

G B Murphy, S D Shawhan, L A Frank, N D'Angelo & D A Gurnett

Department of Physics and Astronomy
University of Iowa, USA

J M Grebowsky

NASA GSFC
Greenbelt, MD, USA

D L Reasoner & N Stone

NASA MSFC
Huntsville, AL, USA

ABSTRACT

The Plasma Diagnostics Package (PDP), which flew as part of the NASA Office of Space Science (OSS-1) payload on STS-3 consisted of an instrument complement capable of characterizing the plasma environment in and around the Space Shuttle Orbiter. These measurements coupled with those made by the Vehicle Charging and Potential (VCAP) experiment also on OSS-1, as well as diagnostics from subsequent flights, provide insight into the effects a large vehicle such as the Orbiter has on the ionospheric plasma. Modification of the environment by contamination such as Orbiter outgassing, thruster operation and water dumps results in altered neutral pressure, modified plasma density and an altered chemical composition. The physical size and velocity of the Orbiter vehicle produces a plasma wake, generates electric fields, results in surface effects and generates broadband electrostatic noise.

Keywords: Large Vehicle Interaction, Wake, Ionospheric Plasma, Shuttle Environment

1. INTRODUCTION

1.1 Background

Until the flight of STS-3 in March 1982 little opportunity was available to study the interactions of a vehicle whose scale was large compared to an ion gyroradius and that was moving at a high velocity with respect to a relatively dense and cool plasma. Table 1 summarizes the plasma parameters in the F2 ionosphere and includes Orbiter parameters of interest.

Extensive theoretical work has been done on the problem of plasma wakes. Stone (Ref. 1) provides an excellent summary of this research and more recently Samir et al (Ref. 2) have studied the expansion of a plasma into a vacuum and discussed such phenomena as ion streams, rarefaction waves, and plasma instabilities and suggest appropriate in situ measurements on the space shuttle.

1.2 Instrumentation

Instruments aboard the Plasma Diagnostics Package (PDP) were designed to measure thermal particle densities and temperatures, energetic particle distribution functions, electric and magnetic fields, and electrostatic and electromagnetic waves. Table 2 lists the complement of instruments aboard this experiment and the parameters they measure. The PDP was designed both for on pallet measurements and as an RMS (Remote Manipulator System) probe. The PDP was lifted out of the bay with the RMS and maneuvered around the Orbiter in sequences designed to measure the electric and magnetic fields, electrostatic and electromagnetic waves as well as the thermal and energetic particle environment.

Table 1.

Plasma Parameters	
Ambient Density	$n_e \equiv 10^5 - 10^6$ cm^{-3}
Ambient Temperature	$T_e \equiv 1200° - 2400°$K
Electron Gyroradius	4.3 cm
Ion Gyrodadius	~ 4m (0^+)
Ion Thermal Speed	1.3 km/sec
Orbiter Parameters	
V_{orb} = 7.8 km/sec	Surface Area:
	Insulator ~ 1400m^2
Mach # 5-8	Conductor ~ 60m^2
Characteristic Length	37m long, 24m wingspan

Other investigations of interest to this discussion that were part of the OSS-1 payload were the VCAP (Vehicle Charging and Potential) experiment and the FPEG (Fast Pulse Electron Gun). (For a complete description of the OSS-1 experiment complement see Neupert et al Ref. 3). The VCAP investigation consisted of charge and current probes (primarily for measuring vehicle capacitance with respect to the plasma), a Langmuir Probe (LP) for measurement of electron density and temperature and a Spherical Retarding Potential Analyzer (SRPA) for ion density and temperature.

1.3 The STS-3 Mission

Since STS-3 was still a flight test mission, the payload had a low priority for selection of flight attitude and the one chosen as a compromise for the payload/orbiter objectives lead to difficulties in sorting out day/night and ram/wake

Proceedings of the 17th ESLAB Symposium on 'Spacecraft/Plasma Interactions and their Influence on Field and Particle Measurements', Noordwijk, The Netherlands, 13-16 Sept. 1983. (ESA SP-198, publ. December 1983).

Table 2.

- LOW ENERGY PROTON AND ELECTRON DIFFERENTIAL ENERGY ANALYZER (LEPEDEA)
  - Nonthermal Electron and Ion Energy Spectra and Pitch Angle Distributions for Particle Energies between 2 eV and 50 keV
- AC MAGNETIC WAVE SEARCHCOIL SENSOR
  - Magnetic Fields with a Frequency Range of 30 Hz to 178 kHz
- TOTAL ENERGETIC ELECTRON FLUXMETER
  - Electron Flux 10^{9} - 10^{14} Electrons/cm^2 Sec
- AC ELECTRIC AND ELECTROSTATIC WAVE ANALYZERS
  - Spectra with a Frequency Range of 30 Hz to 800 MHz
  - Electric Field Strength at S-Band, 2.2 GHz
- DC ELECTROSTATIC DOUBLE PROBE WITH SPHERICAL SENSORS
  - Electric Fields in one axis from 4 mV/m to 4 V/m
- DC TRIAXIAL FLUXGATE MAGNETOMETER
  - Magnetic Fields from 12 Milligauss to 1.5 Gauss
- LANGMUIR PROBE
  - Thermal Electron Densities between 10^3 and 10^7 cm^{-3}
  - Density Irregularities with Frequencies of .5 Hz to 178 kHz
- RETARDING POTENTIAL ANALYZER/DIFFERENTIAL ION FLUX PROBE
  - Ion Number Density from 10^2 to 10^7 cm^{-3}
  - Energy Distribution Function below 6 eV
  - Directed Ion Velocities up to 15 km/sec
- ION MASS SPECTROMETER
  - Mass Ranges of 1 to 64 Atomic Mass Units
  - Ion Densities from 20 to 2 X 10^7 Ions cm^{-3}
- PRESSURE GAUGE
  - Ambient Pressure from 10^{-3} to 10^{-7} Torr

effects. The attitude of the Orbiter for all of the PDP data presented here is referred to as Nose-To-Sun (NTS) with a 2x orb rate roll (see Figure 1). This attitude results in a cyclic ram/wake cycle for instruments in the payload bay such that maximum ram occurs around ascending node and maximum wake at descending node.

Effects of the Space Shuttle Orbiter on the ionospheric plasma will be discussed in two parts. The first is induced contamination which will be treated only briefly and the second are effects induced by the vehicle's size, velocity and electrical properties.

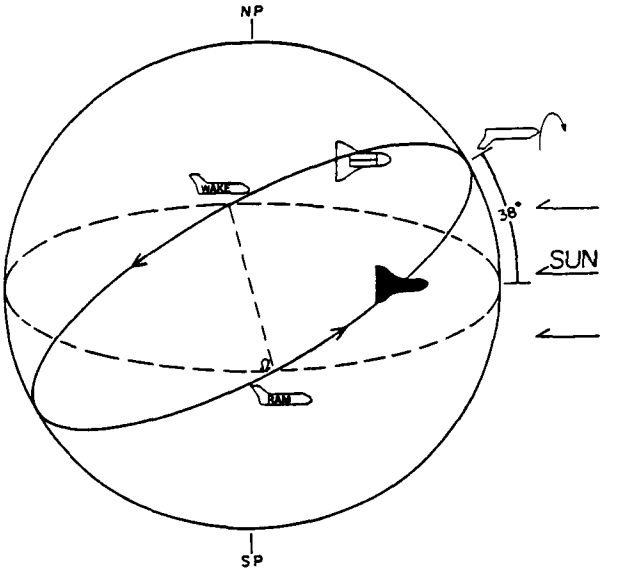

Figure 1. STS-3 Orbit Attitude

2. INTERACTION VIA CONTAMINATION

Electromagnetically, the Orbiter is relatively clean. Shawhan and Murphy (Ref. 4) indicated that both transmitters and unintentional interference are well below Interface Control Document specs. The predominant noise turned out to be the ubiquitous broad band electrostatic noise which will be discussed in the next section.

The principle form of modification via contamination takes the form of chemical releases. These chemicals; water, nitrogen, hydrogen and traces of other heavier molecules, enter the ionosphere as a result of Orbiter outgassing, thruster firings, and water dumps. In a discussion of the pressure environment, Shawhan and Murphy (Ref. 5) pointed to high payload bay outgassing rates that bring neutral pressure to 4 x 10^{-5} torr when the doors are closed in orbit. The gas cloud did not decrease significantly as the mission progressed evidenced by enhanced pressures when the payload bay was turned "Top-To-Sun" on the sixth day of the mission.

A Bennett Ion Mass Spectrometer utilizing retarding potentials was capable of separating the ambient ionospheric ions from those released by the Orbiter. Results reported by Grebowsky et al (Ref. 6) indicate that the expected O^+ ion is predominant, but that there is a significant amount of H_2O^+, NO^+ and CO_2^+. Narcisi et al (Ref. 7) on a subsequent shuttle flight, confirm the presence of high concentrations of H_2O^+ and noted that at times over one-half of the ambient O^+ has been converted to H_2O^+ by a reaction with water vapor in the Orbiter vicinity.

This molecular contamination is accentuated by thruster operation. The dominant neutral species

released by the N_2O_4/hydrazine attitude control thrusters is H_2O (32% mole fraction), N_2 (31%) and H_2 (17%). These neutrals act to deplete the surrounding plasma by means of recombination reactions. Narcisi et al, reported an order of magnitude decrease in ambient O^+ density when thrusters are fired. In a detailed report summarizing the observed effects of thrusters on the local plasma Murphy et al (Ref. 8) pointed to plasma turbulence, momentary increases in pressure and electron density as well as enhancement of broadband electrostatic noise that were associated with thruster events. Abrupt shifts in spacecraft potential were also noted with the admonition that events were extremely variable and depended on Orbiter orientation as well as the location of the thruster with respect to the sensor.

3. INTERACTIONS RESULTING FROM VEHICLE MOTION

3.1 The Plasma Wake

As can be seen in Table 1, the size and speed of the Orbiter enables it to produce a significant plasma wake. Several investigators have measured ion and electron energies and densities in this wake. Raitt and Siskind (Ref. 9) reported four orders of magnitude decreases in the electron density in the near wake and noted elevated temperatures of > 4000°K. They had difficulty in getting reliable temperature measurements because of the severe plasma turbulence present near the Orbiter which had not been seen on small spacecraft. Data reduction for the PDP Langmuir Probe is still in a preliminary state, but comparisons with Raitt's data (Ref. 9) from the VCAP investigation has provided a cross calibration point and qualitative agreement is good. Figure 2 shows the measured electron density as a function of attack angle from the PDP data. An angle of 0° corresponds to ram condition (payload bay pointing into velocity vector) and 180° is wake condition. Since these data have an absolute scale that is uncertain by a factor of 2 to 5, they are primarily noteworthy in that the 4 orders of magnitude depletions are also evident. Measurements made by the PDP on the RMS arm at distances 5 to 10 meters from the payload bay show depletions which are narrower in spatial extent and of only 2 to 3 orders of magnitude. Since maximum ram occurs at approximately sunrise and maximum wake at sunset, the correction for day/night density differences is unnecessary to first order.

Stone et al (Ref. 10) reported differential ion flow measurements made with the PDP while on the RMS. Ion streams up to 40° from the angle of attack and with 10% of the full ram current density were observed. These secondary streams had not been previously observed and are as yet unexplained.

4. VEHICLE CHARGING AND ASSOCIATED ELECTRIC FIELDS

Several experimentors have measured vehicle potential at F2 region altitudes and low inclination orbits. Shawhan and Murphy (Ref. 5) measured the potential of two spherical floating probes with respect to the Orbiter chassis and reported potentials of several volts with no electron gun operation. Murphy et al (Ref. 8) observed a dramatic shift in this vehicle potential accompanied by rapid changes in the electric field when thrusters fire.

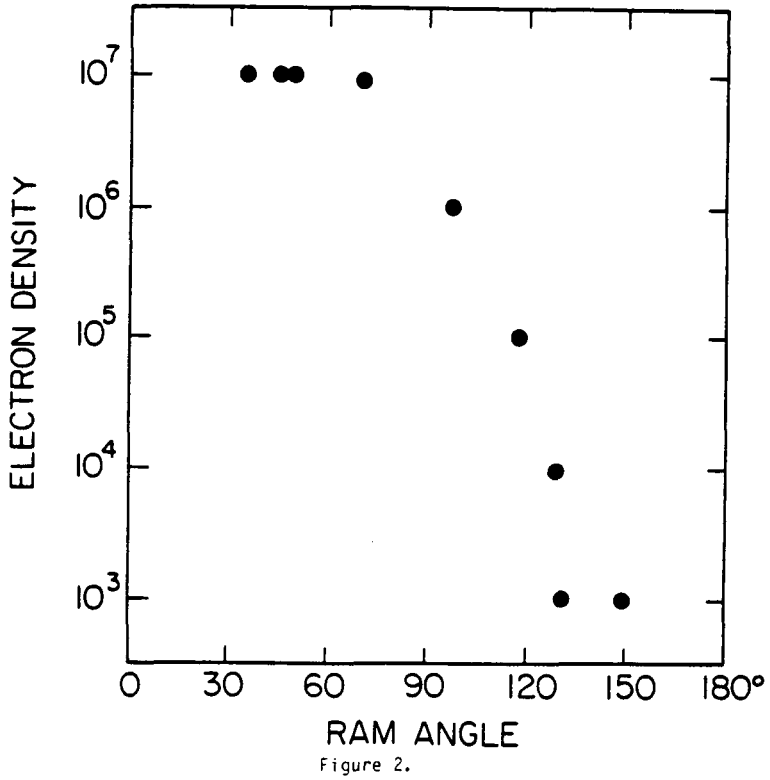

Figure 2.

Both Raitt and Siskind (Ref. 9) and Shawhan and Murphy (Ref. 5) reported the potentials measured by their plasma probes are consistent with V x B · L charging effects where L is the distance between the main engine nozzles (the principle exposed conducting surface) and the probes. Any passive charging due to energetic electrons or similar sources appeared to be negligible and was a minor perturbation to the overall V x B effect.

5. OPTICAL EMISSIONS

One of the surprises of the STS-3, was the discovery by Banks et al (Ref. 11) of the presence of a glow near the ram surface of the vehicle. This glow, which may be due to a chemical reaction near the surface of the vehicle, has a brightness of 10K Rayleighs or greater. The precise brightness depends on the wavelength of the emission. This glow is not entirely unprecedented and has been reported from Atmospheric Explorer (AE) observations at low altitude. Yee and Abreu (Ref. 12) in a detailed study attributed the AE results to an interaction of atomic oxygen with the vehicle surface.

Papadopoulos (Ref. 13) speculated that the shuttle glow was a critical ionization phenomena and proposed a series of measurements to determine if the shuttle behaves like an artificial comet.

PDP observations on STS-3 indicated a surface pressure enhancement on the ram side of the vehicle as great as a factor of 200 over ambient (Ref. 5). These enhanced pressures would be consistent with chemical interaction on or near the vehicle surface since they are 2 to 5 times greater than pressure enhancements in the normal supersonic shock front.

Recent flights of hand-held spectrometers should lead to confirmation of the Yee and Abreu, or Papadopoulos explanation or perhaps to a new theory. The glow seems most pronounced at lower altitudes and Banks et al (Ref. 11) also report that the glow is enhanced during and for a brief period following thruster operations.

6. ELECTROSTATIC NOISE

The most intense emission observed at any frequency by the PDP plasma wave receivers has been called Broadband Orbiter Generated Electro Static (BOGES) noise. The characteristics of this noise as briefly reported by Shawhan and Murphy (Ref. 4) are summarized in Table 3. The Table has been divided into two columns designated "above and "below" the presumed Lower Hybrid Resonance (LHR) frequency. The marked difference in degree of polarization of these electrostatic waves is illustrated in Figure 3. Note the sharp peaks in emissions above LHR at oblique angles to the magnetic field. The lower frequency waves show virtually no polarization. These observations were made while the PDP was being maneuvered on the RMS arm and were well out of the payload bay. At no time did the RMS move the PDP far enough from the Orbiter to see a noticeable decrease in the intensity of this noise. Figure 4 illustrates that BOGES noise is relatively intense anytime the PDP is out of the deep wake and the small variations seen are believed to be local geometry effects not related to the plasma density as measured at the PDP. Note also the data in Figure 4 indicate that high frequencies disappear first and reappear last as the PDP passes through the wake condition. This is generally true for all cases although there is considerable variability from orbit to orbit on the details. For example, if spectrograms like Figure 4 taken 12 hours apart are compared, there are considerable differences in the details of the behavior close to maximum wake. The only difference in these cases is the magnetic field direction at that point in the orbit which infers that the generation or propagation of these waves depends on the magnetic field between the source of the emission and the detector. Another characteristic of this noise is that it is well correlated with $\Delta N/N$ turbulence as measured with the PDP Langmuir Probe. Peak $\Delta N/N$ values of 1-3% are observed when the noise is most intense. This turbulence and associated noise is increased by thruster operations and water dumps.

Waves of a similar nature near and below the LHR frequency have been reported by Koskinen et al (Ref. 14) on the Swedish S29 Barium-GEOS Sounding Rocket.

Table 3

1. Broadband: approximately 30 Hz to 200 kHz with 50 to 70 dB variation over orbit
2. Peak spectral density occurs at 100-300 Hz and is approximately 80 dB $\mu V/M/(Hz)^{1/2}$
3. Well correlated with plasma turbulence as measured by $\Delta N/N$ spectrum
4. Has distinctly different character above and below LHR

Below LHR:	Above LHR:
- Noise present for virtually whole orbit but modulated by attitude and B-field orientation of orbiter	- Evidence of increasing polarization at higher frequencies
- No evidence of significant polarization	- Peak intensities occur when E-field sensor axis is 30-45 degrees from B-field alignment
- Seems to disappear completely only when PDP is in orbiter wake	- E-field intensity as high as .01 V/m at 100 kHz observed
- Primarily electrostatic	

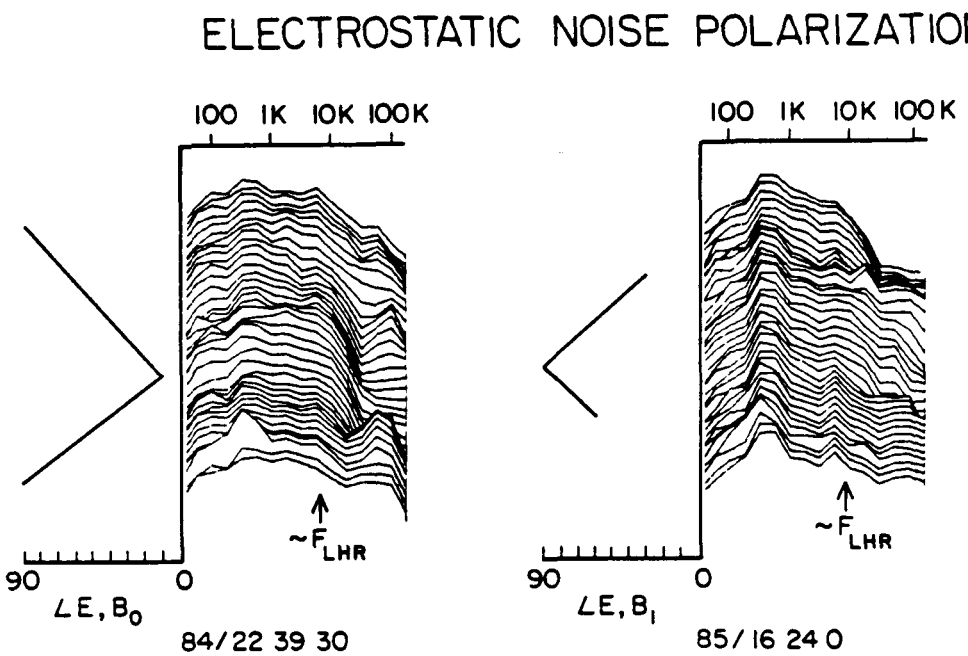

Figure 3

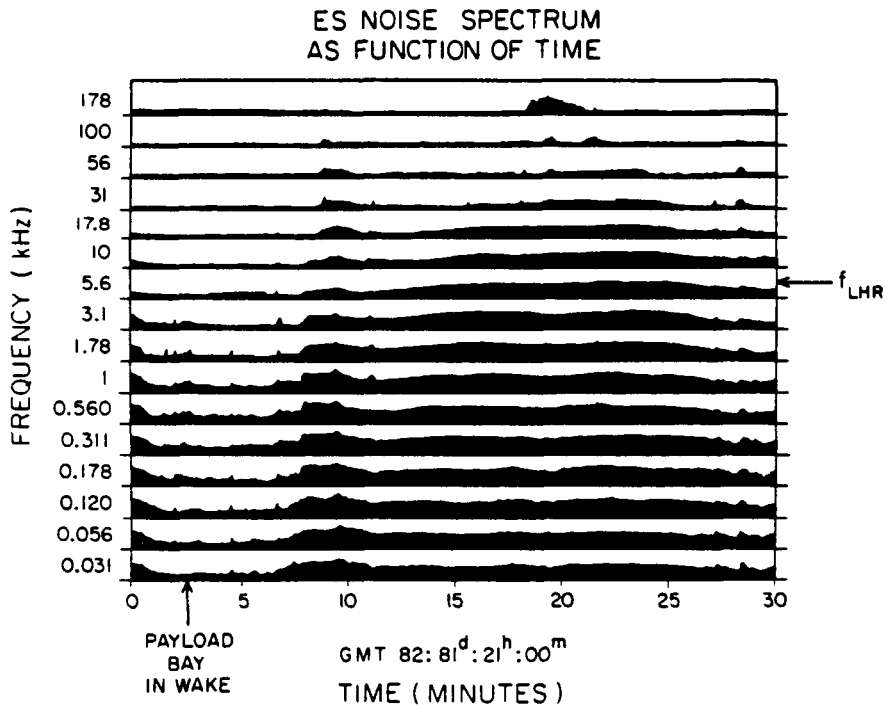

Figure 4

Several explanations are available (Ref. 14) for the phenomenon observed on this and other rocket flights, but they do not adequately explain all characteristics of the BOGES noise observed on the STS Orbiter. Kintner et al (Ref. 15) described ion acoustic noise during a chemical release which they attributed to ion-ion streaming between Cs^+ and ambient ions. Considering the observation of ion streams by Stone (Ref. 10) this may be a candidate for explaining the Shuttle induced noise. It is important to note that neither of these observations have a spectrum quite like the BOGES noise observed on STS-3. Much theoretical work is being done at present dealing with this problem. Papadopoulos (Ref. 16) is working to explain the noise spectrum by a critical ionization velocity phenomena driven by plasma instabilities. Initial agreement looks good and results will soon be published. Parrish et al (Ref. 17) have taken another approach seeking to use strong turbulence theory to produce hydrodynamic or ion acoustic waves. Present observational data may not be sufficient to choose the correct theory but additional experimentation on Spacelab-2 should lead to a better understanding of this phenomena.

7. SUMMARY

The flight of the Shuttle Orbiter through the ionosphere has proved to be an intersting plasma physics experiment. Discovery of the vehicle glow, secondary ion streams, BOGES noise and other associated phenomena are leading to an increased understanding of the F2 ionospheric physics and chemistry. The flights of Spacelab-1 (1983) and Spacelab-2 (1985) carry plasma diagnostics as well as electron and ion guns to stimulate plasma interactions and study Orbiter charging. Further theoretical work on the instabilities creating BOGES noise and the physics of the Orbiter wake will provide further guidance for the experiments on these missions and ultimately for a Space Plasma Lab mission in the 1987 time frame.

8. REFERENCES

1. Stone N H 1981, The aerodynamics of bodies in a rarefied ionized gas with applications to spacecraft environmental dynamics, NASA Technical Paper 1933, November.

2. Samir U et al 1983, The expansion of a plasma into a vacuum--basic phenomena and processes and applications to space plasma physics, submitted to Reviews of Geophysics and Space Physics, NASA MSFC-Space Science Lab Preprint #83-102.

3. Neupert W M 1982, OSS-1 a pathfinder mission for space science on shuttle, 21st Aerospace Science Meeting, AIAA Paper 83-0249.

4. Shawhan S D et al 1983, Measurements of STS-3 electromagnetic interference by the OSS-1 plasma diagnostics package, submitted for publicatio J. Spacecraft & Rockets, special STS-3/OSS-1 issue.

5. Shawhan S D & Murphy G B 1983, Plasma diagnostics package assessment of the STS-3 orbiter plasma environment, submitted for publication J. Spacecraft & Rockets, special STS-3/OSS-1 issue.

6. Grebowsky J M et al 1983, Measured thermal ion environment of STS-3, Fall 1983 AIAA Meeting on Shuttle Environment, AIAA-83-2597-CP.

7. Narcisi R et al 1983, Gaseous and plasma environment around the space shuttle, Fall 1983 AIAA Meeting on Shuttle Environment AIAA-83-2659-CP.

8. Murphy G B et al 1983, Perturbations to the plasma environment induced by orbiter's maneuvering thrusters, Fall 1983 AIAA Meeting on Shuttle Environment, AIAA 83-2599-CP.

9. Raitt W J et al 1983, Measurements of the thermal plasma environment of the space shuttle, submitted to Planet Space Sci., August 1983.

10. Stone N H et al 1983, Multiple ion streams in the near vicinity of the space shuttle, submitted to Geophys. Res. Lett.

11. Banks P M et al 1983, Observations of optical emissions from STS-3, Geophys. Res. Lett., February 1983.

12. Yee J H & Abreu V J 1982, Contamination observed with the atmospheric explorer satellite, Proc. SPIE.

13. Papadopoulos K & Ko K 1983, Electron energization and optical emissions in the space shuttle, Geophys. Res. Lett., submitted for publication.

14. Koskinen E J et al 1983, An observation of LHR noise with banded structure by the sounding rocket S29 Barium-Geos, J. Geophys. Res., Vol. 88, p. 4131-4136, May 1983.

15. Kintner et al 1980, The observation and production of ion acoustic waves during the trigger experiment, J. Geophys. Res., Vol. 85, #A10 p. 5071-5077, October 1, 1980.

16. Papadopoulos K 1983, Shuttle glow (the plasma alternative), SAI Report 84-147-WA.

17. Parrish J 1983, Private Communication, September 1983.

From: Proceedings of the USAF/NASA Spacecraft Environmental Interactions Technology Conference, U. S. Air Force Academy, Colorado Springs, CO, Oct. 4-6, 1983.

SUPRATHERMAL PLASMA OBSERVED ON THE STS-3 MISSION BY THE PLASMA DIAGNOSTICS PACKAGE*

W. Paterson, L. A. Frank, H. Owens,
J. S. Pickett, and G. B. Murphy
University of Iowa

S. D. Shawhan
NASA Headquarters

INTRODUCTION

Artificially produced electron beams have been used extensively during the past decade as a means of probing the magnetosphere (ref. 1), and more recently as a means of actively controlling spacecraft potential (ref. 2). Experimentation in these areas has proven valuable, yet at times confusing, due to the interaction of the electron beam with the ambient plasma. The OSS-1/STS-3 Mission in March 1982 provided a unique opportunity to study beam-plasma interactions at an altitude of 240 km. On board for this mission was a Fast Pulse Electron Generator (FPEG), which served as part of Utah State University's Vehicle Charging and Potential experiment. Measurements made by the Plasma Diagnostics Package (PDP) while extended on the Orbiter RMS show modifications of the ion and electron energy distributions during electron beam injection.

In this paper, some of the observations made by charged particle detectors are discussed and related to measurements of Orbiter potential. The paper is divided into three sections. A brief description of several of the PDP instruments appears first, followed by a section describing the joint PDP/FPEG experiment. The third section consists of observations made during electron beam injection.

INSTRUMENTATION

The PDP carries a wide range of instruments for the measurement of pressure, waves, fields, and particles. A discussion of these instruments and some of the preliminary results of the mission can be found in Shawhan et al. (ref. 3). Of interest for this discussion are the charged particle detectors, and to a lesser extent, instruments used to measure electric potential and the geomagnetic field in the vicinity of the Orbiter.

The Low Energy Proton and Electron Differential Energy Analyzer (LEPEDEA) is a curved plate detector capable of detecting ions and electrons with energies between 2 eV and 36 keV. It is nearly identical to instruments flown on ISEE-1 and ISEE-2. The energy resolution of LEPEDEA is $\Delta E/E = 0.16$, and 1.6 sec. is required for a complete energy scan. The LEPEDEA fields of view are shown in figure 1. The seven detectors are sampled simultaneously and together have a field of view of 6 degrees by 162 degrees.

*This work is supported by NASA/Lewis Research Grant No. NAG3-449

An electron fluxmeter is also included in the PDP for detection of electrons. This instrument samples the electron flux independent of energy ten times per second. The fluxmeter is directed opposite to the LEPEDEA. It has a wide field of view with low angular resolution.

Electric fields were measured by two 20 cm spherical probes separated by 1.6m. The average potential between these spheres was measured relative to Orbiter ground with a range of ±8.2v. When the PDP was extended on the RMS, this potential was a measure of the plasma potential in the vicinity of the PDP.

A triaxial fluxgate magnetometer was used to measure magnetic fields. The magnetometer sampled the magnetic field 10 times each second, along each of its 3 axes with a resolution of ±12 mgauss.

THE JOINT PDP/FPEG EXPERIMENT

Joint operations between the PDP and the FPEG were conducted while the Orbiter was in a nose-to-sun attitude with a roll rate of twice per orbit (see figure 2). For the experiment discussed in this paper, the FPEG emitted a 50-mA, 1-keV, unmodulated electron beam. A total of eleven emissions occurred under both daytime and nighttime conditions and at various injection pitch angles with each emission approximately fifteen minutes in duration. During these injections, the PDP was deployed on the Orbiter RMS and moved about the Orbiter in an effort to locate the beam.

The primary instrument for location of the beam was an electron fluxmeter located on the opposite side of the PDP from the LEPEDEA. During the search for the beam, the fluxmeter was pointed downward toward the FPEG aperture in the Orbiter bay which left the LEPEDEA looking away from the electron beam. Because of this orientation, the LEPEDEA did not detect primary beam electrons. At times, however, the PDP was rotated through 90 degrees about its spin axis (see figure 1) which allowed the LEPEDEA to view a range of particle pitch angles including primary particles.

OBSERVATIONS

Because of changing Orbiter attitude (twice per orbit roll rate) and variations in the geomagnetic field over the course of an orbit, a wide range of injection pitch angles were observed. Calculations by J. Sojka of Utah State University show that for injection pitch angles greater than about 60 degrees (depending on the precise beam-orbiter orientation), the beam intercepted the Orbiter surface. At angles less than this the beam escaped. Qualitative analysis of charged particle and potential measurements made by the PDP support this analysis.

Ambient electrons (photoelectrons) were detected with energies up to about 80 eV during the day and 10 eV at night, while ions were seen at energies principally below 10 eV during both day and night. During beam injection at angles less than 30 degrees, intense fluxes of electrons were detected at energies up to the primary beam energy of 1 keV. Virtually no ions were seen at these times. Enhanced electron fluxes were observed at all points accessible to the PDP. However, due to the limited reach of the RMS, no measurements were made at distances greate

than 7m from the beam. For beam injection, at angles greater than 60 degrees, the measured ion and electron fluxes often resembled the flux seen with the beam off.

Measurements of Orbiter potential during small angle injection also differed from the ambient case. When the beam was off, the Orbiter potential relative to the nearby plasma remained $< \pm 8.2$v consistent with $V \times B \cdot L$ (ref. 3). When the beam was injected at less than 30 degrees, the potential was offscale and positive, and dropped below the maximum measurable value of 8.2v only at the maximum distance from the beam of 7m. Potentials during large angle injections were generally nearer to those measured with the beam off.

The observations tend to support the claim that the beam did escape from the near vicinity of the Orbiter for small angle injection, but did not at larger angles. The enhanced electron flux and elevated potential associated with small angle injection may be due to escape of the beam. If this is so, the large angle conditions which were so similar to ambient conditions could be due to the electron beam impacting the Orbiter rather than escaping. In this case, almost all of the beam current is collected so that the disturbance is localized and the Orbiter does not need to charge.

Figure 3 shows the measured flux during one of these rotations which took place at a distance of 7m from the center of the beam. Since this distance is roughly twice the gyroradius of a 1 keV electron travelling perpendicular to the magnetic field, these measurements must be of electrons outside of the primary beam. The angles shown in figure 3 are the pitch angles of electrons as they were detected by the LEPEDEA. Angles greater than 90 degrees correspond to electrons travelling down the field lines from the direction in which the beam was injected. Angles less than 90 degrees indicate electrons moving up the field in the same direction as the outgoing beam. Although pitch angles less than 30 degrees and greater than 140 degrees were not sampled, this figure seems to show a net return of electrons along the field lines from the direction in which the beam was injected indicating that more current returns from the upper hemisphere during upwards injection than from the lower.

Based on this preliminary analysis of measurements made during electron beam emission, it appears that the electron beam did escape from the Orbiter. These escapes induced positive Orbiter potentials, and were associated with enhanced fluxes of electrons. During escape of the beam, there is evidence that there was a net flow of electrons along the magnetic field from the direction in which the beam was injected.

REFERENCES

1. Winckler, J. R.: The Applications of Artificial Electron Beams to Magnetospheric Research. Rev. Geophys. Space Phys., 18, 659, 1980.

2. Pedersen, A.: Plasma Diagnostics by Electron Guns and Electric Field Probes on ISEE-1. Artificial Particle Beams in Space Plasma Studies, (B. Grandal, ed.), Plenum Press, New York.

3. Shawhan, S. D.; Murphy, G. B.; and Pickett, J. S.: Plasma Diagnostics Package Initial Assessment of the Shuttle Orbiter Plasma Environment. Accepted J. of Spacecraft and Rockets, 1983.

LEPEDEA FIELDS-OF-VIEW

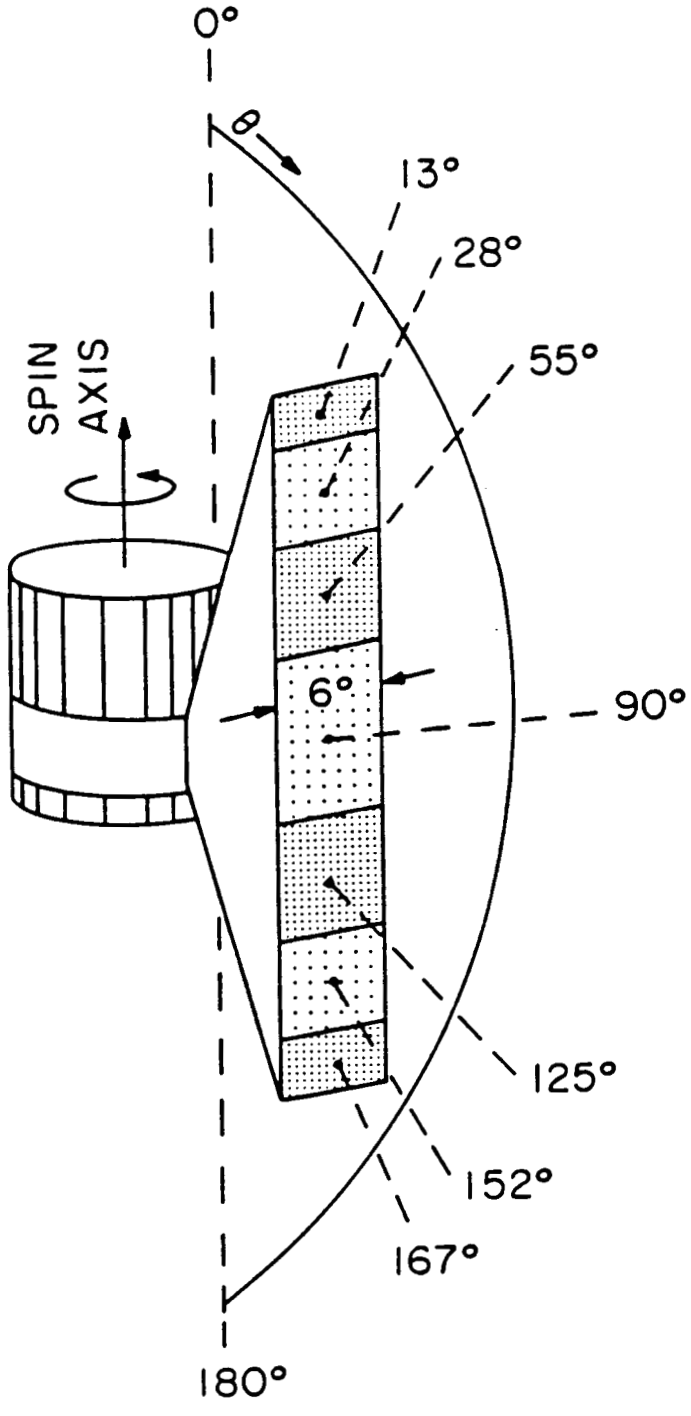

Figure 1

STS-3 ORBIT ATTITUDE
MARCH 24, 1982

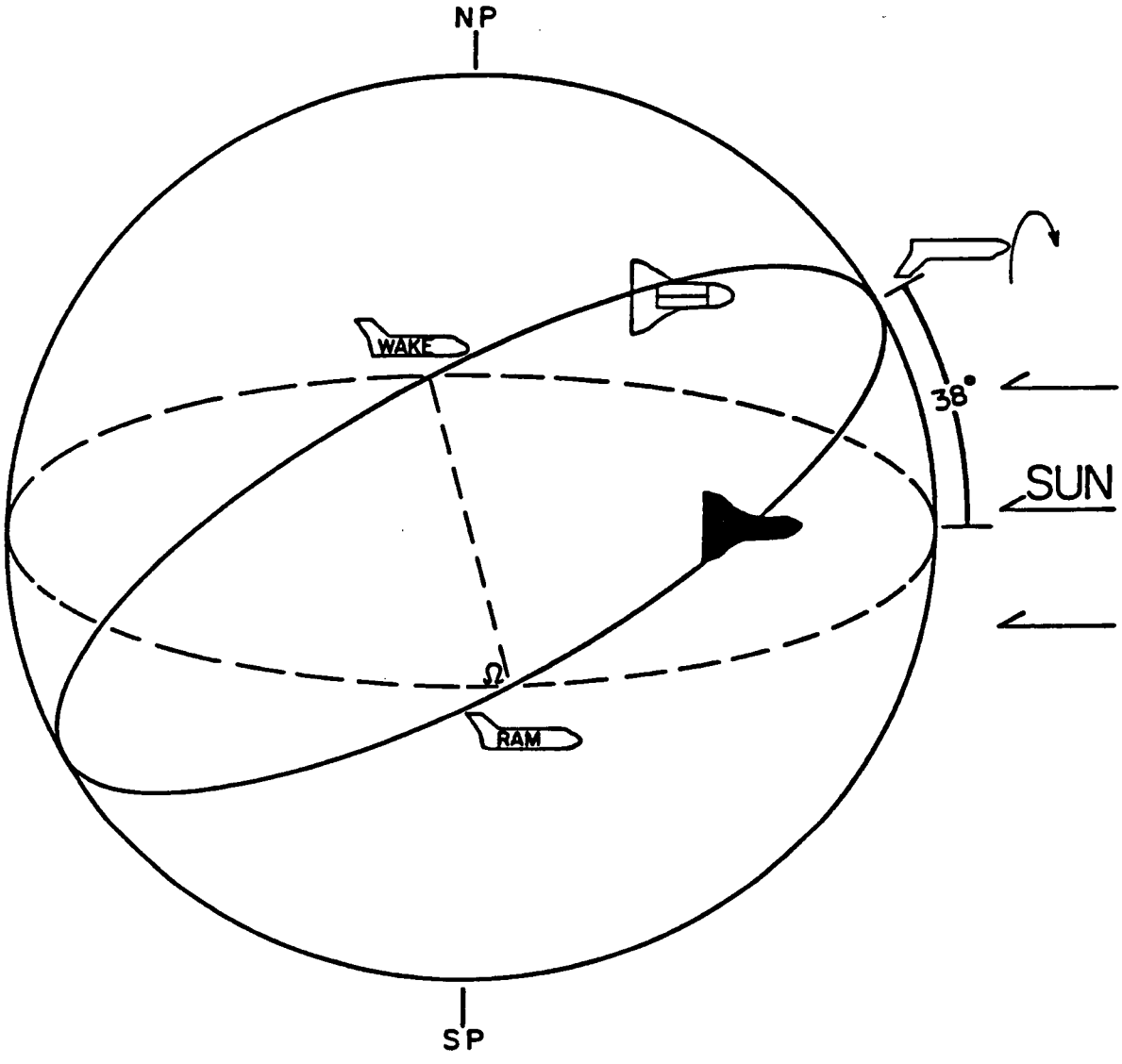

NOSE TO SUN 2x ORB RATE ROLL

Figure 2

Electron flux 7m from the beam (2 eV < E < 36 keV).

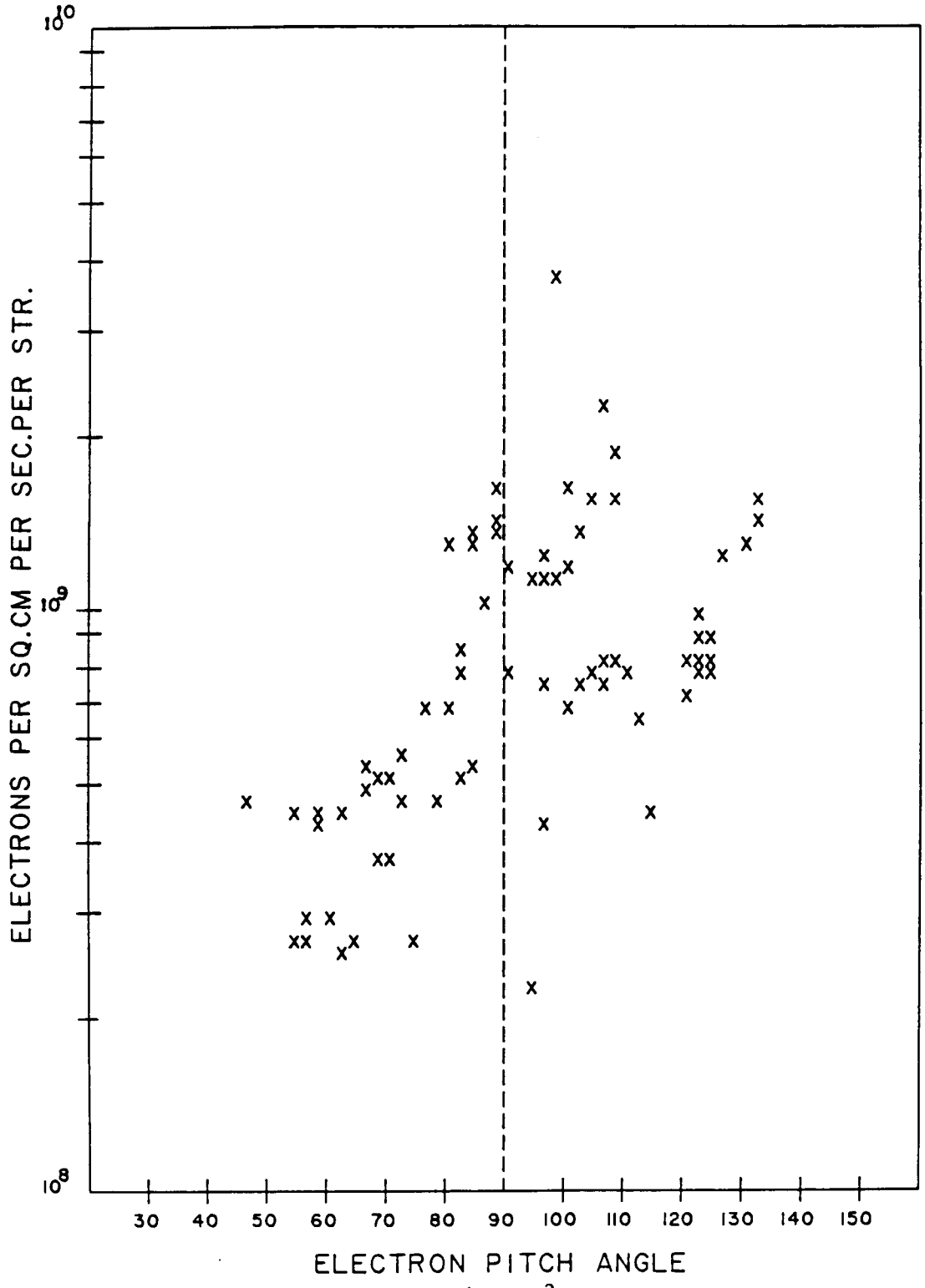

Figure 3

From: Proceedings of the USAF/NASA Spacecraft Environmental Interactions Technology Conference, U. S. Air Force Academy, Colorado Springs, CO, Oct. 4-6, 1983.

ELECTRON AND ION DENSITY DEPLETIONS MEASURED IN THE STS-3 ORBITER WAKE*

G. B. Murphy and J. S. Pickett
University of Iowa

W. S. Raitt
Utah State University

S. D. Shawhan
NASA Headquarters

INTRODUCTION

The third Space Shuttle flight on Columbia carried instrumentation to measure thermal plasma density and temperature. Two separate investigations, the Plasma Diagnostics Package (PDP) and the Vehicle Charging and Potential Experiment (VCAP), carried a Langmuir Probe, and the VCAP also included a Spherical Retarding Potential Analyzer (SRPA). The Langmuir Probe on the PDP made measurements while the PDP was attached to the pallet in the Orbiter bay and while the PDP was articulated by the RMS. Only those measurements made while the PDP is in the payload bay are discussed here since the VCAP instrumentation remains in the payload bay at all times and the two measurements are compared.

Figure 1 illustrates the location of the PDP and VCAP instrumentation on the science payload pallet.

The principle thrust of this paper is to discuss the wake behind a large structure (in this case the Space Shuttle Orbiter) flying through the ionospheric plasma. Much theoretical work has been done regarding plasma wakes (ref. 1) and to a certain extent laboratory plasmas have provided an experimental and measurement basis set for this theory. The instrumentation on this mission gives the first data taken with a large vehicle in the ionospheric laboratory.

First, the PDP Langmuir Probe and its data set will be presented, then the VCAP Langmuir Probe and SRPA with associated data. A discussion of agreement between the two data sets is then followed by some other PDP data which infers an even lower wake density.

Lastly, conclusions, caveats and a description of future work which will further advance the measurement techniques and data set are put forth.

PDP LANGMUIR PROBE RESULTS

The PDP Langmuir Probe is a 6 cm diameter gold-plated sphere which is operated in two modes, the $\Delta N/N$ mode and the swept mode. The swept mode which is of concern

*This work is supported by NASA/Lewis Research Grant No. NAG3-449

The science pallet configuration on STS-3 showing the location of the instrumentation in question.

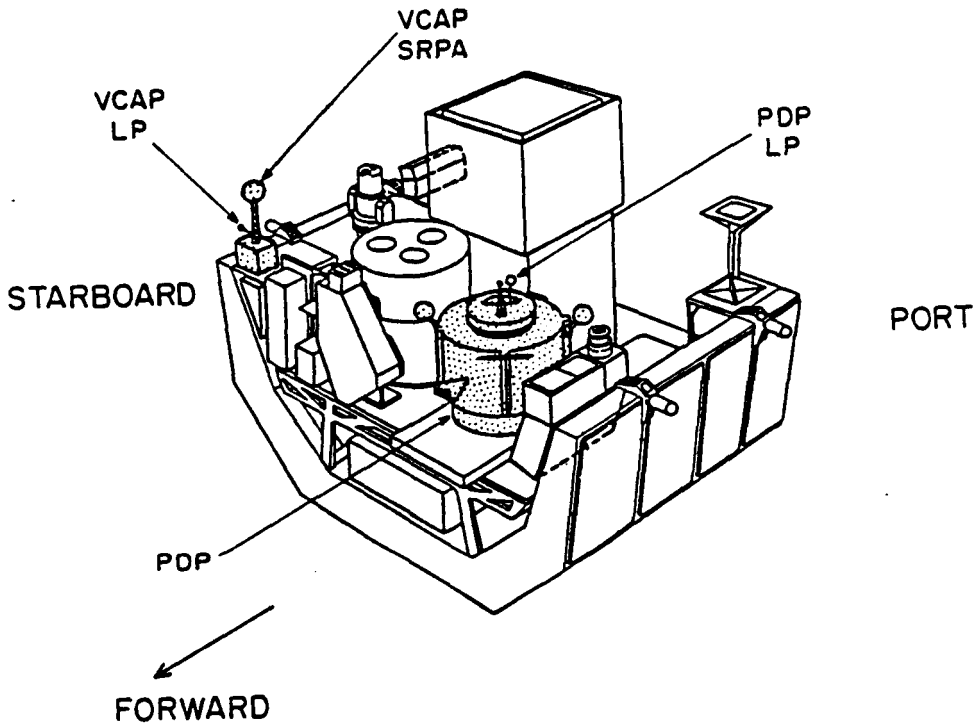

Figure 1

here is a 120 step voltage sweep which lasts 1.2 seconds and is executed 5 times per minute. The nominal density range of the probe is approximately 5×10^2 to $5 \times 10^6 /cm^3$, the precise sensitivity depending on temperature. Operating in this mode, the Langmuir Probe has a current voltage characteristic whose slope is proportional to $1/T_e$ and which has a "knee" in the curve proportional to N_e.

There are two limitations to the PDP Langmuir Probe measurements. The first occurs when the plasma is too dense to really see the entire knee of the curve resulting in instrument saturation and an underestimate of density. The second occurs when the plasma temperature is too high and density too low to get a reliable slope resulting in only an upper bound on density and lower bound on temperature.

Figure 2 illustrates the electron density and temperature for one orbit as a function of vehicle attitude. (The data is repeated for a second orbit to provide clarity for the graph and illustrate a periodicity which is real). The vehicle attitude is described by θ_1 and θ_2 which are illustrated at the top of the figure. Maximum wake occurs when the vehicle flies tail first with the plasma ramming into the Orbiter belly (e.g. GMT 83:20:48). At this point in time, the vehicle is flying a nose-to-sun attitude with a 2 times orbit roll. (See figure 2 in the paper "Suprathermal Plasma Observed on the STS-3 Mission by the Plasma Diagnostics

Package, by Paterson et al. (ref. 2) in this issue for a description of this ttitude.) This results in a once per orbit ram/wake cycle which is evident in figure 2 by the e^- density and neutral density (pressure) measurements.

Several important observations summarize figure 2:

1. Although density is near ambient while the paylaod bay is neither pointing directly into the velocity vector or into the wake, there is evidence that the density may be 2 to 10 times ambient when the bay points close to the velocity vector. The probe saturates making reliable measurement above 2×10^6 difficult. The region cross hatched in figure 2 is where this higher density regime is encountered.

2. Density decreases rapidly as the Orbiter rolls into wake condition.

3. The minimum reliable measurement of density with the PDP probe is approximately $5 \times 10^2/cm^3$. At least another order of magnitude decrease is required to pull the sweep totally offscale which is subsequently observed to happen. The sweep remains offscale for approximately 25 minutes centered around 83:20:48.

4. During all non-wake conditions, the temperature remains relatively constant at about 1000° (±30%).

5. Temperature rises rapidly as density decreases.

6. The highest reliable temperatures occur at 6000°K. However, the trend continues suggesting temperatures in excess of 7000°K in the deep wake.

It is also worthwhile to note that in near ram condition the neutral density (pressure) was almost two orders of magnitude above ambient ionospheric conditions and fell below 10^{-7} torr (the instrument sensitivity limit) during wake conditions.

THE VCAP LANGMUIR PROBE AND SRPA

Data on the characteristics of the ambient thermal plasma are extracted from the probes using a technique similar to that described by Raitt et al. (ref. 3). This AC technique employed for the probes enables direct measurement of the second derivative of the SRPA current-voltage characteristic and the first derivative of the LP current-voltage characteristic.

The SRPA signal is obtained by adding two sinusoidal AC signals (at 8.5 kHz and 10.7 kHz) to a sawtooth sweep voltage. The probe current is passed through a narrow band amplifier that selects the difference freqency of 2.2 kHz, which is a measure of the non-linearity of the probe current-voltage characteristic, and results in a signal proportional to the second derivative of the current-voltage characteristic. Two ac current ranges are available: one from -76 dB to -24 dB and the other from -40 dB to 0 dB relative to 10^{-7} amp rms. Each successive sweep of the probe alternates between the two ranges. Since the sweep period is 17 seconds the complete dynamic range is covered each 34 seconds.

Summary of PDP Langmuir Probe electron density and temperature as function of vehicle attitude. Neutral pressure measurements are included for reference. The cross-hatched areas are where the probe sweep saturates and the routine used to calculate N_e under-estimates density by as much as an order of magnitude.

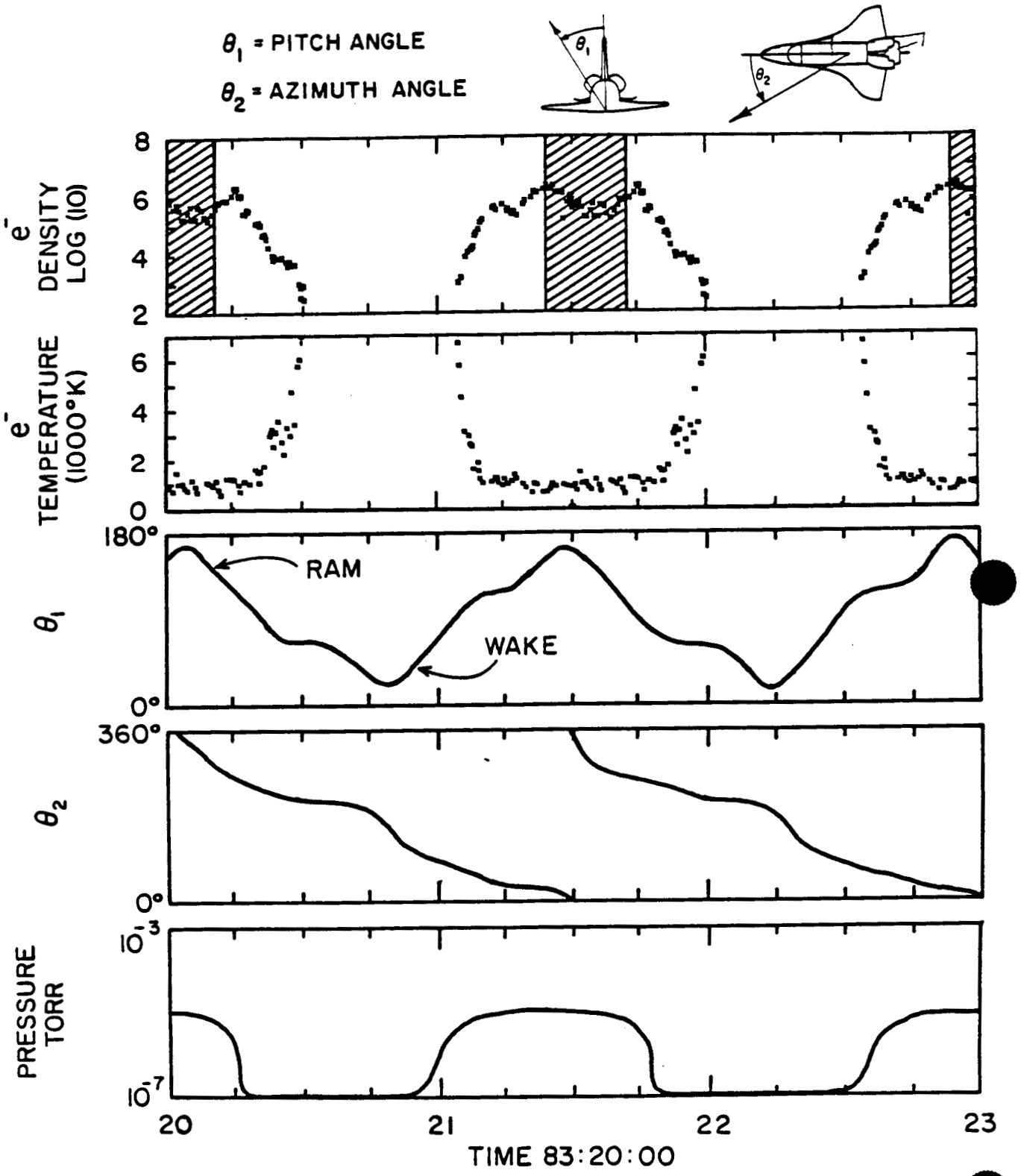

Figure 2

The LP has only one AC signal (at 3.2 kHz) added to the sweep voltage. The amplitude of the alternating component of the probe current derived by using a narrow band amplifier tuned to 3.2 kHz enables the first derivative of the current voltage characteristic to be measured directly. A single dynamic current range, from -80 dB to +10 dB relative to 10^{-6} amp rms, is used for all sweeps. The range of the sawtooth voltage is from -2 V to +3 V, the period and phase of the sweep being synchronized to the SRPA sweep.

Figure 3 illustrates data taken under similar conditions as that taken by the PDP, although at a different time. In this case the vehicle attitude is different, but the same angles are used to characterize the direction of the velocity vector. The addition of the dark bar on this figure serves to show when day and night occur during the orbit.

The results of the Langmuir Probe (dotted line) and SRPA (solid line) generally confirm results of the PDP Langmuir Probe. VCAP Langmuir Probe temperatures are not plotted, but the following results are notable:

1. Close to ambient (1000°K) ionspheric temperatures are measured during non-wake condition.

2. As the Orbiter rolls into wake, a turbulence at all frequencies adds noise to the 3.2 kHz LP first derivative, but measurements indicate an increase in temperature to beyond 4000°K.

VCAP LP densities indicate the following:

1. An upper bound of electron density when the paylaod bay faces close to the velocity vector is $10^7/cm^3$.

2. Density during wake conditions drops to below the instrument sensitivity of 10^4 e/cm^3.

The SRPA measurements are difficult to interpret since the peak in the second derivative as a function of sweep voltage for the dominant ionospheric O^+ ion is often contaminated by locally produced H_2O^+ and NO^+. When the O^+ peak is clearly observable, several observations prevail:

1. Densities consistent with ambient ionospheric O^+ are observed for most conditions which shall be referred to as non-wake.

2. $>$ 2 orders of magnitude depletion occurs in the near wake.

ADDITIONAL EVIDENCE FOR LARGE DEPLETION

Additional evidence for a many order of magnitude depletion in the electron density in the near wake is provided by what amounts to a sounder experiment. Recall that the VCAP SRPA is excited with a signal at 8.5 and 10.7 kHz. The PDP contains a 16 channel (± 15% bandwidth) spectrum analyzer capable of detecting electrostatic or electromagnetic waves over a frequency range from 30 Hz to 178 kHz. The instrument has a saturation of approximately 1 V/m electric field amplitude and a usable dynamic range of about 95 dB.

Summary of VCAP Langmuir Probe (dotted line) and SRPA (solid line) results as a function of vehicle attitude.

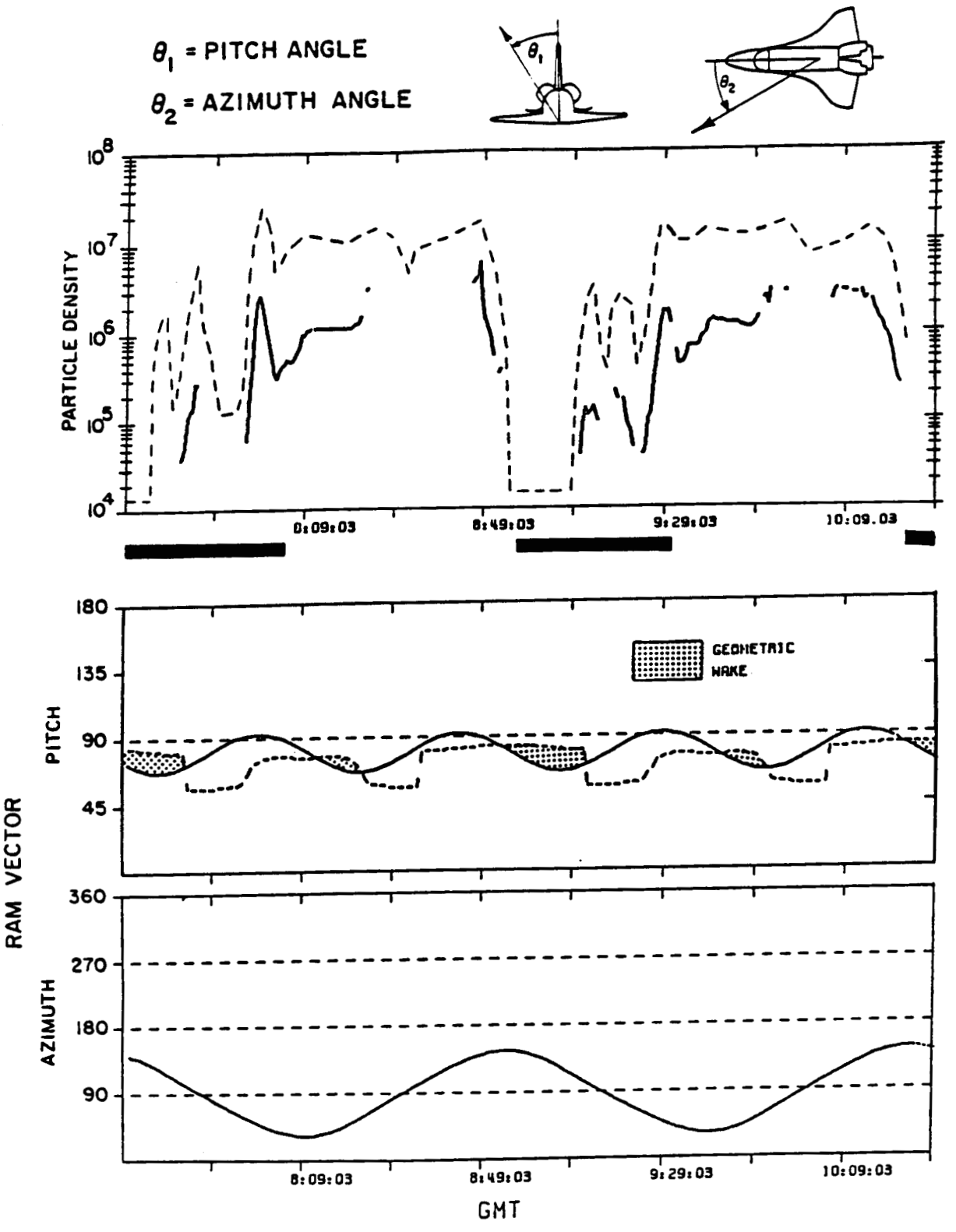

Figure 3

During most of the orbit, the Spectrum Analyzer output is dominated by broad- and orbiter generated electrostatic noise, (ref. 4) thruster firings or other events. Figure 4 illustrates that as the wake boundary is approached, the electrostatic noise disappears in all channels simultaneously and as the payload bay is immersed deeper in the orbiter's wake a signal in the 10 kHz channel grows to a point of dominance in the spectrum. This in fact is the VCAP SRPA signal. As the density drops so that the plasma frequency nears or drops below 10.7 kHz, this signal can propagate to the PDP sensor. Detailed calculations and modeling are being done taking field strengths and sensor separation into account, but preliminary work suggests that although the PDP Langmuir Probe infers densities, $< 50/cm^3$, the density probably drops at least another order of magnitude to $< 5/cm^3$. This would be approximately six orders of magnitude of plasma depletion in the near wake from that measured under ram condition.

The VLF electric field spectrum showing the increasing intensity of the received SRPA signal.

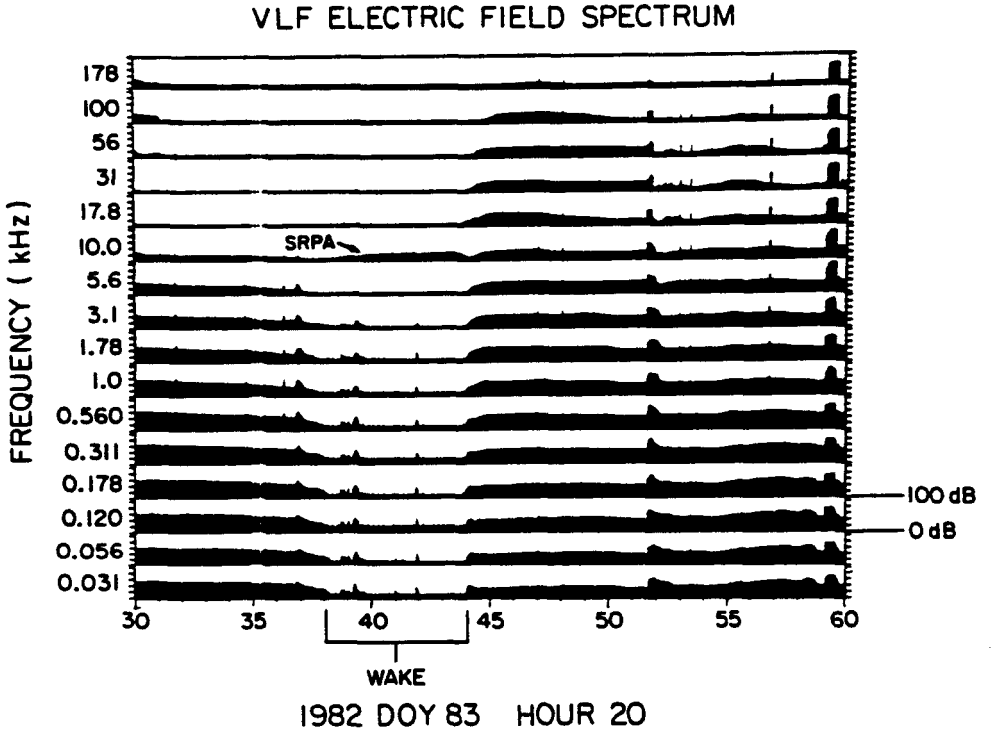

Figure 4

SUMMARY

Although measurements are still in a primitive state, several conclusions can be drawn from the STS-3 PDP and VCAP data.

1. Ram conditions seem to result in a higher than expected electron density.

2. Density depletions of at least 4 orders of magnitude in the wake plasma are observed and there is evidence to suggest this depletion may be as high as six orders of magnitude.

3. Effective temperature measured by the thermal plasma probes indicate an increase in electron temperature in the wake to > 6000°K.

4. The thermal ions are excluded rapidly as the orbiter bay rolls into wake and only those locally produced H_2O^+ and NO^+ are measurable.

5. Both LP's and the SRPA indicate a degree of plasma density or velocity turbulence which peaks in the transition region between ram and wake.

Several concerns about these measurements are that: first, the VCAP probes' outputs are often contaminated by the turbulence which causes bias in the data; second, the ability of the PDP LP to measure density and temperature reliably beyond a certain limited range is questionable; and third, whether the sounder experiment setup between the VCAP SRPA and PDP Spectrum Analyzer is "calibratable" is still an open question.

The first concern is being worked and there is confidence that corrections for the turbulence can be computed. Recall that the PDP LP has a $\Delta N/N$ mode which can provide upper bounds on the turbulence within a given frequency band.

The second concern, which applies to a lesser degree to the VCAP LP, is harder to solve. As the density decreases and temperature increases, the size of the probe in relation to a debye length and thermal electron gyroradius changes drastically. This means that approximations used to derive temperature and density are no longer valid and new formulations must be used. A long-term research effort is underway to better understand the behavior of swept probes in these extreme regimes. (See ref. 5 for a description of the probe theory). Meanwhile, effort has been made to include data in this report derived from regimes where approximations hold. Thus, the densities and temperatures are probably good to a factor of two.

It is encouraging to note that when comparisons are made to measurements made by the DE satellite, which flew through the same altitude and latitude regime within the same day, general agreement is found. The DE data show dayside conditions of $N_e = .9 - 1.1 \times 10^6/cm^3$ and $T_e = 1500° - 2000°$ while the PDP and VCAP data taken dayside out of wake and also out of maximum ram condition indicate $N_e = 2$ to $10 \times 10^6/cm^3$ and $T_e = 1000°$ (±30%).

The third concern is currently being worked and if the "sounder" is calibratable, it should provide valuable input for theory.

The fact that elevated temperatures are observed in the near wake of a spacecraft is not without precedence. Samir et al. (ref. 6) found evidence for elevated electron temperatures in the wake of Explorer 31, a much smaller vehicle than the Shuttle Orbiter.

Additional measurements by the PDP and VCAP instruments will be made on Spacelab-2 where detailed experiments have been designed to study the structure of the wake out to approximately one kilometer from the vehicle.

REFERENCES

1. Samir, U.; Wright, K. H., Jr.; and Stone, N. H.: The Expansion of a Plasma into a Vacuum--Basic Phenomena and Processes and Applications to Space Plasma Physics. Submitted to Reviews of Geophysics and Space Physics Space Science Laboratory, MSFC, Preprint #83-102.

2. Paterson, W.; Frank, L. A.; Owens, H.; Pickett, J. S.; Murphy, G. B.; and Shawhan, S. D.: Suprathermal Plasma Observed on the STS-3 Mission by the Plasma Diagnostics Package. Submitted to Proceedings of the Spacecraft Environmental Interactions Conference, October 4-6, 1983.

3. Raitt, W. J.; Dorling, E. B.; Sheather, P. H.; and Blades, J.: Ionospheric Measurements from the ESRO-4 Satellite. Planet Space Sci., 23, 1085-1101, 1975.

4. Shawhan, S. D.; Murphy, G. B.; and Pickett, J. S.: Plasma Diagnostics Package Initital Assessment of the Shuttle Orbiter Plasma Environment. Accepted for publication, December 1983, J. Spacecraft and Rockets.

5. Rubinstein, J. and Laframboise, J. G.: Theory of a Spherical Probe in a Collisionless Magnetoplasma. Phys. Fluids 25 (7), July 1982, 1174-1182.

6. Samir, U. and Wrenn, G. L.: Experimental Evidence of an Electron Temperature Enhancement in the Wake of an Ionospheric Satellite. Planet. Space Sci., 1972, Vol. 20, 889-904.

From: Proceedings of the AIAA Shuttle Environment and Operations Meeting, Washington, DC, Oct. 31-Nov. 2, 1983

PERTURRATIONS TO THE PLASMA ENVIRONMENT INDUCED BY THE ORBITER'S MANEUVERING THRUSTERS

83-2599

ld R. Murphy
earch Assistant
Department of Physics & Astronomy
Iowa City, IA 52242

Stanley D. Shawhan
Professor of Physics
Department of Physics & Astronomy
Iowa City, IA 52242

Jolene S. Pickett
Research Assistant
Department of Physics & Astronomy
Iowa City, IA 52242

Abstract

A summary of observations made by the Plasma Diagnostics Package (PDP) aboard STS-3 in March 1982 with particular regard to thruster induced effects is presented. Ionospheric chemistry and its relation to plasma hole formation is discussed and comparisons made with previous work which has modeled and measured effects from much larger exhaust masses. Principle attention is focused on local effects observed on or near the Orbiter and on how these disturbances can upset astronomical and space plasma measurements. Since various operational profiles for attitude control are available, several suggestions are offered to help the future experimenter plan a scenario minimizing the data contamination.

Introduction

Effects of rocket exhaust on the atmosphere and ionosphere have been, at various times, a concern from the earliest days of rocket flights. Most recently, attention has been given to the chemical effects of these plumes particulary in F1 and F2 regions. An excellent review of work to date in this field is given by Mendillo[1] where studies of the effects from shuttle OMS engine circularization burns are discussed. Since the Orbiter's primary and vernier Reaction Control System (RCS) thrusters are much smaller than the OMS, it is tempting to assume that they would have no appreciable effect on the ionospheric environment. Such is not the case and data presented in this paper shows that plasma perturba-

FIGURE 1.
SPACE SHUTTLE REACTION CONTROL SUBSYSTEM PLUME VECTORS

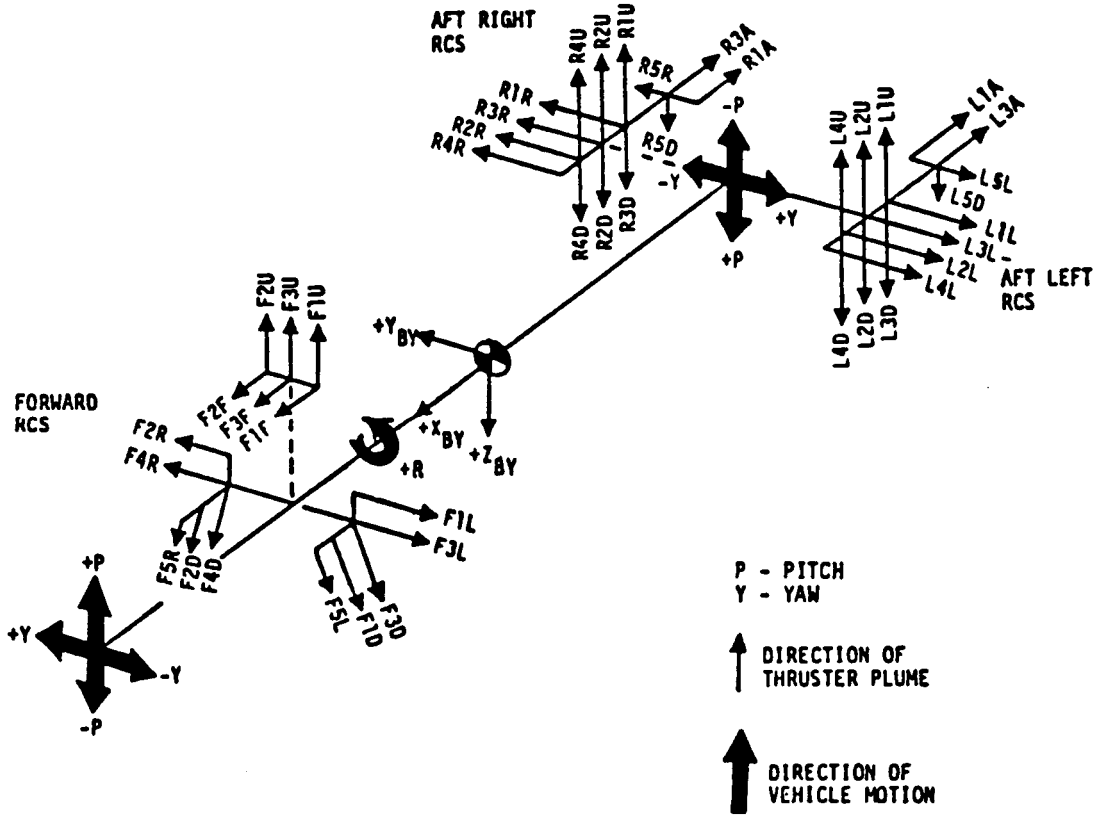

RCS CONSISTS OF 1 FORWARD MODULE AND 2 AFT RCS SUBSYSTEMS IN PODS
38 MAIN THRUSTERS (14 FORWARD, 12 PER AFT POD)
6 VERNIER THRUSTERS (2 FORWARD AND 4 AFT)
PROPELLANTS: OXIDIZER, N_2O_4; FUEL, MMH

tions induced by these small engines can be noticeable and in some cases at least disruptive to measurements.

The discussion is divided into five sections. The first describes the characteristics of the 44 RCS thrusters, their emission patterns, emission rates and exhaust constituents both neutral and charged species. The second gives an overview of the PDP/STS-3 mission profile and reviews the F2 region ionosphere characteristics. The third is the primary observation section. Data collected by the PDP during a large number and variety of thruster events is presented and a tentative hypothesis explaining these effects is offered. References to observations from other experiments which are consistent with these data are also discussed. Section four discusses the chemical reactive potential of these plumes, suggests several modeling problems, and describes experiments which will be carried out on the Spacelab-2 mission. Part five of the paper summarizes the impact of thruster firings to the astronomical or space plasma experiment. Examples of thruster operational scenarios are presented and suggestions for minimizing the impact to these experiments are given.

The STS Orbiter RCS Thrusters

The Reaction Control System (RCS) or attitude control system aboard the Orbiter consists of 38 primary (870 lb.) thrusters and 6 vernier (25 lb.) thrusters. Figure 1 shows the location and designation of these 44 engines. Note that the arrows indicate the direction of thrust and that the short arrows are the verniers. Note also that all verniers point down or sideways, that is, they have no component of their thrust along the Orbiter -Z axis. Several possible operational plans are available for these thrusters and the details are determined by the attitude maneuver required as well as the setting of the Digital Auto Pilot (see last section of this paper).

Two variable sets ultimately determine the effect these thrusters have on the local ionospheric environment. The first is the amount of mass ejected and its direction and velocity of flow; the second is the neutral and ion composition and temperature. Table 1 presents the mass emission characteristics of the vernier and primary engines, as well as sample data from flight 3 indicating typical firing characteristics. The fact that typical vernier mass emission is greater than that of the primaries is due to the fact that the verniers are less efficient at moving the Orbiter because optimal torques are not used and thus more net mass ejection is required. It should be emphasized, however, that the mass ejection rate is much less and therefore the corresponding time of thrust pulses greater. This will be an important consideration operationally. Figure 2 illustrates the mass ejection profile assuming an axially symmetric flow and point source. In reality because of the location of the thrusters, an appreciable amount of exhaust can bounce off Orbiter surfaces including the engine pods, tail and wings.

The rest of the information necessary to characterize the plumes is contained in Table 2. The mole fraction of each major species of neutral and ion is given, as well as the total number of molecules in the typical firing described in Table 1. Although the fraction of ionized exhaust is very low, there is still an appreciable number of ion-electron pairs present when compared with the 10^{20}e/km^3 which is a typical F2 region plasma density.

STS-3 Mission at 240 km

The Plasma Diagnostics Package was carried aboard STS-3 as part of NASA OSS-1 payload. Designed to measure DC electric and magnetic fields, AC electrostatic and electromagnetic waves, particle energies, fluxes and distribution functions, it was used on both the pallet and as

TABLE 1.
MASS EJECTION CHARACTERISTICS FOR VRCS AND PRCS THRUSTERS

	Average Mass Ejected	Average Number of Firings in Event	Duration of Event
Vernier (VRCS) 40.8 g/sec			
*Typical (Attitude Hold)	163g	2	2 sec
Longest (Maneuver)	2100g	14	30 sec
Primary (PRCS) 1419.8 g/sec			
Typical (Attitude Hold)	114g	1	80 msec
Longest (Manuever)	682g	5	720 msec

*Typical firings based on analysis of all available STS-3 thruster event data. This included several different attitudes and DAP settings.

FIGURE 2.
PRIMARY THRUSTER NORMALIZED EJECTION PROFILE

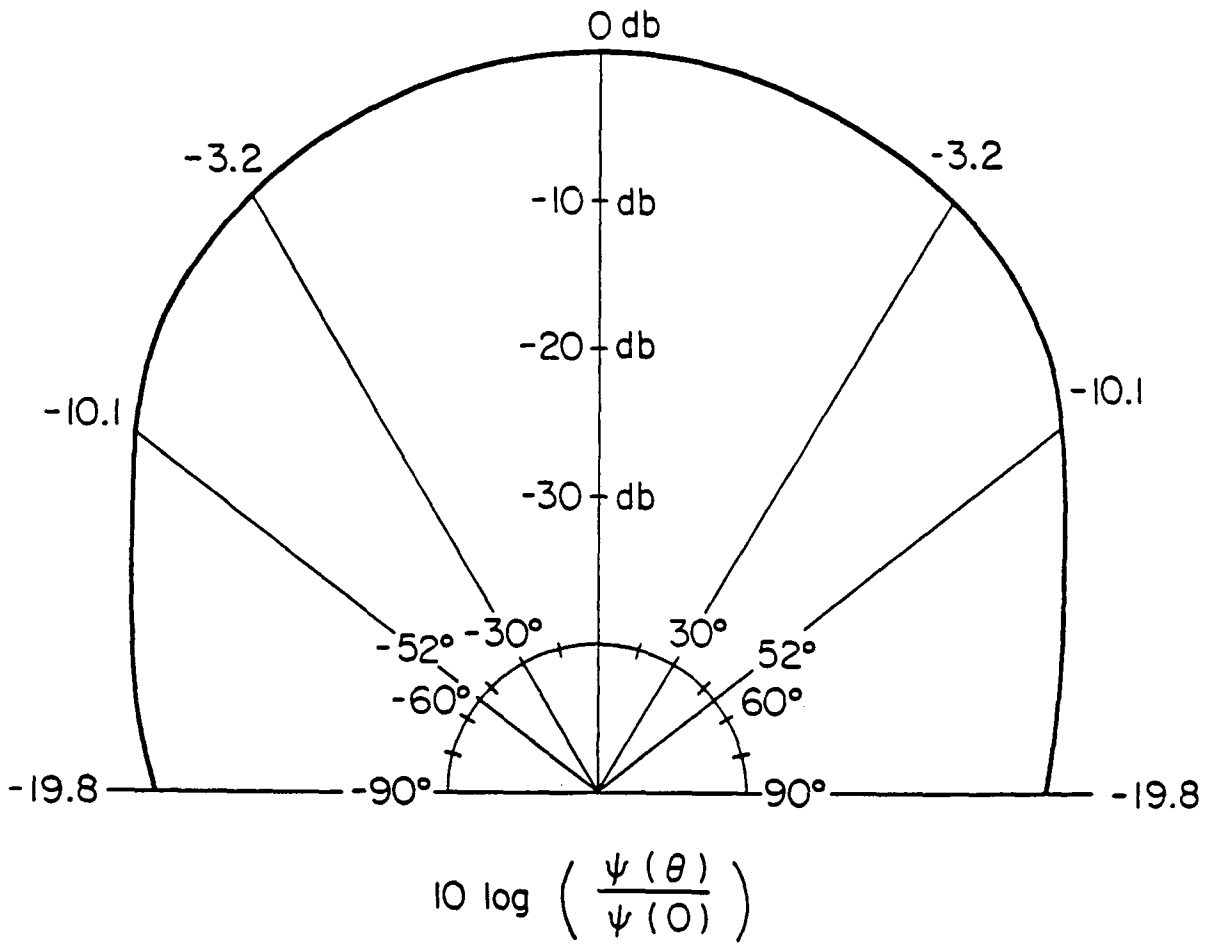

an RMS probe. Detailed descriptions of the instrument complement as well as a good review of other environmental measurements not covered here are available in Shawhan.[2] For those like the OSS-1 scientists who use the Orbiter as a measurement platform for doing Astronomy, earth science, materials testing or space plasma experiments, OSS-1 provided an environmental data base. Realizing that the Orbiter and its associated subsystems do not always provide an environment equivalent to that of the F2 ionosphere, enables better flight preparation. Since this paper deals in particular with temporary thruster modification of this region, it is useful to briefly review the physics and chemistry of the F2 region.

With a neutral component of $< 10^9/cm^3$ and an average plasma density of 10^5 to $10^6/cm^3$, the F2 region extends from approximately 225 to 400 km altitude and marks the layer of the ionosphere of highest plasma density. The dominant ion of the F2 region is O^+ created by ionizing UV < 910A and the dominant neutral is O. Less abundant N_2 and O_2 play an important part in the principle loss process for the O^+ ion. This process concerns the slow formation of the molecular ions N_2^+, NO^+, or O_2^+ and their rapid dissociative recombination as discussed in Banks.[4] From the standpoint of thruster effects, it is important to note that the H_2O and H_2 present in the exhaust plume have been shown to be 100 - 1000 times more efficient at formation of molecular ions with O^+ than the background N_2 and O_2 (for detailed chemistry see Mendillo[5]).

It is also important to compare the temperature and velocity of the exhaust plume with the temperature of the ions and neutrals at this altitude. Self-consistent models as well as satellite measurements have bounded the temperature at 240 km altitude to beween 1000°K and 2000°K. Ions and electrons from the exhaust plume have equivalent kinetic temperature of 22,000°K and 3,000°K respectively. This discrepancy arises because all plume constituents exit at relatively the same velocity giving the heavier ions a much higher equivalent kinetic temperature. With this background on the thrusters' exhaust characteristics and the F2 ionosphere, it is appropriate to discuss the experimental findings of the PDP.

TABLE 2.
THRUSTER PLUME CHARACTERISTICS

Primary Thruster	Vernier Thruster
M = 1419.8 G/S/Engine	M = 40.8 G/S/Engine

Composition - Neutrals

Species	Mol. Wt.	Mole Fraction
H_2O	18	0.328
N_2	28	0.306
CO_2	44	0.036
O_2	32	0.0004
CO	28	0.134
H_2	2	0.17
H	1	0.015
MMH - NO_3	46	0.002

Composition - Dominant Ions

NO^+	30	1.7×10^{-8}
CO_2^-	44	2.7×10^{-10}
OH^-	17	4.3×10^{-10}
Electrons	--	2.4×10^{-9}

Total Number of Neutrals and Ions

	Number of Neutrals	Number of Ions (Electrons)
VRCS		
Typical	1.3×10^{25}	3.1×10^{17}
Longest	1.7×10^{26}	3.8×10^{18}
PRCS		
Typical	9.2×10^{24}	2.1×10^{17}
Longest	5.5×10^{25}	1.2×10^{18}

Observations

Since the PDP on STS-3 was always either on the pallet or on the RMS in the near vicinity of the Orbiter, the measurements taken reflected only the local effects of thruster operations. Figure 3 exemplifies disturbances measured while in the cargo bay. Note first the middle panel labeled "pressure". The cold cathode ionization pressure gauge located near the bottom of the PDP is baffled to be insensitive to ram neutrals and meant to be a sense of the pressure near the surface of the PDP. Note that not all thruster operations are as obvious as the pair that occur at approximately 23:35, however, all but one register at least a small increase. At this particular time, the Orbiter is on the day side of the earth at mid-latitude and with the payload bay in wake. It should be noted that some data samples show a marked increase in pressure while others do not. Since the pressure gauge is only sampled every 1.6 seconds and typical firings (Table 1) of primaries last for only 80 msec it is not possible to give details of the time evolution of pressure.

However, an upper bound of the steady state pressure increase possible can be obtained by analysis of data during a specially scheduled engine test called the L2U burn. This data is

FIGURE 3.
STS-3 THRUSTER PLASMA EFFECTS

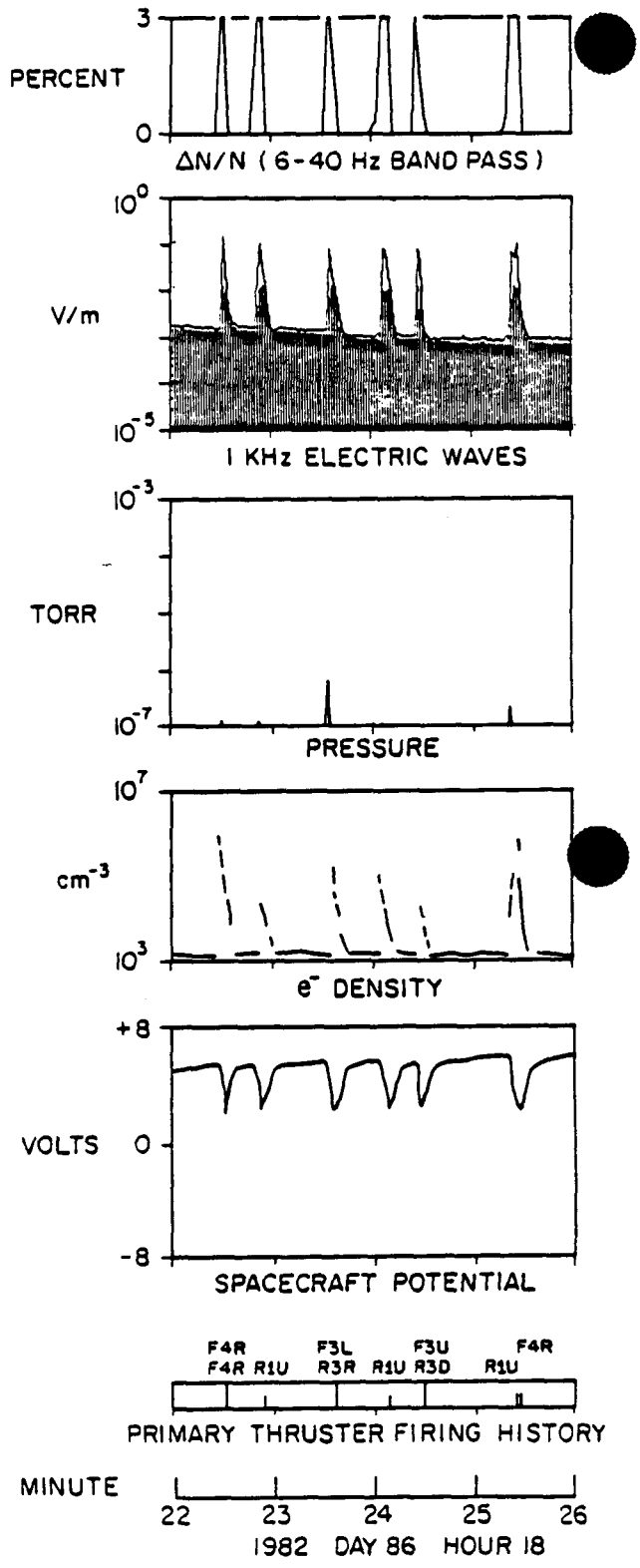

FIGURE 4.
PRESSURE ENHANCEMENT DURING L2U ENGINE TEST

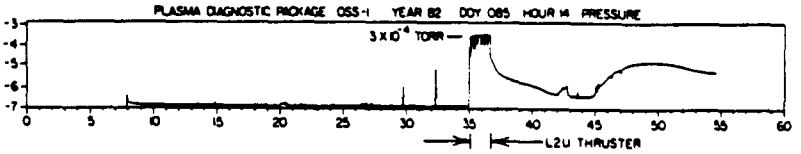

depicted in Figure 4. Note that pressure rose to 3×10^{-4} torr during this burn which lasted for more than a minute and consisted of L2U, R1U and F2U firing with 19 pulses from L2U, 34 from R1U and continuous emission from F2U. Note the large decay time after the engines shut down which is believed to be due to the slow outgassing of adsorbed emission products. In reality, no experiment should see long duration pressure increases of this nature. However, it is possible that any primary thruster firing could momentarily increase pressure to these levels, relaxing to ambient pressure on time scales of 1 second or less.

Next, returning to Figure 3 note the bottom panel which is a measure of PDP potential. Since the PDP is grounded to the Orbiter chassis it is also a measure of Orbiter potential with respect to local plasma as well. This panel is typical of thruster effects on spacecraft charge for this mission. There is an abrupt potential shift towards zero with a slow recovery time (~ 8 seconds for these examples). Vernier thrusters also induce this effect, but the magnitude and duration are less. Potential observations can be summarized as follows: Thrusters always act to push the potential toward negative and is most noticeable when the potential is positive and the PDP is in the plasma wake. Measurement of DC electric field indicates a modification as well, however, this data has yet to be incorporated.

A look at Panels 1, 2 and 4 provide additional clues to the cause of the potential shift. Recall that there is a significant plasma component to the exhaust plume. The top panel is a time history of the magnitude of plasma density irregularities ($\Delta N/N$) in the frequency range 6 - 40 Hz. Thruster operations induce large scale plasma density changes. It is in fact true that virtually every thruster firing documented can be seen by the Langmuir Probe which senses these irregularities. It matters little which thruster fires or for how long, a significant disturbance is always seen. A look at Panel 4 reveals that absolute electron density in these examples can change by several orders of magnitude. Unlike $\Delta N/N$ disturbances, however, this density enhancement is most pronounced with low ambient density that is in the plasma wake. This is understandable if one realizes that the total number of electrons available in a typical firing (Table 1) is similar to the number contained in the ambient F2 plasma approximately 100m on a side.

Panel 2 illustrates that an increase in background electrostatic noise accompanies thruster operation. Although only a 1 kHz (±15% bandwidth) channel of an electrostatic wave analyzer is plotted, this disturbance is evident from approximately 30 Hz to 200 kHz. A background noise level of ~ 10^{-3} V/m is due to the Orbiter plasma interaction and is briefly described in Shawhan.[3] This noise which present theory[6] attributes to lower hybrid drift instabilities driven by plasma density gradients could be amplified by the introduction of yet another plasma which increases those density gradients. This enhanced electrostatic noise is also present to a greater or lesser degree with virtually all vernier and primary thruster operations.

In summary, the local effects seem to have two time scales. A short time scale for the neutral pressure enhancement which for typical thruster operations is on the order of one second, and a longer plasma perturbation time scale associated with enhanced electrostatic emission, increased plasma density, altered electric fields and spacecraft potential. This longer duration disturbance can range from a few seconds to almost half a minute. Recalling the amount of plasma introduced by typical thruster firings (Table 2) and the temperature and density of the plume compared to the ambient ionosphere, it is clear that the RCS engines act almost as a local point source for electrons which are near thermal. The enhanced electron densities observed near the Orbiter and "discharge" of electric potential are consistent with this scenario. Ions which have velocities high compared to thermal ions tend to escape with the net plume velocity and only those scattered from Orbiter surfaces are believed to be seen immediately following a firing. Presently work is underway to analyze the ion energies observed so as to determine if ions seen during thruster operations could be accelerated by electric fields present near the Orbiter. An Ion Mass Spectrometer on the PDP does see order of magnitude enhancements in H_2O^+ and NO^+ which are important constituents of the plume.[7] It is important to note that higher electron densities and neutral pressure are also consistent with enhancement in the shuttle glow phenomenon discovered by Banks et al. on STS-3.[8]

Future Modeling and Experimental Problems

Extensive modeling of the chemical effects of rocket releases have been done by Bernhardt[9] and Mendillo[10] with emphasis on the effects of Shuttle OMS burns and circularization burns of the proposed HLLV. Results indicate that source efficiency factors (the number of ion-electron pairs destroyed compared to the total plume destruction potential) for H_2O - H_2 exhaust plumes tend to increase with smaller mass release and tend to increase with altitude to at least 400 km. Mendillo[10] models a release of 10^{30} molecules to have an efficiency of ~ 1.2% at

TABLE 3.
RELATIVE PLASMA DATA CONTAMINATION OF VERNIER AND PRIMARY RATE HOLD MANEUVERS

	DAP Settings		% Contamination
Vernier	Discrete Rotation Rate	0.135°/sec	5
	Rate Deadband	0.02°/sec	
	Attitude Deadband	1.0°	
	Minimum Pulse	0.01°/sec	
Primary	Discrete Rotation Rate	0.135°/sec	30
	Rate Deadband	0.2°/sec	
	Attitude Deadband	5.0°	
	Minimum Pulse	0.1°/sec	

400 km while a 10^{27} molecule release has an efficiency close to 11%. A PRCS firing or extended VRCS firing releasing 10^{25} -10^{26} molecules over a period of a few seconds to few tens of seconds could have a higher source efficiency because of the lower plume density and the fact that the plume becomes more like a line source.[10] Because of these considerations, it may be worthwhile modeling not just OMS effects, but the plumes of the smaller RCS thrusters as well. Spacelab-2 currently scheduled to fly in March 1985 at an altitude of 400 km includes ionospheric modification measurements to several km beyond the shuttle. The PDP on this mission will have higher resolution pressure measurements, collect plume data as a free-flyer as well as in the Orbiter bay and on the RMS. Coupled with the addition of ground based diagnostics and carefully scheduled OMS burns, a great deal can be gained by these in situ diagnostics. The near Orbiter measurements of STS-3 provide information for experiment design on SL-2, suggest new modeling possibilities and provides a new dimension in time scale studies of chemical releases.

Operational Trade-Offs

Despite the fact that the thrusters and OMS engines provide in themselves an interesting experiment in ionospheric modification, it may be important and even critical in some instances to avoid the plasma effects as much as possible. This is particularly difficult for instruments which may be doing optical observations since they often require accurate pointing which by its nature needs thruster assistance. Previous evidence from Mendillo[1] refers to enhancements in airglow emissions from rocket plumes. Instrumentation aboard Spacelab-1 may be capable of measuring enhanced airglow from the Orbiters' thrusters and determining if it presents an operational problem for experimenters needing optical or infrared data.

Data from STS-3 serves to illustrate that how one chooses to hold an attitude and to what precision greatly determines the frequency and duration of thruster operation. Table 3 shows two examples of digital autopilot settings and the resultant degree of data contamination in a 10-minute interval. Example 1 uses the verniers only to hold a rotation rate of .135°/second with a deadband rate of .02 and minimum Δ pulse of .01°/second. This resulted in little contamination. Example 2 holds the same rate (.135°/second) with primaries using a minimum Δ pulse of 0.1°/second. The difference in number of firings is quite pronounced. In general, it seems better to maneuver with primaries and better to hold attitude with verniers. The tighter the constraint on the deadband in attitude hold or rate of roll, the higher the frequency of thruster operations. By carefully considering these trade-offs, the experimenters working with NASA can best optimize their measurement opportunities while minimizing fuel usage.

References

1. Mendillo, Michael, "The Effect of Rocket Launches on the Ionosphere," Adv. in Space Res., Vol., 1, pp. 275-290, 1981.

2. Shawhan, S. D. and G. B. Murphy, "Plasma Diagnostics Package Assessment of the STS-3 Orbiter Plasma Environment," AIAA Paper 83-0253, Reno, Nevada, 10-13 January 1983, Submitted to J. Spacecraft and Rockets, 1983.

3. Shawhan, S. D., G. B. Murphy and D. L. Fortna, "Measurements of STS-3 Electromagnetic Interference by the OSS-1 Plasma Diagnostics Package, submitted to J. Spacecraft and Rockets, 1983.

4. Banks, P. M. and G. Kockarts, Aeronomy (Part B), Chapter 20, Academic Press, New York, 1973.

5. Mendillo, Michael, Gerald S. Hawkins and John A. Klobuchar, "An Ionospheric Total Electron Content Disturbance Associated with the Launch of NASA's Skylab," Tech. Report 74-0342, AFCRL, Bedford, Mass., 1974.

6. Papadoupolus, K. and K. Ko, "Electron Energization and Optical Emissions in the Space Shuttle," Geophys. Res. Lett., submitted for publication, 1983, and K. Papadoupolus, "Shuttle Glow (The Plasma Alternative)," SAI Report 84-147-WA, 1983.

7. Grebowsky, Joseph, M., "Measured Thermal Ion Environment of STS-3," Paper No. 83-2597 this AIAA Session, 1983.

8. Banks, P. M., P. R. Williamson and W. J. Raitt, "Space Shuttle Glow Observations," Geophys. Res. Letter, Vol. 10, pp. 118-121, 1983.

9. Bernhardt, "Three-Dimensional, Time-Dependent Modeling of Neutral Gas Diffusion in a Nonuniform, Chemically Reactive Atmosphere," J. Geophys. Res., Vol. 84, pp. 793-802, 1979.

10. Mendillo, Michael and Bruce Herniter, "Modification of the Aerospace Environment by Large Space Vehicles, Vol. 17, #3, pp. 226-231, 1980.

From: Proceedings of the AIAA Shuttle Environment and Operations Meeting, Washington, DC, Oct. 31-Nov. 2, 1983.

MEASURED THERMAL ION ENVIRONMENT OF STS-3

J. M. Grebowsky
M. W. Pharo III
H. A. Taylor, Jr.
I. J. Eberstein
NASA Goddard Space Flight Center
Greenbelt, Md. 20771

83-2597

Abstract

The Plasma Diagnostic Package (PDP) on the third Space Shuttle Flight (STS-3) included a Bennett RF ion mass spectrometer which surveyed the positive ion composition in the vicinity of the vehicle. The ion measurements both within and exterior to the Shuttle cargo bay show the pervasive influence of the Shuttle's own gaseous emissions on its immediate plasma environment. Within the bay the ion spectrometer detected copius quantities of ions when the Shuttle was in daylight and when the gas pressure at the surface of the PDP was enhanced. In general few cases of ion detection occurred when the bay was facing toward the Shuttle wake. The plasma near the Shuttle consisted predominately of O^+ (16AMU) ions and ions with atomic masses of 18, 30, 32 and 44 AMU corresponding to H_2O^+, NO^+, O_2^+ and CO_2^+. All of these ions with the exception of H_2O^+ and CO_2^+ are expected ambient ions at the Shuttle's altitude of 240KM. During some thruster firings the 18 and 30 AMU ion concentrations detected within the bay increase by up to an order of magnitude within the 2.4 second sweep of the instrument. During these latter events the O^+ contributions did not show a similar change.

I. Background

Included in the Plasma Diagnostic Package (PDP) flown on the STS-3 Shuttle mission was a Bennett ion mass spectrometer. This spectrometer was similar in construction to those successfully flown on numerous sounding rockets, the Atmosphere Explorer Satellites C and E and on the Pioneer Venus orbiter. The details of the spectrometer operation have been previously discussed in the literature (e.g., Brinton et al.[1]) and hence will not be repeated here. Under ideal conditions the spectrometer is capable of measuring ion species in the range from 1 to 64 atomic mass units with number densities from approximately 20 to 2×10^7 ions/cm^3. The sweep rate of the instrument through the entire range of atomic mass units was approximately 2.4 seconds which as will be seen is fast enough to resolve perturbations in the Shuttle's plasma environment due to attitude variations but not fast enough to detect all the perturbations produced directly by the short period thruster firings.

There are two important advantages in using an ion mass spectrometer to study the immediate environment of the Shuttle. First it is possible to resolve details of how the plasma is perturbed near the Shuttle by the aerodynamical impact of the spacecraft on the ambient ionosphere. Second by the detection of ion species which can only be of Shuttle origin the spectometer can provide some insight into the nature of the gases that envelop the spacecraft. During the course of the STS-3 mission, the PDP was operated while stowed on the pallet within the cargo bay. In addition, a variety of measurements were obtained while the instrument was operated on the Remote Manipulator system arm (RMS). In the latter mode the PDP was put through several complicated maneuvers to determine some of the properties of the Shuttle wake as well as the effects of electron gun firings on the Shuttle's immediate environment. In this paper we will not consider the ion composition detected on the extended RMS, but instead will concentrate on the observations made while the PDP was secured within the Shuttle's bay, where the number of ions collected by the spectrometer were dependent only upon the attitude and location of the Shuttle and the products of Shuttle emissions. The ion spectrometer observations are explored to determine how contaminated the STS-3 plasma environment actually is and to see exactly what type of perturbation the Shuttle's own gaseous emissions have on the plasma within the bay when the bay doors are open.

II. Spectrometer View

For the exact location of the ion mass spectrometer with respect to the other instruments on the PDP as well as a brief overview of the initial PDP measurements the reader is referred to the paper of Shawhan and Murphy[2]. For the present it suffices to note that the orifice of the ion mass spectrometer is not facing unobstructedly into free space. The position of the PDP on the pallet was such that the spectrometer was directed toward the interior port bulkhead of the Shuttle bay (i.e., parallel to the Y axis in Shuttle coordinates — see Figure 1). It was located below the bay door and indeed below the Vehicle Charging and Potential Experiment package which was placed on the side of the pallet toward which the spectrometer faced.

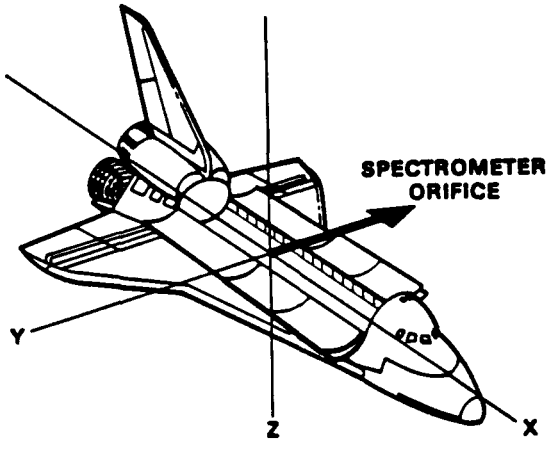

Fig. 1. In the Shuttle coordinate system the ion spectrometer is directed parallel to the Y axis.

Since thermal ion spectrometer measurements of incident ion flux can only accurately be converted into number density when the average speed of the plasma into the spectrometer orifice is known, it is evident that the complex geometry of the barriers surrounding the spectrometer while in the bay makes this a difficult task. Hence instead of specifying the ion number densities explicitly, the collected ion currents will be used to analyze the ion composition within the bay. This will provide a good estimate of the relative ion composition since the current of each ion collected is in general proportional to its density.

III. Shuttle Attitude

The STS-3 flight was primarily a thermal mission and this drove the operational timeline. Attitudes employed were nose-to-sun (with a roll rate two times that of the orbit rate), tail-to-sun, top-to-sun, and Thermal Passive Control —the so called barbecue mode. Most of the PDP observations were taken with the nose-to sun attitude. For simplicity this discussion is confined principally to the nose-to-sun configuration since the length of time spent in this configuration allows one to discern repeatable orbit by orbit variations in the bay ion population.

A schematic drawing of the Shuttle orientation during a typical nose-to-sun orbit is shown in Figure 2. The Shuttle rolls twice per orbit. The STS-3 inclination was 38 degrees with the line of node approximately perpendicular to the sun vector. In this orbital configuration the Shuttle's open bay faces into the ram direction only once per orbit at the ascending node near the dawn terminator. Shawhan and Murphy[2] have indicated the importance of this in understanding the periodic enhancement of the neutral pressure measured by the Pressure Gauge on the PDP — the pressure, as is to be expected, peaks as the ambient gas rams into the bay.

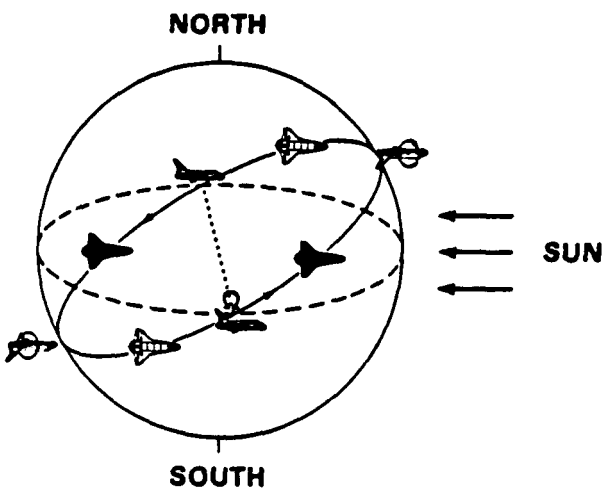

Fig. 2. The Shuttle attitude in the nose-to-sun 2X orbital rate spin configuration has only one region along the orbit at which the bay is toward the ram direction-the ascending node.

IV. Ion Measurements

STS-3 was launched on March 22,1982 (day number 81). The major ion currents detected along an entire orbit within the bay during the first nose-to-sun attitude period are shown in Figure 3. The ion spectrometer was stepped consecutively through 4 different sensitivity modes by varying the retarding voltage in front of the collector. In this paper only one of these modes is considered — the one with the next to the lowest sensitivity — to ensure the maximum mass resolution possible for identifying the more prominent ions present. All of the ion currents to be shown in the plots were obtained during this mode.

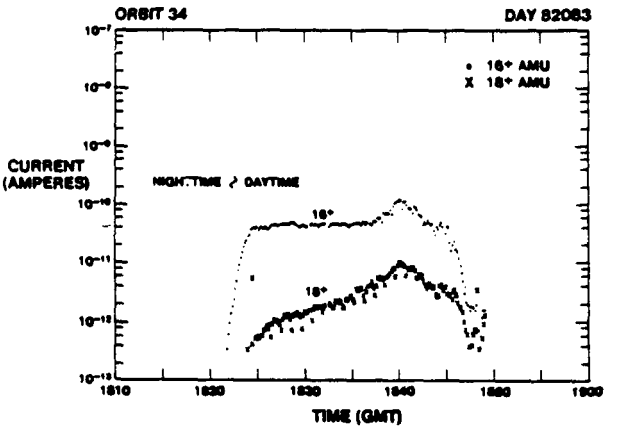

Fig. 3 (a) The collected ion currents in the bay for the ion species with atomic masses of 16 and 18 are shown for orbit 34. The ion currents rise rapidly at sunrise then later in the day abruptly drop below the instrument sensitivity.

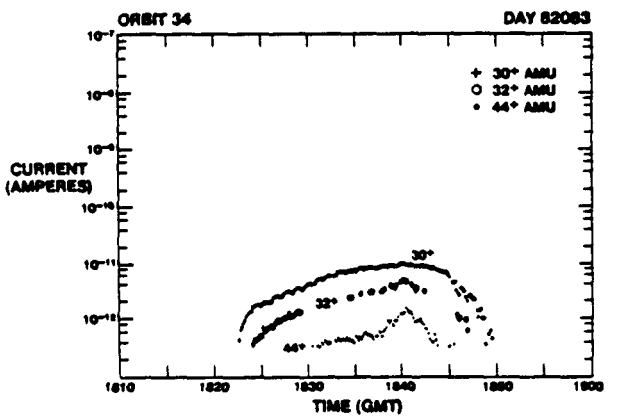

(b) The heavy mass ions measured on the same orbit follow similar variations. The ions with atomic masses of 18 (H_2O^+) and 44 (CO_2^+) are STS-3 borne contaminants.

Figure 3 depicts only a 50 minute period of observations out of an orbital period of approximately 1.5 hours. Thermal ions were not detected on the unplotted portions of the orbi

Figure 3a shows the lower atomic masses observed whereas Figure 3b shows the heavier ions. Although a momentary enhancement of the ion currents (and of course their densities) is seen just after 1815 GMT, the ionization buildup near the spectrometer occurs rapidly at the time the Shuttle crosses into daylight. The aproximate position at which STS-3 crossed the terminator into sunlight is indicated by the wavy line. The most dominant ion observed is mass 16 (O^+) which is typically the dominant ambient ionospheric ion at the STS-3's mean altitude of 244km. Other detected ions, typical of ionospheric species, include the 30 and 32 AMU ions which correspond to ionized NO and O_2 respectively.

Although some of the ions observed on the orbit depicted in Figure 3 have masses characteristic of those in the ambient ionosphere, the overall behavior of the ion composition measured in the bay cannot be explained by ionospheric variations along the STS-3 orbit. The secondary ions with atomic mass numbers 18 and 44 have never been reported to be seen with such prominence at these altitudes in the ionosphere. The most likely ion species corresponding to these masses are H_2O^+ and CO_2^+ respectively — i.e., ions whose neutral molecule counterpart is deposited in the vicinity of the Shuttle by outgassing of materials, by cabin leakage as well as by engine firings. Neutral gas composition changes due to Shuttle emissions have been measured directly on several Shuttle flights by the Neutral Gas Mass Spectrometer as part of the Induced Environment Contamination Monitor (Carignan[3]).

Another feature of the bay composition which cannot be explained by ambient ionosphere variation is the restricted region along the orbit where the collected ion currents rise several orders of magnitude above the instrument limiting sensitivity. Although the bottomside of the F-layer can be very sharp near the equator and result in measured ion densities on a circular orbiting satellite that abruptly increase as the spacecraft moves from the bottomside of the layer into the layer maximum (Brinton[4]), this cannot explain the composition variations shown in Figure 3. Firstly the 16 AMU ions are not the dominant ionospheric species in the bottomside of the sharp layers - the molecular ions NO^+ and O_2^+ are. In the STS-3 observations these molecular ions do not dominate the ion distributions. Secondly, the bay ion densities abruptly dropped near 0210 GMT — at a local time near noon — where, because of photoionization, the bottomside of the F-layer is not sharp. Hence the observed ion concentration variations do not seem to be directly related to expected ambient ionosphere variations.

The region in which significant ion concentrations are seen is not just peculiar to the one orbit depicted in Figure 3. In the nose-to-sun 2X orbital rate roll configuration the ion population within the bay always rose abruptly near the dawn terminator only to decrease later in sunlight about 25 minutes later. Figure 4 shows another example of measurements made on a similar type of orbit taken two and one half days later in the bay. Only the four most dominant ions are plotted here — again, they correspond to species with atomic masses of 16, 18, 30 and 32. The same general orbital variation of the ion current at and after the dawn terminator crossing observed in the earlier example is evident. Another feature found on many orbits is a precursor enhancement of the ion currents followed by a decrease before sunrise. On the orbit depicted in Figure 4 this feature is fairly prominent. In the following section, explainations will be offered for this latter enhancement as well as for the recurring dayside current enhancement. The large drop in the ion currents seen just before 0435 GMT is not related to the undisturbed temporal development of the bay population. Rather, it is caused by the firing of the plasma gun carried on STS-3 which produces a positive spacecraft charge that prevents the thermal ions from entering the spectrometer.

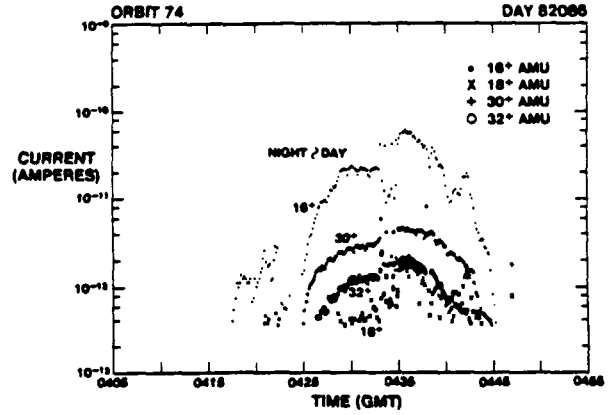

Fig. 4. The collected currents of the 4 dominant ions on orbit 74 show the same basic variation along the orbit as was seen on the previously discussed orbit 34. Note the ionization enhancement before the prominent terminator enhancement.

V. Controlling Processes

As previously mentioned, Shawhan and Murphy[2] showed that there was a diurnal variation in the gas pressure at the PDP surface for the nose-to-sun 2X orbital rate roll orbits. If one compares the measured pressure variations plotted in that paper with the ion variations for the two orbits considered thus far, it becomes evident that the dayside decrease of the ion concentration occurs simultaneously with the decrease in the pressure. However, the pressure at the PDP within the bay shows no rapid increase at the terminator as do the ion concentrations. The pressure rises in its diurnal cycle well before this time. Although the gas pressure enhancements appear to be due to ambient gas colliding with open bay surfaces near the ascending node when the bay is exposed to the ram direction, the ion behavior is noticeably different.

The most plausible source of the ions detected is photoionization of the gas cloud surrounding the space vehicle. Such a mechanism would explain the onset of ionization at the

terminator as well as the drop-off of the ionization when the gas pressure at the PDP drops to its background level. The absence of ionization within the bay during other parts of the orbit arises because the bay is then facing into the wake of the Shuttle.

The precursor enhancement of ions may reflect the expected collected current maximum at that point in the orbit when the ambient ions rammed by the Shuttle can travel to the spectrometer orifice without being shielded by the Shuttle or anything in the bay. This can be seen by consideration of Figure 2 with the spectrometer directed in the starboard direction. At the antisolar point the spectrometer is directed into the spacecraft ram direction and would collect a large flux of ions were it not blocked by the Vehicle Charging and Potential experiment in front of it. On the other hand, at the ascending node the open bay is in the ram direction but the instrument is pointing 90 degrees from it; hence currents will be low. Between these two points is a region where the angle of attack to the orifice is less than 90 degrees and where the plasma incoming has direct access to the spectrometer resulting in a peak in the collected current. Indeed the ion spectrometer, which is sensitive to the flow energy into its orifice, shows a mass spectrum in this region that is characteristic of inflowing ions. Hence the precursor event is consistent with ambient ions flowing directly to the spectrometer.

VI. Short Term Perturbations

In addition to the regular repeatable behavior observed on nose-to-sun attitude orbits there are also short term changes in the ion composition in response to activities of the Space Shuttle. Some of these are evident in the measurements shown in Figure 5. Again we have the typical enhancement of the collected ionization near the terminator. In this instance the mass 18 ions are comparable in concentration to the mass 16 ions on the ascending leg of the current curves until approximately 0150 GMT whereupon the H_2O^+ current drops rapidly. The other ion species do not show this behavior. Also, although not plotted, ions with atomic mass 19 were detected along with the initially enhanced H_2O^+. This feature was not seen to repeat from orbit-to-orbit.

The observed high concentrations of water ions are reminiscent of the behavior of the ion composition observed within "ionosphere holes" that have been created by experimental dumpings of water in the ionosphere. As reported by Sjolander and Szuszczewicz[5] these holes not only correspond to a depletion of O^+ ions with an attendent increase in the H_2O^+ ions, but also are characterized by the presence of mass 19 ions identified as H_3O^+ ions that are the result of interacting neutral water molecules and ions. Indeed a water dump was made from the Shuttle on this orbit approximately a half hour before the observations in Figure 5. In sunlight the water ice associated with the water dump will sublimate and the gaseous water will be ionized. A sharp drop off in the water ion concentration would then be expected as the Shuttle moves through the ionization of this local water enhancement.

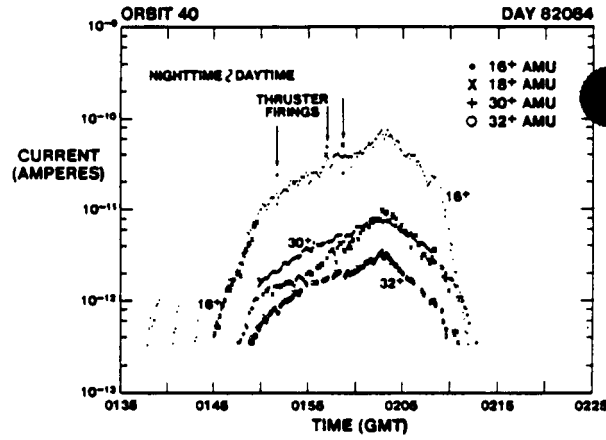

Fig. 5. Another nose to sun oriented orbit is shown. This orbit is unique in that the H_2O^+ ions are comparable in concentration to O^+. A water dump occurred before these measurements were made. Also discrete enhancements are observed in the mass 18 and 30 ion currents that are associated with thruster firings. In addition to the ions shown, ions with atomic mass 19 were also observed during the initial H_2O^+ enhancement and during the thruster events.

Another phenomenon that is commonly seen is the appearance of discrete enhancements in the concentrations of ions with atomic masses 18, 19, and 30. These are singled out in Figure 5 by arrows. On this pass ions of atomic mass 19 also appeared in association with the spikelike enhancements but are not shown in the figure. T perturbations occur on a very short time scale. They are detected on only a single sweep of the ion spectrometer through the entire mass range which takes 2.4 seconds. On the prior and succeeding sweeps these current spikes are noticeably absent.

Thruster firings of either the Primary Reaction Control System or the Vernier Control System can and do produce gaseous emissions on time scales shorter than the spectrometer sweep period. Indeed the three ion current spikes seen in Figure 5 were associated with thruster firings. In this instance the times of the firings were determined from spikes in the VLF electric field strength measured on the PDP (obtained from the PDP survey slides provided by J. Pickett, University of Iowa). Studies by Shawhan and Murphy[2,6] have shown that these VLF bursts correlate with the thruster firings. Although the ion spikes in general are observed only with thruster firings, the converse does not hold. Since the firings can and do take place in times less than one second, the bursts of gas may produce ionization in a time scale much shorter than the instrument sweep period so that the ionization peaks are not observed.

The Shuttle thrusters use monomethyl-hydrazine with hydrogen tetroxide as the oxydizer.

The observations of enhanced H_2O^+, H_3O^+ and NO^+ densities are consistent with the chemical products which can be produced by the combustion (as can be deduced from the studies of Eberstein and Glassman[7], Phillips and Shaw[8], and Hurle et al.[9]) However, at the present time, it is not known whether the observed ionization is due to photoionization of the thruster gases, charge transfer with the ambient ions, ionization produced within the combustion chamber or to the critical ionization mechanism discussed by Papadopoulos[10]. A more detailed study of the ion composition variations observed during the firings in combination with other plasma measurements made in the vicinity of the Shuttle should help resolve this question.

VII. Conclusions

The STS-3 ion composition measurements presented show that the plasma environment within the cargo bay is a very dynamic medium. The wake of the Shuttle is severely depleted of ionization and photoionization of the Shuttle's own gaseous envelope appears to play a role in producing the bay plasma. There is also evidence of plasma flowing into the bay. Water dumps and engine firings are reflected in characteristic changes of the ion composion. Measurements have been presented for only those orbits in which the Shuttle's nose was pointed toward the sun as it rolled twice per orbital period. This configuration resulted in a generally repeatable variation in the bay ion composition from orbit to orbit. We don't want to end leaving the impression that the bay variations are always this regular. The dominant effect of the spacecraft attitude on determining this variation can be seen by referring to the orbit plotted in Figure 6. The Shuttle on this orbit was initially in the nose-to-sun configuration but was then reoriented for a Reaction Control System burn attitude before going back to its original attitude. Prominent engine firing related ion spikes are evident, as are distinct changes in the ion current profiles with the attitude changes.

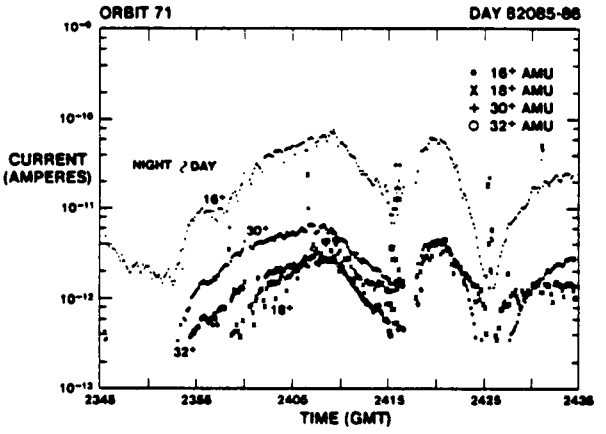

Fig. 6. On this orbit the Shuttle was initially in the nose-to-sun configuration and the ion currents as described earlier began to increase at the terminator. The attitude was changed for a Reaction Control System burn resulting in a more complex variation in the ion measurements and to a greater incidence of thruster related ion enhancements.

References

1. H. C. Brinton, L. R. Scott, M. W. Pharo, III, and J. T. C. Coulson, "The Bennett ion mass spectrometer on Atmosphere Explorer-C and-E", Radio Science, Vol. 8, pp 323-332, 1973.

2. S. D. Shawhan and G. B. Murphy, "Plasma Diagnostic Package Assessment of the STS-3 orbiter environment and systems for science", AIAA 21st Aerospace Sciences Meeting, Reno, Nevada, Paper AIAA-83-0253, January, 1983.

3. C. R. Carignan, "Neutral Gas Mass Spectrometer on the IECM" in The Shuttle Environment Workshop, Prepared for NASA by Systematics General Corporation, pp A139-A146, 1983.

4. H. C. Brinton, "Variations in thermospheric hydrogen and oxygen inferred from ion chemistry", in Proceedings of a Symposium on the Scientific Results Of Atmospheric Explorer, Bryce Resort, National Aeronautics and Space Administration, Washington, D.C. 1977.

5. G. W. Sjolander and E. P. Szuszczewicz, "Chemically depleted F2 ion composition: measurements and theory", J. Geophys. Res., Vol. 84, pp 4393-4399, 1979.

6. S. D. Shawhan and G. Murphy, "STS-3/OSS-1 Plasma Diagnostics Package (PDP) measurements of Orbiter transmitter and subsystem electromagnetic interference", in The Shuttle Environment Workshop, prepared for NASA by Systematics General Corporation, pp A233-A250, 1983.

7. I. J. Eberstein and I. Glassman, "The gas phase decomposition of Hydrazine and its derivatives", Tenth Symposium (International) on Combustion, pp. 365-374, The Combustion Institute, 1965.

8. L. Phillips and R. Shaw, "Reactions of Methyl and Methoxyl Radicals with Nitrogen Dioxide and Nitric Oxide", Tenth Symposium (International) on Combustion, pp. 453-361, 1965.

9. I. R. Hurle, J. M. Sugden, and G. B. Nutt, "Chemi-ionization of nitric oxide in flames containing hydrocarbon additives", Twelfth Symposium (International) on Combustion, pp. 387-394, 1969.

10. K. Papadopoulos, "On the Shuttle glow (the plasma alternative)", Science Applications Inc. Report No. 84-147-WA, Washington, D.C., 1983.